Non-Equilibrium Electron Transport through a Double Quantum Dot System

Study of Two Exchange Coupled Quantum Dots in a 4-Terminal Geometry

Zur Erlangung des akademischen Grades eines
DOKTORS DER NATURWISSENSCHAFTEN
von der Fakultät für Physik der Universität (TH)
Karlsruhe

genehmigte

DISSERTATION

von

Dipl.-Phys. Verena Körting
aus Augsburg

Tag der mündlichen Prüfung	07.12.2007
Referent	Prof. Dr. Peter Wölfle
Korreferent	Prof. Dr. Alexander Mirlin

Abstract

In this thesis we study two quantum dots, coupled by an exchange interaction, with an emphasis on non-equilibrium physics. Both dots are assumed to be in the Coulomb blockade regime, such that the number of particles on the dots is conserved. Assuming a single electron on each quantum dot, the double quantum dot system is characterized by an interplay between the spin-spin coupling of the dots with the leads, the so-called Kondo interaction, and the spin-exchange coupling between the dots. We find that a finite voltage on one quantum dot drives the other quantum dot out of equilibrium. This behavior can be explained in a simple picture: Two coupled spins form singlet and triplet states with an excitation gap given by the spin-spin interaction. In equilibrium it is known that temperature determines the occupation of the states. Out of equilibrium thermodynamic considerations no longer apply. The occupation of the quantum dot states is then determined by a self-consistent equation, which includes the effects of a finite voltage and the corresponding decoherence due to a finite current. If the voltage provides sufficient energy to overcome the singlet-triplet gap, the occupation probability of the ground state decreases and excited states become populated. Since the triplets are current-carrying states and the singlet does not allow for transport in the lowest approximation, the effect of the non-equilibrium distribution functions is visible in the differential conductance. In the case of an antiferromagnetic exchange coupling between the dots a large voltage on one quantum dot leads to a finite occupation of triplet states, which can be probed by a current measurement in the other quantum dot. We expect experiments to observe this transfer of non-equilibrium properties, if it is possible to fabricate a double quantum dot device in a 4-terminal geometry.

In this thesis a setup exhibiting the explained non-equilibrium transfer is discussed. From the Anderson impurity model an effective Kondo model is derived by a Schrieffer-Wolff transformation, and it is explained why the current through the left and the right quantum dot can be treated independently. The physics of the spin Kondo model is calculated to lowest order perturbation theory in the coupling to the leads. Attention has to be paid to the case of very small spin-spin interaction, but the main part of this thesis deals with a large singlet-triplet gap. The magnetization, the polarization, the current, and the T-matrix are calculated to 2nd order in perturbation theory. The exchange coupling from the left to the right quantum dot leads to the above-mentioned non-equilibrium transfer and a new quantity, the transconductance, is introduced to measure this effect. Although the transconductance is observed already in 2nd order perturbation theory, the effect originates indirectly through the voltage-dependent occupation probabilities. In current-current correlations the non-equilibrium transfer can be observed directly. It is shown that the current cross-correlation between the current through the left and right quantum dot is finite due to the decoherence and finite life time of the quantum dot states. Although this calculation is performed to fourth order in the coupling to the leads, the non-zero result is of second order. As is well-known from the Kondo effect at low temperatures logarithmic divergences do not allow for a perturbation expansion. New methods were developed and the non-equilibrium community tries to find a consensus on which method is best suited to describe the Kondo effect with a finite bias voltage. In this thesis two different approaches are presented, based on the poor man's scaling approach and on the flow equation approach. In non-equilibrium all processes in the energy window opened by the voltage contribute to the transport

properties. Therefore it is important to include the frequency of the incoming and outgoing particles of a scattering process into any scaling theory. This is incorporated in both methods discussed here. They only differ in the way the decoherence, which plays a major role in systems out of equilibrium, is included. We find in both approaches that a finite voltage applied to one quantum dot drives an exchange coupled quantum dot out of equilibrium. Whereas the first method is presented with results for the current, the transconductance, and the T-matrix, the second method is on a Hamiltonian level and the non-equilibrium transfer is discussed by its signatures in the flow of the coupling functions. The transconductance is enhanced by the scaling procedure and therefore we hope that it can be measured in experiments in the near future.

Deutsche Zusammenfassung

In dieser Dissertation wird das Verhalten zweier gekoppelter Quantenpunkte untersucht, die zum einen durch eine Austauschwechselwirkung gekoppelt sind und zum anderen durch eine endliche Spannung aus ihrem Gleichgewichtszustand getrieben werden. Des weiteren wird angenommen, dass sich beide Quantenpunkte im Bereich der Coulomb-Blockade befinden, so dass die Anzahl der Teilchen auf den Quantenpunkten erhalten ist. Es wird angenommen, dass jeder Quantenpunkt mit jeweils einem einzelnen Elektron besetzt ist. Damit ist das Verhalten des Doppelquantenpunktsystems geprägt durch ein Wechselspiel zwischen der Spin-Austausch-Wechselwirkung der beiden Quantenpunkte und der Spin-Spin-Wechselwirkung jedes Quantenpunktes mit den Zuleitungen, der sog. Kondo-Wechselwirkung.

Es zeigt sich, dass ein Quantenpunkt aus seinem Gleichgewichtszustand getrieben wird, falls über den anderen Quantenpunkt eine endliche Spannung angelegt wird. Dieses Verhalten kann in wenigen Worten verständlich gemacht werden: Zwei gekoppelte Spins bilden Singulett- und Triplett-Zustände, die durch eine Anregungsenergie, gegeben durch die Spin-Spin-Wechselwirkung, aufgespalten sind. Es ist bekannt, dass im thermischen Gleichgewicht die Besetzung der Zustände durch die Temperatur gegeben ist. Dies gilt nicht mehr für Systeme außerhalb des Gleichgewichts. Die Besetzung der Quantenpunktzustände ist daraufhin durch eine selbstkonsistente Gleichung bestimmt, die den Beitrag einer endlichen Spannung und der entsprechenden Dekohärenz aufgrund eines endlichen Stromflusses enthält. Falls die Spannung genug Energie zur Verfügung stellt, um die Singulett-Triplett-Aufspaltung zu überbrücken, nimmt die Besetzung des Grundzustandsniveaus ab und angeregte Zustände werden zunehmend besetzt. Da die Triplett-Zustände stromtragend sind und der Singulett-Zustand in erster Näherung den Stromkanal blockiert, lässt sich ein Effekt der Nichtgleichgewichtsbesetzung in der Messung der Leitfähigkeit beobachten. Falls die Austauschkopplung zwischen den beiden Quantenpunkten antiferromagnetisch ist, kann eine starke Spannung an einem Quantenpunkt zu einer endlichen Besetzung der Triplett-Zustände führen. Dies kann mit einer Strommessung an dem anderen Quantenpunkt nachgewiesen werden. Wir erwarten, dass diese Übertragung von Nichtgleichgewichtseigenschaften in Experimenten zu beobachten ist, falls es möglich ist, ein Doppelquantenpunktsystem in einer 4-Kontakt Geometrie herzustellen.

In dieser Arbeit behandeln wir ein System, das die erklärte Nichtgleichgewichtsübertragung zeigt. Ausgehend von einem Anderson-Störstellenmodell wird ein effektives Kondomodell mittels einer Schrieffer-Wolff-Transformation hergeleitet und es wird erörtert, warum der Strom durch den linken Quantenpunkt und durch den rechten Quantenpunkt als unabhängig angenommen werden kann. Daraufhin wird die Physik des Spin-Kondomodells mit Hilfe der Störungstheorie in niedrigster Ordnung berechnet. Vorsicht ist geboten im Fall einer kleinen Spin-Spin-Wechselwirkung, aber für den Hauptteil dieser Arbeit liegt der Schwerpunkt auf einer großen Singulett-Triplett-Aufspaltung. Die Magnetisierung, die Polarisierung, der Strom und die T-Matrix werden in zweiter Ordnung Störungstheorie berechnet. Die Austauschkopplung zwischen dem linken und dem rechten Quantenpunkt führt zu der erwähnten Nichtgleichgewichtsübertragung und eine neue Größe, die sog. *transconductance*, wird eingeführt, um diesen Effekt zu messen. Die *transconductance* wird bereits in zweiter Ordnung Störungstheorie beobachtet, aber der Effekt entsteht indirekt durch eine Span-

nungsabhängigkeit der Besetzungszahlen. In den Strom-Strom-Korrelationen kann die Nichtgleichgewichtsübertragung direkt beobachtet werden. Es wird gezeigt, dass eine Kreuzkorrelation zwischen dem Strom durch den linken und durch den rechten Quantenpunkt aufgrund der Dekohärenz und der endlichen Lebenszeit der Quantenpunktzustände existiert. Obwohl diese Rechnung in vierter Ordnung Störungstheorie in der Ankopplung der Quantenpunkte an die Zuleitungen durchgeführt wird, ist das gefundene Ergebnis effektiv von zweiter Ordnung.

Es ist allgemein bekannt, dass im Kondomodell logarithmische Divergenzen zu einem Zusammenbruch der Störungstheorie bei niedrigen Temperaturen führt. Neue Methoden wurden entwickelt und es wird kontrovers diskutiert, welche Methode am besten geeignet ist, um den Kondo-Effekt unter Berücksichtigung einer endlichen Spannung zu beschreiben. In dieser Doktorarbeit werden zwei verschiedene Ansätze vorgeschlagen, aufbauend auf dem *poor man's scaling*-Ansatz und der Flussgleichungsmethode. Im Nichtgleichgewicht tragen alle Prozesse in einem Energiefenster, das durch die Spannung geöffnet wird, bei. Aus diesem Grund ist es wichtig, die Frequenz der einfallenden und auslaufenden Teilchen eines Wechselwirkungsereignisses in jede Renormierungstheorie zu integrieren. Dies trifft auf beide hier behandelten Methoden zu. Der einzige Unterschied besteht in der Behandlung der Dekohärenz, die eine richtige Rolle in Systemen außerhalb des Gleichgewichts spielt. In beiden Ansätzen wird beobachtet, dass ein Quantenpunkt aus dem Gleichgewicht gebracht wird, wenn eine endliche Spannung an einem gekoppelten Quantenpunkt angelegt wird. Mithilfe der ersten Methode, der störungstheoretischen Renormierungsgruppe im Nichtgleichgewicht, werden Ergebnisse für den Strom, die *transconductance*, und die T-Matrix gezeigt. Im Gegensatz dazu basiert die zweite Methode auf einer Diagonalisierung des Hamiltonianoperators und die Nichtgleichgewichtsübertragung wird anhand ihrer Signaturen im Fluss der Kopplungen diskutiert. Die *transconductance* wird durch die Reskalierung verstärkt und aus diesem Grund besteht die Hoffnung, dass diese Größe in naher Zukunft in Experimenten gemessen werden kann.

Contents

List of Figures

1 Introduction

The progress of experimental cooling techniques has made the study of physical phenomena at cryogenic temperatures possible and lead to the discovery of new phenomena. Many-particle effects like superconductivity or the Kondo effect are able to form only at low temperatures. At large temperatures the physics is mostly determined by thermal fluctuations, and only when the temperature is lowered sufficiently quantum effects can become significant.

Improvement of fabrication techniques in the last few years facilitated the production of two-, one-, and even zero-dimensional structures. In lower dimensions the screening of electrons is less significant which opens up the possibility of strong correlations. In recent years more and more emphasis has been put on the spin degree of freedom of the electrons. To manipulate the spin rather than the charge degree of freedom, and to construct circuits utilizing the spin of the electrons is the aim of the "spintronics" community.

In this thesis we study in detail the properties of two coupled spins surrounded by itinerant electrons in a quantum dot setup. The observation that alloys containing transition metals can contain electrons with a large effective mass, the so-called heavy fermions, is claimed to originate from a competing interaction between localized moments and itinerant electrons. The two-spin setup is a first step towards an understanding of this many-particle effect. In addition this setup shows interesting physical behavior on its own. Strong correlations due to the Coulomb repulsion of the two electric charges as well as the spin nature of the two localized electrons are important ingredients to understand the physics of a double quantum dot setup.

Before we study in detail the system of two coupled quantum dots, a general introduction to the physical background and experimental realizations of the Kondo effect in and out of equilibrium is given.

1.1 Introduction to Kondo Physics

Most physical problems can be solved by an appropriate one-particle description. There are a few problems arising from many-particle effects which need to be treated by special methods, one of which is the Kondo effect. This effect was found by experimentalists in the 1930s and received its name from the Japanese physicist Jun Kondo [1], who was the first to explain its physics in 1964. The resistivity of a metal compound at low temperatures depends on the type of the current-carrying particles. For itinerant electrons it decreases with decreasing temperatures and saturates at a finite value ρ_{imp} determined by the potential scattering off embedded impurities, e.g. defects in the crystal lattice. In some metals the resistivity shows an increase at low temperatures followed by a saturation at even lower temperatures. This effect was found to scale with the percentage of magnetic impurity atoms in the metallic compound. For a review of the

Kondo problem we refer the reader to the book of A. C. Hewson [2]. Shorter but more recent reviews can be found in Refs. [3, 4, 5, 6].

After it had been explained how a local moment could form in a Fermi sea in the so-called Anderson impurity model [7], it was the idea of J. Kondo that the spin of the local moment $\vec{S}$ interacts antiferromagnetically with the spin of the conduction electrons $\vec{s}$, $J\vec{S}\vec{s}$. Using this effective Hamiltonian Kondo [1] showed that the resistivity at low temperatures increases logarithmically, which indicates the range of validity of the perturbative calculation. Perturbation theory breaks down since at some point the coupling to the impurity is no longer a small parameter.

The energy level of the local moment is below the Fermi energy. Due to strong correlations between two electrons, the so-called Coulomb energy U, the occupation with a second electron is energetically suppressed. Therefore the impurity level is occupied with a single electron and thus with a spin-1/2 moment. This model is commonly referred to as the Anderson impurity model [7]. The Kondo Hamiltonian can be derived from the Anderson model by a Schrieffer-Wolff transformation [8] as discussed in chapter 2 for a double quantum dot system. The Kondo interaction J can be expressed in terms of the microscopic parameters of the Anderson impurity model. We refer the interested reader to chapter 2 or Refs. [2, 8].

At low temperatures infinitesimal excitations of electrons around the Fermi surface lead to a series of elastic, coherent spin-flip scattering processes. A cloud of scattered conduction electrons builds up in the vicinity of the impurity spin. In the local moment density of states a narrow many-particle resonance of the width of the Kondo temperature T_K, the so-called Abrikosov-Suhl or Kondo resonance, forms at the Fermi edge. This resonance explains the increase of the resistivity since conduction electrons are scattered more strongly with an increasing screening cloud. The Kondo temperature becomes the dominant energy scale of the system, such that two different systems show a universal behavior depending only on the ratio of the involved energies to T_K. The perturbation theory approach breaks down if the interaction between the local moment and the sea of conduction electrons becomes too strong. For even lower temperatures the Kondo system reaches its ground state, a singlet formation of the conduction electron screening cloud with the spin of the local moment. The host metal featuring the compensated impurity spin can thus be described by a Fermi liquid theory as discussed by Nozières [9].

The complexity of the Kondo problem led to the development of new methods to describe the strong coupling regime of the model. A first approach to describe the scaling to strong coupling was the "poor man's scaling" approach by Anderson [10] in 1966. The perturbative renormalization group (RG) method as described in chapter 5 builds on the poor man's scaling approach and therefore this method is discussed in detail in chapter 5. Further developments for example of the numerical renormalization group (NRG) by Wilson [11] in 1975 or the Fermi liquid description of Nozières [9] in 1974 are not considered in this thesis and we refer the reader to the extended literature. A good starting point therefore is the book by A. C. Hewson [2].

1.1.1 The Two Impurity Kondo Model

The Kondo effect in metals arises from local spin moments due to magnetic impurities in a Fermi sea of itinerant electrons. In general these impurities are dilute in their host

metal, but if they are only a few Fermi wavelengths apart new physics arises. Due to the polarization of the surrounding electron background two impurities can interact via an effective spin-spin interaction, denoted the Ruderman-Kittel-Kasuya-Yoshida (RKKY) interaction. It has been claimed that a lattice of Kondo impurities can explain the physics of heavy fermion compounds [4].

The interest in the physics of the two impurity model has not decayed up to recent days, since the two impurity model is a necessary step towards a generalization of the single impurity model towards a Kondo lattice. The main issues of the discussion of the two impurity Kondo model are given here and further reading can be found in Ref. [12, 13, 14, 15, 16, 17].

In the two impurity Kondo model, or more generally, in the so-called two impurity Anderson model, there are two important energy scales: the Kondo temperature T_K and the RKKY interaction K. The Kondo temperature is proportional to $(|\rho J|)^{1/2}\exp(1/\rho J)$ and the RKKY coupling $K \propto (\rho J)^2$, where ρ is the electron density of states [14]. In general the RKKY interaction depends on the distance between the two impurities in units of the Fermi wavelength and due to Friedel oscillations the interaction changes the sign from ferromagnetic to antiferromagnetic periodically, see e.g. [18] for this derivation.

If the RKKY interaction is ferromagnetic and large compared to the Kondo temperature, the two spins form an effective spin 1 state [16]. In contrast, for an antiferromagnetic RKKY interaction in the case of $K \gg T_K$ the two spins form a singlet state. The Kondo interaction favors a singlet state between each impurity spin and the conduction electrons if $T_K \gg K$. These two singlet formations compete with each other. It was found, that for $K/T_K \approx 2.2$ there is a transition between the two different ground states of two Kondo screened impurities or of an uncompensated singlet state, see e.g. Ref. [14]. If the two impurity Kondo model is seen as a toy model for the Kondo lattice the phase with the uncompensated two impurity spin singlet corresponds to an antiferromagnetic ground state.

The works on the two-impurity Kondo model reach from perturbative scaling methods [12] over numerical methods in Refs. [13, 14, 15] to conformal field theory [16]. In the latter is was proven that the quantum critical point between the two competing phases occurs depending of the type of particle-hole symmetry. Up to now consensus has not been achieved as to whether the transition between the two competing ground states is a quantum phase transition or a cross-over if potential scattering is present [17].

In this thesis the energy regime of the quantum phase transition is not discussed, but it is the aim of future calculations to reduce the strength of the spin-spin interaction K down to the Kondo scale T_K to be able to see signatures of this quantum phase transition.

1.2 The Kondo Effect in Quantum Dots

Since the physics of the Kondo effect was predicted in single-electron transistors a lot of effort has been put into the development of these microscopic circuits referred to as quantum dots. In a very small confined region of only a few electrons the quantum nature of electrons becomes important and the spin of the electron can give rise to interesting phenomena like the Kondo effect. Since the first observation of the Kondo effect in quantum dots in 1998 [19, 20] the study of the Kondo effect has undergone a

renaissance [6]. For introductory reading we refer to the original publications [19, 20, 21] as well as to a few recent reviews [3, 4, 5, 6] or the books [2, 22].

In general a quantum dot can be seen as an "artificial atom" or a single-electron transistor. For example in semiconductor quantum dots [19, 20, 21] a two-dimensional electron gas is depleted by an arrangement of gate barriers such that a zero-dimensional region is produced. Transport through this so-called quantum dot takes place through spin-conserving tunnel events. Therefore a quantum dot is well described by an Anderson impurity model [7]. The first theoretical predictions that the Kondo effect should be observable in those and similar structures were given in 1988 [23, 24]. As one of the first realizations we would like to mention Ref. [25].

The Kondo effect is observable in the Coulomb blockade regime, which is similar to the local moment phase explained before. The energy levels in the zero-dimensional system are quantized due to the confinement and the Pauli principle of the electrons plays a major role. In low dimensional systems the Coulomb repulsion between two electrons is large, such that the highest energy level below the Fermi energy of the leads is occupied by only one electron with an uncompensated spin. The energy of the level states can be tuned by a gate potential and a source-drain voltage applied across can lead to a non-equilibrium current. A contour plot of the conductance with respect to the gate voltage and the source-drain voltage, referred to as the stability diagram, shows a diamond-like structure. In the linear conductance a finite current is found only if an energy level is on resonance with the Fermi surface. If the quantum dot is occupied by an odd number of electrons, i.e. it is in the so-called Kondo regime, it shows a zero-bias anomaly. In contrast to the Kondo effect in metallic compounds the Abrikosov-Suhl resonance, which is energetically pinned to the Fermi surface, allows for an elastic transport through the quantum dot, whereas it leads to an increased scattering for a magnetic impurity in an otherwise pure metal. Therefore an increase in the conductivity of the quantum dot is observed while the temperature is lowered. In a symmetric setup the conductivity reaches a value of $2e^2/h$, the so-called unitary limit. If the chemical potential in the leads is shifted by a large voltage Kondo resonances build up at the two different Fermi surfaces. If the two Fermi surfaces match the energy difference between two levels or an internal structure in the quantum dot setup, inelastic tunneling processes are enhanced by Kondo correlations. This is studied in detail in this thesis for the system of two coupled quantum dots.

Quantum dots have a few advantages compared to traditional Kondo systems, as listed for example in Ref. [6]. Among other things a single Kondo impurity and not a statistical average is measured in quantum dots. In these mesoscopic systems most of the parameters are tunable and different setups, e.g. double quantum dots, can be fabricated. Additionally quantum dots provide the possibility to study transport out of equilibrium.

In a quantum dot setup a fine-tuning of the tunneling strength is always necessary. For a large Kondo temperature T_K the coupling to the leads should be chosen sufficiently large, but the particles should also be confined to the quantum dot which sets an upper limit to the magnitude of the coupling. In semiconductor quantum dots it is therefore possible to achieve a T_K of the order of $0.1 - 1K$ [6]. The Kondo effect was also observed in transport through molecules and nanowires, where a larger T_K can be achieved [6].

1.2.1 Double Quantum Dot Systems

Experimental groups all over the world tried to produce a setup which could tune all the parameters of two interacting spins in a double quantum dot setup to be able to study the interesting physics emerging from the two-impurity Kondo model. A general review about the state of experiments on double quantum dots in 2003 is given in Ref. [26]. It is explained that the stability diagram for two quantum dots in series shows a honeycomb lattice rather than the diamond structure of a single quantum dot.

The experiment which drew our attention to the setup of two coupled quantum dots was published by the experimental group in Harvard in April 2004 [27]. It is claimed in Ref. [27] that a "nonlocal spin control by suppressing and splitting Kondo resonances in one quantum dot by changing the electron number and coupling of the other dot" is achieved. In the last three years further experiments followed, for example the work of the Delft group [28] and experiments at the NTT in Japan [29].

In the experimental setup from N. J. Craig *et al.* [27] the parameters measured were an electron temperature of $85mK$ and a Coulomb charging energy of $U = 800\mu eV$. The largest tunnel coupling $\Gamma = 2\pi N(0)|t|^2$ is claimed to be of the same order of magnitude as the level spacing $\Delta = 100\mu eV$ within each quantum dot. From the full width at half maximum Craig *et al.* claim to have a Kondo temperature of $T_K \approx 0.6K \sim 51\mu eV$. The splitting of the Kondo peak is measured to be $0.12meV$, corresponding to the energy 2.2 T_K, where the quantum phase transition from the two-impurity Kondo model is expected to be. In Ref. [27] it was observed that one of the quantum dots could be tuned from a Kondo regime, showing a zero-bias peak, into a split peak if the coupling to the other dot was increased by making the barrier between the dots more transparent.

Some theoretical works relating to the experiment [27] should be mentioned here. Refs. [30, 31] discuss the physics of two quantum dots coupled by RKKY interaction in order to explain the observed conductance characteristics. Among other things we find in this thesis the same current characteristics as discussed in Refs. [30, 31], but in a different energy regime than the approaches used therein.

In the following we neglect the discussion about the use of double quantum dots for quantum computing since we are interested in inelastic and decoherent transport processes. The aim of this thesis is to describe "Non-Equilibrium Electron Transport through a Double Quantum Dot System". The study of this subject was initiated by the experiment of Craig *et al.* as mentioned before. The double quantum dot setup considered here does not completely represent the experiment in [27], but it can be used to give a quantitative description of the experimental results. Furthermore the double quantum dot system discussed here illustrates the transfer of a non-equilibrium situation on one quantum dot to another quantum dot mediated by a spin-spin interaction between the dots. Before we give an outline of this thesis, we introduce very briefly a few theoretical tools useful when dealing with physics out of equilibrium.

1.3 Theoretical Tools Out of Equilibrium

The most general definition one can give for non-equilibrium is that it is not equilibrium. Consequently the rules of thermodynamics do not apply. In this thesis "non-equilibrium" refers to a large voltage applied across a transport region otherwise in equilibrium. The

transient behavior is neglected here and only the stationary state that establishes after the transient is discussed.

In a typical transport setup two leads with different chemical potentials are connected to a quantum mechanical system, e.g. a quantum dot. Even if the coupling between the leads and the transport region is switched on adiabatically, the system does not return to its initial state if the coupling is adiabatically switched off again. It is characteristic for a non-equilibrium setup that the physics of the system is not described solely by the ground state. As explained in detail in chapter 3 one calculational tool reverses the time evolution after some interaction took place at time t such that the system is taken back to $t_0 = -\infty$ where the ground state was known. By doubling the time axis also the space of the Green's functions is doubled and these so-called contour-ordered Green's functions are important out of equilibrium. Whereas the fluctuation and the dissipation of a system are correlated in equilibrium, such a theorem is not valid e.g. if a finite voltage is applied. This is reflected in different determining equations for the contour-ordered Green's functions. We refer the reader to chapter 3 of this thesis for a brief introduction or to the Refs. [22, 32, 33, 34].

As previously mentioned any perturbation theory approach fails to describe the Kondo Hamiltonian at low temperatures. The Kondo resonance is a sharp resonance pinned to the Fermi surface of the leads. In a double quantum dot system a whole range of energy scales is present, e.g. a conduction electron band width of the order of eV whereas the applied voltages are usually in the order of μeV to meV. Anderson proposed in 1966 [10] the so-called "poor man's scaling", which integrates out processes to high-energy states and incorporates their contributions into a change of the couplings in the initial Hamiltonian. This scaling leads to an effective model at low energies. The method is a perturbative renormalization group and therefore it does not describe e.g. the ground state of the Kondo Hamiltonian, but its tendencies show that the Kondo singlet is formed. In non-equilibrium the many-particle resonance builds up due to Kondo correlations at the two different Fermi surfaces of the leads. Inelastic processes can therefore be Kondo enhanced, such that it is necessary to include the incoming frequency of a conduction electron in any theory.

In this thesis we discuss two different ways how to perform a perturbative renormalization group out of equilibrium. In chapter 5 the method developed by A. Rosch *et al.* [35, 36] is introduced and in chapter 6 the non-equilibrium flow equation method of S. Kehrein [37, 38] is discussed. Another approach, based on the functional renormalization group [39, 40], is shortly addressed in chapter 5. All these methods have in common that the frequency dependence of the coupling vertex is important and in a transport setup all processes in the energy window opened by the voltage contribute. For non-equilibrium setups the role of the decoherence [41] is important. It is lively discussed in the physical community, how and to which degree decoherent effects influence a transport setup. The details of the methods and their application to the setup of two coupled quantum dots are discussed in the respective chapters.

1.4 Structure of this Thesis

This thesis consists of four almost independent parts. It was written such that the interested reader can jump to the chapter of interest without the background of a previous

section.

Chapter 2 is a technical chapter. It explains the basic physics of two coupled spins in a first part and afterwards the focus is put on finding an appropriate Hamiltonian. The Schrieffer-Wolff transformation is introduced and it is shown how an effective Kondo model can be derived from an Anderson impurity model. Chapter 2 introduces the Hamiltonian of the double quantum dot system which is discussed in the remaining thesis and it is shown that the transport through each of the quantum dots can be treated independently.

A large part of the thesis is devoted to calculations in perturbation theory. In the first part (chapter 3) the Keldysh Green's functions method is introduced. It is discussed in detail why the lesser Green's function in non-equilibrium has to be determined from a self-consistent equation. The effect of a finite voltage and why it can be seen as an effective temperature out of equilibrium is explained. Although the calculation is included only in appendix C some explanations of why an off-diagonal Green's function arises and how it can be treated is found in chapter 3.

For readers not interested in the calculational method all results for the perturbation theory treatment of a double quantum dot setup are summarized in chapter 4. Each section in this chapter contains in a few lines the derivation of the physical quantity of interest and explicit details of the calculations are given in appendix B. The discussion includes the polarization, the magnetization, the current, the T-matrix, the noise, and a current cross-correlation out of equilibrium. Special focus is put on the observation that a non-equilibrium situation on one quantum dot can be transferred to a coupled quantum dot by a finite spin-spin interaction.

In chapter 5 a schematic derivation of the perturbative RG method as introduced by A. Rosch *et al.* [35, 36] is given. In non-equilibrium the poor man's scaling approach has to be generalized to include the effects of a finite voltage and a finite decoherence. The self-consistent equation for the occupation probabilities also has to be taken into account. Within the perturbative RG we show results for the polarization, the current, and the T-matrix in the case of antiferromagnetic and ferromagnetic coupling between the two quantum dots. The transfer of a non-equilibrium situation from one quantum dot to another is found to be enhanced by the scaling of the Kondo couplings. This provides the hope that the effect can be observed in experiments.

The thesis closes with chapter 6 on the generalization of the flow equation approach to non-equilibrium by S. Kehrein [37, 38]. This renormalization method is one of the few scaling theories which is applicable out of equilibrium. The method is introduced and some results are discussed. The flow equation method is a diagonalization scheme for the Hamiltonian and not for physical observables like the poor man's scaling, and therefore the method can easily be generalized to two-loop order. To higher orders decoherence mechanisms enter the scaling equations naturally. By contrast, the decoherence rates had to be included by hand in chapter 5.

Conclusions regarding the different parts of the thesis are given in chapter 7. We find that a non-equilibrium situation is transferred from one quantum dot to another by a spin-spin interaction. It is discussed in which physical quantities this can be observed and why there is the hope that the effect can be measured in experiments.

2 Model of a Double Quantum Dot System

Quantum dots allow for an isolation of a single spin-1/2 particle and interesting effects in electric charge transport are observed. Generalizing this setup to two electrons on two quantum dots additionally the spin interaction of the electrons can be studied.

In the following section 2.2 we introduce a general Hamiltonian for a double quantum dot and discuss within the framework of a Schrieffer-Wolff transformation how an effective Hamiltonian can be derived for the description of spin properties which occur at a lower energy scale than charge properties. We show that even the simple setup introduced here leads to a spin-spin interaction between the two quantum dots.

2.1 Physics of Two Coupled Spins

Before we discuss the origin of the exchange interaction the physics of two coupled quantum dots is discussed in detail. In this section we introduce the notations which are used in the remaining thesis, discuss different operator structures and the relation between product states and singlet-triplet states.

2.1.1 Product States and Singlet-Triplet States

For the following a setup of two localized spin states denoted by left (L) and right (R) is assumed. Each spin can be described by a state $|\sigma\rangle$ where $\sigma = \pm 1$ refers to up/down ($\uparrow$ / $\downarrow$) spin orientation. The Hilbert space of the two spins is then described by the four product states

$$|1\rangle = |\uparrow\rangle_L|\downarrow\rangle_R, \qquad |2\rangle = |\downarrow\rangle_L|\uparrow\rangle_R, \qquad |3\rangle = |\uparrow\rangle_L|\uparrow\rangle_R, \qquad |4\rangle = |\downarrow\rangle_L|\downarrow\rangle_R.$$

Since these are product states, it is easy to write down the eigenvalues of the single spin operators

$$\vec{S}^z_\alpha|\sigma_L\rangle_L|\sigma_R\rangle_R = \frac{1}{2}\,\sigma_\alpha\,|\sigma_L\rangle_L|\sigma_R\rangle_R,$$
$$\vec{S}^2_\alpha|\sigma_L\rangle_L|\sigma_R\rangle_R = \frac{3}{4}\,|\sigma_L\rangle_L|\sigma_R\rangle_R,$$

where $\alpha = L, R$ and $\hbar = 1$ is assumed. The ladder operators $\vec{S}^{+} = \frac{1}{\sqrt{2}}\left(\vec{S}^{x} + i\vec{S}^{y}\right)$ and $\vec{S}^{-} = \frac{1}{\sqrt{2}}\left(\vec{S}^{x} - i\vec{S}^{y}\right)$ act as follows,

$$\vec{S}_L^{+}|\uparrow\rangle_L|\sigma'\rangle_R = 0, \qquad \vec{S}_L^{+}|\downarrow\rangle_L|\sigma'\rangle_R = \frac{1}{\sqrt{2}}|\uparrow\rangle_L|\sigma'\rangle_R,$$
$$\vec{S}_L^{-}|\downarrow\rangle_L|\sigma'\rangle_R = 0, \qquad \vec{S}_L^{-}|\uparrow\rangle_L|\sigma'\rangle_R = \frac{1}{\sqrt{2}}|\downarrow\rangle_L|\sigma'\rangle_R,$$

and analogous for $\vec{S}_R^{\pm}$.

We assume that the two spins are coupled by a spin-spin or exchange interaction K

$$K\vec{S}_L\vec{S}_R = K\left(\vec{S}_L^{+}\vec{S}_R^{-} + \vec{S}_L^{-}\vec{S}_R^{+} + \vec{S}_L^{z}\vec{S}_R^{z}\right).$$

As known from basic quantum mechanics the product states are thus no longer eigenstates of the system. This leads to the definition of singlet and triplet states,

$$|t_+\rangle = |\uparrow\rangle_L|\uparrow\rangle_R, \tag{2.1a}$$
$$|t_0\rangle = \frac{1}{\sqrt{2}}\left(|\uparrow\rangle_L|\downarrow\rangle_R + |\downarrow\rangle_L|\uparrow\rangle_R\right), \tag{2.1b}$$
$$|t_-\rangle = |\downarrow\rangle_L|\downarrow\rangle_R, \tag{2.1c}$$
$$|s\rangle = \frac{1}{\sqrt{2}}\left(|\uparrow\rangle_L|\downarrow\rangle_R - |\downarrow\rangle_L|\uparrow\rangle_R\right). \tag{2.1d}$$

The singlet $|s\rangle$ and the triplet $|t_0\rangle$, both with a magnetic moment of 0, are no longer product states, but one often refers to them as being entangled.

$$|s\rangle = \frac{1}{\sqrt{2}}\left(|1\rangle - |2\rangle\right), \qquad |1\rangle = \frac{1}{\sqrt{2}}\left(|t_0\rangle + |s\rangle\right),$$
$$|t_0\rangle = \frac{1}{\sqrt{2}}\left(|1\rangle + |2\rangle\right), \qquad |2\rangle = \frac{1}{\sqrt{2}}\left(|t_0\rangle - |s\rangle\right),$$

This is the reason why the study of two quantum dot systems has attracted a lot of scientific interest (for a recent review see Ref. [26]). Not to mention there is also a large interest in the entanglement and deentanglement of two states in the quantum computer community.

The singlet and triplet states have the property

$$\vec{S}_L\vec{S}_R|t_\gamma\rangle = \frac{1}{4}|t_\gamma\rangle, \qquad \vec{S}_L\vec{S}_R|s\rangle = -\frac{3}{4}|s\rangle,$$

where $\gamma = -, 0, +$. Thus the value of the exchange coupling K corresponds to the energy of the excitation gap between singlet and triplet states.

The square total spin moment, $\vec{S}_+ = \vec{S}_L + \vec{S}_R$, can be rewritten by

$$\vec{S}_+^2 = \vec{S}_L^2 + 2\ \vec{S}_L\vec{S}_R + \vec{S}_R^2,$$

and we find

$$\vec{S}_+^z|t_\gamma\rangle = \gamma\ \frac{1}{2}\ |t_\gamma\rangle, \qquad \vec{S}_+^z|s\rangle = 0,$$
$$\vec{S}_+^2|t_\gamma\rangle = 2\ |t_\gamma\rangle, \qquad \vec{S}_+^2|s\rangle = 0.$$

It follows directly that the triplet is a spin 1 ($S(S+1) = 2$) with three different magnetic moments $\gamma \in \{+, 0, -\}$ and the singlet has spin 0. Both are bosonic particles states, since they are composed of two electrons. They are eigenstates of $\vec{S}_+$ and $\vec{S}_L\vec{S}_R$.

2.1.2 Singlet-Triplet Representation

Instead of the spin operators $\vec{S}_L$ and $\vec{S}_R$ we introduce bosonic operators $s^\dagger$, $t_+^\dagger$, $t_0^\dagger$ and $t_-^\dagger$ which create a singlet or triplet state out of the vacuum.[1] Since it is not possible to use common perturbation theory for spin operators, the pseudo particle representation is a nice workaround to be able to do a systemic expansion in a small parameter and use Wick's theorem. By defining these four different states the Hilbert space is enlarged by physically forbidden states. These states, e.g. containing 2 singlet states or a singlet and a triplet state at the same time, have to be projected out. To find physical results we have to enforce that the sum of the occupation probability of all pseudo particle states, $n_s + n_{t_+} + n_{t_0} + n_{t_-} = 1$, equals one. Therefore we use a method usually referred to as the Abrikosov pseudofermion representation [42] in the notation of P. Coleman [43].

In order to fulfill the constraint,

$$Q = s^\dagger s \ + t_+^\dagger t_+ + t_0^\dagger t_0 + t_-^\dagger t_- = 1, \tag{2.2}$$

we introduce a Langragian parameter in form of a chemical potential λ in the Hamiltonian

$$H_\lambda = H + \lambda Q.$$

Every physical quantity $\mathcal{O}$ has to be calculated in the limit of this chemical potential λ going to infinity by the rule

$$\langle \mathcal{O} \rangle_{Q=1} = \lim_{\lambda \to \infty} \frac{\langle Q\mathcal{O} \rangle_\lambda}{\langle Q \rangle_\lambda}, \tag{2.3}$$

where $\langle \ldots \rangle_\lambda$ is the grandcanonical average with respect to the Hamiltonian H_λ. Since $\langle Q \rangle_\lambda$ scales with $e^{-\beta\lambda}$ every physical process with one factor $e^{-\beta\lambda}$ survives the projection while every process containing for example twice this factor, $(e^{-\beta\lambda})^2$, is projected out for $\lambda \to \infty$. Later on this observation is often used to argue that some terms from an expansion need not to be calculated because they will be projected out in the final step of a physical projection.

The impurity spin $\vec{S}_\alpha$ can be written in the singlet-triplet representation by (see for example Ref. [44])

$$\mathbf{S}_L^z = \tfrac{1}{2}\left(t_+^\dagger t_+ - t_-^\dagger t_- + s^\dagger t_0 + t_0^\dagger s \ \right), \tag{2.4a}$$

$$\mathbf{S}_L^+ = \tfrac{1}{2}\left(t_0^\dagger t_- + t_+^\dagger t_0 + s^\dagger t_- - t_+^\dagger s \ \right), \tag{2.4b}$$

$$\mathbf{S}_L^- = \tfrac{1}{2}\left(t_0^\dagger t_+ + t_-^\dagger t_0 - s^\dagger t_+ + t_-^\dagger s \ \right), \tag{2.4c}$$

and

$$\mathbf{S}_R^z = \tfrac{1}{2}\left(t_+^\dagger t_+ - t_-^\dagger t_- - s^\dagger t_0 - t_0^\dagger s \right), \tag{2.5a}$$

$$\mathbf{S}_R^+ = \tfrac{1}{2}\left(t_0^\dagger t_- + t_+^\dagger t_0 - s^\dagger t_- + t_+^\dagger s \right), \tag{2.5b}$$

$$\mathbf{S}_R^- = \tfrac{1}{2}\left(t_0^\dagger t_+ + t_-^\dagger t_0 + s^\dagger t_+ - t_-^\dagger s \right). \tag{2.5c}$$

[1] The pseudo particles are chosen bosonic here, but they can also be chosen fermionic without changing the outcome of the calculation.

In analogy to a spin-1/2 representation we use the notation

$$\vec{S}_\alpha = \frac{1}{2} t^\dagger_{\gamma'} \left(\vec{T}_\alpha\right)_{\gamma'\gamma} t_\gamma,$$

with a 4x4 matrix $\vec{T}_{\gamma'\gamma}$ for $\gamma, \gamma' \in \{s, t_+, t_0, t_-\}$ rather than a Pauli matrix $\vec{\tau}_{\sigma'\sigma}$ for a spin-1/2. The "pseudo Pauli matrices" are defined by

$$\vec{T}^z_L = \begin{pmatrix} 0 & 0 & 1 & 0 \\ 0 & 1 & 0 & 0 \\ 1 & 0 & 0 & 0 \\ 0 & 0 & 0 & -1 \end{pmatrix}, \qquad \vec{T}^+_L = \left(\vec{T}^-_L\right)^\dagger = \begin{pmatrix} 0 & 0 & 0 & 1 \\ -1 & 0 & 1 & 0 \\ 0 & 0 & 0 & 1 \\ 0 & 0 & 0 & 0 \end{pmatrix}, \tag{2.6}$$

and

$$\vec{T}^z_R = \begin{pmatrix} 0 & 0 & -1 & 0 \\ 0 & 1 & 0 & 0 \\ -1 & 0 & 0 & 0 \\ 0 & 0 & 0 & -1 \end{pmatrix}, \qquad \vec{T}^+_R = \left(\vec{T}^-_R\right)^\dagger = \begin{pmatrix} 0 & 0 & 0 & -1 \\ 1 & 0 & 1 & 0 \\ 0 & 0 & 0 & 1 \\ 0 & 0 & 0 & 0 \end{pmatrix}. \tag{2.7}$$

As mentioned before the singlet and triplet states are eigenstates of the total spin $\vec{S}_+ = \vec{S}_L + \vec{S}_R$ and the correlation $\vec{S}_L\vec{S}_R$. In the singlet-triplet representation we find,

$$\begin{aligned} \vec{S}_L\vec{S}_R &= -\frac{3}{4} s^\dagger s + \frac{1}{4} t^\dagger_0 t_0 + \frac{1}{4} t^\dagger_- t_- + \frac{1}{4} t^\dagger_+ t_+, \\ \left(\vec{S}_L + \vec{S}_R\right)^z &= \frac{1}{4} t^\dagger_+ t_+ - \frac{1}{4} t^\dagger_- t_-, \\ \left(\vec{S}_L + \vec{S}_R\right)^2 &= 2 \sum_\gamma t^\dagger_\gamma t_\gamma. \end{aligned}$$

Please note that the ladder operators of the total spin,

$$\begin{aligned} \left(\vec{S}_L + \vec{S}_R\right)^+ &= t^\dagger_0 t_- + t^\dagger_+ t_0, \\ \left(\vec{S}_L + \vec{S}_R\right)^- &= t^\dagger_0 t_+ + t^\dagger_- t_0, \end{aligned}$$

contain only processes between triplet states. In contrast to the singlet with total spin 0 the triplet states have a total spin 1 and thus three different magnetic moments $S^z_+ = \{0, \pm 1\}$. Consequently the total spin acts only on the triplet states and the singlet state is conserved. This leads for example to a suppression of the current in the antiferromagnetic case and is discussed in detail later on. It is shown in the next section, that any process involving a singlet state is a transition from a singlet to a triplet or vice versa with an energy cost of the excitation gap K.

2.1.3 Inelastic Processes

In the previous section it was demonstrated, that the singlet and triplets are eigenstates of the total spin $\vec{S}_+ = \vec{S}_L + \vec{S}_R$ and the spin-spin interaction $\vec{S}_L\vec{S}_R$. The two spins can also interact via the spin difference $\vec{S}_- = \vec{S}_L - \vec{S}_R$ and the vector product $2i(\vec{S}_L \times \vec{S}_R)$.

The singlet and triplet states are not eigenstates of those operators and consequently a representation of $\vec{S}_-$ and $2i(\vec{S}_L \times \vec{S}_R)$ in the singlet-triplet basis destroys a state e.g. a singlet and creates a triplet state or vice versa.

From Eqs. (2.4) and (2.5) we find immediately

$$\begin{aligned}\left(\vec{S}_L - \vec{S}_R\right)^z &= s^\dagger t_0 + t_0^\dagger s,\\ \left(\vec{S}_L - \vec{S}_R\right)^+ &= s^\dagger t_- - t_+^\dagger s,\\ \left(\vec{S}_L - \vec{S}_R\right)^- &= -s^\dagger t_+ + t_-^\dagger s.\end{aligned}$$

Not directly from the definition of singlet-triplet states but also straightforwardly one can derive

$$\begin{aligned}2i\left(\vec{S}_L \times \vec{S}_R\right)^z &= 2\vec{S}_L^-\vec{S}_R^+ - 2\vec{S}_L^+\vec{S}_R^- = t_0^\dagger s - s^\dagger t_0,\\ 2i\left(\vec{S}_L \times \vec{S}_R\right)^+ &= 2\vec{S}_L^+\vec{S}_R^z - 2\vec{S}_L^z\vec{S}_R^+ = -s^\dagger t_- - t_+^\dagger s,\\ 2i\left(\vec{S}_L \times \vec{S}_R\right)^- &= 2\vec{S}_L^z\vec{S}_R^- - 2\vec{S}_L^-\vec{S}_R^z = s^\dagger t_+ + t_-^\dagger s.\end{aligned}$$

These processes show a change of the total spin from 0 to 1 in contrast to $\vec{S}_+$ and $\vec{S}_L\vec{S}_R$ which do not change the total spin. Please note that the operator structure is antihermitian $[2i(\vec{S}_L \times \vec{S}_R)]^\dagger = -2i(\vec{S}_L \times \vec{S}_R)$.

The combinations $(\vec{S}_L - \vec{S}_R) \pm 2i(\vec{S}_L \times \vec{S}_R)$

$$\left(\vec{S}_L - \vec{S}_R\right)^z + 2i\left(\vec{S}_L \times \vec{S}_R\right)^z = 2t_0^\dagger s, \tag{2.8a}$$

$$\left(\vec{S}_L - \vec{S}_R\right)^+ + 2i\left(\vec{S}_L \times \vec{S}_R\right)^+ = -2t_+^\dagger s, \tag{2.8b}$$

$$\left(\vec{S}_L - \vec{S}_R\right)^- + 2i\left(\vec{S}_L \times \vec{S}_R\right)^- = 2t_-^\dagger s, \tag{2.8c}$$

$$\left(\vec{S}_L - \vec{S}_R\right)^z - 2i\left(\vec{S}_L \times \vec{S}_R\right)^z = 2s^\dagger t_0, \tag{2.8d}$$

$$\left(\vec{S}_L - \vec{S}_R\right)^+ - 2i\left(\vec{S}_L \times \vec{S}_R\right)^+ = 2s^\dagger t_-, \tag{2.8e}$$

$$\left(\vec{S}_L - \vec{S}_R\right)^- - 2i\left(\vec{S}_L \times \vec{S}_R\right)^- = -2s^\dagger t_+, \tag{2.8f}$$

appear quite often for a setup with two spins (see for example Ref. [45]).

Eqs. (2.8) become important when we compare the results from the flow equation method to the results of the perturbative RG. Since the flow equation is a calculation on the Hamiltonian basis it does not need to represent the spins in a singlet-triplet basis like the perturbative RG which is derived from Green's functions.

The singlet-triplet representation is used since it diagonalizes the Hamiltonian and therefore perturbation theory using Wick's Theorem is possible. The Kondo coupling addresses only the spin $\vec{S}_L$ and $\vec{S}_R$ and not the singlet and triplet states. If the excitation gap K between the singlet s and the triplet t_0 is of the order of their level broadening, such that the two states have a finite overlap, then the product basis rather than the singlet-triplet basis provides diagonality in the Hamiltonian. As is discussed later on, this implies the need of a degenerate perturbation theory.

We want to point out one important property of the system. The interaction between the conduction electron spin and the impurity spin leads to the Kondo effect via resonant spin flip processes. Elastic transport processes are usually available through a non spin-flip interaction $\vec{S}^z\vec{s}^z$. For example the impurity spin $\vec{S}^z_L$ in the singlet-triplet representation is given by $\frac{1}{2}\left(s^\dagger t_0 + t_0^\dagger s + t_+^\dagger t_+ - t_-^\dagger t_-\right)$. If the ground state is one of the triplets, t_+ or t_-, then the operation $\vec{S}^z_L$ does not cost any energy. A process like $s^\dagger t_0$ is accompanied by a change of the total spin of the double quantum dot system and costs an energy of K. This simple argument indicates, that there is no transport at zero temperature as long as the voltage does not support sufficient energy for a spin-flip from the singlet to a triplet state. At finite temperature thermodynamically generated excitations of higher-lying states may contribute to a finite transport current even for small voltages.

2.2 Schrieffer-Wolff Transformation

In this section an Anderson model of two quantum dots which are capacitively coupled is introduced and an effective Hamiltonian is derived for the lower energy physics where the number of electrons on each dot is conserved. This Schrieffer-Wolff transformation produces new coupling constants like the Kondo coupling, a potential scattering, and a spin exchange interaction special to the chosen setup. This section intents to provide the reader with an insight into the underlying physics of the double quantum dot system, which we discuss in the remaining parts of the thesis. Especially deviations from this model for example a leakage over the double quantum dot are derived.

After introducing the Hamiltonian of a model system in section 2.2.1 we explain the idea behind the Schrieffer-Wolff transformation in section 2.2.2. Following up on the definitions of the generators of the transformation we first derive the effective Hamiltonian in second order (section 2.2.4) followed by a derivation of the third order leakage in section 2.2.5.

2.2.1 Model of the Double Quantum Dot System

The most general case we consider, is the set of two quantum dots as depicted in Fig. 2.1. The setup consists of two quantum dots denoted by left (L) and right (R). Each dot itself is described by an Anderson model

$$H_\alpha = \sum_\sigma \epsilon_{\alpha\sigma} d^\dagger_{\alpha\sigma} d_{\alpha\sigma} + \frac{1}{2} U_\alpha n_{\alpha\sigma} n_{\alpha\overline{\sigma}}, \tag{2.9}$$

where $\alpha = L, R$. The fermionic operator $d^\dagger_{\alpha\sigma}/d_{\alpha\sigma}$ creates/annihilates an electron with spin σ on the quantum dot α. One electron can be placed at the energy $\epsilon_\alpha < 0$, but an additional electron is subject to a Coulomb repulsion and has to pay the energy U_α if it occupies the same dot.

We assume that the dots are close in space such that there is additionally a Coulomb repulsion U_{LR} between electrons in the left dot and electrons in the right dot,

$$H_{\text{cap}} = U_{LR} \sum_{\sigma,\sigma'} n_{L\sigma} n_{R\sigma'}. \tag{2.10}$$

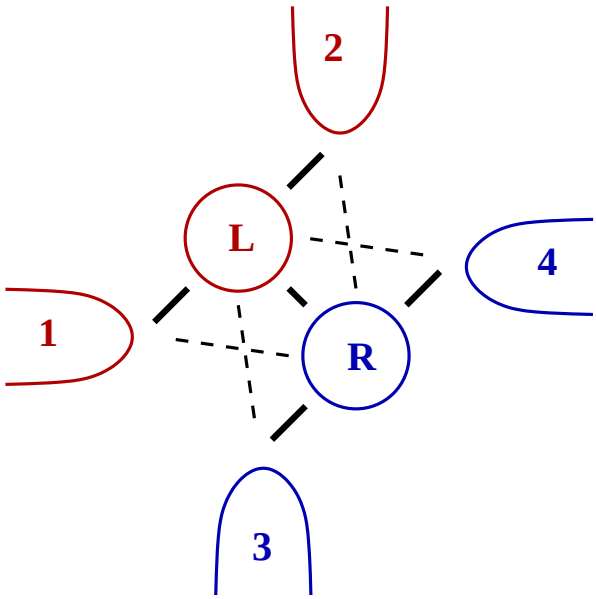

Figure 2.1: Basic model for a double quantum dot system: a left (L) and a right (R) quantum dot connected to four leads denoted by $1, 2, 3$ and 4. A hopping between the quantum dots is allowed and it is assumed that the hopping between lead $1, 2$ $(3, 4)$ and the right (left) quantum dot is negligible (dashed lines).

This Hamiltonian is often referred to as capacitively coupled quantum dots (see e.g. Ref. [46, 47]). In an atom or molecule with degenerate levels it is known from Hunds rule that electrons prefer to align their spin parallel

$$H_{\text{Hund}} = -J_H \left(n_{L\uparrow} n_{R\uparrow} + n_{L\downarrow} n_{R\downarrow} \right). \tag{2.11}$$

The Hund coupling J_H is mainly introduced to allow for a distinction between different spin configurations in the calculation.

Since the dots are assumed to be in close proximity we have to allow for hopping between them,

$$H_{LR} = \sum_{\sigma} \left(t_{LR} d^{\dagger}_{R\sigma} d_{L\sigma} + t_{RL} d^{\dagger}_{L\sigma} d_{R\sigma} \right), \tag{2.12}$$

but the hopping parameter t_{LR} is assumed to be small. Since the Hamiltonian has to be hermitian, the relation $t_{LR} = t^{\dagger}_{RL}$ holds and it is usually assumed that t_{LR} and t_{RL} are identical.

To measure a current and therefore properties of the quantum dots, the left and right quantum dots are contacted by four leads which we denote by $n = 1, 2, 3, 4$. We describe the leads by a kinetic term

$$H_n = \frac{1}{N} \sum_{nk\sigma} \epsilon_{nk\sigma} c^{\dagger}_{nk\sigma} c_{nk\sigma}, \tag{2.13}$$

where N is the number of band states. The fermionic operator $c^{\dagger}_{nk\sigma}/c_{nk\sigma}$ creates/annihilates an electron in the lead n with momentum k and spin σ. Each lead can be at a different potential $\epsilon_{nk\sigma} = \epsilon_{k\sigma} - \mu_n$. For most of the calculations we assume that the

density of states is constant $\mathcal{N}(\epsilon) = \mathcal{N}(0)\Theta(D - |\epsilon|)$, where $\mathcal{N}(0) = 1/2D$ and the half bandwidth D is the largest energy scale of the system. This is motivated by experiments using GaAs quantum dots, where the leads are an electron gas in two dimensions.

The coupling between the leads and the quantum dots is given by a hopping Hamiltonian,

$$H_{\alpha n} = \frac{1}{N} \sum_{nk\sigma} \left(t_{n\alpha} d^\dagger_{\alpha\sigma} c_{nk\sigma} + t_{\alpha n} c^\dagger_{nk\sigma} d_{\alpha\sigma} \right), \tag{2.14}$$

for $n = 1, 2, 3, 4$. Please note that the spin is conserved during a hopping process. Due to hermiticity $t_{n\alpha} = t^\dagger_{\alpha n}$ and it is assumed that these two couplings are identical. As the hopping between the dots t_{LR} also the hopping parameters $t_{n\alpha}$ to the leads are assumed to be small.

Experimentally double quantum dots are realized for example by a sophisticated setup of tunnel barriers. We assume that the hopping between leads and dots $t_{\alpha n}$ is of the same order as the hopping between the dots t_{LR} themselves and thus small. Therefore we separate the Hamiltonian into an uncoupled part,

$$H_0 = H_n + H_L + H_R + H_{\text{cap}} + H_{\text{Hund}}, \tag{2.15}$$

and a coupling part,

$$H_{\text{int}} = H_{LR} + H_{Ln} + H_{Rn}, \tag{2.16}$$

which provides a perturbation to H_0.

This is a simple example for a double quantum dot setup. A similar setup but including a strong t_{LR} is discussed in Ref. [46, 47]. We present the derivation of an effective low-energy Hamiltonian to justify the assumptions that we use in the course of this thesis.

Although the model is treated as general as possible, we will later concentrate on the special case of $t_{L3} = t_{L4} = t_{R1} = t_{R2} = 0$. This assumption is equivalent to neglecting all dashed coupling lines in Fig. 2.1. It provides an interesting setup since the leads 1 and 2 then only probe the left quantum dot and the leads 3 and 4 are coupled to the right quantum dot solely. In section 2.2.5 we derive to third order in the hopping energies a so-called leakage from the left leads over the quantum dot system to the right leads and it is shown that the leakage is negligibly small or vanishes completely in a symmetric setup.

2.2.2 Idea behind the Schrieffer-Wolff Transformation

A finite current through the quantum dot is found for example if the number of electrons on the double quantum dot system changes. This so-called sequential tunneling takes place at large energy scales proportional to the charging energy. Here we concentrate on the case of cotunneling with a fixed number of electrons, which occurs at low energy scales.

The idea of a Schrieffer-Wolff transformation is to apply a unitary transformation $\tilde{H} = \mathrm{e}^{iS} H \mathrm{e}^{-iS}$ to the Hamiltonian H to produce an effective Hamiltonian $\tilde{H}$ approximated by

$$\tilde{H} \approx H + [iS, H] + \frac{1}{2}[iS, [iS, H]] + \frac{1}{3!}[iS, [iS, [iS, H]]] + \ldots.$$

Using the separation $H = H_0 + H_{\text{int}}$ the rotation can be written by

$$\begin{aligned}\tilde{H} \approx\, & H_0 + H_{\text{int}} + [iS, H_0] + [iS, H_{\text{int}}] + \frac{1}{2}[iS, [iS, H_0]] \\ & + \frac{1}{2}[iS, [iS, H_{\text{int}}]] + \frac{1}{3!}[iS, [iS, [iS, H_0]]] + \dots . \end{aligned} \tag{2.17}$$

Thus a sophisticated generator S can be found such that the condition,

$$H_{\text{int}} + [iS, H_0] = 0, \tag{2.18}$$

is fulfilled. If H_{int} is of the order of t, then all processes to order t vanish in the transformation. Consequently S is of the order of t and the expansion of e^{iS} in the small quantity t is justified. By inserting Eq. (2.18) in Eq. (2.17) we find

$$\begin{aligned}\tilde{H} \approx & H_0 + H_{\text{int}} - H_{\text{int}} + [iS, H_{\text{int}}] - \frac{1}{2}[iS, H_{\text{int}}] + \frac{1}{2}[iS, [iS, H_{\text{int}}]] \\ & - \frac{1}{3!}[iS, [iS, H_{\text{int}}]] + \dots \\ \approx & H_0 + \frac{1}{2}[iS, H_{\text{int}}] + \frac{1}{3}[iS, [iS, H_{\text{int}}]] + \dots . \end{aligned}$$

After the rotation the lowest order process in the effective Hamiltonian $\tilde{H}$ is of the order of t^2. This procedure is commonly referred to as Schrieffer-Wolff transformation [8]. The idea presented here will furthermore be utilized for the method of flow equations (see chapter 6 or Ref. [38]). Therefore the Hamiltonian is rotated to an energy-diagonal representation with a series of infinitesimal unitary transformations which cancel out a perturbation term like explained above.

If the hopping t is small, we can neglect higher orders and therefore find an effective model for further considerations. Nevertheless the third order contribution is also calculated to show that the leakage which is created initially in 3rd order can be neglected.

The low-energy physics we consider does not allow for a change in the particle number. This has to be enforced additionally. Thus in a next step we have to project onto the particle state of interest

$$H_{\text{eff}} = \mathcal{P}\tilde{H}\mathcal{P} \approx \mathcal{P}H_0\mathcal{P} + \frac{1}{2}\mathcal{P}[iS, H_{\text{int}}]\mathcal{P} + \frac{1}{3}\mathcal{P}[iS, [iS, H_{\text{int}}]]\mathcal{P} + \dots \tag{2.19}$$

The specific form of the projection $\mathcal{P}$ will be defined later on. A few useful relations for the calculation of the commutators are given in appendix A.1.1.

2.2.3 Generators of the Transformation

In order to perform the Schrieffer-Wolff transformation we have to find a generator S that fulfills

$$H_{LR} + H_{Ln} + H_{Rn} + [iS, H_0] = 0.$$

Since the latter condition is linear, we can make a separation in $S = S_{LR} + S_{Ln} + S_{Rn}$ as to cancel term by term,

$$\begin{aligned} H_{LR} + [iS_{LR}, H_0] &= 0, \\ H_{\alpha n} + [iS_{\alpha n}, H_0] &= 0 \quad \text{for} \quad \alpha = \{L, R\}. \end{aligned}$$

Please note, that the operator (iS) has to be antihermitian such that $[iS, H_0]$ is hermitian. The next two subsections are devoted to the two different generators S_{LR} and $S_{\alpha n}$ respectively.

Generator S_{LR}

To cancel the hopping H_{LR} between the two different quantum dots we propose a generator

$$S_{LR} = i \sum_{\sigma} \left(t_{LR} \hat{E}_{LR}(\sigma) d^{\dagger}_{R\sigma} d_{L\sigma} - t_{RL} \hat{E}_{LR}(\sigma) d^{\dagger}_{L\sigma} d_{R\sigma} \right), \tag{2.20}$$

where

$$\begin{aligned} \hat{E}_{LR}(\sigma) = & \frac{1}{\epsilon_{L\sigma} - \epsilon_{R\sigma}} \left(1 - n_{L\overline{\sigma}}\right) \left(1 - n_{R\overline{\sigma}}\right) \\ & + \frac{1}{\epsilon_{L\sigma} - \epsilon_{R\sigma} + U_{LR} - U_R} \left(1 - n_{L\overline{\sigma}}\right) n_{R\overline{\sigma}} \\ & + \frac{1}{\epsilon_{L\sigma} - \epsilon_{R\sigma} + U_L - U_{LR}} n_{L\overline{\sigma}} \left(1 - n_{R\overline{\sigma}}\right) \\ & + \frac{1}{\epsilon_{L\sigma} - \epsilon_{R\sigma} + U_L - U_R} n_{L\overline{\sigma}} n_{R\overline{\sigma}}. \end{aligned} \tag{2.21}$$

(iS_{LR}) is antihermitian as required. Please note, that in the first term of S_{LR} the inverse energy term $\hat{E}_{LR}(\sigma)$ is implicitly multiplied by $n_{R\sigma}\left(1 - n_{L\sigma}\right)$ and in the second term by $n_{L\sigma}\left(1 - n_{R\sigma}\right)$. Since $\hat{E}_{LR}(\sigma)$ is an operator, it is important that it acts after $d^{\dagger}_{R\sigma} d_{L\sigma}$. We choose this convention since the expression can now be interpreted as the gain of hopping t_{LR} at the cost of an intermediate state defined by the combination of occupation operators with an energy difference to the initial state as defined in the corresponding denominator.

It has to be proven that $[iS_{LR}, H_0] = -H_{LR}$. The proof is shown for one example in appendix A.1.2

Generator $S_{\alpha n}$

Similarly it has to be shown for the generator $S_{\alpha n}$ that $-i[S_{\alpha n}, H_0] = H_{\alpha n}$. The lengthy proof is left out here. The interested reader can look up how it should work in appendix A.1.2 or for example the corresponding chapter in Ref. [22]. The generator $S_{\alpha n}$ is given by

$$S_{\alpha n} = i \frac{1}{N} \sum_{nk\sigma} \left(t_{\alpha n} \hat{E}_L(\sigma) c^{\dagger}_{nk\sigma} d_{\alpha\sigma} - t_{n\alpha} \hat{E}_L(\sigma) d^{\dagger}_{\alpha\sigma} c_{nk\sigma} \right), \tag{2.22}$$

where

$$\begin{aligned}
\hat{E}_\alpha(\sigma) = & \frac{1}{\epsilon_{\alpha\sigma} - \zeta} \left(1 - n_{\alpha\overline{\sigma}}\right) \left(1 - n_{\overline{\alpha}\sigma}\right) \left(1 - n_{\overline{\alpha\sigma}}\right) \\
& + \frac{1}{\epsilon_{\alpha\sigma} + U_{LR} - J_H - \zeta} \left(1 - n_{\alpha\overline{\sigma}}\right) n_{\overline{\alpha}\sigma} \left(1 - n_{\overline{\alpha\sigma}}\right) \\
& + \frac{1}{\epsilon_{\alpha\sigma} + U_{LR} - \zeta} \left(1 - n_{\alpha\overline{\sigma}}\right) \left(1 - n_{\overline{\alpha}\sigma}\right) n_{\overline{\alpha\sigma}} \\
& + \frac{1}{\epsilon_{\alpha\sigma} + 2U_{LR} - \zeta} \left(1 - n_{\alpha\overline{\sigma}}\right) n_{\overline{\alpha}\sigma}\ n_{\overline{\alpha\sigma}} \\
& + \frac{1}{\epsilon_{\alpha\sigma} + U_\alpha - \zeta} n_{\alpha\overline{\sigma}}\ \left(1 - n_{\overline{\alpha}\sigma}\right) \left(1 - n_{\overline{\alpha\sigma}}\right) \\
& + \frac{1}{\epsilon_{\alpha\sigma} + U_\alpha + U_{LR} - \zeta} n_{\alpha\overline{\sigma}}\ n_{\overline{\alpha}\sigma} \left(1 - n_{\overline{\alpha\sigma}}\right) \\
& + \frac{1}{\epsilon_{\alpha\sigma} + U_\alpha + U_{LR} + J_H - \zeta} n_{\alpha\overline{\sigma}}\ \left(1 - n_{\overline{\alpha}\sigma}\right) n_{\overline{\alpha\sigma}} \\
& + \frac{1}{\epsilon_{\alpha\sigma} + U_\alpha + 2U_{LR} - \zeta} n_{\alpha\overline{\sigma}}\ n_{\overline{\alpha}\sigma}\ n_{\overline{\alpha\sigma}}, \qquad (2.23)
\end{aligned}$$

with $\alpha = L/R$ and $\overline{\alpha} = R/L$, respectively. The energy change ζ of the conduction electron is given with respect to the Fermi energy. Usually the Coulomb energy U_α is the largest energy scale and the energy of the involved conduction electron ζ is neglected in comparison with it.

Having found the right generators of the transformation we can calculate the effective interaction to higher orders in the hopping parameters $t_{\alpha n}$ and t_{LR}.

2.2.4 Effective Hamiltonian in 2nd Order

With the correct choice of generators, the Schrieffer-Wolff transformation provides a cancellation to linear order of the hopping in and out of the quantum dots and instead an effective interaction $\frac{1}{2} i \left[S, H_{\text{int}}\right]$ of second order in the hopping. We now focus on processes which conserve the particle number on the quantum dot. After the projection we find that the two terms,

$$\mathcal{P} \left[S_{LR}, H_{\alpha n}\right] \mathcal{P} = \mathcal{P} \left[S_{\alpha n}, H_{LR}\right] \mathcal{P} = 0,$$

can be neglected since $H_{\alpha n}$ always changes the number of electrons on the dot.

Still the model does not constrict properties of the double quantum dot system itself. There can still be from 0 to 4 electrons present and there are many interesting regimes in this setup. We refer the interested reader for example to Ref. [48] and [49]. We limit ourselves to a double quantum dot system with two electrons, especially with one electron on each quantum dot, since this setup models the situation of two interacting Kondo impurities.

In total there are two electrons in the double quantum dot system and we neglect the higher lying singlet if both electrons are in one quantum dot (see Ref. [48]). Out of these four states, the two with same spin direction are additionally shifted in energy by the Hund coupling J_H. After the calculation J_H is set to zero and it is assumed that all four states have the same energy.

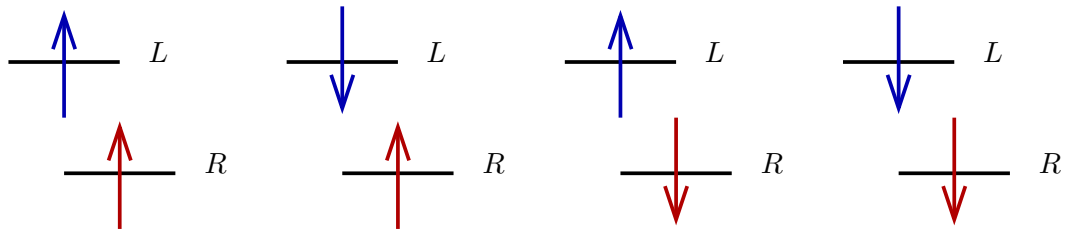

Figure 2.2: When there is only one electron allowed on each of the quantum dots, these are the four possible spin states of the double quantum dot system.

The states with two electrons on one quantum dot with an energy of $2\epsilon_\alpha + U_\alpha$ for either $\alpha = L$ or R have to be energetically unfavorable in comparison to a state with one electron on each quantum dot and an energy of $\epsilon_L + \epsilon_R + U_{LR}$. We can always tune the double quantum dot setup into this limit by choosing

$$U_L, U_R > U_{LR}.$$

This is physically the most reasonable assumption since $U_{LR} < U_\alpha$ corresponds to a Coulomb interaction for two electron on different quantum dots that is smaller than the energy cost if they are placed on the same.

Furthermore we demand that the number of electrons on each quantum dot remains unchanged, and consequently the contributions from

$$\mathcal{P}\left[S_{Ln}, H_{Rm}\right]\mathcal{P} = \mathcal{P}\left[S_{Rn}, H_{Lm}\right]\mathcal{P} = 0$$

can be discarded as well.

Finally the effective Hamiltonian consists of one term which deals only with the interactions on the double quantum dot system $[S_{LR}, H_{LR}]$ and a term including interactions with the leads. These are summarized in the commutator $[S_{\alpha n}, H_{\alpha m}]$ for $\alpha = L, R$.

Effective interaction from $[S_{LR}, H_{LR}]$

The interaction between the two quantum dots is described by strong repulsions U_L, U_R, U_{LR} and a small hopping t_{LR}. In this limit we can do a perturbation calculation in t_{LR} and find the effective correlation from the term $[S_{LR}, H_{LR}]$ in the Schrieffer-Wolff transformation. By contrast, if t_{LR} would be large and a perturbation in it is not possible, then one would have to diagonalize H_{LR} and $H_L + H_R$ to find new hybridized eigenstates, see e.g. Refs. [46, 47]. In the following it is assumed that the hopping t_{LR} is small which corresponds to the experimental situation where a tunnel barrier separates

the two dots. Then $[S_{LR}, H_{LR}]$ contains three different terms,

$$\begin{aligned}
[S_{LR}, H_{LR}] = i \Bigg[& \sum_{\sigma} \left(t_{LR} \hat{E}_{LR}(\sigma) d^{\dagger}_{R\sigma} d_{L\sigma} - t_{RL} \hat{E}_{LR}(\sigma) d^{\dagger}_{L\sigma} d_{R\sigma} \right), \\
& \sum_{\sigma'} \left(t_{LR} d^{\dagger}_{R\sigma'} d_{L\sigma'} + t_{RL} d^{\dagger}_{L\sigma'} d_{R\sigma'} \right) \Bigg] \\
= i \sum_{\sigma\sigma'} \Big\{ & (t_{LR})^2 \left[\hat{E}_{LR}(\sigma), d^{\dagger}_{R\sigma'} d_{L\sigma'} \right] d^{\dagger}_{R\sigma} d_{L\sigma} \\
& - (t_{RL})^2 \left[\hat{E}_{LR}(\sigma), d^{\dagger}_{L\sigma'} d_{R\sigma'} \right] d^{\dagger}_{L\sigma} d_{R\sigma} \Big\} \qquad (2.24) \\
+ i \sum_{\sigma\sigma'} & 2 t_{LR} t_{RL} \hat{E}_{LR}(\sigma) \delta_{\sigma\sigma'} \left(d^{\dagger}_{R\sigma} d_{R\sigma} - d^{\dagger}_{L\sigma} d_{L\sigma} \right) \qquad (2.25) \\
+ i \sum_{\sigma\sigma'} & t_{LR} t_{RL} \Big\{ \left[\hat{E}_{LR}(\sigma), d^{\dagger}_{L\sigma'} d_{R\sigma'} \right] d^{\dagger}_{R\sigma} d_{L\sigma} \\
& - \left[\hat{E}_{LR}(\sigma), d^{\dagger}_{R\sigma'} d_{L\sigma'} \right] d^{\dagger}_{L\sigma} d_{R\sigma} \Big\}, \qquad (2.26)
\end{aligned}$$

differing by their physical content.

Eq. (2.24) involves two particle excitations and contributes only if there is already a doubly occupied state either in the left or in the right quantum dot.

Eq. (2.25) is spin conserving and proportional to the difference in occupation number on the left and right quantum dot.

Eq. (2.26) conserves the number of electrons on each quantum dot, but the spin quantum number is not conserved. This term leads to spin-flip processes and therefore to an effective spin-spin interaction.

At this stage one should remember that the considerations here are limited to two-particle physics – one electron in the left quantum dot and one electron in the right quantum dot. An immediate consequence of this is that any contribution of Eq. (2.24) is projected out in this configuration space and only Eq. (2.25) and (2.26) contribute. Obviously a hopping process which does not change the spin state is not possible for the two states with identical spin direction. Thus the only contribution of Eq. (2.25) arises from the projection $n_{L\sigma}(1 - n_{L\overline{\sigma}}) n_{R\overline{\sigma}}(1 - n_{R\sigma})$ for $\sigma = \uparrow, \downarrow$. After performing the spin summation of the term

$$\begin{aligned}
& i \sum_{\sigma\sigma'} 2 t_{LR} t_{RL} \hat{E}_{LR}(\sigma) \delta_{\sigma\sigma'} \left(n_{R\sigma} - n_{L\sigma} \right) \\
= i \sum_{\sigma} 2 t_{LR} t_{RL} & \left(\frac{1}{\epsilon_{L\sigma} - \epsilon_{R\sigma} + U_L - U_{LR}} n_{R\sigma} \left(1 - n_{R\overline{\sigma}}\right) n_{L\overline{\sigma}} \left(1 - n_{L\sigma}\right) \right. \\
& \left. - \frac{1}{\epsilon_{L\sigma} - \epsilon_{R\sigma} + U_{LR} - U_R} n_{L\sigma} \left(1 - n_{L\overline{\sigma}}\right) n_{R\overline{\sigma}} \left(1 - n_{R\sigma}\right) \right),
\end{aligned}$$

we find a first contribution to the new effective Hamiltonian $\tilde{H} = \frac{1}{2} [iS, H_{\text{int}}]$

$$\frac{1}{2} i \left[S_{LR}, H_{LR} \right] = \frac{1}{2} K \left(n_{L\uparrow} n_{R\downarrow} + n_{L\downarrow} n_{R\uparrow} \right) + \ldots \qquad (2.27)$$

where

$$K = \left(\frac{2t_{LR}t_{RL}}{\epsilon_{L\sigma} - \epsilon_{R\sigma} + U_L - U_{LR}} - \frac{2t_{LR}t_{RL}}{\epsilon_{L\sigma} - \epsilon_{R\sigma} + U_{LR} - U_R} \right). \tag{2.28}$$

Before we discuss Eq. (2.27) in further detail, we study Eq. (2.26) in the configuration subspace.

$$\begin{aligned} & i \sum_{\sigma\sigma'} t_{LR}t_{RL} \left\{ \left[\hat{E}_{LR}(\sigma), d^\dagger_{L\sigma'} d_{R\sigma'} \right] d^\dagger_{R\sigma} d_{L\sigma} - \left[\hat{E}_{LR}(\sigma), d^\dagger_{R\sigma'} d_{L\sigma'} \right] d^\dagger_{L\sigma} d_{R\sigma} \right\} \\ & = i \sum_{\sigma} \frac{1}{2} K d^\dagger_{L\overline{\sigma}} d_{R\overline{\sigma}} d^\dagger_{R\sigma} d_{L\sigma} - \frac{1}{2} K d^\dagger_{R\overline{\sigma}} d_{L\overline{\sigma}} d^\dagger_{L\sigma} d_{R\sigma}. \end{aligned}$$

This provides another contribution to the Hamiltonian $\tilde{H}$

$$\frac{1}{2} i \left[S_{LR}, H_{LR} \right] = \frac{1}{2} K \left(d^\dagger_{L\uparrow} d_{L\downarrow} d^\dagger_{R\downarrow} d_{R\uparrow} + d^\dagger_{L\downarrow} d_{L\uparrow} d^\dagger_{R\uparrow} d_{R\downarrow} \right) \ldots, \tag{2.29}$$

which in contrast to Eq. (2.27) is a spin-flip term.

To combine the two parts effective spin operators for the two quantum dots are introduced,

$$\begin{aligned} S^z_\alpha &= \frac{1}{2} \left(n_{\alpha\uparrow} - n_{\alpha\downarrow} \right), \\ S^+_\alpha &= \frac{1}{\sqrt{2}} \left(\vec{S}^x_\alpha + i \vec{S}^y_\alpha \right) = \frac{1}{\sqrt{2}} d^\dagger_{\alpha\uparrow} d_{\alpha\downarrow}, \\ S^-_\alpha &= \frac{1}{\sqrt{2}} \left(\vec{S}^x_\alpha - i \vec{S}^y_\alpha \right) = \frac{1}{\sqrt{2}} d^\dagger_{\alpha\downarrow} d_{\alpha\uparrow}. \end{aligned}$$

Furthermore we can use the constraint, that there is only one electron on each quantum dot, to represent the occupation numbers $n_{\alpha\sigma}$ by spin operators,

$$\begin{aligned} & n_{\alpha\uparrow} + n_{\alpha\downarrow} = 1, \\ \Rightarrow \qquad & n_{\alpha\uparrow} = \frac{1}{2} + S^z_\alpha, \qquad\qquad n_{\alpha\downarrow} = \frac{1}{2} - S^z_\alpha. \end{aligned} \tag{2.30}$$

Finally the combination of Eq. (2.27) and (2.29) gives

$$\frac{1}{2} i \left[S_{LR}, H_{LR} \right] = K \vec{S}_L \vec{S}_R - \frac{1}{4} K. \tag{2.31}$$

Please note that so far this is only valid for two of the four states in the configuration space. Taking a closer look at the two states with the same spin direction on the left and right quantum dot we find

$$\left(K \vec{S}_L \vec{S}_R - \frac{1}{4} K \right) |\sigma\rangle_L |\sigma\rangle_R = K \left(\frac{1}{2}\sigma \cdot \frac{1}{2}\sigma + 0 + 0 - \frac{1}{4} \right) |\sigma\rangle_L |\sigma\rangle_R = 0,$$

such that the expression does not have an influence on those states. The expression in Eq. (2.31) is thus the general result for the effective low-energy interaction between the two dots.

To understand this result from physical arguments we study the virtual processes. In Fig. 2.3 one such exchange process is illustrated. With an energy of t_{LR} an electron can be excited to a doubly occupied state in one quantum dot which costs the energy $\epsilon_L - \epsilon_R + U_L - U_{LR}$. Please note, that this process is only possible if the two spins in the two quantum dots are antiparallel. Another hopping process of energy t_{RL} results in the original state or in a state where both spins are flipped. We will later on refer to

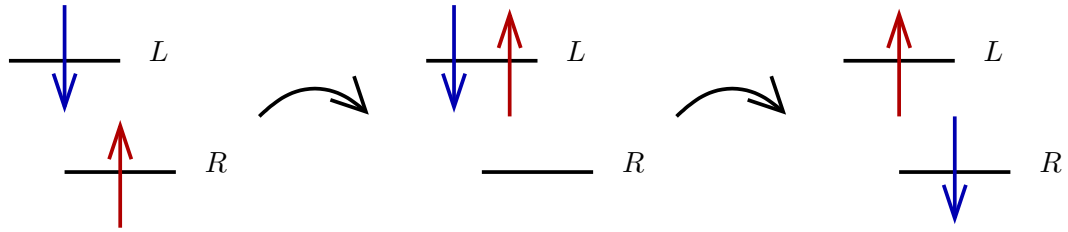

Figure 2.3: Illustration of the effective spin-spin interaction via an intermediate excited state. The second process can lead to a spin flip or can leave the system in the initial state.

this exchange interaction as a spin-spin interaction.

The Hund rule coupling does not play a role in the expression for K since only the states with spin $\uparrow$ and $\downarrow$ are shifted in energy by the spin-spin interaction. Please note that applying a magnetic field does not change the interaction since the difference $\epsilon_{L\sigma} - \epsilon_{R\sigma}$ of the initial and intermediate state is of the same spin species and a shift by $\frac{1}{2}\sigma B$ cancels out.

Effective Interaction from $[S_{Ln}, H_{Lm}]$ and $[S_{Rn}, H_{Rm}]$

In the previous section we found that the Schrieffer-Wolff transformation produces in 2nd order an exchange interaction between the spins of the two quantum dots. Due to the similar coupling Hamiltonians we expect that the two terms $[S_{Ln}, H_{Lm}]$ and $[S_{Rn}, H_{Rm}]$ lead similarly to an effective spin-spin interaction between the electron on the quantum dot and electrons in the leads.

The commutator $[S_{\alpha n}, H_{\alpha m}]$ for $\alpha = L, R$ is given by,

$$[S_{\alpha n}, H_{\alpha m}] = i \left[\frac{1}{N} \sum_{nk\sigma} \left(t_{\alpha n} \hat{E}_\alpha(\sigma) c^\dagger_{nk\sigma} d_{\alpha\sigma} - t_{n\alpha} \hat{E}_\alpha(\sigma) d^\dagger_{\alpha\sigma} c_{nk\sigma} \right), \right.$$
$$\left. \frac{1}{N} \sum_{mk'\sigma'} \left(t_{\alpha m} c^\dagger_{mk'\sigma'} d_{\alpha\sigma'} + t_{m\alpha} d^\dagger_{\alpha\sigma'} c_{mk'\sigma'} \right) \right].$$

We separate the particle-conserving contributions

$$it_{\alpha n} t_{m\alpha} \frac{1}{N^2} \sum_{nk\sigma} \sum_{mk'\sigma'} \left[\hat{E}_\alpha(\sigma) c^\dagger_{nk\sigma} d_{\alpha\sigma}, d^\dagger_{\alpha\sigma'} c_{mk'\sigma'} \right]$$
$$- it_{n\alpha} t_{\alpha m} \frac{1}{N^2} \sum_{nk\sigma} \sum_{mk'\sigma'} \left[\hat{E}_\alpha(\sigma) d^\dagger_{\alpha\sigma} c_{nk\sigma}, c^\dagger_{mk'\sigma'} d_{\alpha\sigma'} \right],$$

from the non-particle-conserving contributions

$$it_{\alpha n}t_{\alpha m}\frac{1}{N^2}\sum_{nk\sigma}\sum_{mk'\sigma'}\left[\hat{E}_\alpha(\sigma)c^\dagger_{nk\sigma}d_{\alpha\sigma},c^\dagger_{mk'\sigma'}d_{\alpha\sigma'}\right]$$
$$-it_{n\alpha}t_{m\alpha}\frac{1}{N^2}\sum_{nk\sigma}\sum_{mk'\sigma'}\left[\hat{E}_\alpha(\sigma)d^\dagger_{\alpha\sigma}c_{nk\sigma},d^\dagger_{\alpha\sigma'}c_{mk'\sigma'}\right].$$

The latter can be directly neglected due to the projection $\mathcal{P}$ into the two-particle subspace since it does not conserve the number of electrons on the quantum dot system. We find similar to the commutator $[S_{LR},H_{LR}]$ a spin conserving contribution

$$\frac{i}{N^2}\sum_{nk\sigma}\sum_{mk'\sigma'}t_{\alpha n}t_{m\alpha}\hat{E}_\alpha(\sigma)\left\{c^\dagger_{nk\sigma}c_{mk'\sigma}\delta_{\sigma\sigma'}-\delta_{kk'}\delta_{mn}\delta_{\sigma\sigma'}d^\dagger_{\alpha\sigma'}d_{\alpha\sigma}+h.c.\right\},\tag{2.32}$$

and a spin-flip contribution

$$\frac{i}{N^2}\sum_{nk\sigma}\sum_{mk'\sigma'}\left\{t_{\alpha n}t_{m\alpha}\left[\hat{E}_\alpha(\sigma),d^\dagger_{\alpha\sigma'}\right]c_{mk'\sigma'}c^\dagger_{nk\sigma}d_{\alpha\sigma}\right.$$
$$\left.-t_{n\alpha}t_{\alpha m}c^\dagger_{mk'\sigma'}\left[\hat{E}_\alpha(\sigma),d_{\alpha\sigma'}\right]d^\dagger_{\alpha\sigma}c_{nk\sigma}\right\}.\tag{2.33}$$

First we concentrate on the contribution from Eq. (2.32). The term with $1/N^2\sum_{k'k}\delta_{k,k'}$ is of order $1/N$ where N is the number of states in the leads, and is negligible small in the thermodynamic limit $N\to\infty$ in comparison with all other terms. Thus it is neglected in the following. The terms in $\hat{E}_\alpha$, which are compatible with the projection to the two particle subspace, lead to a contribution to the interacting Hamiltonian $\frac{1}{2}i\left[S_{\alpha n},H_{\alpha m}\right]$ of the form

$$-\frac{1}{2}\frac{1}{N^2}\sum_{nk\sigma}\sum_{mk'\sigma'}c^\dagger_{nk\sigma}c_{mk'\sigma}$$
$$\left\{\frac{t_{\alpha n}t_{m\alpha}}{\epsilon_{\alpha\sigma}+U_{LR}-J_H-\zeta}n_{\alpha\sigma}\left(1-n_{\alpha\overline{\sigma}}\right)n_{\overline{\alpha}\sigma}\left(1-n_{\overline{\alpha\sigma}}\right)\right.$$
$$+\frac{t_{\alpha n}t_{m\alpha}}{\epsilon_{\alpha\sigma}+U_{LR}-\zeta}n_{\alpha\sigma}\left(1-n_{\alpha\overline{\sigma}}\right)\left(1-n_{\overline{\alpha}\sigma}\right)n_{\overline{\alpha\sigma}}$$
$$+\frac{t_{\alpha n}t_{m\alpha}}{\epsilon_{\alpha\sigma}+U_\alpha+U_{LR}-\zeta}\left(1-n_{\alpha\sigma}\right)n_{\alpha\overline{\sigma}}\,n_{\overline{\alpha}\sigma}\left(1-n_{\overline{\alpha\sigma}}\right)$$
$$\left.+\frac{t_{\alpha n}t_{m\alpha}}{\epsilon_{\alpha\sigma}+U_\alpha+U_{LR}+J_H-\zeta}\left(1-n_{\alpha\sigma}\right)n_{\alpha\overline{\sigma}}\;\left(1-n_{\overline{\alpha}\sigma}\right)n_{\overline{\alpha\sigma}}\right\}+h.c.\tag{2.34}$$

To bring this expression into a short form spin operators for the conduction electrons are introduced,

$$\vec{s}_{nm}=\frac{1}{N^2}\sum_{k'k}\sum_{\sigma'\sigma}c^\dagger_{nk\sigma}\frac{1}{2}\vec{\tau}_{\sigma'\sigma}c_{mk'\sigma'}.\tag{2.35}$$

Thus we can reformulate

$$c^\dagger_{nk\uparrow}c_{mk'\uparrow}=\frac{1}{2}\sum_\sigma c^\dagger_{nk\sigma}c_{mk'\sigma}+s^z_{nm},$$
$$c^\dagger_{nk\downarrow}c_{mk'\downarrow}=\frac{1}{2}\sum_\sigma c^\dagger_{nk\sigma}c_{mk'\sigma}-s^z_{nm},$$

to separate the potential scattering from the spin interaction part. By performing the sum in Eq. (2.34) over spin indices rigorously many different coupling terms are created. A sketch of this calculation is given in appendix A.1.3. In the following the Hund coupling $J_H = 0$ is set to zero and we neglect the spin dependence of the bare energy levels $\epsilon_{\alpha\sigma} = \epsilon_\alpha$, which is justified for zero or negligibly small magnetic field.

Then the commutator $\frac{1}{2}i\left[S_{\alpha n}, H_{\alpha m}\right]$ gives

$$\begin{aligned}&= \frac{1}{2}\sum_{mn} J_{\alpha nm} s^z_{nm} S^z_\alpha + h.c. \\ &+ \frac{1}{2}\sum_{mn\sigma}\frac{1}{N^2}\sum_{kk'} V_{\alpha nm} c^\dagger_{nk\sigma} c_{mk'\sigma} + h.c.,\end{aligned}$$

where

$$J_{\alpha nm} = \frac{2t_{\alpha n}t_{m\alpha}}{\epsilon_\alpha + U_\alpha + U_{LR} - \zeta} - \frac{2t_{\alpha n}t_{m\alpha}}{\epsilon_\alpha + U_{LR} - \zeta}, \tag{2.36}$$

$$V_{\alpha nm} = -\frac{1}{2}\left(\frac{t_{\alpha n}t_{m\alpha}}{\epsilon_\alpha + U_\alpha + U_{LR} - \zeta} + \frac{t_{\alpha n}t_{m\alpha}}{\epsilon_\alpha + U_{LR} - \zeta}\right). \tag{2.37}$$

Additionally there is a contribution from the spin flip part in Eq. (2.33). Leaving out the actual calculation we state the result

$$\begin{aligned}i\sum\Bigg\{ &\frac{t_{\alpha n}t_{m\alpha}}{\epsilon_\alpha + U_{LR} - J_H - \zeta} n_{\overline{\alpha}\sigma}\left(1 - n_{\overline{\alpha\sigma}}\right) \\ &+ \frac{t_{\alpha n}t_{m\alpha}}{\epsilon_\alpha + U_{LR} - \zeta}\left(1 - n_{\overline{\alpha}\sigma}\right) n_{\overline{\alpha\sigma}} \\ &- \frac{t_{\alpha n}t_{m\alpha}}{\epsilon_\alpha + U_\alpha + U_{LR} - \zeta} n_{\overline{\alpha}\sigma}\left(1 - n_{\overline{\alpha\sigma}}\right) \\ &- \frac{t_{\alpha n}t_{m\alpha}}{\epsilon_\alpha + U_\alpha + U_{LR} + J_H - \zeta}\left(1 - n_{\overline{\alpha}\sigma}\right) n_{\overline{\alpha\sigma}}\Bigg\} c^\dagger_{nk\sigma} c_{mk'\overline{\sigma}} d^\dagger_{\alpha\overline{\sigma}} d_{\alpha\sigma} + h.c.\end{aligned}$$

Using again the spin representation of the operators we find a contribution to the interacting Hamiltonian $\tilde{H}$, again in the case of $J_H = 0$,

$$\frac{1}{2}\sum J_{\alpha nm}\left(s^+_{nm} S^-_\alpha + s^-_{nm} S^+_\alpha\right) + h.c..$$

Summary of Effective Hamiltonian

Collecting all terms from the two previous sections we find the new effective Hamiltonian $\tilde{H} = H_0 + \tilde{H}_{\text{int}}$ with $H_0 = H_L + H_R + H_{\text{cap}} + H_{\text{Hund}}$ and

$$\begin{aligned}\tilde{H}_{\text{int}} = &K\vec{S}_L\vec{S}_R - \frac{1}{4}K \\ &+ \sum_{nm} J_{Lnm}\vec{S}_L\vec{s}_{nm} + \sum_{nm} J_{Rnm}\vec{S}_R\vec{s}_{nm} \\ &+ \sum_{nm\sigma}\frac{1}{N^2}\sum_{k,k'} V_{Lnm} c^\dagger_{nk\sigma} c_{mk'\sigma} + \sum_{nm\sigma}\frac{1}{N^2}\sum_{k,k'} V_{Rnm} c^\dagger_{nk\sigma} c_{mk'\sigma},\end{aligned}$$

where it is assumed that $t_{\alpha n} = t_{n\alpha}$. With this assumption *h.c.* and the sum over m, n cancels the prefactor of 1/2.

The coupling strengths are given in terms of the initial hopping matrix elements $t_{\alpha n}$ and t_{LR} and the interaction energies U_{LR} and U_α,

$$\begin{aligned} J_{\alpha nm} =& \frac{2t_{\alpha n}t_{\alpha m}}{\epsilon_\alpha + U_\alpha + U_{LR} - \zeta} - \frac{2t_{\alpha n}t_{\alpha m}}{\epsilon_\alpha + U_{LR} - \zeta}, \\ V_{\alpha nm} =& -\frac{1}{2}\left(\frac{t_{\alpha n}t_{\alpha m}}{\epsilon_\alpha + U_\alpha + U_{LR} - \zeta} + \frac{t_{\alpha n}t_{\alpha m}}{\epsilon_\alpha + U_{LR} - \zeta}\right), \\ K =& \frac{2t_{LR}t_{RL}}{\epsilon_L - \epsilon_R + U_L - U_{LR}} - \frac{2t_{LR}t_{RL}}{\epsilon_L - \epsilon_R + U_{LR} - U_R}. \end{aligned}$$

A discussion of these terms follows in section 2.3.

Please note, that the spin-spin interaction $J_{\alpha nm}$ is proportional to $t_{\alpha n}^2$. Thus in the case of interest when $t_{L3} = t_{L4} = 0$ there exists no coupling between the spin in the left quantum dot and the right leads. The same applies for the right quantum dot and the left leads in the case of $t_{R1} = t_{R2} = 0$. Since this independent spin control is an interesting setup, it should be checked if a leakage exists in higher order and how strong its influence could be.

2.2.5 Contributions from 3rd Order

So far all terms of higher order than t^2 were neglected using the assumption that the hopping is small. In this section we study the so-called leakage, which denotes a coupling between the leads connected to the left quantum dot to the leads connected to the right. Such a term is created to 3rd order in the coupling t and the aim of this section is to compare its magnitude to the other terms from 2nd order.

The 3rd order contribution is given by

$$\begin{aligned} &\frac{1}{3}\left[iS, [iS, H_{\text{int}}]\right] \\ &= \frac{i^2}{3}\left[S_{LR} + S_{Ln} + S_{Rn}, [S_{LR} + S_{Lm} + S_{Rm}, H_{LR} + H_{L\nu} + H_{R\nu}]\right]. \end{aligned}$$

Since the system is projected onto a double quantum dot system with 2 electrons in total and a fixed number of one electron on each quantum dot, a few terms can be neglected. For example all commutators contributing to the 2nd order in the Schrieffer-Wolff transformation are projected out in the 3rd order term, since they conserve the particle number only in a 2nd order process,

$$\mathcal{P}\frac{i^2}{3}\left[S_{LR} + S_{Ln} + S_{Rn}, [S_{LR}, H_{LR}] + [S_{\alpha m}, H_{\alpha\nu}]\right]\mathcal{P} = 0.$$

Thus 9 terms are projected out while there are 18 which could potentially be important. Fortunately even more processes are projected out,

$$\begin{aligned} &\mathcal{P}\frac{i^2}{3}\left[S_{LR}, [S_{LR}, H_{L\nu} + H_{R\nu}] + [S_{Lm} + S_{Rm}, H_{LR}]\right]\mathcal{P} = 0, \\ &\mathcal{P}\frac{i^2}{3}\left[S_{Ln} + S_{Rn}, [S_{Lm}, H_{R\nu}] + [S_{Rm}, H_{L\nu}]\right]\mathcal{P} = 0, \\ &\mathcal{P}\frac{i^2}{3}\left[S_{\alpha n}, [S_{LR}, H_{\alpha\nu}] + [S_{\alpha m}, H_{LR}]\right]\mathcal{P} = 0, \quad \text{for} \quad \alpha = L, R, \end{aligned}$$

since they do not conserve the electron number on the quantum dots. Finally we have to take into account only the following contributions

$$\begin{aligned}\frac{1}{3}\left[iS,\left[iS,H_{\text{int}}\right]\right] =& \frac{i^2}{3}\left[S_{LR},\left[S_{Lm},H_{R\nu}\right]+\left[S_{Rm},H_{L\nu}\right]\right]\\ &+\frac{i^2}{3}\left[S_{Ln},\left[S_{LR},H_{R\nu}\right]+\left[S_{Rm},H_{LR}\right]\right]\\ &+\frac{i^2}{3}\left[S_{Rn},\left[S_{LR},H_{L\nu}\right]+\left[S_{Lm},H_{LR}\right]\right].\end{aligned}$$

Thus any contribution to third order in the coupling is of the type $t_{nL}t_{LR}t_{Rm}$ and corresponds to a "leakage" from the left to the right leads. In general we expect two different types of processes as depicted in Fig. 2.4. In one process (left panel) an electron is trans-

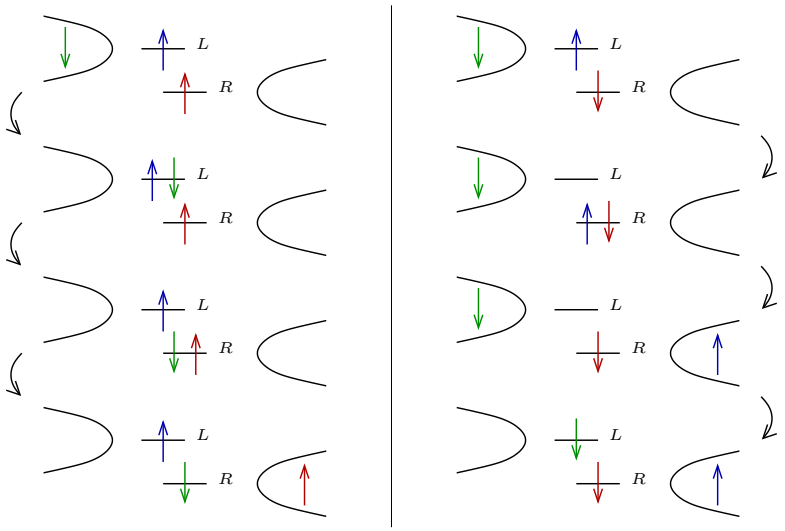

Figure 2.4: Two different processes can contribute to the leakage of an electron in one of the left leads to an electron in one of the right leads over the double quantum dot system. The two types of processes are discussed in the text.

ferred from a left electrode m to a right electrode n over virtual three-particle states. In this type of leakage an electron from one of the leads hops onto the dot. It is obvious that the same process can take place over virtual one-electron states when the first process is a hopping out of one dot into one of the leads. It is observed later that the path of the particle and the hole cancel each other in a symmetric setup. This type of leakage is possible for any state of the double quantum dot system and it can leave the original state unchanged or lead to a spin-flip like shown in Fig. 2.4 (left panel).

The other type of process involves first a virtual state inside the double quantum dot system as depicted in the right panel of Fig. 2.4. This process is only possible in the case of antiparallel oriented spins. Two interaction processes with the leads lead to a non-zero leakage, but the two processes with the leads are uncorrelated and independent of the spin orientation. It is found later on that also in this type of leakage two paths cancel each other in a symmetric setup such that the contribution vanishes completely.

The calculation of the leakage is shown in appendix A.2. In the derivation of leakage terms we focus on the derivation of a spin interaction similar to a Kondo coupling J_{nm}

in second order, but with one electron created in the left leads and one destroyed in the right leads or vice versa. In appendix A.2 an indirect Kondo coupling of the left leads to the right leads via the double quantum dot $\vec{S}_\alpha \vec{s}_{nm}$ where $m \in \{1,2\}$ and $n \in \{3,4\}$ is calculated. There are further types of couplings created to third order. Nevertheless we focus on the magnitude to which the leakage contributes to the coupling part of the effective Hamiltonian.

In order to compare this term with the 2nd order contributions analytically we concentrate on the special case of two identical quantum dots, i.e. $\epsilon_L = \epsilon_R = \epsilon$ and $U_L = U_R = U$. Summarizing thus the calculation to third order we find a contribution to the Hamiltonian

$$J_{nm}^{\text{leakage}} \vec{S}_\alpha^- \vec{s}_{nm}^+$$

of the order of

$$\begin{aligned} J_{nm}^{\text{leakage}} =& \frac{2}{3} t_{mL} t_{LR} t_{Rn} \\ & \left\{ \frac{1}{\epsilon + U_{LR} - \zeta} \left(\frac{1}{\epsilon + U - \zeta} - \frac{1}{\epsilon + U_{LR} - \zeta} \right) \right. \\ & + \frac{1}{U - U_{LR}} \left(\frac{1}{\epsilon + 2U_{LR} - \zeta} + \frac{1}{\epsilon + U - \zeta} \right) \\ & + 2 \frac{1}{U - U_{LR}} \left(\frac{1}{\epsilon + U_{LR} - \zeta} + \frac{1}{\epsilon + U + U_{LR} - \zeta} \right) \\ & \left. + \frac{1}{\epsilon + U + U_{LR} - \zeta} \left(\frac{1}{\epsilon + U + U_{LR} - \zeta} - \frac{1}{\epsilon + 2U_{LR} - \zeta} \right) \right\}. \end{aligned} \tag{2.38}$$

This term gives rise to an interaction which moves an electron from a left lead to a right lead or vice versa over the double quantum dot system even if $t_{L3} = t_{L4} = t_{R1} = t_{R2} = 0$ is assumed. In the next section the importance of this term compared to the other interactions is discussed.

2.3 Effective Hamiltonian and Discussion

We derived an effective Hamiltonian for the low energy properties of the double quantum dot system as illustrated in Fig. 2.1. In the new interaction Hamiltonian $\tilde{H}_{\text{int}}$ the number of particles on the quantum dot is conserved and the interaction takes place only via a spin-spin interaction or a potential scattering. Using a Schrieffer-Wolff transformation we derived a Kondo model from the Anderson model. In the following it is assumed that the Hund coupling $J_H = 0$ does not split up the four spin states of the double quantum dot system and that the bare energy levels are not spin dependent $\epsilon_{\alpha\sigma} = \epsilon_\alpha$. Furthermore it is assumed that the two quantum dots are identical,

$$\epsilon_L = \epsilon_R = \epsilon \qquad \text{and} \qquad U_L = U_R = U.$$

With these assumptions it is possible to discuss the spin exchange interaction, the Kondo coupling J and the leakage coupling quantitatively.

2.3.1 Spin Exchange Interaction

The spin exchange interaction in the symmetric setup is given by

$$K = 4\frac{t_{LR}t_{RL}}{U - U_{RL}}.$$

Since we are in the regime where $U_{LR} < U$ the interaction is positive and therefore the two quantum dot spins align antiferromagnetically.

This can be understood from a simple argument as already depicted in Fig. 2.3: Two parallel oriented spins are fixed on each quantum dot since hopping is forbidden from the Pauli principle. Two antiparallel oriented spins can have a virtual transition to the other quantum dot thus gaining the kinetic energy t_{LR} while the virtual doubly occupied state costs the energy $U - U_{RL}$. Through this process the two states can lower their energy.

Please note that in a lot of experiments the spin exchange interaction is observed to be ferromagnetic. It is not aim of this thesis to generalize the model such that it is additionally capable of describing ferromagnetism. Usually the quantum dots are further apart such that there is no direct hopping, but the interaction is mediated by an electron bath. In experiments this can be for example a larger (metallic) quantum dot like in [27] or a nanowire like in [29]. The intermediate region leads to an RKKY interaction between the two quantum dots, which can be ferromagnetic or antiferromagnetic depending on the distance. For an explanation of the RKKY interaction see for example Ref. [18].

In this thesis we want to discuss the properties of a double quantum dot system coupled to a set of leads. It was shown that even a simple hopping and capacitative coupling between the two dots leads to an exchange interaction. The presence of a spin-spin interaction is assumed from now on without further mentioning where it comes from and how it is created.

2.3.2 Particle-Hole Symmetry

The interactions of the quantum dots with the leads in the symmetric setup are given by

$$\begin{aligned} J_{nm} =& 2t_n t_m \left(\frac{1}{\epsilon + U + U_{LR} - \zeta} - \frac{1}{\epsilon + U_{LR} - \zeta} \right), \\ V_{nm} =& -\frac{1}{2} t_n t_m \left(\frac{1}{\epsilon + U + U_{LR} - \zeta} + \frac{1}{\epsilon + U_{LR} - \zeta} \right). \end{aligned}$$

In an experimental setup the level energy ϵ can be tuned by a gate voltage. This has the advantage that this parameter can be chosen such that the potential scattering vanishes. Then the paths of a particle and a hole have the same energy and cancel each other. The particle-hole symmetric energy of the quantum dot,

$$\epsilon_{\mathrm{PH}} = -U/2 - U_{LR},$$

depends on the capacitance U_{LR}. Inserting the energy ϵ_{PH} in the expression for the couplings we find

$$J_{nm}^{\mathrm{PH}} = 4t_n t_m / U \qquad \text{and} \qquad V_{nm}^{\mathrm{PH}} = 0,$$

where the intermediate energy ζ of a conduction electron is neglected in comparison with the energy scale of the Coulomb repulsion. The Kondo coupling J_{nm}^{PH} does not depend on U_{LR} in contrast to the exchange interaction K. Later on it is assumed that the spin exchange interaction is sufficiently large such that the two spins are locked into singlet and triplet states while the coupling to the leads is still treated perturbatively. This is not justified from this simple model, but as mentioned before there are several mechanisms which can create a spin-spin interaction. Since the results of this model are comparable to experimental results it is justified to assume that the spin-spin interaction locks the double quantum dot into singlet and triplet states while the spin-spin coupling to the leads is just a small perturbation, which leads to a finite current through either the left or the right quantum dot.

2.3.3 Discussion of the Leakage

For the remaining thesis it is further assumed that there is no tunneling from the left to the right leads and vice versa. Therefore the leakage term in the effective Hamiltonian has to be small. For the symmetric setup of two identical quantum dots in the particle-hole symmetric case we find

$$J_{nm}^{\mathrm{PH,leakage}} = 0,$$

such that all paths cancel each other. This can be understood from Fig. 2.4: For each particle traveling from the left to the right lead there is a hole which takes the opposite way with the same energy cost in a particle-hole symmetric setup. Similarly a process involving an excited singlet state costs the same energy on the left quantum dot as on the right quantum dot in the case of left-right symmetry. In the calculation we find that the phases of the two processes are of opposite sign and therefore the paths cancel each other.

In a not particle-hole symmetric case the leakage is given in Eq. (2.38). For two asymmetric quantum dots $J_{nm}^{\mathrm{leakage}}$ has to be derived along the lines of the calculation in appendix A.2. We find numerically for typical values of a quantum dot experiment[2] that the leakage is an order of magnitude smaller than the Kondo coupling since it is of the order of t^3 and t is assumed to be a small parameter. Thus it can be claimed that there is no leakage from a left lead to a right lead, especially in the preferred particle-hole symmetric case.

2.4 Summary and Outlook

In this section we introduced the double quantum dot setup, which is studied in the remaining part of the thesis. Two quantum dots are occupied by one electron each and coupled via a spin-spin interaction K. The origin of the spin-spin interaction is for example an exchange interaction or an RKKY interaction as discussed in section 2.3.

Both dots are coupled to two leads which allow for an electronic transport. We proved that for two identical quantum dots in the particle-hole symmetric case there is no leakage from the left to the right leads and argued that away from particle-hole

[2] This numerical comparison is not explicitly shown here.

symmetry the leakage is still small. Thus we can treat the current through the left and the current through the right quantum dot independently.

For a strong spin-spin interaction the two electrons on the left and right quantum dot are entangled. In section 2.1 we introduced singlet-triplet states and pseudo bosons, which create those states out of the vacuum. Using the pseudo-particle-representation common perturbation theory is possible.

Some physical insights have been gained from this introductory chapter. For example we learned that the interaction between the leads and for example the left quantum dot is via an interaction with the spin $\vec{S}_L$ and not via an interaction with the singlet-triplet states. We introduced a representation for the spin $\vec{S}_L$ and $\vec{S}_R$ in the singlet-triplet representation. An important observation is, that we do not find a singlet-singlet interaction. A singlet can only interact with the cost of K to a triplet state. Thus if we have for example a singlet ground state we do not expect any non-zero current until an energy scale like the voltage or the temperature provides sufficient energy to overcome the singlet-triplet excitation gap K.

We also like to mention at this point that the singlet-triplet representation is only valid if the spin-spin interaction is strong. The singlet and triplet states are in competition with product states if the gap K and the broadening of the resonance Γ become of the same order of magnitude. This problem is addressed in chapter 3 and appendix C is devoted to perturbation theory in the case of degenerate states.

After setting up a model, deriving an effective Hamiltonian and introducing the framework of singlet-triplet states we now proceed and discuss the physics of the double quantum dot system. Therefore we start with the lowest order approach - perturbation theory to 2nd order - although it is known that it fails in the Kondo regime, it gives some insight into physical behavior and a first quantitative description of the physics of a double quantum dot system at high temperatures.

3 Perturbation Theory – Part I: Method

In this chapter we discuss in detail the physics of a double quantum dot system in lowest order perturbation theory. Some ideas of perturbation theory in non-equilibrium were already given in the introduction in section 1.3. Since this method is a well-known concept we mention here only some of the most important definitions and refer the reader to the literature on the subject.

After having introduced the principles of perturbation theory out of equilibrium we define the Hamiltonian of the double quantum dot system of interest. In section 3.2 the Green's functions of the system are defined and their lowest order expression is written down. Building on the first two sections we calculate the perturbative correction to the double quantum dot system when the coupling to the leads is small. The result of the self energy from section 3.3 is then used in the Dyson equation for the retarded Green's function in section 3.4. The major impact of a finite self energy is reflected in a finite life time of the pseudo particles, i.e. a finite level broadening Γ. Even more significant is the effect of a finite self energy on the lesser Green's function. It is discussed in detail in section 3.5 that this leads to a quantum Boltzmann equation for the occupation probability of the double quantum dot states. Some complications in solving this equation are mentioned. For a discussion of results we refer the reader to chapter 4.

3.1 Introduction

Perturbation theory is closely related to the interaction picture in quantum mechanics. It is assumed that there is a part H_0 of the Hamiltonian which can be solved exactly and a perturbation or interacting part H_{int} which is coupled to the system H_0 by a small quantity. The idea is to treat H_{int} approximately by performing a series expansion in this small quantity. In this thesis we calculate e.g. the current properties, thus the double quantum dot setup and the leads are treated exactly and we perform a perturbation expansion in the coupling from the dots to the leads which allows for transport. An introduction to perturbation theory and further references can be found for example in the books Refs. [33, 22, 34].

In order to apply perturbation theory we have to choose a physical observable that should be described approximately. As mentioned before this can be the current or in general the Green's function for a single particle. There are different types of Green's functions, for example the retarded Green's function

$$G^r(t,t') = -i\Theta(t-t') \left\langle \left\{ f(t), f^\dagger(t') \right\} \right\rangle .$$

The retarded Green's function $G^r(t,t')$ describes the dynamics of a fermion f which is created at time t', interacts with the system until it is taken out again at time t. In the

interaction picture the time evolution of the ground state $|\Phi_0\rangle$ of H_0 at $t = -\infty$ to the interacting state at time t is described by $|\Psi(t)\rangle = S(t, -\infty)|\Phi_0\rangle$, where the S-matrix is given by

$$S(t, t') = T_t \ \exp\left[-i \int_{t'}^{t} dt_1 H_{\text{int}}(t_1)\right].$$

T_t stands for the time-ordering of the operators on the time axis, such that the latest time stands to the left. For a detailed derivation please see Ref. [33]. In the interaction picture the time evolution of the states is determined only by the interaction Hamiltonian $H_{\text{int}}(t)$.

The expectation value of the retarded Green's function G^r can be expressed in terms of the ground state at $t = \pm\infty$ by including $T_t S(\infty, -\infty)$ in the expression for the Green's function.[1] Usually it is assumed that the perturbation is switched on adiabatically at some time and switched off again in the far future. The assumption that the ground state of the system is the same at $t = -\infty$ before switching on and at $t = +\infty$ after switching off the interaction fails sometimes. Especially in the case of a finite voltage it is immediately obvious that the particles which have been transported from one lead to the other do not flow back if the coupling is switched off. In this situation a perturbation theory which originates from Keldysh [50] and Kadanoff & Baym [51] applies. The notation used in the following goes back to a review article of Rammer & Smith [32]. The way this introductory section is structured is closely related to some chapters of the book by Haug & Jauho [34].

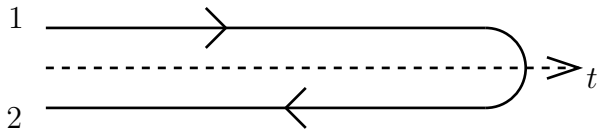

Figure 3.1: Picture of the Keldysh contour, where the time evolution is taken back to infinity $t \to -\infty$. The upper contour is usually denoted by 1 and the lower with opposite time direction by 2.

Keldysh doubled the time axes as illustrated in Fig. 3.1. The system is prepared in a known initial state. After switching on the coupling adiabatically, the interaction of a particle with the system is probed and afterwards the time is taken back on the contour 2 to the far past where the initial state is known. Using this trick the Green's function is in general a 2×2 matrix in the indices 1 and 2. In a short notation the Green's function matrix is written as $G(\tau, \tau') = -i\langle T_c f(\tau) f^\dagger(\tau')\rangle$, where τ is a time on the contour and T_c refers to the time-ordering along the contour. After the projection onto one of the contours τ is replaced by t since then it refers to a physical time.

[1] This is a sloppy formulation, but we present only the rough idea of perturbation theory. The interested reader should consult Ref. [33] for a rigorous derivation.

In the Keldysh language it is distinguished between four different Green's functions

$$\begin{aligned}
G^{11}(t,t') &= G^{t}(t,t') = -i\left\langle T_t\ f(t)f^\dagger(t')\right\rangle, \\
G^{22}(t,t') &= G^{\tilde{t}}(t,t') = -i\left\langle \tilde{T}_t\ f(t)f^\dagger(t')\right\rangle, \\
G^{21}(t,t') &= G^{>}(t,t') = -i\left\langle f(t)f^\dagger(t')\right\rangle, \\
G^{12}(t,t') &= G^{<}(t,t') = \pm i\left\langle f^\dagger(t')f(t)\right\rangle,
\end{aligned}$$

where the upper sign is for fermions and the lower for bosons. The time-ordered Green's function $G^t(t,t')$ is the same as in usual perturbation theory. T_t is the time-ordering on contour 1 as defined before, such that the latest time stands to the left. The anti-time-ordered Green's function $G^{\tilde{t}}$ is time-ordered on contour 2. These two functions are related by $[G^{\tilde{t}}(t,t')]^\dagger = G^t(t,t')$. The lesser Green's function $G^<(t,t')$ has a fixed order of operators. It is proportional to the occupation number $G^<(t,t) = \pm in$. The greater Green's function $G^>(t,t')$ at $t' = t$ can be interpreted as the occupation of a hole state.

The four Green's functions are not independent. They are related by

$$G^{11}(t,t') + G^{22}(t,t') = G^<(t,t') + G^>(t,t').$$

Sometimes also the Keldysh Green's function $G^K(t,t')$ is used which is defined by

$$G^K(t,t') = G^<(t,t') + G^>(t,t').$$

The time-ordered, anti-time-ordered, and also Keldysh Green's functions are not considered in the following, rather relations to the retarded and advanced Green's function are used,

$$\begin{aligned}
G^{11}(t,t') &= G^r(t,t') + G^<(t,t'), \\
G^{22}(t,t') &= G^<(t,t') - G^a(t,t'),
\end{aligned}$$

where the retarded and the advanced Green's function are defined like in equilibrium perturbation theory

$$\begin{aligned}
G^r(t,t') &= -i\Theta(t-t')\langle\{f(t), f^\dagger(t')\}\rangle = \Theta(t-t')\left(G^>(t,t') - G^<(t,t')\right), \\
G^a(t,t') &= i\Theta(t'-t)\langle\{f(t), f^\dagger(t')\}\rangle = \Theta(t'-t)\left(G^<(t,t') - G^>(t,t')\right).
\end{aligned}$$

It follows immediately that

$$G^r(t,t') - G^a(t,t') = G^>(t,t') - G^<(t,t'),$$

and the spectral function $A = i(G^r - G^a) = 2i\mathrm{Im}[G^r]$ can be expressed as well by the difference of the greater and lesser Green's function. As illustrated in e.g. Ref. [34, 32] the relation,

$$G^<(\omega) = -\mathrm{e}^{-\beta(\omega-\mu)}G^>(\omega),$$

holds in equilibrium, where the density matrix is determined by $\mathrm{e}^{\beta H}$. It follows directly from this equation that

$$\begin{aligned}
G^<(\omega)\left(1+\mathrm{e}^{-\beta(\omega-\mu)}\right) &= -\mathrm{e}^{-\beta(\omega-\mu)}\left(G^r(\omega) - G^a(\omega)\right) \\
\Rightarrow G^<(\omega) &= i\frac{1}{1+\mathrm{e}^{\beta(\omega-\mu)}}A(\omega).
\end{aligned}$$

Thus in equilibrium the lesser Green's function $G^<$ and the spectral function A or more generally the retarded Green's function G^r are related by what it usually referred to as a fluctuation-dissipation theorem. We use the ansatz of the lesser Green's function to be a product of a distribution function and the spectral function in the rest of the thesis. For further reading we refer to Refs. [34, 32].

For a finite voltage or another non-equilibrium situation we find that the retarded and lesser Green's function are no longer related by a fluctuation-dissipation theorem. Thus both have to be calculated by different determining equations. As included in the name the only information we have about a non-equilibrium state is, that it is not in equilibrium. Thermodynamic properties like the magnetization are now determined by the voltage V (and decoherence rate Γ) instead of by the temperature T.

After having introduced the Green's function, which is treated perturbatively, we now explain very shortly the principles of perturbation theory. More thorough explanations can be found in introductory books like Refs. [33, 22, 34]. As already mentioned the time evolution in the interaction picture is carried by the S-matrix, which in non-equilibrium is time-ordered by T_c on the Keldysh contour[2]. The expansion of the exponential gives a series in H_{int},

$$\begin{aligned} S_c &= T_c \exp\left[-i \int_c d\tau_1 H_{\text{int}}(\tau_1)\right] \\ &\approx T_c \left[1 - i \int_c d\tau_1 H_{\text{int}}(\tau_1) + \frac{(-i)^2}{2} \int_c d\tau_1 \int_c d\tau_2 H_{\text{int}}(\tau_1) H_{\text{int}}(\tau_2) \pm \ldots\right]. \end{aligned}$$

The first term is the non-interacting result, the second term is the first order correction and so on and so forth. This expansion provides the perturbation series to any order of the interaction Hamiltonian H_{int}.

In the model of a double quantum dot system the small parameter in the perturbative expansion is the coupling to the leads. Perturbation theory is used to calculate the Green's functions of the system, the current, the T-matrix and current-current correlations. To perform this calculation the concepts of Wick's theorem and the self energy have to be introduced, although a derivation or closer explanation is avoided due to length reasons.

Wick's theorem allows to reduce all higher-order Green's function with more than 2 operators to the single-particle Green's functions as introduced before. Wick's theorem is only valid for example if the non-interacting Hamiltonian H_0 is quadratic.[3] Since these conditions are fulfilled for the Hamiltonian chosen for the double quantum dot system Wick's theorem is applicable.

If one performs the expansion in the interacting Hamiltonian as described above, one would find a series of various contributions conveniently represented by Feynman diagrams. As illustrated in Fig. 3.2 some diagrams appear repeatedly. Consequently the Green's function can be written in a self-consistent equation, which includes an infinite order of the so-called self energy Σ. The self energy Σ is a collection of all irreducible

[2]This calculation contains a lot of technical pitfalls and needs a careful derivation. We refer the interested reader to the review [32] for further reading.

[3]See one of the references [33, 22] for further details.

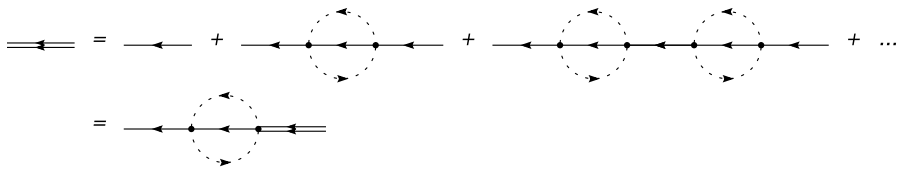

Figure 3.2: Diagrammatic illustration of the Dyson equation.

diagrams in the perturbation expansion. The Dyson equation,

$$G(\tau,\tau') = G^{(0)}(\tau,\tau') + \int_c d\tau_1 \int_c d\tau_2 \; G^{(0)}(\tau,\tau_1)\Sigma(\tau_1,\tau_2)G(\tau_2,\tau'),$$

is illustrated in Fig. 3.2. The diagrams which enter the self energy Σ can be determined by calculating the expansion series and identifying the irreducible diagrams in the corresponding order of perturbation theory. Please see section 3.3 for a typical derivation and Refs. [33, 22, 34] for further reading.

For example the calculation of the self energy contains products of Keldysh Green's functions and the lesser or retarded part of these products has to be determined. For this purpose one either has to sum over all possible contour diagrams (see for example section 4.6) or use the so-called Langreth rules of analytical continuation.

We will use repeatedly the Langreth rules for $A(\tau,\tau') = B(\tau,\tau')C(\tau',\tau)$,

$$\begin{aligned} A^{</>}(t,t') &= B^{</>}(t,t')C^{>/<}(t',t), \\ A^{r/a}(t,t') &= B^{<}(t,t')C^{a/r}(t',t) + B^{r/a}(t,t')C^{<}(t',t), \end{aligned}$$

and $A(\tau,\tau') = B(\tau,\tau')C(\tau,\tau')$,

$$\begin{aligned} A^{</>}(t,t') &= B^{</>}(t,t')C^{</>}(t',t), \\ A^{r}(t,t') &= B^{<}(t,t')C^{r}(t',t) + B^{r}(t,t')C^{<}(t',t) + B^{r}(t,t')C^{r}(t',t). \end{aligned}$$

All these rules are derived in Ref. [34] or can be calculated straightforwardly.

A further combination that arises frequently is $A(\tau,\tau') = \int_c d\tau_1 B(\tau,\tau_1)C(\tau_1,\tau')$ and can be written as

$$\begin{aligned} A^{<}(t,t') &= \int dt_1 \left(B^{r}(t,t_1)C^{<}(t_1,t') + B^{<}(t,t_1)C^{a}(t_1,t')\right), \\ A^{r}(t,t') &= \int dt_1 B^{r}(t,t_1)C^{r}(t_1,t'). \end{aligned}$$

In future calculations we always refer to this section and the rules written down here.

As already mentioned in the introduction 1.1 a Kondo coupling is accompanied by a failure of perturbation theory. For low temperatures a many-body effect with the leads produces a term in higher order perturbation theory that diverges logarithmically. Special treatment is therefore necessary to understand the physics at low temperatures. Renormalization methods for non-equilibrium situations are discussed in chapters 5 and 6. Nevertheless, at finite temperatures or in the case of another finite energy scale in the system, the perturbation theory is valid. In any case it provides a first qualitative insight into the physics of the double quantum dot system at hand.

3.2 Notations and Definitions

In this section we introduce the basic notation used in this chapter and for the rest of the thesis. After introducing the Hamiltonian and the model system, we summarize the ansatz for the Green's functions and write down their 0th order expressions. We comment on some conservation rules and how they can be used to simplify parts of the calculations in appendix B.1.

3.2.1 Hamiltonian of the Double Quantum Dot System

As already explained in the introduction the system of two Kondo impurities exhibits interesting physics. After the experimental breakthrough in producing quantum dots the study of two coupled quantum dots has found renewed interest, as well in the connection of quantum phase transitions as in the context of quantum computing. Here we study a double quantum dot which is in neither of these regimes, but focus on strongly coupled dots and the influence of decoherence on the system for large applied voltages.

In the following the setup of two coupled quantum dots is used as motivated in section 2.2.

$$\begin{aligned} H =& H_0 + H_{\text{int}}, \\ H_0 =& \sum_{n,k,\sigma} \epsilon_k c^\dagger_{nk\sigma} c_{nk\sigma} + \sum_{\gamma} \epsilon_\gamma t^\dagger_\gamma t_\gamma + \lambda Q, \qquad (3.1) \\ H_{\text{int}} =& \sum_{m,n=1,2} J_{mn} \vec{S}_L \, \vec{s}_{mn} + \sum_{m,n=3,4} J_{mn} \vec{S}_R \, \vec{s}_{mn}, \qquad (3.2) \\ Q =& s^\dagger s \; + t^\dagger_0 t_0 + t^\dagger_+ t_+ + t^\dagger_- t_-. \qquad (3.3) \end{aligned}$$

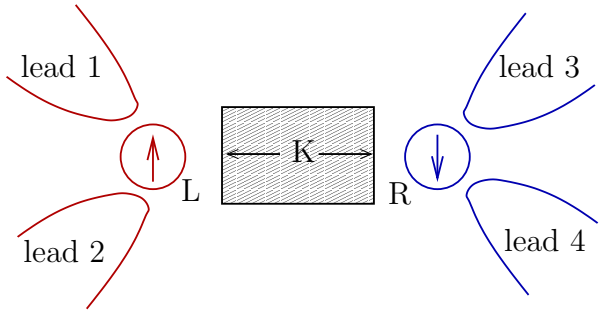

Figure 3.3: Double quantum dot system: Two Kondo impurities denoted L, R each connected to two leads $1, 2$ and $3, 4$, respectively, and coupled to each other by a not further defined spin exchange interaction K.

The operator $c_{nk\sigma}$ creates a conduction electron in the lead n with spin σ and momentum k. To describe the coupled double quantum dots singlet and triplet states are used. The bosonic operator $t_\gamma(t^\dagger_\gamma)$ destroys (creates) a singlet or triplet state. The states are ordered by $t_\gamma \in \{s, t_+, t_0, t_-\}$. The corresponding eigenenergies including a finite magnetic field $-B\,(S^z_L + S^z_R)$ are

$$\epsilon_s = -\frac{3}{4}K, \qquad \epsilon_{t_+} = \frac{1}{4}K - B, \qquad \epsilon_{t_0} = \frac{1}{4}K, \qquad \epsilon_{t_-} = \frac{1}{4}K + B.$$

To enforce that only one state is occupied at a time ($Q = 1$), we use the Abrikosov pseudo fermion representation [42] as introduced in section 2.1.2.

The perturbative part of the Hamiltonian H_{int} contains the spin-spin interaction between the impurity spin and the spin of the conduction electrons defined by

$$\vec{s}_{mn} = \frac{1}{2} \sum_{k,k',\sigma,\sigma'} c^{\dagger}_{mk'\sigma'} \vec{\tau}_{\sigma'\sigma} c_{nk\sigma}. \tag{3.4}$$

For $m \neq n$ the operators $\vec{s}_{mn}$ are tunneling operators and the corresponding interaction J_{mn} is responsible for the electronic transport. If a finite voltage is applied to two of the leads, e.g. 1 and 2, then a current can flow over the quantum dot due to processes given in the interaction Hamiltonian H_{int}, Eq. (3.2), to orders of the coupling J_{mn}. The spin of the left or right quantum dot is defined by

$$\vec{S}_{\alpha} = \frac{1}{2} t^{\dagger}_{\gamma'} \left(\vec{T}_{\alpha} \right)_{\gamma'\gamma} t_{\gamma},$$

where $\alpha = L, R$ and the pseudo Pauli matrices as defined in Eqs. (2.6) and (2.7) in section 2.1.

Please note, that the quantum dot spin $\vec{S}_{\alpha}$ interacts due to the definition in Eq. (3.4) with the sum over momentum states in the leads.[4] It is therefore convenient to use the momentum integrated conduction electron Green's function.

Please note, that the leads $1, 2$ and $3, 4$ are decoupled from each other. There is no current flowing over the double quantum dot system, but only through each of the quantum dots. The only connection between the two dots is the spin-spin interaction K. As has been shown the leakage over the two quantum dots is negligibly small in the case of two close-by quantum dots even if a hopping between the dots is allowed. Please see section 2.2 in the previous chapter for more details.

3.2.2 Green's Functions

We define the Green's function for the conduction electrons by

$$G_{nk\sigma}(\tau, \tau') = -i \langle T_c c_{nk\sigma}(\tau) c^{\dagger}_{nk\sigma}(\tau') \rangle.$$

In the following calculations it is assumed, that the leads are in equilibrium and the influence of a magnetic field on the conduction electrons is neglected.[5] We explicitly take into account a chemical potential $\mu = \mu_0 \pm eV/2$ which corresponds to the thermodynamic chemical potential $\mu_0 \approx \epsilon_F$ and an additional shift due to the applied voltage. We will occasionally refer to V as an energy such that a factor of e is implied but not explicitly written.

Since the pseudo-particles interact with electrons of all momentum k, usually the momentum integrated expression for the conduction electron Green's function is used. The band structure is assumed to be constant $N(\epsilon) = N(0)\Theta(D - |\epsilon|)$ as illustrated in Fig. 3.4. The band cutoff D is assumed to be the largest energy scale of the system. The spectral function is given by

$$A(\epsilon) = 2\pi N(0) \Theta(D - |\epsilon|).$$

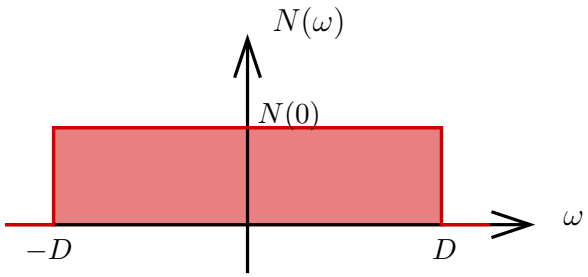

Figure 3.4: Illustration of the constant density of states $N(\omega) = N(0)\Theta(D - |\omega|)$.

Normalization of $A(\omega)$ fixes $N(0)$ to the value $N(0) = 1/2D$. The real part of the retarded or advanced Green's function is given by

$$\mathrm{Re}\sum G^{r/a}_{nk}(\omega) = \sum_k P\frac{1}{\omega - \epsilon_k} = \int d\epsilon N(0)\Theta(D - |\epsilon|)P\frac{1}{\omega - \epsilon} = N(0)\ln\frac{D-\omega}{D+\omega}.$$

Since typical frequencies of the system are much smaller than the band cutoff, $\omega \ll D$, the real part $\mathrm{Re}[G^{r/a}]$ is neglected in the following.

The ansatz used throughout the thesis for the conduction electron Green's functions are

$$\sum_k G^{<}_{nk}(\omega) = if(\omega - \mu_n)2\pi N(0)\Theta\left(D - |\omega|\right), \tag{3.5a}$$

$$\sum_k G^{>}_{nk}(\omega) = -i(1 - f(\omega - \mu_n))2\pi N(0)\Theta\left(D - |\omega|\right), \tag{3.5b}$$

$$\mathrm{Im}\sum_k G^{r}_{nk}(\omega) = -i\pi N(0)\Theta\left(D - |\omega|\right), \tag{3.5c}$$

$$\mathrm{Im}\sum_k G^{a}_{nk}(\omega) = i\pi N(0)\Theta\left(D - |\omega|\right), \tag{3.5d}$$

where μ_n is the chemical potential of lead n.

The double quantum dot is driven into a non-equilibrium state by the applied voltage. It is the purpose of this work to calculate the effect of an arbitrary voltage applied to the transport region. The contour-ordered Green's functions for the double quantum dot system are defined by

$$G_{\gamma\gamma'}(\tau, \tau') = -i\langle T_c t_\gamma(\tau) t^\dagger_{\gamma'}(\tau')\rangle.$$

Please note, that the singlet and triplet states s, t_+, t_0, t_- are chosen bosonic. We explicitly write down γ and γ' since the calculation shows, that between the singlet s and the triplet t_0, both with magnetic moment 0, the average in higher order perturbation theory does not vanish $\langle s^\dagger t_0\rangle \neq 0$. For a small level splitting between the singlet and the triplet there exists an ambiguity to the product states as discussed in section 2.1. In a self-consistent calculation those effects have to be taken into account very carefully.

[4] In the following a prefactor $1/N^2$ is neglected.

[5] In realistic setups the g-factor in the leads is negligible small, see discussion in Ref. [52].

Rewriting the Green's functions $G_{\gamma\gamma'}(\omega)$ for all possible γ, γ' in form of the matrix $\mathcal{G}$,

$$\mathcal{G}(\omega) = \begin{pmatrix} G_{ss}(\omega) & 0 & G_{st_0(\omega)} & 0 \\ 0 & G_{t_+t_+}(\omega) & 0 & 0 \\ G_{t_0s}(\omega) & 0 & G_{t_0t_0}(\omega) & 0 \\ 0 & 0 & 0 & G_{t_-t_-}(\omega) \end{pmatrix}, \tag{3.6}$$

allows us later to express e.g. the self energy in a short and descriptive way.

Since the pseudo particles for the singlet and triplet states are bosonic the 0th order ansatz is given by

$$\left(G_\gamma^{(0)}\right)^< (\omega) = -in_\gamma A_\gamma(\omega), \tag{3.7a}$$

$$\left(G_\gamma^{(0)}\right)^> (\omega) = -i(1+n_\gamma) A_\gamma(\omega), \tag{3.7b}$$

$$\left(G_\gamma^{(0)}\right)^{r/a} (\omega) = \frac{1}{\omega - \epsilon_\gamma \pm i\delta}, \tag{3.7c}$$

$$A_\gamma^{(0)}(\omega) = 2\pi\delta(\omega - \epsilon_g). \tag{3.7d}$$

It is assumed in the following that the lesser Green's function $G^<(\omega)$ can be written as the product of the spectral function $A(\omega)$ and an in general frequency-dependent occupation function $n(\omega)$. Since the spectral function is strongly peaked, it is further assumed that the occupation is just a number with the value $n_\gamma = n_\gamma(\omega_\gamma)$.

In this section we introduced the Hamiltonian for the double quantum dot system which is discussed in the remaining part of the thesis. We defined the Green's functions for the conduction electrons and the pseudo particles in the uncoupled case. If the interaction with the leads is switched on, the Green's functions for the double quantum dot system change as is discussed in the following. Some additional information on the matrix Green's function from sum rule considerations are given in appendix B.1.

3.3 Self Energy Calculation of the Pseudo Particles

Now corrections to the isolated double quantum dot system are calculated as we turn on the coupling J to the leads and consequently drive a current through the system if the leads are at different chemical potentials. The perturbation theory in the Kondo coupling J is valid as long as J is small such that the order $\mathcal{O}(N+1)$ contributions can be neglected in comparison with the $\mathcal{O}(N)$ contribution. It is known from Kondo physics that perturbation theory fails at low temperatures, but it provides a first insight into the double quantum dot setup and is correct at higher temperatures.

The Dyson equation,

$$\mathcal{G}(\tau, \tau') = \mathcal{G}^{(0)}(\tau, \tau') + \int_c d\tau_1 \int_c d\tau_2 \mathcal{G}^{(0)}(\tau, \tau_1)\Sigma(\tau_1, \tau_2)\mathcal{G}(\tau_2, \tau'),$$

determines the influence of the self energy Σ on the Green's function $\mathcal{G}$. The Green's function $\mathcal{G}^{(0)}$ is the unperturbed Green's function of the isolated double quantum dot system. The contour-ordered Green's function were defined in Eqs. (3.7). Please note, that the Dyson equation as written down here is a matrix equation for the matrix Green's

function and the matrix self energy,

$$\Sigma = \begin{pmatrix} \Sigma_{ss} & 0 & \Sigma_{st_0} & 0 \\ 0 & \Sigma_{t_+t_+} & 0 & 0 \\ \Sigma_{t_0s} & 0 & \Sigma_{t_0t_0} & 0 \\ 0 & 0 & 0 & \Sigma_{t_-t_-} \end{pmatrix}. \tag{3.8}$$

In the next section it is shown, tht the self energy is not diagonal but block diagonal with respect to the s-t_0 and t_+-t_- sectors.

The first correction $\Sigma^{(1)}$ to the unperturbed result originates from the first order expansion in the interaction Hamiltonian,

$$\int d\tau_1 \langle T_c t_\gamma(\tau) H_{\text{int}}(\tau_1) t^\dagger_{\gamma'}(\tau')\rangle.$$

Since the conduction electron contribution can be separated from the pseudo boson part, this expectation value only is non-zero if $\langle \mathbf{s}_{mn}(\tau_1)\rangle \neq 0$. The expectation value

$$\langle \mathbf{s}_{mn}(\tau_1)\rangle = \langle c^\dagger_{mk'\sigma'}(\tau_1)\tau_{\sigma'\sigma}c_{nk\sigma}(\tau_1)\rangle = \tau^z_{\sigma\sigma}\delta_{m,n}n_{nk\sigma},$$

is proportional to $n_{nk\uparrow} - n_{nk\downarrow}$. If the occupation number of the conduction electrons is not spin dependent, then $\text{Tr}[\tau^z_{\sigma\sigma}] = 0$. The influence of the magnetic field on the leads is neglected in this calculation here. Consequently, the first order in the perturbation expansion does not contribute to the self energy. The first finite contribution is thus of 2nd order.

3.3.1 Calculation of 2nd Order Self Energy

In order to calculate the second order self energy $\Sigma^{(2)}_{\gamma\gamma'}$, we have to calculate the expectation value

$$\begin{aligned} &\langle T_c t_\gamma(\tau) H_{\text{int}}(\tau_1) H_{\text{int}}(\tau_2) t^\dagger_{\gamma'}(\tau')\rangle \\ &= \sum \frac{1}{4}\vec{\tau}^i_{\sigma'\sigma}\vec{\tau}^j_{s's} J^i_{mn}J^j_{MN}\langle t_\gamma(\tau)\vec{S}^i(\tau_1)\vec{S}^j(\tau_2)t^\dagger_{\gamma'}(\tau')\rangle \\ &\langle c^\dagger_{mk'\sigma'}(\tau_1)c_{nk\sigma}(\tau_1)c^\dagger_{Mp's'}(\tau_2)c_{Nps}(\tau_2)\rangle, \end{aligned}$$

where the sum is over all variables, that appear at least twice (Einstein summation convention) and the whole expression is integrated over the contour-times $\int_c d\tau_1$ and $\int_c d\tau_2$. Since the leads $1, 2$ and $3, 4$ are decoupled, no contribution from $\langle S_L S_R\rangle$ is found. For the perturbation calculation the indices i and j in the Kondo couplings J^i_{mn} and J^j_{MN} are of no importance. They are dragged along only since they become important in the context of perturbative RG, see chapter 5.

One should not forget that when calculating the self energy factor of $\frac{1}{2}(-i)^3$ from the perturbative expansion has to be included. The contraction of the conduction electrons is straightforward and leads to

$$\frac{1}{2}(-i)^3\frac{1}{4}\tau^i_{\sigma'\sigma}\tau^j_{\sigma\sigma'}J^i_{mn}J^j_{nm}\frac{-1}{(-i)^2}\,G_{nk\sigma}(\tau_1,\tau_2)G_{mk'\sigma'}(\tau_2,\tau_1)\langle t_\gamma(\tau)\vec{S}^i(\tau_1)\vec{S}^j(\tau_2)t^\dagger_{\gamma'}(\tau')\rangle.$$

We introduce a useful abbreviation for the conduction electron loop, which is similar to the spin susceptibility

$$X_m^n(\tau_1,\tau_2) = \frac{1}{(-i)^2}\sum_{k,k'} G_{nk'}(\tau_1,\tau_2)G_{mk}(\tau_2,\tau_1). \tag{3.9}$$

This quantity is calculated and discussed in detail in appendix B.2.

Since Wick's theorem applies we find by inserting the pseudo particle representation into the expression for the self energy

$$\begin{aligned}-\frac{1}{2}\frac{1}{16}\sum \tau^i_{\sigma'\sigma}\tau^j_{\sigma\sigma'}J^i_{mn}J^j_{nm}X^n_m(\tau_1,\tau_2)\\ \times\Big(G_{\gamma\gamma_1'}(\tau,\tau_1)\vec{T}^i_{\gamma_1'\gamma_1}G_{\gamma_1,\gamma_2'}(\tau_1,\tau_2)\vec{T}^j_{\gamma_2'\gamma_2}G_{\gamma_2,\gamma'}(\tau_2,\tau')\\ +G_{\gamma\gamma_2'}(\tau,\tau_2)\vec{T}^j_{\gamma_2'\gamma_2}G_{\gamma_2,\gamma_1'}(\tau_2,\tau_1)\vec{T}^i_{\gamma_1'\gamma_1}G_{\gamma_1,\gamma'}(\tau_1,\tau')\Big).\end{aligned}$$

Since the summation is over all internal variables, the second contribution is identical to the first one as can be seen using the variable shift $\tau_1 \leftrightarrow \tau_2$, $i \leftrightarrow j$, $m \leftrightarrow n$, and $\sigma' \leftrightarrow \sigma$.

The self energy $\Sigma^{(2)}$ can now be extracted from

$$\begin{aligned}&\frac{(-i)^3}{2!}\int_c d\tau_1\int_c d\tau_2\langle t_\gamma(\tau)H_{\rm int}(\tau_1)H_{\rm int}(\tau_2)t^\dagger_{\gamma'}(\tau')\rangle\\ &=\int_c d\tau_1\int_c d\tau_2 G_{\gamma,\gamma_1'}(\tau,\tau_1)\Sigma_{\gamma_1',\gamma_2}(\tau_1,\tau_2)G_{\gamma_2,\gamma'}(\tau_2,\tau'),\end{aligned}$$

where

$$\begin{aligned}\Sigma_{\gamma_1',\gamma_2}(\tau_1,\tau_2) = -\frac{1}{2}\frac{1}{16}\sum 2J^i_{mn}J^j_{nm}\tau^i_{\sigma'\sigma}\tau^j_{\sigma\sigma'}X^n_m(\tau_1,\tau_2)\\ \vec{T}^i_{\gamma_1'\gamma_1}G_{\gamma_1,\gamma_2'}(\tau_1,\tau_2)\vec{T}^j_{\gamma_2'\gamma_2}.\end{aligned} \tag{3.10}$$

To second order perturbation theory in the Kondo couplings J, diagrams like the one shown in Fig. 3.5 enter the self energy.

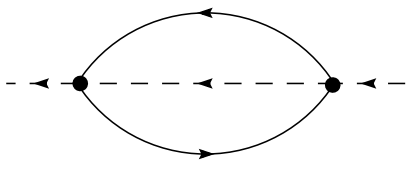

Figure 3.5: Typical diagram which enters the self energy in second order perturbation theory. Solid lines: conduction electron Green's functions; dashed lines: pseudo particles of the double quantum dot system.

In the summation over all lead indices it has to be distinguished between the left and

the right side:

$$\begin{aligned} Y_L(\tau_1,\tau_2) &= \sum_{m,n=1,2} 2J_{mn}J_{nm}G_{nk\sigma}(\tau_1,\tau_2)G_{mk'\sigma'}(\tau_2,\tau_1) \\ &= \sum_{m,n=1,2} 2J_{mn}J_{nm}\; X_n^m(\tau_1,\tau_2), \qquad (3.11) \\ Y_R(\tau_1,\tau_2) &= \sum_{m,n=3,4} 2J_{mn}J_{nm}G_{nk\sigma}(\tau_1,\tau_2)G_{mk'\sigma'}(\tau_2,\tau_1) \\ &= \sum_{m,n=3,4} 2J_{mn}J_{nm}\; X_n^m(\tau_1,\tau_2). \qquad (3.12) \end{aligned}$$

The following relations for $\alpha = L, R$ are useful in the calculation,

$$X_m^n(\tau_2,\tau_1) = \frac{1}{(-i)^2}\sum_{k,k'} G_{nk'}(\tau_2,\tau_1)G_{mk}(\tau_1,\tau_2) = X_n^m(\tau_1,\tau_2)$$

and $\qquad Y_\alpha(\tau_2,\tau_1) = Y_\alpha(\tau_1,\tau_2).$

With this abbreviations and making use of the matrix representation for the self energy Σ and the Green's function $\mathcal{G}$, the general result for the second order self energy gives

$$\Sigma(\tau_1,\tau_2) = -\frac{1}{2}\frac{1}{16}\tau^i_{\sigma'\sigma}\tau^j_{\sigma\sigma'}\sum_{\alpha=L,R} Y_\alpha(\tau_1,\tau_2)\vec{T}^i_\alpha\mathcal{G}(\tau_1,\tau_2)\vec{T}^j_\alpha. \qquad (3.13)$$

After performing the spin summation and using $\mathrm{Tr}[\tau^i\tau^j] = 2\delta_{i,j}$ the self energy simplifies to

$$\Sigma(\tau_1,\tau_2) = -\frac{1}{16}\sum_\alpha Y_\alpha(\tau_1,\tau_2)\vec{T}_\alpha\mathcal{G}(\tau_1,\tau_2)\vec{T}_\alpha,$$

where $\vec{T}\mathcal{G}\vec{T}$ is short for $T^+\;\mathcal{G}\;T^- + T^-\;\mathcal{G}\;T^+ + T^z\;\mathcal{G}\;T^z$.

3.3.2 Results for the 2nd Order Self Energy

The result in Eq. (3.13) is as general as possible. It is valid for any Kondo system coupled to leads if one replaces the pseudo Pauli matrices $\vec{T}$ by the corresponding spin representation for the interacting system, e.g. for a spin-1/2 system by the usual Pauli matrices $\vec{T} = \vec{\tau}$. For the double quantum dot system of interest, we use the spin matrices

as defined in section 2.1. The following self energies are found

$$\begin{aligned}\Sigma_{ss}(\tau_1,\tau_2) = -\frac{1}{16}\big[&\big(G_{t_0t_0}(\tau_1,\tau_2)+G_{t_+t_+}(\tau_1,\tau_2)+G_{t_-t_-}(\tau_1,\tau_2)\big)\\ &(Y_L(\tau_1,\tau_2)+Y_R(\tau_1,\tau_2))\big], \qquad (3.14)\\ \Sigma_{t_0t_0}(\tau_1,\tau_2) = -\frac{1}{16}\big[&\big(G_{ss}(\tau_1,\tau_2)+G_{t_+t_+}(\tau_1,\tau_2)+G_{t_-t_-}(\tau_1,\tau_2)\big)\\ &(Y_L(\tau_1,\tau_2)+Y_R(\tau_1,\tau_2))\big], \qquad (3.15)\\ \Sigma_{t_+t_+}(\tau_1,\tau_2) = -\frac{1}{16}\big[&\big(G_{ss}(\tau_1,\tau_2)+G_{t_0t_0}(\tau_1,\tau_2)+G_{t_+t_+}(\tau_1,\tau_2)\big)\\ &(Y_L(\tau_1,\tau_2)+Y_R(\tau_1,\tau_2))\\ &-(G_{st_0}(\tau_1,\tau_2)+G_{t_0s}(\tau_1,\tau_2))\,(Y_L(\tau_1,\tau_2)-Y_R(\tau_1,\tau_2))\big], \qquad (3.16)\\ \Sigma_{t_-t_-}(\tau_1,\tau_2) = -\frac{1}{16}\big[&\big(G_{ss}(\tau_1,\tau_2)+G_{t_0t_0}(\tau_1,\tau_2)+G_{t_-t_-}(\tau_1,\tau_2)\big)\\ &(Y_L(\tau_1,\tau_2)+Y_R(\tau_1,\tau_2))\\ &+(G_{st_0}(\tau_1,\tau_2)+G_{t_0s}(\tau_1,\tau_2))\,(Y_L(\tau_1,\tau_2)-Y_R(\tau_1,\tau_2))\big], \qquad (3.17)\end{aligned}$$

and

$$\begin{aligned}\Sigma_{st_0}(\tau_1,\tau_2) = -\frac{1}{16}\big[&\big(G_{t_-t_-}(\tau_1,\tau_2)-G_{t_+t_+}(\tau_1,\tau_2)\big)\,(Y_L(\tau_1,\tau_2)-Y_R(\tau_1,\tau_2))\\ &+G_{t_0s}(\tau_1,\tau_2)\,(Y_L(\tau_1,\tau_2)+Y_R(\tau_1,\tau_2))\big], \qquad (3.18)\\ \Sigma_{t_0s}(\tau_1,\tau_2) = -\frac{1}{16}\big[&\big(G_{t_-t_-}(\tau_1,\tau_2)-G_{t_+t_+}(\tau_1,\tau_2)\big)\,(Y_L(\tau_1,\tau_2)-Y_R(\tau_1,\tau_2))\\ &+G_{st_0}(\tau_1,\tau_2)\,(Y_L(\tau_1,\tau_2)+Y_R(\tau_1,\tau_2))\big]. \qquad (3.19)\end{aligned}$$

There exists an off-diagonal self energy contribution in second order. As a consequence there also exists an off-diagonal Green's function $G^{(2)}_{st_0} = G^{(0)}_{ss}\Sigma^{(2)}_{st_0}G^{(0)}_{t_0t_0}$. Before the importance and consequences of the off-diagonal self energy is discussed, a few remarks are given about the actual calculation and it is commented on some usual assumptions,

In the following we only need the lesser self energy $\Sigma^<$ and the spectral weight Γ. The broadening Γ_γ gives a finite life time of the pseudo particle t_γ and is also proportional to the rate of tunneling out of the singlet or triplet state. The lesser self energy $\Sigma^<_\gamma$ is important in the context of the quantum Boltzmann equation discussed in section 3.5 and can be interpreted as the sum of all rates that end in the state t_γ.

Time-translational invariance is assumed and that all quantities have reached a stationary state such that they depend only on the time difference $t - t'$.

After Fourier transformation all quantities depend only on one frequency ω and we find

$$\begin{aligned}(X^n_m)^<(\omega) =& -2\pi N(0)^2 n_B(\omega+\mu_n-\mu_m)[\omega+\mu_n-\mu_m], \qquad (3.20)\\ Y^<_L(\omega) =&(-2\pi)\left[\left(g^2_{11}+g^2_{22}\right)2\omega n_B(\omega)\right.\\ &\left.+2g_{12}g_{21}\left((\omega+eV_L)n_B(\omega+eV_L)+(\omega-eV_L)n_B(\omega-eV_L)\right)\right], \qquad (3.21)\\ Y^<_R(\omega) =&(-2\pi)\left[\left(g^2_{33}+g^2_{44}\right)2\omega n_B(\omega)\right.\\ &\left.+2g_{34}g_{43}\left((\omega+eV_R)n_B(\omega+eV_R)+(\omega-eV_R)n_B(\omega-eV_R)\right)\right], \qquad (3.22)\end{aligned}$$

where $g_{mn} = N(0)J_{mn}$ is the dimensionless Kondo coupling and $n_B(x) = 1/(\exp[x/T] - 1)$ is the Bose distribution function. For a derivation of these quantities please see appendix B.2. The relation $X_m^n(\tau_1, \tau_2) = X_n^m(\tau_2, \tau_1)$ for the time arguments translates to

$$(X_m^n)^<(\omega) = (X_n^m)^>(-\omega), \tag{3.23}$$
$$Y_\alpha^>(\omega) = Y_\alpha^<(-\omega). \tag{3.24}$$

The function $Y_\alpha^<(\omega)$ for $\alpha = L, R$ is related to $Y_\alpha^<(-\omega)$ by

$$Y_\alpha^<(-\omega) = Y_\alpha^<(\omega) + (-2\pi)2g_\alpha^2 w, \tag{3.25}$$

where the following abbreviations are introduced also for later

$$4g_L^2 = g_{11}^2 + g_{22}^2 + 2g_{12}g_{21}, \tag{3.26}$$
$$4g_R^2 = g_{33}^2 + g_{44}^2 + 2g_{34}g_{43}, \tag{3.27}$$
$$g_{\text{all}}^2 = 4g_L^2 + 4g_R^2. \tag{3.28}$$

With these definitions and relations we can now write down the Fourier transform of the lesser self energy $\Sigma^<$ and the broadening Γ. We find with the Langreth rules from section 3.1

$$\Sigma^<(\omega) \propto \int \frac{d\epsilon}{2\pi} \vec{T}\mathcal{G}^<(\omega - \epsilon)\vec{T}Y^<(\epsilon) = \int \frac{d\epsilon}{2\pi} \vec{T}\mathcal{G}^<(\epsilon)\vec{T}Y^<(\omega - \epsilon), \tag{3.29}$$

$$\begin{aligned} -i\Gamma(\omega) &= \Sigma^>(\omega) - \Sigma^<(\omega) = \Sigma^r(\omega) - \Sigma^a(\omega) \\ &\propto \int \frac{d\epsilon}{2\pi} \left[\vec{T}\mathcal{G}^>(\epsilon)\vec{T}Y^>(\omega - \epsilon) - \vec{T}\mathcal{G}^<(\epsilon)\vec{T}Y^<(\omega - \epsilon)\right] \\ &= \int \frac{d\epsilon}{2\pi} \left[\vec{T}\left(\mathcal{G}^<(\epsilon) - iA(\epsilon)\right)\vec{T}Y^<(-\omega + \epsilon) - \vec{T}\mathcal{G}^<(\epsilon)\vec{T}Y^<(\omega - \epsilon)\right] \\ &\approx -i \int \frac{d\epsilon}{2\pi} \vec{T}A(\epsilon)\vec{T}Y^<(\epsilon - \omega) + \mathcal{O}(\mathrm{e}^{-\beta\lambda}). \end{aligned} \tag{3.30}$$

Due to the constraint, Eq. (3.3), the terms in Γ which are proportional to the lesser Green's function $G^<$ are neglected. To extract physical quantities we have to project observables onto the physical Hilbert space. Since $G^<$ is already proportional to $e^{-\beta\lambda}$, the combination with any physical quantity e.g. with n in the quantum Boltzmann equation is projected out, see section 2.1 or [42]. To simplify the calculation this term is neglected already during the calculation.

3.3.3 Discussion of the Off-Diagonal Self Energy Σ_{st_0}

The self energy, Eq. (3.13), of a double quantum dot state is determined by the excitation of an intermediate state by means of a particle-hole pair in the leads (see also Fig. 3.5). The intermediate state decays to the initial state when the electron-hole pair recombines. If the broadening is larger than the splitting between different levels, it can happen that the recombination of the electron-hole pair leaves the system in a different state. This is general for every system with two nearly degenerate energy levels and one or more additional levels which are allowed as intermediate states. Or more generally: if there

are more spin and orbital degrees of freedom in the impurity structure than there are in the electron leads, the off-diagonal contributions can be finite.

For example for the double quantum dot system we find a non-zero self energy Σ_{st_0} from Eq. (3.18),

$$\Sigma_{st_0}(\tau_1,\tau_2) = -\frac{1}{16}\left[G_{t_0 s}(\tau_1,\tau_2)\left(Y_L(\tau_1,\tau_2)+Y_R(\tau_1,\tau_2)\right)\right.$$
$$\left.+\left(G_{t_-t_-}(\tau_1,\tau_2)-G_{t_+t_+}(\tau_1,\tau_2)\right)\left(Y_L(\tau_1,\tau_2)-Y_R(\tau_1,\tau_2)\right)\right].$$

The off-diagonal contribution is created by the term $(G_{t_-t_-}-G_{t_+t_+})(Y_L-Y_R)$ because $G_{t_0 s}$ does not exist in lowest order. Consequently the self energy is non-zero if the symmetry of the setup is broken due to a finite magnetic field $t_+ \neq t_-$ (spin symmetry broken) and due to a left-right asymmetry $Y_L \neq Y_R$. The left-right symmetry is broken if the coupling to the left lead J_L is not identical to the coupling to the right lead J_R, see therefore the definition of Y_L and Y_R in Eqs. (3.21) and (3.22).

This can be understood from a simple argument: Starting from a singlet state the

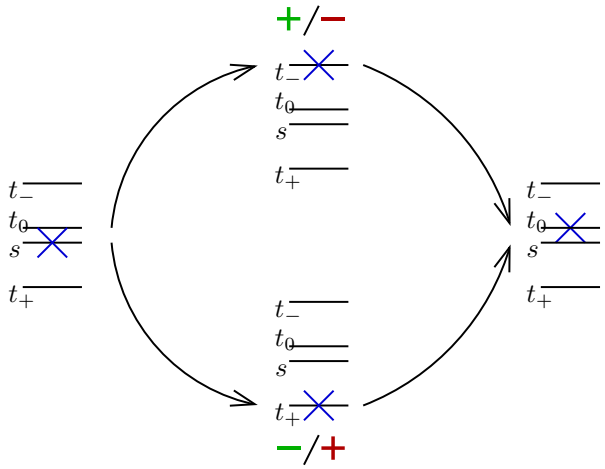

Figure 3.6: Illustration of the symmetries in the off-diagonal self energy. There are two different paths with different signs which can lead from the singlet to the triplet t_0. Green/left sign for interaction with left leads. Red/right sign for interaction with right leads.

interaction part of the Hamiltonian allows the transition to an intermediate/excited state by changing the spin of either the left or the right quantum dot. Changing the left spin of a singlet state

$$S_L^-|s\rangle = +\frac{1}{\sqrt{2}}|t_-\rangle, \qquad S_L^+|s\rangle = -\frac{1}{\sqrt{2}}|t_+\rangle,$$

creates an intermediate state with $S^z_{\text{tot}} \neq 0$ and the two triplet states t_+ and t_- arise with a different sign, as illustrated in Fig. 3.6. If the excited triplets decay back into the singlet the same sign appears and cancels out finally. By contrast, if they decay into the $S^z_{\text{tot}} = 0$ triplet the sign remains the same. This is the reason why the off-diagonal self energy Σ_{st_0} vanishes for zero magnetic field. In that case the two paths are identical but with opposite phase and destructive interference leads to a cancellation.

The observed symmetry with respect to left and right leads can be understood along the same line of argument. If the spin state of the right quantum dot is changed starting

from a singlet state, we find

$$S_R^-|s\rangle = -\frac{1}{\sqrt{2}}|t_-\rangle, \qquad S_R^+|s\rangle = +\frac{1}{\sqrt{2}}|t_+\rangle.$$

Thus if the coupling to the left and the right leads is identical and the creation of an electron-hole pair in the leads costs the same amount of energy, then these two path interfere with each other destructively.

Please note that these two symmetrical points are special to the double quantum dot setup discussed here. Off-diagonal contributions can always appear as soon as there are two levels close in energy and one or more intermediate states available. The double quantum dot setup studied here is known to show a quantum phase transition at small values of the singlet-triplet gap K as discussed in chapter 1. Additionally it is known for example from conformal field theory (see e.g. Ref. [16]) that the operator $\vec{S}_L - \vec{S}_R$ destroys this property. It is also obvious that for a finite magnetic field the system can no longer form a Kondo singlet. These two broken symmetries are thus well-known in the community working with double quantum dots.

In this section we derived and discussed the second order self energy of a double quantum dot system coupled to leads by the small parameter J. We showed that in a setup where there are more spin and orbital degrees of freedom in the quantum dot than degrees of freedom in the leads, off-diagonal entries in the self energy are found to higher orders in perturbation theory. Now the influence of this self energy is studied, first on the retarded Green's function in section 3.4 and then on the lesser Green's function for a finite voltage in section 3.5.

3.4 Retarded Green's Function

The retarded Green's function has to fulfill the Dyson equation

$$\mathcal{G}^r = \mathcal{G}_0^r + \mathcal{G}_0^r \Sigma^r \mathcal{G}^r \qquad \text{or} \qquad \mathcal{G}^r = \left[(\mathcal{G}_0^r)^{-1} - \Sigma^r \right]^{-1}, \tag{3.31}$$

with the self energy Σ^r given in the previous section. The real part of the self energy $\mathrm{Re}[\Sigma^r]$ shifts the energy of the level and the imaginary part $i\mathrm{Im}[\Sigma^r]$ is a measure for the finite life time of the pseudo particle states due to an interaction with the leads. The imaginary part of the retarded self energy is often also referred to as the broadening of the level $\Gamma = 2\mathrm{Im}[\Sigma^r]$. The advanced Green's function G^a is the conjugate of the retarded Green's function $G^r = [G^a]^\dagger$. It contains the same physics and therefore the discussion here is limited to the retarded Green's function.

We find for the retarded Green's function matrix,

$$\left[(\mathcal{G}_0^r)^{-1} - \Sigma^r \right]^{-1} = \begin{pmatrix} \left(\omega - \omega_{t_0} - \Sigma^r_{t_0 t_0}\right)/\det & 0 & \Sigma^r_{s t_0}/\det & 0 \\ 0 & G^r_{t_+ t_+}(\omega) & 0 & 0 \\ \Sigma^r_{t_0 s}/\det & 0 & \left(\omega - \omega_s - \Sigma^r_{ss}\right)/\det & 0 \\ 0 & 0 & 0 & G^r_{t_- t_-}(\omega) \end{pmatrix}, \tag{3.32}$$

where

$$\begin{aligned} \det &= \left(\omega - \omega_{t_0} - \Sigma^r_{t_0 t_0}\right)\left(\omega - \omega_s - \Sigma^r_{ss}\right) - \Sigma^r_{st_0}\Sigma^r_{t_0 s}, \\ G^r_{t_\pm t_\pm}(\omega) &= \left(\omega - \omega_{t_\pm} - \Sigma^r_{t_\pm t_\pm}\right)^{-1}. \end{aligned} \tag{3.33}$$

There are now two different cases, which are discussed in the following: the off-diagonal self energy $\Sigma^r_{st_0} = 0$ or $\Sigma^r_{st_0} \neq 0$.

3.4.1 Special Case: $\Sigma^r_{st_0} = 0$

In the case of zero magnetic field $B = 0$ or symmetric coupling $J_L = J_R$, the self energy $\Sigma^r_{st_0} = 0$ is zero as discussed in section 3.3.3. It follows immediately, that the off-diagonal retarded Green's function $G^r_{st_0} = 0$ vanishes and is not created to all orders of perturbation theory, i.e. no off-diagonals complications appear in the calculation. The diagonal retarded Green's functions can be expressed for $\gamma = \{s, t_+, t_0, t_-\}$ as

$$G^r_{\gamma\gamma}(\omega) = \frac{1}{\omega - \omega_\gamma + i\Gamma_{\gamma\gamma}/2}.$$

The shift of the real part of the retarded self energy $\mathrm{Re}[\Sigma^r]$ is usually neglected. Since it is quadratic in the small property J^2 it is only a small correction to the actual level energy ω_γ which is of the order of $\mathcal{O}(J^0)$. Though the shift can be important in some special cases (see Ref. [53]), it is not important in the parameter space discussed in this thesis.

Additionally in most of the calculations here the influence of a retarded self energy on the broadening of the level is neglected. It is assumed that all other physical properties change on a larger energy scale than the broadening Γ. Effectively the broadening is treated infinitesimally small such that the spectral function is a δ-function,

$$G^r_{\gamma\gamma}(\omega) = P\frac{1}{\omega - \omega_\gamma} + i\pi\delta(\omega - \omega_\gamma).$$

Due to this "on-shell" assumption most of the calculations simplify, for example integral equation turn into linear equations. The real part of the retarded Green's function is usually neglected.

In the perturbative RG in chapter 5 we include the broadening again, since the physics of a finite lifetime destroys the Kondo effect. For the 2nd order perturbation theory in this chapter, the broadening is of the order g^2_{all}. All other physical quantities change on a much larger energy scale and thus the effect of a finite retarded self energy on the diagonal Green's functions is often neglected. In section 4.2 there is a small remark on how a finite broadening Γ influences the outcome of a current calculation.

3.4.2 Finite Off-Diagonal Self Energy $\Sigma^r_{st_0} \neq 0$

If both the left-right symmetry $J_L \neq J_R$ and the spin symmetry $B \neq 0$ are broken, we find a non-zero off-diagonal self energy $\Sigma^r_{st_0}$. Since the Dyson equation for the retarded

Green's function can be solved exactly, Eq. (3.31), this is not a principle problem. From Eq. (3.32) the solution for the retarded Green's function is given by

$$G^r_{st_0}(\omega) = \frac{\Sigma^r_{st_0}(\omega)}{\left(\omega - \omega_{t_0} - \Sigma^r_{t_0t_0}(\omega)\right)\left(\omega - \omega_s - \Sigma^r_{ss}(\omega)\right) - \Sigma^r_{st_0}(\omega)\Sigma^r_{t_0s}(\omega)}. \tag{3.34}$$

In comparison with the diagonal Green's function this is not a Lorentzian, but a more complex frequency dependent function. It can be written as the difference between two Lorentzians as illustrated in appendix C. Note that the spectral weight on resonance at ω_s or ω_{t_0} is finite. For example at $\omega = \omega_s$ we find for the off-diagonal retarded Green's function

$$G^r_{st_0}(\omega_s) = \frac{\Sigma^r_{st_0}(\omega_s)}{\Sigma^r_{ss}(\omega_s)\left(K + \Sigma^r_{t_0t_0}(\omega_s)\right) - \Sigma^r_{st_0}(\omega_s)\Sigma^r_{t_0s}(\omega_s)}.$$

This value is suppressed by a large K such that the off-diagonal components only become important at vanishingly small singlet-triplet gap K. A detailed calculation of the retarded Green's function in the case of $K = 0$ and for finite K can be found in appendix C.1.1 and C.1.2, respectively. For the calculations in the main part of the thesis, two remarks are in place. First, there exists an off-diagonal retarded Green's function $G^r_{st_0}$ if there are more spin or orbital degrees on freedom in the transport region, e.g. in a double quantum dot setup, than in the leads. Second, the off-diagonal retarded Green's function is of the order $\Sigma^r_{st_0}/K$. It can be neglected in the case of a large singlet-triplet splitting and vanishes in the case of left-right symmetry $J_L = J_R$ or magnetic field $B = 0$.

3.5 Lesser Green's Function and the Quantum Boltzmann Equation

In an equilibrium situation the lesser Green's function would be connected to the spectral function via a fluctuation-dissipation theorem as discussed in section 3.1. The thermodynamic result is shown in section 3.5.1. In a non-equilibrium case, for example with a finite applied voltage, the lesser Green's function has to be determined independently. The dynamics of the system is no longer described by $e^{\beta H}$. Most of this section is devoted to this non-equilibrium effect. In section 3.5.2 we derive the determining equation for $\mathcal{G}^<$ and emphasize why it is a self-consistent equation. Although the self energy corrections are of 2nd order in the coupling J, they give rise to a 0th order correction to $\mathcal{G}^<$. The results are discussed in chapter 4.

3.5.1 In Equilibrium

In equilibrium the system is not coupled to the leads and there is no transport through the dots. The occupation of the singlet and triplet states is determined assuming that the double quantum dot system is coupled to a thermal bath. We find in the canonical

representation

$$n_s = \frac{\mathrm{e}^{K/T}}{1+\mathrm{e}^{B/T}+\mathrm{e}^{-B/T}+\mathrm{e}^{K/T}},$$
$$n_{t_\gamma} = \frac{\mathrm{e}^{-\gamma B/T}}{1+\mathrm{e}^{B/T}+\mathrm{e}^{-B/T}+\mathrm{e}^{K/T}}.$$

Although the singlet and triplet states are bosonic particles, their occupation is not given by the Bose distribution function. The occupation numbers contain the information that in the antiferromagnetic case $K > 0$ the singlet is the ground state. If $K < 0$ and $B > 0$, the triplet t_+ is the ground state, and in the special case of $B = 0$ the three triplets form a degenerate ground state.

The occupation numbers n_s and n_{t_γ} are not observables which can be measured in experiment, but correlation functions like the polarization $\langle \vec{S}_L \vec{S}_R \rangle$ or the magnetization $M = \langle \vec{S}_L^z + \vec{S}_R^z \rangle$ are measurable observables.

3.5.2 Derivation of the Quantum Boltzmann Equation

If a finite voltage V is applied to the setup, the dynamics is no longer described by the temperature T, see Refs. [52, 54]. A determining equation for the occupation number n is derived from the Dyson equation for the lesser Green's function $G^<$. This equation is called the quantum Boltzmann equation most of the time but sometimes also referred to as the quantum kinetic equation. To 2nd order this equation is identical to the rate or master equation where the transition rates are determined from Fermi's golden rule.

The Dyson equation for the lesser Green's function $G^<$,

$$G_0^{-1}\, G^< = \Sigma^r G^< + \Sigma^< G^a, \tag{3.35}$$

can be rewritten as

$$\left[G_0^{-1} - \Sigma^r\right]\, G^< = \Sigma^<\, G^a$$
$$\Rightarrow \quad (G^r)^{-1}\, G^< = \Sigma^<\, G^a.$$

Further on a symmetrized version is used. Starting from

$$G^<\left[G_0^{-1} - \Sigma^a\right] = G^r\, \Sigma^<$$
$$\Rightarrow \quad G^<\, (G^a)^{-1} = G^r\, \Sigma^<,$$

the difference of the two latter equations is taken, which gives

$$(G^r)^{-1}\, G^< - G^<\, (G^a)^{-1} = \Sigma^<\, G^a - G^r\, \Sigma^<. \tag{3.36}$$

By taking this difference the transient behavior is disregarded and only information on the stationary state is obtained, which is the limit here considered (see also Ref. [34]).

If off-diagonal contributions are neglected in Eq. (3.36) we have to solve the following equations

$$\left[(G^r)^{-1} - (G^a)^{-1}\right]_{\gamma\gamma}(\omega)\, G^<_{\gamma\gamma}(\omega) = \Sigma^<_{\gamma\gamma}(\omega)\, \left[G^a - G^r\right]_{\gamma\gamma}(\omega) \tag{3.37}$$
$$\Rightarrow \quad G^<_{\gamma\gamma}(\omega) = \frac{\Sigma^<_{\gamma\gamma}(\omega)}{\Gamma_{\gamma\gamma}(\omega)}\, A_{\gamma\gamma}(\omega).$$

Using the ansatz $G^<_{\gamma\gamma} = -in_\gamma(\omega)A_{\gamma\gamma}(\omega)$ the expression (3.37) corresponds to a self-consistent equation for the occupation number $n_\gamma(\omega) = i\Sigma^<_{\gamma\gamma}(\omega)/\Gamma_{\gamma\gamma}(\omega)$ [52]. In general n_γ is a frequency dependent function, but it is assumed that it deviates from the value on resonance on a larger energy scale than the energy scale on which the spectral function A_γ changes. Usually the spectral function is approximated by a δ-distribution. Consequently the occupation number is described by the constant value $n_\gamma = n_\gamma(\omega_\gamma)$ at the resonance $\omega = \omega_\gamma$. Since Eq. (3.37) is an equation for the distribution function of the pseudo particle states, it is plausible why it is called the quantum Boltzmann equation.

Eq. (3.36) is a self-consistent equation for the occupation numbers, or probability distributions, of the singlet and triplet states. The dependence on the occupation number enters through the lesser self energy $\Sigma^<_{\gamma\gamma}$ which is an integral over the lesser Green's functions $G^<_{\gamma'\gamma'}$, see Eq. (3.29). Although the rates $\Gamma_{\gamma\gamma}$ are calculated to 2nd order perturbation theory the effect on the occupation number from the self-consistent equation is a 0th order effect.

The off-diagonal lesser Green's function is defined by

$$G^<_{st_0}(t,t') = -i\left\langle t_0^\dagger(t')s(t)\right\rangle.$$

The function $G^<_{st_0}$ is zero for the unperturbed system in contrast to the diagonal Green's functions for example $G^{(0)}_{ss} = -in_s\ 2\pi\delta(\omega-\omega_s)$, but $G^<_{st_0}$ is created to second order in the perturbation theory. Still it cannot be neglected like the retarded off-diagonal Green's function. The calculation of the non-equilibrium distribution functions with the quantum Boltzmann equation has to be self-consistent in second order. Thus the off-diagonal terms contribute to the same amount as the rates of diagonal terms do, and both are 0th order in the coupling J to the leads.

Including the off-diagonal elements the quantum Boltzmann equation becomes a complex structure. We write down the equation (3.36) for $G^<_{st_0}$ explicitly with the frequency dependence

$$\begin{aligned}&(G^r)^{-1}_{ss}(\omega)\,G^<_{st_0}(\omega) - G^<_{ss}(\omega)\,(G^a)^{-1}_{st_0}(\omega) + (G^r)^{-1}_{st_0}(\omega)\,G^<_{t_0t_0}(\omega) - G^<_{st_0}(\omega)\,(G^a)^{-1}_{t_0t_0}(\omega)\\ =&\Sigma^<_{ss}(\omega)\,G^a_{st_0}(\omega) - G^r_{ss}(\omega)\,\Sigma^<_{st_0}(\omega) + \Sigma^<_{st_0}(\omega)\,G^a_{t_0t_0}(\omega) - G^r_{st_0}(\omega)\,\Sigma^<_{t_0t_0}(\omega).\end{aligned}$$

The equation mixes $G^<_{st_0}(\omega)$ with the singlet $G^<_{ss}(\omega)$ and triplet $G^<_{t_0t_0}(\omega)$ components. Additionally the spectral weight is distributed at different frequencies. In the discussion of the retarded Green's function we found that the off-diagonal Green's function has a complicated frequency dependence. The self energy in the quantum Boltzmann equation is given by a convolution of the Green's functions with a contribution from the leads.

In principle the quantum Boltzmann equation for the off-diagonal Green's function can be solved if one finds a correct ansatz for $G^<_{st_0}$ and if one manages to solve the integral equation. Here we suggest a different approach. As explained in detail in appendix C we perform a transformation of the singlet-triplet basis and solve the quantum Boltzmann equation in a new basis. Since the calculation contains a lot of details, it is included in the appendix. Here only the main ideas of the calculation in chapter C are presented.

3.5.3 Idea behind the Degenerate Perturbation Theory

The problem of the self-consistent quantum Boltzmann equation in the limit of small exchange interaction K is the frequency-dependence. In case the off-diagonals can be

neglected, the ansatz that the spectral function is strongly peaked can be used, i.e. the occupation number is calculated on resonance only. We want to be able to make the same ansatz in the case when there are non-zero off-diagonal Green's functions.

In a first step we therefore transform the retarded Green's function matrix $\mathcal{G}^r$ by $U^{-1}\mathcal{G}^r U$ to a diagonal retarded Green's function matrix $\tilde{\mathcal{G}}^r$. The transformation gives two new retarded Green's functions at the two frequencies ω_1 and ω_2. These Green's functions G_1^r and G_2^r are orthonormal since they are eigenvectors of the retarded Green's function matrix. The quantum Boltzmann equation can be thus treated independently at the two frequencies ω_1 and ω_2. The retarded Green's functions G^r_{ss}, $G^r_{t_0t_0}$, and $G^r_{st_0}$ consist of sums or differences of G_1^r and G_2^r. The explicit calculation can be found in appendix C.1.2. It is found that in the case of $K = 0$ the new eigenstates of the system after the rotation correspond to the product basis as introduced in section 2.1. This is obvious from a simple physical argument: if there is no spin-spin interaction K, the product states describe the system exactly. The singlet s and the triplet t_0 are not pure states in this case. On the other hand if $K \neq 0$ the singlet and triplet states rather than the product states are pure states, since they provide an eigenbasis to $K\vec{S}_L\vec{S}_R$. The idea behind the rotation is to get rid of the corresponding entanglement and find the correct eigenbasis for the Hamiltonian depending on the strength of K. Please note, that the rotation is only important if K becomes of the order of the broadening Γ.

The advanced Green's function is rotated differently. From the sum rule consideration $[G^a_{st_0}]^\dagger = G^r_{t_0 s}$ the rotation is in principle given by U^*. This is discussed in more detail in section C.1.4.

In non-equilibrium it is necessary to solve the quantum Boltzmann equation. Therefore we rotate the retarded and the advanced Green's function in Eq. (3.36) correspondingly. This produces a transformed lesser Green's function $\tilde{G}^<$ and also a rotated self energy $\tilde{\Sigma}^<$. Details of this calculation are found in appendix C.2.2. In the transformed self energy the rotation can be included into the pseudo Pauli matrices $\vec{T}$. With the diagonal retarded Green's function in the eigenspace the quantum Boltzmann equation can be written again as a linear equation and the self-consistent set of equations for the occupation numbers can be solved in the rotated basis. The initial lesser Green's functions $G^<_{ss}$, $G^<_{t_0t_0}$ and $G^<_{st_0}$ are found by a back-transformation. In the case of $K = 0$ as discussed in section C.2.1 the occupation of the singlet and triplet states are given as the sum or difference of the occupation numbers of the product states. The more general case of finite K is discussed in appendix C.2.2. To simplify the calculation we utilize the results from section B.1. How to create an ansatz for the transformed lesser Green's function is described in the appendix in section C.2.2.

Finally the reader should be reminded that the transformation is necessary only in the limit when K is of the order of the broadening Γ. If the spin-spin interaction is stronger and the singlet-triplet gap has opened sufficiently, then the off-diagonal self energy can be neglected in the quantum Boltzmann equation.

For the parameter regimes discussed in the remaining part of this thesis the off-diagonal elements are neglected and the interested reader is referred to the chapter C in the appendix.

3.6 Summary and Outlook

In part I of the topic perturbation theory we discussed the basic concepts of perturbation theory out of equilibrium. Physical observables and results of the quantum Boltzmann equation are discussed in part II in chapter 4.

In section 3.1 the most important concepts of perturbation theory in non-equilibrium were mentioned. If a finite voltage is applied to the double quantum dot system, the lesser and the retarded Green's function do not obey a fluctuation-dissipation theorem as in equilibrium. They have to be determined independently by solving two different Dyson equations. Section 3.4 is devoted to the retarded Green's function. Its Dyson equation can be solved exactly, but since the retarded self energy is a 2nd order correction to the unperturbed result, the effect of a finite retarded self energy is usually neglected. In chapter 5 this is reconsidered and we discuss the effect of a finite imaginary part of the retarded self energy, because it leads to a finite life time of the pseudo particle states and therefore to decoherence effects.

The lesser Green's function obeys a self-consistent equation as derived in section 3.5. The rates to 2nd order in perturbation theory contribute to 0th order in the perturbative expansion. It is assumed that the lesser Green's function $G^<(\omega) = -inA(\omega)$ can be written by a product of the spectral function, as determined from the imaginary part of the retarded Green's function, and an occupation number, which obeys the self-consistent quantum Boltzmann equation. The solution for the occupation numbers and a discussion of the results follows in section 4.1.

4 Perturbation Theory – Part II: Results

After having introduced the calculational method in chapter 3, we continue with discussions of the results in chapter 4. The voltage-dependent occupation numbers and related thermodynamic properties are studied in section 4.1. As a physical observable which is easily accessible in experiment the current through one of the quantum dots is discussed in section 4.2. By tuning the parameters of the double quantum dot system we show interesting effects that appear only out of equilibrium, for example the so-called transconductance. Since it is a quantity that is comparable to the impurity density of states of an Anderson model, the T-matrix of the conduction electrons is discussed in section 4.3. Performing the same calculation within the framework of perturbative RG in chapter 5 opens the possibility to compare the results with NRG calculations. So far it was assumed that the spin-spin interaction between the two quantum dot spins is antiferromagnetic, because this case shows interesting physics due to competing ground states as discussed in chapter 1. Results for the ferromagnetic case are shown in section 4.4 and the difference to the antiferromagnetic setup is discussed.

Motivated by the observation that there is a communication between the left and the right quantum dot in non-equilibrium, we study current-current correlations: In section 4.5 the noise is introduced and results of the current-current correlation in one lead are shown. In section 4.6 we prove that the cross-correlation between the current in the left and the current in the right lead is non-zero.

4.1 Polarization and Magnetization

The occupation numbers for the singlet and triplet states are not physical observables, but they determine the voltage dependence of thermodynamic quantities like the polarization p and the magnetization M. We discuss results for $B = 0$ in section 4.1.1 and for finite magnetic field in section 4.1.2.

In this chapter the contributions from the off-diagonal self energy $\Sigma_{st_0} = \Sigma_{t_0 s}$ are neglected. This approximation is exact for symmetrically coupled quantum dots even if the magnetic field is non-zero. It fails in the case of asymmetric coupling $J_L \neq J_R$ and finite magnetic field $B \neq 0$. This failure is shown at the end of this section and as discussed in the previous chapter a resolution to this problem is presented in appendix C.

As discussed in section 3.5.2 we have to solve the set of equations (3.37),

$$\Gamma_{\gamma\gamma}(\omega_\gamma) n_\gamma = i\Sigma^<_{\gamma\gamma}(\omega_\gamma),$$

for $\gamma \in \{s, t_+, t_0, t_-\}$. To derive this equation the ansatz $G^<_\gamma = -i n_\gamma A_\gamma(\omega)$ was used and it was assumed that the frequency dependence is dominated by a strongly peaked spectral function $A_\gamma(\omega)$. The self-consistency of the equation is hidden in $\Sigma^<_{\gamma\gamma}$ which

explicitly depends on the occupation numbers n_γ. The system of the four equations for $\gamma \in \{s, t_+, t_0, t_-\}$ is underdetermined. In order to find a non-trivial solution for the occupation numbers we need additionally the constraint

$$n_s + n_{t_+} + n_{t_0} + n_{t_-} = 1.$$

Taking this constraint into account we find voltage-dependent solutions for the states of the double quantum dot system n_s, n_{t_+}, n_{t_0} and n_{t_-}. The calculation and the solutions are given in detail in appendix B.3.

We restrict ourselves to the case of degenerate triplet states in the next section. This case is studied in great detail, since the calculations in the framework of the perturbative RG in section 5, and of the flow equation method in chapter 6 do not include a finite magnetic field either.

4.1.1 Polarization in the Case of Vanishing Magnetic Field $B = 0$

In the case of $B = 0$ all triplet states are degenerate and $n_{t_+} = n_{t_0} = n_{t_-} \equiv n_t$. The following system of equation has to be solved,

$$\begin{aligned} Y^<_{L+R}(-K) n_s &= Y^>_{L+R}(K) n_t, \\ n_s + 3n_t &= 1, \end{aligned}$$

and the solution can be written down immediately. We find for the occupation numbers,

$$n_{s/t} = \frac{Y^<_{L+R}(\mp K)}{Y^<_{L+R}(-K) + 3Y^<_{L+R}(K)},$$

where $Y^<_{L+R}(\omega) = Y^<_L(\omega) + Y^<_R(\omega)$. The derivation of Y_α is shown in appendix B.2. The function $Y^<_\alpha(\omega)$ for $\alpha = L, R$ depends on the voltage V_α and on the coupling to the left or right leads, as given in Eqs. (3.21) or (3.22) respectively.

Since the pseudo particles do not correspond to a physical observable, rather the polarization p is discussed, which is a measure for the spin-spin correlation,

$$\langle \vec{S}_L \vec{S}_R \rangle = -\frac{3}{4}(n_s - n_t) = -\frac{3}{4} p.$$

The polarization $p = n_s - n_t$ is given by

$$p = n_s - n_t = \frac{Y^<_{L+R}(-K) - Y^<_{L+R}(K)}{Y^<_{L+R}(-K) + 3Y^<_{L+R}(K)} = 1 - 4\,\frac{Y^<_{L+R}(K)}{Y^<_{L+R}(-K) + 3Y^<_{L+R}(K)}. \tag{4.1}$$

For voltage $V_L = 0$ we find

$$p = n_s - n_t = \frac{1 - e^{-K/T}}{1 + 3e^{-K/T}} = 1 - 4\,\frac{1}{e^{K/T} + 3}.$$

In Fig. 4.1 we illustrate the difference between the voltage dependence of the polarization p (Fig. 4.1(a)) and the temperature dependence (Fig. 4.1(b)).

In an equilibrium setup with $V_L = V_R = 0$ the exponential factor $e^{-K/T}$ is asymptotically 1 in the limit of $T > K$. The polarization decreases in this limit as

$$p \propto \frac{1}{4}\left(1 - \ e^{-K/T}\right)$$

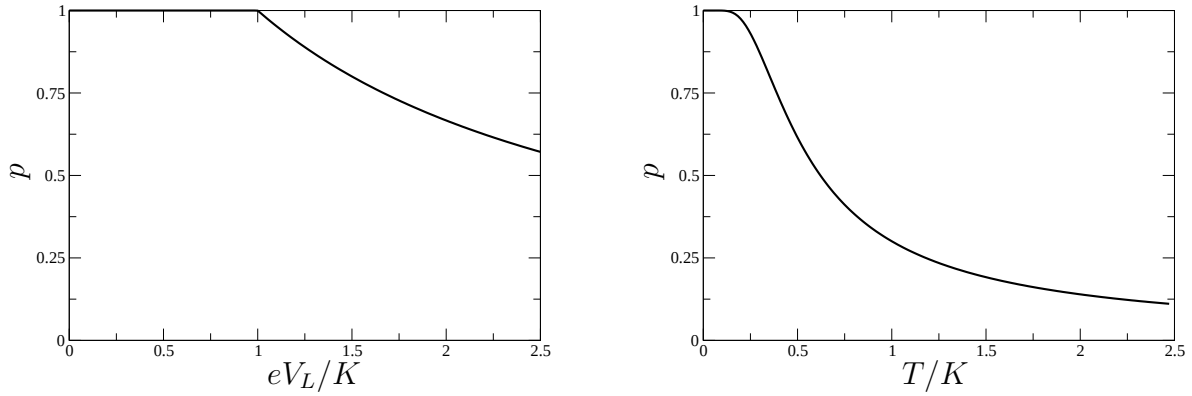

(a) Dependence of p on the voltage.

(b) Dependence of p on the temperature.

Figure 4.1: Dependence of the polarization p on the voltage eV_L/K (left panel) for $T/K = 0.001$ and on the temperature (right panel) for $eV_L/K = 0$. Both plots use $V_R = 0$, $B = 0$ and small coupling $g_L = g_R = 0.1$.

to the value 0 if the singlet and triplet states are equilibrated and both have an occupation probability of 1/4. For even larger temperatures, $T \gg K$, the behavior goes over to a $1/T$ Curie-like decay, which is obvious from a further expansion of the exponential $p \propto (1 - 1 + K/T + \ldots)/4 \approx K/4T$.

By contrast in the finite voltage case the quantity $Y^<_{L+R} = Y^<_L + Y^<_R$ for $V_R = 0$ is given by

$$\begin{aligned} Y^<_{L+R}(\pm K) = &\left(g_{11}^2 + g_{22}^2 + 4g_R^2\right) 2(\pm K) n_B(\pm K) \\ &+ 2g_{12}g_{21}\left[(\pm K + eV_L) n_B(\pm K + eV_L) + (\pm K - eV_L) n_B(\pm K - eV_L)\right]. \end{aligned}$$

Assuming that the temperature is the smallest energy scale in the system and using the approximation $n_B(x) = e^{-\beta x} \approx 0$ for $x > 0$ and $n_B(x) \approx -1$ for $x < 0$, we find for $V_L \gg K > 0$

$$\begin{aligned} Y^<_{L+R}(K) &\approx 2g_{12}g_{21}(eV_L - K), \\ Y^<_{L+R}(-K) &\approx 2\left(g_{11}^2 + g_{22}^2 + 4g_R^2\right) K + 2g_{12}g_{21}(eV_L + K) \\ &= 2\left(4g_L^2 + 4g_R^2\right) K + 2g_{12}g_{21}(eV_L - K). \end{aligned}$$

Inserting into the expression for the polarization we find in the large voltage limit

$$p \propto \frac{(4g_L^2 + 4g_R^2)\, K}{(4g_L^2 + 4g_R^2)\, K + 2 \cdot 2g_{12}g_{21}(eV_L - K)}.$$

The dependence of p on the voltage is thus algebraic. This is in contrast to the dependence on the temperature T which is exponential. For very large voltages $V_L \gg K$ the polarization falls off like

$$p \approx \frac{g_{\text{all}}^2}{4g_{12}g_{21}eV_L} K.$$

This behavior is similar to a Curie law, but with an effective temperature of $(g_{12}g_{21}/g_{\text{all}}^2)eV_L$. It is important to notice that the effect of a finite voltage on the

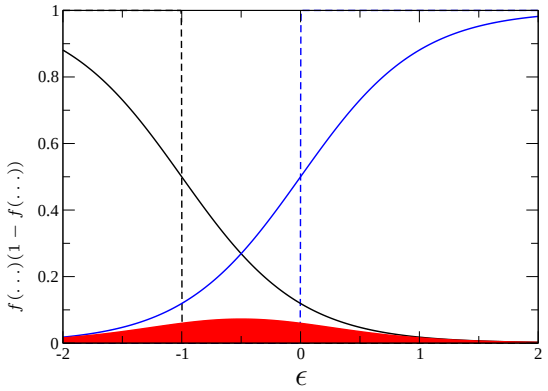

(a) Kernel for $V = 0$ and the two different temperatures $T/K = 0.001$ and $T/K = 0.5$.

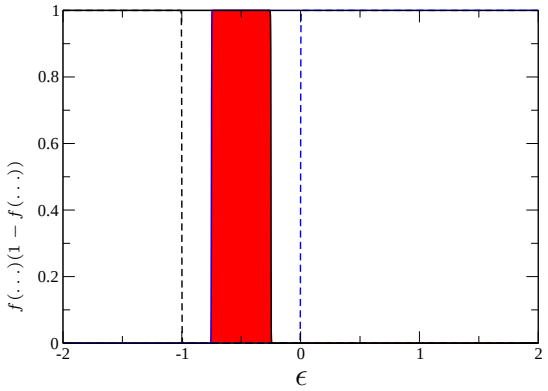

(b) Kernel for $T/K = 0.001$ and the two different voltages $V = 0$ and $eV/K = 1.5$.

Figure 4.2: Kernel $f(\epsilon + K - eV/2)(1 - f(\epsilon + eV/2))$ at $K = 1$ for two different temperatures T/K in the left panel and for different voltages eV/K in the right panel.

polarization is of 0th order in the perturbative expansion to orders of the coupling g to the leads.

To illustrate where the difference from the equilibrium to the non-equilibrium result originates from, we have to refer to an analytical detail in the calculation. As already discussed in the derivation of the self energy (section 3.3) the 2nd order contribution originates from an electron-hole pair which is created and recombined in the leads during two interaction processes. The function $Y^{<}_{\mathrm{L+R}}(\omega)$ contains this contribution from the leads. As can be seen from the derivation in appendix B.2 $Y^{<}_{\alpha}(\omega)$ is proportional to the convolution

$$\int_{-D}^{D} d\epsilon f(\epsilon + \omega - \mu_m)\left(1 - f(\epsilon - \mu_n)\right),$$

where the chemical potential is $\mu_{m,n} = \pm eV_\alpha/2$ in the leads m, n and $\alpha = L, R$. The kernel of this integral is sketched in Fig. 4.2. The integral is non-zero if the distribution of the electron $f(\epsilon + \omega - \mu_m)$ overlaps with the distribution of the hole $(1 - f(\epsilon - \mu_n))$. The frequency ω in $Y^{<}_{\alpha}(\omega)$ takes the values $\omega = \pm K$ in Eq. (4.1) for the polarization. For $\omega = -K$ the distribution f of the electron and $(1 - f)$ of the hole have a finite overlap. The observed dependencies therefore arise from the contribution of $\omega = K$. In this case the temperature T or the voltage V have to be large to provide a finite overlap (see in Fig. 4.2). The temperature enters the exponential and smoothens the step in the Fermi distribution function. The voltage shifts the onset of $(1 - f)$ and the offset of f, respectively. This explains the exponential and algebraic dependence of the polarization on the temperature and voltage, respectively.

In Fig. 4.3 it is shown that the polarization p does not only depend on the voltage V_L applied to the left quantum dot, but that also the voltage V_R affects the non-equilibrium distribution of the double quantum dot system. If the voltage V_R reaches the threshold $eV_R \approx K$, a finite current through the right quantum dot leads to an occupation of the excited triplet states via decoherent processes. Thus the value of the polarization $p(eV_L < K)$ deviates from the value 1. Since we chose a symmetric setup the value for

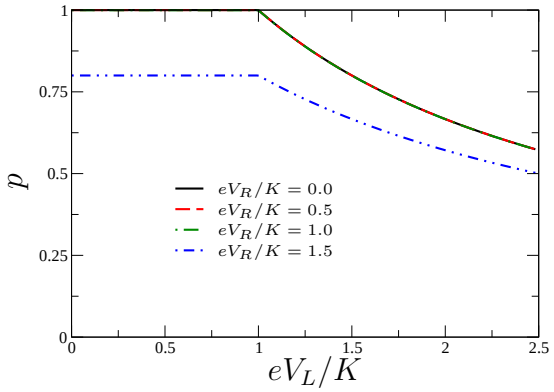

Figure 4.3: Dependence of the polarization $p = n_s - n_t$ on the voltage eV_L/K if the voltage V_R applied to the right quantum dot is varied. The plots for $eV_R/K = 0.0, 0.5, 1.0$ lie on top of each other. The other parameters are $g_L = g_R = 0.1$, $T/K = 0.001$, and $B = 0$.

$eV_R/K = 1.5$ and $V_L = 0$ is the same as for $eV_L/K = 1.5$ and $V_R = 0$ as can be seen in Fig. 4.3.

The voltage is sometimes interpreted as an effective temperature. As in thermodynamic considerations the finite occupation of excited states is possible if sufficient energy is provided to overcome the gap. While in thermodynamics this process is described by the Boltzmann factor $e^{\beta \hat{H}}$ here it is described by the quantum Boltzmann equation in non-equilibrium. The transition rates between the pseudo particle states play an important role in this context and the finite life times of the states is induced by a current driven through the system. The decoherence rates Γ are proportional to the coupling g^2 to the leads, the singlet-triplet gap K and the finite voltages V_L and V_R in left and right leads, respectively. Although the rates are of 2nd order in the coupling, the effect on the occupation number is of 0th order. The decrease of p seen in Fig. 4.3 is clearly not proportional to $g^2 \approx 0.01$, rather the polarization falls off like $1/V_L$.

This discussion is general for every microscopic system where a finite voltage is applied [52, 54]. Consequently we find the same behavior even if we apply a finite magnetic field to the quantum dot system.

4.1.2 Polarization and Magnetization for Finite Magnetic Field $B \neq 0$

In the case of finite magnetic field the solutions of the non-equilibrium distribution functions, n_s, n_{t_+}, n_{t_0} and n_{t_-}, are given in appendix B.3. In the symmetric case, when the coupling J_L to the left leads is identical to the coupling J_R to the right leads, we can perform the calculation without any assumptions.[1] We show in Fig. 4.4(a) how the occupation numbers of the singlet and triplet states depend on the voltage for a finite magnetic field $B/K = 0.5$. The singlet remains the ground state of the system but the triplet t_+ is already occupied for $eV_L = K - B$. Then sequentially the triplet t_0 at $eV_L = K$ and t_- at $eV_L = K + B$ become occupied when increasing V_L.

If there is a magnetic field $B \neq 0$, the magnetization is finite. The magnetization M

[1] If the left-right symmetry is conserved, the off-diagonal entries of the self energy $\Sigma_{st_0} = \Sigma_{t_0 s} = 0$ are exactly zero.

is defined by[2],

$$M = \langle \vec{S}_L^z + \vec{S}_R^z \rangle = n_{t_+} - n_{t_-}.$$

For a finite magnetic field the polarization p is redefined according to section 2.1 by

$$p = -\frac{4}{3}\langle \vec{S}_L \vec{S}_R \rangle = n_s - \frac{1}{3}\left(n_{t_+} + n_{t_0} + n_{t_-}\right).$$

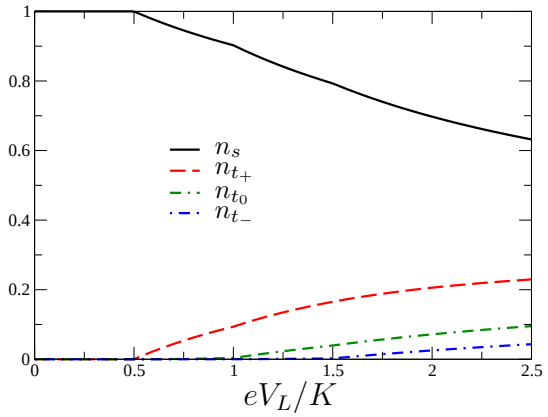

(a) Non-equilibrium occupation numbers vs. voltage.

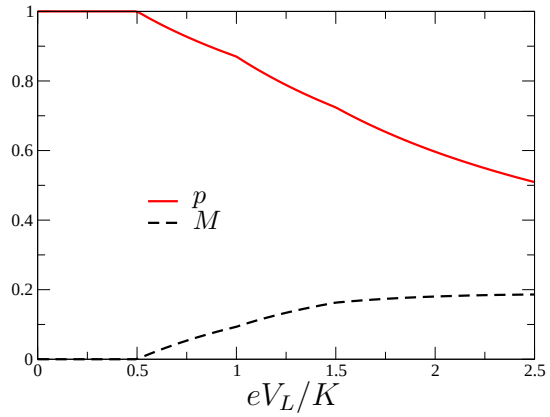

(b) Polarization and magnetization vs. voltage.

Figure 4.4: Non-equilibrium occupation numbers, the polarization p and the magnetization M dependent on the voltage for vanishing temperature $T/K = 0.001$, small coupling $g_L = g_R = 0.1$, finite magnetic field $B/K = 0.5$, and $V_R = 0$.

Then it has to be distinguished between three different cases: magnetic field B lesser, greater or identical to the spin-spin interaction K.

For two coupled quantum dots with a strong spin-spin interaction $K > B$, the singlet is the ground state and the polarization p has the value 1. If the magnetic field $B > K$ is stronger than the spin-spin interaction K then the triplet t_+ is the ground state and the polarization is $-1/3$ as can be seen in Fig. 4.5. The transition between these two cases happens at $K = B$ when the singlet s and triplet t_+ are degenerate and both are occupied with a probability 1/2. The polarization is then $+1/3$. The transitions between the three values of $p = 1, 1/3, -1/3$ happen on a scale set by the temperature. A finite voltage provides the energy to occupy excited states. In the large voltage limit the system tends to equilibrate in the sense that all states become populated with the same probability. As can be seen from Fig. 4.4(b) and Fig. 4.5 the polarization always increases or decreases like $1/V_L$ to 0.

Similar statements hold for the magnetization of the system. It reaches the first non-zero value at $B = K$ when the triplet t_+ becomes the ground state of the system. From the value of 0 in Fig. 4.4(b) it changes over the value of 0.5 to 1 in Fig. 4.5 in a energy window which is determined by the temperature. The voltage provides sufficient energy to occupy the excited triplet t_- and consequently the magnetization M tends to 0 like $1/V$.

[2]This definition is related to the total magnetization $M_{\text{tot}} = 2\langle S_L^z + S_R^z \rangle = 2M$. The factor of 2 is left out due to convenience.

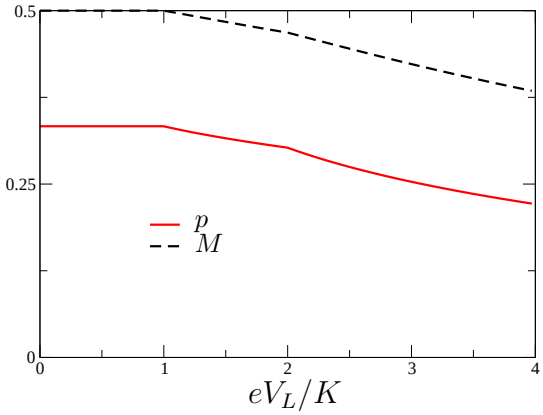

(a) Polarization and magnetization for $B/K = 1$.

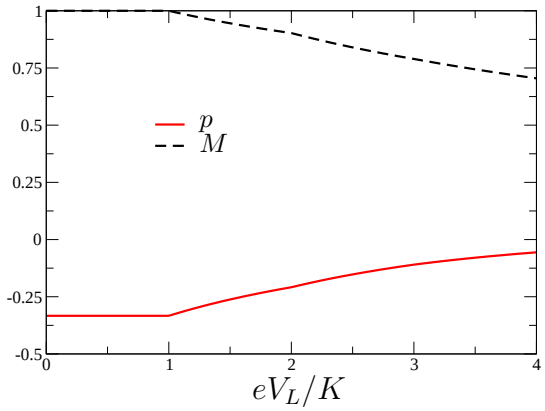

(b) Polarization and magnetization for $B/K = 2$.

Figure 4.5: Polarization and magnetization for magnetic field $B = K$ and degenerate ground state (left panel), and for magnetic field $B = 2K$ and a triplet ground state (right panel).

4.1.3 Magnetization in the Case of Spin-Spin Interaction $K = 0$

The approximation that the off-diagonal self energy contributions can be neglected, fails in the case of small spin-spin interaction $K < \Gamma$. This failure is illustrated here in the case of $K = 0$.

In the case of $K = 0$ we find that the occupation for the singlet s and triplet t_0 are identical, $n_s = n_{t_0}$. Thus the following system of coupled equations has to be solved,

$$\begin{aligned} 2Y^<_{L+R}(\pm B)n_{t_\pm} &= 2Y^<_{L+R}(\mp B)n_s, \\ 2n_s + n_{t_+} + n_{t_-} &= 1. \end{aligned}$$

The solution is

$$\begin{aligned} n_s &= \frac{Y^<_{L+R}(B)Y^<_{L+R}(-B)}{\left(Y^<_{L+R}(B) + Y^<_{L+R}(-B)\right)^2}, \\ n_{t_\pm} &= \left(\frac{Y^<_{L+R}(\pm B)}{Y^<_{L+R}(B) + Y^<_{L+R}(-B)}\right)^2. \end{aligned}$$

The magnetization of the left quantum dot is thus given by

$$\begin{aligned} M_L &= 2\langle S^z_L\rangle = n_{t_+} - n_{t_-} \\ &= \frac{\left(Y^<_{L+R}(B)\right)^2 - \left(Y^<_{L+R}(-B)\right)^2}{\left(Y^<_{L+R}(B) + Y^<_{L+R}(-B)\right)^2} = \frac{Y^<_{L+R}(B) - Y^<_{L+R}(-B)}{Y^<_{L+R}(B) + Y^<_{L+R}(-B)}. \end{aligned} \tag{4.2}$$

The magnetization M_L of the left quantum dot should be decoupled from the right side when $K = 0$. The solution of M_L in Eq. (4.2) depends on $Y^<_R(\pm B)$ and consequently on the voltage V_R and the coupling of the right quantum dot to the leads 3 and 4. Thus the calculation fails since the magnetization of a quantum dot depends on the properties of another quantum dot which is decoupled.

The result for the magnetization M_L for $K = 0$ in Eq. (4.2) is not wrong in the case of conserved spin symmetry or conserved left-right symmetry. In those cases the

off-diagonal self energy Σ_{st_0} is identical to 0 as discussed in section 3.3.3. In the case of $B = 0$ the magnetization is $M_L = 0$ as expected, since for $B = K = 0$ all pseudo states are occupied by the same probability of $\frac{1}{4}$. In the case of $Y_L = Y_R$, Y_{L+R} can be rewritten by $2Y_L$. Then the result Eq. (4.2) is identical to the result for a single quantum dot with a finite magnetic field see Ref. [52].

For a finite magnetic field and for asymmetric coupling of the quantum dots to the left and right leads care must be taken regarding the off-diagonal contributions. How to include the off-diagonal contributions in the quantum Boltzmann equation was already discussed in section 3.5.3 and is described in detail in appendix C.

In section 4.1 we showed that the pseudo particle occupation numbers depend on the voltage applied to the quantum dot system to 0th order in the perturbation expansion. The non-equilibrium situation also affects thermodynamic quantities like the polarization and magnetization of the double quantum dot system. Instead of a Curie $1/T$-law these observables decrease like $1/V$ for large voltages. Due to a finite current the states in the double quantum dot system are subject to decoherent processes.

4.2 Non-Equilibrium Current

The magnetization M and the polarization p are physical observables, but they are not easily accessible in experiments. By contrast the current can be measured directly. We discuss the differential conductance dI/dV in detail in this section. This quantity gives a measure of the level distribution in a mesoscopic device and is therefore studied extensively. In experiments of double quantum dot setups, e.g. Ref. [27, 29], the applied voltages are of the order or larger than internal energy scales of the mesoscopic system. To describe the experimental results it is therefore necessary to include non-equilibrium effects into the calculation.

We discuss the current and related derivatives for vanishing magnetic field $B = 0$ (section 4.2.2) and finite magnetic field $B \neq 0$ (section 4.2.3). The calculation of the current expression in section 4.2.1 follows along the lines of Refs. [55, 56, 57], see also Ref. [34].

4.2.1 Derivation of the Non-Equilibrium Current

The current through the left quantum dot is defined by the charge of an electron times the change in the charge carrier density of for example the first lead,

$$\begin{aligned} I_L &= -e \sum_\sigma \frac{d}{dt} n_{1\sigma} = -e \sum_\sigma \frac{1}{i\hbar} \left[\sum_k c^\dagger_{1k\sigma} c_{1k\sigma}, H \right] \\ &= i\frac{e}{\hbar} \left[J_{12} \vec{S}_L \vec{s}_{12} - J_{21} \vec{S}_L \vec{s}_{21} \right]. \end{aligned}$$

Defining the correlation function

$$D_{12}(\tau, \tau') = -i \left\langle T_c \vec{S}_L(\tau) \vec{s}_{12}(\tau') \right\rangle, \tag{4.3}$$

the current becomes proportional to the real part of $D_{12}^{>}$,

$$\begin{aligned} I_L &= -\frac{e}{\hbar}\left(J_{12}D_{12}^{>}(t,t) - J_{21}[D_{21}^{>}]^{\star}(t,t)\right) \\ &= -2\frac{e}{\hbar}J_{12}\int\frac{d\omega}{2\pi}\,\mathrm{Re}\left[D_{12}^{>}(\omega)\right], \qquad \text{if } J_{12}=J_{21}. \end{aligned} \tag{4.4}$$

In 0th order $D_{12}^{(0)}$ does not contribute since the expectation value of $\langle c^{\dagger}_{1k'\sigma'}\frac{1}{2}\vec{\tau}_{\sigma'\sigma}c_{2k\sigma}\rangle$ is zero. The lowest order contribution originates from

$$D_{12}^{(1)}(\tau,\tau') = (-i)^2\int d\tau_1\left\langle T_c\vec{S}_L(\tau)H_{\mathrm{int}}(\tau_1)\vec{s}_{12}(\tau')\right\rangle.$$

Wick's theorem applied to the conduction electron part implies, that there are only the following three terms,

$$\begin{aligned} D_{12}^{(1)}(\tau,\tau') = (-i)^2J_{21}\int d\tau_1\,\big[&\left\langle T_cS_L^{+}(\tau)S_L^{-}(\tau_1)s_{21}^{+}(\tau_1)s_{12}^{-}(\tau')\right\rangle \\ &+\left\langle T_cS_L^{-}(\tau)S_L^{+}(\tau_1)s_{21}^{-}(\tau_1)s_{12}^{+}(\tau')\right\rangle \\ &+\left\langle T_cS_L^{z}(\tau)S_L^{z}(\tau_1)s_{21}^{z}(\tau_1)s_{12}^{z}(\tau')\right\rangle\big]. \end{aligned}$$

The lowest order diagram for the current has the form given in Fig. (4.6). As is obvious

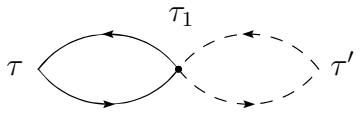

Figure 4.6: First order diagram for the correlation function D_{12} (Eq. (4.3)), which determines the current. Solid line: conduction electrons, dashed line: singlet-triplet states.

from the expression for $D_{12}^{(1)}$ and the diagram, it is effectively the conduction electron spin susceptibility $\langle T_c\vec{s}_{21}(\tau_1)\vec{s}_{12}(\tau')\rangle$ and the quantum dot spin susceptibility $\langle T_c\vec{S}_L(\tau)\vec{S}_L(\tau_1)\rangle$ which enter the formula for the current.

After applying Wick's theorem we find

$$\begin{aligned} D_{12}^{(1)}(\tau,\tau') =& \frac{1}{16}J_{21}\int d\tau_1\tau^{i}_{\sigma'\sigma}\tau^{j}_{\sigma\sigma'}T^{i}_{\gamma'\gamma}T^{j}_{\gamma_1'\gamma_1} \\ &\frac{1}{(-i)^2}\sum_{kk'}G_{2k\sigma}(\tau',\tau_1)G_{1k'\sigma'}(\tau_1,\tau') \\ &\frac{1}{(-i)^2}G_{\gamma_1\gamma'}(\tau_1,\tau)G_{\gamma\gamma_1'}(\tau,\tau_1). \end{aligned}$$

The spin susceptibility of the conduction electrons is defined as[3],

$$X_2^1(\tau_1,\tau') = \frac{1}{(-i)^2}\sum_{k,k'}G_{1k'}(\tau_1,\tau')G_{2k}(\tau',\tau_1),$$

[3]Please compare to the definition of X_m^n in Eq. (3.9) on page 43.

where the spin index is neglected since the conduction electrons are independent of the spin state. For a derivation and discussion of this conduction electron spin susceptibility we refer to the appendix B.2. Since the change of the particles number is calculated in the first lead, the indices m and n are restricted to 1 and 2. Furthermore we define the spin susceptibility for the double quantum dot system (DQD),

$$X_{\mathrm{DQD}}(\tau,\tau_1) = \sum \tau^i_{\sigma'\sigma}\tau^j_{\sigma\sigma'}T^j_{\gamma_1'\gamma_1}G_{\gamma_1\gamma'}(\tau_1,\tau)T^i_{\gamma'\gamma}G_{\gamma\gamma_1'}(\tau,\tau_1) = 2\mathrm{Tr}\left[\vec{T}\mathcal{G}\vec{T}\mathcal{G}\right], \tag{4.5}$$

where the sum is over all indices (Einstein summation convention). The sum over all indices is equivalent to the trace of the matrix product.

Using these notations we can rewrite the correlation function as

$$D^{(1)}_{12}(\tau,\tau') = -\frac{1}{16}J_{21}\int d\tau_1 X_{\mathrm{DQD}}(\tau,\tau_1)X^1_2(\tau_1,\tau').$$

To derive the current we need the greater component, which can be extracted using the Langreth rules given in section 3.1,

$$D^{>}_{12}(t,t') = -\frac{1}{16}J_{21}\int dt_1 \left(X^r_{\mathrm{DQD}}(t,t_1)\left(X^1_2\right)^{>}(t_1,t') + X^{>}_{\mathrm{DQD}}(t,t_1)\left(X^1_2\right)^{a}(t_1,t')\right).$$

Only $D^{>}(t,t')$ at $t'=t$ enters the expression for the current. To simplify the calculation we perform a Fourier transformation and transform back at a later stage. In frequency space we thus find

$$D^{>}_{12}(\omega) = -\frac{1}{16}J_{21}\left(X^r_{\mathrm{DQD}}(\omega)\left(X^1_2\right)^{>}(\omega) + X^{>}_{\mathrm{DQD}}(\omega)\left(X^1_2\right)^{a}(\omega)\right). \tag{4.6}$$

Similar to the rules for single particle Green's functions, there are also relations between the susceptibilities. For the conduction electron spin susceptibility we find the relation

$$\left(X^1_2\right)^{a}(\omega) \approx -\frac{1}{2}\left(X^1_2\right)^{>}(\omega) + \frac{1}{2}\left(X^1_2\right)^{<}(\omega). \tag{4.7}$$

This is closely related to $G^a \approx \frac{1}{2}iA = -\frac{1}{2}(G^{>}-G^{<})$, since $A = i(G^r-G^a) = i(G^{>}-G^{<})$ and consequently $-iA = G^{>}-G^{<}$. A proof of this relation can be found in appendix B.2. Since the current is proportional to the real part of the correlation function $D^{>}_{12}(\omega)$, the real part of the conduction electron Green's functions can be neglected.

A similar relation holds for X^r_{DQD},

$$X^r_{\mathrm{DQD}}(\omega) = \frac{1}{2}X^{>}_{\mathrm{DQD}}(\omega) - \frac{1}{2}X^{<}_{\mathrm{DQD}}(\omega). \tag{4.8}$$

The derivation of Eq. (4.8) can be found in appendix B.4.

Using Eq. (4.7) and Eq. (4.8) the expression for $D^{>}_{12}(\omega)$ in Eq. (4.6) simplifies to

$$D^{>}_{12}(\omega) = -\frac{1}{16}J_{21}\frac{1}{2}\left(X^{>}_{\mathrm{DQD}}(\omega)\left(X^1_2\right)^{<}(\omega) - X^{<}_{\mathrm{DQD}}(\omega)\left(X^1_2\right)^{>}(\omega)\right).$$

Inserting further $D^{>}_{12}(\omega)$ into the expression for the current, Eq. (4.4), we find

$$I_L = \frac{e}{h}\int d\omega \frac{1}{4}J_{12}\frac{1}{4}J_{21}\left(X^{>}_{\mathrm{DQD}}(\omega)\left(X^1_2\right)^{<}(\omega) - X^{<}_{\mathrm{DQD}}(\omega)\left(X^1_2\right)^{>}(\omega)\right).$$

The next step is to calculate the spin susceptibility of the double quantum dot system within the singlet-triplet representation.

If the contributions of Σ_{st_0} and $\Sigma_{t_0 s}$ are neglected no off-diagonal terms appear. The well-known ansatz for the lesser Green's functions $G^<_\gamma(\omega) = -in_\gamma A_\gamma(\omega)$ is used, where the spectral function $A_\gamma(\omega) = i\left(G^r_\gamma(\omega) - G^a_\gamma(\omega)\right) = 2\pi\delta(\omega - \epsilon_\gamma)$[4] is assumed to be strongly peaked. Since all other physical quantities change on a larger energy scale we can neglect the finite width and assume a δ-function rather than a Lorentz peak. Directly related to this sharp structure of the spectral function $A_\gamma(\omega)$ is the assumption that the occupation number n_γ can be assumed to be frequency independent since it does not change rapidly within the width of the spectral function[5]. The value of the occupation number itself has to be calculated from a quantum Boltzmann equation as explained in section 4.1.

The calculation of the spin susceptibility of the double quantum dot system is now straightforward. Later on we refer back to the derivation here when it appears in further calculations. Note that a contribution from $G^< \times G^<$ is projected out since it is proportional to $\mathrm{e}^{-2\beta\lambda}$ and is thus neglected in the following.

$$\begin{aligned}
X^>_{\mathrm{DQD}}(\omega) &= \sum \tau^i_{\sigma'\sigma}\tau^j_{\sigma\sigma'} \int \frac{d\epsilon}{2\pi} \mathrm{Tr}\left[G^<(\epsilon)T^i G^>(\epsilon+\omega)T^j\right] \\
&\approx \sum \tau^i_{\sigma'\sigma}\tau^j_{\sigma\sigma'} \int \frac{d\epsilon}{2\pi} G^<_{\gamma'}(\epsilon)T^i_{\gamma'\gamma}\left(G^r_\gamma(\epsilon+\omega) - G^a_\gamma(\epsilon+w)\right)T^j_{\gamma\gamma'} \\
&= \sum \tau^i_{\sigma'\sigma}\tau^j_{\sigma\sigma'} \int \frac{d\epsilon}{2\pi} (-i)2\pi n_{\gamma'}\delta\left(\epsilon - \epsilon_{\gamma'}\right) T^i_{\gamma'\gamma}(-i)2\pi\delta\left(\epsilon+\omega-\epsilon_\gamma\right)T^j_{\gamma\gamma'} \\
&= -\sum 2\pi\delta\left(\omega - \epsilon_\gamma + \epsilon_{\gamma'}\right)\tau^i_{\sigma'\sigma}\tau^j_{\sigma\sigma'}T^j_{\gamma\gamma'}n_{\gamma'}T^i_{\gamma'\gamma},
\end{aligned}$$

and analogously we get

$$\begin{aligned}
X^<_{\mathrm{DQD}}(\omega) &\approx \sum \tau^i_{\sigma'\sigma}\tau^j_{\sigma\sigma'} \int \frac{d\epsilon}{2\pi}\left(G^r_{\gamma'}(\epsilon-\omega) - G^a_{\gamma'}(\epsilon-w)\right)T^i_{\gamma'\gamma}G^<_\gamma(\epsilon)T^j_{\gamma\gamma'} \\
&= -\sum 2\pi\delta\left(\omega - \epsilon_\gamma + \epsilon_{\gamma'}\right)\tau^i_{\sigma'\sigma}\tau^j_{\sigma\sigma'}T^i_{\gamma'\gamma}n_\gamma T^j_{\gamma\gamma'}.
\end{aligned}$$

We find explicitly that the symmetry $X^>_{\mathrm{DQD}}(\omega) = X^<_{\mathrm{DQD}}(-\omega)$ is fulfilled. This result is only valid if the spectral function is assumed to be a δ-function. A finite broadening will be discussed later.

The corresponding expression for the current is thus

$$\begin{aligned}
I_L =& 2\pi\frac{e}{h}\left(\frac{1}{4}J_{12}\tau^i_{\sigma'\sigma}T^i_{\gamma'\gamma}\right)\left(\frac{1}{4}J_{21}\tau^j_{\sigma\sigma'}T^j_{\gamma\gamma'}\right) \\
&\int d\omega\left(-n_{\gamma'}\left(X^1_2\right)^<(\omega) + n_\gamma\left(X^1_2\right)^>(\omega)\right)\delta\left(\omega - \epsilon_\gamma + \epsilon_{\gamma'}\right). \qquad (4.9)
\end{aligned}$$

The expression in Eq. (4.9) is generalized to calculate the current using the perturbative RG method in chapter 5.

[4] Here a factor of $\hbar$ is understood such that the frequency ω has the unit of an energy, $\hbar\omega$.

[5] In section 4.2.2 we show one result of the current including a finite decoherence rate Γ.

The conduction electron spin susceptibility X_2^1 is calculated in appendix B.2 and inserted into Eq. (4.9). After a summation over all indices the result is

$$\begin{aligned} I_L =&(2\pi)^2 \frac{e}{h} \frac{1}{16} g_{12} g_{21} \tau^i_{\sigma'\sigma} \tau^j_{\sigma\sigma'} T^i_{\gamma'\gamma} n_\gamma T^j_{\gamma\gamma'} \\ &\left((\epsilon_{\gamma'} - \epsilon_\gamma - eV_L)\, n_B\left(\epsilon_{\gamma'} - \epsilon_\gamma - eV_L\right) - (\epsilon_{\gamma'} - \epsilon_\gamma + eV_L)\, n_B\left(\epsilon_{\gamma'} - \epsilon_\gamma + eV_L\right)\right), \end{aligned}$$

where g refers to the dimensionless coupling $g = N(0)J$ and the voltage is defined by

$$eV_L = \mu_1 - \mu_2. \tag{4.10}$$

The current is antisymmetric with respect to the voltage. Using the relation $n_B(x) = \frac{1}{2}\coth(\frac{1}{2}\beta x) - \frac{1}{2}x$, we define the function $F_3(x, V)$,

$$F_3(x, V) = \frac{1}{2}(x - eV)\coth\left(x - eV\right) - \frac{1}{2}(x + eV)\coth\left(x + eV\right), \tag{4.11}$$

which reflects the antisymmetry since $F_3(x, -V) = -F_3(x, V)$. This leads immediately to the conclusion that the current vanishes if the voltage is zero, $F_3(x, V = 0) = 0$. The same symmetry arguments apply to the first argument of the function $F_3(x, V)$

$$F_3(-x, V) = -F_3(x, V), \qquad F_3(0, V) = F_3(x, 0) = 0.$$

Using the function $F_3(x, V)$ the current can be written in the final form,

$$I_L = \frac{1}{16}(2\pi)^2 \frac{e}{h}\, g_{12} g_{21} \tau^i_{\sigma'\sigma} \tau^j_{\sigma\sigma'} T^i_{\gamma'\gamma} n_\gamma T^j_{\gamma\gamma'} \left(eV_L + F_3(\epsilon_{\gamma'} - \epsilon_\gamma, V_L)\right). \tag{4.12}$$

Since this current expression is general, any setup of quantum dots with the corresponding pseudo-spin matrix $\vec{T}$ can be calculated in this framework. The only assumptions entering the result of the current in Eq. (4.12) are, that the Green's functions $G_{\gamma\gamma'} = G_\gamma$ are diagonal and the ansatz for the lesser Green's function, $G^<(\omega) = -inA(\omega)$, applies.

4.2.2 Discussion of the Current for Vanishing Magnetic Field $B = 0$

In the case of vanishing magnetic field $B = 0$ all triplet states are degenerate, $n_{t_0} = n_{t_-} = n_{t_+} \equiv n_t$. The energy eigenvalues of the states are given by $\omega_{t_0} = \omega_{t_+} = \omega_{t_-} = \frac{1}{4}K$ and $\omega_s = -\frac{3}{4}K$. After summation of the conduction electron and quantum dot indices in Eq. (4.12) the current I_L through the left quantum dot is given by

$$I_L = \frac{1}{8}(2\pi)^2 \frac{e}{h} g_{12} g_{21} \left[3eV_L - 3\left(n_t - n_s\right) F_3\left(K, V_L\right)\right]. \tag{4.13}$$

The first term in Eq. (4.13) is linear in the voltage and the second term is a function proportional to the polarization $p = n_s - n_t$.

In Fig. 4.7(a) the current I_L versus the voltage eV_L/K applied to the left quantum dot is shown at low temperatures $T/K = 0.001$ and a small coupling $g_L = g_R = 0.1$. If not stated differently the couplings to the leads are assumed to be identical $g_{11} = g_{22} = g_{12} = g_{21} = g_L$ and $g_{33} = g_{44} = g_{34} = g_{43} = g_R$. The result is shown only for $V_L > 0$ since the current for $V_L < 0$ is given according to $I(-V_L) = -I_L(V_L)$. In the case of an antiferromagnetic coupling $K > 0$ between the two quantum dots, the singlet is the

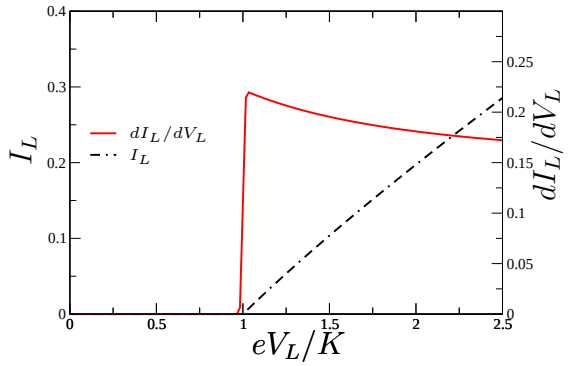

(a) Current I_L in comparison with differential conductance dI_L/dV_L.

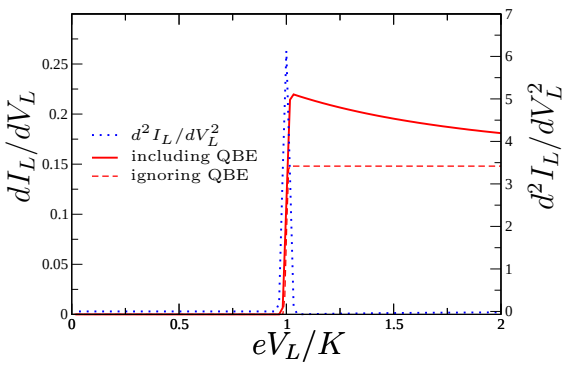

(b) Differential conductance dI_L/dV_L and the second derivative d^2I_L/dV_L^2.

Figure 4.7: Current $I_L[e/h]$, differential conductance $dI_L/dV_L[e^2/h]$ and the second derivative of the current d^2I_L/dV_L^2 versus voltage eV_L/K for $B = V_R = 0$, $g_L = g_R = 0.1$ and small temperature $T/K = 0.001$. The right panel includes the result for dI_L/dV_L if the physics of the quantum Boltzmann equation (QBE) is ignored.

ground state of the system. The ferromagnetic case and its different physics is discussed separately in section 4.4. As already mentioned in chapter 2 there is no current through the quantum dot if the singlet is the ground state. Any process involves a transition to a triplet state. This is only possible if the energy gap can be overcome by an energy of the system like a temperature or a voltage of the order of the singlet-triplet gap. This argument is valid in the particle-hole symmetric case if potential scattering is not present (see section 2.2). Otherwise the current would have a finite slope and would not be suppressed for voltages below the singlet-triplet gap.

The threshold behavior is more pronounced in the differential conductance dI_L/dV_L. As it is obvious from Fig. 4.7(a) the conductance displays the level structure of the mesoscopic system which is attached to the leads. The differential conductance is symmetric with respect to the voltage and we show only the positive voltage axis. Contrary to the common expectation the maximum is not at $eV_L = K$. In non-equilibrium the voltage at the inflection point corresponds to the value of the energy gap. Alternatively the level splitting can be determined from the second derivate of the current as illustrated in Fig. 4.7(b). In the same panel we also illustrate the effect of the self-consistent calculation of the occupation numbers. If the quantum Boltzmann equation is ignored, the differential conductance has a step rather than a cusp at $eV_L = K$. As was shown in Ref. [52] the voltage-dependent occupation probabilities are necessary to describe experimental results.

In Fig. 4.8(a) the influence of the temperature on the differential conductance is illustrated. We observe that the width of the cusp becomes broader for higher temperatures, since there are electron excitations present within an energy of $2T$ around the Fermi edge. In Fig. 4.8(b) the effect of different couplings to the leads is illustrated. The derivation of the Kondo model from an underlying Anderson model implies

$$J_{12}J_{21} = (4t_1t_2/U)^2 = J_{11}J_{22},$$

with the expression derived for J_{nm} in section 2.3.2 in the particle-hole symmetric case. Therefore the parameters in Fig. 4.8(b) go beyond the Anderson model. We define a

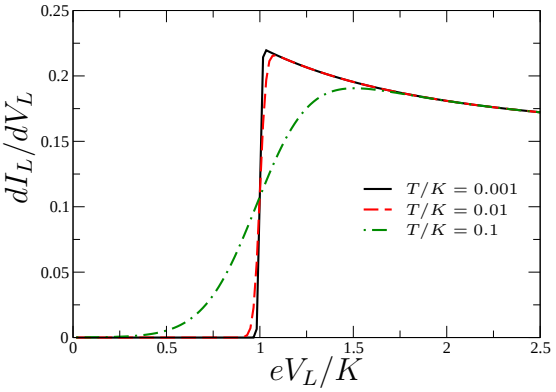

(a) Differential conductance for different values of the temperature.

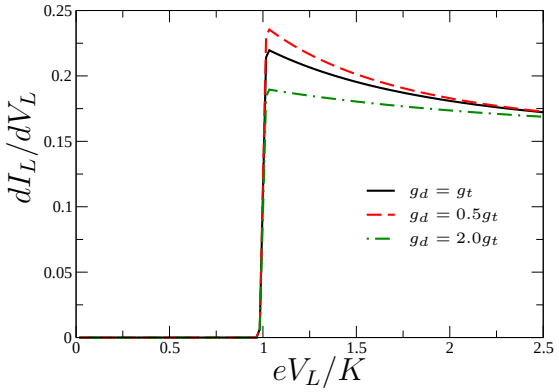

(b) Differential conductance for different values of the Kondo coupling to the leads.

Figure 4.8: Differential conductance $dI_L/dV_L[e^2/h]$ vs. voltage eV_L/K for $B = V_R = 0$. In the left panel different values of the temperature $T/K = 0.001, 0.01, 0.1$ are shown and the coupling $g_L = g_R = 0.1$ is kept constant. In the right panel the temperature is constant $T/K = 0.001$ and we vary the Kondo coupling to the leads, while the transport coupling $g_{12} = g_{21} = g_t$ is kept constant to the value 0.1.

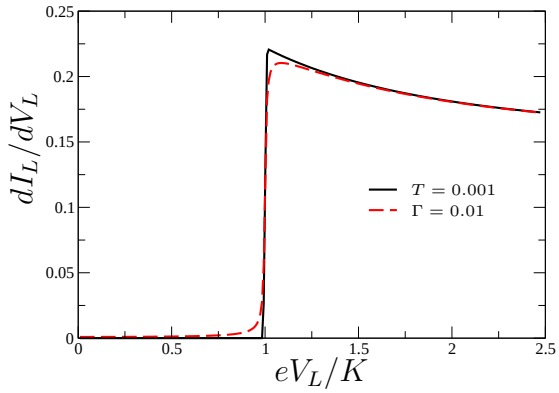

Figure 4.9: Differential conductance dI_L/dV_L vs. eV_L/K for finite, but small temperature $T/K = 0.001$ in comparison with a calculation including the finite level broadening Γ of the pseudo particles. The other parameters are $B = V_R = 0$, $g_L = g_R = 0.1$.

diagonal Kondo coupling $g_d = g_{11} = g_{22}$ and a transport Kondo coupling $g_t = g_{12} = g_{21}$. It is obvious from Eq. (4.13) that the transport is governed by the coupling g_t. In Fig. 4.8(b) the coupling g_d is changed while g_t is kept constant. The cusp at $eV_L = K$ is enhanced if $g_t = 2g_d$ and lowered if $g_d = 2g_t$ compared to the symmetric case $g_d = g_t$. Apart from that the structure of the peak does not change. This observation originates in the dependence of the non-equilibrium occupation on the ratio g_d/g_t.

In Fig. 4.9 it is taken into account that the singlet and triplet states gain a finite life time due to the interaction with the leads. This hybridization is reflected in a finite broadening Γ. The effect of a finite decoherence due to the non-equilibrium situation is discussed in more detail in chapter 5. Here we only illustrate that the physics is dominated by Γ instead of by the temperature T, if $\Gamma > T$. In this limit the spectral function $A(\omega)$ is approximated by a Lorentzian $1/\pi\ \Gamma/((\omega - \epsilon_\gamma)^2 + \Gamma^2)$ instead of a δ-function in the convolution with X_1^2. The calculation is given in appendix B.2. In

analogy to $n_B(x) = \frac{1}{2}(\coth(\beta x/2) - 1)$ we define the broadened $n_B^\Gamma(x) = \frac{1}{2}(\tilde{c}(x) - 1)$, where

$$\begin{aligned}\tilde{c}(x) = &\frac{1}{\pi}\left(\arctan\left(\frac{x+2T}{\Gamma}\right) + \arctan\left(\frac{x-2T}{\Gamma}\right)\right)\\ &+ \frac{2T}{x}\frac{1}{\pi}\left(\arctan\left(\frac{x+2T}{\Gamma}\right) - \arctan\left(\frac{x-2T}{\Gamma}\right)\right)\\ &- \frac{\Gamma}{2x}\frac{1}{\pi}\left(\ln\left[(x+2T)^2+\Gamma^2\right] + \ln\left[(x-2T)^2+\Gamma^2\right]\right).\end{aligned}$$

This expression is valid for $T \ll x, \Gamma$, since the derivation makes use of the expansion of $xn_B(x)$ at $T \ll x$. In Fig. 4.9 we show a comparison of the result of the conductance if the broadening is neglected and if a finite Γ of the order of $g^2K = 0.01$ is taken into account. Please note that the resonance is broadened and additionally the shape changes.

The effect of a finite decoherence can also be studied indirectly via the effect of a finite voltage V_R applied to the right quantum dot on the current through the left quantum dot. In Fig. 4.10 it is shown that as soon as the voltage V_R reaches the threshold

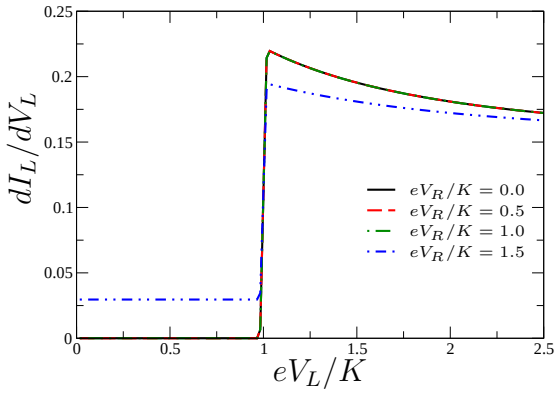

Figure 4.10: Dependence of the differential conductance dI_L/dV_R on the voltage eV_L/K if the voltage V_R applied to the right quantum dot is varied. The plots for $eV_R/K = 0.0, 0.5$ and 1.0 lie on top of each other. Further parameters are $g_L = g_R = 0.1$, $T/K = 0.001$, and $B = 0$.

$eV_R > K$, triplet states become occupied. The non-equilibrium situation on the right quantum dot is transferred by the spin-spin interaction K to the left quantum dot and a finite conductance dI_L/dV_L is observed even in the linear regime $eV_L < K$.

In Fig. 4.11 we study the differential dependence of the current through the left quantum dot on the voltage applied to the right quantum dot. The current I_L depends on V_R via the polarization $p = n_s - n_t$. In the inset of Fig. 4.11 we plot the rescaled quantity $(K/eV_L)dI_L/dV_R$. This so-called transconductance does not dependent on the voltage V_L or the spin-spin interaction K, as long as V_L is below the threshold $eV_L < K$.

From the expression for the current in Eq. (4.13) we can derive an expression for the transconductance,

$$\begin{aligned}\frac{dI_L}{dV_R} &= \frac{3}{8}(2\pi)^2\frac{e}{h}g_{12}g_{21}\left(-\frac{dp}{dV_R}\right)F_3(K,V_L)\\ &= \frac{3}{4}(2\pi)^2\frac{e}{h}\frac{2g_{12}g_{21}}{g_{\text{all}}^2}\frac{2g_{34}g_{43}}{K}\,p^2\,F_3(K,V_L)\left(\frac{dF_1}{dV_R}(K,V_R)\right),\end{aligned} \tag{4.14}$$

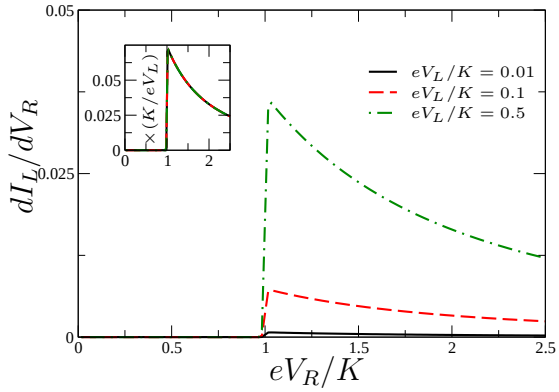

Figure 4.11: Transconductance $dI_L/dV_R[e^2/h]$ vs. eV_R/K for various values of $eV_L/K = 0.01, 0.1, 0.5$ and $g_L = g_R = 0.1$, $B = 0$ and $T/K = 0.001$. Inset: transconductance rescaled with a factor of K/eV_L.

since

$$\left(-\frac{dp}{dV_R}\right) = p^2 \frac{1}{2g_{\text{all}}^2 K} 4 \frac{d}{dV_R} Y_{L+R}(K) = 4p^2 \frac{2g_{34}g_{43}}{2g_{\text{all}}^2 K} \frac{d}{dV_R} F_1(K, V_R),$$

and where $F_1(K, V_R) = (K + eV_R)n_B(K + eV_R) + (K - eV_R)n_B(K - eV_R)$.

The increase of dI_L/dV_R at the voltage $eV_R = K$ originates from $d/dV_R F_1(K, V_R)$ and the decrease in Fig. 4.11 is then due to p^2. Both effects are closely related to the non-equilibrium occupation number of the pseudo particle states. The transconductance is a capacitive effect which becomes obvious from the combination of the couplings to the left and right leads. If we assume that all couplings are derived from an underlying Anderson model such that $g_{12}g_{21} = g_{11}g_{22}$ and additionally $g_{11} = g_{22} = g_L$ (and analogously for the leads 3 and 4), the expression for dI_L/dV_R is proportional to

$$1/\left(\frac{1}{g_L^2} + \frac{1}{g_R^2}\right).$$

The transconductance $(K/eV_L)dI_L/dV_R$ is thus finite and reaches its largest value if the couplings g_L and g_R are identical.

As a last point in this section it should be mentioned, that although the current through the left quantum dot can be tuned by a voltage applied to the right quantum dot, the chosen setup of a double quantum dot system can not be used as a switch. This conclusion is proven in appendix B.4.

4.2.3 Current in the Case of a Finite Magnetic Field $B \neq 0$

If the coupling is left-right-symmetric, the off-diagonals are exactly zero.[6] Performing the same steps to calculate the current as in the case for zero magnetic field, we can derive an expression for the current in finite magnetic field B.

[6] In the antisymmetric case $J_L \neq J_R$ the off-diagonal contributions can only be neglected for $K \gg \Gamma$.

Evaluating the spin product $T^i_{\gamma'\gamma} n_\gamma T^j_{\gamma\gamma'}$ in Eq. (4.12) we obtain

$$I_L = \frac{1}{8}(2\pi)^2 \frac{e}{h} g_{12} g_{21} \left[3eV_L - (n_{t_+} - n_{t_-}) F_3(B, V_L) - (n_{t_+} - n_s) F_3(K + B, V_L) \right.$$
$$\left. - (n_{t_0} - n_s) F_3(K, V_L) - (n_{t_-} - n_s) F_3(K - B, V_L) \right]. \quad (4.15)$$

This result is only valid in the regime where off-diagonal contributions are negligible.

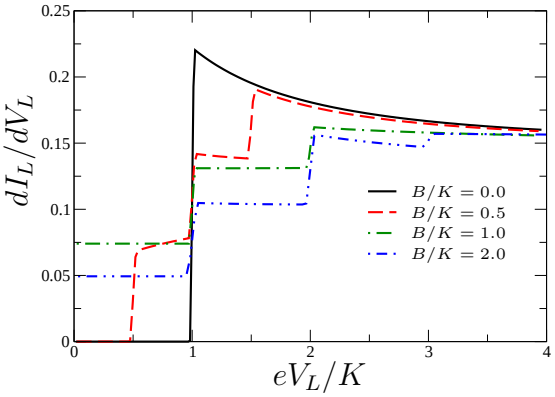

(a) Differential conductance vs. voltage for different values of B/K.

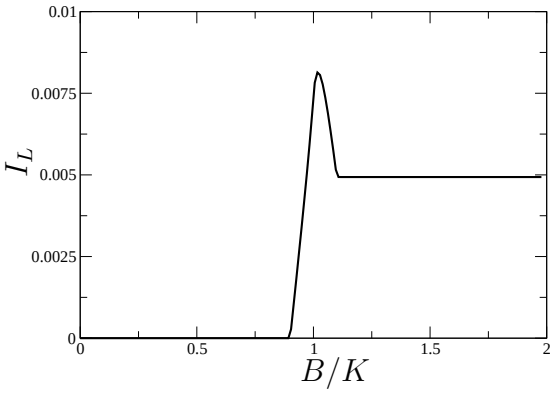

(b) Current vs. magnetic field.

Figure 4.12: In the left panel we show the differential conductance dI_L/dV_L vs. eV_L/K for finite values of the magnetic field $B/K = 0.0, 0.5, 1.0, 2.0$ at low temperature $T/K = 0.001$, $V_R = 0$ and $g_L = g_R = 0.1$. In the right panel the dependence of the current on the magnetic field B is shown at $eV_L/K = 0.1$ and same set of parameters as in left panel.

In Fig. 4.12(a) we show the differential conductance for finite magnetic field B. As in the calculation of the magnetization in section 4.1.2 the current shows different physical behavior for $B < K$, $B = K$, and $B > K$. A degenerate ground state e.g. for $B = K$ as well as a triplet ground state show a finite current in the linear regime $eV_L < K$. From Fig. 4.12(b) it is obvious that the crossover between singlet and triplet ground states happens on the energy scale given by the temperature T.[7] The differential conductance can thus be used to analyze the energy spectrum of an unknown sample, since the series of peaks is linked to the level structure of the transport region, see therefore also the discussion in Refs. [31, 30].

In the limit of $K \to 0$ the current in Eq. (4.15) depends on the total magnetization $M_{\text{tot}} = 2\langle \vec{S}^z_L + \vec{S}^z_R \rangle$ rather than on $M_L = 2\langle \vec{S}^z_L \rangle$ solely. Consequently the current depends on the voltage V_R although the two quantum dots are decoupled, see therefore the discussion in section 4.1.3. The assumption that the off-diagonal contributions can be neglected fails in the limit $K \to 0$. It is explained in appendix C how the current can be calculated in that special case.

In this section we derived the expression for the current through one of the quantum dots. The differential conductance dI/dV shows the same qualitative behavior as the results of various experiments (e.g. Ref. [27, 29]). The shape of the resonance is affected by the non-equilibrium occupation numbers. Besides the temperate T the broadening of the cusp depends on the broadening Γ. A finite voltage V_R applied to the right

[7] As discussed in Ref. [45] the differential conductance at $B = K$ is Kondo enhanced.

quantum dot creates a non-equilibrium situation for the whole quantum dot system. This effect can be probed by the transconductance $(K/eV_L)dI_L/dV_R$, which illustrates that the current I_L through the left quantum dot can be tuned by the voltage V_R. Without solving the quantum Boltzmann equation this effect would not be present and it originates exclusively from the decoherence of singlet and triplet states due to a large voltage.

4.3 T-Matrix

So far we discussed mainly the properties of the double quantum dot system. In this section we focus on the scattering of conduction electrons off the Kondo impurities. A useful quantity in scattering problems is the so-called T-matrix or reducible self energy of the conduction electron Green's function (see e.g. Ref. [2, 58, 59]). It is defined by the perturbative expansion of the conduction electron Green's function,

$$G^r = G_0^r + G_0^r T^r G_0^r.$$

By writing the expansion one can derive a self-consistent equation for the T-matrix,

$$\begin{aligned} T &= H_{\text{int}} + H_{\text{int}} G_0 H_{\text{int}} + H_{\text{int}} G_0 H_{\text{int}} G_0 H_{\text{int}} + \dots \\ &= H_{\text{int}} + H_{\text{int}} G_0 T. \end{aligned} \tag{4.16}$$

It was shown e.g. in Ref. [59] for a quantum dot subject to a magnetic field, that the T-matrix links the Anderson model for the double quantum dot system, that was discussed in section 2.2, to the Kondo model studied in chapters 3 and 4. The low frequency part of the d-level density of states (DOS) in the Anderson model can be identified with the T-matrix by

$$A_d(\omega, T, K) = -\frac{1}{\pi} \text{Im}\left[N(0)\, T^r(\omega, T, K)\right]. \tag{4.17}$$

This relation is imperfect in the case of 2nd order perturbation theory, but the T-matrix is discussed again in the context of perturbative RG in chapter 5. With the knowledge of the spectral function the linear response conductance can be calculated as (see Ref. [58])

$$G = \frac{dI}{dV}\Big|_{V\to 0} = \frac{e^2}{\hbar} \sum_\sigma \int d\omega A_{d\sigma}(\omega) \left(-\frac{\partial f}{\partial \omega}\right).$$

Since we already derived the differential conductance for a finite voltage in the previous section, the comparison of the T-matrix from the Kondo model with the spectral function of the Anderson model is the main issue of this section.

4.3.1 Calculation of the T-Matrix

In second order perturbation theory the T-matrix or reducible self energy is identical to the irreducible self energy of the conduction electron Green's function. On the Keldysh contour the Green's function is defined as

$$G_{nk\sigma}(\tau, \tau') = -i\langle T_c c_{nk\sigma}(\tau) c^\dagger_{nk\sigma}(\tau')\rangle.$$

In the following we concentrate on the case of vanishing magnetic field, $B = 0$. The first order of perturbation theory does not contribute in this case since it is proportional to $\langle \vec{S}_L \rangle$. The leading contribution originates from 2nd order perturbation theory,

$$\frac{1}{2}(-i)^3 \int d\tau_1 \int d\tau_2 \langle T_c c_{nk\sigma}(\tau) H_{\rm int}(\tau_1) H_{\rm int}(\tau_2) c^\dagger_{nk\sigma}(\tau') \rangle .$$

In the following we consider only one of the left leads (n = 1, 2). Since the calculation is similar to the derivation of the self energy it is not shown here. After applying Wick's theorem we can extract the expression for the T-matrix in 2nd order perturbation theory,

$$T_n(\tau_1, \tau_2) = \frac{1}{4} J^i_{nm} J^j_{mn} \tau^i_{\sigma\sigma'} \tau^j_{\sigma'\sigma} G_{mk'\sigma'}(\tau_1, \tau_2) \langle S^i_L(\tau_1) S^j_L(\tau_2) \rangle . \tag{4.18}$$

The corresponding diagram is illustrated in Fig. 4.13. Eq. (4.18) can be rewritten by

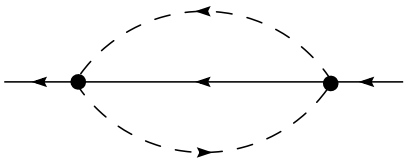

Figure 4.13: Typical diagram which determines the T-matrix to second order perturbation theory. Solid lines: conduction electron Green's functions; dashed lines: pseudo particles of the double quantum dot system.

introducing the spin susceptibility for the double quantum dot system (DQD),

$$T_n(\tau_1, \tau_2) = -\frac{1}{16} J_{nm} J_{mn} G_{mk'\sigma'}(\tau_1, \tau_2) X_{\rm DQD}(\tau_2, \tau_1), \tag{4.19}$$

where $X_{\rm DQD}$ for the singlet-triplet states is given by

$$X_{\rm DQD}(\tau_2, \tau_1) = \sum \tau^i_{\sigma\sigma'} \tau^j_{\sigma'\sigma} G_{\gamma'}(\tau_2, \tau_1) T^i_{\gamma'\gamma} G_\gamma(\tau_1, \tau_2) T^j_{\gamma\gamma'} .$$

This is identical to the definition in Eq. (4.5) in section 4.2. By using the Langreth rules from section 3.1 we find the expression for the retarded T-matrix,

$$T^r_n(t_1, t_2) = -\frac{1}{16} J_{nm} J_{mn} \left(G^<(t_1, t_2) X^a_{\rm DQD}(t_2, t_1) + G^r(t_1, t_2) X^<_{\rm DQD}(t_2, t_1) \right) .$$

After Fourier transformation the frequency dependent T-matrix is given by the convolution

$$T^r_n(\omega) = -\frac{1}{16} J_{nm} J_{mn} \int \frac{d\epsilon}{2\pi} \left(G^<(\epsilon + \omega) X^a_{\rm DQD}(\epsilon) + G^r(\epsilon + \omega) X^<_{\rm DQD}(\epsilon) \right) .$$

By inserting the usual ansatz for the conduction electron Green's functions and the results of $X_{\rm DQD}$ as known from previous sections we find

$$\begin{aligned} -\frac{1}{\pi} {\rm Im} \left[N(0) T^r_n(\omega) \right] = & \frac{1}{16} g_{nm} g_{mn} \tau^i_{\sigma'\sigma} \tau^j_{\sigma\sigma'} T^i_{\gamma'\gamma} T^j_{\gamma\gamma'} \\ & \left[f(\omega + \epsilon_{\gamma'} - \epsilon_\gamma - \mu_m) (n_\gamma - n_{\gamma'}) - n_{\gamma'} \right] . \end{aligned} \tag{4.20}$$

This result is generally valid for any setup of quantum dots. In the case of two coupled quantum dots the pseudo Pauli matrices from Eq. (2.6) in section 2.1 are inserted and thus we obtain

$$\begin{aligned} &-\frac{1}{\pi}\mathrm{Im}\left[N(0)T^r(\omega)\right] \\ &=-\frac{3}{8}\sum_m g_{nm}g_{mn}\left[1+(n_s-n_t)\left(f(\omega+K-\mu_m)-f(\omega-K-\mu_m)\right)\right]. \end{aligned} \tag{4.21}$$

The T-matrix is symmetric with respect to the frequency, $T^r(-\omega)=T^r(\omega)$, which can be seen by rewriting the difference of the two Fermi distribution functions as $2f(x)=(1-\tanh(\beta x/2))$.

4.3.2 Discussion of Results for the T-Matrix

In the case of antiferromagnetic spin-spin interaction $K>0$ the singlet is the ground state. In Fig. 4.14 it is observed that the T-matrix is zero until the frequency ω reaches the value K. Since $T^r(\omega)$ is symmetric in ω only the values for $\omega>0$ are shown. In Fig. 4.14 the effect of an increasing temperature is illustrated, when the Fermi function becomes smeared over the energy scale of $2T$. Thermodynamically excited states con-

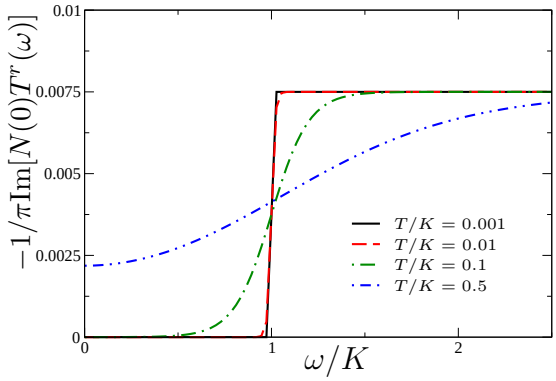

Figure 4.14: T-matrix $-1/\pi\mathrm{Im}[N(0)T^r(\omega)]$ of one of the left leads at $g_L=g_R=0.1$, $V_L=V_R=0$, and different temperatures T/K.

tribute and the T-matrix at low frequencies has a finite value. The shape of this curve is due to Eq. (4.17) identical to the low frequency spectrum of the d-level density of states in the Anderson model. The step-like behavior corresponds to the gap due to singlet and triplet states, but the peak structure due to a Kondo enhancement is not observed since the calculation is only to lowest (2nd) order perturbation theory.

A finite voltage provides a non-equilibrium situation (see Fig. 4.15). We distinguish between a direct effect and an indirect effect. If the T-matrix is studied in one of the left leads and a finite voltage V_L is applied to the left leads, the T-matrix is directly effected by V_L. If a finite voltage V_R is applied to the right leads, the T-matrix shows an indirect dependence on V_R. In both cases an effect is observed which is different to the temperature broadening as illustrated in Fig. 4.14. In Fig. 4.15(a) the chemical potential in lead $n=1$ is shifted by $+eV_L/2$. With increasing voltage two steps appear at $\omega=K\mp eV_L/2$. Since the chemical potential in lead 1 is $\mu_1=eV_L/2$, we expect

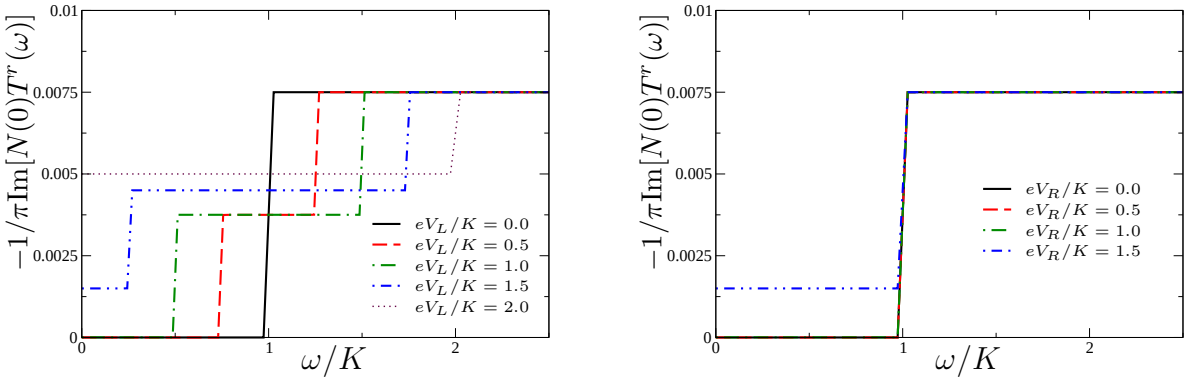

(a) T-matrix for different values of the voltage V_L.

(b) T-matrix for different values of the voltage V_R.

Figure 4.15: T-matrix of one of the left leads in 2nd order perturbation theory for different values of the voltage eV_L/K (and $V_R = 0$) in the left panel and voltage eV_R/K (and $V_L = 0$) in the right panel. The plots for $eV_R/K = 0.0, 0.5$, and 1.0 lie on top of each other. Further parameters of the system are $g_L = g_R = 0.1$, $T/K = 0.001$ and $B = 0$.

the singlet-triplet splitting to vanish at an energy of $eV_L = 2K$ such that the value of the T-matrix at $\omega = 0$ is non-zero. A typical feature of a non-equilibrium situation is the voltage-dependent occupation numbers. This effect can be observed in Fig. 4.15(a). Since the triplet states become occupied as soon as the voltage reaches the threshold $eV_L = K$, the zero-frequency value of $\mathrm{Im}[T^r]$ is finite already before eV_L reaches the value $2K$.

The effect of non-equilibrium occupation numbers also manifests itself in the plot of the T-matrix of one of the left leads while changing the voltage V_R applied to the right leads. In Fig. 4.15(b) the resonance does not split like in the case with finite V_L, but we observe the effect of non-equilibrium occupation numbers as soon as V_R reaches the threshold K. The T-matrix at frequencies $\omega < K$ is finite and therefore deviates from the equilibrium value. As for the transconductance in the previous section this increase is only observable if the quantum Boltzmann equation is taken into account. The decoherent processes due to a finite current in the system provide the basis for this physical behavior.

In this section the T-matrix was calculated and the effect of a finite voltage on its behavior was shown. The results discussed here are limited to the case where $K > 0$, i.e. when the singlet is the ground state of the double quantum dot system.

4.4 Ferromagnetic Spin-Spin Coupling

So far the spin-spin interaction K between the left and right quantum dot spins was assumed to be antiferromagnetic. In the low temperature limit the singlet ground state is then in competition with the Kondo singlet of a quantum dot spin and the spin of the leads. Since this competition gives rise to interesting physics the ferromagnetic case coupling was ignored so far. Experiments observe both parallel and anti-parallel orientation of quantum dot spins[8]. Therefore we shortly address this case as well and

[8]How a ferromagnetic interaction can arise is discussed in section 2.2.

show the differences to the antiferromagnetic case, and how these two cases can be distinguished in an experiment.

In the case of a ferromagnetic coupling between the two quantum dots, the triplets are the ground state of the system. They are threefold degenerate, but split up in a finite magnetic field such that the triplet t_+ with both spins in the direction of the magnetic field $\vec{B}$ is the ground state.

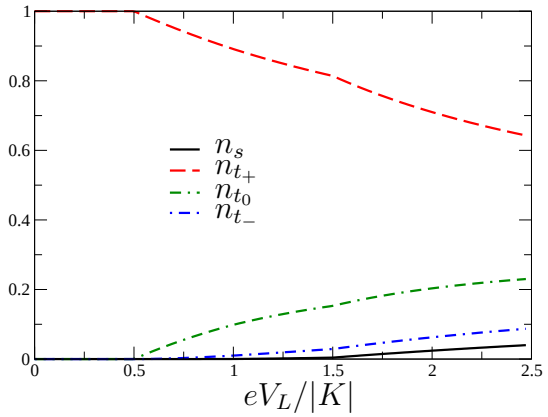

(a) Voltage-dependent occupation numbers for $B/|K| = 0.5$.

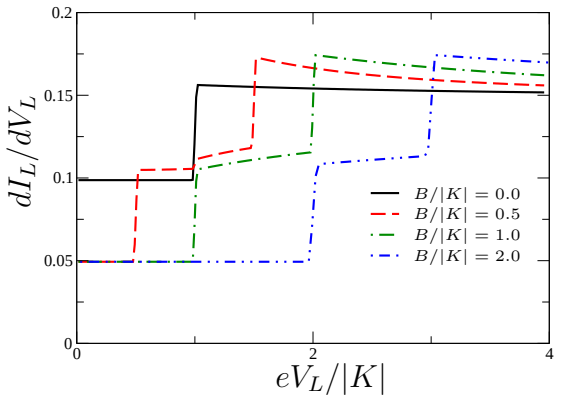

(b) Differential conductance for various values of the magnetic field $B/|K|$.

Figure 4.16: For ferromagnetic spin-spin coupling, $K < 0$, the occupation numbers and the differential conductance dI_L/dV_L behave different than the antiferromagnetic case. Parameters of the plots are $V_R = 0$, $g_L = g_R = 0.1$, $T/|K| = 0.001$.

For antiferromagnetic coupling and $B/K = 0.5$ the level distributions was shown in Fig. 4.4(b) on page 60. There the singlet was the ground state and t_+ the first excited state, with a gap of $K - B$. In the ferromagnetic case in Fig. 4.16(a) the triplet t_+ is the ground state and the first excited state is the triplet t_0, separated by the energy B. In agreement with the antiferromagnetic case the occupations of the singlet and triplet states tend towards equilibration and fall off algebraicly with $1/V$ for large values of the voltage.

In the antiferromagnetic case in Fig. 4.12(a) on page 71 transport is suppressed in the linear voltage regime for $eV_L < K$. Since the singlet is the ground state, all transport channels are blocked due to a finite excitation energy to a triplet state. In the ferromagnetic case with zero magnetic field, the ground state is three-fold degenerate and we find a finite current flowing even in the linear regime. In an experimental setup of two coupled quantum dots one can therefore read out from the linear conductance regime if the coupling is ferromagnetic or antiferromagnetic, see also discussion in Refs. [30, 31].

Applying a magnetic field to the double quantum dot lifts the degeneracy of the triplet ground state. The level structure of the transport region can be measured by the differential conductance as illustrated in Fig. 4.16. Note that the triplet t_+ does not block the transport in contrast to a singlet ground state, since elastic tunneling is allowed.[9]

A similar behavior can be observed in the T-matrix in the case of ferromagnetic coupling $K < 0$, as can be seen in Fig. 4.17 for $B = 0$. We find a finite value at $\omega = 0$

[9] An elastic transport process involves $\vec{S}_L^z \propto t_+^\dagger t_+$.

and a step at $\omega = |K|$. The double quantum dot system is a two-level structure with an energy gap of K both in the case of a singlet and in the case of a threefold degenerate triplet ground state. In Fig. 4.17 it can be seen that the excited singlet state becomes populated for $eV_L > |K|$, but the effect is less significant than in the antiferromagnetic case. There is also a finite transconductance in the ferromagnetic setup, but with the same argument as before the effect is less pronounced if three triplet states loose some weight to one singlet state than vice versa.

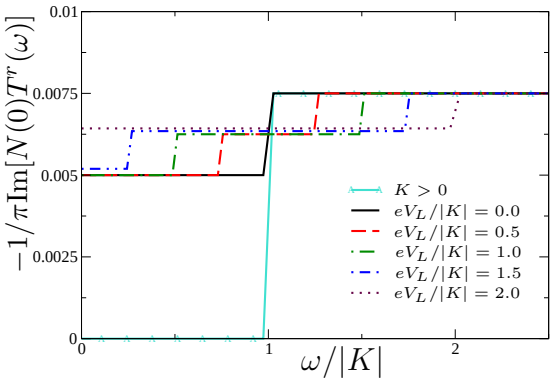

Figure 4.17: T-matrix $-1/\pi \mathrm{Im}[N(0)T^r(\omega)]$ of one of the left leads for different values of the voltage $eV_L/|K|$. For comparison the T-matrix for $V_L = 0$ and $K > 0$ is added to the graph. Parameters is this plot are $g_L = g_R = 0.1$, $T/|K| = 0.001$ and $V_R = B = 0$.

4.5 Non-Equilibrium Shot Noise

In this section we study the fluctuation of the current through one of the quantum dots. The current was studied in detail in section 4.2. More information on the nature of the transport and on the correlation between particles carrying the current can be found in the noise spectrum. After defining the noise and introducing the notations which are used in that community, we calculate the shot noise in 2nd order perturbation theory in section 4.5.2. The introduction is kept short and most of the explanations to the physical background of the noise are given in section 4.5.3 accompanied with results. Shown here are only a few results and a sorrow investigation of the whole parameter space will be the aim of future work. The introduction in section 4.5.1 is based mainly on Refs. [60] and [61].

4.5.1 Introduction to Shot Noise

The current measured in experiment is the average value of a dynamic observable that fluctuates due to finite temperatures and the stochastic nature of electron transport.

The noise in general is defined as the fluctuations of the current around its average value[10]

$$\delta I(t) = I(t) - \langle I(t) \rangle, \tag{4.22}$$

$$S(t-t') = \langle \delta I(t)\delta I(t') + \delta I(t')\delta I(t) \rangle = \langle I(t)I(t') + I(t')I(t) \rangle - 2\langle I(0) \rangle^2. \tag{4.23}$$

[10]Please note that there are different definitions for this quantity, which differ by factors of 2.

Often $S(t-t')$ is referred to as the current-current correlation function and its Fourier transform $S(\omega)$ is denoted the noise spectrum. As for the current we discuss only the stationary state, and the frequency dependent noise is determined by

$$S(\omega) = \int d(t-t')\ \mathrm{e}^{i\omega(t-t')}\ S(t-t'). \tag{4.24}$$

The noise at zero temperature $T = 0$ is commonly referred to as the shot noise. Its finite value is a consequence of the stochastic nature of the electron transport (fluctuation in the occupation number).

The noise provides information about the correlation between individual transport processes, which can not be accessed in a current measurement.

A finite temperature provides a source of noise. Fluctuations of the average occupation number for electrons are given by $f(1-f)$, where f is the Fermi distribution function. The equilibrium current ($V = 0$) is proportional to the change of the electron occupation number. The thermal noise, also denoted the Nyquist-Johnson noise, is related to the conductance $G = I/V$ via a fluctuation-dissipation theorem

$$S(\omega) = 4k_B T\ G \qquad \text{for} \qquad \hbar\omega \ll k_B T.$$

Only the shot noise provides new information about the transport process, but it has to be studied in a non-equilibrium situation with a finite applied voltage.

If successive, elementary transport processes are uncorrelated, such that the electrons are transmitted randomly and independent with a small transmission rate $T \ll 1$, then the shot noise is related to the current by

$$S = 2e\langle I\rangle.$$

This relation was found in 1918 by W. Schottky. It follows straightforward assuming that the arrival of particles obeys a Poisson statistics.

In connection with the Schottky noise the Fano factor, defined as

$$F = \frac{S}{2e\langle I\rangle}, \tag{4.25}$$

is often discussed. In the case of uncorrelated and rare transport events, the Fano factor is 1 and the shot noise is referred to as Poissonian. If $F > 1$ then the shot noise is super-poissonian, and if $F < 1$ it is called subpoissonian.

Electrons experience a repulsion by the Pauli principle, which leads in general to subpoissonian values of the Fano factor. This is derived from scattering theory in a semi-classical approach and phenomena like cotunneling are not included in this theory. There are a few cases where correlations can enhance the noise (see Ref. [62, 63]). This is discussed in detail in the results, section 4.5.3, and the physical explanations are given correspondingly.

Additionally it is observed in experiments that the noise at low frequencies generally depends inversely on the frequency f. The reviews Ref. [60, 61] claim that to this point the physics of the so-called $1/f$-noise is not fully understood.

In the next section the shot noise spectrum $S(\omega)$ is calculated to lowest order in perturbation theory. The derivation is kept short and more emphasis is put on the discussion of the results given in section 4.5.3.

4.5.2 Calculation of Shot Noise

In this section the noise in the left lead of the double quantum dot setup is calculated. Therefore we study the current-current correlation as defined in Eq. (4.23) and generalize it to the Keldysh space to be able to treat non-equilibrium situations,

$$S_L(\tau,\tau') = \langle T_c I_L(\tau) I_L(\tau')\rangle.$$

Since the noise calculation is performed only to 2nd order in the coupling, the term $\langle I(0)\rangle^2$ does not appear since the current is finite only in 2nd or higher orders. For the rest of the calculation we are interested only in the noise power,

$$S_L^>(\omega) = \int dt\ \mathrm{e}^{i\omega t}\ S_L^>(t,0),$$

and pay special attention to the shot noise $S(0)$ at frequency $\omega = 0$.

The noise in transport through the right quantum dot follows analogously and we treat only $S_L(\omega)$ since we also only discussed the current through the left quantum dot in section 4.2.

The current I_L through the left quantum dot is defined by

$$I_L(\tau) = i\frac{e}{\hbar}\left(J_{12}\vec{S}_L(\tau)\vec{s}_{12}(\tau) - J_{21}\vec{S}_L(\tau)\vec{s}_{21}(\tau)\right).$$

It is antisymmetric in the leads 1 and 2 and therefore antisymmetric with respect to the voltage V_L since $\mu_1 = -\mu_2 = eV_L/2$. The noise on the other hand is symmetric in the voltage since it is quadratic in the current.

The lowest order expectation value of the current $\langle I_L(0)\rangle_0$ is zero. Contrary the product of two current operators in the definition of the noise is finite,

$$\begin{aligned} S_L(\tau,\tau') = \left(i\frac{e}{\hbar}\right)^2 \langle T_c \Big(&J_{12}\vec{S}_L(\tau)\vec{s}_{12}(\tau) - J_{21}\vec{S}_L(\tau)\vec{s}_{21}(\tau)\Big) \\ &\Big(J_{12}\vec{S}_L(\tau')\vec{s}_{12}(\tau') - J_{21}\vec{S}_L(\tau')\vec{s}_{21}(\tau')\Big)\rangle. \end{aligned}$$

Since the derivation of the noise is similar to the calculation of the current, we state the result immediately. The calculation is given in appendix B.5. We find the result

$$S_L^>(\omega) = \frac{(2\pi)^2}{8}\frac{e^2}{h} J_{12}J_{21}\vec{T}^j_{\gamma\gamma'} n_{\gamma'} \vec{T}^i_{\gamma'\gamma} \left[\left(X_2^1\right)^<(\epsilon_\gamma - \epsilon_{\gamma'} - \hbar\omega) + \left(X_1^2\right)^<(\epsilon_\gamma - \epsilon_{\gamma'} - \hbar\omega)\right], \tag{4.26}$$

where $\vec{T}$ are the pseudo Pauli matrices of the singlet-triplet states and X_n^m the conduction electron spin susceptibilities as defined in appendix B.2.

The result in Eq. (4.26) is similar to the expression for the current as is obvious from the lowest order diagram as illustrated in Fig. 4.18. In contrast to the current there is no integration over an internal time. This has the consequence that the noise is symmetric in the voltage while the current in antisymmetric. This is seen when the summation over the pseudo particle indices is performed explicitly,

$$\begin{aligned} S_L^>(\omega) = \frac{(2\pi)^2}{8}\frac{e^2}{h} g_{12}g_{21} \big[&n_s\left(\mathcal{F}_2(K - B - \hbar\omega) + \mathcal{F}_2(K + B - \hbar\omega) + \mathcal{F}_2(K - \hbar\omega)\right) \\ &+n_{t_+}\left(\mathcal{F}_2(-K + B - \hbar\omega) + \mathcal{F}_2(B - \hbar\omega) + \mathcal{F}_2(-\hbar\omega)\right) \\ &+n_{t_0}\left(\mathcal{F}_2(-K - \hbar\omega) + \mathcal{F}_2(B - \hbar\omega) + \mathcal{F}_2(-B - \hbar\omega)\right) \\ &+n_{t_-}\left(\mathcal{F}_2(-K - B - \hbar\omega) + \mathcal{F}_2(-B - \hbar\omega) + \mathcal{F}_2(-\hbar\omega)\right)\big], \end{aligned}$$

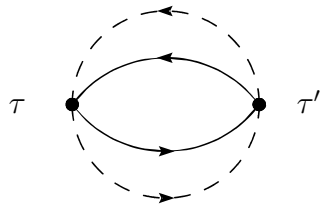

Figure 4.18: Diagram for the lowest order contribution to the shot noise $S(\tau, \tau')$ in perturbation theory. Solid line: conduction electrons, dashed line: singlet-triplet states.

where

$$\mathcal{F}_2(x) = n_B(x + eV_L)(x + eV_L) + n_B(x - eV_L)(x - eV_L).$$

The function $\mathcal{F}_2(x)$ is symmetric in the voltage,

$$\mathcal{F}_2(x) = \frac{1}{2}(x + eV_L)\coth\left(\frac{1}{2}\beta(x + eV_L)\right) + \frac{1}{2}(x - eV_L)\coth\left(\frac{1}{2}\beta(x - eV_L)\right) - x,$$

and for $V_L = 0$ it reduces to the finite value $2xn_B(x) = x(\coth(\beta x/2) - 1)$. This temperature dependent value is related to the thermal noise. From the definition of the noise in Eq. (4.23) the noise $S_L(\omega)$ consists of the sum of the greater $S_L^>(\omega)$ and lesser component $S_L^<(\omega)$ in non-equilibrium.

In the case of a vanishing magnetic field, $B = 0$, the noise is given by

$$\begin{aligned} S_L(\omega) = \frac{(2\pi)^2}{8}\frac{e^2}{h} g_{12}g_{21}3\,[&n_s\left(\mathcal{F}_2(K - \hbar\omega) + \mathcal{F}_2(K + \hbar\omega)\right) \\ &+n_t\left(\mathcal{F}_2(-K - \hbar\omega) + \mathcal{F}_2(-K + \hbar\omega)\right) \\ &+2n_t\left(\mathcal{F}_2(-\hbar\omega) + \mathcal{F}_2(\hbar\omega)\right)]\,. \end{aligned} \tag{4.27}$$

Eq. (4.27) is discussed in detail in the next section.

4.5.3 Discussion of Results for the Shot Noise

The noise is defined in terms of the current-current correlation. If the singlet is the ground state of the double quantum dot system, there is no current flowing through neither the left quantum dot nor the right quantum dot. Consequently we expect the noise to show no signal until the voltage V_L reaches the threshold K and excited triplet states allow for a transport through the left quantum dot.

This behavior is indeed observed in Fig. 4.19(a) for $B = 0$. As long as the singlet is the ground state the noise is zero and becomes finite at the energy scale of the voltage where the first triplet state is occupied. If the magnetic field B is larger than the spin-spin interaction K the triplet t_+ is the ground state of the system. In that case a finite current is flowing and the noise has a finite value as also seen in Fig. 4.19(a).

As can be seen from Fig. 4.19(a) the noise shows a similar behavior to the current in section 4.2. The Fano factor[11] shows the characteristic thermal divergence $\coth(\beta V/2)$ at small voltages. The noise is most often Poissonian, but close to the transitions between

[11] A preliminary calculation of the Fano factor can be found in appendix B.5.1.

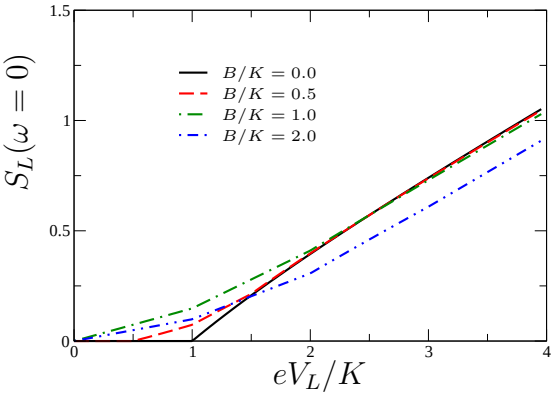

(a) Noise $S_L(\omega = 0)$ vs. eV_L/K for different values of B/K.

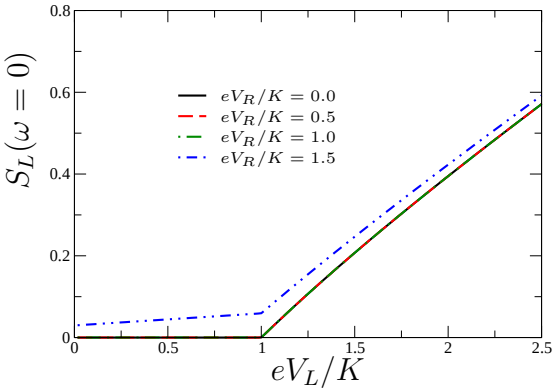

(b) Noise $S_L(\omega = 0)$ vs. eV_L/K for different values of eV_R/K.

Figure 4.19: Noise $S_L(\omega = 0)[e^3/h]$ vs. eV_L/K for finite values of the magnetic field $B/K = 0.0, 0.5, 1.0, 2.0$ and $V_R = 0$ in left panel, and dependence of $S_L(\omega = 0)$ on the voltage eV_L/K for different values of the voltage V_R applied to the right quantum dot and $B = 0$ in the right panel. The plots for $eV_R/K = 0.0, 0.5$, and 1.0 lie on top of each other. Further parameters are $g_L = g_R = 0.1$, and $T/K = 0.001$.

two pseudo particle states we observe a super-poissonian value. In analogy to Ref. [62, 63] we interpret this result as the existence of two states with finite life time. For example if the singlet state is occupied the current is 0 and if the triplet t_+ is occupied the current is finite. The measured current jumps between these two states with a time indirect proportional to the life time of the states. At low frequencies $\omega \to 0$ this enhances the noise power.

Again we observe that a non-equilibrium situation on one quantum dot has an impact on the transport through the other quantum dot. In Fig. 4.19(b) we show the noise $S_L(\omega = 0)$ for different values of the voltage V_R applied to the right quantum dot. The transconductance effect becomes visible as soon as the voltage reaches the threshold $eV_R = K$. Thus triplet states become populated and a current can flow. A finite current leads to a finite noise as observed in Fig. 4.19(b) for $eV_R/K = 1.5$.

The results given here are preliminary. Thus the calculation and interpretation of the effect of a finite voltage applied to either the left or right quantum dot and the corresponding Fano factor is the aim of future work. The study of the interplay between finite frequency noise and a finite voltage could also provide new insights into the physics of the transport through a double quantum dot system.

4.6 Current Cross-Correlation

It was observed in the previous calculations that the current flowing through the right quantum dot is correlated to the current through the left quantum dot and vice versa. In the calculation of the left current I_L the voltage V_R on the right quantum dot enters via the non-equilibrium occupation number. The non-equilibrium occupation number is a 0th order contribution and the lowest contribution to the current is of 2nd order in the coupling to the leads. Thus this current cross-correlation is so far observed indirectly. Now we study directly the correlation between the current through the left quantum dot

I_L and the current through the right quantum dot I_R. Therefore the following correlation function is investigated

$$\mathcal{D}(\tau,\tau') = \langle T_c I_L(\tau) I_R(\tau')\rangle, \tag{4.28}$$

where the currents are given by

$$\begin{aligned} I_L(\tau) &= i\frac{e}{\hbar}\left(J_{12}\vec{S}_L(\tau)\vec{s}_{12}(\tau) - J_{21}\vec{S}_L(\tau)\vec{s}_{21}(\tau)\right), \\ I_R(\tau') &= i\frac{e}{\hbar}\left(J_{34}\vec{S}_R(\tau')\vec{s}_{34}(\tau') - J_{43}\vec{S}_R(\tau')\vec{s}_{43}(\tau')\right). \end{aligned}$$

Since $\langle \vec{s}_{mn}\rangle = 0$ for $m \neq n$, both the 0th and the 1st order do not contribute to $\mathcal{D}(\tau,\tau')$. Please note that the current I_α for $\alpha = L, R$ is antisymmetric in the applied voltage V_α and therefore $\mathcal{D}$ is antisymmetric in V_L and V_R. The 2nd order term,

$$\mathcal{D}^{(2)}(\tau,\tau') = \frac{(-i)^2}{2}\int_C d\tau_1 \int_C d\tau_2 \, \langle T_c I_L(\tau) H_{\text{int}}(\tau_1) H_{\text{int}}(\tau_2) I_R(\tau')\rangle, \tag{4.29}$$

gives a finite contribution to the current cross-correlation. Since the current is already linear in the coupling to the leads the expression in Eq. (4.29) is 4th order in the Kondo coupling J.

4.6.1 Derivation of the Current Cross-Correlation

In the correlation function $\mathcal{D}$ we find that only the following terms contribute,

$$\begin{aligned} \mathcal{D}^{(2)}(\tau,\tau') = \frac{(-i)^2}{2}\left(\frac{e}{\hbar}\right)^2 \sum \int d\tau_1 \int d\tau_2 \Big\{ &\Big\langle T_c \vec{S}_L^{\,i}(\tau)\vec{S}_L^{\,i_1}(\tau_1)\vec{S}_R^{\,j_2}(\tau_2)\vec{S}_R^{\,j}(\tau') \\ &\left[\left(J_{12}\vec{s}_{12}^{\,i}(\tau) - J_{21}\vec{s}_{21}^{\,i}(\tau)\right) J_{mn}\vec{s}_{mn}^{\,i_1}(\tau_1)\right] \\ &\left[J_{MN}\vec{s}_{MN}^{\,j_2}(\tau_2)\left(J_{34}\vec{s}_{34}^{\,j}(\tau') - J_{43}\vec{s}_{43}^{\,j}(\tau')\right)\right]\Big\rangle \\ + \Big\langle T_c \vec{S}_L^{\,i}(\tau)\vec{S}_R^{\,j_1}(\tau_1)\vec{S}_L^{\,i_2}(\tau_2)\vec{S}_R^{\,j}(\tau') \\ &\left[\left(J_{12}\vec{s}_{12}^{\,i}(\tau) - J_{21}\vec{s}_{21}^{\,i}(\tau)\right) J_{MN}\vec{s}_{MN}^{\,i_2}(\tau_2)\right] \\ &\left[J_{mn}\vec{s}_{mn}^{\,j_1}(\tau_1)\left(J_{34}\vec{s}_{34}^{\,j}(\tau') - J_{43}\vec{s}_{43}^{\,j}(\tau')\right)\right]\Big\rangle\Big\}, \end{aligned}$$

where the sum goes over all indices. By changing the summation indices, it can be shown that the second term is identical to the first term. This cancels the prefactor of $\frac{1}{2}$ from the perturbative expansion.

Conduction Electron Contribution

We define two different conduction electron contributions, one for the left quantum dot

$$\begin{aligned} \chi_L(\tau,\tau_1) &= \left\langle T_c\left[\left(J_{12}\vec{s}_{12}^{\,i}(\tau) - J_{21}\vec{s}_{21}^{\,i}(\tau)\right) J_{mn}s_{mn}^{i_1}(\tau_1)\right]\right\rangle \\ &= \frac{1}{4}J_{12}J_{21}\vec{\tau}_{\sigma'\sigma}^{\,i}\vec{\tau}_{\sigma\sigma'}^{\,i_1}\left(G_{2k\sigma}(\tau,\tau_1)G_{1k'\sigma'}(\tau_1,\tau) - G_{1k'\sigma'}(\tau,\tau_1)G_{2k\sigma}(\tau_1,\tau)\right), \end{aligned} \tag{4.30}$$

and one for the right quantum dot,

$$\begin{aligned}\chi_R(\tau', \tau_2) &= \left\langle T_c \left[J_{MN} s^{j_2}_{MN}(\tau_2) \left(J_{34} \vec{s}^{\,j}_{34}(\tau') - J_{43} \vec{s}^{\,j}_{43}(\tau') \right) \right] \right\rangle \\ &= \frac{1}{4} J_{34} J_{43} \vec{\tau}^{\,j}_{s's} \vec{\tau}^{\,j_2}_{ss'} \left(G_{4ps}(\tau', \tau_2) G_{3p's'}(\tau_2, \tau') - G_{3p's'}(\tau', \tau_2) G_{4ps}(\tau_2, \tau') \right). \quad (4.31)\end{aligned}$$

Both terms are polarization bubbles and the calculation is given in appendix B.2. Please note the special asymmetry of these bubbles,

$$\chi_L(\tau, \tau_1) = -\chi_L(\tau_1, \tau), \quad (4.32)$$

$$\chi_R(\tau', \tau_2) = -\chi_R(\tau_2, \tau'), \quad (4.33)$$

which reflects the antisymmetry with respect to the voltage $eV_L = \mu_1 - \mu_2$ and $eV_R = \mu_3 - \mu_4$.

Thus the correlation function can be expressed by

$$\mathcal{D}^{(2)}(\tau, \tau') = -\left(2\pi \frac{e}{h}\right)^2 \int d\tau_1 \int d\tau_2 \left\langle T_c \vec{S}^i_L(\tau) \vec{S}^{i_1}_L(\tau_1) \vec{S}^{j_2}_R(\tau_2) \vec{S}^j_R(\tau') \right\rangle \chi_L(\tau, \tau_1) \chi_R(\tau', \tau_2). \quad (4.34)$$

The physics of a coupled double quantum dot system manifests itself in a finite expectation value of the left and right impurity spins in Eq. (4.34).

Double Quantum Dot Contribution

The conduction electrons of the left and the right leads are decoupled, thus the only mediation of a current cross-correlation is via the spin-spin interaction K. We calculate

$$\langle T_c \vec{S}^i_L(\tau) \vec{S}^{i_1}_L(\tau_1) \vec{S}^{j_2}_R(\tau_2) \vec{S}^j_R(\tau') \rangle \quad (4.35)$$

in the singlet-triplet representation. Eq. (4.35) is explicitly written down in appendix B.6.

In general Eq. (4.35) gives 24 different contributions without taking the pseudo particle constraint into account. The projection mechanism as explained in section 2.1 projects out all diagrams with a product of two or more occupation numbers, since they correspond to unphysical states. Using this projection all diagrams with two independent pseudo particle loops can be neglected. The singlet-triplet states are pseudo bosonic states and the setup allows only for transitions between them; it is not possible to create two singlet and triplet states in the double quantum dot system and thus two independent loops are unphysical. For example the contribution from $\langle I_L \rangle_\lambda \langle I_R \rangle_\lambda$[12] does not have to be taken into account since it consists of two independent diagrams.

After the projection six different diagrams remain which contribute to the current cross-correlation. We divide them into two groups:

- two "vertex", or "virtual interaction", diagrams (see section 4.6.2)
- four "self energy" diagrams (see section 4.6.3)

[12] In contrast, the product of $\langle I_L \rangle_{Q=1} \langle I_R \rangle_{Q=1}$ is finite since the projection already took place.

We will furthermore simplify the calculation by assuming, that either the spin symmetry ($B = 0$) or the left-right symmetry ($g_L = g_R$) is fulfilled, such that all pseudo particle Green's functions are diagonal. It is also assumed that the pseudo particle Green's functions can be represented by the ansatz $G^<_\gamma(\omega) = in^\lambda_\gamma A_\gamma(\omega)$ and $G^r_\gamma(\omega) - G^a_\gamma(\omega) = -iA_\gamma(\omega)$, where $A_\gamma(\omega) = 2\pi\delta(\omega - \epsilon_\gamma)$.

For a shorter notation the function $d(\tau, \tau')$ is introduced which corresponds to the correlation function without the prefactor,

$$\mathcal{D}(\tau, \tau') = -\left(2\pi\frac{e}{h}\right)^2 d(\tau, \tau').$$

Before performing the spin index summation, the Green's function structure on the Keldysh contour is worked out. In the following the lesser correlation function,

$$\mathcal{D}^<(t, t') = \mathcal{D}^{12}(t, t'),$$

is studied. This implies that $\tau \to t$ is on the upper contour (1) and $\tau' \to t'$ is on the lower contour (2). The two contour times τ_1 and τ_2 can be either on the upper or lower contour, and all four possibilities have to be taken into account. Note that a vertex on the lower contour (2) is accompanied by a minus sign.

Since it is easier to do the calculation with retarded and advanced Green's functions than with time-ordered and anti-time-ordered Green's functions the following equalities are utilized (compare section 3.1),

$$G^{11}(t, t') = G^r(t, t') + G^<(t, t'), \tag{4.36}$$
$$G^{22}(t, t') = G^<(t, t') - G^a(t, t'). \tag{4.37}$$

Furthermore we use that the system of four Keldysh Green's functions is over-determined and express the greater Green's function $G^>$ in terms of the lesser Green's function $G^<$,

$$G^{21}(t, t') = G^>(t, t') = G^<(t, t') + G^r(t, t') - G^a(t, t'). \tag{4.38}$$

Please note, that the pseudo particle constraint allows only for one lesser Green's function in the whole expression. A product of two lesser Green's functions is immediately proportional to $e^{-2\beta\lambda}$ and will be projected out in any calculation of a physical observable (see section 2.1 for an explanation of the pseudo particle projection [42, 43]).

4.6.2 Contributions from the "Vertex" Diagrams

The two diagrams, which are denoted as "vertex" diagrams, are summarized in Fig. 4.20. An electron-hole pair in the left leads, $\chi_L(\tau, \tau_1)$, travels between the times τ and τ_1, while another electron-hole pair in the right leads, $\chi_R(\tau', \tau_2)$ propagates independently between times τ' and τ_2. The current cross-correlation is finite due to a closed loop of four singlet-triplet scattering processes with the leads. In the "vertex" diagram such a series of processes consists of a pseudo particle interacting with the left leads, then the right leads, again with a left lead and finally with the right leads.

We call these diagrams "vertex" diagrams, since they contain the structure of a vertex correction, which is illustrated in Fig. 4.21(a). The diagram in Fig. 4.20 is produced when

Figure 4.20: Diagrams for the so-called "vertex" contributions to the current cross-correlation. Solid lines: conduction electrons, dashed line: singlet and triplet states.

(a) Diagram for a vertex correction.

(b) Diagram for effective or "virtual" spin-spin interaction.

Figure 4.21: Schematic diagrams for a vertex contribution (left panel) and for an effective interaction (right panel). Dashed lines represent pseudo particles and solid lines stand for conduction electrons.

the external legs of a renormalized vertex are closed with an additional pure interaction vertex at a fourth time.

Alternatively one could also interpret the diagrams in Fig. 4.20 as a "virtual" interaction $\vec{S}_L\vec{S}_L$ or $\vec{S}_R\vec{S}_R$ mediated over the conduction electrons in the respective leads. A combination of two "virtual" interactions of the type of Fig. 4.21(b) produces the current cross-correlation diagrams in Fig. 4.20.

There are two different "vertex" diagrams as illustrated in Fig. 4.20. The full calculation can be found in appendix B.6.2. Here we show only the result of one of the two "vertex" diagrams d_v since the other one gives a similar but time-reserved expression.

From one "vertex" diagram we find the following contribution to the current cross-correlation

$$\begin{aligned} d_v^<(\omega) =& \frac{1}{16}\left(\vec{T}_L^i\right)_{\gamma'\gamma} n_\gamma \left(\vec{T}_R^j\right)_{\gamma g}\left(\vec{T}_L^{i_1}\right)_{g\gamma_1}\left(\vec{T}_R^{j_2}\right)_{\gamma_1\gamma'} \\ & \int\frac{d\tilde{\omega}}{2\pi}\Big\{G^r_{\gamma_1}(\tilde{\omega}+[\omega-\epsilon_\gamma+\epsilon_g])G^r_{\gamma'}(\tilde{\omega})\chi_L^{11}(\tilde{\omega}-\epsilon_\gamma+\omega)\chi_R^>(-\omega+\epsilon_\gamma-\epsilon_g) \\ & \quad + G^a_g(-\tilde{\omega}+[-\omega+\epsilon_\gamma+\epsilon_{\gamma_1}])G^r_{\gamma'}(\tilde{\omega})\chi_L^<(\tilde{\omega}-\epsilon_\gamma+\omega)\chi_R^>(\tilde{\omega}-\epsilon_{\gamma_1}) \\ & \quad + G^a_g(\tilde{\omega})G^a_{\gamma_1}(\tilde{\omega}+[\omega-\epsilon_\gamma+\epsilon_{\gamma'}])\chi_L^<(\omega-\epsilon_\gamma+\epsilon_{\gamma'})\chi_R^{22}(-\tilde{\omega}+\epsilon_\gamma-\omega)\Big\}\,. \end{aligned}$$

Note that each of the three terms has the residual of the retarded or advanced Green's function on the same half plane. The integration can thus be closed over the other half plane and the integral is zero if we assume that χ_L and χ_R do not have residuals.[13] The contribution from d_v to the current cross-correlation is negligibly small.

The purpose of calculating a current cross-correlation was to find a direct coupling between the current through the left quantum dot and the current through the right quantum dot. In previous sections we found that there is e.g. a finite transconductance

[13] See therefore also discussion of vertex diagrams in Ref. [41].

due to the decoherence of the pseudo particle states, which is created by a finite current in a finite voltage situation. The "vertex" diagram contribution to the current cross-correlation was discussed to be negligible. This could be understood from the structure of the interaction, see Fig. 4.20. A pseudo particle which interacts with an electron-hole pair in the left leads at time τ, creates another electron-hole pair in the right leads at time τ_2 before an interaction and recombination of the left electron-hole pair takes place at time τ_1. Finally the electron hole-pair in the right leads recombines with the initial and final pseudo particle. No decoherent processes took place in this series of events.

Although a vertex is usually associated with decoherence, the process explained here is not sufficient to find a non-zero current cross-correlation in lowest order. We expect diagrams in higher order perturbation theory to have a finite contribution.

4.6.3 Contributions from the "Self Energy" Diagrams

Since the first two diagrams were shown to give only a negligible contribution to the current cross-correlation we concentrate now on the remaining contributions. The diagrams in Fig. 4.22, denoted as "self energy" diagrams, consist of two different types with each a time-reversed partner. In contrast to the "vertex" diagrams a pseudo particle creates and recombines with an electron hole pair e.g. in the left leads in the course of two interaction processes before an interaction with the right leads takes place. These diagrams are therefore more promising to give a finite contribution for the decoherent correlation effect we want to describe. It is observed that every diagram shows a combi-

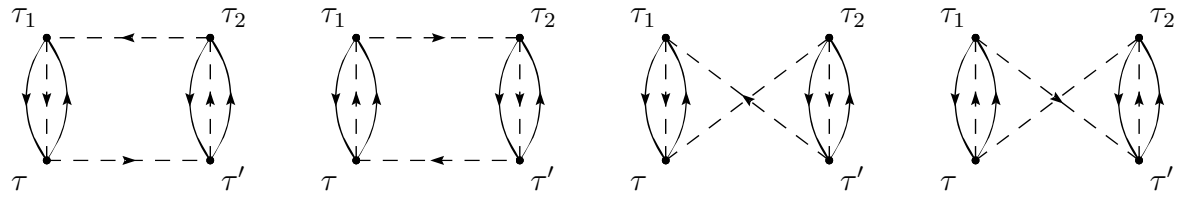

Figure 4.22: Diagrams for the so-called "self energy" contributions to the current cross-correlation. Solid lines: conduction electrons; dashed lines: double quantum dot states.

nation of $\chi_\alpha(\tau,\tau_i)G(\tau,\tau_i)$. The "self energy" like structure $\mathcal{S}$ is defined for the left and right leads, respectively, by

$$(\mathcal{S}_L)_{\gamma'\gamma_1}(\tau,\tau_1) = \frac{1}{4}\left(\vec{T}_L^{i}\right)_{\gamma'\gamma} G_\gamma(\tau,\tau_1)\left(\vec{T}_L^{i_1}\right)_{\gamma\gamma_1}\chi_L(\tau,\tau_1), \tag{4.39}$$

$$(\mathcal{S}_R)_{g'\gamma_2}(\tau',\tau_2) = \frac{1}{4}\left(\vec{T}_R^{j}\right)_{g'g} G_g(\tau',\tau_2)\left(\vec{T}_R^{j_2}\right)_{g\gamma_2}\chi_R(\tau',\tau_2). \tag{4.40}$$

The function $\mathcal{S}_\alpha$ for $\alpha = L,R$ is strictly speaking not a self energy. The diagram looks similar, but $\mathcal{S}_\alpha$ contains only electron-hole pairs in two different leads, e.g. 1 and 2 for $\alpha = L$, and no processes within the same lead. In addition, the function $\mathcal{S}_\alpha$ is antisymmetric with respect to the voltage V_α or an exchange of the lead indices 1 and 2, which originates from the antisymmetry of χ_α (see Eqs. (4.32) and (4.33)).

As every function in Keldysh space the function $\mathcal{S}_\alpha$ fulfills for example $\mathcal{S}_\alpha^> - \mathcal{S}_\alpha^< = \mathcal{S}_\alpha^r - \mathcal{S}_\alpha^a$. It is important to notice that

$$\mathcal{S}_\alpha^<(t_i,t_j) = \frac{1}{4}\vec{T}\,\mathcal{G}^<(t_i,t_j)\,\vec{T}\,\chi_\alpha^<(t_i,t_j)$$

Figure 4.23: Diagram of the "self energy" like structure $\mathcal{S}$.

is proportional to the lesser Green's function and therefore proportional to $e^{-\beta\lambda}$ in the pseudo particle constraint.

The result of the current cross-correlation $\mathcal{D}$ is given by the sum of all diagrams in Fig. 4.22. The calculation can be found in appendix B.6.3. In the result we distinguish between two different kind of contributions, d_{s0} and d_s. In d_{s0} all terms that cancel each other at zero frequency $\omega = 0$ are collected,

$$\begin{aligned} d_{s0}^{<}(\omega) = \int \frac{d\tilde{\omega}}{2\pi} \big\{ & \left[\mathcal{S}_L^{11}(\tilde{\omega}+\omega) - \mathcal{S}_L^{11}(\tilde{\omega})\right] \\ & \times \left[\mathcal{G}^{12}(\tilde{\omega}+\omega)\mathcal{S}_R^{21}(\tilde{\omega})\mathcal{G}^{11}(\tilde{\omega}) - \mathcal{G}^{11}(\tilde{\omega}+\omega)\mathcal{S}_R^{12}(\tilde{\omega}+\omega)\mathcal{G}^{21}(\tilde{\omega})\right] \\ & + \left[\mathcal{S}_R^{22}(\tilde{\omega}+\omega) - \mathcal{S}_R^{22}(\tilde{\omega})\right] \\ & \times \left[\mathcal{G}^{22}(\tilde{\omega})\mathcal{S}_L^{21}(\tilde{\omega})\mathcal{G}^{12}(\tilde{\omega}+\omega) - \mathcal{G}^{21}(\tilde{\omega})\mathcal{S}_L^{12}(\tilde{\omega}+\omega)\mathcal{G}^{22}(\tilde{\omega}+\omega)\right] \\ & - \left[\mathcal{S}_L^{11}(\tilde{\omega}+\omega) - \mathcal{S}_L^{11}(\tilde{\omega})\right]\mathcal{G}^{12}(\tilde{\omega}+\omega) \\ & \times \left[\mathcal{S}_R^{22}(\tilde{\omega}) - \mathcal{S}_R^{22}(\tilde{\omega}+\omega)\right]\mathcal{G}^{21}(\tilde{\omega})\big\}\,. \end{aligned}$$

In d_s there are only two contributions from the "self energy" diagrams, which are finite in the case of $\omega = 0$,

$$\begin{aligned} d_s^{<}(\omega) &= \int \frac{d\tilde{\omega}}{2\pi} \big\{ -\mathcal{S}_L^{12}(\tilde{\omega}+\omega)\mathcal{G}^{22}(\tilde{\omega}+\omega)\mathcal{S}_R^{21}(\tilde{\omega})\mathcal{G}^{11}(\tilde{\omega}) \\ &\qquad -\mathcal{S}_L^{21}(\tilde{\omega})\mathcal{G}^{11}(\tilde{\omega}+\omega)\mathcal{S}_R^{12}(\tilde{\omega}+\omega)\mathcal{G}^{22}(\tilde{\omega})\big\} \\ &\approx \int \frac{d\tilde{\omega}}{2\pi} \{\mathcal{S}_L^{<}(\tilde{\omega}+\omega)\mathcal{G}^{a}(\tilde{\omega}+\omega)\mathcal{S}_R^{>}(\tilde{\omega})\mathcal{G}^{r}(\tilde{\omega}) \\ &\qquad +\mathcal{S}_L^{>}(\tilde{\omega})\mathcal{G}^{r}(\tilde{\omega}+\omega)\mathcal{S}_R^{<}(\tilde{\omega}+\omega)\mathcal{G}^{a}(\tilde{\omega})\}\,. \end{aligned}$$

It should be noticed that these two finite contributions originate solely from the two right diagrams in Fig. 4.22.

Finally we can write down the result for the current cross-correlation $\mathcal{D}(\omega)$ in the zero frequency limit[14],

$$D^{<}(\omega \to 0) = -\frac{e^2}{h}\int d\tilde{\omega}\mathrm{Tr}\left[\mathcal{S}_L^{<}(\tilde{\omega})\mathcal{G}^{a}(\tilde{\omega})\mathcal{S}_R^{>}(\tilde{\omega})\mathcal{G}^{r}(\tilde{\omega}) + \{L \leftrightarrow R\}\right]. \tag{4.41}$$

Please note that this is a general result that can be applied to any quantum dot setup with a pseudo Pauli matrix. For the rest of this section Eq. (4.41) is worked out in the case of two coupled quantum dots.

[14]The result is corrected by a factor of $\hbar$ since the frequency ω is treated implicitly as an energy $\hbar\omega$.

4.6.4 Calculation of $D^<(\omega = 0)$

If the ansatz $G_\gamma = -in_\gamma A_\gamma(\omega)$ is used and $\mathcal{S}^>_\alpha \approx \mathcal{S}^r_\alpha - \mathcal{S}^a_\alpha$ is approximated due to the pseudo-particle projection, we find the two expressions

$$(\mathcal{S}_L)^<_{\gamma'\gamma_1}(\tilde{\omega}) = \frac{1}{4} i \left(\vec{T}^i_L\right)_{\gamma'\gamma} n_\gamma \chi^<_L(\tilde{\omega} - \epsilon_\gamma) \left(\vec{T}^{i_1}_L\right)_{\gamma\gamma_1},$$
$$(\mathcal{S}_R)^>_{g'\gamma_2}(\tilde{\omega}) \approx \frac{1}{4} i \left(\vec{T}^j_R\right)_{g'g} \chi^<_R(\epsilon_g - \tilde{\omega}) \left(\vec{T}^{j_2}_R\right)_{g\gamma_2}.$$

For the explicit calculation of χ_α we refer to section B.2. In frequency space the expression gives,

$$\chi^<_L(\tilde{\omega}) = -2\frac{2\pi}{4} g_{12} g_{21} \left(n_B(\tilde{\omega} + eV_L)(\tilde{\omega} + eV_L) - n_B(\tilde{\omega} - eV_L)(\tilde{\omega} - eV_L)\right), \tag{4.42}$$
$$\chi^<_R(\tilde{\omega}) = -2\frac{2\pi}{4} g_{34} g_{43} \left(n_B(\tilde{\omega} + eV_R)(\tilde{\omega} + eV_R) - n_B(\tilde{\omega} - eV_R)(\tilde{\omega} - eV_R)\right), \tag{4.43}$$

where $eV_L = \mu_1 - \mu_2$ and $eV_R = \mu_3 - \mu_4$. The factor of 2 originates from the spin summation and the dimensionless couplings $g = N(0)J$ is used. The Bose distribution function $n_B(x) = 1/(\mathrm{e}^{-\beta x} - 1)$ is singular at $x = 0$, but the product $xn_B(x)$ is finite and in the limit of $x/T \ll 1$ it can be approximated by

$$xn_B(x) = \begin{cases} 0 & \text{if } x > 2T \\ T - \frac{1}{2}x & \text{if } |x| < 2T \\ |x| & \text{if } x < -2T \end{cases}. \tag{4.44}$$

Consequently $\chi^<_L(\tilde{\omega} - \epsilon_\gamma)$ in $\mathcal{S}^>_L(\tilde{\omega})$ provides an upper cutoff and $\chi^<_R(\epsilon_g - \tilde{\omega})$ in $\mathcal{S}^>_R(\tilde{\omega})$ provides a lower cutoff for the integration over the frequency $\tilde{\omega}$ in Eq. (4.41). The cutoff is determined by system parameters like the voltages V_L and V_R, the singlet-triplet gap K, the temperature T, and in general the magnetic field B. In the following it is assumed, that there is no magnetic field $B = 0$. Thus the self energy, and hence also the function $\mathcal{S}$, is a diagonal matrix.

In this case the trace in Eq. (4.41) can be carried out and yields

$$D^<(\omega = 0) = \frac{e^2}{h}\frac{3}{16}\int d\tilde{\omega} \left[3n_t \chi^<_L(\tilde{\omega} - \epsilon_t)\mathcal{G}^a_s(\tilde{\omega})\chi^<_R(\epsilon_t - \tilde{\omega})\mathcal{G}^r_s(\tilde{\omega}) + s^<_L(\tilde{\omega})\mathcal{G}^a_t(\tilde{\omega})s^>_R(\tilde{\omega})\mathcal{G}^r_t(\tilde{\omega}) + \{L \leftrightarrow R\}\right], \tag{4.45}$$

where

$$s^<_L(\tilde{\omega}) = n_s \chi^<_L(\tilde{\omega} - \epsilon_s) + 2n_t \chi^<_L(\tilde{\omega} - \epsilon_t),$$
$$s^>_R(\tilde{\omega}) = \chi^<_R(\epsilon_s - \tilde{\omega}) + 2\chi^<_R(\epsilon_t - \tilde{\omega}).$$

For the derivation of this expression we used that the spectral function $A_\gamma(\omega)$ is a δ-function in the calculation of $\mathcal{S}_L$ and $\mathcal{S}_R$. This implies, that the pseudo particle Green's functions were so far used in the lowest, unperturbed order.

0th order retarded Green's functions

If we attempt to calculate the integral in Eq. (4.45) with the unperturbed pseudo particle Green's functions $G^{r/a}(\tilde{\omega}) = 1/(\tilde{\omega} - \epsilon_\gamma \pm i\eta)$, we encounter a divergence. η is an infinitesimally small convergence factor. The limit $\eta \to 0$ sends the width of the pseudo particle resonance to zero. Thus the spectral function is a δ-function and the life time of the particles is infinite. Without a coupling to the leads this assumption is justified.

The product $G^r_\gamma(\tilde{\omega})G^a_\gamma(\tilde{\omega})$, can be expressed by the spectral function $A_\gamma(\tilde{\omega})$ by

$$G^r_\gamma(\tilde{\omega})G^a_\gamma(\tilde{\omega}) = \frac{1}{\tilde{\omega} - \epsilon_\gamma + i\eta}\frac{1}{\tilde{\omega} - \epsilon_\gamma - i\eta} = \frac{1}{2i\eta}\frac{2i\eta}{(\tilde{\omega} - \epsilon_\gamma)^2 + \eta^2} = \frac{1}{2\eta}A_\gamma(\tilde{\omega}).$$

The limit of the life time $1/\eta$ to infinity has to be taken after the integration over $\tilde{\omega}$ of the spectral function $A_\gamma(\tilde{\omega})$ in Eq. (4.45). Consequently the expression for the current cross-correlation diverges. We suspect that this problem is correlated with the discussions in Ref. [63, 62]. A related work which derives cross-correlations in a three-terminal setup can be found in Ref. [64]. It is the aim of future work to study the current cross-correlation in more detail, especially also for finite frequencies $\omega \neq 0$.

2nd order retarded Green's functions

It is therefore important to include the finite life time of the pseudo particle states into the calculation. If a finite broadening of the retarded and advanced self energy is assumed, e.g. from the second order self energy, we find

$$G^r_\gamma(\tilde{\omega})G^a_\gamma(\tilde{\omega}) = \frac{1}{\Sigma^r_\gamma(\tilde{\omega}) - \Sigma^a_\gamma(\tilde{\omega})}\left(G^r_\gamma(\tilde{\omega}) - G^a_\gamma(\tilde{\omega})\right) = \frac{1}{\Gamma_\gamma(\tilde{\omega})}A_\gamma(\tilde{\omega}),$$

where the broadening due to the leads is given by $\Gamma_\gamma(\tilde{\omega}) = i(\Sigma^r_\gamma(\tilde{\omega}) - \Sigma^a_\gamma(\tilde{\omega}))$ and the spectral function $A_\gamma(\tilde{\omega})$ is thus a Lorentzian of width Γ_γ. A broadening is always present for finite temperatures and finite voltages.

As in all previous calculations it is assumed, that the broadening of the spectral function is smaller than other system parameters, e.g. the singlet-triplet energy gap K, and that all the other functions vary on a slower energy scale than the spectral function. Then we can approximate the Lorentzian inside the integration by a δ-function.

Using these considerations in Eq. (4.45) we find the result for the current cross-correlation in the zero-frequency limit,

$$D^<(\omega = 0) = 2\pi\frac{e^2}{h}\frac{3}{16}\left[\frac{(2n_t\ \chi^<_L(0) + n_s\ \chi^<_L(K))\,(2\chi^<_R(0) + \chi^<_R(-K))}{\Gamma_t(\epsilon_t)} + 3n_t\frac{\chi^<_L(-K)\chi^<_R(K)}{\Gamma_s(\epsilon_s)} + \{L \leftrightarrow R\}\right]. \tag{4.46}$$

Including the hybridization of the double quantum dot states with the leads, a finite current cross-correlation exists.

4.6.5 Discussion of Results for the Current Cross-Correlation

The current cross-correlation was calculated in Eq. (4.45) to fourth order in perturbation theory. It was found that the expression diverges if the life time of the particles is

assumed to be infinite and thus a finite broadening Γ of the spectral function was included in the calculation, Eq. (4.46). Since Γ is calculated to 2nd order in the perturbation theory, the result of the current cross-correlation in Eq. (4.46) is effectively of 2nd order in the perturbation theory.[15]

In Fig. 4.24 it is shown that there is a non-zero current cross-correlation. Since the current $I_R(V_R = 0) = 0$ is always zero, we find in the case of $V_R = 0$ a trivial result $\langle I_L I_R \rangle = 0$ for all V_L. As long as the voltage $V_R > 0$ applied to the right quantum dot is below the threshold $eV_R < K$, the current cross-correlation $D^<(\omega = 0)$ also shows a threshold behavior. After either the voltage V_R or the voltage V_L reaches the threshold, there is enough energy in the system to populate triplet states. A finite occupation of triplet states opens the possibility to have a current through both quantum dots, and the current cross-correlation $\langle I_L I_R \rangle$ becomes finite, see Fig. 4.24.

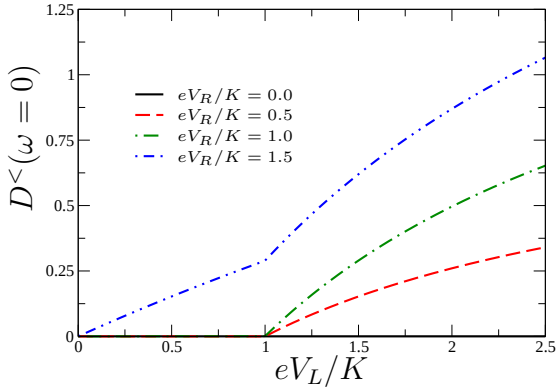

Figure 4.24: Dependence of the current cross-correlation $D^<(\omega = 0)$ on the voltage eV_L/K if the voltage eV_R/K applied to the right quantum dot is varied. $D^<(\omega = 0) \equiv 0$ for $V_R = 0$ as explained in the text. Further parameters are $g_L = g_R = 0.1$, $T/K = 0.001$, and $B = 0$.

In the previous section we observed a correlation between the current in the left quantum dot and the voltage applied to the right (see discussion of the transconductance in section 4.2), mediated by the voltage-dependence of the non-equilibrium occupation numbers. The purpose of this section was to find a quantity which shows the correlation directly. Strikingly we did not find a direct correlation between the current through the left and the right quantum dot. The result as it is shown in Fig. 4.24 is non-zero due to a finite life time of the pseudo particle states. As in the case of the transconductance the decoherence is the driving force out of equilibrium. The same transition rates are involved in the self-consistent equation for the non-equilibrium distribution functions and in the finite life time for the singlet and triplet states in the calculation of $D^<(\omega = 0)$. Both dI_L/dV_R and $\langle I_L I_R \rangle$ are non-zero in 2nd order perturbation theory and both are strongly connected to a non-equilibrium situation, where a voltage larger than a threshold is applied.

4.7 Summary and Outlook

This chapter was devoted to results for selected physical properties of a double quantum dot setup in lowest order perturbation theory. As will be discussed in the following

[15] Schematically one can say: $\chi_L \cdot \chi_R/\Gamma \propto g^2 \cdot g^2/g^2 \propto g^2$.

chapters the perturbation theory fails at low temperatures and new methods to cope with this problem are introduced. Some of the physical insights we achieved from the discussion in this chapter are included in the approaches further on.

The most important finding from non-equilibrium perturbation theory is the dependence of the singlet and triplet occupation numbers on the current through, or the voltage across, the double quantum dot system. This dependence originates from finite decoherence rates due to a hybridization with the leads, but since the 2nd order rates are used in a self-consistent equation the effect on the occupation probability is to 0th order in the perturbative expansion. A finite voltage can, like a finite temperature, provide the energy to excite states above the ground state. Thermodynamic properties like the polarization or magnetization (see section 4.1) fall off inversely proportional to the voltage V, similar to a Curie-law with an effective temperature.

This has an immediate effect on the current characteristic. For two antiferromagnetically coupled quantum dots the ground state is a singlet and as explained before (see section 2.1 or 4.2) all transport channels are blocked due to a finite excitation gap to the triplet states. A finite voltage applied to the left or right quantum dot can provide sufficient energy to occupy the excited triplet states and thus allow a finite current. We discussed in detail in section 4.2 the quantity $(K/eV_L)dI_L/dV_R$, referred to as transconductance. The transconductance is non-zero in a non-equilibrium situation solely due to the discussed non-equilibrium distribution functions. Since the current is a quantity which is easily accessible in experiments, there is the possibility that by a measurement of the transconductance also the voltage-dependence of the level distributions can be probed.

In this chapter also the T-matrix as in the scattering problem for conduction electrons was discussed and we found an effect similar to the transconductance. We studied the case of a ferromagnetic coupling between the two quantum dots and found a different current characteristic than for an antiferromagnetic coupling. This allows to distinguish between the ferro- and antiferromagnetic case in an experiment and the magnitude of the singlet-triplet gap can be read off from the peak structure in the differential conductance. It was discussed that the transconductance is less significant in the ferromagnetic case, since the triplet ground state does not block the transport like the singlet ground state in the antiferromagnetic case.

Finally we studied certain current-current correlations. The shot noise, i.e. the current-current correlation $\langle I_L I_L \rangle$, as found in section 4.5 is Poissonian, i.e. proportional to the current since the tunneling events which lead to the transport are uncorrelated. Consequently we can observe the same effect in the noise as found in the current. More thorough investigations are needed to understand the result of the current cross-correlation in section 4.6. We find that $\langle I_L I_R \rangle$ is finite if one of the voltages eV_L or eV_R is larger than the threshold K. Although the calculation is done to 4th order perturbation theory, the result is effectively proportional to 2nd order in the coupling J. Therefore the observation of a finite current cross-correlation is, as the transconductance, an indirect effect, which originates from the finite life time of the singlet and triplet states due to a hybridization with the leads. To measure the noise in experiment is difficult because of the small values of the order of e^3/h. We hope that the current cross-correlation is more easily accessible in experiments since it involves two current measurements and not the measurement of fluctuations around the mean value of the current.

The appearance of a non-zero transconductance is by now well understood and using the perturbative RG method it was published in Ref. [65]. By contrast the interpretation of the noise and the current cross-correlation needs more thorough investigations, but the preliminary results shown here are promising. It is the aim of future work to study these quantities also at finite frequencies $\omega \neq 0$. Recently a new experimental setup was presented and current cross-correlation were measured for a double quantum dot system at the charge degeneracy point [66, 67]. Since this setup is similar to the model studied here we hope that the measurement of a current cross-correlation will soon be realized in experiments.

In conclusion, we found for several physical quantities that the spin-spin interaction K in a double quantum dot setup can transfer a non-equilibrium situation from one quantum dot to another quantum dot, which is not subject to a large voltage.

5 Perturbative Renormalization Group

The perturbative treatment of the Kondo model fails at low temperatures. The physical concept of a perturbative renormalization group (RG) theory is explained in section 5.1. We spend some time on motivating the origin of the renormalization group (RG) equation out of equilibrium in section 5.2. The difference to equilibrium properties is discussed and the frequency dependent flow of the couplings is derived in section 5.3.

The non-equilibrium occupation numbers were shown to play an important role in the perturbation theory (chapters 3 and 4) and are discussed in the framework of perturbative RG in section 5.4. An emphasis is put on the effect of a finite decoherence that appears due to a finite voltage across or a finite current through one quantum dot. As an example of a measurable quantity the current is discussed in section 5.5 and we show that the transconductance is not only non-zero but also enhanced by the scaling. To compare the result of the rescaled T-matrix with the result from numerical renormalization group (NRG) is an ongoing project. A discussion of this subject is found in section 5.6. Finally the case of ferromagnetic coupling between the two quantum dots is discussed in section 5.7 and it is illustrated why this case reaches the limits of the perturbative RG out of equilibrium.

5.1 Introduction

The enhancement of the resistivity found in some metals with magnetic impurities was first explained by Jun Kondo [1] using perturbation theory. The T-Matrix (see section 4.3), which can be used to calculate transport, shows a logarithmic enhancement at low temperatures. This logarithmic behavior is one of the major features of the Kondo interaction $H_{\text{int}} = J\vec{S}\vec{s}$ between the impurity spin and the conduction electron spin, but the divergence is not physical. Due to a factor of $\ln(D/T)$ the contribution from 3rd order perturbation theory becomes larger than the 2nd order at low temperatures indicating the break-down of perturbation theory. By contrast experiments show, that after a logarithmic increase the resistivity saturates again at even lower temperatures below the so-called Kondo temperature T_K. This behavior can not be explained using perturbation theory.

By now the physical background of the Kondo divergence is well established. The spin of the conduction electrons $\vec{s}$ scatters with the impurity spin $\vec{S}$. The resistivity increases at lower temperatures when the impurity spin becomes localized. Due to a series of coherent scattering processes a screening cloud forms around the impurity which can be seen as a sharp resonance of the density of states at the Fermi energy, the so-called Abrikosov-Suhl resonance. At zero temperature the impurity spin is completely screened and the system can be described by an effective Fermi liquid theory with a spin-singlet ground state as found by Nozières [9]. A lot of work has been done on the Kondo model and new methods were developed, which are now also used for other condensed matter

or particle physics problems as discussed in the introduction, section 1.

One of the first attempts to go beyond perturbation theory was an approach from Anderson [10] called the "poor man's scaling". This method was recently generalized to the non-equilibrium problem of transport at a finite bias voltage by A. Rosch *et al.* [35].

The poor man's scaling method uses the separation of energy scales in the system. The spin-scattering processes at low temperatures take place in a small energy window around the Fermi surface. By contrast, the energy of the electrons available for scattering processes reaches from the lower cutoff $-D$ to the upper cutoff D, where D is orders of magnitudes larger than other system parameters like the temperature.[1] The scaling procedure integrates out scattering to high-lying energy states and includes the changes into renormalized couplings, as illustrated in Fig. 5.1. By further decreasing

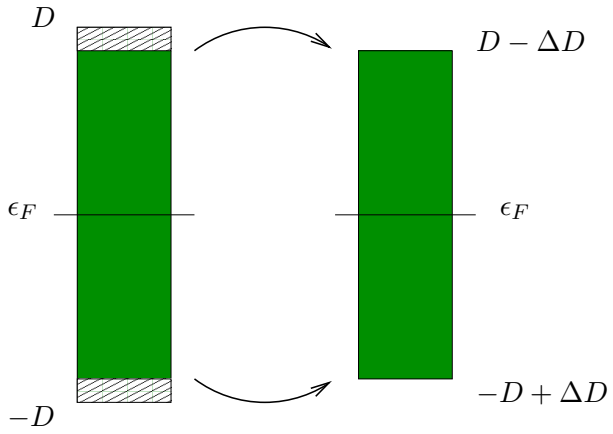

Figure 5.1: Schematic scaling step in poor man's scaling.

the band cutoff in infinitesimal steps, an effective model for the physics at low energies is generated. This effective model in poor man's scaling is of the same form as the initial Hamiltonian H_{int}, but the value of the coupling J is renormalized. This scaling is described by a flow equation for the coupling $J(D)$ depending on the change of the band cutoff D. For the Kondo model of a single impurity in a metallic host the flow equation is, as derived in Ref. [2],

$$\frac{\partial J(D)}{\partial \ln D} = -2N(0)\left(J(D)\right)^2 .$$

If the cutoff is reduced from D_0 to some cutoff $D < D_0$, the coupling flows according to

$$N(0)J(D) = \frac{1}{\frac{1}{N(0)J(D_0)} + 2\ln\frac{D}{D_0}} = \frac{N(0)J(D_0)}{1 + 2N(0)J(D_0)\ln\frac{D}{D_0}}.$$

Since the band cutoff is lowered, the ratio $D/D_0 < 1$ is smaller than one such that the logarithm $\ln(D/D_0) < 0$ has a negative sign. For antiferromagnetic coupling $J > 0$ the denominator is zero at the energy scale denoted as the Kondo temperature T_K, where

$$T_K = D_0\, e^{-\frac{1}{2N(0)J(D_0)}}.$$

[1] Typical values of the bandwidth are $D \approx 1eV$ and temperatures of $T = 4K \sim 0.3\ meV$.

The cutoff-dependent coupling $J(D)$ diverges logarithmically at the energy scale of T_K,

$$N(0)J(D) = \frac{1}{2\ln\frac{D}{T_K}}.$$

The poor man's scaling is a perturbative method since the change of the coupling is calculated by a perturbative series. The perturbative RG is valid only as long as $T \gg T_K$. It can be seen as an infinite summation of the leading logarithmic order diagrams, i.e. the "parquet" diagrams see Ref. [2]. Thus the Kondo temperature T_K depends exponentially on the coupling. This non-analytical dependence can not be described by standard perturbation theory.

A finite temperature or another energy of the system can cut off the flow of the coupling $J(D)$ even before D is reduced to the Kondo temperature. For example in a magnetic field the energy levels of the spin are split up by the Zeeman effect. Resonant spin flip processes are thus no longer possible since a spin flip costs the energy B. The spin-flip coupling at the Fermi energy is no longer logarithmically divergent. The flow of this coupling is therefore cut off and prevented to flow to strong-coupling. On the contrary the coupling at a finite frequency of $\omega = B$ is logarithmically divergent and the physical system contains information on finite energy scales away from the ground state Fermi energy.

In the case of a finite bias voltage and thus different chemical potentials a similar argument applies. In this case the Kondo resonance builds up at the two Fermi surfaces and the couplings at the finite frequencies $\omega = \pm eV/2$ diverge logarithmically. Taking into account the frequency dependence of coupling functions, allows us to calculate non-equilibrium properties for example the non-equilibrium current through a Kondo impurity. A finite voltage and therefore a finite current leads to a finite decoherence as discussed already in the previous chapters. To capture all effects of non-equilibrium the decoherence has to be taken into account as an additional energy scale of the system. It is important that the occupation probabilities of the impurity states are dependent on the transition rates and obey a quantum Boltzmann equation as discussed in section 3.5. In the following it is discussed how the perturbative RG method introduced by A. Rosch *et al.* [35, 36] includes these effects.

5.2 RG Equations

We consider the double quantum dot system as introduced in chapters 3 and 4. Taking into account the frequency dependence of the coupling functions, the interacting Hamiltonian is rewritten as

$$H_{\text{int}} = \sum \frac{1}{4}\left(\vec{T}_\alpha\right)_{\gamma'\gamma} \vec{\tau}_{\sigma'\sigma} J^{nk\sigma,\omega_c;mk'\sigma',\omega_c'}_{\gamma,\omega_\gamma;\gamma',\omega_{\gamma'}} t^\dagger_{\gamma'} t_\gamma c^\dagger_{mk'\sigma'} c_{nk\sigma},$$

where the sum is over all indices (Einstein summation convention). For the coupling J the convention is used, that the index of the incoming energy is written to the left, and the outgoing to the right, as illustrated in Fig. 5.2. A conduction electron in the lead n with momentum k and spin σ, which comes in with a frequency ω_c, interacts with a pseudo particle of the double quantum dot system with index $\gamma \in \{s, t_+, t_0, t_-\}$, and frequency ω_γ. After the scattering event a conduction electron with momentum k' and

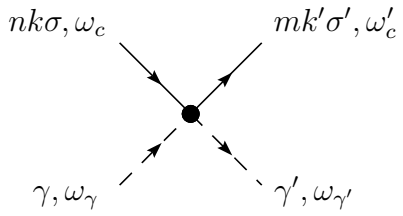

Figure 5.2: Schematic illustration of the pure vertex $\mathcal{V}^{nk\sigma,\omega_c;mk'\sigma',\omega_c'}_{\gamma,\omega_\gamma;\gamma',\omega_{\gamma'}}$.

spin σ' leaves with an energy of ω_c' in the lead m while the double quantum dot system is left in the pseudo particle state γ' with frequency $\omega_{\gamma'}$. The energy is conserved such that the energy of the two incoming particles is equal to the energy of the two outgoing particles, $\omega_c + \omega_\gamma = \omega_c' + \omega_{\gamma'}$. The interaction is local in time and thus takes place on the same time contour. In case the time is on the anti-time ordered contour (2), the interaction gains a minus sign.

The vertex $\mathcal{V}$ flows as the cutoff is reduced. The initial condition for $\mathcal{V}$ is given by the initial Hamiltonian,

$$\mathcal{V}^{nk\sigma,\omega_c;mk'\sigma',\omega_c'}_{\gamma,\omega_\gamma;\gamma',\omega_{\gamma'}}(D = D_0) = \frac{1}{4} N(0) J_{mn} \left(\vec{T}_\alpha\right)_{\gamma'\gamma} \vec{\tau}_{\sigma'\sigma}.$$

The interaction always takes place either on the left quantum dot $n, m = 1, 2$ or on the right quantum dot $m, n = 3, 4$. An interaction from a left lead with the right quantum dot is not allowed and will hence not be generated in the poor man's scaling approach.

5.2.1 Derivation of the Scaling Equations

For the derivation of the scaling equations in the poor man's scaling approach the steps of P.W. Anderson in Ref. [68] are followed and generalized to non-equilibrium. Anderson described the poor man's scaling as a technique "to eliminate successively the higher energy regions in favor of an effective interaction" [68].

The idea is to scale down the band cutoff D and change the coupling correspondingly such that physical quantities do not change their value. As a typical physical quantity the T-matrix is studied. As derived in section 4.3 the T-matrix obeys a self-consistent equation of the type,

$$T = H_{\text{int}} + H_{\text{int}} G^{(0)} T. \tag{5.1}$$

We introduce a projection $P_{\Delta D}$ on the states with the energy $\pm(D - \Delta D)$ in the vicinity of the upper or lower band edge $\pm D$, respectively. Then we find by resubstituting $T = H_{\text{int}} + H_{\text{int}} P_{\Delta D} G^{(0)} T + H_{\text{int}}(1 - P_{\Delta D}) G^{(0)} T$ into the equation (5.1) for T,

$$\begin{aligned} T =& H_{\text{int}} + H_{\text{int}} P_{\Delta D} G^{(0)} H_{\text{int}} \\ &+ (H_{\text{int}} + H_{\text{int}} P_{\Delta D} G^{(0)} H_{\text{int}})(1 - P_{\Delta D}) G^{(0)} T + H_{\text{int}} P_{\Delta D} G^{(0)} H_{\text{int}} P_{\Delta D} G^{(0)} T \\ =& \tilde{H}_{\text{int}} + \tilde{H}_{\text{int}}(1 - P_{\Delta D}) G^{(0)} T, \end{aligned}$$

where $\tilde{H}_{\text{int}} = H_{\text{int}} + \Delta H_{\text{int}}$ and

$$\Delta H_{\text{int}} = H_{\text{int}} P_{\Delta D} G^{(0)} H_{\text{int}}. \tag{5.2}$$

This is the idea of renormalization: by using a new cutoff $(D - \Delta D)$ the T-matrix is calculated self-consistently as in Eq. (5.1), but with a coupling $\tilde{H}_{\rm int}$ which incorporates the contribution of the states in the energy regime $[D - \Delta D, D]$ and $[-D, -D + \Delta D]$. To derive the effective interaction in Eq. (5.2) a term which is proportional to $(\Delta D)^2$ is neglected. This is justified since the renormalization step can be made arbitrarily small.

In the case of a finite voltage and non-equilibrium Green's functions this approach has to be modified. The interaction Hamiltonian $H_{\rm int} \propto J\ \vec{S}_\alpha \vec{\tau}_{\sigma'\sigma}\ c^\dagger_{mk'\sigma'} c_{nk\sigma}$ describes a spin scattering from a conduction electron state k to a state k'. We define the projection $P_{\Delta D}$ that projects the conduction electron state into the energy regimes $[D - \Delta D, D]$ and $[-D, -D + \Delta D]$.

In the perturbation theory expansion in the Keldysh language (section 3.1) we find an expression for the T-matrix (compare section 4.3) from an expansion of the conduction electron Green's function,

$$\begin{aligned} iG_{nk\sigma}(\tau, \tau') =& \langle c_{nk\sigma}(\tau) c^\dagger_{nk\sigma}(\tau')\rangle + \langle c_{nk\sigma}(\tau)(-i) \left[\int_c d\tau_1 H_{\rm int}(\tau_1)\right] c^\dagger_{nk\sigma}(\tau')\rangle \\ &+ \langle c_{nk\sigma}(\tau) \frac{(-i)^2}{2!} \left[\int_c d\tau_1 \int_c d\tau_2 H_{\rm int}(\tau_1) H_{\rm int}(\tau_2)\right] c^\dagger_{nk\sigma}(\tau')\rangle + \ldots . \end{aligned}$$

Translating the idea of scaling from Ref. [68] to this expression we aim at writing the whole series with an effective interaction Hamiltonian $\tilde{H}_{\rm int}(\tau_1)$ in the projected subspace. Inserting $H_{\rm int} = [P_{\Delta D} + (1 - P_{\Delta D})] H_{\rm int} [P_{\Delta D} + (1 - P_{\Delta D})]$ we find, that $\tilde{H}_{\rm int}$

$$\begin{aligned} \int_c d\tau_1 \tilde{H}_{\rm int}(\tau_1) =& \int_c d\tau_1 (1 - P_{\Delta D}) H_{\rm int}(\tau_1)(1 - P_{\Delta D}) \\ &+ \frac{-i}{2} \int_c d\tau_1 \int_c d\tau_2 (1 - P_{\Delta D}) H_{\rm int}(\tau_1) P_{\Delta D} H_{\rm int}(\tau_2)(1 - P_{\Delta D}), \end{aligned}$$

reproduces a first order contribution in the perturbative series with an effective interaction $\tilde{H}_{\rm int}$. Again ΔD is assumed to be small such that scattering within the energy window $[D - \Delta D, D]$ and $[-D, -D + \Delta D]$ can be neglected. In general the poor man's scaling is a perturbative expansion in the interaction Hamiltonian $H_{\rm int}$, but higher orders are usually not taken into account. In the following we calculate the expansion for an effective Hamiltonian $\tilde{H}_{\rm int}$ by

$$\tilde{H}_{\rm int}(\tau_1) - H_{\rm int}(\tau_1) = -\frac{i}{2} H_{\rm int}(\tau_1) H_{\rm int}(\tau_2). \tag{5.3}$$

Instead of the projection of particles to the band edges, the change of the Hamiltonian $\Delta H_{\rm int}(D) = H_{\rm int} - \tilde{H}_{\rm int}$ is calculated for the full bandwidth and afterwards the change of $i/2 H_{\rm int}(\tau_1) H_{\rm int}(\tau_2)$ is determined by a derivation with respect to the cutoff D.[2] If the derivative $D\partial/\partial D = \partial/\partial \ln D$ of Eq. (5.3) is taken, we find a scaling equation for the cutoff dependent Hamiltonian

$$\frac{\partial H_{\rm int}(D)}{\partial \ln D} = D \frac{\partial}{\partial D} \left[\frac{i}{2} H_{\rm int}(\tau_1) H_{\rm int}(\tau_2)\right]. \tag{5.4}$$

[2] In other words, the minus sign from $-i/2$ is cancelled since the band cutoff is reduced: $(D - \Delta D) - D = -\Delta D$.

The cutoff D is reduced in infinitesimal steps until an energy scale D^* is reached which cuts off the flow and the Hamiltonian $H_{\rm int}(D^*)$ provides an effective model for the physics on this low energy scale. The first correction $H_{\rm int}(\tau_1)H_{\rm int}(\tau_2)$ to the interacting Hamiltonian $\tilde{H}_{\rm int}(D)$ for the double quantum dot system is now studied in detail.

The poor man's scaling is a renormalization group treatment to lowest order. The summation of the leading logarithmic order diagrams is also referred to as one-loop order. In chapter 6 the flow equation method to two-loop order is discussed and although this scaling method is differently structured than the perturbative RG a discussion of the physical content of higher order diagrams is given there.

5.2.2 Generating the Scaling Equations

In the following derivation we focus on the coupling of the left quantum dot to the leads. The derivation here explains how the RG equations in Ref. [36] arise. Currently we are working on a rigorous derivation of the scaling equations and here only the cornerstones of the calculation are given. A rigorous derivation can be produced along the lines of functional RG (e.g. Ref. [40, 39]).

To calculate the correction to the vertex in second order we have to contract one conduction electron line and one pseudo particle line in $H_{\rm int}(\tau_1)H_{\rm int}(\tau_2)$. As mentioned before only the renormalization of the vertices which exist before the rescaling steps are taken into account. On the Keldysh contour the interaction can take place either on the first contour or on the second contour, where the interaction on the anti-time-ordered axis gains a minus sign. In the following it is assumed, that the times τ_1 and τ_2 are on the first contour, since the calculation for the second contour follows analogously.

In the following equations the notation γ is used for γ, ω_γ and n stands for $nk\sigma, \omega_c$ etc. We find for $i/2 H_{\rm int}(\tau_1)H_{\rm int}(\tau_2)$,

$$\begin{aligned}
&\frac{i}{2}H_{\rm int}(\tau_1)H_{\rm int}(\tau_2) = \frac{i}{2}\frac{1}{16}J^{n;m}_{\gamma_1;\gamma_1'}J^{\nu;\mu}_{\gamma_2;\gamma_2'}\left(\vec{T}_\alpha\right)^{i}_{\gamma_1'\gamma_1}\tau^{i}_{\sigma'\sigma}\left(\vec{T}_\alpha\right)^{j}_{\gamma_2'\gamma_2}\tau^{j}_{s's} \\
&\times\left(t^\dagger_{\gamma_1'}(\tau_1)\left\langle t_{\gamma_1}(\tau_1)t^\dagger_{\gamma_2'}(\tau_2)\right\rangle t_{\gamma_2}(\tau_2) + t^\dagger_{\gamma_2'}(\tau_2)\left\langle t_{\gamma_2}(\tau_2)t^\dagger_{\gamma_1'}(\tau_1)\right\rangle t_{\gamma_1}(\tau_1)\right) \\
&\times\left(c^\dagger_{mk'\sigma'}(\tau_1)\left\langle c_{nk\sigma}(\tau_1)c^\dagger_{\mu p's'}(\tau_2)\right\rangle c_{\nu ps}(\tau_2) + c^\dagger_{\mu p's'}(\tau_2)\left\langle c_{\nu ps}(\tau_2)c^\dagger_{mk'\sigma'}(\tau_1)\right\rangle c_{nk\sigma}(\tau_1)\right).
\end{aligned}$$

The contraction leads to the two different diagrams illustrated in Fig. 5.3. The factor of 1/2 from the perturbative expansion cancels since each diagram appears twice.

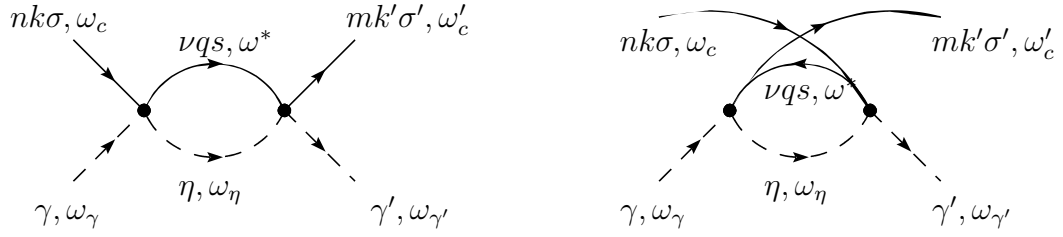

(a) "Cooper" contribution. (b) "Peierls" contribution.

Figure 5.3: Illustration of the two diagrams which lead to Kondo physics. Left diagram is referred to as the " Cooper" contribution and right diagram as the "Peierls" contribution.

As mentioned before τ_1 and τ_2 are assumed to be on the first Keldysh contour. In the following only the frequency dependence of the vertices is discussed. In frequency space the interaction Hamiltonian is renormalized by the term

$$\begin{aligned} &i^3\frac{1}{16}J^{\nu;m}_{\eta;\gamma'}J^{n;\nu}_{\gamma;\eta'}\left(\vec{T}_\alpha\right)^i_{\gamma'\eta}\vec{\tau}^i_{\sigma's}\left(\vec{T}_\alpha\right)^j_{\eta\gamma}\vec{\tau}^j_{s\sigma}t^\dagger_{\gamma'}t_\gamma c^\dagger_{m\sigma'}c_{n\sigma}G^{11}_\eta(\omega_\eta)G^{11}_{\nu qs}(\omega^*) \\ +&i^3\frac{1}{16}J^{n;\nu}_{\eta;\gamma'}J^{\nu;m}_{\gamma;\eta'}\left(\vec{T}_\alpha\right)^i_{\gamma'\eta}\vec{\tau}^i_{s\sigma}\left(\vec{T}_\alpha\right)^j_{\eta\gamma}\vec{\tau}^j_{\sigma's}t^\dagger_{\gamma'}t_\gamma c^\dagger_{m\sigma'}c_{n\sigma}G^{11}_\eta(\omega_\eta)G^{11}_{\nu qs}(\omega^*). \end{aligned} \tag{5.5}$$

The first term corresponds to the diagram in Fig. 5.3(a), where both Green's functions point in the same direction. This part is from now on referred to as the "Cooper" contribution, since both particles travel in the same direction in time. The second term corresponds to the diagram in Fig. 5.3(b). Here the Green's functions propagate in opposite directions. This diagram is denoted the "Peierls" contribution.

Eq. (5.5) needs to be integrated over the internal frequencies. Due to the energy conservation on the two pure vertices the frequency ω^* is fixed, but its value is different for the Cooper and the Peierls contribution. In the following sections these two different terms are discussed.

Calculation of the Cooper Contribution

The contribution of the Cooper diagram (Fig. 5.3(a) or first term in Eq. (5.5)) is defined by

$$\mathbf{C}^{\nu qs}_\eta = -i\int\frac{d\omega_\eta}{2\pi}G^{11}_\eta(\omega_\eta)G^{11}_{\nu qs}(\omega^*), \tag{5.6}$$

where ω^* is determined by the energy conservation at one of the two pure vertices, e.g. the vertex of the incoming particles gives $\omega^* = \omega_c + \omega_\gamma - \omega_\eta$. The time-ordered Green's function $G^{11} = G^< + G^r$ can be expressed in terms of the lesser and retarded Green's functions. In general the convolution of $(G^<_\eta G^<_{\nu qs} + G^<_\eta G^r_{\nu qs} + G^r_\eta G^<_{\nu qs} + G^r_\eta G^r_{\nu qs})$ has to be calculated. Nevertheless for the scaling equation only the terms that are dependent on the cutoff D contribute. To leading order we therefore neglect all terms besides the contribution from $\mathrm{Re}[G^r_\eta]\ G^<_{\nu q\sigma}$. The correction to the interaction vertex is thus real. In higher orders imaginary parts have to be accounted for, but they are neglected in this framework. The perturbative RG method is thus consistent only to leading logarithmic order and it is valid only above the Kondo temperature T_K.

A short side remark is added here about the possible contributions of the off-diagonal retarded Green's functions $G^r_{st_0}$ and $G^r_{t_0s}$ as found in section 3.4. Both are of the order Γ/K and therefore they can be neglected to leading logarithmic order if K is finite. For the scaling equations, it is not important to take into account off-diagonal components. Only to 0th order, like in the calculation of the non-equilibrium distribution functions, they can not be neglected. It is assumed in the calculation here, that the retarded Green's functions are diagonal and all off-diagonal self energy contributions can be neglected.

The Cooper term in Eq. (5.6) is given to leading logarithmic order by

$$\begin{aligned}\mathbf{C}_{\eta}^{\nu qs} &= -i\int \frac{d\omega_\eta}{2\pi}\,\mathrm{Re}[G_\eta^r(\omega_\eta)]G^<_{\nu qs}(\omega_c+\omega_\gamma-\omega_\eta)\\ &\approx -\frac{1}{2}N(0)\int dx \frac{1}{\Delta\omega_C - x}\tanh\left(\frac{x}{2T}\right)\Theta\left(D-|x|\right)\\ &= -\frac{1}{2}N(0)\int_{-D}^{D} dx \frac{1}{\Delta\omega_C - x}\tanh\left(\frac{x}{2T}\right),\end{aligned}$$

where $\Delta\omega_C = \omega_c+\omega_\gamma-\mu_\nu-\epsilon_\eta$ and $x=\omega^*-\mu_\nu=\omega_c+\omega_\gamma-\omega_\eta-\mu_\nu$. Only $\frac{1}{2}\tanh(\omega^*/2T)$, the asymmetric part of the Fermi function $f(\omega^*)=(1-\tanh(\omega^*/2T))/2$ in $G^<_{\nu s}(\omega^*)=if(\omega^*)A(\omega^*)$, is taken into account since the other terms do not contribute to leading logarithmic order. The spectral function of the conduction electron Green's function $A(\omega^*)=2\pi\Theta(D-|\omega^*|)$ is assumed to have a sharp cutoff at the two band edges D and $-D$.

The derive the cutoff dependence for the renormalization flow of the interaction Hamiltonian the derivative $D\partial/\partial D$ of Eq. (5.5) is taken. The incoming and outgoing operators $t^\dagger_{\gamma'}t_\gamma c^\dagger_{m\sigma'}c_{n\sigma}$ and the spin structure due to $\left(\vec{T}_\alpha\right)^i_{\gamma'\eta}\vec{\tau}^i_{\sigma' s}\left(\vec{T}_\alpha\right)^j_{\eta\gamma}\vec{\tau}^j_{s\sigma}$ are assumed to be independent of the cutoff. The cutoff dependence of the Cooper contribution is therefore determined by

$$\begin{aligned}&\frac{\partial}{\partial\ln D}J^{\nu qs,\omega^*;mk'\sigma',\omega'_c}_{\eta,\omega_\eta;\gamma',\omega_{\gamma'}}J^{nk\sigma,\omega_c;\nu qs,\omega^*}_{\gamma,\omega_\gamma;\eta,\omega_\eta}\mathbf{C}^{\nu qs}_\eta\\ &\quad= -\frac{1}{2}N(0)D\left[J^{\nu qs,\omega^*=D+\mu_\nu;mk'\sigma',\omega'_c}_{\eta,\omega_\eta;\gamma',\omega_{\gamma'}}J^{nk\sigma,\omega_c;\nu qs,\omega^*=D+\mu_\nu}_{\gamma,\omega_\gamma;\eta,\omega_\eta}\frac{1}{\Delta\omega_C-D}\right.\\ &\qquad\left.-J^{\nu qs,\omega^*=-D+\mu_\nu;mk'\sigma',\omega_c}_{\eta,\omega_\eta;\gamma',\omega_{\gamma'}}J^{nk\sigma,\omega_c;\nu q\sigma,\omega^*=-D+\mu_\nu}_{\gamma,\omega_\gamma;\eta',\omega_{\eta'}}\frac{(-1)}{\Delta\omega_C+D}\right],\end{aligned}$$

where $\tanh(x/2T)$ is approximated by $\mathrm{sign}(x)$ since the temperature T is assumed to be negligibly small compared to every other energy scale of the system. So far the calculation is equivalent to the calculation of Anderson [10]. In the original paper on poor man's scaling the frequency $\Delta\omega_C$ is neglected in comparison to the cutoff D, since the cutoff is the largest energy scale of the system.

During the renormalization the cutoff D is sent to zero. As long as $D>\Delta\omega_C$ the ratio,

$$\frac{D}{\Delta\omega_C-D}\approx -1 \quad \text{for} \quad D\gg\Delta\omega_C,$$

can be approximated by -1. At some energy scale the cutoff D is reduced below $\Delta\omega_C$. Since the ratio,

$$\frac{D}{\Delta\omega_C-D}\approx 0 \quad \text{for} \quad D\ll\Delta\omega_C,$$

is then negligibly small, the flow of the coupling is stopped by the energy scale $\Delta\omega_C$, which is given by internal energies scales of the system. In the following the ratio

$D/(\Delta\omega_C - D)$ is approximated by a step function,

$$-\frac{D}{D \mp \Delta\omega_C} \approx -\Theta(D - |\Delta\omega_C|).$$

The absolute value of $\Delta\omega_C$ is taken such that this assumption is also valid for the ratio $-D/(D+\Delta\omega_C)$. The approximation of a step-like behavior fails if the cutoff D and $\Delta\omega_C$ are of the same order of magnitude. A more rigorous derivation of the cutoff function $\Theta(D - |\Delta\omega_C|)$ is needed to deal with this energy regime of the flow, e.g. in functional RG or in the flow equation method (see chapter 6).

The Cooper contribution to the RG equation thus gives

$$\begin{aligned}&\frac{\partial}{\partial \ln D} J^{\nu qs,\omega^*;mk'\sigma',\omega_c'}_{\eta,\omega_\eta;\gamma',\omega_{\gamma'}} J^{nk\sigma,\omega_c;\nu qs,\omega^*}_{\gamma,\omega_\gamma;\eta,\omega_\eta} \mathbf{C}^{\nu qs}_{\eta} \\ =&\frac{1}{2} N(0)\Theta(D - |\omega_c + \omega_\gamma - \mu_\nu - \epsilon_\eta|) \sum_{\lambda=\pm 1} J^{\nu qs,\lambda D+\mu_\nu;mk'\sigma',\omega_c'}_{\eta,\omega_\eta;\gamma',\omega_{\gamma'}} J^{nk\sigma,\omega_c;\nu qs,\lambda D+\mu_\nu}_{\gamma,\omega_\gamma;\eta,\omega_\eta}. \end{aligned} \tag{5.7}$$

The cutoff D is reduced to 0 and therefore $\lambda D \to 0$ in Eq. (5.7) is approximated by zero. This is valid under the assumption that the frequency dependence of the Θ-function is stronger than the frequency dependence of the coupling functions. Then Eq. (5.7) simplifies to

$$\begin{aligned}&\frac{\partial}{\partial \ln D} J^{\nu qs,\omega^*;mk'\sigma',\omega_c'}_{\eta,\omega_\eta;\gamma',\omega_{\gamma'}} J^{nk\sigma,\omega_c;\nu qs,\omega^*}_{\gamma,\omega_\gamma;\eta,\omega_\eta} \mathbf{C}^{\nu qs}_{\eta} \\ =&N(0)\Theta(D - |\omega_c + \omega_\gamma - \mu_\nu - \epsilon_\eta|) J^{\nu qs,\mu_\nu;mk'\sigma',\omega_c'}_{\eta,\omega_\eta;\gamma',\omega_{\gamma'}} J^{nk\sigma,\omega_c;\nu qs,\mu_\nu}_{\gamma,\omega_\gamma;\eta,\omega_\eta}. \end{aligned} \tag{5.8}$$

Calculation of the Peierls Contribution

The same derivation has now to be done for the Peierls contribution of the scaling equation (5.5). In contrast to the Cooper contribution the two intermediate particles in the Peierls contribution propagate in different directions in time as illustrated in Fig. 5.3(b). The Peierls contribution is given by

$$\mathbf{P}^{\nu qs}_{\eta} = -i \int \frac{d\omega_\eta}{2\pi} G^{11}_{\eta}(\omega_\eta) G^{11}_{\nu qs}(\omega^*),$$

where $\omega^* = \omega_c + \omega_\eta - \omega_{\gamma'}$ in this case.

Analogous to the derivation of the Cooper contribution we find

$$\begin{aligned}\mathbf{P}^{\nu qs}_{\eta} &= -i \int \frac{d\omega_\eta}{2\pi} \operatorname{Re}[G^{r}_{\eta}(\omega_\eta)] G^{<}_{\nu qs}(\omega_c + \omega_\eta - \omega_{\gamma'}) \\ &\approx -\frac{1}{2} N(0) \int_{-D}^{D} dx \frac{1}{x - \Delta\omega_P} \tanh\left(\frac{x}{2T}\right), \end{aligned}$$

where $\Delta\omega_P = \omega_{\gamma'} - \omega_c + \mu_\nu - \epsilon_\eta$. Since a hole is involved in the Peierls contribution, the conduction energy ω_c enters with a different sign in $\Delta\omega_P$ compared to $\Delta\omega_C$ in the Cooper contribution.

With the same assumptions as used in the derivation of Eq. (5.7) we obtain

$$\begin{aligned}&\frac{\partial}{\partial \ln D} J^{nk\sigma,\omega_c;\nu qs,\omega^*}_{\eta,\omega_\eta;\gamma',\omega_{\gamma'}} J^{\nu qs,\omega^*;mk'\sigma',\omega'_c}_{\gamma,\omega_\gamma;\eta,\omega_\eta} \mathbf{P}^{\nu qs}_{\eta} \\ &= -\frac{1}{2} N(0)\Theta(D - |\omega_{\gamma'} - \omega_c + \mu_\nu - \epsilon_\eta|) \sum_{\lambda=\pm 1} J^{nk\sigma,\omega_c;\nu qs,\lambda D+\mu_\nu}_{\eta,\omega_\eta;\gamma',\omega_{\gamma'}} J^{\nu qs,\lambda D+\mu_\nu;mk'\sigma',\omega'_c}_{\gamma,\omega_\gamma;\eta,\omega_\eta}. \end{aligned} \tag{5.9}$$

In the limit of $D \to 0$ and if the frequency dependence of the coupling function is neglected, Eq. (5.9) simplifies to

$$\begin{aligned}&\frac{\partial}{\partial \ln D} J^{nk\sigma,\omega_c;\nu qs,\omega^*}_{\eta,\omega_\eta;\gamma',\omega_{\gamma'}} J^{\nu qs,\omega^*;mk'\sigma',\omega'_c}_{\gamma,\omega_\gamma;\eta,\omega_\eta} \mathbf{P}^{\nu qs}_{\eta} \\ &= -N(0)\Theta(D - |\omega_{\gamma'} - \omega_c + \mu_\nu - \epsilon_\eta|) J^{nk\sigma,\omega_c;\nu qs,\mu_\nu}_{\eta,\omega_\eta;\gamma',\omega_{\gamma'}} J^{\nu qs,\mu_\nu;mk'\sigma',\omega'_c}_{\gamma,\omega_\gamma;\eta,\omega_\eta}. \end{aligned} \tag{5.10}$$

Summary and General RG Equation

Using the result of Eq. (5.7) and (5.9) in Eq. (5.5) the RG equation for the general vertex $\mathcal{V}$ is given by

$$\begin{aligned}\frac{\partial \mathcal{V}^{nk\sigma,\omega_c;mk'\sigma',\omega'_c}_{\gamma,\omega_\gamma;\gamma',\omega_{\gamma'}}}{\partial \ln D} =& \frac{1}{2} \sum_{\lambda=\pm 1} \sum_{\eta,\nu,s} \\ &\times \Big(\mathcal{V}^{\nu qs;\lambda D+\mu_\nu;mk'\sigma',\omega'_c}_{\eta,\omega_\eta;\gamma',\omega_{\gamma'}} \Theta_{|\omega_c+\omega_\gamma-\mu_\nu-\epsilon_\eta|} \mathcal{V}^{nk\sigma,\omega_c;\nu qs,\lambda D+\mu_\nu}_{\gamma,\omega_\gamma;\eta,\omega_\eta} \\ &- \mathcal{V}^{nk\sigma,\omega_c;\nu qs,\lambda D+\mu_\nu}_{\eta,\omega_\eta;\gamma',\omega_{\gamma'}} \Theta_{|\omega_{\gamma'}-\omega_c+\mu_\nu-\epsilon_\eta|} \mathcal{V}^{\nu qs,\lambda D+\mu_\nu;mk'\sigma',\omega'_c}_{\gamma,\omega_\gamma;\eta,\omega_\eta} \Big), \end{aligned} \tag{5.11}$$

where we introduced the notation $\Theta_x = \Theta(D - |x|)$. The general vertex is defined by

$$\mathcal{V}^{nk\sigma,\omega_c;mk'\sigma',\omega'_c}_{\gamma,\omega_\gamma;\gamma',\omega_{\gamma'}} = \frac{1}{4} \vec{\tau}_{\sigma'\sigma} \left(\vec{T}_\alpha \right)_{\gamma'\gamma} N(0) J^{nk\sigma,\omega_c;mk'\sigma',\omega'_c}_{\gamma,\omega_\gamma;\gamma',\omega_{\gamma'}}.$$

Eq. (5.11) is the generalization of Eq. (6) in the paper of A. Rosch *et al.* [36].

The expression (5.11) can be applied to every Kondo model with a number of leads and some level structure of the Kondo dot if the interaction can be written as a general vertex $\mathcal{V}$. To derive the scaling equation for a specific problem, the first step is to perform the spin product of the conduction electron spin. One has to be careful since the spin matrices appear in a different order in the Cooper and the Peierls contributions. The RG equations are specialized to e.g. the double quantum dot system when the pseudo Pauli-matrices $\vec{T}$ are inserted in Eq. (5.11).

A finite current through a quantum dot system leads to fluctuations in the occupation probabilities and the impurity states gain a finite life time. Since the Kondo effect is sensitive to the coherence of scattering processes, the broadening Γ has to be included in the RG flow to compensate for the fact that the flow of the running couplings, if not stopped by a system parameter before, is stopped at the energy scale of the dephasing Γ. This mechanism including self energy and vertex corrections has been discussed in detail in Ref. [41]. Here it is only motivated how an additional cutoff arises in the poor man's scaling framework. The real part of the retarded Green's function with a finite

width Γ leads to a Cooper contribution $\mathbf{C}_\eta^{\nu qs}$ of

$$\begin{aligned}\frac{\partial}{\partial \ln D}\mathbf{C}_\eta^{\nu qs} &= -\frac{1}{2}N(0)D\frac{\partial}{\partial D}\int_{-D}^{D} dx \frac{\Delta\omega_C - x}{(\Delta\omega_C - x)^2 + (\Gamma/2)^2}\tanh\left(\frac{x}{2T}\right) \\ &= -\frac{1}{2}N(0)D\frac{\Delta\omega_C - D}{(\Delta\omega_C - D)^2 + (\Gamma/2)^2} + \frac{1}{2}N(0)D\frac{\Delta\omega_C + D}{(\Delta\omega_C + D)^2 + (\Gamma/2)^2}.\end{aligned}$$

If $\Delta\omega_c \pm D \gg \Gamma/2$ the decoherence does not play a role and we find the step-like cutoff as discussed before, whereas in the case of $\Delta\omega_c \pm D \ll \Gamma/2$ we find

$$\frac{\partial}{\partial \ln D}\mathbf{C}_\eta^{\nu qs} \approx N(0)\frac{(\Delta\omega_C)^2 + D^2}{(\Gamma/2)^2} \ll 1.$$

The finite life time of the pseudo particle states provides an additional cutoff in the RG scheme. Since the decoherence is large in the case of a finite voltage, this additional cutoff is important in a non-equilibrium calculation. In the following we redefine the cutoff function Θ_x as

$$\Theta_x = \Theta\left(D - \sqrt{x^2 + \Gamma^2}\right). \tag{5.12}$$

The decoherence provides also an additional cutoff in equilibrium if the coupling diverges at a finite frequency, e.g. the singlet-triplet gap K. A detailed discussion of this and to which leading order the decoherence enters the scaling equations can be found in Ref. [41].

5.2.3 Calculation and Assumptions for the RG Equations of the Double Quantum Dot System

The derivation of the RG equations for the double quantum dot system is shown for one coupling as an example in appendix D.1. For a spin-flip process where the double quantum dot state changes from the triplet t_+ to the singlet s the spin of the involved conduction electron changes correspondingly from $\downarrow$ to $\uparrow$. The flow of this coupling is given by

$$\begin{aligned}\frac{\partial g^{nk\downarrow,\omega_c;mk'\uparrow,\omega_c'}_{t_+,\omega_{t_+};s,\omega_s}}{\partial \ln D} = -\frac{1}{2}\Big(& g^{\nu q\downarrow,\omega^*;mk'\uparrow,\omega_c'}_{t_+,\omega_{t_+};s,\omega_s} g^{nk\downarrow,\omega_c;\nu q\downarrow,\omega^*}_{t_+,\omega_{t_+};t_+,\omega_{t_+}} \Theta_{\omega_c+\omega_{t_+}-\mu_\nu-\omega_{t_+}} \\ & + g^{nk\downarrow,\omega_c;\nu q\uparrow,\omega^*}_{t_+,\omega_{t_+};s,\omega_s} g^{\nu q\uparrow,\omega^*;mk'\uparrow,\omega_c'}_{t_+,\omega_{t_+};t_+,\omega_{t_+}} \Theta_{\omega_s-\omega_c+\mu_\nu-\omega_{t_+}} \\ & + g^{\nu q\uparrow,\omega^*;mk'\uparrow,\omega_c'}_{t_0,\omega_{t_0};s,\omega_s} g^{nk\downarrow,\omega_c;\nu q\uparrow,\omega^*}_{t_+,\omega_{t_+};t_0,\omega_{t_0}} \Theta_{\omega_c+\omega_{t_+}-\mu_\nu-\omega_{t_0}} \\ & + g^{nk\downarrow,\omega_c;\nu q\downarrow,\omega^*}_{t_0,\omega_{t_0};s,\omega_s} g^{\nu q\downarrow,\omega^*;mk'\uparrow,\omega_c'}_{t_+,\omega_{t_+};t_0,\omega_{t_0}} \Theta_{\omega_s-\omega_c+\mu_\nu-\omega_{t_0}}\Big).\end{aligned} \tag{5.13}$$

In general the coupling vertex has four different frequencies, one for each incoming and each outgoing leg. It is assumed that the pseudo particle energies can be approximated by their values on resonance, i.e. on-shell. This approximation is justified since the broadening of the spectral weight is much smaller than other physical quantities of the system, especially in comparison with the band width of the conduction electron density

of states. If the frequencies of the double quantum dot states are assumed to be on resonance, we can rewrite

$$g^{nk\sigma,\omega_c;mk'\sigma',\omega_c'}_{t_+,\omega_{t_+};s,\omega_s} \to g^{nk\sigma,\omega_c;mk'\sigma',\omega_c'}_{t_+,\frac{1}{4}K-B;s,-\frac{3}{4}K}.$$

After assuming the pseudo particle energies to be on-shell the vertex thus only depends on two frequencies. The energy conservation on the vertex determines one of these two frequencies and it is assumed in the following, that the frequency of a vertex is always given by the incoming frequency, i.e. ω_c in $g^{nk\sigma,\omega_c;mk'\sigma',\omega_c'}_{t_+,\frac{1}{4}K-B;s,-\frac{3}{4}K}$. For this example we replace in the coupling function $\omega_c \to \omega$ and $\omega_c' \to \omega_c + \omega_s - \omega_{t_+} = \omega + K - B$. In the following the coupling function is written as

$$g^{nk\sigma,\omega_c;mk'\sigma',\omega_c'}_{t_+,\frac{1}{4}K-B;s,-\frac{3}{4}K} \to g^{nk\sigma;mk'\sigma'}_{t_+;s}(\omega).$$

With these assumptions the RG equation (5.13) simplifies to

$$\begin{aligned}\frac{\partial g^{n\downarrow;m\uparrow}_{t_+;s}(\omega)}{\partial \ln D} = -\frac{1}{2}\Big(& g^{\nu\downarrow;m\uparrow}_{t_+;s}(\omega) g^{n\downarrow;\nu\downarrow}_{t_+;t_+}(\omega)\Theta_{\omega-\mu_\nu} \\ & + g^{n\downarrow;\nu\uparrow}_{t_+;s}(\omega) g^{\nu\uparrow;m\uparrow}_{t_+;t_+}(\omega+K-B)\Theta_{\omega-\mu_\nu+K-B} \\ & + g^{\nu\uparrow;m\uparrow}_{t_0;s}(\omega-B) g^{n\downarrow;\nu\uparrow}_{t_+;t_0}(\omega)\Theta_{\omega-\mu_\nu-B} \\ & + g^{n\downarrow;\nu\downarrow}_{t_0;s}(\omega) g^{\nu\downarrow;m\uparrow}_{t_+;t_0}(\omega+K)\Theta_{\omega-\mu_\nu+K}\Big).\end{aligned}$$

The derivation of this scaling equation is shown in detail in appendix D.1. In general one can derive all scaling equations analogously, even in the case of a finite magnetic field B, but we restrict ourselves to the discussion of the case $B = 0$. The study of a finite magnetic field applied to a double quantum dot setup is the aim of future work.

It was observed in chapter 3 that the self energy can have off-diagonal contributions in the limit of $K \ll \Gamma$. Nevertheless, the leading logarithmic order as discussed above originates from a convolution of a conduction electron Green's function with the retarded Green's function for the double quantum dot system. As discussed in section 3.4 the off-diagonal retarded Green's function is proportional to Γ/K and $\Gamma \propto g^2 \propto 1/\ln^2$ can thus be neglected to leading logarithmic order. As discussed in section 3.5 the quantum Boltzmann equation is difficult to solve in the case of vanishing K. It is not the scope of this thesis to discuss this subject further. In future work one would have to rederive the scaling equations in the rotated subspace as explained in chapter C in the appendix to avoid the problems mentioned there.

5.2.4 RG Equations of the Double Quantum Dot System

In the case of zero magnetic field $B = 0$ the three triplet states are degenerate. As discussed previously the complications due to off-diagonal contributions do not appear. We assume further a symmetric Kondo setup such that the spin conserving J^z and the spin-flip $J^\perp$ couplings are not distinct. This assumption is justified since the spin symmetry is conserved in zero magnetic field.

Consequently there are only three different RG equations,

$$\begin{aligned}
\frac{\partial g_{ts}^{nm}(\omega)}{\partial \ln D} &= -\frac{1}{2}\,(2g_{ts}^{\nu m}(\omega)g_{tt}^{n\nu}(\omega)\Theta_{\omega-\mu_\nu} \\
&\quad +2g_{ts}^{n\nu}(\omega)g_{tt}^{\nu m}(\omega+K)\Theta_{\omega-\mu_\nu+K})\,, \\
\frac{\partial g_{st}^{nm}(\omega)}{\partial \ln D} &= -\frac{1}{2}\,(2g_{tt}^{\nu m}(\omega-K)g_{st}^{n\nu}(\omega)\Theta_{\omega-\mu_\nu-K} \\
&\quad +2g_{tt}^{n\nu}(\omega)g_{st}^{\nu m}(\omega)\Theta_{\omega-\mu_\nu})\,, \\
\frac{\partial g_{tt}^{nm}(\omega)}{\partial \ln D} &= -\frac{1}{2}\,(g_{st}^{\nu m}(\omega+K)g_{ts}^{n\nu}(\omega)\Theta_{\omega-\mu_\nu+K} \\
&\quad +g_{st}^{n\nu}(\omega)g_{ts}^{\nu m}(\omega-K)\Theta_{\omega-\mu_\nu-K} \\
&\quad +2g_{tt}^{\nu m}(\omega)g_{tt}^{n\nu}(\omega)\Theta_{\omega-\mu_\nu})\,.
\end{aligned}$$

The chemical potential is defined by $\mu_{1/2} = \pm eV_L/2$ for the leads 1 and 2 on the left side and $\mu_{3,4} = \pm eV_R/2$ for the leads 3 and 4 on the right side. A summation over the internal lead index ν is implicitly understood. Please note, that these RG equations are only valid to leading logarithmic order.

Further Assumptions

The dependence on the frequency appears in the coupling function $g(\omega)$ and in the cutoff function Θ_ω. At the initial cutoff D_0 the couplings are not frequency dependent and the flow is the same for every frequency ω. If the band cutoff D is reduced below some energy scale like the exchange interaction K then the flow of the coupling function is stopped for certain frequencies while the flow for other frequencies continues. Below this energy scale the coupling function is not a constant but explicitly frequency dependent. In the following it is assumed, that the frequency dependence of the coupling function is negligible in comparison to the strong frequency dependence of the Θ-function. The approximation,

$$f(\Delta\omega)\Theta(D-|\Delta\omega|) \to f(0)\Theta(D-|\Delta\omega|),$$

is used and it is assumed, that the frequency argument of the couplings functions is determined by the corresponding Θ-function.

Using these assumptions the RG equations of the double quantum dot system in the case of zero magnetic field are

$$\begin{aligned}
\frac{\partial g_{ts}^{nm}(\omega)}{\partial \ln D} &= -\ \tfrac{1}{2}\ (2g_{ts}^{\nu m}(\mu_\nu)g_{tt}^{n\nu}(\mu_\nu)\Theta_{\omega-\mu_\nu} \\
&\quad +2g_{ts}^{n\nu}(\mu_\nu-K)g_{tt}^{\nu m}(\mu_\nu)\Theta_{\omega-\mu_\nu+K})\,, && \text{(5.14a)} \\
\frac{\partial g_{st}^{nm}(\omega)}{\partial \ln D} &= -\ \tfrac{1}{2}\ (2g_{tt}^{\nu m}(\mu_\nu)g_{st}^{n\nu}(\mu_\nu+K)\Theta_{\omega-\mu_\nu-K} \\
&\quad +2g_{tt}^{n\nu}(\mu_\nu)g_{st}^{\nu m}(\mu_\nu)\Theta_{\omega-\mu_\nu})\,, && \text{(5.14b)} \\
\frac{\partial g_{tt}^{nm}(\omega)}{\partial \ln D} &= -\ \tfrac{1}{2}\ (g_{st}^{\nu m}(\mu_\nu)g_{ts}^{n\nu}(\mu_\nu-K)\Theta_{\omega-\mu_\nu+K} \\
&\quad +g_{st}^{n\nu}(\mu_\nu+K)g_{ts}^{\nu m}(\mu_\nu)\Theta_{\omega-\mu_\nu-K} \\
&\quad +2g_{tt}^{\nu m}(\mu_\nu)g_{tt}^{n\nu}(\mu_\nu)\Theta_{\omega-\mu_\nu})\,. && \text{(5.14c)}
\end{aligned}$$

These RG equations are similar to the scaling equations for the Kondo effect in a singlet-triplet setup [45] and for the double quantum dot considerations in Refs. [46, 69]. However, none of these works includes the frequency dependence of the coupling functions.

Symmetry Relations

Due to the hermiticity of the Hamiltonian symmetry arguments between the three coupling functions have to hold,

$$g_{tt}^{nm}(\omega) = g_{tt}^{mn}(\omega), \tag{5.15a}$$
$$g_{st}^{nm}(\omega) = g_{ts}^{mn}(\omega - K), \tag{5.15b}$$
$$g_{ts}^{nm}(\omega) = g_{st}^{mn}(\omega + K). \tag{5.15c}$$

Consequently there are only two independent coupling functions, because the coupling g_{ts}^{nm} can be represented by the coupling g_{st}^{mn} with different frequency argument or vice versa.

5.3 Flow of the Couplings

The RG equations for a system of two coupled quantum dots are given in Eq. (5.14). In the following we concentrate on the couplings to the left quantum dot. A detailed derivation of the flow of the couplings is given in appendix D.2 assuming that $V_L = 0$. The general case can be worked out straightforwardly in the same manner. In this section the physical content of the scaling equations is addressed. It is assumed that $K \gg \Gamma$ and the temperature T is negligibly small compared to the decoherence rate Γ. One has to distinguish between three different energy regimes for the flowing cutoff D: $D_0 > D > K$, $K > D > \Gamma$, and $\Gamma > D$. These originate from the two different cut off regimes in Eq. (5.14), $\Theta(D - |K|)$ and $\Theta(D - |\Gamma|)$.

5.3.1 Flow in the Energy Regime $D_0 > D > K$

The cutoff D_0 is the largest energy scale of the system. The initial couplings at $D = D_0$ are frequency independent and until the scale $D^* = K$ no frequency dependence is created by the flow, and thus the frequency argument of the coupling functions can be neglected. All Θ-functions have the value one in the regime $D_0 > D > K$ and the RG equations (5.14) in that regime are given by

$$\frac{\partial g_{ts}^{nm}}{\partial \ln D} = -\frac{1}{2}\left(2g_{ts}^{\nu m} g_{tt}^{n\nu} + 2g_{ts}^{n\nu} g_{tt}^{\nu m}\right), \tag{5.16}$$
$$\frac{\partial g_{tt}^{nm}}{\partial \ln D} = -\frac{1}{2}\left(g_{st}^{\nu m} g_{ts}^{n\nu} + g_{st}^{n\nu} g_{ts}^{\nu m} + 2g_{tt}^{\nu m} g_{tt}^{n\nu}\right). \tag{5.17}$$

The coupling g_{st} is related to g_{ts} by the symmetry relation $g_{st}^{mn}(\omega) = g_{ts}^{nm}(\omega - K)$. In this regime the frequency dependence can be neglected and consequently it follows that $g_{st}^{nm} = g_{ts}^{mn}$. The couplings $g_{\gamma\gamma'}^{11} = g_{\gamma\gamma'}^{22}$, denoted the diagonal coupling $g_{\gamma\gamma'}^{d}$, obey a different scaling equation than the couplings $g_{\gamma\gamma'}^{12} = g_{\gamma\gamma'}^{21}$, defined as the transport coupling $g_{\gamma\gamma'}^{t}$.

The equations for the couplings g^d_{ts}, g^t_{ts}, g^d_{tt} and g^t_{tt} can be decoupled by defining symmetrized couplings as

$$g^{\pm}_{+} = (g^d_{tt} \pm g^t_{tt}) + (g^d_{st} \pm g^t_{st}),$$
$$g^{\pm}_{-} = (g^d_{tt} \pm g^t_{tt}) - (g^d_{st} \pm g^t_{st}).$$

Then the equations for the four different couplings $g^{\pm}_{\pm}$ have the same form,

$$\frac{\partial g^{\pm}_{\pm}}{\partial \ln D} = -\left(g^{\pm}_{\pm}\right)^2. \tag{5.18}$$

Eq. (5.18) is the typical flow of a Kondo coupling. The solution for the differential equation (5.18) is

$$g^{\pm}_{\pm}(D) = \frac{1}{\frac{1}{g^{\pm}_{\pm}(D_0)} + \ln\left(D/D_0\right)}.$$

This expression diverges if the cutoff D is reduced to the energy scale T_K, where

$$T_K = D_0\, \mathrm{e}^{-1/g^{\pm}_{\pm}(D_0)}.$$

Altogether there are four different energy scales on which the four different couplings $g^{\pm}_{\pm}$ become divergent. The largest energy scale determines the breakdown of the perturbation. From the definitions of $g^{\pm}_{\pm}$ it is obvious, that g^{+}_{+} is the largest coupling, since it is the sum of four couplings. Therefore the Kondo temperature is determined by the initial value of $g^{+}_{+}(D = D_0)$. In appendix D.2 the general case of different initial couplings is discussed. The discussion here is limited to the special case of symmetric couplings,

$$g(D) \equiv g^d_{tt}(D) = g^t_{tt}(D) = g^d_{st}(D) = g^t_{st}(D) = \frac{g^{+}_{+}(D)}{4},$$

where

$$g^{+}_{+}(D) = \frac{1}{\ln(D/T_K)},$$
$$T_K = D_0\, \mathrm{e}^{-1/4g(D_0)}.$$

Since the double quantum dot system has four degrees of freedom due to the singlet and triplet states and the diagonal and transport processes, the Kondo temperature is given by $D_0 \mathrm{e}^{-1/(4g_{\mathrm{DQD}})}$ instead of $D_0 \mathrm{e}^{-1/(2g_{\mathrm{1QD}})}$ as in a setup with only one quantum dot.

5.3.2 Flow in the Energy Regime $K > D > \Gamma$

When the cutoff is reduced below the energy scale of K, the frequency dependence of the coupling plays a role. In the RG equations Eq. (5.14) either $\Theta(D - \sqrt{\omega^2 + \Gamma})$ or $\Theta(D - \sqrt{(\omega \pm K)^2 + \Gamma})$ cuts off the flow.

In the regime $K > D > \Gamma$ and for $V_L = 0$ the RG equations (5.14) are given by

$$\begin{aligned}\frac{\partial g_{ts}^{nm}(\omega)}{\partial \ln D} &= -\frac{1}{2}\left(2g_{ts}^{\nu m}(0)g_{tt}^{n\nu}(0)\Theta_{\omega}\right.\\ &\quad \left.+2g_{ts}^{n\nu}(-K)g_{tt}^{\nu m}(0)\Theta_{\omega+K}\right), \qquad (5.19)\\ \frac{\partial g_{tt}^{nm}(\omega)}{\partial \ln D} &= -\frac{1}{2}\left(g_{st}^{\nu m}(0)g_{ts}^{n\nu}(-K)\Theta_{\omega+K}\right.\\ &\quad +g_{st}^{n\nu}(K)g_{ts}^{\nu m}(0)\Theta_{\omega-K}\\ &\quad \left.+2g_{tt}^{\nu m}(0)g_{tt}^{n\nu}(0)\Theta_{\omega}\right). \qquad (5.20)\end{aligned}$$

In Eqs. (5.19) and (5.20) the triplet-triplet coupling $g_{tt}(\omega)$ appears on the right hand side only with the frequency $\omega = 0$. As in the regime $D_0 > D > K$ the diagonal $g_{tt}^{d}(\omega = 0) = g_{tt}^{11}(\omega = 0) = g_{tt}^{22}(\omega = 0)$ and the transport coupling $g_{tt}^{t}(\omega = 0) = g_{tt}^{12}(\omega = 0) = g_{tt}^{21}(\omega = 0)$ obey each an RG equation. As before their flow equations are coupled, but can be decoupled by using the sum and difference $g_{tt}^{\pm} = g_{tt}^{d} \pm g_{tt}^{t}$, respectively,

$$\frac{\partial g_{tt}^{\pm}(\omega = 0, D)}{\partial \ln D} = -\left(g_{tt}^{\pm}(\omega = 0, D)\right)^2.$$

Since we assumed symmetric coupling, $g_{tt}^{t}(\omega = 0, D^* = K) = g_{tt}^{d}(\omega = 0, D^* = K)$, the coupling $g_{tt}^{-}(\omega = 0, D^* = K) = 0$ is initially zero and is not created during the flow. The solution of the differential equation for g_{tt}^{+} is

$$g_{tt}^{+}(0, D) = \frac{1}{\ln\left(\frac{D}{T^*}\right)},$$

where

$$T^* = D^* \mathrm{e}^{-1/g_{tt}^{+}(\omega=0,D=D^*)} = K\mathrm{e}^{-2\ln\left(\frac{K}{T_K}\right)} = K\left(\frac{1}{K/T_K}\right)^2 = T_K\,\frac{T_K}{K},$$

and $D^* = K$ is the energy scale where the flow of the coupling functions becomes frequency dependent.

We find for the flow of the triplet-triplet coupling in the regime $K > D > \Gamma$,

$$g_{tt}^{d}(\omega = 0, D) = g_{tt}^{t}(\omega = 0, D) = \frac{1}{2\,\ln\left(\frac{D}{T^*}\right)}.$$

On the right hand side of equations (5.19) and (5.20) only the couplings $g_{ts}^{nm}(\omega = 0)$ and $g_{ts}^{nm}(\omega = -K)$ appear, since $g_{st}^{nm}(\omega = 0) = g_{ts}^{mn}(\omega = -K)$ and $g_{st}^{nm}(\omega = K) = g_{ts}^{mn}(\omega = 0)$. The flow of $g_{ts}^{nm}(\omega = 0, D)$ and $g_{ts}^{nm}(\omega = -K, D)$ is dependent on the flow of $g_{tt}(0, D)$. The transport and the diagonal couplings are defined analogous to the triplet-triplet couplings. From the initial condition at $D^* = K$ it follows immediately that $g_{ts}^{-}(\omega, D) = g_{ts}^{d}(\omega, D) - g_{ts}^{t}(\omega, D) = 0$ and these couplings are not created during the flow.

Thus only the flow of $g_{ts}^{+}(\omega = 0, D) = g_{ts}^{d}(\omega = 0, D) + g_{st}^{t}(\omega = 0, D)$ and $g_{ts}^{+}(\omega = -K, D) = g_{ts}^{d}(\omega = -K, D) + g_{ts}^{t}(\omega = -K, D)$ has to be calculated, for example

$$\frac{\partial g_{ts}^{+}(\omega = 0, D)}{\partial \ln D} = -g_{ts}^{+}(\omega = 0, D)\frac{1}{\ln(D/T^*)}.$$

This differential equation is solved straightforwardly and we find

$$g_{ts}^{+}(\omega = 0, D) = g_{ts}^{+}(\omega = 0, D^*)\frac{\ln D^*/T^*}{\ln D/T^*} = \frac{1}{\ln\left(\frac{D}{T^*}\right)}.$$

The coupling $g_{ts}^{d/t}(\omega = -K, D)$ has the same initial value and obeys the same scaling equation. Thus it also flows like

$$g_{ts}^{+}(\omega = -K, D) = \frac{1}{\ln\left(\frac{D}{T^*}\right)}.$$

The couplings $g_{ts}^{+}(\omega = 0, D)$, $g_{ts}^{+}(\omega = -K, D)$ and $g_{tt}^{+}(\omega = 0, D)$ follow the identical flow. Assuming that all coupling functions start with the same initial value, also in the regime of $K > D > \Gamma$ the frequency dependent couplings at $\omega = 0, \pm K$ flow to the same value,

$$\begin{aligned} g_{ts}^{d/t}(\omega = 0, D) = g_{ts}^{d/t}(\omega = -K, D) = g_{tt}^{d/t}(\omega = 0, D) &= \frac{1}{2\ln D/T^*} \\ &= \frac{1}{2(\ln D/T_K + \ln K/T_K)}. \end{aligned}$$

5.3.3 Flow in the Energy Regime $D < \Gamma$

If the band width D is reduced below the lowest energy scale of the system, none of the couplings flows any more. The couplings scale to a constant value given by the energy scale Γ. The decoherence destroys an infinite series of coherent scattering events that could lead to the strong-coupling behavior of the Kondo couplings. If the band cutoff D is reduced to 0, the coupling functions converge to the value

$$g_{ts}^{d}(\omega = 0, D \to 0) = g_{ts}^{t}(\omega = -K, D \to 0) = g_{tt}^{t}(0, D \to 0) = \frac{1}{2(\ln \Gamma/T_K + \ln K/T_K)}.$$

5.3.4 Illustration of the Flow of the Couplings

The flow of the coupling functions is illustrated in Fig. 5.4 for the parameters of the double quantum dot system used in this thesis. The discussion of the parameters follows in section 5.4.2.

An apparent frequency dependence of the coupling functions is observed in Fig. 5.4. For a large band cutoff $D > K$ the coupling functions follow the same flow at every frequency, but at later stages of the flow the peak structure becomes pronounced. In g_{st} and g_{ts} there are two resonances, which are shifted by the energy K with respect to each other. This confirms the symmetry relation of Eq. (5.15). As discussed in the previous section the peaks flow with the same logarithmic dependence. There are satellite peaks in g_{tt}, which are less pronounced than the peak in g_{ts} at finite frequency. The parameters are chosen with a large decoherence Γ such that the flow of the couplings stops at $g \ll 1$. Therefore the calculation of the current or other physical quantities in second order is justified.

Fig. 5.4 illustrates the flow of characteristic values chosen for the double quantum dot setup considered here. It is found in chapter 6 that the scaling in the flow equation method shows a similar behavior. After the development of the perturbative RG by

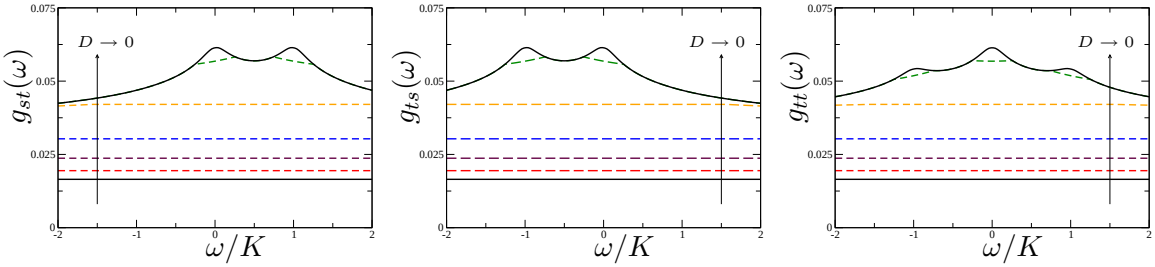

(a) $g_{st}(\omega)$ (b) $g_{ts}(\omega)$ (c) $g_{tt}(\omega)$

Figure 5.4: Flow of the frequency-dependent couplings $g_{st}(\omega)$, $g_{ts}(\omega)$, and $g_{tt}(\omega)$ for the different values of the cutoff $D = 1000, 100, 10, 1, 0.1, 0.01, 0.001$. The flow of the coupling stops when the energy scale of the decoherence is reached. The parameters $1/\ln(K/T_K) = 0.2$, $T/T_K = 0.1$, $B = V_L = V_R = 0$, and $g_0 = 0.0165$ result in a decoherence rate $\Gamma = 0.0063$.

A. Rosch *et al.* [35, 36], the method was applied to other setups as well, here should be mentioned only a few like the singlet-triplet Kondo effect [48], a electrostatically coupled double quantum dot setup in Ref. [70] and the application to the two-channel Kondo model [53].

5.4 Polarization

A detailed discussion of the polarization, $p = n_s - n_t$, is found in section 4.1, where this thermodynamic quantity was shown to depend on the finite voltage to 0th order in a perturbative expansion of the coupling J to the leads. The quantum Boltzmann equation is equivalent to a rate equation of the form

$$\Gamma_{s\to t} n_s = \Gamma_{t\to s} n_t,$$

where $\Gamma_{s\to t}$ is the rate for a transition from a singlet state to a triplet state and analogous for $\Gamma_{t\to s}$. In 2nd order perturbation theory these rates are equivalent to the expressions derived from Fermi's golden rule. The rate $\Gamma_{s\to t}$ corresponds to the broadening $\Gamma_{ss}(\omega_s)/3$ of the singlet state in the notation used in chapters 3 and 4.

Thus the finite life time of the singlet state $1/\Gamma_{ss}(\omega_s)$ is responsible both for a broadening of the singlet resonance and for a non-equilibrium occupation probability of the singlet level. In this section it is discussed how to take both effects into account.

In the following the effect of a finite magnetic field is not addressed. As was discussed in chapter 3 contributions from off-diagonal singlet-triplet Green's functions and self energies can not be neglected for a double quantum dot system with finite magnetic field $B \neq 0$ and left-right asymmetry $g_L \neq g_R$. Since these off-diagonal contributions additionally are important only in the case of $K \ll \Gamma$, this small parameter space is left out of discussion in this part of the thesis.

5.4.1 Self Energy Σ and Spectral Weight Γ

A non-zero self energy of the pseudo particles has two consequences. On the one hand the retarded self energy shifts the resonance by the value of the real part of $\mathrm{Re}\Sigma^r$ and on the other hand it leads to a broadening $\Gamma = i\left(\Sigma^> - \Sigma^<\right) = 2i\mathrm{Im}\Sigma^r$ of the spectral

function. The pseudo particles gain a finite life time due to interactions with the leads. Resonant processes only take place within a time $1/\Gamma$. The Kondo effect itself arises due to resonant spin-flip processes and is destroyed by a finite life time of the pseudo particle states. The broadening Γ has to be included into perturbative RG in order to compensate for the fact that the flow of the running couplings, if not stopped by a system parameter before, is stopped by the decoherence rate Γ.[3] Since the broadening Γ provides a cutoff for the flow of the coupling functions and the coupling functions enter the derivation of the broadening Γ, the flow of the couplings has to be calculated self-consistently. In the routine used here this is done by a few iterative steps until convergence is reached.

On the other hand the lesser self energy plays a major role in a non-equilibrium situation due to a large applied voltage. In this case the lesser and retarded Green's function do no longer fulfill a fluctuation-dissipation theorem as in equilibrium and have to be calculated independently. The lesser Green's functions are derived from a quantum Boltzmann equation, see section 3.5 for a more detailed discussion. The concepts of the non-equilibrium perturbation theory in chapters 3 and 4 are here generalized to the perturbative renormalization group.

In perturbative RG the contour-ordered self energy is given by

$$\Sigma_{\gamma_1',\gamma_2}(\tau_1,\tau_2) = -\frac{1}{16}\sum J^{nk\sigma,\omega_c;mk'\sigma',\omega_c'}_{\gamma_1,\omega_{\gamma_1};\gamma_1',\omega_{\gamma_1'}} J^{mk'\sigma',\omega_c';nk\sigma,\omega_c}_{\gamma_2,\omega_{\gamma_2};\gamma_1,\omega_{\gamma_1}} \vec{\tau}^i_{\sigma'\sigma}\vec{T}^i_{\gamma_1'\gamma_1} X^n_m(\tau_1,\tau_2) G_{\gamma_1}(\tau_1,\tau_2)\vec{T}^j_{\gamma_1\gamma_2}\vec{\tau}^j_{\sigma\sigma'}. \tag{5.21}$$

One has to distinguish between the lesser self energy $\Sigma^<$, which enters the quantum Boltzmann equation, and the broadening $\Gamma = i(\Sigma^> - \Sigma^<)$ that provides a finite life time of the double quantum dot states. In the following only the diagonal parts of the self energy are taken into account. As discussed in the beginning of this section the rates Γ enter as well the retarded Green's functions as the quantum Boltzmann equation in non-equilibrium. Using this information derived in chapter 4 the calculation of the lesser self energy $\Sigma^<$ is redundant.

With the assumptions for the coupling functions $g(\omega)$ as discussed in section 5.3 the spectral weight Γ is given by

$$\begin{aligned}\Gamma_{\gamma\gamma}(\omega) &= i\left(\Sigma^>_{\gamma\gamma}(\omega) - \Sigma^<_{\gamma\gamma}(\omega)\right)\\ &\approx \frac{1}{16}\int\frac{d\epsilon}{2\pi} J^{nk\sigma;mk'\sigma'}_{\gamma';\gamma}(\epsilon') J^{mk'\sigma';nk\sigma}_{\gamma;\gamma'}(\epsilon'+\omega-\epsilon)\\ &\qquad (X^n_m)^>(\omega-\epsilon)\vec{\tau}^i_{\sigma'\sigma}\vec{T}^i_{\gamma\gamma'}A_{\gamma'}(\epsilon)\vec{T}^j_{\gamma'\gamma}\vec{\tau}^j_{\sigma\sigma'}.\end{aligned}$$

The definition and the derivation of the conduction electron spin susceptibility, X^n_m, is found in section B.2. The function X^n_m allows only processes within an energy window according to the chosen frequency of the involved physical processes and also determines the energy of the conduction electrons in the particle-hole loop. This is seen from the

[3] Compare to the definition of the cutoff in Eq. (5.12).

definition,

$$\begin{aligned}(X_m^n)^> (\omega-\epsilon) &= -\int \frac{d\epsilon'}{2\pi} G^<_{nk\sigma}(\epsilon') G^>_{mk'\sigma'}(\epsilon'+\omega-\epsilon) \\ &= -2\pi N(0)^2 \int' d\epsilon' \ \mathrm{ferm}[\epsilon-\omega+\mu_m,\mu_n](\epsilon'),\end{aligned}$$

where

$$\begin{aligned}\mathrm{ferm}[a,b](\omega) &= (1-f(\omega-a))\, f(\omega-b), \\ \int' d\epsilon' &= \int d\epsilon' \Theta(D-|\epsilon'|)\Theta(D-|\epsilon'+\omega-\epsilon|).\end{aligned}$$

The function $\mathrm{ferm}[a,b](\omega)$ equals zero if $a > b$. In the case $a < b$ and for zero tem-

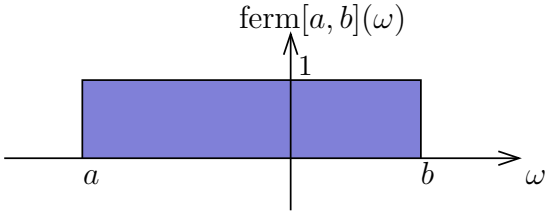

Figure 5.5: Illustration of the function $\mathrm{ferm}[a,b](\omega)$ for $a < b$.

perature $T = 0$, $\mathrm{ferm}[a,b](\omega)$ is equivalent to a box of height one between a and b as illustrated in Fig. 5.5. A finite voltage V shifts the chemical potentials in the leads $\mu_{n,m}$ to $\pm eV/2$. If the energy transfer between the state γ' ($\equiv \epsilon$) and γ ($\equiv w$) takes place in the window opened by the voltage, then this process contributes to the self energy. This behavior was already discussed in the context of the voltage-dependence of the polarization in section 4.1.

It is straightforward to simplify the expression for Γ using the approximation, that the ω-dependence in the integration limits $\pm D + \omega$ can be neglected, since the band cutoff is larger than any other energy scale of the system. We thus find that the broadening Γ in perturbative RG is given by

$$\begin{aligned}\Gamma_{\gamma\gamma}(\omega) = -\frac{1}{16}\int d\epsilon \int_{-D}^{D} d\epsilon' \ g^{nk\sigma;mk'\sigma'}_{\gamma';\gamma}(\epsilon') g^{mk'\sigma';nk\sigma}_{\gamma;\gamma'}(\epsilon'+\omega-\epsilon) \\ \mathrm{ferm}[\epsilon-\omega+\mu_m,\mu_n](\epsilon') \ \vec{\tau}^i_{\sigma'\sigma}\vec{T}^i_{\gamma\gamma'} A_{\gamma'}(\epsilon)\vec{T}^j_{\gamma'\gamma}\vec{\tau}^j_{\sigma\sigma'}.\end{aligned}$$

Remark about the Numerical Calculation

As illustrated in Fig. 5.5 the function $\mathrm{ferm}[a,b]$ is a box of the height one between a and b. Rather than a convolution with the function ferm the Kondo couplings are approximated by their average in the interval from a to b

$$g^{nk\sigma;mk'\sigma'}_{\gamma';\gamma}(\epsilon') g^{mk'\sigma';nk\sigma}_{\gamma;\gamma'}(\epsilon'+\omega-\epsilon) \approx \frac{1}{b-a} \ \overline{g^{nk\sigma;mk'\sigma'}_{\gamma';\gamma} g^{mk'\sigma';nk\sigma}_{\gamma;\gamma'}}(a,b),$$

where

$$\overline{g^{nk\sigma;mk'\sigma'}_{\gamma';\gamma}\, g^{mk'\sigma';nk\sigma}_{\gamma;\gamma'}}(a,b) = \int_a^b d\epsilon' g^{nk\sigma;mk'\sigma'}_{\gamma';\gamma}(\epsilon') g^{mk'\sigma';nk\sigma}_{\gamma;\gamma'}(\epsilon' + \epsilon_\gamma - \epsilon_{\gamma'}).$$

Accordingly we approximate

$$\mathrm{ferm}[a,b] \approx \frac{1}{b-a}\int_a^b d\epsilon' \mathrm{ferm}[a,b](\epsilon').$$

The incoming frequency $\omega \to \epsilon_\gamma$ and the intermediate frequency $\epsilon \to \epsilon_{\gamma'}$ are approximated by the energy of the pseudo particle states on resonance. Using the average of the coupling functions the integrals in the spectral weight Γ can be separated,

$$\Gamma_{\gamma\gamma}(\epsilon_\gamma) = -\frac{1}{16} \int\limits_{\epsilon_{\gamma'}-\epsilon_\gamma+\mu_m}^{\mu_n} d\epsilon'\ g^{nk\sigma;mk'\sigma'}_{\gamma';\gamma}(\epsilon') g^{mk'\sigma';nk\sigma}_{\gamma;\gamma'}(\epsilon' + \epsilon_\gamma - \epsilon_{\gamma'}) \int d\epsilon\ \mathrm{ferm}[\epsilon - \epsilon_\gamma + \mu_m, \mu_n]\ \vec{\tau}^i_{\sigma'\sigma}\vec{T}^i_{\gamma\gamma'} A_{\gamma'}(\epsilon)\vec{T}^j_{\gamma'\gamma}\vec{\tau}^j_{\sigma\sigma'}. \tag{5.22}$$

The approximation that the pseudo particle frequency can be taken on resonance is used again in the expression (5.22) and it is assumed that $\Gamma_{\gamma\gamma}(\omega)$ is calculated on resonance $\omega = \epsilon_\gamma$. The broadening of $A_{\gamma'}$ is neglected in the integration over the coupling functions, but it enters the convolution with $\mathrm{ferm}[\epsilon - \epsilon_\gamma + \mu_m, \mu_n]$.

The expression for $\Gamma_{\gamma\gamma}(\epsilon_\gamma)$ in Eq. (5.22) has to be calculated self-consistently. The spectral weight Γ determines the life time of the pseudo particles and therefore prevents the flow to strong-coupling since the Kondo resonance is destroyed by a non-zero decoherence. The broadening of the spectral function $A_\gamma(\omega) = \pi\Gamma/((\omega - \epsilon_\gamma)^2 + (\Gamma/2)^2)$ is in comparison with the perturbation theory calculation in chapter 4 not neglected and as shown later the broadening Γ determines the width of the resonances. Finally, the rate Γ determines the non-equilibrium distribution function of the singlet and triplet states in a self-consistent equation.

5.4.2 Discussion of the Chosen Parameter Set

If not stated differently the following parameter set is used throughout this chapter

$$\begin{aligned} g_{mn} &= 0.0165, \\ D_0 &= 1000, \\ T_K &= D_0 \mathrm{e}^{-1/(4g)}, \\ T &= 0.1\ T_K, \\ 1/\ln(K/T_K) &= 0.2, \\ V_L = V_R = B &= 0. \end{aligned}$$

In Fig. 5.6 we show the different energy scales of the system. It is found in a renormalization group treatment of the Kondo model, that the energy scale T_K determines the physics of the whole system. All energy scale are thus given in units of T_K. The Kondo

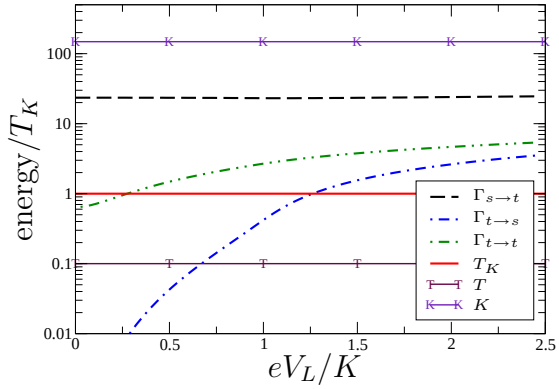

Figure 5.6: Energy comparison and voltage dependence of the decoherence rates $\Gamma_{s\to t}$, $\Gamma_{t\to s}$, and $\Gamma_{t\to t}$ for typical parameters of the system $1/\ln(K/T_K) = 0.2$, $T = 0.1T_K$, $g_L = g_R = 0.0165$ and $V_R = B = 0$. Explanations are given in the text.

temperature T_K was calculated in the previous section. The band cutoff D_0 is assumed to be of the order of $1000meV$ motivated by experimental values. The coupling g_{mn} is chosen such that the system does not flow to strong-coupling before the reduced band cutoff D reaches the energy scale of the decoherence Γ. Since there is a finite decoherence present in the system the temperature is chosen below the Kondo temperature and is thus negligibly small. On the other hand the singlet-triplet gap K has then to be large.

For an antiferromagnetic coupling the ground state of the system is a singlet. The rate $\Gamma_{s\to t}$ is the largest decoherence rate in Fig. 5.6 since the phase space of the singlet states is larger than of the triplet states. Since there are no singlet-singlet processes allowed in the double quantum dot setup, every process includes a transition from a singlet to a triplet state. Thus the rate $\Gamma_{s\to t}$ is involved in all physical process. A singlet-triplet transition is allowed for voltages eV_L above the threshold K. At this energy scale the other rates, $\Gamma_{t\to s}$ and $\Gamma_{t\to t}$, are comparable or larger than the Kondo temperature. In the following calculations of the current and the T-matrix it is thus assumed that all physical quantities are cut off by the rate $\Gamma_{s\to t}$, which is justified in the case of antiferromagnetic coupling. In section 5.7 the ferromagnetic case is discussed and different decoherence rates of singlet and triplet processes are taken into account.

An applied voltage leads to a finite current. Transport processes lead to an increase of the decoherence rates with increasing voltage. Since these decoherence rates also enter the quantum Boltzmann equations, they are responsible for a non-equilibrium occupation number. The voltage dependence of Γ therefore leads to the voltage dependence of thermodynamic properties like the polarization.

Here we only discussed the self energy as a source of decoherence, although in general there are further sources like vertex renormalizations (see Ref. [41]). The vertex corrections can be treated in higher orders or other scaling methods, but are left out in the discussion here.

5.4.3 Discussion of the Polarization

Since no magnetic field is applied, the magnetization equals zero. Nevertheless thermodynamic properties of the double quantum dot system can be studied in the spin-spin correlation $\langle \vec{S}_L \vec{S}_R \rangle$. The spin-spin correlation is proportional to the difference in the

occupation of singlet and triplet states,

$$\langle \vec{S}_L \vec{S}_R \rangle = \frac{3}{4} (n_t - n_s) .$$

Therefore this quantity indicates deviations from the singlet ground state, as discussed in detail in section 4.1.

In the following we discuss the properties of the polarization p using perturbative RG instead of perturbation theory. The polarization,

$$p\,(T, K, V_L, V_R) = n_s - n_t,$$

depends on the temperature T, the exchange interaction K, and the two different voltages V_L and V_R applied to the left and the right quantum dots, respectively.

In Fig. 5.7 the dependence of p on the voltage V_L applied to the left quantum dot is shown. The voltage applied to the right quantum dot is assumed to be zero, $V_R = 0$. The value of p at $V_L = 0$ is close to one, which is the thermodynamic value from equilibrium physics. A special feature of the non-equilibrium situation is the dependence of p on the voltage. As soon as the voltage reaches a value of the order of the exchange interaction K the channel for singlet-triplet processes is opened, and the value of p deviates from 1. For higher voltages not only the singlet is occupied but also triplet states are populated, as illustrated in Fig. 5.7(a). For $eV_L \gg K$ the polarization decreases inversely proportional

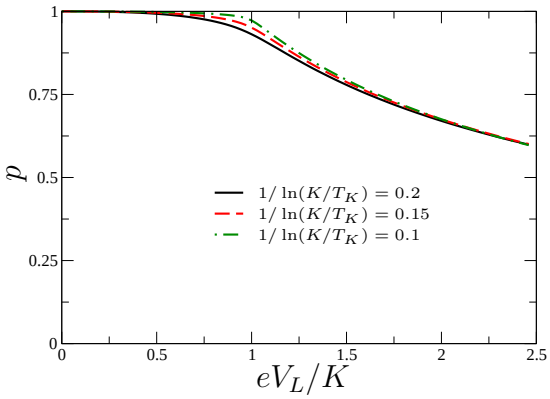

(a) Polarization p vs. voltage eV_L/K.

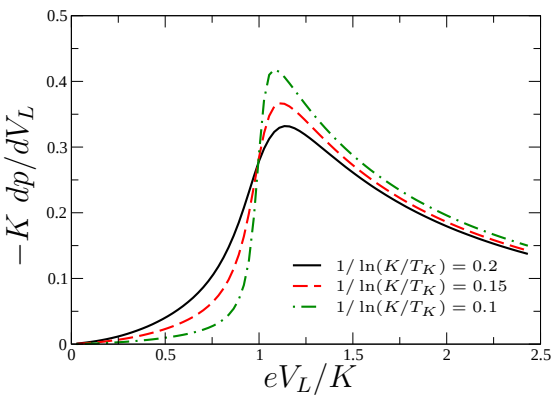

(b) Derivative of the polarization $-K\ dp/dV_L$ vs. voltage eV_L/K.

Figure 5.7: Polarization $p = n_s - n_t$ in dependence of eV_L/K for different values of $\ln(K/T_K)$ when the temperature $T/T_K = 0.1$ is negligibly small. The Kondo coupling on the left and right side is assumed to be identical, $g_L = g_R = 0.00165$.

to the voltage V_L as discussed in detail in section 4.1. This threshold behavior is generic, but in contrast to the perturbation theory calculation the polarization p in perturbative RG depends on the value of the coupling K.

This is studied in Fig. 5.7(b) where the derivative of p with respect to the voltage is shown. The derivative dp/dV_L is inversely proportional to the spin-spin coupling K such that Kdp/dV_L is shown in Fig. 5.7(b) for a better comparison. The derivative is negative, since the polarization decreases. For large voltages the decrease is proportional to $1/V_L^2$ since the polarization falls off like $1/V_L$. We find a pronounced feature at the

threshold $eV_L = K$, where the polarization starts to deviate from the equilibrium value. The width of the structure is given by the decoherence rate Γ. It is observed that the smaller the values of K the broader the resonance, since the coupling flows to larger values. In this case the decoherence is larger since it is roughly proportional to g^2K. This explains the smearing of the threshold with increasing decoherence rate Γ.

In Fig. 5.8 the dependence of the polarization p on the two different voltages V_L and V_R is shown. If the voltage eV_R reaches the threshold K it has an influence on the

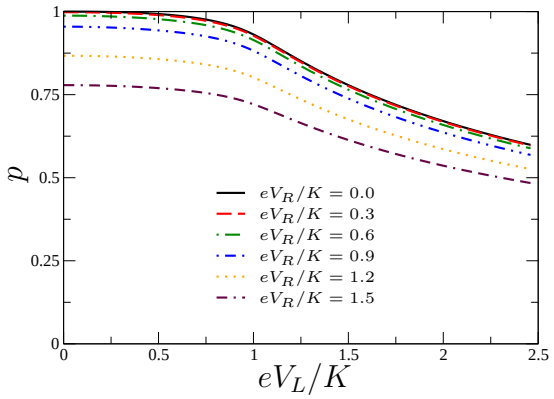

Figure 5.8: Polarization for a negligibly small temperature of $T/T_K = 0.1$ and fixed interaction $1/\ln(K/T_K) = 0.2$. The Kondo coupling on the left and right side is assumed to be identical, $g_L = g_R = 0.0165$. The voltage V_R applied to the right quantum dot is changed and the behavior of p on the voltage eV_L/K is shown.

behavior of p with V_L. This threshold corresponds to the energy necessary for a spin-flip process which in the double quantum dot system is always connected to a singlet-triplet process. A finite value of V_R can provide the energy to populate the triplet states in the same way as V_L does. Since we have assumed the Kondo temperature to be the same on both quantum dots, the left-right symmetry is preserved and V_L can be interchanged by V_R in all figures. Similar to the discussion in perturbation theory we expect the voltage dependence of the polarization to influence the currents through the two coupled quantum dots significantly.

5.5 Non-Equilibrium Current

In this section we discuss the current in perturbative RG as an example of a physical quantity which can be measured in experiment. As was shown in Ref. [35] the perturbative RG method is to leading logarithmic order comparable with experimental data for a single Kondo impurity. After an expression for the current in derived we discuss in detail the properties of the current through a double quantum dot system. An emphasis is put on the transconductance, which was defined in section 4.2 to measure the effect of a voltage applied to the right quantum dot on the current through the left quantum dot. Using the perturbative RG method it is shown that all resonances, also in the transconductance, are enhanced by taking the scaling of the couplings into account.

5.5.1 Calculation of the Non-Equilibrium Current

To derive the expression for the current in the perturbative RG approach we use the result for the current to second order in perturbation theory in Eq. (4.9) in the previous chapter. Including a few straightforward generalizations it is given by

$$\begin{aligned} I =&(2\pi)^2\frac{e^2}{h}\left(\frac{1}{4}N(0)J_{L12}\tau^i_{\sigma'\sigma}T^i_{\gamma'\gamma}\right)\left(\frac{1}{4}N(0)J_{L21}\tau^j_{\sigma\sigma'}T^j_{\gamma\gamma'}\right)\\ &\int_{-D}^{D}d\epsilon\int d\omega\int\frac{d\omega_\gamma}{2\pi}A_\gamma(\omega_\gamma)A_{\gamma'}(\omega_\gamma-\omega)\\ &\left(n_{\gamma'}f(\epsilon+\omega-\mu_1)\left(1-f(\epsilon-\mu_2)\right)-n_\gamma f(\epsilon-\mu_2)\left(1-f(\epsilon+\omega-\mu_1)\right)\right), \end{aligned} \tag{5.23}$$

where $X_2^1(\omega)=-2\pi N(0)f(\epsilon+\omega-\mu_1)(1-f(\epsilon-\mu_2))$ and the analogous expression for $X_1^2(\omega)$ was inserted. The spectral functions are assumed to be Lorentzians rather than δ-functions to take into account the effect of a finite broadening. The convolution of two Lorentzians gives another Lorentzian with a new width of $\Gamma_\gamma+\Gamma_{\gamma'}$ and a modified resonance position. This justifies the approximation that $\Gamma_{s\to t}$ can be used as an averaged broadening, since any process involves a transition of a singlet to a triplet state in the case of antiferromagnetic coupling $K>0$.

The coupling constants are generalized to coupling functions or rather general vertices, but this is straightforward in Eq. (5.23). The replacements are given by

$$\begin{aligned}\left(\frac{1}{4}N(0)J_{L12}\tau^i_{\sigma'\sigma}T^i_{\gamma'\gamma}\right)&\to\mathcal{V}^{2\sigma,\epsilon;1\sigma',\epsilon+\omega}_{\gamma,\omega_\gamma;\gamma',\omega_{\gamma'}},\\ \left(\frac{1}{4}N(0)J_{L21}\tau^j_{\sigma\sigma'}T^j_{\gamma\gamma'}\right)&\to\mathcal{V}^{1\sigma',\epsilon+\omega;2\sigma,\epsilon}_{\gamma',\omega_{\gamma'};\gamma,\omega_\gamma},\end{aligned}$$

where the first index in the vertex refers to the incoming and the second to the outgoing particles of the interaction.

After some straightforward steps the current in the perturbative RG approach is given by

$$\begin{aligned} I =&(2\pi)^2\frac{e^2}{h}\frac{1}{16}\tau^i_{\sigma'\sigma}T^i_{\gamma'\gamma}\,n_\gamma\,T^j_{\gamma\gamma'}\tau^j_{\sigma\sigma'}\\ &\int d\epsilon\int d\omega\Big[A_\gamma(\omega+\omega_{\gamma'})\mathrm{ferm}[-\omega+\mu_2,\mu_1](\epsilon)g^{1\sigma;2\sigma'}_{\gamma,\omega_\gamma;\gamma',\omega_{\gamma'}}(\epsilon)g^{2\sigma';1\sigma}_{\gamma',\omega_{\gamma'};\gamma,\omega_\gamma}(\epsilon+\omega)\\ &-A_\gamma(\omega+\omega_{\gamma'})\mathrm{ferm}[-\omega+\mu_1,\mu_2](\epsilon)g^{2\sigma;1\sigma'}_{\gamma,\omega_\gamma;\gamma',\omega_{\gamma'}}(\epsilon)g^{1\sigma';2\sigma}_{\gamma',\omega_{\gamma'};\gamma,\omega_\gamma}(\epsilon+\omega)\Big]. \end{aligned} \tag{5.24}$$

The first part in Eq. (5.24) describes electrons flowing from lead 2 to lead 1. The second term in Eq. (5.24) with the opposite sign diminishes the current by the flow from lead 1 to lead 2, such that the total current is the difference between these two parts. In order to calculate the current numerically including the flowing coupling functions the same approximations as for the calculation of the self energy are used.

Therefore the energy of the spectral function $A_\gamma(\omega+\omega_{\gamma'})$ is shifted to $A_\gamma(\omega)$. Effectively the integral limits, $-D$ and D, would thus be shifted by $\omega_{\gamma'}$, but it is assumed

that $\omega_{\gamma'}$ is as smaller than the cutoff and therefore the shift is neglected,

$$I\frac{h}{e} = (2\pi)^2 \frac{1}{16} \tau^i_{\sigma'\sigma} T^i_{\gamma'\gamma}\, n_\gamma\, T^j_{\gamma\gamma'} \tau^j_{\sigma\sigma'} \int d\epsilon \int d\omega A_\gamma(\omega) \mathrm{ferm}[-\omega + \omega_{\gamma'} + \mu_2, \mu_1](\epsilon) \; g^{1\sigma;2\sigma'}_{\gamma,\omega_\gamma;\gamma',\omega_{\gamma'}}(\epsilon) g^{2\sigma';1\sigma}_{\gamma',\omega_{\gamma'};\gamma,\omega_\gamma}(\epsilon + \omega - \omega_{\gamma'}) - \{1 \leftrightarrow 2\}. \tag{5.25}$$

It is also assumed that it is sufficient to use the average of the couplings in the window opened by the function ferm similar to the approximations in the calculation of Γ. Therefore the two integrals can be calculated independently. This approximation is justified since we are only interested in the leading logarithmic order.

Finally the current in the numerical routine is calculated by

$$I\frac{h}{e} = (2\pi)^2 \sum \frac{1}{16} \tau^i_{\sigma'\sigma} T^i_{\gamma'\gamma}\, n_\gamma\, T^j_{\gamma\gamma'} \tau^j_{\sigma\sigma'} \left[\int_{\omega_{\gamma'} - \omega_{\gamma'} + \mu_1}^{\mu_2} d\epsilon \; g^{1\sigma;2\sigma'}_{\gamma,\omega_\gamma;\gamma',\omega_{\gamma'}}(\epsilon) g^{2\sigma';1\sigma}_{\gamma',\omega_{\gamma'};\gamma,\omega_\gamma}(\epsilon + \omega - \omega_{\gamma'}) \right] \left[\int d\omega A_\gamma(\omega) \mathrm{ferm}[-\omega + \omega_{\gamma'} + \mu_2, \mu_1] \right] - \{1 \leftrightarrow 2\}.$$

The results and the physical content of the current of a double quantum dot system are discussed in the following section.

5.5.2 Current through a Double Quantum Dot System

The expression (5.25) is specialized to the double quantum dot system. Assuming all triplets to be degenerate for zero magnetic field $B = 0$, the evaluation of the summation over all spin degrees of freedom gives the current

$$\begin{aligned} I = \frac{e^2}{h}(2\pi)^2 \frac{1}{8} \int d\epsilon \, \{ \quad & 3n_t \mathrm{ferm}[-K + \mu_2, \mu_1](\epsilon) g^{12}_{ts}(\epsilon) g^{21}_{st}(\epsilon + K) \\ & + 3n_s \mathrm{ferm}[K + \mu_2, \mu_1](\epsilon) g^{12}_{st}(\epsilon) g^{21}_{ts}(\epsilon - K) \\ & + 6n_t \mathrm{ferm}[\mu_2, \mu_1](\epsilon) g^{12}_{tt}(\epsilon) g^{21}_{tt}(\epsilon) \\ & - \{1 \leftrightarrow 2\} \, \}. \end{aligned} \tag{5.26}$$

The chemical potentials are shifted by a finite voltage, $\mu_1 = +eV_L/2$ and $\mu_2 = -eV_L/2$. The function ferm appears in Eq. (5.26) with six different arguments. Only a few give a finite contribution. In the following considerations the spin-spin coupling is assumed to be antiferromagnetic $K > 0$. A discussion of the ferromagnetic case $K < 0$ follows in section 5.7. At $V = 0$ the current is zero by symmetry. In the following we assume that the voltage V is in the linear regime, i.e. it is smaller than the singlet-triplet excitation gap K such that the threshold or Kondo enhanced resonance is not reached.

Then $\mathrm{ferm}[\mu_2, \mu_1]$ is proportional to the voltage V_L or temperature T in the case of $V_L = 0$, but the temperature is assumed to be negligibly small. The functions $\mathrm{ferm}[\mu_1, \mu_2]$ and $\mathrm{ferm}[K + \mu_1, \mu_2]$ are identically zero, and also the contribution from $\mathrm{ferm}[K + \mu_2, \mu_1]$ vanishes as long as $eV_L < K$. The function $\mathrm{ferm}[-K + \mu_1, \mu_2]$ is non-zero in the energy

window between $-K + eV_L/2$ and $-eV_L/2$. Finally the most important contribution comes from ferm$[-K + \mu_2, \mu_1]$ in the energy window between $-K - eV_L/2$ and $+eV_L/2$.

Using the relations $g^{n,m}_{s,t}(\epsilon + K) = g^{m,n}_{t,s}(\epsilon)$ and $g^{n,m}_{t,t}(\epsilon) = g^{m,n}_{t,t}(\epsilon)$ and neglecting a finite broadening of the decoherence or the temperature, the current can be written by

$$I_L \frac{h}{e^2} = (2\pi)^2 \frac{3}{8} n_t \left\{ \int_{-K-V/2}^{V/2} d\epsilon \left(g^{12}_{ts}(\epsilon)\right)^2 + 2 \int_{-V/2}^{V/2} d\epsilon \left(g^{12}_{tt}(\epsilon)\right)^2 - \int_{-K+V/2}^{-V/2} d\epsilon \left(g^{21}_{ts}(\epsilon)\right)^2 \right\}. \tag{5.27}$$

It is observed that the current in the linear voltage regime is proportional to n_t. If the exchange interaction K is antiferromagnetic, the singlet is the ground state and there is only a non-zero current below the threshold if there is a finite occupation of the triplet states due to e.g. a large voltage $eV_R > K$ applied to the right quantum dot.

5.5.3 Discussion of the Current Properties

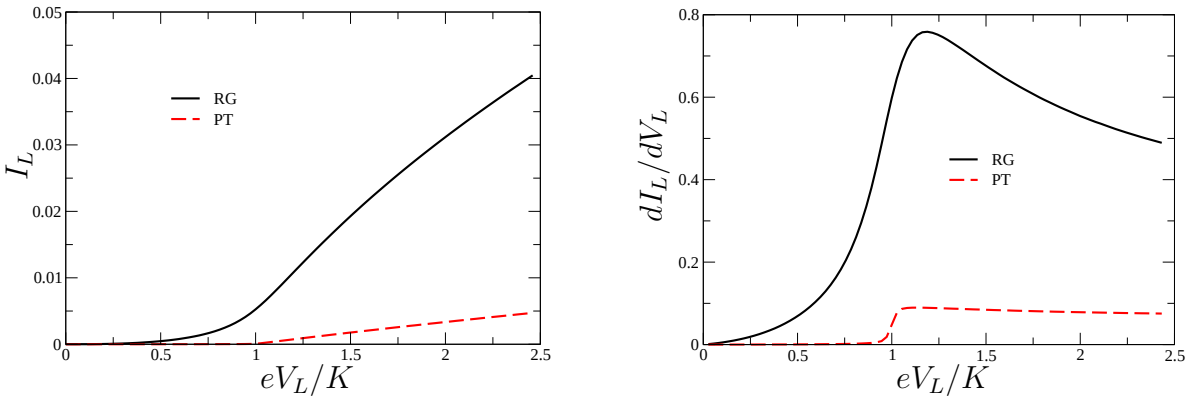

(a) Current I_L vs. voltage eV_L/K.

(b) Differential conductance dI_L/dV_L vs. voltage eV_L/K.

Figure 5.9: Current $I_L[e^2/h]$ characteristic for the left quantum dot and differential conductance $dI_L/dV_L[e^2/h]$ from this curve for $B = V_R = 0$, $g_L = g_R = 0.0165$ and exchange interaction of $1/\ln(K/T_K) = 0.2$. The temperature is chosen to be small $T/T_K = 0.1$ such that the broadening originates only from the dephasing. For comparison the result of the 2nd order perturbation theory (PT) is shown.

In Fig. 5.9(a) we show a typical current characteristic for a double quantum dot system in the case of zero magnetic field. The current is antisymmetric with respect to the applied voltage, and thus only the positive voltage axis is shown. It is assumed that there is no difference in the chemical potentials on the right side ($V_R = 0$). For a small applied voltage the current is approximately zero and only thermodynamically excited processes contribute to a small transport current. As soon as the voltage becomes of the order of the exchange interaction K the current starts to increase, because the voltage provides the energy for inelastic processes. This threshold behavior is better seen in the derivative of the current. The dI/dV curve in Fig. 5.9(b) shows a resonance close to $eV_L \sim K$. Although $eV_L = K$ is the inflection point and not the maximum of the

curve. As discussed in section 4.2 the maximum in the 2nd derivative of the current with respect to the voltage, d^2I_L/dV_L^2, is equivalent to the exchange coupling K.

As illustrated in Fig. 5.9 the perturbative RG and the perturbation theory results show certain differences. Both differential conductance dI_L/dV_L curves show a resonance around K, but the value of the differential conductance at the resonance is Kondo enhanced in the perturbative RG approach. At the negligibly small temperature chosen in Fig. 5.9 the broadening originates only from decoherence processes in the singlet-triplet channel and is not given by the temperature T as in the perturbation theory. It can be shown, although not illustrated here, that including a finite broadening in the current calculation and using a rescaled coupling constant fails to describe the current characteristic found in perturbative RG. At a finite energy, e.g. $\omega = K$, the conduction electrons can provide the energy for coherent spin-flip processes. The coupling flows logarithmically at this certain frequency and thus the step in the differential conductance is significantly enhanced. This confirms that the frequency dependence of the coupling functions is important.

For temperatures larger than the Kondo temperature T_K the broadening is determined by the temperature and not by the dephasing, as illustrated in Fig. 5.10(a). A finite

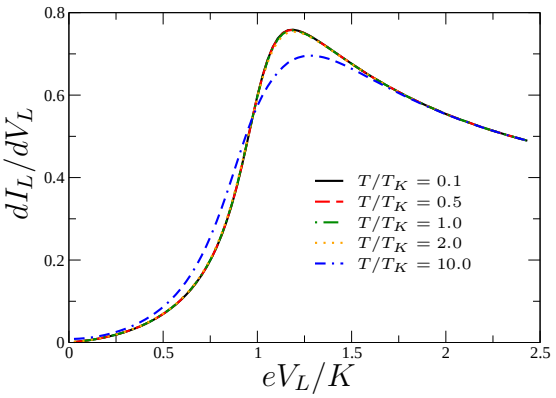

(a) Differential conductance vs. voltage for different values of the temperature.

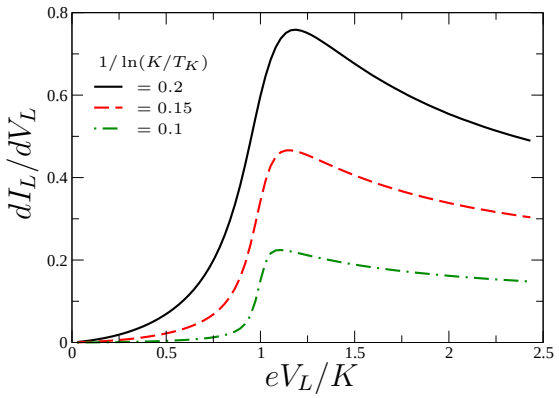

(b) Differential conductance vs. voltage for different values of the coupling K.

Figure 5.10: Differential conductance $dI_L/dV_L[e^2/h]$ through the left quantum dot for zero magnetic field $B = 0$ and voltage $V_R = 0$. In the left panel the temperature is changed from below the Kondo temperature $T/T_K = 0.1$ to values above T_K while the interaction is kept constant at $1/\ln(K/T_K) = 0.2$. In the right panel different values of the exchange interaction $\ln(K/T_K)$ are shown, which are chosen such that the perturbative approach is still valid. The temperature here is negligibly small $T/T_K = 0.1$.

temperature smears the Fermi surface of the conduction electrons and therefore destroys the coherent scattering processes which lead to the Kondo divergence. The value at the resonance is lower than the unitary value of $2e^2/h$. For temperatures close to and below the Kondo temperature T_K one expects a Kondo resonance to form, i.e. the resonance reaches the unitary limit. The transport through the quantum dot destroys the coherence which is important for the build-up of the Kondo effect and the behavior is determined by the finite broadening Γ of the double quantum dot levels. As observed in Fig. 5.10(a) the differential conductance dI_L/dV_L does not depend on the temperature of the system for temperatures T lower than Γ.

In Fig. 5.10(b) the dependence of the differential conductance through the left quantum dot on the voltage is shown for different strength of the interaction K/T_K. The perturbative RG is a perturbative method, such that we are not able to calculate physical properties within the Kondo regime. The flow has to be cut off to keep the coupling in the perturbative regime. For a double quantum dot setup there are three parameters which provide a cutoff for the flow. First there is the temperature which is assumed to be negligibly small, $T/T_K = 0.1$ in Fig. 5.10(b). The applied voltage also cuts off the flow indirectly through the mechanism of dephasing. Besides the voltage dependence of the different broadenings Γ it was shown in Fig. 5.6 that the energy scale which cuts off the flow is on average given by the decoherence rate $\Gamma = \Gamma_{s\to t}$. Due to the finite phase space $\Gamma_{s\to t}$ is always larger than T_K, but for example $\Gamma_{t\to t}$ is only comparable to T_K at $eV_L \sim K$, see also discussion in sections 5.4.2 and 5.7. The exchange coupling K leads to a level splitting of the singlet and triplet states and it also provides a cutoff. As discussed in section 5.3 the couplings in a symmetric setup flow to the value of $\frac{1}{2\ln(\Gamma K/T_K^2)}$. The effect of the cutoff by K is observed in Fig 5.10(b). For larger values of K the flow is stopped at a smaller values of the coupling and the absolute value of dI/dV decreases further below the unitary value $2e^2/h$.

Transconductance

It was observed in the differential conductance that no transport takes place as long as the voltage V_L is below the threshold given by the singlet-triplet excitation gap K. For an antiferromagnetic exchange interaction the singlet is the ground state. There are no spin-conserving processes which allow for a transport without changing the singlet to a triplet state. Only if the voltage V_L provides sufficient energy, a finite dI_L/dV_L is observed. If triplet states are occupied for example due to a finite temperature, elastic processes contribute to a small current signal even within the linear voltage regime.

In section 5.4.3 it was observed that the polarization $p = n_s - n_t$ deviates from one if a sufficiently large voltage is applied to the right quantum dot. A finite voltage provides the energy to populate triplet states. If triplet states are available for transport, there is a finite current for small voltages V_L, as discussed in Eq. (5.27). In Fig. 5.11

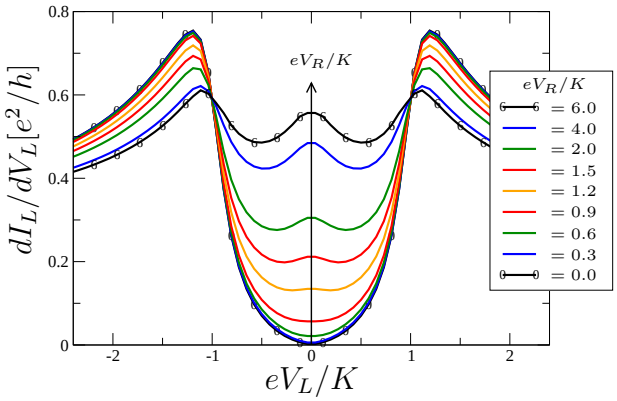

Figure 5.11: Differential current dI_L/dV_L versus eV_L/K for an spin-spin interaction $1/\ln(K/T_K) = 0.2$ while the voltage eV_R/K is changed. The Kondo couplings on the left and right side are assumed to be the identical to $g_L = g_R = 0.0165$ and temperature $T/T_K = 0.1$ is chosen negligibly small.

this effect is observed. As long as the voltage V_R across the right quantum dot is smaller than the exchange interaction K, only an increase in the width of the resonance due to a larger decoherence rate is observed. As soon as the voltage V_R reaches the threshold, the dI_L/dV_L characteristic changes. This is a pure non-equilibrium effect and originates from the 0th order correction of the occupation numbers due to the quantum Boltzmann equation. A comparison of the zero bias value of dI_L/dV_L with the slope of the polarization p with increasing voltage shows a good agreement, see Fig. 5.7(a). A double quantum dot setup therefore provides the possibility to measure the voltage-dependence of the double quantum dot states within a current measurement. Since the current is more easily accessible in experiments than a correlation like $\langle \vec{S}_L \vec{S}_R \rangle$, this provides an interesting experimental means.

An expression for the differential conductance dI_L/dV_L is derived from the expression for the current in Eq. (5.27). In the linear regime of the voltage $eV_L < K$ it is assumed that the triplet occupation does not depend on V_L and thus $dn_t/dV_L = 0$. Therefore we find

$$\begin{aligned}\frac{dI_L}{dV_L}\frac{h}{e^2} = (2\pi)^2 \frac{3}{8} n_t \frac{1}{2} \Big\{ &\left(g_{ts}^{12}(V_L/2)\right)^2 + \left(g_{ts}^{12}(-K - V_L/2)\right)^2 \\ &+ \left(g_{ts}^{21}(-V_L/2)\right)^2 + \left(g_{ts}^{21}(-K + V_L/2)\right)^2 \\ &+ 2\left(g_{tt}^{12}(V_L/2)\right)^2 + 2\left(g_{tt}^{12}(V_L/2)\right)^2 \Big\}. \end{aligned} \tag{5.28}$$

The voltage V_R enters through the occupation of the triplet states $n_t = \frac{1}{4}(1-p)$. The polarization $p = n_s - n_t$ was discussed in detail in the previous section and also in section 5.4.

In Fig. 5.11 the differential conductance develops a zero-bias peak due to Kondo correlations. This originates from the coupling g_{tt} in Eq. (5.28). Since the triplet states are degenerate for $B = 0$ and thus coherent spin-flip processes can take place, the coupling g_{tt} at $\omega = 0$ diverges logarithmically as illustrated in Fig. 5.4. For large values of the voltage $eV_R > K$ there is a sufficient population of triplet states such that this effect becomes visible.

We suggested in Ref. [65] to measure in experiment the so-called transconductance as illustrated in Fig. 5.12. The transconductance $(K/eV_L)dI_L/dV_R$ is defined as the renormalized derivative of the current I_L through the left quantum dot with respect to the voltage V_R applied to the right quantum dot. This quantity was already discussed in detail in section 4.2 and an analytical expression for it was given in Eq. (4.14) to second order in perturbation theory ($\mathcal{O}(2)$). Whereas the differential conductance dI_L/dV_L at zero bias voltage increases proportional to the occupation of triplet states and therefore the polarization p, the transconductance $(K/eV_L)dI_L/dV_R$ increases proportional to Kdp/dV_R. as illustrated in Fig. 5.7(b) this slope shows a similarity to the behavior observed in Fig. 5.12. The peak is enhanced by the scaling of the couplings in perturbative RG compared to the result in perturbation theory. In contrast to the second order result the transconductance depends additionally on the strength of K, see therefore discussion of the dependence of the differential conductance dI_L/dV_L on K. It was shown in section 4.2 that the transconductance to second order in perturbation theory is generic for all voltages below the threshold. As illustrated in Fig. 5.12(b) this is not valid using the perturbative RG approach. The deviations in Fig. 5.12(b) originate from the non-zero decoherence rate. On one hand a different voltage also leads to a different decoherence.

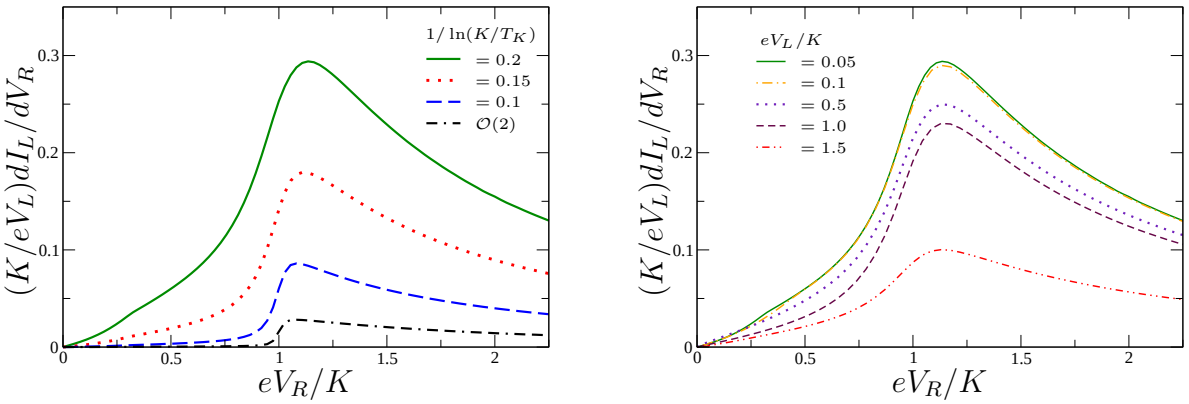

(a) Transconductance for different values of $\ln(K/T_K)$.

(b) Transconductance for different values of eV_L/K.

Figure 5.12: Transconductance $(K/eV_L)dI_L/dV_R[e^2/h]$ versus eV_R/K for different coupling strength $\ln(K/T_K)$ and different voltages eV_L/K. The parameters are chosen $g_L = g_R = 0.0165$, $T = 0.1T_K$, and $B = 0$.

On the other hand this leads to a smearing of the threshold such that there is already a occupations probability for triplet states in the vicinity of Γ around the threshold.

The perturbative RG facilitates a comparison with experiments. There are already some experimental setups, e.g. [27, 29], which provide the possibility to compare the theoretical results for the differential conductance. As mentioned before a qualitative comparison with experiment is possible such that we can describe the structure of the split Kondo peak. Since the perturbative RG is limited to the weak-coupling regime we are not able to discuss the transition from a Kondo screened quantum dot to a double quantum dot singlet, see therefore the discussion in Refs. [30, 31]. We hope that a finite transconductance will be observed in the near future.

5.6 T-Matrix

As explained in section 4.3 the T-matrix in a Kondo model is equivalent to the low-frequency limit of the density of states of the impurity level of a corresponding Anderson impurity model. A calculation of the T-matrix using the perturbative RG approach thus allows for a comparison with numerical methods like the NRG [59]. The numerical RG can provide exact results in the strong-coupling limit, but the method is based on ground state properties and can therefore not be generalized to non-equilibrium. The comparison of the two methods is therefore interesting and an ongoing project exists with Prof. Chung-Hou Chung [71] from the National Chiao-Tung University, Taiwan.

5.6.1 Calculation of the T-Matrix

In section 4.3 an expression for the T-matrix to 2nd order in perturbation theory was derived. This expression, Eq. (4.19), is generalized to coupling functions in the framework of perturbative RG, similar to the expression for the current in the previous section. Leaving out a few steps of the calculation we find the general expression for the T-matrix

in perturbative RG,

$$\begin{aligned}
&-\frac{1}{\pi}\mathrm{Im}\left[N(0)T^r(\omega)\right] \\
=&\mathcal{V}^{m\sigma',\omega+\epsilon_{\gamma'}-\epsilon_\gamma;n\sigma,\omega}_{\gamma,\epsilon_\gamma;\gamma',\epsilon_{\gamma'}}\mathcal{V}^{n\sigma,\omega;m\sigma',\omega+\epsilon_{\gamma'}-\epsilon_\gamma}_{\gamma',\epsilon_{\gamma'};\gamma,\epsilon_\gamma} \\
&\int_{-D}^{D} d\epsilon \int d\epsilon_1 \left(\left[n_\gamma - n_{\gamma'}\right] f(\omega+\epsilon-\mu_m) + n_{\gamma'}\right) A_{\gamma'}(\epsilon_1+\epsilon) A_\gamma(\epsilon_1),
\end{aligned} \tag{5.29}$$

where it is assumed that the leads are in equilibrium such that their distribution is given by the Fermi function $f(\omega)$. The pseudo particle energies are assumed to be on-resonance such that the general vertex $\mathcal{V}$ can be taken out of the integration in Eq. (5.29). As discussed in the previous sections the influence of a finite decoherence becomes important out of equilibrium. Therefore the spectral function in Eq. (5.29) is not approximated by a δ-function.

The T-matrix is given by a convolution of the Fermi function with two spectral functions of the pseudo particle states. The convolution of two Lorentzians in Eq. (5.29) gives another Lorentzian with the resonance at $\epsilon_{\gamma'}-\epsilon_\gamma$ and a width given by the sum of the broadenings. This justifies that the term $\Gamma_{s\to t}$ is used as an averaged broadening Γ in the numerical routine. The first part of the integral in Eq. (5.29) over the Lorentzian equals one due to normalization. The second part of the integral is a convolution of $f(\omega)=\frac{1}{2}(1-\tanh(\omega/2T))$ with the Lorentzian of the width Γ. This convolution can be approximated by a broadened Fermi-function,

$$f_\Gamma(\omega) = \frac{1}{2}\left(1-\frac{2}{\pi}\arctan\left(\frac{\omega}{\Gamma}\right)\right). \tag{5.30}$$

This expression is only valid for a negligibly small temperature T. A derivation of Eq. (5.30) is found in appendix B.2. The function $f_\Gamma(\omega)$ is proportional to $(-\arctan(\omega/\Gamma))$ where the width is determined by Γ rather than to $(-\tanh(\omega/2T))$ which is broadened by the temperature T. The frequency dependence of Γ is neglected, since it is only important if the integration takes place over a large energy scale. A discussion of a frequency dependent spectral width is given in appendix A of Ref. [52].

Using the definition of $f_\Gamma(\omega)$, Eq. (5.30), the T-matrix can be written without an integration,

$$\begin{aligned}
-\frac{1}{\pi}\mathrm{Im}\left[N(0)T^r(\omega)\right] =&\mathcal{V}^{m\sigma',\omega+\epsilon_{\gamma'}-\epsilon_\gamma;n\sigma,\omega}_{\gamma,\epsilon_\gamma;\gamma',\epsilon_{\gamma'}}\mathcal{V}^{n\sigma,\omega;m\sigma',\omega+\epsilon_{\gamma'}-\epsilon_\gamma}_{\gamma',\epsilon_{\gamma'};\gamma,\epsilon_\gamma} \\
&\left[\frac{1}{2}\left[n_\gamma+n_{\gamma'}\right]+\frac{1}{2}\left[n_\gamma-n_{\gamma'}\right]\left(2f_\Gamma(\omega+\epsilon_{\gamma'}-\epsilon_\gamma-\mu_m)-1\right)\right].
\end{aligned} \tag{5.31}$$

Eq. (5.31) is generally valid for any setup of quantum dots, and the explicit properties of the system are given by the structure of the general vertex $\mathcal{V}$.

Explicit Formula

In order to calculate a specific expression for the T-matrix of a double quantum dot system the summation over the corresponding vertices $\mathcal{V}$ is performed in equation (5.31).

If the magnetic field vanishes, $B = 0$, the triplet states are degenerated and the symmetry in spin space is conserved. The sum over n_γ thus gives

$$\begin{aligned}&\frac{1}{16}T^i_{\gamma'\gamma}n_\gamma T^j_{\gamma\gamma'}\tau^i_{\sigma\sigma'}\tau^j_{\sigma'\sigma}g^{n\sigma,\omega;m\sigma',\omega+\epsilon_{\gamma'}-\epsilon_\gamma}_{\gamma',\epsilon_{\gamma'};\gamma,\epsilon_\gamma}g^{m\sigma',\omega+\epsilon_{\gamma'}-\epsilon_\gamma;n\sigma,\omega}_{\gamma,\epsilon_\gamma;\gamma',\epsilon_{\gamma'}}\\ =&\frac{2\cdot 3}{16}\left[n_t\, g^{mn}_{ts}(\omega-K)g^{nm}_{st}(\omega)+n_s\, g^{mn}_{st}(\omega+K)g^{nm}_{ts}(\omega)+2n_t\, g^{mn}_{tt}(\omega)g^{nm}_{tt}(\omega)\right].\end{aligned}$$

Using the hermiticity of the Hamiltonian (e.g. $g^{mn}_{ts}(\omega-K) = g^{nm}_{st}(\omega)$) this expression simplifies to

$$\frac{3}{8}\left[n_t\left(g^{nm}_{st}(\omega)\right)^2+n_s\left(g^{nm}_{ts}(\omega)\right)^2+2n_t\left(g^{nm}_{tt}(\omega)\right)^2\right].$$

Analogously to the previous calculation the sum over $n_{\gamma'}$ gives

$$\begin{aligned}&\frac{1}{16}T^j_{\gamma\gamma'}n_{\gamma'}T^i_{\gamma'\gamma}\tau^j_{\sigma'\sigma}\tau^i_{\sigma\sigma'}g^{m\sigma',\omega+\epsilon_{\gamma'}-\epsilon_\gamma;n\sigma,\omega}_{\gamma,\epsilon_\gamma;\gamma',\epsilon_{\gamma'}}g^{n\sigma,\omega;m\sigma',\omega+\epsilon_{\gamma'}-\epsilon_\gamma}_{\gamma',\epsilon_{\gamma'};\gamma,\epsilon_\gamma}\\ =&\frac{3}{8}\left[n_s\left(g^{nm}_{st}(\omega)\right)^2+n_t\left(g^{nm}_{ts}(\omega)\right)^2+2n_t\left(g^{nm}_{tt}(\omega)\right)^2\right].\end{aligned}$$

In the T-matrix a factor of 2 originates from the spin summation of the conduction electron spin, $\mathrm{Tr}\left[\vec{\tau}\vec{\tau}\right] = 2$, and the factor of 3 originates from the three room coordinates since for zero magnetic field the spin symmetry is conserved.

Consequently Eq. (5.31) gives

$$\begin{aligned}-\frac{1}{\pi}\mathrm{Im}\left[N(0)T^r(\omega)\right] = \frac{3}{8}\Big[&\frac{1}{2}\left(g^{nm}_{ts}(\omega)\right)^2\left[n_s-n_t\right]\left(2f_\Gamma(\omega+K-\mu_m)-1\right)\\ &-\frac{1}{2}\left(g^{nm}_{st}(\omega)\right)^2\left[n_s-n_t\right]\left(2f_\Gamma(\omega-K-\mu_m)-1\right)\\ &+n_t\left(\frac{1}{2}\left(g^{nm}_{st}(\omega)\right)^2+\frac{1}{2}\left(g^{nm}_{ts}(\omega)\right)^2+2\left(g^{nm}_{tt}(\omega)\right)^2\right)\\ &+n_s\left(\frac{1}{2}\left(g^{nm}_{st}(\omega)\right)^2+\frac{1}{2}\left(g^{nm}_{ts}(\omega)\right)^2\right)\Big].\end{aligned} \tag{5.32}$$

5.6.2 Discussion of Results for the T-Matrix

The difference between the perturbation theory calculation to 2nd order and the perturbative RG is illustrated in Fig. 5.13(a) using the same set of parameters as used in the current calculation. We observe two major differences, first of all the perturbative RG calculation is non-zero for $\omega = 0$. This originates from a finite broadening since the value is identical to zero if a different broadening, e.g. $\Gamma = T$, is used. Additionally the T-matrix in perturbative RG is logarithmically enhanced at the step and decreases for larger values of ω whereas in perturbation theory the step stays constant at a finite value. If the broadening is given by the temperature, the value at $\omega = 0$ is zero and the resonance is logarithmically enhanced as seen in Fig. 5.13(a). For $\Gamma = T$ in Fig. 5.13(a) also the cutoff of the flowing coupling functions is provided by the negligibly small temperature. Thus the divergence of the coupling $g_{st}(\omega = K)$ is stopped at a later stage in the flow compared to the flow with finite Γ. For a comparison of perturbative RG with

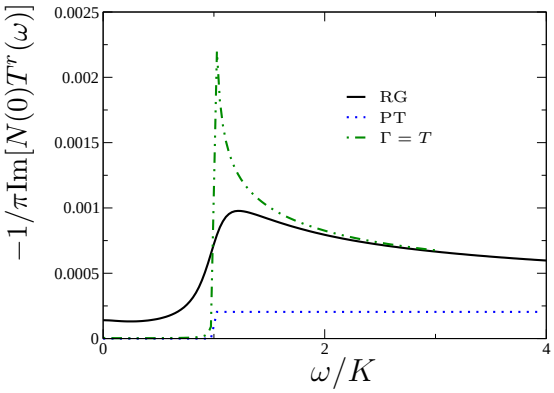

(a) Comparison between T-matrix in perturbation theory and perturbative RG, with and without finite broadening.

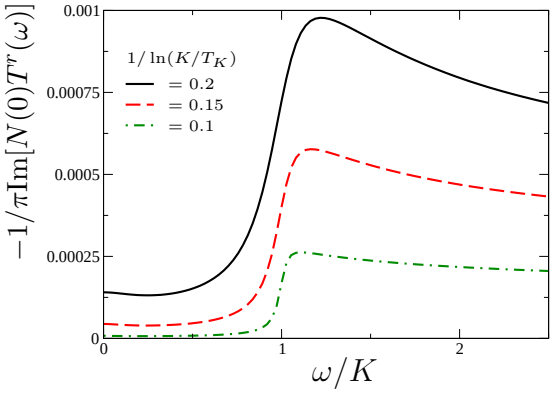

(b) T-matrix vs. frequency ω/K for various interaction strength K.

Figure 5.13: T-matrix $-1/\pi \mathrm{Im}[N(0)T^r(\omega)]$ versus frequency ω/K at temperature $T/T_K = 0.1$, voltages $V_L = V_R = 0$, and initial coupling $g_L = g_R = 0.0165$. The difference between the calculation to second order in perturbation theory (PT) and perturbative RG is illustrated in the left panel for $1/\ln(K/T_K) = 0.2$. For comparison a result is shown assuming that the decoherence is given solely by the temperature. In the right panel the T-matrix $T^r(\omega)$ is shown for different values of the exchange interaction K/T_K.

NRG [71] it is therefore important to find the equivalent broadening schemes, since the result depends significantly on the choice of Γ.

In contrast to perturbation theory the T-matrix in perturbative RG also depends on the exchange interaction K as shown in Fig. 5.13(b). The flow is cut off at different energy scales dependent on the singlet-triplet gap and the decoherence rate. This explains the difference between the different exchange interactions K/T_K, see also discussion of the dependence of the current on different coupling strength.

The behavior of the T-matrix changes if we apply a finite voltage either across the left or the right quantum dot. As discussed in section 4.3 this leads to a direct or an indirect effect. For a voltage applied across the left quantum dot it is observed in Fig. 5.14(a) that the step moves into the valley. Since in non-equilibrium the Kondo coupling is enhanced at both Fermi edges, rather a peak than a step is found at the energies $\omega = K \pm eV_L/2$. For a voltage above the threshold, $eV_L > K$, triplet states become populated and the value of the T-matrix at low frequencies increases.

In Fig. 5.14(b) the T-matrix is plotted for equilibrium ($V_L = 0$) at the probed leads and a finite shift of the chemical potential $\pm V_R/2$ at the other leads. A non-equilibrium situation on the right dot increases the population of triplet states. In perturbative RG this leads to a small zero-bias peak due to Kondo enhanced processes from the triplet-triplet coupling g_{tt} at zero frequency as seen in Fig. 5.14(b).

We found in the study of the T-matrix that interesting physical behavior arises if a finite voltage is applied to a system of two coupled quantum dots. As in the discussion of the previous section we found signatures in the T-matrix that a non-equilibrium situation e.g. on the right quantum dot is transferred to the left quantum dot. Since the T-matrix of the studied Kondo model is identical to the low-frequency spectral function of the corresponding Anderson impurity model [59], this calculation provides the possibility to compare the results of the perturbative RG with NRG. Such a comparison is an

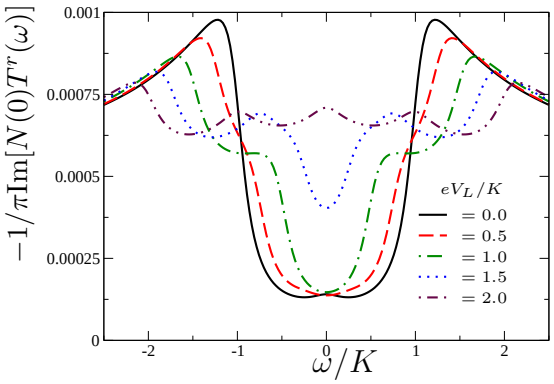

(a) T-matrix vs. ω/K for different values of the voltage V_L and $V_R = 0$.

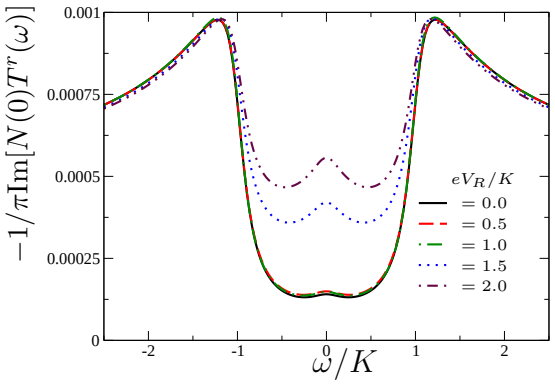

(b) T-matrix vs. ω/K for different values of the voltage V_R and $V_L = 0$.

Figure 5.14: T-matrix $-1/\pi \mathrm{Im}[N(0)T^r(\omega)]$ versus frequency ω/K at $1/\ln(K/T_K) = 0.2$, temperature $T = 0.1\,T_K$, and $B = 0$. The chemical potentials of the left leads are shifted by $\pm eV_L/2$ in the left panel while $V_R = 0$ and V_R is changed in the right panel while $V_L = 0$.

on-going project with Prof. Chung-Hou Chung. The perturbative RG can resolve the resonances at finite frequencies and the NRG is able to describe the Kondo ground state beyond the weak-coupling limit. In non-equilibrium further aspects become important as for example the voltage-dependent occupation numbers and the finite life time of the states. For a comparison between both methods it is important to find a consistent broadening mechanism.

5.7 Ferromagnetic Spin-Spin Coupling

Throughout this chapter the magnetic field is assumed to be zero. In the case of ferromagnetic coupling the triplet ground state is therefore threefold degenerate. Consequently there is a finite conductance in the linear voltage regime, since elastic cotunneling between triplet states is not energetically suppressed. The voltage is assumed to be in the linear regime, i.e. $eV_L < |K|$. In contrast to the antiferromagnetic coupling the term $\mathrm{ferm}[K + \mu_2, \mu_1]$ in Eq. (5.26) gives a finite contribution while $\mathrm{ferm}[-K + \mu_2, \mu_1]$ does not contribute.

For voltages $eV_L < |K|$ the current is given by

$$I_L \frac{h}{e} = (2\pi)^2 \frac{3}{8} \left\{ 2n_t \int_{-eV_L/2}^{eV_L/2} d\epsilon \left(g_{tt}^{12}(\epsilon)\right)^2 + n_s \int_{-|K|-eV_L/2}^{eV_L/2} d\epsilon \left(g_{st}^{12}(\epsilon)\right)^2 - n_s \int_{-|K|+eV_L/2}^{-eV_L/2} d\epsilon \left(g_{st}^{12}(\epsilon)\right)^2 \right\}. \tag{5.33}$$

Including the scaling of the triplet-triplet coupling g_{tt} in perturbative RG a zero-bias peak in the conductance is found, as is seen in the expression for the current in Eq. (5.33). If the flow of the coupling g_{tt} is not stopped by a finite temperature or decoherence, g_{tt} diverges to strong-coupling. Additionally we expect a transconductance effect from the

terms proportional to n_s in Eq. (5.33). The perturbative RG method provides reliable results for the current if the Kondo couplings do not flow to strong-coupling. Both the spin-spin interaction K and the temperature T have to be large to provide a cutoff in the scaling equations.

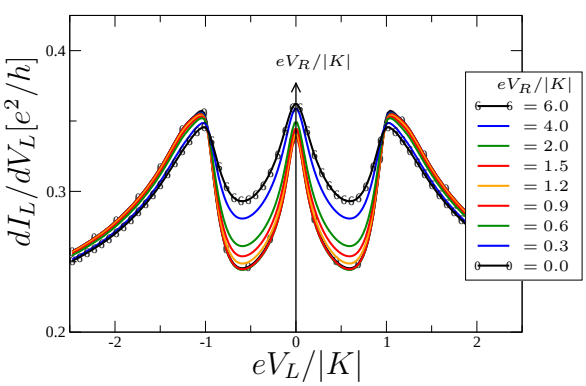

(a) Differential conductance dI_L/dV_L vs. $eV_L/|K|$ for different values of $eV_R/|K|$.

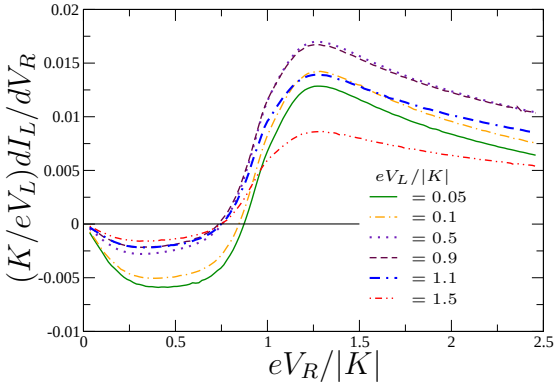

(b) Transconductance $(K/eV_L)dI_L/dV_R$ vs. $eV_R/|K|$ for different values of $eV_L/|K|$.

Figure 5.15: Differential conductance dI_L/dV_L and transconductance $(K/eV_L)dI_L/dV_R$ vs. $eV_L/|K|$ and $eV_R/|K|$, respectively. The temperature $1/\ln(T/T_K) = 0.25$ and the ferromagnetic spin-spin interaction $1/\ln(-K/T_K) = 0.15$ are large.

The differential conductance dI_L/dV_L in Fig. 5.15(a) shows a pronounced zero-bias peak. In Fig. 5.15(a) each coupling is cut off by the corresponding transition rate, i.e. g_{tt} by $\Gamma_{t\to t}$. Please note, that this is different than the broadening scheme used the antiferromagnetic case, where every process involved a singlet-triplet excitation and therefore the decoherence rate $\Gamma_{s\to t}$ provided an average broadening. Therefore the zero-bias peak and the satellite peaks have a different width in the ferromagnetic case.

The effect of a finite voltage V_R in Fig. 5.15(a) is not as pronounced as for the antiferromagnetic case, see Fig. 5.11. Whereas the singlet is an off-state and does not allow for an elastic transport processes, the threefold degenerate triplet states allow for a finite current flow. For ferromagnetic coupling the singlet is the excited state, it becomes populated due to a large voltage V_R on the right impurity. In contrast to Fig. 5.11 we find that the zero-bias peak decreases initially. This behavior originates from an enhanced decoherence due to a finite voltage applied to the right leads. Therefore the transconductance is negative in the linear voltage regime, as illustrated in Fig. 5.15(b). It changes around $eV_R \sim K$ to a positive value. For $eV_R > K$ all channels, singlet and triplet states, contribute to the transport and thus the current I_L is increased compared to $eV_R < K$ where only the triplet states contribute. As in the antiferromagnetic case this transconductance is only observable since the non-equilibrium occupation numbers of the double quantum dot states are taken into account. In the ferromagnetic case the increased decoherence due to a finite V_R additionally diminishes the zero-bias peak.

The T-matrix of two ferromagnetically coupled quantum dots is shown in Fig. 5.16 for different values of the voltage. Using perturbative RG the T-matrix shows a sharp resonance at $\omega = 0$ in contrast to the perturbation theory calculations in section 4.4. Since the T-matrix of a Kondo model can be identified with the spectral function of an Anderson impurity model, see Ref. [59] or section 5.6, the resonance at $\omega = 0$ corresponds

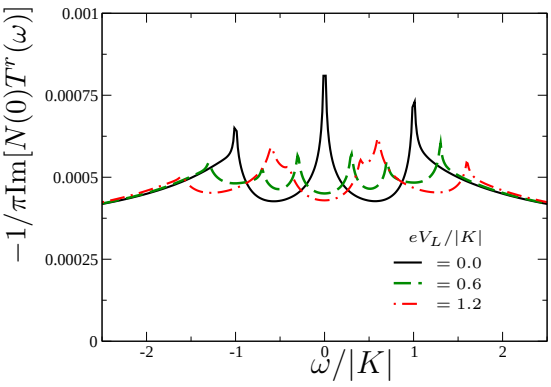

Figure 5.16: T-matrix $-1/\pi \mathrm{Im}[N(0)T^r(\omega)]$ versus frequency $\omega/|K|$ for a ferromagnetic coupling $1/\ln(-K/T_K) = 0.15$, a large temperature $1/\ln(T/T_K) = 0.25$, $V_R = B = 0$ and three different values of the voltages $eV_L/|K| = 0, 0.6, 1.2$.

to a Kondo resonance at the Fermi surface. In the perturbative RG method it is not possible to calculate T^r for ferromagnetic coupling $K < 0$ at the point $\omega = 0$ in the case of small K, T, V_R, and V_L. The numerical RG is able to calculate the spectral function exactly beyond the perturbation approach used here. In contrast, NRG is not able to capture a non-equilibrium situation where the perturbative RG provides reliable results. Thus it is observed in Fig. 5.16 for a finite voltage, that the resonance at $\omega = 0$ is split and two resonances show up at the two Fermi surfaces $\pm eV_L/2$. Also the resonance at finite frequency is split. It is also observed that the decoherence is stronger for larger voltages since the value of the T-matrix on resonance is smaller. In the antiferromagnetic case an additional feature was observed if the voltage reaches the threshold $eV_L > |K|$. Also in the ferromagnetic case the voltage thus provides the energy to populate the excited singlet state. Since the ground state is already a three-fold degenerate triplet, this effect is hardly visible in Fig. 5.16.

In this section we discussed the case of ferromagnetically coupled quantum dots. Coherent spin-flip processes are possible for the three-fold degenerate triplet ground state and thus a Kondo resonance builds up at zero-bias in the differential conductance or at zero frequency in the T-matrix. The perturbative RG method provides only reliable results if the triplet-triplet coupling stays in the weak-coupling regime. Thus the temperature has to be chosen large since the voltage and the singlet-triplet gap do not provide a cutoff for the triplet-triplet coupling. The transfer of a non-equilibrium situation from e.g. the right quantum dot to the left is present, but less pronounced than in the case of antiferromagnetic coupling. This parameter space is interesting in another aspect, since it provides the possibility to compare the exact result from a numerical RG calculation for example in equilibrium with the perturbative RG calculation which becomes valid in the non-equilibrium regime when a finite voltage provides a decoherence to prevent the system to flow to strong-coupling. As mentioned before this is an existing project developed together with Prof. Chung-Hou Chung.

5.8 Summary and Outlook

A perturbative expansion in the coupling to the leads fails for the Kondo model as shown in 1964 by J. Kondo [1]. Therefore methods beyond the perturbation theory were invented. In section 5.1 we discussed the poor man's scaling [10] and generalized the approach to a non-equilibrium situation. In the poor man's scaling approach scattering processes involving energies at the band cutoff are integrated out. The reduction of the band cutoff D leads to a scaling of the Kondo coupling. For the single-impurity Kondo model the Kondo coupling $g = N(0)J$ flows to strong-coupling and the perturbative renormalization approach is no longer valid. In a double quantum dot system further energy scales like the singlet-triplet energy gap enter the flow of the couplings.

If a finite voltage is applied and a current flows through the system, the decoherence originating from fluctuations due to transport processes becomes important. The existence of a finite decoherence rate is not element of the common poor man's scaling. It was included by A. Rosch *et al.* [35, 36] in the framework of a perturbative renormalization group. It is important that the coupling constants g are treated as coupling functions $g(\omega)$ with a finite frequency argument. If a finite voltage is applied to the leads, the Kondo resonance builds up at the two different Fermi edges. All coupling functions $g(\omega)$ in the energy range opened by the voltage enter the transport properties. In section 5.3 the RG equations and their frequency dependence are discussed in detail.

As mentioned in the previous chapters, the rate equation of the distribution probabilities is important in non-equilibrium. The population of triplet states is possible if a large enough voltage is applied e.g. to the right quantum dot. In section 5.4 a similar behavior to the polarization p calculated to second order perturbation theory is observed, but the behavior is qualitatively different since the decoherence Γ takes over the role of the temperature T in the chosen parameter regime. The non-equilibrium occupation of triplet states leads to a finite current in the left quantum dot in the linear conductance regime, since the triplet states do not block the transport channel in contrast to the singlet ground state. This effect leads to a finite transconductance $(K/eV_L)dI_L/dV_R$, which is found in section 5.5 to be enhanced by the Kondo scaling in comparison to the result from perturbation theory. Thus there will be hopefully soon experiments that can confirm a finite transconductance and therefore measure the non-equilibrium distribution function and the decoherence properties of a double quantum dot system. The transconductance resonance is broadened by the decoherence and is therefore broader compared to the one in perturbation theory.

The differential conductance dI_L/dV_L shows a resonance around $eV_L \sim K$ similar to the perturbation theory result, but the finite spectral width Γ broadens the resonance and Γ takes over the role of the temperature. For the shape of the differential conductance the frequency dependence of the couplings is important. The current in the antiferromagnetic case shows a split zero bias peak in contrast to the ferromagnetic case. The value $2K$, i.e. twice the singlet-triplet gap, is not given by the distance between the maximum, but by the difference in the inflection points or the peaks in the second derivative of the current. We also studied the shot noise in the framework of perturbative RG. The results are not shown here, since the Fano factor is mostly Poissonian and therefore no new physics is found in this calculation.

Besides the current through one of the quantum dot, we also studied the T-matrix for one of the left leads. The T-matrix is equivalent to the density of states for the

impurity levels of the Anderson impurity model in the low frequency regime [59]. The project on the T-matrix is closely related to the work of Prof. Chung-Hou Chung [71] and effort is put into a comparison of the perturbative RG with results from numerical RG (NRG). The numerical RG can calculate the ground state properties of the Kondo problem exactly, but fails in non-equilibrium when the properties of the system are not determined solely by the ground state. The perturbative RG includes those non-equilibrium properties but it is valid only for $T \gg T_K$. Thus the comparison is especially interesting in the case of ferromagnetic coupling between the two quantum dots where the perturbative RG fails at low temperatures since the triplet-triplet coupling flows to strong-coupling.

6 The Flow Equation Method

In this chapter the flow equation method out of equilibrium [37, 38] is introduced. The flow equation method is a scaling method which is able to include the frequency of the incoming and outgoing particle in the procedure. This was discussed in the previous chapter to be important for the calculation of transport phenomena.

Here only a brief introduction to the flow equation method is given. We refer the reader to the book of S. Kehrein [38] which provides a nice introduction. The main ideas and the basic equations for the flow equation approach are given in section 6.1. The Hamiltonian of the double quantum dot system is introduced in section 6.2. The representation is slightly changed in comparison to the previous chapters since the flow equation method can treat the spin operator exactly whereas the spin operators were represented by singlet-triplet states in the perturbative treatment.

For the system of two coupled quantum dots the linear, second and third order contributions to the flow equation are discussed. In section 6.3 the linear order, also denoted the kinetic order, is calculated and it is shown that the flow makes the energy processes in the Hamiltonian successively energy-diagonal. To second or one-loop order in the coupling the scaling equations show the characteristic Kondo scaling. Some common assumptions and approximations are discussed in section 6.4 and results for the different couplings of the double quantum dot system are shown. A further issue of section 6.4 is the flow equation method out of equilibrium and the comparison with the non-equilibrium perturbative RG method [35, 36]. The third order or two-loop contribution is a correction to the flow in second order, whereas in a non-equilibrium situation it can dominate the lower order contributions. The different mechanisms of decoherence and how they enter the flow equations are discussed in section 6.5. The results to 3rd order are preliminary, but it is already obvious that a non-equilibrium situation is transferred from one quantum dot to a coupled quantum dot.

6.1 Introduction to the Flow Equation Method

6.1.1 The Idea of Renormalization

The concept of renormalization is used to derive an effective model on a low energy scale for systems which have contributions from a large energy range. The poor man's scaling approach (see section 5.1) by P. W. Anderson [10] succeeded in describing the physics of a Kondo system. Therein scattering processes at the band cutoff, which is large compared to energy scales at the Fermi energy, are integrated out and their contribution leads to a change of the coupling (see Fig. 5.1 on page 94). The coupling of a quantum dot with the leads flows to strong-coupling and the Kondo impurity builds a many-particle state with the surrounding electron cloud.

The poor man's scaling approach eliminates high-energy states by integrating out

degrees of freedom. By iteratively reducing the band cutoff D, also denoted ultraviolet cutoff Λ_{RG} in the following, we receive an effective Hamiltonian at a low energy scale and a running coupling constant. By the successive integration of high-lying energy states a lot of information on the Hilbert space gets lost and after some steps information of the physics only in a reduced space around the Fermi energy is kept. This is illustrated in Fig. 6.1(a) for the renormalized energy space of an interaction involving an incoming k' and outgoing k particle.

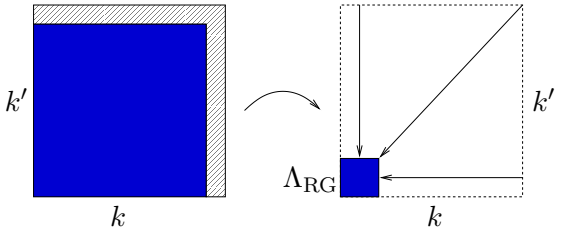

(a) Illustration of poor man's scaling in a 2D energy plot.

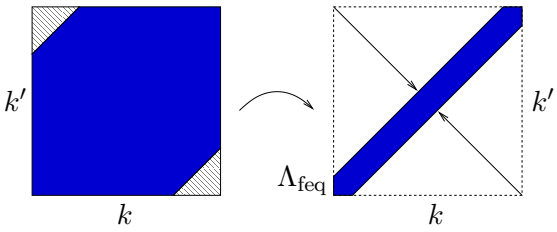

(b) Illustration of the flow equation approach in a 2D energy plot.

Figure 6.1: Comparison of the two different renormalization schemes, poor man's scaling and flow equation approach, in a two-dimensional (2D) energy plot for an incoming particle k' that scatters into an outgoing particle k.

On the contrary the flow equation method does not integrate out higher lying states, but makes the interaction processes successively more energy-diagonal as illustrated in Fig. 6.1(b). After a series of infinitesimal steps the coupling Hamiltonian becomes energy-diagonal by iteratively reducing the energy-diagonality parameter Λ_{feq}. The information on processes with a high energy transfer is lost during the scaling, whereas the contributions of these scattering events are included in the energy-diagonal processes. The phase space of the Hamiltonian is thus not reduced and a calculation of dynamical quantities on all energy scales is possible.

This becomes important for the study of transport problems. As illustrated in Fig. 6.2 for a finite voltage it is important to include all processes in the energy regime provided by the voltage, denoted as the voltage window. The flow equation method includes

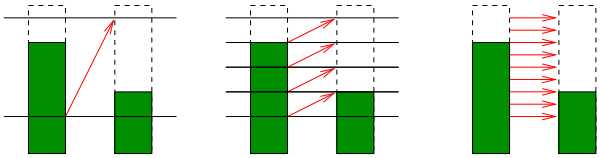

Figure 6.2: During the flow the coupling Hamiltonian becomes energy-diagonal. Since the information is kept on all energy scales, the flow equation method is applicable to transport problems with a finite voltage.

by construction all processes in the energy window, which are energy-diagonal, and therefore gives a first approximation to the problem of non-equilibrium transport. In the next section we discuss the generating equations of the flow equation method and discuss the physics of it on the example of a double quantum dot setup.

6.1.2 The Flow Equation Approach

As illustrated in Fig. 6.1(b) we like to find a transformation such that the Hamiltonian becomes successively more energy-diagonal during the flow. A nice derivation is given in Ref. [38]. Thus only the main lines are discussed here.

Since the scaling should leave the energy spectrum unchanged, the transformation of the Hamiltonian has to be unitary. The separation of energy scales is an important ingredient for the scaling theory. Since the higher energy processes should not mix with the low energy physics, the unitary transformation has to take infinitesimal steps.

We define a family of unitarily equivalent Hamiltonians $H(B)$,

$$\frac{dH(B)}{dB} = [\eta(B), H(B)]\,, \tag{6.1}$$

where B is a not further defined flow parameter and the initial Hamiltonian is given by

$$H(B=0) = H.$$

The generator of the flow $\eta(B)$ is anti-hermitian,

$$\eta(B) = -\eta(B)^\dagger,$$

since the Hamiltonian $H(B)$ has to be hermitian. This provides a good consistency check during the calculation.

The flow equation is similar to the idea of the Schrieffer-Wolff transformation as discussed in section 2.2.2. Parts of the coupling Hamiltonian are eliminated by an appropriate transformation. In the flow equation approach the transformation of the Hamiltonian $dH(B)/dB$ is carried out in infinitesimal steps. In contrast to the poor man's scaling we eliminate successively interaction matrix elements that couple states with an energy transfer $\Delta E \in [\Lambda_{\text{feq}} - \delta\Lambda_{\text{feq}}, \Lambda_{\text{feq}}]$, rather than eliminating the states within this energy window.

6.1.3 The Canonical Generator

The flow parameter B is given by the choice of the generator η. As in the interaction picture the Hamiltonian is separated into a diagonal part H_0 and an interaction part H_{int}, which is not diagonal.

The so-called canonical generator is given by

$$\eta(B) = [H_0(B), H_{\text{int}}(B)]\,. \tag{6.2}$$

It was suggested by F. Wegner. In the following the notation of Ref. [38][1] is used.

If the two conditions

$$\begin{aligned} \text{Tr}\,[H_0(B)H_{\text{int}}(B)] &= 0 \\ \text{and} \quad \text{Tr}\left[\frac{dH_0(B)}{dB}H_{\text{int}}(B)\right] &= 0 \end{aligned}$$

[1] Please see for references of the original papers therein.

are fulfilled, it can be shown that[2]

$$\frac{d}{dB}\mathrm{Tr}\left[H_{\mathrm{int}}^2(B)\right] \leq 0.$$

Thus the Hamiltonian $H(B)$ becomes successively more energy-diagonal during the flow. This is the expected behavior of the flow equations, see section 6.1.1.

The canonical generator in Eq. (6.2) is quadratic in the energy since it is a product of two Hamiltonians. Consequently the flow parameter is inversely proportional to the square of the energy. We define the energy cutoff

$$\Lambda_{\mathrm{feq}} = B^{-1/2}.$$

The flow parameter B flows from 0 to ∞, while the cutoff in the energy Λ_{feq} starts at ∞ and flows to 0, where all energy processes are diagonal.

The canonical generator is linear in the interaction H_{int}. Typically higher and higher order interactions are generated during the flow. At some point there is the need to truncate the series. Similar to the poor man's scaling the flow equation approach is truncated to some order in expansion series of the running coupling constant. In the Kondo model the coupling J is assumed to be small and the solution of the flow equation is valid only in the regime where the coupling $J \ll 1$. If Λ_{feq} reaches the Kondo temperature, the flow becomes uncontrolled and the coupling diverges, i.e. flows to strong-coupling.

As a last remark in this section it should be mentioned that the low energy physics of the flow equation method and the poor man's scaling approach are identical. Therefore the conventional scaling is a limiting case of flow equation, as obvious from the comparison of Fig. 6.1(b) and Fig. 6.1(a).

6.2 A Double Quantum Dot System

The same model of a double quantum dot system as discussed in the previous chapters is now discussed using the flow equation approach. The two quantum dots L and R are coupled each to two leads. The two quantum dots are both occupied by a spin-1/2 and coupled via a spin-spin interaction K. A hopping between them is not allowed. In the following it is assumed that the coupling K is antiferromagnetic.

The coupling of the quantum dot spins to the leads is assumed to be a Kondo spin-spin interaction, denoted J^{ij}. A derivation of this model is given in chapter 2. As illustrated in Fig. 6.3 and explained later in this section the quantum dots are assumed to be coupled to a linear combination of the two left leads and two right leads, denoted as L and R respectively. The initial Hamiltonian H_0,

$$H_0 = \sum_{j=L,R}\sum_{k,\sigma} \epsilon_{\mathrm{k,j}} : c_{kj\sigma}^{\dagger} c_{kj\sigma} : + K\ \vec{S}_L \vec{S}_R, \tag{6.3}$$

is diagonal since it does not change the particle number. Therefore the canonical generator can be applied in the framework of the flow equations method. The operators are

[2]The proof is given in Ref. [38].

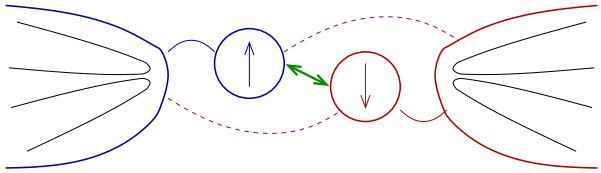

Figure 6.3: Geometry of the double quantum dot system; explanations are given in the text.

normal ordered, such that non-vanishing contractions, e.g. the occupation number, contribute to the commutator of two normal-ordered operators. An introduction to normal ordering can be found in Ref. [38].

Each of the two quantum dots L or R is connected to the leads L or R, respectively. The interacting Hamiltonian is given by

$$\begin{aligned} H_{\text{int}} = & \sum_{j=L,R} \sum_{k'k} J^{Lj}_{k'k} : \vec{S}_L \vec{s}_{(k'j)(kj)} : \\ & + \sum_{j=L,R} \sum_{k'k} J^{Rj}_{k'k} : \vec{S}_R \vec{s}_{(k'j)(kj)} : \\ & + \sum_{j=L,R} \sum_{k'k} Q^{j}_{k'k} : 2i \left(\vec{S}_L \times \vec{S}_R \right) \vec{s}_{(k'j)(kj)} : . \end{aligned}$$

As illustrated in Fig. 6.3, there could be a finite coupling between the left quantum dot and the right leads $J^{LR}_{k'k}$ or vice versa. Even if the couplings $J^{LR}_{k'k}$ and $J^{RL}_{k'k}$ do not exist initially, we find that they are created during the flow. Additionally the coupling $Q^{j}_{k'k}$ is created to lowest order in the flow and thus has to be taken into account in the interaction Hamiltonian to every order.

We assume that the Kondo interaction is obtained from an Anderson impurity model. For the two leads, e.g. 1 and 2 on the left side, the asymmetry r_L is defined by

$$r_L = \frac{g_{11}}{g_{22}}, \tag{6.4}$$

and analogously for the right side: $r_R = g_{33}/g_{44}$. The interlead coupling fulfills the relation,

$$g_{12}^2 = g_{11}\ g_{22}. \tag{6.5}$$

Using Eq. (6.4) and Eq. (6.5) we introduce even and odd combinations of the lead operators. The odd combination,

$$\hat{c}_{Lk\sigma} = \sqrt{\frac{r_L}{1+r_L}}\ c_{2k\sigma} - \sqrt{\frac{1}{1+r_L}}\ c_{1k\sigma},$$

decouples from the Hamiltonian if $\epsilon_{1k\sigma} = \epsilon_{2k\sigma}$. Thus the model can be simplified to a double quantum dot system coupled only to the even combination of the leads,

$$\tilde{c}_{Lk\sigma} = \sqrt{\frac{1}{1+r_L}}\ c_{2k\sigma} + \sqrt{\frac{r_L}{1+r_L}}\ c_{1k\sigma}.$$

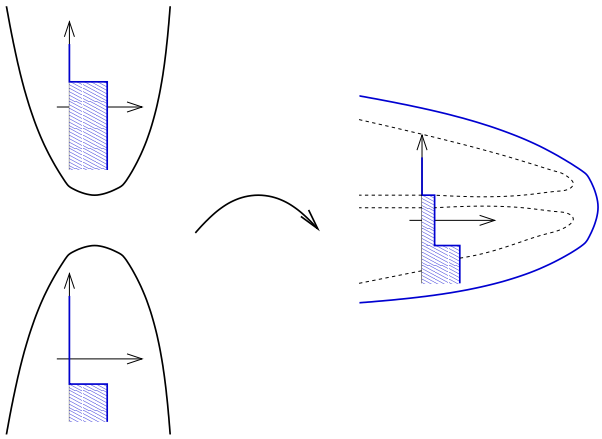

Figure 6.4: The even combination of the conduction electron leads contains information about a finite voltage in the distribution of states.

In the following we refer to $\tilde{c}_{Lk\sigma}$ as $c_{Lk\sigma}$ for the left side. The operator $c_{Lk\sigma}$ obeys the usual Fermi statistics. The same applies analogously for the right side.

A finite voltage effects the distribution function of the electrons, as illustrated in Fig. 6.4. Due to a voltage the two chemical potentials in leads 1 and lead 2 are shifted by $\mu_{1/2} = \pm eV_L/2$, respectively. Consequently the distribution function of the even combination is for zero temperature, $T = 0$, given by

$$n_L(\epsilon) = \begin{cases} 0 & \text{if } \epsilon > eV_L/2 \\ r_L/(1+r_L) & \text{if } |\epsilon| < eV_L/2 \\ 1 & \text{if } \epsilon < -eV_L/2 \end{cases} . \tag{6.6}$$

The distribution function enters the calculation later on via normal ordering of the operators. The flow of the interaction has an influence on n only to higher orders in the flow, thus it is assumed in the following that the leads are not affected by the flow.[3]

Current transport takes place through either the left or the right quantum dot. Due to a strong spin-spin interaction the two quantum dots form singlet and triplet states. As has been discussed in detail in section 2.1 the operators $\left(\vec{S}_L + \vec{S}_R\right)$ and $\left(\vec{S}_L \vec{S}_R\right)$ refer to elastic processes, because they do not change the spin state.

The singlet $|s\rangle = |S^2_{\text{sum}} = 0, S^z_{\text{sum}} = 0\rangle$ and triplet states $|t_{0,\pm}\rangle = |S^2_{\text{sum}} = 1, S^z_{\text{sum}} \in \{-1, -0, 1\}\rangle$ are eigenstates of total spin moment $\vec{S}_{\text{sum}} = \left(\vec{S}_L + \vec{S}_R\right)$. The scalar product of the two spins,

$$2\left(\vec{S}_L \cdot \vec{S}_R\right)^2 = \left(\vec{S}_L + \vec{S}_R\right)^2 - \vec{S}_L^2 - \vec{S}_R^2,$$

does also not change the spin state. Therefore the spin-spin interaction $K\vec{S}_L\vec{S}_R$ is a diagonal part of the Hamiltonian H_0 and can not be treated as a perturbation H_{int}.

The spin operator structures $\left(\vec{S}_L - \vec{S}_R\right)$ and $\left(\vec{S}_L \times \vec{S}_R\right)$ do not conserve the spin,

[3] The first contribution to n originates from two-loop order and the feedback to the flow of the coupling J is of order J^4, see discussion in Ref. [38].

such that we denote them as inelastic processes. It was shown in section 2.1 that

$$\left(\vec{S}_L - \vec{S}_R + 2i\vec{S}_L \times \vec{S}_R\right)|0,0\rangle \to |1,\{0,\pm\}\rangle,$$
$$\left(\vec{S}_L - \vec{S}_R - 2i\vec{S}_L \times \vec{S}_R\right)|1,\{0,\pm\}\rangle \to |0,0\rangle.$$

These processes always involve a change from a triplet to a singlet state. Consequently each process costs the energy of the singlet-triplet gap K and therefore those processes are inelastic.

In the off-diagonal part of the Hamiltonian we rearrange the couplings according to the discussed spin operator structures,

$$\begin{aligned} H_{\text{int}} = &\sum_{j=L,R}\sum_{k'k} J^{\text{sum},j}_{k'k}(B) : \left(\vec{S}_L + \vec{S}_R\right)\vec{s}_{(k'j)(kj)} : \\ &+ \sum_{j=L,R}\sum_{k'k} J^{\text{diff},j}_{k'k}(B) : \left(\vec{S}_L - \vec{S}_R\right)\vec{s}_{(k'j)(kj)} : \\ &+ \sum_{j=L,R}\sum_{k'k} Q^{j}_{k'k}(B) : 2i\left(\vec{S}_L \times \vec{S}_R\right)\vec{s}_{(k'j)(kj)} : . \end{aligned} \tag{6.7}$$

There are three running couplings. $J^{\text{sum},j}_{k'k}$ is the elastic one, which allows for energy-diagonal interaction processes of the double quantum dot system. $J^{\text{diff},j}_{k'k}$ and $Q^{j}_{k'k}$ include processes from singlet to triplet states and consequently every interaction process costs an energy of K.

The initial values are defined by

$$J^{\text{sum},j}_{k'k}(B=0) = \frac{1}{2}\left(J^{Lj}_{k'k}(B=0) + J^{Rj}_{k'k}(B=0)\right), \tag{6.8a}$$
$$J^{\text{diff},j}_{k'k}(B=0) = \frac{1}{2}\left(J^{Lj}_{k'k}(B=0) - J^{Rj}_{k'k}(B=0)\right), \tag{6.8b}$$
$$Q^{j}_{k'k}(B=0) = 0. \tag{6.8c}$$

If we start from a setup with only the left(right) leads coupled to the left(right) quantum dot, then the initial condition additionally enforces

$$J^{LR}_{k'k}(B=0) = J^{RL}_{k'k}(B=0) = 0.$$

Please note that the Hamiltonian has to be hermitian $H^\dagger = H$. This leads immediately to some symmetries of the couplings,

$$J^{\text{sum},j}_{k'k} = J^{\text{sum},j}_{kk'}, \tag{6.9a}$$
$$J^{\text{diff},j}_{k'k} = J^{\text{diff},j}_{kk'}, \tag{6.9b}$$
$$Q^{j}_{k'k} = -Q^{j}_{kk'}. \tag{6.9c}$$

The relation (6.9c) is valid only if $\vec{S}_L$ and $\vec{S}_R$ exchange, because then $[i\left(\vec{S}_L \times \vec{S}_R\right)]^\dagger = -i\epsilon_{abc}\vec{S}^b_R\vec{S}^c_L = -i\left(\vec{S}_L \times \vec{S}_R\right)$.[4] Using the diagonal Hamiltonian H_0 defined in Eq. (6.3) and the interaction Hamiltonian H_{int}, Eq. (6.7), the flow equations are generated in the following to linear, second and third order in the coupling of the quantum dots to the leads, $J^{ij}_{k'k}$ in H_{int}.

[4] See also discussion in section 2.1.

6.3 Linear Order and Generic Behavior

Since the non-interacting part of the Hamiltonian H_0 is diagonal, we can use the canonical generator of the flow equation in this double quantum dot setup. The definition of η, Eq. (6.2), gives the generator

$$\eta = \sum_{i,j=L,R} \sum_{k'k} \eta^{ij}_{k'k} : \vec{S}_i \vec{s}_{(k'j)(kj)} : + \sum_{j=L,R} \sum_{k'k} \gamma^{j}_{k'k} : 2i \left(\vec{S}_L \times \vec{S}_R \right) \vec{s}_{(k'j)(kj)} :, \tag{6.10}$$

where

$$\eta^{Lj}_{k'k} = (\epsilon_{k'} - \epsilon_k)\, J^{Lj}_{k'k} + K Q^{j}_{k'k}, \tag{6.11a}$$

$$\eta^{Rj}_{k'k} = (\epsilon_{k'} - \epsilon_k)\, J^{Rj}_{k'k} - K Q^{j}_{k'k}, \tag{6.11b}$$

$$\gamma^{j}_{k'k} = (\epsilon_{k'} - \epsilon_k)\, Q^{j}_{k'k} + \frac{1}{2} K \left(J^{Lj}_{k'k} - J^{Rj}_{k'k} \right). \tag{6.11c}$$

Some generic behavior can be drawn from this equations. The canonical generator has the same operator structure as the interaction Hamiltonian H_{int} multiplied by an energy which describes the transition between two states,

$$\eta \propto (\text{energy}) \cdot \text{coupling}.$$

The energy transfer between two processes is for example the energy of two conduction electrons, but it can also be the energy of the singlet-triplet gap K.

Please note that the generator has to be antihermitian. This implies

$$\eta^{ij}_{k'k} = -\eta^{ij}_{kk'},$$
$$\gamma^{j}_{k'k} = \gamma^{j}_{kk'}.$$

The lowest order of flow equations is given by $dH(B)/dB = [\eta(B), H_0]$. For the double quantum dot system this leads to a flow of the Hamiltonian $H(B)$ of

$$\begin{aligned}
\frac{dH(B)}{dB} = &- \sum_{i,j=L,R} \sum_{k'k} (\epsilon_{k'} - \epsilon_k)\, \eta^{ij}_{k'k} : \vec{S}_i \vec{s}_{(k'j)(kj)} : \\
&- \sum_{j=L,R} \sum_{k'k} (\epsilon_{k'} - \epsilon_k)\, \gamma^{j}_{k'k} : 2i \left(\vec{S}_L \times \vec{S}_R \right) \vec{s}_{(k'j)(kj)} : \\
&- \sum_{j=L,R} \sum_{k'k} \frac{1}{2} K \left(\eta^{Lj}_{k'k} - \eta^{Rj}_{k'k} \right) : 2i \left(\vec{S}_L \times \vec{S}_R \right) \vec{s}_{(k'j)(kj)} : \\
&- \sum_{j=L,R} \sum_{k'k} K \gamma^{j}_{k'k} : \left(\vec{S}_L - \vec{S}_R \right) \vec{s}_{(k'j)(kj)} : .
\end{aligned}$$

Immediately the flow of the various couplings can be identified, for example the elastic coupling $J^{\text{sum},j}_{k'k}$ is given by

$$\frac{dJ^{\text{sum},j}_{k'k}(B)}{dB} = -\frac{1}{2} (\epsilon_{k'} - \epsilon_k) \left(\eta^{Lj}_{k'k}(B) + \eta^{Rj}_{k'k}(B) \right) = - (\epsilon_{k'} - \epsilon_k)^2 J^{\text{sum},j}_{k'k}(B).$$

This is the typical generic behavior of flow equations to the lowest order using the canonical generator $\eta = [H_0, H_{\text{int}}]$,

$$\frac{d\,\text{coupling}}{dB} \propto -(\text{energy})^2 \cdot \text{coupling}.$$

Therefore the linear order is also referred to as the kinetic term. The generic behavior incorporates the expected behavior of the flow equation, since the coupling flows like

$$J^{\text{sum},j}_{k'k}(B) = \mathrm{e}^{-B(\epsilon_{k'}-\epsilon_k)^2} J^{\text{sum},j}_{k'k}(B=0). \tag{6.12}$$

For $B \to \infty$ any process is exponentially suppressed if it is not diagonal in energy $\epsilon_{k'} = \epsilon_k$. As obvious from Eq. (6.12) the flow parameter B is of the unit $1/\epsilon^2$. The energy cutoff $\Lambda_{\text{feq}} = B^{-1/2}$ describes the cutoff of the energy scale, $\mathrm{e}^{-((\epsilon_{k'}-\epsilon_k)/\Lambda_{\text{feq}})^2}$. Eq. (6.12) serves as a starting point for approximations in further calculations.

The flow for the inelastic couplings is not diagonal as $J^{\text{sum},j}_{k'k}$, but given by

$$\begin{aligned}
\frac{dJ^{\text{diff},j}_{k'k}(B)}{dB} &= -(\epsilon_{k'}-\epsilon_k)\frac{1}{2}\left(\eta^{Lj}_{k'k}(B) - \eta^{Rj}_{k'k}(B)\right) - K\gamma^j_{k'k}(B), \\
\frac{dQ^j_{k'k}(B)}{dB} &= -(\epsilon_{k'}-\epsilon_k)\gamma^j_{k'k}(B) - K\frac{1}{2}\left(\eta^{Lj}_{k'k}(B) - \eta^{Rj}_{k'k}(B)\right).
\end{aligned}$$

The couplings $J^{\text{diff},j}_{k'k}$ and $Q^j_{k'k}$ are given by coupled differential equations. This motivates the definition of new couplings which are the sum or difference of $J^{\text{diff},j}_{k'k}$ and $Q^j_{k'k}$. We define

$$P^j_{k'k} = \frac{1}{2}\left(J^{\text{diff},j}_{k'k} + Q^j_{k'k}\right), \tag{6.13}$$

$$M^j_{k'k} = \frac{1}{2}\left(J^{\text{diff},j}_{k'k} - Q^j_{k'k}\right). \tag{6.14}$$

The new parameters refer the coupling of the lead electrons to $(\vec{S}_L - \vec{S}_R) \pm 2i(\vec{S}_L \times \vec{S}_R)$, i.e. to the transition between singlet and triplet states.

In the calculation of $J^{\text{diff},j}_{k'k}$ and $Q^j_{k'k}$ half of the values of $k'k$ are given by the symmetry relations of Eqs. (6.9). For the couplings $P^j_{k'k}$ and $M^j_{k'k}$ the symmetry relations are different,

$$\left(P^j_{k'k}\right)^\dagger = \frac{1}{2}\left(J^{\text{diff},j}_{kk'} + Q^j_{kk'}\right) = \frac{1}{2}\left(J^{\text{diff},j}_{k'k} - Q^j_{k'k}\right) = M^j_{k'k}. \tag{6.15}$$

Thus all values of $M^j_{k'k}$ can be extracted from a calculation of $P^j_{k'k}$ due to Eq. (6.15). In the following only the coupling $P^j_{k'k}$ is discussed for brevity of expressions.

The two new couplings $P^j_{k'k}$ and $M^j_{k'k}$ fulfill two independent differential equations,

$$\frac{dP^j_{k'k}(B)}{dB} = -(\epsilon_{k'}-\epsilon_k+K)^2 P^j_{k'k}(B), \tag{6.16}$$

$$\frac{dM^j_{k'k}(B)}{dB} = -(\epsilon_{k'}-\epsilon_k-K)^2 M^j_{k'k}(B). \tag{6.17}$$

The symmetry $P^j_{kk'} = M^j_{k'k}$ is clearly visible in equation (6.16) and (6.17). It is also obvious from those equations that a process proportional to the coupling $P^j_{k'k}$ involves

a transition between a singlet and a triplet states and the energy difference in the lead electrons, $\epsilon_{k'} - \epsilon_k$, has to provide the energy of the singlet-triplet gap K.

We can immediately write down the solution of the kinetic flow equation for $P^j_{k'k}$,

$$P^j_{k'k}(B) = \mathrm{e}^{-B(\epsilon_{k'}-\epsilon_k+K)^2} P^j_{k'k}(B=0), \tag{6.18}$$

where the initial value is

$$P^j_{kk}(B=0) = \frac{1}{2}\left(J^{\mathrm{diff},j}_{k'k}(B=0) + Q^j_{k'k}(B=0)\right).$$

For $B \to \infty$ and $\epsilon_{k'} = \epsilon_k$, which corresponds to energy-diagonal processes, the coupling is exponentially suppressed by the energy gap K of the singlet-triplet excitation. This justifies the notation as an inelastic coupling.

The solutions for $J^{\mathrm{diff},j}_{k'k}(B)$ and $Q^j_{k'k}(B)$ are given by the solution of $P^j_{k'k}$ and we find

$$\begin{aligned} J^{\mathrm{diff},j}_{k'k}(B) =& \mathrm{e}^{-B(\epsilon_{k'}-\epsilon_k)^2} 2\cosh\left(2K\left(\epsilon_{k'}-\epsilon_k\right)B\right)\mathrm{e}^{-BK^2}\ J^{\mathrm{diff},j}_{k'k}(B=0) \\ &+ \mathrm{e}^{-B(\epsilon_{k'}-\epsilon_k)^2} 2_n h\left(2K\left(\epsilon_{k'}-\epsilon_k\right)B\right)\mathrm{e}^{-BK^2}\ Q^j_{k'k}(B=0), \qquad (6.19) \\ Q^j_{k'k}(B) =& \mathrm{e}^{-B(\epsilon_{k'}-\epsilon_k)^2} 2_n h\left(2K\left(\epsilon_{k'}-\epsilon_k\right)B\right)\mathrm{e}^{-BK^2}\ J^{\mathrm{diff},j}_{k'k}(B=0) \\ &+ \mathrm{e}^{-B(\epsilon_{k'}-\epsilon_k)^2} 2\cosh\left(2K\left(\epsilon_{k'}-\epsilon_k\right)B\right)\mathrm{e}^{-BK^2}\ Q^j_{k'k}(B=0). \qquad (6.20) \end{aligned}$$

From the lowest order contribution to the flow we find an exponential suppression of off-diagonal energy processes. At early stages of the flow the off-diagonal matrix elements in the interaction Hamiltonian are thus eliminated. At later stages of the flow the feedback of higher order terms becomes important.

6.4 Second Order or One-Loop Result

Additionally to the contribution $[\eta(B), H_0]$ we include $[\eta(B), H_{\mathrm{int}}(B)]$ into the flow $dH(B)/dB$ of the Hamiltonian. The new term includes two interaction processes, one from η and one from H_{int}. Therefore there is one intermediate process involved with a conduction electron of the energy ϵ_{qv}. This energy has to be integrated over the whole band width from $-D$ to $+D$. Thus it gives rise to e.g. the strong-coupling scaling of the Kondo model. The left and the right side are decoupled to this order since no process exists that leaves the left leads, interacts virtually with the right quantum dot, and enters the left leads again.

In the following we write down only major steps of the calculation to explain the underlying physics and leave out details of the calculation. After having calculated $[\eta(B), H_{\mathrm{int}}(B)]$ we sort the terms corresponding to the contributions in $H_{\mathrm{int}}(B)$. For

example the coupling to the left quantum dot $J^{Lj}_{k'k}$ obeys the equation,

$$\begin{aligned}\frac{dJ^{Lj}_{k'k}}{dB} =& -(\epsilon_{k'}-\epsilon_k)\,\eta^{Lj}_{k'k} - K\gamma^j_{k'k}\\ &-\frac{1}{2}\sum_v\left(\eta^{Lj}_{k'v}J^{Lj}_{vk} - J^{Lj}_{k'v}\eta^{Lj}_{vk}\right)(1-2n(vj))\\ &-\frac{1}{2}\sum_v\left(\left(\gamma^j_{k'v}J^{Rj}_{vk} - Q^j_{k'v}\eta^{Rj}_{vk}\right)+\left(J^{Rj}_{k'v}\gamma^j_{vk} - \eta^{Rj}_{k'v}Q^j_{vk}\right)\right)\\ &+\frac{1}{2}\sum_v\left(\gamma^j_{k'v}Q^j_{vk} - Q^j_{k'v}\gamma^j_{vk}\right),\end{aligned} \tag{6.21}$$

and the coupling to the right quantum dot $J^{Rj}_{k'k}$ flows like

$$\begin{aligned}\frac{dJ^{Rj}_{k'k}}{dB} =& -(\epsilon_{k'}-\epsilon_k)\,\eta^{Rj}_{k'k} + K\gamma^j_{k'k}\\ &-\frac{1}{2}\sum_v\left(\eta^{Rj}_{k'v}J^{Rj}_{vk} - J^{Rj}_{k'v}\eta^{Rj}_{vk}\right)(1-2n(vj))\\ &-\frac{1}{2}\sum_v\left(\left(\gamma^j_{k'v}J^{Lj}_{vk} - Q^j_{k'v}\eta^{Lj}_{vk}\right)+\left(J^{Lj}_{k'v}\gamma^j_{vk} - \eta^{Lj}_{k'v}Q^j_{vk}\right)\right)\\ &+\frac{1}{2}\sum_v\left(\gamma^j_{k'v}Q^j_{vk} - Q^j_{k'v}\gamma^j_{vk}\right).\end{aligned} \tag{6.22}$$

Both are renormalized to first loop order. If there is no spin-spin interaction $K = 0$ and consequently $Q^j_{k'k} = \gamma^j_{k'k} = 0$, then all terms besides the first proportional to $\eta^{ij}_{k'v}J^{ij}_{vk}$ vanish in the flow equation of the couplings $J^{ij}_{k'k}$. The remaining term is the common Kondo scaling of the left(right) quantum dot with the left(right) leads. Please compare to the calculation in Ref. [38].

The coupling $Q^j_{k'k}$, which is created in linear order, continues to flow in first loop order. The flow equation gives

$$\begin{aligned}\frac{dQ^j_{k'k}}{dB} =& -(\epsilon_{k'}-\epsilon_k)\,\gamma^i_{k'k} - \frac{1}{2}K\left(\eta^{Lj}_{k'k} - \eta^{Rj}_{k'k}\right)\\ &+\frac{1}{4}\sum_v\left(\left(\eta^{Lj}_{k'v}J^{Rj}_{vk} + J^{Rj}_{k'v}\eta^{Lj}_{vk}\right)-\left(\eta^{Rj}_{k'v}J^{Lj}_{vk} + J^{Lj}_{k'v}\eta^{Rj}_{vk}\right)\right)\\ &+\frac{1}{4}\sum_v\left(\left(\gamma^j_{k'v}J^{Rj}_{vk} - Q^j_{k'v}\eta^{Rj}_{vk}\right)-\left(J^{Rj}_{k'v}\gamma^j_{vk} - \eta^{Rj}_{k'v}Q^j_{vk}\right)\right)(1-2n(vj))\\ &-\frac{1}{4}\sum_v\left(\left(\gamma^j_{k'v}J^{Lj}_{vk} - Q^j_{k'v}\eta^{Lj}_{vk}\right)-\left(J^{Lj}_{k'v}\gamma^j_{vk} - \eta^{Lj}_{k'v}Q^j_{vk}\right)\right)(1-2n(vj)).\end{aligned}$$

The flow equations fulfill the symmetry relations of Eqs. (6.9), which provides a nice check of the results.

6.4.1 Flow of the Coupling $J^{\mathrm{sum},j}_{k'k}$

The interaction with the total spin moment is defined by $J^{\mathrm{sum},j}_{k'k}(B) = \frac{1}{2}(J^{Lj}_{k'k}(B) + J^{Rj}_{k'k}(B))$. If we take the sum of the two equations for $J^{Lj}_{k'k}(B)$ and $J^{Rj}_{k'k}(B)$ and insert

the definition of the canonical generator η (see Eqs. (6.10)) we receive the flow equation Eq. (E.1) in the appendix. Since the expression is lengthy the terms of order e^{-BD^2} are left out in the following expression,

$$\begin{aligned}\frac{dJ^{\mathrm{sum},j}_{k'k}(B)}{dB} =& -(\epsilon_{k'}-\epsilon_k)^2 J^{\mathrm{sum},j}_{k'k}(B)\\ &-\frac{1}{2}\sum_v (1-2n(vj))\left((\epsilon_{k'}-\epsilon_v)-(\epsilon_v-\epsilon_k)\right) J^{\mathrm{sum},j}_{k'v}(B)J^{\mathrm{sum},j}_{vk}(B)\\ &-\frac{1}{2}\sum_v (1-2n(vj))\left((\epsilon_{k'}-\epsilon_v+K)-(\epsilon_v-\epsilon_k+K)\right) P^{j}_{k'v}(B)P^{j}_{vk}(B)\\ &-\frac{1}{2}\sum_v (1-2n(vj))\left((\epsilon_{k'}-\epsilon_v+K)-(\epsilon_v-\epsilon_k-K)\right) P^{j}_{k'v}(B)M^{j}_{vk}(B)\\ &-\frac{1}{2}\sum_v (1-2n(vj))\left((\epsilon_{k'}-\epsilon_v-K)-(\epsilon_v-\epsilon_k+K)\right) M^{j}_{k'v}(B)P^{j}_{vk}(B)\\ &-\frac{1}{2}\sum_v (1-2n(vj))\left((\epsilon_{k'}-\epsilon_v-K)-(\epsilon_v-\epsilon_k-K)\right) M^{j}_{k'v}(B)M^{j}_{vk}(B)\\ &+\ldots. \end{aligned} \tag{6.23}$$

The linear contribution $-(\epsilon_{k'}-\epsilon_k)^2 J^{\mathrm{sum},j}_{k'k}(B)$ enforces an exponential damping of the momentum dependent coupling $J^{\mathrm{sum},j}_{k'k}(B)$. Therefore the so-called diagonal parametrization, see also section 6.4.3, is introduced and the elastic coupling is written by

$$J^{\mathrm{sum},j}_{k'k}(B) = \mathrm{e}^{-B(\epsilon_{k'}-\epsilon_k)^2}\,\overline{J^{\mathrm{sum},j}_{k'k}}(B). \tag{6.24}$$

The exponential behavior originates to linear order and the scaling of the second order determines the flow of the coupling $\overline{J^{\mathrm{sum},j}_{k'k}}(B)$, which in general depends on k' and k. In the diagonal parametrization it is further assumed that $k'=k$, since the exponential prefactor suppresses all other contributions of $J^{\mathrm{sum},j}_{k'k}(B)$ in Eq. (6.24).

Using the outcome of the calculation in linear order a similar expression is defined for the diagonal parametrization of the coupling $P^{j}_{k'k}(B)$. From Eq. (6.18) the inelastic coupling,

$$P^{j}_{k'k}(B) = \mathrm{e}^{-B(\epsilon_{k'}-\epsilon_k+K)^2}\,\overline{P^{j}_{k'k}}(B), \tag{6.25}$$

is not diagonal in the energy, but each interaction process costs an energy of the singlet-triplet gap K.

If we insert the diagonal parametrization, Eqs. (6.24) and (6.25), into the flow equation of the coupling $J^{\mathrm{sum},j}_{k'k}$ each term is similar to

$$\begin{aligned}&\left((\epsilon_{k'}-\epsilon_v+\alpha K)-(\epsilon_v-\epsilon_k+\beta K)\right)\mathrm{e}^{-B(\epsilon_{k'}-\epsilon_v+\alpha K)^2}\mathrm{e}^{-B(\epsilon_v-\epsilon_k+\beta K)^2}\\ =&\frac{1}{2B}\frac{d}{d\,\epsilon_v}\mathrm{e}^{-B(\epsilon_{k'}-\epsilon_v+\alpha K)^2}\mathrm{e}^{-B(\epsilon_v-\epsilon_k+\beta K)^2},\end{aligned}$$

where $\alpha,\beta=0,\pm 1$. The diagonal representation simplifies in this way the integration $\sum_{qv}=\rho\int d\epsilon_{qv}$ over the intermediate state v. The leads are modeled by a constant density of states $\rho(\epsilon)=\rho\,\Theta(D-|\epsilon|)$ centered around the Fermi energy $\epsilon_F\equiv 0$, where

the band width is $2D$ and the constant density of states $\rho = 1/2D$.[5] The dispersion relation $\epsilon_k(k)$ is approximated by a linear dependence, which is a good approximation in the vicinity of the Fermi energy. In the following the indices k', k and q are assumed to represent the energies $\epsilon_{k'}$, ϵ_k and ϵ_q correspondingly.

Assuming vanishing temperature $T = 0$ and vanishing voltage $V = 0$ the integration over the intermediate process gives

$$\begin{aligned}\sum_v (1 - 2\,n(vj))\,\frac{d}{d\,\epsilon_v} f(\epsilon_v) &= \int_{-D}^{0} d\epsilon_v \rho\,(1 - 2\cdot 1)\,\frac{d}{d\,\epsilon_v} f(\epsilon_v) + \int_{0}^{D} d\epsilon_v \rho\,(1 - 2\cdot 0)\,\frac{d}{d\,\epsilon_v} f(\epsilon_v) \\ &= -2\rho\, f(\epsilon_v = 0) + \rho\, f(\epsilon_v = -D) + \rho\, f(\epsilon_v = D).\end{aligned}$$

This term is typical for the Kondo spin interaction. Due to the spin algebra and the discontinuity at the Fermi surface the function $f(\epsilon_v = 0)$ does not cancel out, but provides a finite contribution in the flow equations.

Using this knowledge we find the flow equation of the dimensionless coupling $g^{\mathrm{sum},j}_{k'k} = \rho J^{\mathrm{sum},j}_{k'k}$ of the total spin moment,

$$\begin{aligned}\mathrm{e}^{-B(\epsilon_{k'}-\epsilon_k)^2}\,\frac{d\overline{g^{\mathrm{sum},j}_{k'k}}(B)}{dB} &= \frac{1}{2B}\,\mathrm{e}^{-B(\epsilon_{k'})^2}\mathrm{e}^{-B(-\epsilon_k)^2}\overline{g^{\mathrm{sum},j}_{k'0}}(B)\;\overline{g^{\mathrm{sum},j}_{0k}}(B) \\ &\quad + \frac{1}{2B}\left(\mathrm{e}^{-B(\epsilon_{k'}+K)^2}\overline{p^j_{k'0}}(B) + \mathrm{e}^{-B(\epsilon_{k'}-K)^2}\overline{m^j_{k'0}}(B)\right) \\ &\qquad \left(\mathrm{e}^{-B(-\epsilon_k+K)^2}\overline{p^j_{0k}}(B) + \mathrm{e}^{-B(-\epsilon_k-K)^2}\overline{m^j_{0k}}(B)\right), \qquad (6.26)\end{aligned}$$

neglecting additional terms which include the band cutoff and scale like e^{-2BD^2}. As soon as the flow parameter B becomes of the order of $1/D^2$ these boundary terms are exponentially suppressed. In the following the flow is assumed to start at

$$B_0 = \frac{1}{D^2} \qquad (6.27)$$

with an initial value $J^{\mathrm{sum},j}_{k'k}(B_0)$. The flow of the coupling to the total spin momentum is thus given solely by Eq. (6.26) using the new initial condition.

6.4.2 Flow of the Coupling $P^j_{k'k}(B)$

We leave out all steps of the calculation that were already explained for $g^{\mathrm{sum},j}_{k'k}(B)$ and write down only the result for dimensionless coupling $\overline{p^j_{k'k}}(B) = \rho\overline{P^j_{k'k}}(B)$ for $B > B_0 =$

[5] These conditions are fulfilled for example for a two-dimensional electron gas.

$1/D^2$,

$$\begin{aligned}
\mathrm{e}^{-B(\epsilon_{k'}-\epsilon_k+K)^2}\,\frac{d\overline{p^j_{k'k}}(B)}{dB} &= \frac{1}{2}\,\frac{1}{2B}\,\left(\mathrm{e}^{-B(\epsilon_{k'}+K)^2}\overline{p^j_{k'0}}(B)+\mathrm{e}^{-B(\epsilon_{k'}-K)^2}\overline{m^j_{k'0}}(B)\right)\\
&\qquad \mathrm{e}^{-B(-\epsilon_k)^2}\overline{g^{\mathrm{sum},j}_{0k}}(B)\\
&\quad+\frac{1}{2}\,\frac{1}{2B}\,\mathrm{e}^{-B(\epsilon_{k'})^2}\overline{g^{\mathrm{sum},j}_{k'0}}(B)\\
&\qquad \left(\mathrm{e}^{-B(-\epsilon_k+K)^2}\overline{p^j_{0k}}(B)+\mathrm{e}^{-B(-\epsilon_k-K)^2}\overline{m^j_{0k}}(B)\right)\\
&\quad+\frac{1}{2B}\,\mathrm{e}^{-B(\epsilon_{k'}+K)^2}\mathrm{e}^{-B(-\epsilon_k+K)^2}\overline{p^j_{k'0}}(B)\;\overline{p^j_{0k}}(B)\\
&\quad-\frac{1}{2B}\,\mathrm{e}^{-B(\epsilon_{k'}-K)^2}\mathrm{e}^{-B(-\epsilon_k-K)^2}\overline{m^j_{k'0}}(B)\;\overline{m^j_{0k}}(B). \qquad (6.28)
\end{aligned}$$

In the diagonal representation Eq. (6.25) only the terms with $\epsilon_{k'} - \epsilon_k + K = 0$ are not exponentially suppressed. In the following we discuss analytical and numerical results of the two flow equations Eqs. (6.26) and (6.28).

6.4.3 Approximations and Results

Exact Solution

The exact solution of the Eqs. (6.26) and (6.28) is given in Fig. 6.5 and Fig. 6.6, respectively. It is assumed that $J^{LR} = J^{RL} = 0$ and thus the initial value of $J^{\mathrm{sum},j}_{k'k}$ is identical to $P^j_{k'k}/2$. In Fig. 6.5 the energies k and k' are chosen to be a two-dimensional

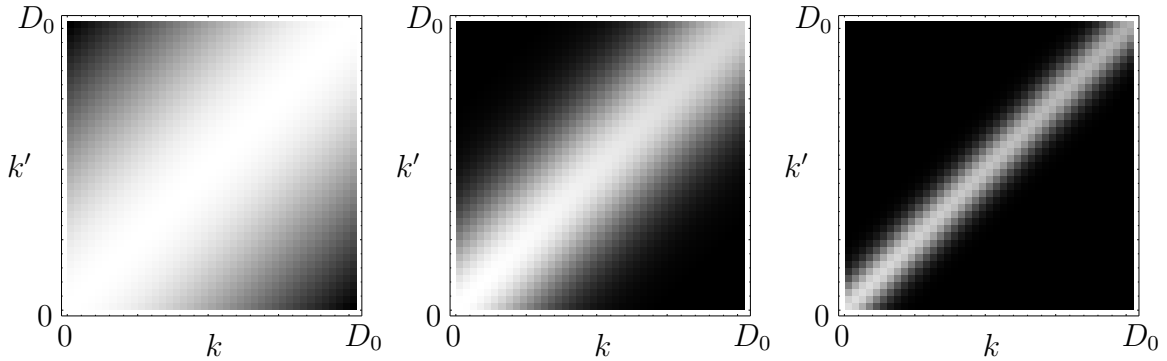

(a) $B = B_0$ (b) $BK^2 = 0.1$ (c) $BK^2 = 1.0$

Figure 6.5: Flow of the coupling $g^{\mathrm{sum},j}_{k'k}$, exactly calculated, on a two-dimensional energy plot.

grid and the strength of the coupling is illustrated by a grey scale code, where light corresponds to strong and dark to negligible coupling strength. For values of the flow parameter B from B_0 to $1/K^2$ a diagonal structure emerges. The exponential envelope originates from the linear order contribution to the flow equation. A substructure develops on the energy-diagonal $\epsilon_k = \epsilon_{k'}$ such that at $\epsilon_k = \epsilon_{k'} = 0$ the coupling flows to a higher value compared to a finite $\epsilon_k \neq 0$. This substructure given by the one-loop order terms is included in the discussion of the diagonal parametrization whereas the infrared parametrization is focused on the value at zero energy.

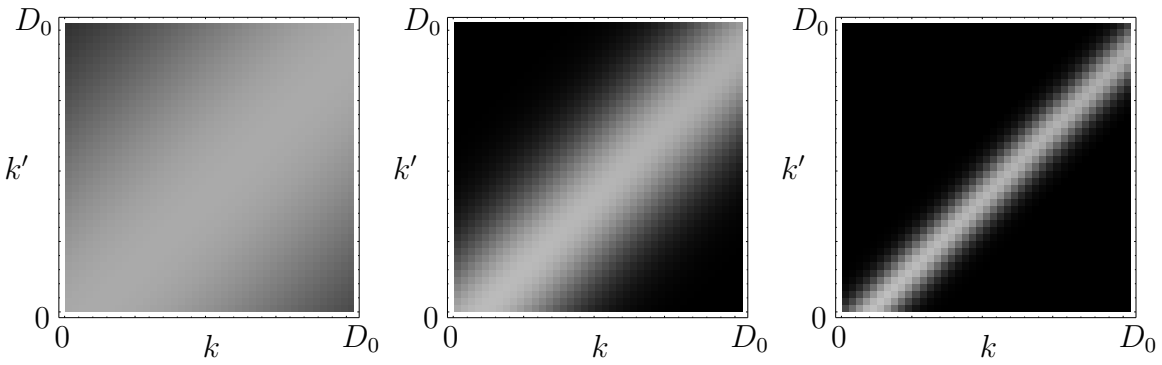

(a) $B = B_0$ (b) $BK^2 = 0.1$ (c) $BK^2 = 1.0$

Figure 6.6: Flow of the coupling $p^j_{k'k}$, exactly calculated, on a two-dimensional energy plot.

In Fig. 6.6 the same calculation as for elastic coupling $J^{\mathrm{sum},j}_{k'k}$ is shown for the inelastic coupling $P^j_{k'k}$. Similarly a large range of the couplings in the k'-k space is suppressed exponentially. In contrast to Fig. 6.5 the energy values of $\epsilon_{k'} - \epsilon_k + K = 0$ flow the strongest. Any process involving the coupling $P^j_{k'k}$ costs an energy of K.

Diagonal Parametrization

The assumptions used in the diagonal parametrization have already been written down in Eqs. (6.24) and (6.25). For example the elastic coupling $J^{\mathrm{sum},j}_{k'k}$ with an arbitrary value of $\epsilon_{k'}$ and ϵ_k is assumed to be exponentially suppressed by $\mathrm{e}^{-B(\epsilon_{k'}-\epsilon_k)^2}$ and its prefactor given by the mean value $(\epsilon_{k'} - \epsilon_k)/2$ [38].

In Fig. 6.7 it is shown how the flow of the coupling $\overline{J^{\mathrm{sum},j}_{k'k}}$ and $\overline{P^j_{k'k}}$ evolves numerically for different energies ϵ_k. As in the exact solution, the starting value is the same for all

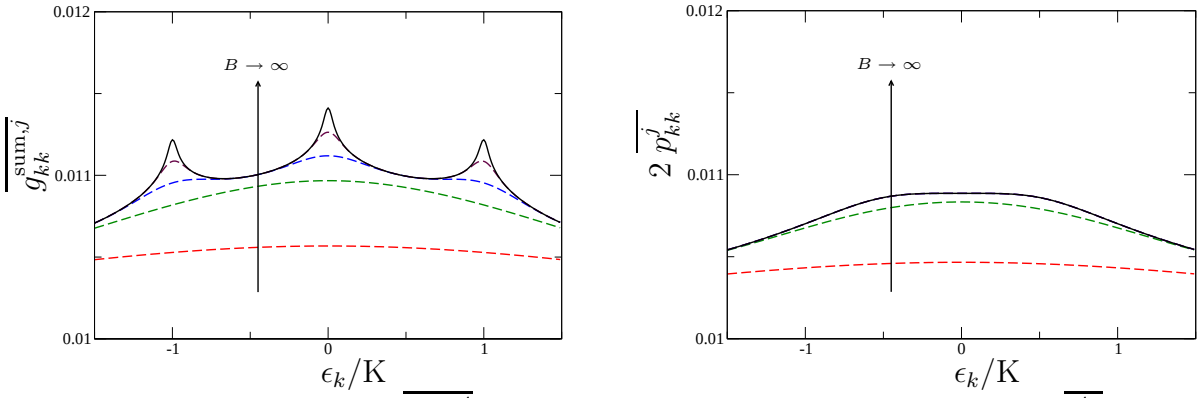

(a) Flow of the coupling $\overline{g^{\mathrm{sum},j}_{kk}}$. (b) Flow of the coupling $2\ \overline{p^j_{kk}}$.

Figure 6.7: Value of the elastic $\overline{g^{\mathrm{sum},j}_{kk}}$ and inelastic coupling $2\ \overline{p^j_{kk}}$ in the diagonal parametrization vs. the energy ϵ_k for increasing values of the flow parameter $BK^2 = 0.01, 0.1, 1.0, 10, 10^2, 10^3$.

couplings at every energy. As the flow parameter increases a frequency structure starts to develop. Please note that in Fig. 6.7 the flow of the couplings without the exponential prefactor is shown. In the flow of $\overline{J^{\mathrm{sum},j}_{kk}}$ the two energies $\epsilon_k = 0$ and $\epsilon_k = \pm K$ are

pronounced. This scaling is similar to the behavior observed in Fig. 5.4 in the previous section about perturbative RG. A comparison of the two methods is the scope of an upcoming section. As discussed before the coupling is most interesting on the energy-diagonal. For $\epsilon_{k'} = \epsilon_k$ the coupling in diagonal parametrization is equivalent to the general coupling,

$$\overline{g^{\mathrm{sum},j}_{k'k}}(B) = g^{\mathrm{sum},j}_{k'k}(B) \qquad \text{if} \qquad \epsilon_{k'} = \epsilon_k.$$

The flow of the coupling $\overline{p^j_{k'k}}$[6] is shown only for values of $\epsilon_{k'} = \epsilon_k$. Therefore the value saturates as soon as the flow parameter reaches the energy scale $B = 1/K^2$. Afterwards the flow does no longer evolve, but this should not be misunderstood such that the coupling saturates. In Fig. 6.7 only the prefactor of the diagonal parametrization is shown, the inelastic coupling is additionally suppressed by the exponential prefactor of e^{-BK^2}. In contrast to other scaling methods the regime of $B > 1/K^2$ is not ill-defined. The flow equation methods makes the Hamiltonian increasingly energy-diagonal. As illustrated

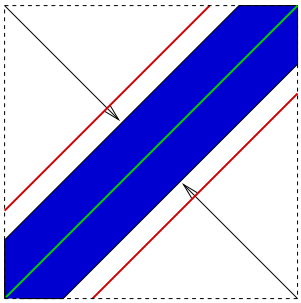

Figure 6.8: The flow equation method is sensible to energy scales. A coupling does no longer flow if the energy-diagonalization reaches the value of the energy transfer of the corresponding process. The scaling equation thus changes, see discussion in the text.

in Fig. 6.8 at some stage inelastic processes are not included in the Hamiltonian and only scattering on the energy-diagonal is taken into account. The scaling equation for the coupling changes and it is shown in detail in one of the next sections that the flow in 2nd order is negligibly small if a finite voltage is applied to the system. Thus third order contributions have to be calculated which include decoherence mechanisms that are important out of equilibrium. The subject of a finite temperature is not discussed in this thesis and we refer the reader to the corresponding chapter in the book [38].

Infrared Parametrization

The flow of the coupling $g^{\mathrm{sum},j}_{k'k}$ is determined by the exponential dependence on $\mathrm{e}^{-B(\epsilon_{k'}-\epsilon_k)^2}$. As discussed in the previous section only the couplings on the energy-diagonal are not suppressed during the flow. The Hamiltonian for $B \to \infty$ is energy-diagonal. It was also observed that the couplings at the energy $\epsilon_{k'} = \epsilon_k = 0$ and $\epsilon_{k'} = \epsilon_k = \pm K$ continue to flow while the flow saturates at other energy scales.

[6] The coupling $p^j_{k'k}$ in Fig. 6.7 is multiplied by a factor of 2 such that it is directly comparable to the coupling $g^{\mathrm{sum},j}_{k'k}$.

In some cases it is sufficient to study the physics only at the zero energy scale, which corresponds to the Fermi energy of the leads. For the coupling $g_{00}^{\mathrm{sum},j}$ the flow is given by inserting $\epsilon_{k'} = \epsilon_k = 0$ in the flow equation (6.26) and (6.28),

$$\frac{d\overline{g_{00}^{\mathrm{sum},j}}(B)}{dB} = \frac{1}{2B}\left(\overline{g_{00}^{\mathrm{sum},j}}(B)\right)^2 + 4\frac{1}{2B}\mathrm{e}^{-2BK^2}\left(\overline{p_{00}^{j}}(B)\right)^2, \tag{6.29}$$

$$\frac{d\overline{p_{00}^{j}}(B)}{dB} = 2\frac{1}{2B}\,\overline{p_{00}^{j}}(B)\overline{g_{00}^{\mathrm{sum},j}}(B), \tag{6.30}$$

where we inserted $p_{00}^{j} = m_{00}^{j}$.

The flow of the couplings in the infrared parametrization $g_{00}^{\mathrm{sum},j}(B) = g_{IR}^{\mathrm{sum},j}(B)$ and $p_{00}^{j}(B) = \mathrm{e}^{-BK^2}p_{IR}^{j}(B)$ is shown in Fig. 6.9. Whereas the coupling p_{IR}^{j} saturates at a

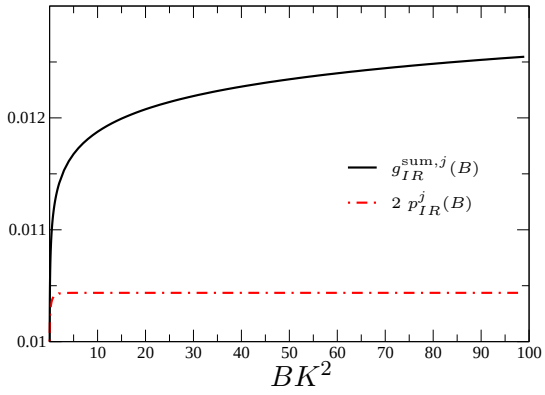

Figure 6.9: Flow of the coupling $g_{IR}^{\mathrm{sum},j}(B)$ and $2\ p_{IR}^{j}(B)$ in the infrared parametrization.

constant value after the flow reached $1/K^2$, the coupling for $g_{IR}^{\mathrm{sum},j}$ continues to flow logarithmically. Notice that only the prefactor of the coupling p_{00}^{j} without the exponential dependence by e^{-BK^2} is shown. In the coupling $g_{IR}^{\mathrm{sum},j}$ the exponential prefactor is equal to unity.

At later stages of the flow, i.e. for $B > B_K$ where $B_K = 1/K^2$, the contribution of the inelastic coupling is exponentially suppressed in the flow equation. For $B > B_K$ the differential equation for $g_{IR}^{\mathrm{sum},j}$ is solved by

$$\begin{aligned} \frac{dg_{IR}^{\mathrm{sum},j}(B)}{dB} &= \frac{1}{2B}\left(g_{IR}^{\mathrm{sum},j}(B)\right)^2 \\ \Rightarrow \qquad \frac{1}{g_{IR}^{\mathrm{sum},j}(B)} &= \frac{1}{g_{IR}^{\mathrm{sum},j}(B_K)} - \frac{1}{2}\ln\left(\frac{B}{B_K}\right) \\ g_{IR}^{\mathrm{sum},j}(B) &= \frac{1}{\frac{1}{2}\ln\left(B_c/B\right)}, \end{aligned} \tag{6.31}$$

with a critical value of the flow parameter $B_c = B_K \exp\left[2/g_{IR}^{\mathrm{sum},j}(B_K)\right]$. As long as $B < B_c$ the ratio $B_c/B > 1$. Approaching the critical value, the coupling diverges logarithmically.

This divergence is characteristic for the Kondo coupling between the quantum dots and the leads. Instead of a spin-1/2 here a degenerate triplet state with spin-1 is studied and the elastic coupling $g_{k'k}^{\mathrm{sum},j}$ describes the flow of the total spin moment. The flow

parameter B, which has the unit 1/energy^2, is translated to an energy cutoff by $B = 1/\Lambda_{\text{feq}}^2$. Therefore we find,

$$\Lambda_{\text{feq}}^c = K \exp\left[-1/g_{00}^{\text{sum},j}(K)\right],$$
$$g_{00}^{\text{sum},j}(B) = \frac{1}{\ln\left(\Lambda_{\text{feq}}/\Lambda_{\text{feq}}^c\right)},$$

equivalently a divergent behavior if the energy cutoff is lowered below the critical value of Λ_{feq}^c, which corresponds to the Kondo temperature as discussed in the previous chapter.

The calculation is controlled as long as the coupling stays small during the flow. If the flow parameter B reaches the critical value the couplings diverge. In the infrared parametrization the flow equation approach is therefore equivalent to the poor man's scaling approach, since it covers the correct physics at the Fermi edge. The strong-coupling in the Kondo problem does not exist if e.g. a finite voltage is applied to the system as is discussed in the next section. The chemical potentials of the leads are shifted by a finite voltage and therefore the infrared parametrization is no longer sufficient, since it provides results only at the energy scale $\epsilon_{k'} = \epsilon_k = 0$. As in the discussion of the previous chapter, the frequency dependence of the couplings is important in non-equilibrium and the flow equation approach should be solved in the diagonal representation.

6.4.4 The Flow Equation Method Out of Equilibrium

The infrared parametrization fails if the double quantum dot setup is subject to a finite voltage, since there are two Fermi surfaces present at $\pm eV/2$. For transport processes all couplings in the energy window opened by the voltage contribute as illustrated in Fig. 6.10. Two Kondo resonances evolve at the two Fermi surfaces, such that the elastic

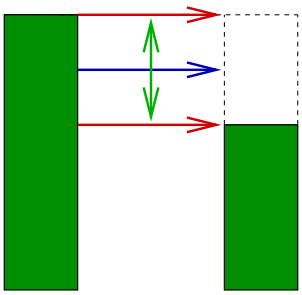

Figure 6.10: If a finite voltage is applied, two Fermi surfaces at $\pm eV/2$ show strong-coupling behavior. Important for transport quantities is the coupling averaged over the voltage window.

coupling $\overline{g_{k'k}^{\text{sum},j}}$ at the energies $\epsilon_k = \epsilon_{k'} = \pm eV/2$ flows to strong-coupling.

This can be seen from the flow equation Eq. (6.23) calculated including a finite voltage. The voltage enters the flow equations via the step-like distribution function of the leads as defined in Eq. (6.6). The integration over the intermediate state in non-equilibrium

gives

$$\begin{aligned}
&\sum_v (1-2n(vj))\,\frac{d}{d\epsilon_v} f(\epsilon_v) \\
&= (1-2)\int_{-D}^{-V_j/2} d\epsilon\rho\ \frac{d}{d\epsilon} f(\epsilon) + \left(1-2\frac{r_j}{1+r_j}\right)\int_{-V_j/2}^{V_j/2} d\epsilon\rho\ \frac{d}{d\epsilon} f(\epsilon) + (1-0)\int_{V_j/2}^{D} d\epsilon\rho\ \frac{d}{d\epsilon} f(\epsilon) \\
&\approx -2\frac{r_j}{1+r_j}\rho f(\epsilon = V_j/2) - 2\frac{1}{1+r_j}\rho f(\epsilon = -V_j/2).
\end{aligned}$$

Since the couplings to the left and the right leads are independent of each other to this order, the index $j = L, R$ is not always written explicitly. Using this integration we find the flow equation for the elastic coupling $\overline{g^{\mathrm{sum},j}_{k'k}}(B)$ in non-equilibrium,

$$\begin{aligned}
&\mathrm{e}^{-B(\epsilon_{k'}-\epsilon_k)^2}\ \frac{d\overline{g^{\mathrm{sum},j}_{k'k}}(B)}{dB} \\
&\quad= \frac{1}{2B}\frac{r_j}{1+r_j}\mathrm{e}^{-B(\epsilon_{k'}-eV_j/2)^2}\mathrm{e}^{-B(eV_j/2-\epsilon_k)^2}\overline{g^{\mathrm{sum},j}_{k'+}}(B)\ \overline{g^{\mathrm{sum},j}_{+k}}(B) \\
&\quad+\frac{1}{2B}\frac{1}{1+r_j}\mathrm{e}^{-B(\epsilon_{k'}+eV_j/2)^2}\mathrm{e}^{-B(-eV_j/2-\epsilon_k)^2}\overline{g^{\mathrm{sum},j}_{k'-}}(B)\ \overline{g^{\mathrm{sum},j}_{-k}}(B) \\
&\quad+\frac{1}{2B}\frac{r_j}{1+r_j}\left(\mathrm{e}^{-B(\epsilon_{k'}-eV_j/2+K)^2}\overline{p^j_{k'+}}(B)+\mathrm{e}^{-B(\epsilon_{k'}-eV_j/2-K)^2}\overline{m^j_{k'+}}(B)\right) \\
&\qquad\left(\mathrm{e}^{-B(eV_j/2-\epsilon_k+K)^2}\overline{p^j_{+k}}(B)+\mathrm{e}^{-B(eV_j/2-\epsilon_k-K)^2}\overline{m^j_{+k}}(B)\right) \\
&\quad+\frac{1}{2B}\frac{1}{1+r_j}\left(\mathrm{e}^{-B(\epsilon_{k'}+eV_j/2+K)^2}\overline{p^j_{k'-}}(B)+\mathrm{e}^{-B(\epsilon_{k'}+eV_j/2-K)^2}\overline{m^j_{k'-}}(B)\right) \\
&\qquad\left(\mathrm{e}^{-B(-eV_j/2-\epsilon_k+K)^2}\overline{p^j_{-k}}(B)+\mathrm{e}^{-B(-eV_j/2-\epsilon_k-K)^2}\overline{m^j_{-k}}(B)\right), \qquad (6.32)
\end{aligned}$$

where $v = \pm$ corresponds to the momentum with energy $\epsilon_v = \pm eV_j/2$.

In contrast to the perturbative RG in the previous section, where the derivation of the RG equations is differently in the case of equilibrium and non-equilibrium, the flow equation is the same in both cases and the difference enters only through a different distribution function of the leads.

The flow of the elastic coupling $\overline{g^{\mathrm{sum},j}_{k'k}}$ is illustrated in Fig. 6.11 in the diagonal representation for a voltage $eV_j/K = 0.25$ smaller than the exchange interaction K. Therefore the inelastic coupling $\overline{p^j_{k'k}}(B)$ is not shown, since it is exponentially suppressed for $B > 1/K^2$ even before the flow parameter B reaches $1/V^2$ and the effects of a finite voltage become important.

In comparison to Fig. 6.7 the flow in Fig. 6.11 shows a divergent coupling at six different energy values. In second order these couplings flow to strong-coupling as soon as B reaches the critical scale B_c. The failure of the infrared parametrization is obvious in Fig. 6.11 since the coupling at the energy scale $\epsilon_{k'} = \epsilon_k = 0$ saturates at a constant value while strong-coupling divergences develop at $\epsilon_{k'} = \epsilon_k = \pm eV_j/2$. This can also be seen in the flow equation (6.32), where the coupling at the energy scale $\epsilon_{k'} = \epsilon_k = 0$ is exponentially suppressed by $\mathrm{e}^{-2B(eV_j/2)^2}$.

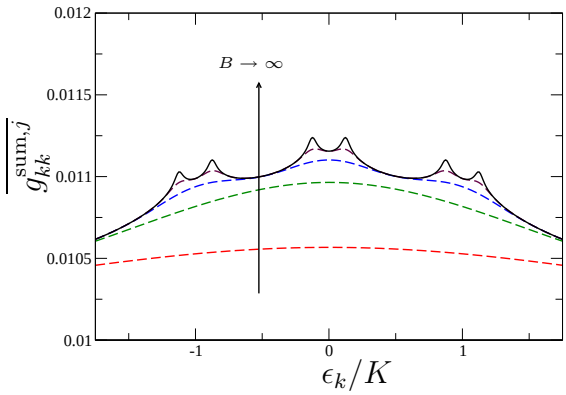

Figure 6.11: Value of the elastic $\overline{g_{kk}^{\mathrm{sum},j}}$ in the diagonal parametrization vs. the energy ϵ_k for increasing values of the flow parameter $BK^2 = 0.01, 0.1, 1.0, 10, 10^2, 10^3$. The finite voltage is chosen $eV_j/K = 0.25$.

All processes within the energy window opened by the voltage contribute to transport processes, as illustrated in Fig. 6.10. It is an advantage of the flow equation that during the flow the Hamiltonian becomes more energy-diagonal while the information on all energy scales is kept, see also discussion in the introductory section of this chapter. In contrast contributions from higher energy scales are integrated out in the standard poor man's scaling approach.

We define a transport coupling,

$$g_t^{\mathrm{sum},j}(B) = \frac{1}{V} \int_{-V/2}^{V/2} d\epsilon_k \overline{g_{kk}^{\mathrm{sum},j}}(B), \tag{6.33}$$

which is the average of all couplings in the voltage window.

In the following we discuss the scaling equation for the transport coupling assuming that the flow parameter B already exceeded the scale $1/K^2$ up to which the inelastic couplings contribute. The flow parameter B is related to an energy cutoff $\Lambda_{\mathrm{feq}} = B^{-1/2}$. During the flow only coupling processes with an energy transfer less than Λ_{feq} are included in the interaction Hamiltonian.

If $\Lambda_{\mathrm{feq}} \gg V$ the transport coupling obeys the usual scaling equation of a Kondo coupling,

$$\frac{dg_t^{\mathrm{sum},j}}{d\ln\Lambda_{\mathrm{feq}}} = -\left(g_t^{\mathrm{sum},j}\right)^2.$$

As mentioned previously the flow equations are not ill-defined if the energy cutoff Λ_{feq} is reduced below the energy scale of the voltage. It is observed, that the flow equation for the transport coupling changes. For an energy cutoff of $\Lambda_{\mathrm{feq}} \ll V$ it is given by

$$\frac{dg_t^{\mathrm{sum},j}}{d\ln\Lambda_{\mathrm{feq}}} = -\left(g_t^{\mathrm{sum},j}\right)^2 \frac{\sqrt{\pi}}{2\sqrt{2}} \frac{\Lambda_{\mathrm{feq}}}{V} \approx 0.$$

If the energy processes in the Hamiltonian are made energy-diagonal to a degree that the energy difference between two scattering states does not exceed the voltage window,

the coupling $g_t^{\mathrm{sum},j}$ does no longer flow and its derivative is negligibly small. A higher order contribution e.g. from two-loop order can now dominate the flow of the coupling since the contribution from one-loop order vanishes. Before it is discussed in section 6.5 how decoherence effects can enter to third order in the coupling, the perturbative RG method as introduced in chapter 5 is compared with the flow equation approach.

6.4.5 Comparison with Perturbative RG

The method of perturbative RG as introduced by A. Rosch *et al.* in Ref. [35, 36] was discussed in detail in the previous chapter. The method generalizes the poor man's scaling approach to non-equilibrium by taking into account a frequency dependence of the couplings. It also includes a voltage-dependence of the distribution functions which becomes important if physical quantities like a non-equilibrium current is calculated. In this section we compare the perturbative RG to the flow equation method to second order. If a finite voltage is applied to a transport regime, decoherence effects play a major role. They are included in the perturbative RG by a finite life time of the quantum dot states [41] and in the flow equation method they enter in two-loop order. Since the comparison of the two methods here is only to second order, the discussion of how decoherence effects enter the different scaling equations is not subject of this section.

As discussed in section 2.1 a comparison between the singlet-triplet representation used in the perturbative RG with the spin representation used in the flow equation approach is possible in the following way: the elastic coupling $g_{k'k}^{\mathrm{sum},j}$ corresponds to the triplet-triplet coupling g_{tt}^{mn}, the inelastic coupling $p_{k'k}^{j}$ corresponds to a singlet-triplet transition g_{st}^{mn}. In the following we compare the elastic coupling g_{tt}^{nm} with $g_{k'k}^{\mathrm{sum},j}$ of only one of the quantum dots, e.g. the left, such that $j = L$ and $m, n \in \{1, 2\}$ is assumed implicitly.

A visual comparison of the flow of the coupling g_{tt} in Fig. 5.4 on page 110 and $g_{k'k}^{\mathrm{sum}}$ in Fig. 6.7 supports the equivalence of the two results. An analytical comparison of the two different scaling equations in Eq. (5.14c) and Eq. (6.32) shows the similarities and the differences of the two approaches.

The flow parameter B starts at $B_0 = 1/D^2$ and flows to infinity whereas the energy cutoff $\Lambda_{\mathrm{feq}} = B^{-1/2}$ reduced the energy transfer of a scattering from D to 0, such that the Hamiltonian is energy-diagonal at later stages of the flow. The definition of the flow parameter, $2BdB = -d\ln\Lambda_{\mathrm{feq}}$, explains the different signs in the two scaling equations. The contributions from two different Fermi surfaces enters the flow equation method by the two different steps in the non-equilibrium distribution function. The summation over the internal energy ϵ_v corresponds to the summation over the lead index v in the perturbative RG approach. Therefore the two scaling equations are the same besides a different cutoff scheme.

The cutoff function $\Theta(\Lambda_{\mathrm{RG}} - x)$ in perturbative RG is an approximation of the different scaling behavior for the ratio between the involved energy x and the running cutoff Λ_{RG}, $x \ll \Lambda_{\mathrm{RG}}$ and $x \gg \Lambda_{\mathrm{RG}}$. The cutoff $\mathrm{e}^{-(x/\Lambda_{\mathrm{feq}})^2}$ in the flow equation approach in contrast is exact for every value of x even in the intermediate regime. The two different cutoff regimes are identical in the limits $x \ll \Lambda$ and $x \gg \Lambda$ as illustrated in Fig. 6.12.

In both methods the frequency dependence is crucial to describe the physics out of equilibrium. Without decoherence effects both methods show strong-coupling behavior

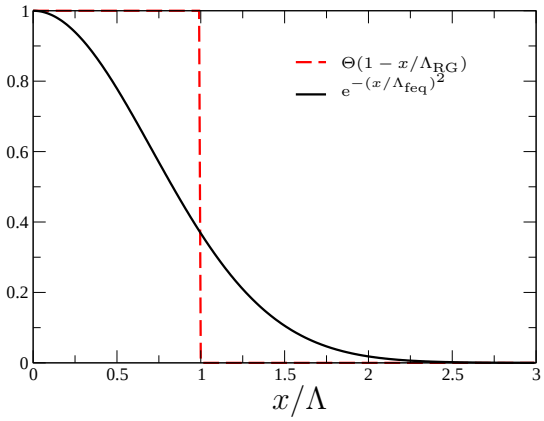

Figure 6.12: The flow equation uses a cutoff of $e^{-(x/\Lambda_{\rm feq})^2}$ in contrast to the cutoff $\Theta(1-x/\Lambda_{\rm RG})$ in perturbative RG.

at special energies. The couplings diverge logarithmically. The perturbative RG and the flow equation method in the diagonal parametrization are consistent to leading logarithmic order. It is assumed that the frequency dependence of the cutoff function dominates such that the frequency dependence of the coupling is neglected on the right side of the scaling equations.

In non-equilibrium decoherence effects prevent the Kondo coupling to flow to strong-coupling. This observation is included in the perturbative RG method by a finite life time of the quantum dot states or by finite vertex corrections [41]. In the flow equation approach it was shown that the second order contributions become negligibly small if the cutoff $\Lambda_{\rm feq}$ is reduced below the voltage, such that contributions from higher orders can dominate the flow. How decoherence terms enter the flow equations is now discussed in detail.

6.5 Third Order or Two-Loop Contributions

It is the aim of this section to explain the origin of decoherence effects to two-loop order in the flow equations. Two intermediate states contribute in the flow to the third order. We discuss in the following the physical ingredient of the higher order contributions. For the interested reader some steps of the calculation are given in appendix E.3.

The flow of the Hamiltonian is given by $dH(B)/dB = [\eta(B), H(B)]$. So far the interaction Hamiltonian $H_{\rm int}(B)$ as well as the generator $\eta(B) = [H_0(B), H_{\rm int}(B)]$ were of linear order in the coupling. To create a flow to third order in the coupling to the leads, we have to include interaction terms, which are created to second order in the coupling, into an Hamiltonian $H_{\rm int}^{(2)}$.

6.5.1 Higher Order Contributions from 2nd Order

In the first-loop calculation new interaction terms are created. To second order in the coupling J we find for example a potential scattering. Additionally the singlet-triplet gap K is renormalized and a constant energy term arises. To study these couplings in more detail will be the task of future investigations. For the rest of this thesis those

couplings are neglected since the flow of the potential scattering or the coupling K does not contribute to leading logarithmic order.[7]

To describe decoherence effects we are interested in couplings involving four conduction electrons, since they describe an effective two-particle interaction mediated by the quantum dot system. To calculate the third order or two-loop correction of $H_{\rm int}$ we include the second order couplings into the interacting Hamiltonian,

$$\begin{aligned} H_{\rm int}^{(2)} = & \sum_{i,j,n=L,R} \sum_{k'k} \sum_{p'p} K^i_{(k'j)(kj);(p'n)(pn)} : i\vec{S}_i \left(\vec{s}_{(k'j)(kj)} \times \vec{s}_{(p'n)(pn)} \right) : \\ & + \sum_{i,j,n=L,R} \sum_{k'k} \sum_{p'p} {}^{(2)}K^i_{(k'j)(kj);(p'n)(pn)} : 2 \left(\vec{S}_{!i} \vec{s}_{(k'j)(kj)} \right) \left(\vec{S}_i \vec{s}_{(p'n)(pn)} \right) : \\ & + \sum_{j,n=L,R} \sum_{k'k} \sum_{p'p} {}^{(3)}K_{(k'j)(kj);(p'n)(pn)} : 2 \left(\vec{S}_L \vec{S}_R \right) \left(\vec{s}_{(k'j)(kj)} \vec{s}_{(p'n)(pn)} \right) : . \end{aligned} \tag{6.34}$$

For example the higher order term $\vec{S}_L : \vec{s}_{(k'j)(kj)} \vec{s}_{(p'n)(pn)} :$ is created out of two interaction processes with the left spin, $\vec{S}_L : \vec{s}_{(k'j)(kj)} :$ and $\vec{S}_L : \vec{s}_{(p'n)(pn)} :$, as schematically illustrated in Fig. 6.13. It can be interpreted as a two-particle interaction of conduction electrons via the impurity spin. The setup of two coupled quantum dots shows a more

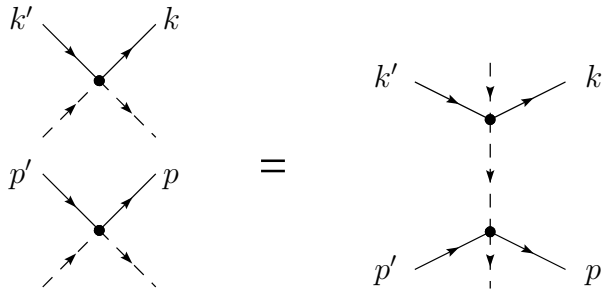

Figure 6.13: Illustration of the higher order coupling $: \vec{S}_L \vec{s}_{(k'j)(kj)} \vec{s}_{(p'n)(pn)} :$, which is created out of twice the Kondo coupling $: \vec{S}_L \vec{s}_{(k'j)(kj)} :$. Solid (dashed) lines refer to conduction electrons (spin states).

complicated interaction structure than a single quantum dot. The calculation of the flow equation to third order is straightforward, see Ref. [38], and some steps of it are given in appendix E.3.

6.5.2 Canonical Generator and Flow of the Coupling to 3rd Order

Since the interaction Hamiltonian has been changed by adding higher-order terms, $H_{\rm int}^{(2)}$, the canonical generator $\eta = [H_0, H_{\rm int}]$ has to be calculated correspondingly. The second order term $\eta^{(2)}$ in the canonical generator $\eta' = \eta + \eta^{(2)}$ is given in Eq. (E.5) in the appendix. It shows the same interaction structure as $H_{\rm int}^{(2)}$ in Eq. (6.34).

The flow of the Hamiltonian is given by $dH(B)/dB = [\eta'(B), H(B)]$, where the Hamiltonian is now defined by $H = H_0 + H_{\rm int} + H_{\rm int}^{(2)}$. Contributions to third order in the coupling originate from $[\eta, H_{\rm int}^{(2)}]$ and $[\eta^{(2)}, H_{\rm int}]$. Since $K_{(k'j)(kj);(q'v)(qv)}$ is generated to

[7] The potential scattering contributes only to order J^4, see discussion in Ref. [38].

2nd order in the initial coupling $J^{ij}_{k'k}$ the term $[\eta^{(2)}, H^{(2)}_{\rm int}]$ is of fourth order in the coupling and is therefore neglected in the following discussion. There is also a contribution of J^3 to the flow of the couplings in $H^{(2)}_{\rm int}$. Since the effect of a J^3 term in the flow of the initial couplings J is to forth order J^4 this contribution can thus be neglected to leading order.

We are interested in the contribution of the higher-order couplings in $H^{(2)}_{\rm int}$ to the initial couplings in the Hamiltonian $H_{\rm int}$. Therefore we define symmetric combinations of the higher order couplings as they appear in the flow equations. The new definitions take respect to the symmetry relations as discussed in appendix E.3. Using the notation $K^{L\pm R} = K^L \pm K^R$ we find

$$\begin{aligned}
(k^a_1)_{(k'j)(kj);(q'\nu)(q\nu)} &= K^{L+R}_{(k'j)(kj);(q'\nu)(q\nu)} - K^{L+R}_{(q'\nu)(q\nu);(k'j)(kj)},\\
(k^a_2)_{(k'j)(kj);(q'\nu)(q\nu)} &= K^{L-R}_{(k'j)(kj);(q'\nu)(q\nu)} - K^{L-R}_{(q'\nu)(q\nu);(k'j)(kj)},\\
(k^s_3)_{(k'j)(kj);(q'\nu)(q\nu)} &=^{(2)} K^{L+R}_{(k'j)(kj);(q'\nu)(q\nu)} +^{(2)} K^{L+R}_{(q'\nu)(q\nu);(k'j)(kj)},\\
(k^a_4)_{(k'j)(kj);(q'\nu)(q\nu)} &=^{(2)} K^{L-R}_{(k'j)(kj);(q'\nu)(q\nu)} -^{(2)} K^{L-R}_{(q'\nu)(q\nu);(k'j)(kj)},\\
(k^s_5)_{(k'j)(kj);(q'\nu)(q\nu)} &=^{(3)} K_{(k'j)(kj);(q'\nu)(q\nu)} +^{(3)} K_{(q'\nu)(q\nu);(k'j)(kj)},
\end{aligned}$$

where s denotes a symmetric and a an asymmetric combination of couplings with respect to interchanging the index $(q'\nu)(q\nu)$ with $(k'j)(kj)$.

So far all couplings are denoted by the energy $(k'j)(kj);(q'\nu)(q\nu)$. In the flow equations we also find contributions from the combination $(k'j)(qj);(q'j)(kj)$ and define

$$\begin{aligned}
k_6 &=^{(3)} K_{(k'j)(qj);(q'j)(kj)} +^{(3)} K_{(q'j)(kj);(k'j)(qj)},\\
k'_6 &=^{(2)} K^{L+R}_{(k'j)(qj);(q'j)(kj)} +^{(2)} K^{L+R}_{(q'j)(kj);(k'j)(qj)}.
\end{aligned}$$

As shown in the appendix, the coupling $k^s_3 = -k^s_5$ and $k_6 = -k'_6$ are related, respectively.

The flow equations for the couplings k_1 to k_6 are shown in appendix E.3. Here only the flow equations of the initial couplings in $H_{\rm int}$ are discussed. After some lengthy but straightforward algebra the flow equation of the elastic coupling $g^{{\rm sum},j}_{k'k}$ to the total spin is found to third order,

$$\begin{aligned}
\frac{dg^{{\rm sum},j}_{k'k}}{dB} &= \ldots +\\
&\quad [n(q'v)(1-n(qv)) + n(qv)(1-n(q'v))]\\
&\quad \Big\{ \frac{1}{4}\left(\epsilon_{k'} - \epsilon_k + \epsilon_{q'} - \epsilon_q - (\epsilon_q - \epsilon_{q'})\right) k^a_1 g^{{\rm sum},v}_{qq'}\\
&\quad + \frac{1}{4}\left(\epsilon_{k'} - \epsilon_k + \epsilon_{q'} - \epsilon_q - K - (\epsilon_q - \epsilon_{q'} + K)\right)(k^a_2 - k^a_4)\, p^v_{qq'}\\
&\quad + \frac{1}{4}\left(\epsilon_{k'} - \epsilon_k + \epsilon_{q'} - \epsilon_q + K - (\epsilon_q - \epsilon_{q'} - K)\right)(k^a_2 + k^a_4)\, m^v_{qq'} \Big\}. \qquad (6.35)
\end{aligned}$$

The inelastic coupling which costs an energy of K is given by

$$\begin{aligned}\frac{dp^j_{k'k}}{dB} = &\ldots + \\ &[n(q'v)(1-n(qv)) + n(qv)(1-n(q'v))] \\ &\left\{ \frac{1}{8}\left(\epsilon_{q'} - \epsilon_q + \epsilon_{k'} - \epsilon_k + K - (\epsilon_q - \epsilon_{q'})\right)\left(k^a_2 + k^a_4\right) g^{\mathrm{sum},v}_{qq'} \right. \\ &+ \frac{1}{4}\left(\epsilon_{q'} - \epsilon_q + \epsilon_{k'} - \epsilon_k - (\epsilon_q - \epsilon_{q'} + K)\right)\left(k^a_1 - 3k^s_3\right) p^v_{qq'} \\ &\left. +\frac{1}{4}\delta_{v,j}\left(\epsilon_{q'} - \epsilon_q + \epsilon_{k'} - \epsilon_k - (\epsilon_q - \epsilon_{q'} + K)\right)\left(2k'_6 + k_6\right) p^j_{qq'} \right\}. \end{aligned} \tag{6.36}$$

There is also a contribution from $(n(q'\nu) - n(q\nu))$ to the flow in third order. Since terms including $(n(q'\nu) - n(q\nu))$ are only proportional to the phase space between q' and q, these terms are neglected, see discussion in Ref. [38].

The newly generated couplings are illustrated in Fig. 6.13. They correspond to an interaction between two incoming particles k' and p' with the quantum dot spin resulting in two outgoing particles k and p. The flow equation in third order contains the integration over two intermediate states q and q'. Depending on which of the incoming or outgoing particles of the two-particle coupling interacts with another particle-hole pair, $J^{ij}_{qq'}$, the third order contribution is a self energy or a vertex correction, as illustrated in Fig. 6.14. As discussed in detail in chapter 5, these third order contributions stop the flow to strong-coupling in the case of a finite voltage. Thus these terms are often referred to as decoherence terms. There are different types of decoherence. The elastic coupling $g^{\mathrm{sum},j}_{k'k}$ in Eq. (6.35) has only contributions from an interaction structure like $(k'j)(kj); (q'\nu)(q\nu) \times (q\nu)(q'\nu)$. As illustrated in Fig. 6.14(b) this corresponds to a self energy correction, i.e. due to hybridization with the leads the quantum dot spins gain a finite life time. If this effect is sufficiently large, for example for a large voltage as discussed in detail in section 6.5.4, the coupling $g^{\mathrm{sum},j}_{k'k}$ does no longer flow to strong-coupling. By contrast, the inelastic coupling contains a combination of couplings with $(k'j)(qj); (q'j)(kj) \times (qj)(q'j)$. This is a vertex correction as illustrated in Fig. 6.14(a).

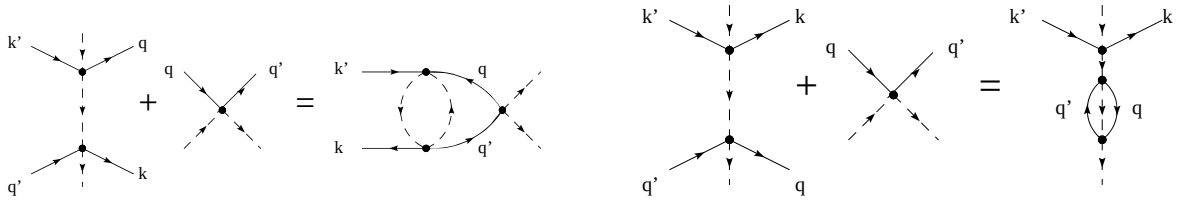

(a) Contribution of a vertex corrections. (b) Contribution of a self energy correction.

Figure 6.14: Two-loop contributions to the flow of the Kondo couplings. Left panel: contribution from k_6 or k'_6; right panel: contributions from k_1-k_5.

In general one has to solve the set of differential equations for $g^{\mathrm{sum},j}_{k'k}$, $p^j_{k'k}$, $k_1, \ldots k_6$. For an analytical result we perform the calculation in two steps. First the couplings $k_1 - k_5$ are integrated over B and then the result is inserted into the differential equation for $g^{\mathrm{sum},j}_{k'k}$. It is assumed that the coupling depends only weakly on the flow parameter,

since it diverges only logarithmically. The dependence of the coupling on B is neglected in the integration over B and thus the result is only valid to leading logarithmic order.

Furthermore it is assumed that the frequency dependence of the coupling is dominated by the exponential prefactors. That the diagonal representation is a good approximation to the third order calculation has been shown for the Kondo model in Ref. [38]. The proof for the double quantum dot setup is the aim of future work.

6.5.3 Discussion of the Flow to 3rd Order

The flow equation for the elastic coupling $g^{\mathrm{sum},j}_{k'k}$ is shown in Eq. (E.6) in the appendix. Here we concentrate on the first term in the flow equation since the other terms are proportional to e^{-BK^2}. To discuss the physical content of the third order contribution in the flow equation we thus concentrate on the limit $B \gg 1/K^2$ where these further contributions can be neglected. The full numerical solution is shown in Fig. 6.15 and discussed at the end of this section.

For a discussion of the leading terms in the differential equation of $g^{\mathrm{sum},j}_{k'k}$ it is useful to define the function $F(y)$,

$$F(y) = \frac{y}{8B}\frac{\sqrt{\pi}}{\sqrt{2B}}\,\mathrm{erf}\left(\sqrt{2B}\,y\right) + \frac{1}{2(2B)^2}\,\mathrm{e}^{-2By^2}.$$

The function $F(y)$ is the result of the integration

$$\begin{aligned}&\int_{l_3}^{l_4} d\epsilon_{q'} \int_{l_1}^{l_2} d\epsilon_q (\epsilon_{q'} - \epsilon_q + \alpha K)^2 \mathrm{e}^{-2B\left(\epsilon_{q'}-\epsilon_q+\alpha K\right)^2} \\ &= F\left(l_4 - l_1 + \alpha K\right) - F\left(l_4 - l_2 + \alpha K\right) - F\left(l_3 - l_1 + \alpha K\right) + F\left(l_3 - l_2 + \alpha K\right),\end{aligned}$$

where $\alpha = 0, \pm 1$. The function $F(y)$ is symmetric in its argument $F(-y) = F(y)$.

In equilibrium the limits of the integration over the two intermediate energy states, ϵ_q and $\epsilon_{q'}$, are given for temperature $T = 0$ by the Fermi energy $\epsilon_F \equiv 0$ and the band cutoff $\pm D$,

$$\int d\epsilon_q \int d\epsilon_{q'} [n(qv)(1 - n(q'v)) + n(q'v)(1 - n(qv))] = \int_{-D}^{0} d\epsilon_q \int_{0}^{D} d\epsilon_{q'} + \int_{0}^{D} d\epsilon_q \int_{-D}^{0} d\epsilon_{q'}.$$

In analogy to the calculation in second order all contributions of the band cutoff vanish for $B \gg 1/D^2$ and can thus be neglected by introducing a new initial value of the coupling at $B_0 = 1/D^2$. The integration simplifies to

$$\begin{aligned}&\int d\epsilon_{q'} \int d\epsilon_q [n(qv)(1 - n(q'v)) + n(q'v)(1 - n(qv))](\epsilon_{q'} - \epsilon_q + \alpha K)^2 \mathrm{e}^{-2B\left(\epsilon_{q'}-\epsilon_q+\alpha K\right)^2} \\ &= 2F(\alpha K) + \mathcal{O}\left(\mathrm{e}^{-BD^2}\right).\end{aligned}$$

Consequently we find the flow equation of the elastic coupling $g^{\mathrm{sum},j}_{k'k}$ in the limit $B \gg 1/K^2$

$$\frac{d\overline{g^{\mathrm{sum},j}_{k'k}}}{dB} = \ldots - 2BF(0)\overline{g^{\mathrm{sum},j}_{k'k}}\;\overline{g^{\mathrm{sum},v}_{q'q}}\;\overline{g^{\mathrm{sum},v}_{qq'}} + \mathcal{O}\left(\mathrm{e}^{-BK^2}\right).$$

Using the definition of $F(y)$ and inserting the result from one-loop order, the coupling of the total spin to the leads $j = L, R$ is given at $\epsilon_k = \epsilon_{k'} = 0$ by

$$2\frac{dg_{IR}^{\mathrm{sum},j}}{d\ln B} = \left(g_{IR}^{\mathrm{sum},j}\right)^2 - \frac{1}{2}g_{IR}^{\mathrm{sum},j}\left(g_{IR}^{\mathrm{sum},v}\right)^2. \tag{6.37}$$

Please note that this is only valid for $B \gg 1/K^2$ or $\Lambda_{\mathrm{feq}} \ll K$.

Eq. (6.37) is the same result as found for the Kondo coupling in poor man's scaling, see e.g. [2]. We find that the third order contribution is a correction to the flow in second order in the coupling. It reduces the flow but the coupling still shows a strong-coupling behavior. Fig. 6.15 is the numerical solution for the flow of the elastic coupling

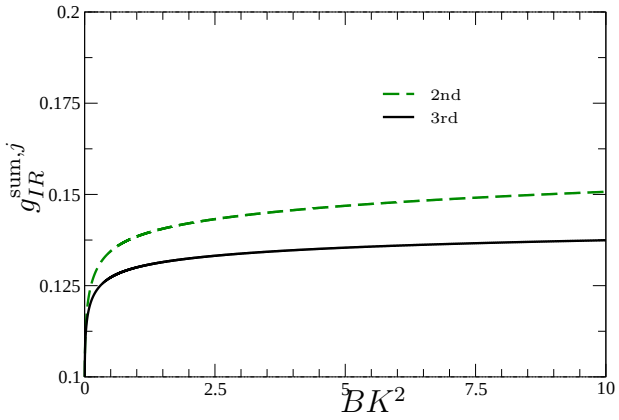

Figure 6.15: Flow of the coupling $g_{IR}^{\mathrm{sum},L}$ to 2nd and 3rd order in the coupling to the leads. The voltage $V_L = V_R = 0$, $K = 1$ and the initial value of the coupling is $g_0 = 0.1$.

$g_{k'k}^{\mathrm{sum},j}$ for $\epsilon_{k'} = \epsilon_k = 0$. The analytical behavior discussed above is valid for $BK^2 \gg 1$. It is observed that in the calculation to 3rd order the increase of the coupling is less pronounced, but the coupling still flows to strong-coupling, see therefore also Ref. [38].

6.5.4 Flow Out of Equilibrium

In contrast to the linear and one-loop order there are two intermediate states involved in a third order contribution. Therefore it is possible that the coupling of the leads to the left quantum dot can have an influence on the right quantum dot. In analogy to the transconductance in the previous chapters some preliminary results are presented which show that a finite voltage applied to one quantum dot prevents the other quantum dot to flow to strong-coupling since a finite decoherence is induced.

In non-equilibrium the occupation numbers are given according to Eq. (6.6). The integration over the two intermediate states provides thus

$$\begin{aligned}&\int d\epsilon_{q'} \int d\epsilon_q [n(qv)(1-n(q'v)) + n(q'v)(1-n(qv))](\epsilon_{q'} - \epsilon_q + \alpha K)^2 \mathrm{e}^{-2B\left(\epsilon_{q'}-\epsilon_q+\alpha K\right)^2} \\ &= 2\frac{1+r_v^2}{(1+r_v)^2}F(\alpha K) + \frac{2r_v}{(1+r_v)^2}\left(F(\alpha K + eV_v) + F(\alpha K - eV_v)\right) + \mathcal{O}\left(\mathrm{e}^{-BD^2}\right),\end{aligned}$$

where $\alpha = 0, \pm 1$.

If the voltage eV is larger than K, then the contribution from $P^j_{k'k}$ and $M^j_{k'k}$ are already negligible when the flow enters the regime of the voltage. The coupling $g^{\mathrm{sum},j}_{k'k}$ flows then according to

$$\frac{dg^{\mathrm{sum},j}_{k'k}}{dB} = \ldots - 2B\frac{1+r_v^2}{(1+r_v)^2}F(0)\overline{g^{\mathrm{sum},j}_{k'k}}\ \overline{g^{\mathrm{sum},v}_{q'q}}\ \overline{g^{\mathrm{sum},v}_{qq'}} - 2B\frac{2r_v}{(1+r_v)^2}F(V_v)\overline{g^{\mathrm{sum},j}_{k'k}}\ \overline{g^{\mathrm{sum},v}_{q'q}}\ \overline{g^{\mathrm{sum},v}_{qq'}} + \mathcal{O}\left(\mathrm{e}^{-BK^2}\right).$$

It was already discussed in detail in section 6.4.4 that the infrared parametrization is not applicable in the case of a finite voltage, since energy processes take place at two different Fermi surfaces shifted by $\pm eV_v/2$ from the equilibrium Fermi energy. In non-equilibrium it is more appropriate to study the transport coupling $g^{\mathrm{sum},j}_t$ defined in Eq. (6.33), which is an average over all energy processes contributing in the energy window opened by the voltage. It was shown in section 6.4.4 that the flow of the coupling to second order is negligibly small in the limit of $B \gg 1/V^2$. In this regime the 3rd order contribution determines the flow of the coupling. As illustrated in Fig. 6.16(a) decoherent processes lead to a stagnation and finally the coupling of the spin to the leads decreases to zero. The physical meaning of this decrease is discussed in the outlook, section 6.6.

For example if a finite voltage V_L is applied to the left quantum dot, the transport coupling of the total spin to the leads $j = L, R$ is given by

$$\frac{dg^{\mathrm{sum},j}_t}{dB} \approx \frac{1}{2B}\left(g^{\mathrm{sum},j}_t\right)^2\frac{\sqrt{\pi}}{\sqrt{8B}V_j} - \frac{1}{4B}\frac{1}{(1+r_v)^2}g^{\mathrm{sum},j}_t\ \left(g^{\mathrm{sum},v}_t\right)^2\left[1+r_v^2+2r_v^2\mathrm{e}^{-2BV_v^2}\right] - \frac{V_v}{4}\frac{\sqrt{\pi}}{\sqrt{2B}}\frac{2r_v}{(1+r_v)^2}g^{\mathrm{sum},j}_t\ \left(g^{\mathrm{sum},v}_t\right)^2 + \mathcal{O}\left(\mathrm{e}^{-BK^2}\right). \tag{6.38}$$

In the limit $B \gg 1/V^2$ the right hand side of Eq. (6.38) is dominated by the term that flows proportional to $1/\sqrt{2B}$. The ansatz $g = g^*/\sqrt{1+\sqrt{B\Gamma^2}}$ solves the differential equation,

$$\frac{dg^{\mathrm{sum},j}_t}{dB} \approx -\frac{V_j}{4}\frac{\sqrt{\pi}}{\sqrt{2B}}\frac{2r_j}{(1+r_j)^2}\ \left(\overline{g^{\mathrm{sum},j}_t}\right)^3,$$

where the decoherence rate Γ_j for the elastic coupling to the lead $j = L, R$ is given by

$$\Gamma_j = \sqrt{\frac{\pi}{2}}\ \frac{2r_j}{(1+r_j)^2}\ (g^*)^2\ V_j,$$

and the initial coupling g^* is determined by the flow of the coupling at the stage where the term proportional to the voltage starts to dominate. This is obvious from a simple argument: The decoherence rate Γ provides a new energy scale of the system. It is of the order of J^2. Thus the third order term in the flow equation transfers to a linear term,

$$\frac{dg^{\mathrm{sum},j}_t}{d\ln\Lambda_{\mathrm{feq}}} \approx \frac{\Gamma_j}{2\Lambda_{\mathrm{feq}}}\overline{g^{\mathrm{sum},j}_t}.$$

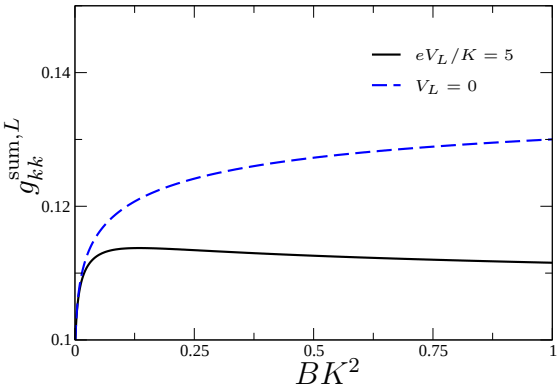

(a) Flow of the coupling $g^{\mathrm{sum},L}_{kk}$ for finite voltage V_L and $\epsilon_k = eV_L/2$.

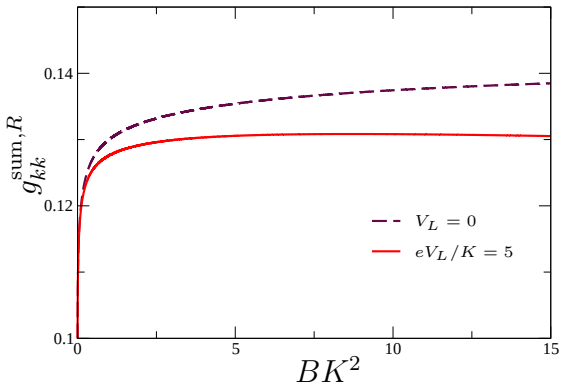

(b) Flow of the coupling $g^{\mathrm{sum},R}_{kk}$ for finite voltage V_L and $\epsilon_k = 0$.

Figure 6.16: Flow in third order of the coupling $g^{\mathrm{sum},L}_{kk}$ and $g^{\mathrm{sum},R}_{kk}$ for finite voltage $eV_L/K = 5$ in comparison with the flow in equilibrium $V_L = 0$. The initial value is $g^{\mathrm{sum},j}_{kk} = 0.1$ and the asymmetry is $r_L = r_R = 1$.

A term linear in the coupling dominates over a contribution to second order and thus the physics of the system is described by the decoherence rate Γ when the energy cutoff is lowered sufficiently, $\Lambda_{\mathrm{feq}} \ll \Gamma$. For a detailed discussion we refer the reader to Ref. [38].

A numerical solution for the flow of the elastic coupling $g^{\mathrm{sum},j}_{kk}$ in and out of equilibrium is given in Fig. 6.16. An exact implementation of the flow equations is work in progress, but the first preliminary results shown here already promise interesting physical behavior. For the coupling $g^{\mathrm{sum},L}_{kk}$ shown for the energy $\epsilon_k = eV_L/2$ in Fig. 6.16(a) an increase is observed in the coupling independently if a finite voltage is applied or not. As soon as the flow parameter B reaches $1/\Gamma^2$ the coupling $g^{\mathrm{sum},L}_{kk}$ saturates and for later stages of the flow the value starts to decrease. This can be explained by an entanglement of the impurity spin with the environment on the energy scale of the dephasing Γ, as is discussed in section 6.6. This is the characteristic behavior of a Kondo coupling subject to a finite voltage, see also discussion in Ref. [38].

In the double quantum dot setup studied here the total spin moment couples to the left leads, as illustrated in Fig. 6.16(a), and to the right leads. The flow of the coupling $g^{\mathrm{sum},R}_{kk}$ for $\epsilon_k = 0$ is shown in Fig. 6.16(b). It is expected that this coupling shows strong-coupling behavior since there is no current through the right quantum dot. Due to the summation over the two lead indices v in Eq. (6.38) the voltage V_L enters the flow equation of $g^{\mathrm{sum},R}_{kk}$. It is observed in the numerical solution, that the coupling to the right leads is prevented to flow to strong-coupling if a large voltage is applied to the left leads. It is the aim of future work to find an analytical expression for this phenomenon, and discuss the whole parameter regime of the double quantum dot system. The two quantum dots are coupled by a spin-spin interaction and it is assumed that no particle transfer takes place. In Fig. 6.16(b) it is illustrated that a decoherence due to current-noise is transferred from one quantum dot to a coupled quantum dot. This effect was discussed in details in the previous chapters of this thesis and has the direct consequence that the transconductance $(K/eV_L)dI_L/dV_R$ is finite.

In conclusion we found that a finite voltage prevents the Kondo coupling to show strong-coupling behavior. The system is dominated by decoherence due to current-

noise. The coherent spin-flip processes which lead to the Kondo effect are prohibited due to a finite life time of the quantum dot spin states. In the flow equation for the coupling of the total spin moment to the leads, Eq. (6.35), only self energy contributions as illustrated in Fig. 6.14(b) enter. Due to a hybridizaton with the leads the spin states gain a finite life time and the coherence of scattering events is lost. In the flow equation for the inelastic coupling, Eq. (6.36), there are also contributions from vertex corrections, as illustrated in Fig. 6.14(a). For example the coupling of the left spin to the left leads, $J^{LL}_{k'k} = J^{\mathrm{sum},L}_{k'k} + P^{L}_{k'k} + P^{L}_{kk'}$, is a combination of the elastic and inelastic couplings. It will be studied in future work how this coupling is influenced by the different mechanisms of decoherence.

6.6 Summary and Outlook

This chapter was devoted to the flow equation method out of equilibrium. A brief introduction to the method is given in section 6.1 and for further reading we refer the reader to the book of S. Kehrein [38]. The main purpose of this chapter was the discussion of the scaling of the different couplings in a double quantum dot system. In section 6.2 the two different kinds of couplings between the double quantum dot system and the leads were discussed: the elastic one, which interacts with the total magnetic moment of the two spins, and the inelastic one, which involves a transition from a singlet to a triplet state and therefore the energy difference of the singlet-triplet gap K has to be provided by the incoming and outgoing conduction electrons.

To linear order in the coupling to the leads the flow equations for the couplings incorporate this behavior such that the elastic coupling $J^{\mathrm{sum},j}_{k'k}$ is proportional to $\mathrm{e}^{-B(\epsilon_{k'}-\epsilon_k)^2}$ while the inelastic coupling $P^{j}_{k'k}$ is exponentially suppressed for $\epsilon_{k'} = \epsilon_k$ due to the factor $\mathrm{e}^{-B(\epsilon_{k'}-\epsilon_k+K)^2}$. The coupling Hamiltonian becomes successively energy-diagonal with increasing flow parameter B or decreasing frequency cutoff $\Lambda_{\mathrm{feq}} = B^{-1/2}$. At later stages of the flow higher order contributions become important, and as examples the second (one-loop) and third (two-loop) order contributions are discussed here. In general the flow equation method is exact, whereas in practice it is perturbative since new couplings are created during the flow and the series has to be truncated. The flow equation method keeps the information on all energy scales since the Hamiltonian becomes successively energy-diagonal during the flow. In non-equilibrium all coupling contributions in the energy window opened by the voltage are important and thus the flow equation method is applicable. One advantage of the energy-diagonalization procedure is that the derivation of the flow equations is identical in and out of equilibrium.

Various approximations to solve the scaling equations to second order in the couplings were discussed in section 6.4. It is possible to solve the flow equations exactly in a numerical framework as shown in section 6.4.3. The diagonal parametrization approximates e.g. the coupling $J^{\mathrm{sum},j}_{k'k}$ by a product of an exponential factor $\mathrm{e}^{-B(\epsilon_{k'}-\epsilon_k)^2}$ with an average coupling $\overline{J^{\mathrm{sum},j}_{k'k}}$ where k' and k are determined by the energy conservation at the vertex, $\epsilon_{k'} = \epsilon_k$. For the energy at the Fermi surface, i.e. the infrared parametrization, the flow equation method and the poor man's scaling approach give identical results. It is shown in section 6.4 that the coupling of the total spin to the leads diverges if the frequency cutoff is reduced below a critical value. This strong-coupling behavior is characteristic for a system with Kondo interactions.

In chapter 5 the perturbative RG method was introduced since it is applicable to the Kondo problem out of equilibrium. In section 6.4.5 the two different non-equilibrium scaling methods are compared. It is found that in the diagonal parametrization the same approximations are used as in the perturbative RG. The two methods differ by the energy cutoff mechanism, which is given by $\mathrm{e}^{-(x/\Lambda_{\mathrm{feq}})^2}$ in the flow equation method and by $\Theta(1-x/\Lambda_{RG})$ in the perturbative RG. Apart from that the way the decoherence is included is quite different. Whereas a finite life time of the double quantum dot states is included by hand in the cutoff scheme in chapter 5, decoherence mechanisms enter the flow equation method naturally to third order in the coupling.

The third order contributions to the scaling equations were discussed in section 6.5. There are no imaginary contributions in the flow equations, thus the question arises why this method can describe a finite life time of the quantum dot states.[8] Decoherence mechanisms arise in this framework when including two-particle interactions of the type $\vec{S}\,(\vec{s}_{k'k}\times\vec{s}_{p'p})$, which are created to second order in the coupling to the leads. To understand how these terms lead to decoherence it is important to consider the scaling equation both for the Hamiltonian as well as for the operators of the system. While the Hamiltonian becomes successively more energy-diagonal, hence "simple",[9] the operator structure can become complicated since any operator $\mathcal{O}$ is also transformed unitarily by the same scaling equation as the Hamiltonian in Eq. (6.1),

$$\frac{d\mathcal{O}(B)}{dB} = [\eta(B), \mathcal{O}(B)]\,,$$

where $\mathcal{O}(B=0)=\mathcal{O}$. For example in the spin-1/2 Kondo model the spin of the Kondo impurity shows a scaling behavior. As discussed in detail in Ref. [38] the spin $\vec{S}(B)$ is given by

$$\vec{S}(B) = h(B)\vec{S} + i\sum \gamma_{k'k}(B)\left(\vec{S}\times\vec{s}_{k'k}\right).$$

It is found that the prefactor $h(B)$ vanishes for $B\to\infty$. The spin $\vec{S}$ is then given by the operator structure $(\vec{S}\times\vec{s}_{k'k})$ and thus becomes entangled with the environment, i.e. the spin $\vec{s}_{k'k}$ in the leads. In non-equilibrium the entanglement is present when the frequency cutoff Λ_{feq} is reduced below the energy scale of the decoherence rate Γ. This explains why the decoherence enters the scaling equations by the newly created couplings to second order. When the spin in the Kondo coupling $\vec{S}\;\vec{s}_{p'p}$ becomes entangled with the environment, the Kondo interaction changes to $\left(\vec{S}\times\vec{s}_{k'k}\right)\vec{s}_{p'p}$, which is the coupling taken into account to calculate the third order contribution in the flow equations. The decoherence rate Γ is a new energy scale of the system. Since this energy is proportional to the phase space and of second order in the coupling, J^2V, the third order contribution is effectively of linear order: $J^3V\sim J\Gamma$. Therefore the third order contribution can dominate the scaling behavior given otherwise by the second order term.

To study the flow of the spin operators using the flow equation method is a natural extension of this work. First preliminary results for the decoherence of a double quantum dot system were given in section 6.5. It was explained that there are two different

[8] The finite life time in perturbation theory originates from the imaginary part of the self energy.

[9] The energy-diagonality of the Hamiltonian $H(B\to\infty)$ provides a tool to study the time evolution of the Hamiltonian or observables, see also Ref. [38].

decoherence mechanisms which prevent the elastic Kondo coupling to flow to strong-coupling. An analytical discussion of the different contributions is the aim of future work. By a numerical analysis we could show that a finite voltage applied to e.g. the left quantum dot stops the flow of the coupling between the total spin and the left leads. It is also observed that the flow of the coupling to the right leads does not show strong-coupling behavior although the right leads are not subject to a large voltage. As also observed in the previous chapters the spin-spin interaction between two coupled quantum dots can transfer a non-equilibrium situation between the dots. In the flow equation method this effect is observed to two-loop order when decoherence effects enter the scaling equations. An experimental observable like the transconductance as discussed in the previous sections is not calculated here since a new flow equation has to be solved for every observable. The signatures of the non-equilibrium transfer that were found in the scaling equations indicate that a finite transconductance can be found in a current measurement, however this has to be verified explicitly in the future.

7 Conclusions

A quantum dot subject to a large voltage can drive a second, coupled dot out of equilibrium, although there is no particle exchange between the dots. We studied the effect of a finite voltage applied to the system of two coupled quantum dots and found that this non-equilibrium transfer manifests itself in different physical quantities. Before we discuss explicit examples the principle idea of the non-equilibrium mediation is explained.

In the Kondo model a quantum dot is described solely by its spin configuration. The setup of two coupled quantum dots is connected to four leads to allow for a transport through each of the dots independently. A finite voltage applied to the right quantum dot drives a finite current through the dot. Repeated transport processes lead to a finite life time of the spin state in this quantum dot. The occupation of the spin ground state decays inversely proportional to the applied voltage for large voltages. The other (left) quantum dot is coupled to the right quantum dot by a pure spin-spin interaction. For an antiferromagnetic coupling of the spin system the ground state is a spin singlet. A finite current applied to the right quantum dot leads to a decoherence of the spin state on the right quantum dot as well as a decoherence of the coupled quantum dot system. Even if the leads coupled to the left quantum dot are not subject to a finite voltage, the non-equilibrium situation on the right side has an influence on the left quantum dot. This can be observed in various physical quantities. It was the aim of this thesis to discuss this effect and further the physical behavior of a double quantum dot system out of equilibrium using perturbation theory and various scaling approaches.

7.1 Conclusions to "Model of a Double Quantum Dot System"

We motivated the Kondo spin model for two coupled quantum dots by deriving an effective model from a microscopic Hamiltonian of two Anderson impurities. We showed that the two quantum dots can be coupled via an exchange interaction process and discussed other mechanism which lead to a spin-spin coupling. Two coupled spin states form singlet and triplet states and we introduced a pseudo particle representation, which provides the means for performing perturbation calculations for a system of coupled quantum dots. As an important detail it was shown in section 2.2, that the leakage between leads attached to the left quantum dot and leads connected to the right quantum dot can be neglected. For two identical quantum dots which are tuned to particle-hole symmetry the leakage is even zero and the currents through the left and the right quantum dot can be treated independently. Therefore we hope that the double quantum dot setup we investigated here can soon be realized in experimental setups (similar setups have already been discussed in Ref. [27, 29]). The magnitude of the parameters for the double quantum dot system of interest depend on microscopic parameters, which could be determined from experiments on these systems.

7.2 Conclusions to "Perturbation Theory"

The well-known method of Green's functions has to be generalized to non-equilibrium. In the case of a finite voltage the retarded and the lesser Green's functions fulfill two independent Dyson equations. It was shown that the determining equation for the lesser Green's function leads to a self-consistent equation for the occupation number of the double quantum dot states. A finite voltage influences the distribution functions to 0th order in the perturbative expansion. Like an effective temperature a finite voltage can provide the energy to occupy excited states. If the voltage reaches a threshold given by the singlet-triplet gap, a finite current and therefore decoherent processes lead to a finite occupation of triplet states, in case the two quantum dots are in a singlet ground state due to an antiferromagnetic coupling. We studied the thermodynamic quantities polarization $\langle \vec{S}_L \vec{S}_R \rangle$ and magnetization $2\langle \vec{S}_L^z + \vec{S}_R^z \rangle$ as a function of voltage and observed in both cases that the ground state becomes depopulated, if large voltages are applied either across the left or the right quantum dot. The decay from the initial value is inversely proportional to the applied voltage.

This can be measured in a current measurement. Since the singlet state blocks the transport through a single quantum dot, the excitation of triplet states opens a channel for transport. In section 4.2 we studied in detail the so-called transconductance (see Ref. [65]). The differential dependence of the current through the left quantum dot in dependence on the voltage applied to the right quantum dot may be measured in experiments and provides a proof of the voltage-dependence of the singlet and triplet states and an indirect measure of the decoherence properties of the double quantum dot system.

The transfer of the non-equilibrium situation on one quantum dot to another coupled dot can also be seen in the T-matrix and the noise. It is even observed for ferromagnetic coupling, but the effect is less pronounced. The calculation of the noise properties and the current cross-correlation $\langle I_L I_R \rangle$ is on-going work, but preliminary results showed that the correlation between the current through the left and the current through the right quantum dot is given solely by a finite life time of the double quantum dot states.

7.3 Conclusions to "Perturbative Renormalization Group"

The perturbation theory fails to describe the physics of the Kondo model at low temperatures. In chapter 5 we introduced a recent generalization of poor man's scaling, the perturbative RG [35, 36], which is able to describe, for example current transport for large applied voltages. While reducing the cutoff, the model can be mapped on an effective Hamiltonian on a low energy scale. In non-equilibrium the frequency argument of the coupling function cannot be neglected and the flow stops at the energy given by the decoherence rate, if it is not stopped by an energy scale of the double quantum dot. The rate equation for the level occupation probabilities is also taken into account including the renormalized rates.

We discussed the method and the flow of the couplings in detail and showed in analogy to the perturbation theory the results for the polarization and current. We found that the effect of transconductance is enhanced by the scaling of the couplings [65]. This

increases the possibility to measure in experiment the transfer of a non-equilibrium situation from one quantum dot to another. As ongoing projects we also proposed the calculation of the T-matrix in perturbative RG, with the aim to compare the results with calculations of the spectral function in NRG. The special case of ferromagnetic coupling was also discussed and some limitations of the perturbative RG approach were shown.

7.4 Conclusions to "Flow Equation Method"

Although the perturbative RG incorporates all ingredients of a non-equilibrium scaling theory, the important effect of a finite decoherence has to be inserted by hand. In the last chapter of this thesis we therefore discussed the flow equation method out of equilibrium [37, 38]. We applied this scaling approach to the setup of two coupled quantum dots and found in lowest order that the couplings in the Hamiltonian flow to strong-coupling. The flow equation method is also perturbative in the coupling of the quantum dot to the leads, but in contrast to the perturbative RG higher orders can be calculated straightforwardly. We showed explicitly that a decoherence scale appears naturally in this approach. As in the other chapters we observed that due to the finite voltage applied to the left quantum dot the couplings on the right side do no longer flow to strong-coupling. Two antiferromagnetically coupled quantum dots undergo a quantum phase transition from an uncompensated spin singlet to two Kondo screened impurities for a small exchange coupling of the order of the Kondo temperature. An intensive study of the parameter regime of this model is the aim of future work. The perturbative RG approach fails already at couplings of one order of magnitude larger than the Kondo temperature. The hope is that the regime of the quantum phase transition can be approached, or signatures of it can be identified, using the flow equation method.

A Additional Calculations to Chapter 2

A.1 Calculation to 2nd order in the Hopping Parameter t

A.1.1 Important Commutators

For the following calculation we use repeatedly the following relations

$$[AB, C] = A\{B, C\} - \{C, A\}B,$$
$$[AB, C] = A[B, C] - [C, A]B,$$

and

$$[AB, CD] = A\{B, C\}D - C\{D, A\}B + CA\{B, D\} - \{C, A\}BD,$$
$$[AB, CD] = A[B, C]D - C[D, A]B + CA[B, D] - [C, A]BD.$$

We will often encounter

$$[d_\sigma, n_{d\sigma'}] = \delta_{\sigma\sigma'}\ d_\sigma, \qquad [n_{d\sigma'}, d_\sigma] = -\delta_{\sigma\sigma'}\ d_\sigma, \qquad [1 - n_{d\sigma'}, d_\sigma] = \delta_{\sigma\sigma'}\ d_\sigma,$$

and analogously

$$\left[d^\dagger_\sigma, n_{d\sigma'}\right] = -\delta_{\sigma\sigma'}\ d^\dagger_\sigma, \qquad \left[n_{d\sigma'}, d^\dagger_\sigma\right] = \delta_{\sigma\sigma'}\ d^\dagger_\sigma, \qquad \left[1 - n_{d\sigma'}, d^\dagger_\sigma\right] = -\delta_{\sigma\sigma'}\ d^\dagger_\sigma.$$

Immediately it follows

$$[d_\sigma, n_{d\sigma'}n_{d\overline{\sigma}'}] = \delta_{\sigma,\overline{\sigma}'}\ n_{d\sigma}\ d_\sigma + \delta_{\sigma,\sigma'}\ n_{d\overline{\sigma}}\ d_\sigma.$$

Also useful are the facts

$$[n_{d\sigma}, n_{d\sigma'}] = 0 \quad \text{and} \quad n^2_{d\sigma} = n_{d\sigma}$$

for fermions.

A.1.2 Check of the Generator S_{LR}

It has to be proven that $[iS_{LR}, H_0] = -H_{LR}$. Here we show only one example, namely for the first term in $\hat{E}_{LR}(\sigma)$ contributing to S_{LR} as $\frac{t_{LR}}{\epsilon_{L\sigma} - \epsilon_{R\sigma}}(1 - n_{L\overline{\sigma}})(1 - n_{R\overline{\sigma}})d^\dagger_{R\sigma}d_{L\sigma}$. Since the intermediate state is occupied by only one electron, we can forget the contribution from H_{cap} and H_{Hund} and only have to calculate

$$i[S_{LR}, H_n] = 0 \quad \text{and}$$
$$i[S_{LR}, H_\alpha] = i\sum_{\sigma\sigma'}\big[t_{LR}\hat{E}_{LR}(\sigma)d^\dagger_{R\sigma}d_{L\sigma} - t_{LR}\hat{E}_{LR}(\sigma)d^\dagger_{L\sigma}d_{R\sigma},$$
$$\epsilon_{\alpha\sigma'}n_{\alpha\sigma'} + \frac{1}{2}U_\alpha n_{\alpha\sigma'}n_{\alpha\overline{\sigma}'}\big].$$

For example in the case of $\alpha = R$

$$
\begin{aligned}
& i\sum_{\sigma\sigma'}\left[\frac{t_{LR}}{\epsilon_{L\sigma}-\epsilon_{R\sigma}}(1-n_{L\overline{\sigma}})(1-n_{R\overline{\sigma}})d^{\dagger}_{R\sigma}d_{L\sigma},\epsilon_{R\sigma'}n_{R\sigma'}+\frac{1}{2}U_R n_{R\sigma'}n_{R\overline{\sigma}'}\right] \\
&= i\sum_{\sigma\sigma'}t_{LR}\frac{\epsilon_{R\sigma'}}{\epsilon_{L\sigma}-\epsilon_{R\sigma}}(1-n_{L\overline{\sigma}})(1-n_{R\overline{\sigma}})\left[d^{\dagger}_{R\sigma},n_{R\sigma'}\right]d_{L\sigma} \\
&\quad + t_{LR}\frac{\frac{1}{2}U_R}{\epsilon_{L\sigma}-\epsilon_{R\sigma}}(1-n_{L\overline{\sigma}})(1-n_{R\overline{\sigma}})\left[d^{\dagger}_{R\sigma},n_{R\sigma'}n_{R\overline{\sigma}'}\right]d_{L\sigma} \\
&= i\sum_{\sigma}t_{LR}\frac{-\epsilon_{R\sigma}}{\epsilon_{L\sigma}-\epsilon_{R\sigma}}(1-n_{L\overline{\sigma}})(1-n_{R\overline{\sigma}})d^{\dagger}_{R\sigma}d_{L\sigma} \\
&\quad - t_{LR}\frac{\frac{1}{2}U_R}{\epsilon_{L\sigma}-\epsilon_{R\sigma}}(1-n_{L\overline{\sigma}})(1-n_{R\overline{\sigma}})2n_{R\overline{\sigma}}\; d^{\dagger}_{R\sigma}d_{L\sigma} \\
&= i\sum_{\sigma}t_{LR}\frac{-\epsilon_{R\sigma}}{\epsilon_{L\sigma}-\epsilon_{R\sigma}}(1-n_{L\overline{\sigma}})(1-n_{R\overline{\sigma}})d^{\dagger}_{R\sigma}d_{L\sigma},
\end{aligned}
$$

where one term cancels out since $n_{R\overline{\sigma}}(1-n_{R\overline{\sigma}}) = n_{R\overline{\sigma}} - n^2_{R\overline{\sigma}} = 0$ - a state cannot be occupied and empty at the same time. The commutator with H_L works similarly, but provides a different sign

$$
\begin{aligned}
& i\sum_{\sigma\sigma'}\left[\frac{t_{LR}}{\epsilon_{L\sigma}-\epsilon_{R\sigma}}(1-n_{L\overline{\sigma}})(1-n_{R\overline{\sigma}})d^{\dagger}_{R\sigma}d_{L\sigma},\epsilon_{L\sigma'}n_{L\sigma'}+\frac{1}{2}U_L n_{L\sigma'}n_{L\overline{\sigma}'}\right] \\
&= i\sum_{\sigma}t_{LR}\frac{\epsilon_{L\sigma}}{\epsilon_{L\sigma}-\epsilon_{R\sigma}}(1-n_{L\overline{\sigma}})(1-n_{R\overline{\sigma}})d^{\dagger}_{R\sigma}d_{L\sigma}.
\end{aligned}
$$

Consequently the first term results in

$$
i\left[S_{LR},H_\alpha\right] = i^2\sum t_{LR}(1-n_{L\overline{\sigma}})(1-n_{R\overline{\sigma}})d^{\dagger}_{R\sigma}d_{L\sigma}+\ldots
$$

and together with all other terms finally $i\left[S_{LR},H_\alpha\right]$ cancels H_{LR}.

A.1.3 General Operator Structure to 2nd Order in the Schrieffer-Wolff Transformation

In the section 2.2.4 we found the general result for the interacting Hamiltonian from the spin-conserving part of $\frac{1}{2}i\left[S_{\alpha n},H_{\alpha m}\right]$ to be

$$
\begin{aligned}
& -\frac{1}{2}\frac{1}{N^2}\sum_{nk\sigma}\sum_{mk'\sigma'}c^{\dagger}_{nk\sigma}c_{mk'\sigma} \\
&\qquad \left\{\frac{t_{\alpha n}t_{m\alpha}}{\epsilon_{\alpha\sigma}+U_{LR}-J_H-\zeta}n_{\alpha\sigma}\left(1-n_{\alpha\overline{\sigma}}\right)n_{\overline{\alpha}\sigma}\left(1-n_{\overline{\alpha}\overline{\sigma}}\right)\right. \\
&\qquad +\frac{t_{\alpha n}t_{m\alpha}}{\epsilon_{\alpha\sigma}+U_{LR}-\zeta}n_{\alpha\sigma}\left(1-n_{\alpha\overline{\sigma}}\right)\left(1-n_{\overline{\alpha}\sigma}\right)n_{\overline{\alpha}\overline{\sigma}} \\
&\qquad +\frac{t_{\alpha n}t_{m\alpha}}{\epsilon_{\alpha\sigma}+U_{\alpha}+U_{LR}-\zeta}\left(1-n_{\alpha\sigma}\right)n_{\alpha\overline{\sigma}}\;n_{\overline{\alpha}\sigma}\left(1-n_{\overline{\alpha}\overline{\sigma}}\right) \\
&\qquad \left.+\frac{t_{\alpha n}t_{m\alpha}}{\epsilon_{\alpha\sigma}+U_{\alpha}+U_{LR}+J_H-\zeta}\left(1-n_{\alpha\sigma}\right)n_{\alpha\overline{\sigma}}\;\left(1-n_{\overline{\alpha}\sigma}\right)n_{\overline{\alpha}\overline{\sigma}}\right\}+h.c.
\end{aligned}
$$

For this expression we now evaluate the spin summation and after using some spin relations we find some contributions to the potential scattering and the spin interaction part. To simplify the expressions it is assumed that the energy level $\epsilon_{\alpha\sigma}$ does not dependent on the spin σ of the electron on the dot. Thus we find,

$$\begin{aligned}\frac{1}{2}i\left[S_{\alpha n}, H_{\alpha m}\right] = &\frac{1}{2}\sum_{m,n}\sum_{k,k'}\left(J_{\alpha nm}s^z_{nm}S^z_\alpha + h.c.\right)\\ &+\frac{1}{2}\sum_{m,n}\sum_{k,k'}\left(J^{\overline{\alpha}}_{\alpha nm}s^z_{nm}S^z_{\overline{\alpha}} + h.c.\right)\\ &+\frac{1}{2}\sum_{m,n}\sum_{k,k'}\left(V_{\alpha nm}c^\dagger_{nk\sigma}c_{mk'\sigma} + h.c.\right)\\ &+\frac{1}{2}\sum_{m,n}\sum_{k,k'}\left(V^{SS}_{\alpha nm}c^\dagger_{nk\sigma}c_{mk'\sigma}S^z_L S^z_R + h.c.\right),\end{aligned}$$

where the Kondo interactions are given by

$$\begin{aligned}J_{\alpha nm} =&\frac{t_{\alpha n}t_{m\alpha}}{\epsilon_{\alpha\sigma}+U_\alpha+U_{LR}+J_H-\zeta}+\frac{t_{\alpha n}t_{m\alpha}}{\epsilon_{\alpha\sigma}+U_\alpha+U_{LR}-\zeta}\\ &-\frac{t_{\alpha n}t_{m\alpha}}{\epsilon_{\alpha\sigma}+U_{LR}-J_H-\zeta}-\frac{t_{\alpha n}t_{m\alpha}}{\epsilon_{\alpha\sigma}+U_{LR}-\zeta},\end{aligned}\tag{A.1}$$

$$\begin{aligned}J^{\overline{\alpha}}_{\alpha nm} =&\frac{t_{\alpha n}t_{m\alpha}}{\epsilon_{\alpha\sigma}+U_\alpha+U_{LR}+J_H-\zeta}-\frac{t_{\alpha n}t_{m\alpha}}{\epsilon_{\alpha\sigma}+U_\alpha+U_{LR}-\zeta}\\ &-\frac{t_{\alpha n}t_{m\alpha}}{\epsilon_{\alpha\sigma}+U_{LR}-J_H-\zeta}+\frac{t_{\alpha n}t_{m\alpha}}{\epsilon_{\alpha\sigma}+U_{LR}-\zeta},\end{aligned}\tag{A.2}$$

and the potential scattering terms yield

$$\begin{aligned}V_{\alpha nm} =&-\frac{1}{4}\left(\frac{t_{\alpha n}t_{m\alpha}}{\epsilon_{\alpha\sigma}+U_\alpha+U_{LR}+J_H-\zeta}+\frac{t_{\alpha n}t_{m\alpha}}{\epsilon_{\alpha\sigma}+U_\alpha+U_{LR}-\zeta}\right.\\ &\left.+\frac{t_{\alpha n}t_{m\alpha}}{\epsilon_{\alpha\sigma}+U_{LR}-J_H-\zeta}+\frac{t_{\alpha n}t_{m\alpha}}{\epsilon_{\alpha\sigma}+U_{LR}-\zeta}\right),\end{aligned}\tag{A.3}$$

$$\begin{aligned}V^{SS}_{\alpha nm} =&-\frac{t_{\alpha n}t_{m\alpha}}{\epsilon_{\alpha\sigma}+U_\alpha+U_{LR}+J_H-\zeta}+\frac{t_{\alpha n}t_{m\alpha}}{\epsilon_{\alpha\sigma}+U_\alpha+U_{LR}-\zeta}\\ &-\frac{t_{\alpha n}t_{m\alpha}}{\epsilon_{\alpha\sigma}+U_{LR}-J_H-\zeta}+\frac{t_{\alpha n}t_{m\alpha}}{\epsilon_{\alpha\sigma}+U_{LR}-\zeta}.\end{aligned}\tag{A.4}$$

Additionally we have the spin-flip part from Eq. (2.33).

$$=i\sum\left\{t_{\alpha n}t_{m\alpha}\left[\hat{E}_\alpha, d^\dagger_{\alpha\sigma'}\right]c_{mk'\sigma'}c^\dagger_{nk\sigma}d_{\alpha\sigma} - t_{n\alpha}t_{\alpha m}c^\dagger_{mk'\sigma'}\left[\hat{E}_\alpha, d_{\alpha\sigma'}\right]d^\dagger_{\alpha\sigma}c_{nk\sigma}\right\}.$$

Leaving out the actual calculation we write down the result of the spin-flip scattering contribution

$$\begin{aligned}&\frac{1}{2}\sum J_{\alpha nm}\left(s^+_{nm}S^-_\alpha + s^-_{nm}S^+_\alpha\right) + h.c.\\ &+\sum J^x_{\alpha nm}\left(s^+_{nm}S^-_\alpha S^z_{\overline{\alpha}} - s^-_{nm}S^+_\alpha S^z_{\overline{\alpha}}\right) + h.c.,\end{aligned}$$

where

$$J^x_{\alpha nm} = V^{SS}_{\alpha nm}. \tag{A.5}$$

Collecting all terms we find the new Hamiltonian $H = H_0 + H_{\text{int}} + H_{\text{Hund}}$ with $H_0 = H_L + H_R + H_{\text{cap}} + H_{J_H}$ and

$$\begin{aligned}
H_{\text{int}} =& K\vec{S}_L\vec{S}_R - \frac{1}{4}K \\
&+ \sum_{nm} J_{Lnm}\vec{S}_L\vec{s}_{nm} + \sum_{nm} J_{Rnm}\vec{S}_R\vec{s}_{nm} \\
&+ \frac{1}{N^2}\sum_{nm}\sum_{\sigma}\sum_{k,k'} V_{Lnm}c^\dagger_{nk\sigma}c_{mk'\sigma} + \frac{1}{N^2}\sum_{nm}\sum_{\sigma}\sum_{k,k'} V_{Rnm}c^\dagger_{nk\sigma}c_{mk'\sigma}, \\
H_{J_H} =& \sum_{nm} J^R_{Lnm}\vec{S}^z_R\vec{s}^z_{nm} + \sum_{nm} J^L_{Rnm}\vec{S}^z_L\vec{s}^z_{nm} \\
&+ \sum J^x_{Lnm}\left(s^+_{nm}S^-_L S^z_R - s^-_{nm}S^+_L S^z_R\right) + \sum J^x_{Rnm}\left(s^+_{nm}S^-_R S^z_L - s^-_{nm}S^+_R S^z_L\right) \\
&+ \sum_{nm}\sum_{\sigma}\sum_{k,k'}\left(V^{SS}_{Lnm} + V^{SS}_{Rnm}\right)c^\dagger_{nk\sigma}c_{mk'\sigma}S^z_L S^z_R,
\end{aligned}$$

if we assume $t_{\alpha n} = t_{n\alpha}$ to be real, since then *h.c.* provides just a factor of 2.

Please note, that if $J_H = 0$ all couplings in H_{J_H} are zero and

$$\begin{aligned}
J_{\alpha nm} =& \frac{2t_{\alpha n}t_{\alpha m}}{\epsilon_{\alpha\sigma} + U_\alpha + U_{LR} - \zeta} - \frac{2t_{\alpha n}t_{\alpha m}}{\epsilon_{\alpha\sigma} + U_{LR} - \zeta}, \\
V_{\alpha nm} =& -\frac{1}{2}\left(\frac{t_{\alpha n}t_{\alpha m}}{\epsilon_{\alpha\sigma} + U_\alpha + U_{LR} - \zeta} + \frac{t_{\alpha n}t_{\alpha m}}{\epsilon_{\alpha\sigma} + U_{LR} - \zeta}\right), \\
K =& \frac{2t_{LR}t_{RL}}{\epsilon_L - \epsilon_R + U_{LR} - U_R} - \frac{2t_{LR}t_{RL}}{\epsilon_L - \epsilon_R + U_L - U_{LR}}.
\end{aligned}$$

These coupling are used in the the main text of this thesis.

A.2 Calculation of the 3rd Order Contribution to the Leakage

From a calculational point of view we can state that to third order we only get contributions from the following terms, omitting the summation over all intermediate indices $\sum_\sigma 1/N^2 \sum_{nk'\sigma'} \sum_{mk''\sigma''}$

$$
\begin{aligned}
&\frac{1}{3}t_{mL}t_{LR}t_{Rn}\Big\{\Big[\hat{E}_{LR}(\sigma)d^\dagger_{R\sigma}d_{L\sigma},\Big[\hat{E}_R(\sigma')c^\dagger_{nk'\sigma'}d_{R\sigma'},d^\dagger_{L\sigma''}c_{mk''\sigma''}\Big]\Big]\\
&\qquad+\Big[\hat{E}_R(\sigma')c^\dagger_{nk'\sigma'}d_{R\sigma'},\Big[\hat{E}_{LR}(\sigma)d^\dagger_{R\sigma}d_{L\sigma},d^\dagger_{L\sigma''}c_{mk''\sigma''}\Big]\Big]\\
&\qquad-\Big[\hat{E}_R(\sigma')c^\dagger_{nk'\sigma'}d_{R\sigma'},\Big[\hat{E}_L(\sigma'')d^\dagger_{L\sigma''}c_{mk''\sigma''},d^\dagger_{R\sigma}d_{L\sigma}\Big]\Big]\Big\},\\
-&\frac{1}{3}t_{nL}t_{LR}t_{Rm}\Big\{\Big[\hat{E}_{LR}(\sigma)d^\dagger_{R\sigma}d_{L\sigma},\Big[\hat{E}_L(\sigma')d^\dagger_{L\sigma'}c_{nk'\sigma'},c^\dagger_{mk''\sigma''}d_{R\sigma''}\Big]\Big]\\
&\qquad+\Big[\hat{E}_L(\sigma')d^\dagger_{L\sigma'}c_{nk'\sigma'},\Big[\hat{E}_{LR}(\sigma)d^\dagger_{R\sigma}d_{L\sigma},c^\dagger_{mk''\sigma''}d_{R\sigma''}\Big]\Big]\\
&\qquad+\Big[\hat{E}_L(\sigma')d^\dagger_{L\sigma'}c_{nk'\sigma'},\Big[\hat{E}_R(\sigma'')c^\dagger_{mk''\sigma''}d_{R\sigma''},d^\dagger_{R\sigma}d_{L\sigma}\Big]\Big]\Big\},\\
+&\frac{1}{3}t_{nR}t_{RL}t_{Lm}\Big\{\Big[\hat{E}_{LR}(\sigma)d^\dagger_{L\sigma}d_{R\sigma},\Big[\hat{E}_R(\sigma')d^\dagger_{R\sigma'}c_{nk'\sigma'},c^\dagger_{mk''\sigma''}d_{L\sigma''}\Big]\Big]\\
&\qquad+\Big[\hat{E}_R(\sigma')d^\dagger_{R\sigma'}c_{nk'\sigma'},\Big[\hat{E}_{LR}(\sigma)d^\dagger_{L\sigma}d_{R\sigma},c^\dagger_{mk''\sigma''}d_{L\sigma''}\Big]\Big]\\
&\qquad-\Big[\hat{E}_R(\sigma')d^\dagger_{R\sigma'}c_{nk'\sigma'},\Big[\hat{E}_L(\sigma'')c^\dagger_{mk''\sigma''}d_{L\sigma''},d^\dagger_{L\sigma}d_{R\sigma}\Big]\Big]\Big\},\\
-&\frac{1}{3}t_{mR}t_{RL}t_{Ln}\Big\{\Big[\hat{E}_{LR}(\sigma)d^\dagger_{L\sigma}d_{R\sigma},\Big[\hat{E}_L(\sigma')c^\dagger_{nk'\sigma'}d_{L\sigma'},d^\dagger_{R\sigma''}c_{mk''\sigma''}\Big]\Big]\\
&\qquad+\Big[\hat{E}_L(\sigma')c^\dagger_{nk'\sigma'}d_{L\sigma'},\Big[\hat{E}_{LR}(\sigma)d^\dagger_{L\sigma}d_{R\sigma},d^\dagger_{R\sigma''}c_{mk''\sigma''}\Big]\Big]\\
&\qquad+\Big[\hat{E}_L(\sigma')c^\dagger_{nk'\sigma'}d_{L\sigma'},\Big[\hat{E}_R(\sigma'')d^\dagger_{R\sigma''}c_{mk''\sigma''},d^\dagger_{L\sigma}d_{R\sigma}\Big]\Big]\Big\}.
\end{aligned}
$$

For the moment we concentrate on the first term in the series proportional to $t_{mL}t_{LR}t_{Rn}$. First of all the conduction electron term is filtered out by repeated use of

$$
\begin{aligned}
c_{mk''\sigma''}c^\dagger_{nk'\sigma'} =&\delta_{m,n}\delta_{k',k''}\delta_{\sigma\sigma''}-c^\dagger_{nk'\sigma'}c_{mk''\sigma''}\\
\approx&-c^\dagger_{nk'\sigma'}c_{mk''\sigma''}.
\end{aligned}
$$

The $\delta_{k',k''}$ contribution is neglected since it is of the order of $1/N$ (summation over only one momentum) in comparison with all order terms. This assumption was already used in the calculation of the 2nd order contribution.

As an example the first term proportional to $t_{mL}t_{LR}t_{Rn}$ is shown,

$$
\begin{aligned}
&\frac{1}{3}t_{mL}t_{LR}t_{Rn}\Big\{\Big[\hat{E}_{LR}(\sigma)d^\dagger_{R\sigma}d_{L\sigma},\hat{E}_R(\sigma')d_{R\sigma'}d^\dagger_{L\sigma''}+d^\dagger_{L\sigma''}\hat{E}_R(\sigma')d_{R\sigma'}\Big],\\
&\qquad+\hat{E}_R(\sigma')d_{R\sigma'}\cdot\hat{\alpha}+\hat{\alpha}\cdot\hat{E}_R(\sigma')c^\dagger_{nk'\sigma'}d_{R\sigma'}\Big\}c^\dagger_{nk'\sigma'}c_{mk''\sigma''}\\
&\text{where}\qquad\hat{\alpha}=\Big[\hat{E}_{LR}(\sigma)d^\dagger_{R\sigma}d_{L\sigma},d^\dagger_{L\sigma''}\Big]-\Big[\hat{E}_L(\sigma'')d^\dagger_{L\sigma''},d^\dagger_{R\sigma}d_{L\sigma}\Big].
\end{aligned}
$$

Extracting term by term we can write down the result

$$
\begin{aligned}
&\frac{1}{3}t_{mL}t_{LR}t_{Rn}\Big\{c_1\,d^\dagger_{L\overline{\sigma}}d_{L\overline{\sigma}''}d^\dagger_{R\sigma}d_{R\sigma'}-c_2\,d^\dagger_{L\sigma''}d_{L\sigma}d^\dagger_{R\sigma}d_{R\sigma'}\\
&\qquad+c_3\,d^\dagger_{L\overline{\sigma}}d_{L\overline{\sigma}''}d^\dagger_{R\overline{\sigma}'}d_{R\overline{\sigma}}-c_4\,d^\dagger_{L\sigma''}d_{L\sigma}d^\dagger_{R\overline{\sigma}'}d_{R\overline{\sigma}}\Big\}c^\dagger_{nk'\sigma'}c_{mk''\sigma''},
\end{aligned}
$$

where

$$
\begin{aligned}
c_1 &= \frac{1}{\epsilon_L - \epsilon_R + U_L - U_{LR}} \left(\frac{1}{\epsilon_R + U_{LR} - \zeta} + \frac{1}{\epsilon_R + 2U_{LR} - \zeta} \right) \\
&\quad + \frac{1}{\epsilon_R + U_{LR} - \zeta} \left(\frac{1}{\epsilon_L - \epsilon_R + U_L - U_{LR}} + \frac{1}{\epsilon_L + U_L - \zeta} \right), \\
c_2 &= \frac{1}{\epsilon_R + U_{LR} - \zeta} \left(\frac{1}{\epsilon_L - \epsilon_R} + \frac{1}{\epsilon_L + U_{LR} - \zeta} \right), \\
c_3 &= \frac{1}{\epsilon_R + U_R + U_{LR} - \zeta} \left(\frac{1}{\epsilon_L - \epsilon_R + U_L - U_R} + \frac{1}{\epsilon_L + U_L + U_{LR} - \zeta} \right), \\
c_4 &= \frac{1}{\epsilon_L - \epsilon_R + U_{LR} - U_R} \left(\frac{1}{\epsilon_R + U_R - \zeta} + \frac{1}{\epsilon_R + U_R + U_{LR} - \zeta} \right) \\
&\quad + \frac{1}{\epsilon_R + U_R + U_{LR} - \zeta} \left(\frac{1}{\epsilon_L - \epsilon_R + U_{LR} - U_R} + \frac{1}{\epsilon_L + 2U_{LR} - \zeta} \right).
\end{aligned}
$$

Please note that the expressions are simplified by assuming $J_H = 0$ and that the bare energy levels are not spin-dependent $\epsilon_{\alpha\sigma} = \epsilon_\alpha$.

The couplings c_1 and c_4 start or result in the state $|\sigma\rangle_L|\overline{\sigma}\rangle_R$ allowing only antiparallel spin pairs on the double quantum dot. By contrast the couplings c_2 and c_3 do not depend on the spin. These two different kinds of leakage were already illustrated in Fig. 2.4.

To compare this result to the 2nd order contributions we concentrate on one special spin interaction $\vec{s}^{+}_{nm}$ and find for $\sigma' = \uparrow$ and $\sigma'' = \downarrow$ a contribution to the effective Hamiltonian $\tilde{H}$ of

$$
\frac{1}{3} t_{mL} t_{LR} t_{Rn} \frac{1}{2} \left(c_1 - c_2 + c_3 - c_4 \right) \left(\vec{S}^{-}_L + \vec{S}^{-}_R \right).
$$

There is a bunch of other couplings which are created to third order like $\left(\vec{S}_L \times \vec{S}_R \right) \vec{s}_{nm}$ and also potential scattering terms. Nevertheless here we do not discuss the general case, but find out to which magnitude the leakage contributes to the coupling part of the effective Hamiltonian. Therefore we focus on the indirect Kondo coupling of the left leads to the right leads via the double quantum dot $\vec{S}_\alpha \vec{s}_{nm}$ where $m \in \{1, 2\}$ and $n \in \{3, 4\}$.

Since the summation is over all possible lead indices m and n the term proportional to $t_{nL} t_{LR} t_{Rm}$ contributes to the same amount as the one discussed before. The general minus sign cancels out by the different order of the lead electron creation and annihilation operator. Leaving out details of the calculation we find

$$
\begin{aligned}
&\frac{1}{3} t_{mL} t_{LR} t_{Rn} \Big\{ k_1 d^\dagger_{L\overline{\sigma}} d_{L\overline{\sigma}''} d^\dagger_{R\sigma} d_{R\sigma'} + k_2 d^\dagger_{L\sigma''} d_{L\sigma} d^\dagger_{R\sigma} d_{R\sigma'} \\
&\qquad + k_3 d^\dagger_{L\overline{\sigma}} d_{L\overline{\sigma}''} d^\dagger_{R\overline{\sigma}'} d_{R\overline{\sigma}} + k_4 d^\dagger_{L\sigma''} d_{L\sigma} d^\dagger_{R\overline{\sigma}'} d_{R\overline{\sigma}} \Big\} c^\dagger_{nk'\sigma'} c_{mk''\sigma''},
\end{aligned}
$$

where

$$
\begin{aligned}
k_1 &= \frac{1}{\epsilon_L - \epsilon_R + U_L - U_{LR}} \left(\frac{1}{\epsilon_L + U_L - \zeta} + \frac{1}{\epsilon_L + U_L + U_{LR} - \zeta} \right) \\
&\quad + \frac{1}{\epsilon_L + U_L + U_{LR} - \zeta} \left(\frac{1}{\epsilon_L - \epsilon_R + U_L - U_{LR}} - \frac{1}{\epsilon_R + 2U_{LR} - \zeta} \right), \\
k_2 &= \frac{1}{\epsilon_L + U_{LR} - \zeta} \left(\frac{1}{\epsilon_L - \epsilon_R} - \frac{1}{\epsilon_R + U_{LR} - \zeta} \right), \\
k_3 &= \frac{1}{\epsilon_L + U_L + U_{LR} - \zeta} \left(\frac{1}{\epsilon_R + U_R + U_{LR} - \zeta} - \frac{1}{\epsilon_L - \epsilon_R + U_L - U_R} \right), \\
k_4 &= -\frac{1}{\epsilon_L - \epsilon_R + U_{LR} - U_R} \left(\frac{1}{\epsilon_L + U_{LR} - \zeta} + \frac{1}{\epsilon_L + 2U_{LR} - \zeta} \right) \\
&\quad + \frac{1}{\epsilon_L + U_{LR} - \zeta} \left(\frac{1}{\epsilon_R + U_R - \zeta} - \frac{1}{\epsilon_L - \epsilon_R + U_{LR} - U_R} \right).
\end{aligned}
$$

In this example of a spin flip we find that a hopping from the left leads to the right leads is of the order

$$
\frac{1}{3} t_{mL} t_{LR} t_{Rn} \frac{1}{2} \left(c_1 + k_1 - c_2 + k_2 + c_3 + k_3 - c_4 + k_4 \right) \left(\vec{S}_L^- + \vec{S}_R^- \right) \vec{s}_{nm}^+.
$$

The other two terms contributing with $t_{nR} t_{RL} t_{Lm}$ and $t_{mR} t_{RL} t_{Ln}$ can be calculated as well and give an analogous result to the two mentioned terms with the replacement $L \leftrightarrow R$ and $(\epsilon_L - \epsilon_R + U_{LR} - U_R) \leftrightarrow (\epsilon_L - \epsilon_R + U_L - U_{LR})$.

In order to compare this term with the 2nd order contributions we concentrate on the special case of two identical quantum dots. With $\epsilon_L = \epsilon_R = \epsilon$ and $U_L = U_R = U$ we find first of all that the two divergent terms $1/(\epsilon_L - \epsilon_R)$ and $1/(\epsilon_L - \epsilon_R + U_L - U_R)$ cancel each other and finally

$$
\begin{aligned}
&\frac{1}{2} \left(c_1 + k_1 - c_2 + k_2 + c_3 + k_3 - c_4 + k_4 \right) \\
=&\frac{1}{U - U_{LR}} \left(\frac{1}{\epsilon + U_{LR} - \zeta} + \frac{1}{\epsilon + 2U_{LR} - \zeta} + \frac{1}{\epsilon + U - \zeta} + \frac{1}{\epsilon + U + U_{LR} - \zeta} \right) \\
&+ \frac{1}{\epsilon + U_{LR} - \zeta} \left(\frac{1}{U - U_{LR}} + \frac{1}{\epsilon + U - \zeta} \right) \\
&+ \frac{1}{\epsilon + U + U_{LR} - \zeta} \left(\frac{1}{U - U_{LR}} - \frac{1}{\epsilon + 2U_{LR} - \zeta} \right) \\
&+ \left(\frac{1}{\epsilon + U + U_{LR} - \zeta} \right)^2 - \left(\frac{1}{\epsilon + U_{LR} - \zeta} \right)^2.
\end{aligned}
$$

Additionally to the left-right symmetry it is assumed that the couplings $t_{LR} = t_{RL}$ are identical without a phase. Consequently the other two terms contributing with $t_{nR} t_{RL} t_{Lm}$ and $t_{mR} t_{RL} t_{Ln}$ can be taken into account by multiplying the upper result with a factor 2. The leakage coupling $J_{nm}^{\text{leakage}} = c_1 + k_1 - c_2 + k_2 + c_3 + k_3 - c_4 + k_4$ is discussed in detail in the section 2.2.5.

B Explicit Calculations Referring to Chapters 3 and 4

B.1 Relations for the Matrix Green's Function from Sum Rule Considerations

We find the following sum rules for a general Green's function $G_{\gamma\gamma'}$,

$$\delta_{\gamma\gamma'} = \left\langle [t_\gamma, t^\dagger_{\gamma'}] \right\rangle = i \int \frac{d\omega}{2\pi} \left(G^>_{\gamma\gamma'}(\omega) - G^<_{\gamma\gamma'}(\omega) \right) = \int \frac{d\omega}{2\pi} A_{\gamma\gamma'}(\omega). \tag{B.1}$$

Thus a diagonal spectral function $A_{\gamma\gamma}(\omega)$ has a total weight of 1 whereas an off-diagonal spectral function $A_{\gamma\gamma'}(\omega)$ has a total weight of 0. As shown later on the off-diagonal spectral function is non-zero, but contains some negative contributions which make the total weight vanish.

Furthermore we find

$$\begin{aligned}
\left[G^r_{\gamma\gamma'}(t)\right]^\dagger &= \left[-i\Theta(t) \left\langle \left[t_\gamma(t), t^\dagger_{\gamma'}(0) \right] \right\rangle \right]^\dagger \\
&= i\Theta(t) \left\langle \left[t_{\gamma'}(-t), t^\dagger_\gamma(0) \right] \right\rangle = G^a_{\gamma'\gamma}(-t) \\
\Rightarrow \qquad \left[G^r_{\gamma\gamma'}(\omega)\right]^\dagger &= G^a_{\gamma'\gamma}(\omega) \\
\Rightarrow \qquad \mathrm{Re}\left\{G^r_{\gamma\gamma'}(\omega)\right\} &= \mathrm{Re}\left\{G^a_{\gamma'\gamma}(\omega)\right\}, \\
\mathrm{Im}\left\{G^r_{\gamma\gamma'}(\omega)\right\} &= -\mathrm{Im}\left\{G^a_{\gamma'\gamma}(\omega)\right\}.
\end{aligned} \tag{B.2}$$

For the diagonal part this reveals no new information, but for the off-diagonal we find

$$A_{st_0}(\omega) = A_{t_0 s}(\omega), \tag{B.3}$$

i.e. the spectral functions for st_0 and $t_0 s$ are identical. The spectral function matrix obeys $A^T = A$ such that A is symmetric. Please note that this is a general statement from a conservation rule. This statement still holds if we perform a perturbation theory and thus it is used frequently in the course of the calculation.

In non-equilibrium the lesser Green's function contains different information than the retarded Green's function and thus we also consider

$$\begin{aligned}
\left[G^<_{\gamma\gamma'}(t)\right]^\dagger &= \left[-i \left\langle t^\dagger_{\gamma'}(0) t_\gamma(t) \right\rangle \right]^\dagger = i \left\langle t^\dagger_\gamma(0) t_{\gamma'}(-t) \right\rangle = -G^<_{\gamma'\gamma}(-t) \\
\Rightarrow \qquad \left[G^<_{\gamma\gamma'}(\omega)\right]^\dagger &= -G^<_{\gamma'\gamma}(\omega) \\
\Rightarrow \qquad \mathrm{Re}\left\{G^<_{\gamma\gamma'}(\omega)\right\} &= -\mathrm{Re}\left\{G^<_{\gamma'\gamma}(\omega)\right\}, \\
\mathrm{Im}\left\{G^<_{\gamma\gamma'}(\omega)\right\} &= \mathrm{Im}\left\{G^<_{\gamma'\gamma}(\omega)\right\}.
\end{aligned} \tag{B.4}$$

The real part of a diagonal lesser Green's function is exactly zero and the imaginary part contains the physical information. For the off-diagonal lesser Green's function we can not make such a statement. Whereas these relations can be used to make an ansatz for the lesser off-diagonal Green's function, see appendix C.

B.2 Conduction Electron Spin Susceptibility

The conduction electron spin susceptibility is defined by Eq. (3.9),

$$X_n^m(\tau_1,\tau_2) = \frac{1}{(-i)^2}\sum_{k,k'} G_{mk'}(\tau_1,\tau_2)G_{nk}(\tau_2,\tau_1).$$

It corresponds to an electron-hole pair which is created in the leads m and n. Therefore it contributes to the self energy in second order. Due to a finite self energy the double quantum dot states gain a finite life time. The broadening originates in a hybridization of the system with the leads.

The conduction electron spin susceptibility enters the current through the combination $X_2^1 - X_1^2$ and thus also the current cross-correlation. The noise is proportional to current fluctuations which are proportional to $f(1-f)$, i.e. $X_1^2 + X_2^1$. Therefore it is often claimed that the decoherence in non-equilibrium is due to current-noise.

Useful for the calculation are the relations

$$f(x)\left(1-f(y)\right) = n_B(x-y)\left(f(y)-f(x)\right),$$
$$\int_{-\infty}^{\infty} dx\left(f(x+a)-f(x)\right) = -a,$$

where $f(x)$ is the Fermi function and $n_B(x)$ is the Bose function in equilibrium. Furthermore we find

$$n_B(x) = \frac{1}{2}\left(\coth\left(\frac{1}{2}\beta x\right) - 1\right),$$
$$f(x) = \frac{1}{2}\left(1 - \tanh\left(\frac{1}{2}\beta x\right)\right).$$

The different contributions from X_n^m on the contour are given by the Langreth rules in section 3.1,

$$\left(X_n^m\right)^{<}(t,t') = -\sum_{k,k'} G^{<}_{mk'\sigma'}(t,t')G^{>}_{nk\sigma}(t',t),$$
$$\left(X_n^m\right)^{>}(t,t') = -\sum_{k,k'} G^{>}_{mk'\sigma'}(t,t')G^{<}_{nk\sigma}(t',t),$$
$$\left(X_n^m\right)^{r}(t,t') = -\sum_{k,k'} \left(G^{<}_{mk'\sigma'}(t,t')G^{a}_{nk\sigma}(t',t) + G^{r}_{mk'\sigma'}(t,t')G^{<}_{nk\sigma}(t',t)\right),$$
$$\left(X_n^m\right)^{a}(t,t') = -\sum_{k,k'} \left(G^{<}_{mk'\sigma'}(t,t')G^{r}_{nk\sigma}(t',t) + G^{a}_{mk'\sigma'}(t,t')G^{<}_{nk\sigma}(t',t)\right).$$

We use the ansatz for the momentum integrated conduction electron Green's function as given in Eq. 3.5 in section 3.2.2.

We calculate X_n^m in Fourier space. For example $(X_n^m)^> (\omega)$ is given by

$$\begin{aligned}(X_n^m)^> (\omega) &= -2\pi N(0)^2 \int_{-D}^{D} d\epsilon f(\epsilon - \mu_n)\,(1 - f(\epsilon + \omega - \mu_m)) \\ &= -2\pi N(0)^2 n_B(-\omega + \mu_m - \mu_n) \int_{-D}^{D} d\epsilon\,(f(\epsilon + \omega - \mu_m) - f(\epsilon - \mu_n)) \\ &\approx -2\pi N(0)^2 n_B(-\omega + \mu_m - \mu_n) \int_{-\infty}^{\infty} d\epsilon'\,(f(\epsilon' + \omega - \mu_m + \mu_n) - f(\epsilon')) \\ &= -2\pi N(0)^2 n_B(-\omega + \mu_m - \mu_n)\,[-\omega + \mu_m - \mu_n]\,.\end{aligned}$$

Therefore it is assumed that the band cutoff D is the largest energy scale in the system such that the integration limits can be sent to infinity and a frequency in those limits can be neglected.

For $(X_m^n)^< (\omega)$ we find

$$\begin{aligned}(X_n^m)^< (\omega) &= -2\pi N(0)^2 \int_{-D}^{D} d\epsilon f(\epsilon + \omega - \mu_m)\,(1 - f(\epsilon - \mu_n)) \\ &= -2\pi N(0)^2 n_B(\omega - \mu_m + \mu_n) \int_{-D}^{D} d\epsilon\,(f(\epsilon - \mu_n) - f(\epsilon + \omega - \mu_m)) \\ &\approx -2\pi N(0)^2 n_B(\omega - \mu_m + \mu_n) \int_{-\infty}^{\infty} d\epsilon'\,(f(\epsilon' - \omega + \mu_m - \mu_n) - f(\epsilon')) \\ &= -2\pi N(0)^2 n_B(\omega - \mu_m + \mu_n)\,[\omega - \mu_m + \mu_n]\,.\end{aligned}$$

Note that the symmetry is fulfilled,

$$(X_m^n)^< (\omega) = (X_n^m)^> (-\omega). \tag{B.5}$$

The result for $(X_n^m)^r (\omega)$ is also shown here,

$$\begin{aligned}(X_n^m)^r (\omega) &= -\pi N(0)^2 \int_{-D}^{D} d\epsilon\,(f(\epsilon - \mu_n) - f(\epsilon + \omega - \mu_n)) \\ &\approx -\pi N(0)^2 \int_{-\infty}^{\infty} d\epsilon'\,(f(\epsilon' - \omega + \mu_m - \mu_n) - f(\epsilon')) \\ &= -\pi N(0)^2\,[\omega - \mu_m + \mu_n]\,.\end{aligned}$$

Analogous we find

$$(X_n^m)^a (\omega) = \pi N(0)^2\,[\omega - \mu_m + \mu_n]\,.$$

The contributions of the leads to the self energy are given by Eqs. (3.11) and (3.12)

$$\begin{aligned}Y_L(\tau_1, \tau_2) &= \sum_{m,n=1,2} 2J_{mn}J_{nm}\; X_n^m(\tau_1, \tau_2), \\ Y_R(\tau_1, \tau_2) &= \sum_{m,n=3,4} 2J_{mn}J_{nm}\; X_n^m(\tau_1, \tau_2).\end{aligned}$$

After Fourier transformation we find

$$\begin{aligned} Y_L^<(\omega) =&(-2\pi)\left[\left(g_{11}^2+g_{22}^2\right)2\omega n_B(\omega)\right. \\ &\left.+2g_{12}g_{21}\left((\omega+eV_L)n_B(\omega+eV_L)+(\omega-eV_L)n_B(\omega-eV_L)\right)\right], \qquad \text{(B.6)} \\ Y_R^<(\omega) =&(-2\pi)\left[\left(g_{33}^2+g_{44}^2\right)2\omega n_B(\omega)\right. \\ &\left.+2g_{34}g_{43}\left((\omega+eV_R)n_B(\omega+eV_R)+(\omega-eV_R)n_B(\omega-eV_R)\right)\right]. \qquad \text{(B.7)} \end{aligned}$$

Due to $(X_m^n)^<(\omega) = (X_n^m)^>(-\omega)$ the following relation holds,

$$Y_\alpha^>(\omega) = Y_\alpha^<(-\omega).$$

Since $1+n_B(x) = -n_B(-x)$ the function $Y^<(\omega)$ is related to $Y^<(-\omega)$ by

$$Y_\alpha^<(-\omega) = Y_\alpha^<(\omega) + (-2\pi)2g_\alpha^2 w.$$

B.2.1 Relation between $\left(X_2^1\right)^a$ and $-\frac{1}{2}\left(X_2^1\right)^>(\omega)+\frac{1}{2}\left(X_2^1\right)^<(\omega)$

For the conduction electron spin susceptibility we find the relation

$$\left(X_2^1\right)^a(\omega) \approx -\frac{1}{2}\left(X_2^1\right)^>(\omega)+\frac{1}{2}\left(X_2^1\right)^<(\omega). \qquad \text{(B.8)}$$

This is closely related to $G^a \approx \frac{1}{2}iA = -\frac{1}{2}(G^>-G^<)$, since $A = i(G^r-G^a) = i(G^>-G^<)$ and consequently $-iA = G^>-G^<$. We will now prove this correlation. From the Langreth rules we find

$$\begin{aligned} \left(X_2^1\right)^>(\omega) &= \frac{1}{(-i)^2}\int\frac{d\epsilon}{2\pi}G_{1k'}^>(\epsilon+\omega)G_{2k}^<(\epsilon), \\ \left(X_2^1\right)^<(\omega) &= \frac{1}{(-i)^2}\int\frac{d\epsilon}{2\pi}G_{1k'}^<(\epsilon+\omega)G_{2k}^>(\epsilon), \\ \left(X_2^1\right)^a(\omega) &= \frac{1}{(-i)^2}\int\frac{d\epsilon}{2\pi}\left(G_{1k'}^<(\epsilon+\omega)G_{2k}^r(\epsilon)+G_{1k'}^a(\epsilon+\omega)G_{2k}^<(\epsilon)\right). \end{aligned}$$

To prove Eq. (B.8) we calculate

$$\begin{aligned} \left(X_2^1\right)^>(\omega) &= -\int d\epsilon 2\pi N(0)^2\left(1-f(\epsilon+\omega-\mu_1)\right)f(\epsilon-\mu_2)\Theta(D-|\epsilon|)\Theta(D-|\epsilon+\omega|) \\ &= -2\pi N(0)^2\int_{-D}^{D}d\epsilon f(\epsilon-\mu_2)\left(1-f(\epsilon+\omega-\mu_1)\right), \qquad \text{(B.9)} \end{aligned}$$

and analogous

$$\begin{aligned} \left(X_2^1\right)^<(\omega) &= -\int d\epsilon 2\pi N(0)^2 f(\epsilon+\omega-\mu_1)\left(1-f(\epsilon-\mu_2)\right)\Theta(D-|\epsilon|)\Theta(D-|\epsilon+\omega|) \\ &= -2\pi N(0)^2\int_{-D}^{D}d\epsilon f(\epsilon+\omega-\mu_1)\left(1-f(\epsilon+\mu_2)\right). \qquad \text{(B.10)} \end{aligned}$$

Here we already made the first assumption that ω is always much smaller than the band cutoff D, $\omega \ll D$, and therefore ω can be neglected in the limits of the integral. Furthermore we have

$$\begin{aligned}\mathrm{Re}\left(X_2^1\right)^a(\omega) = -\int \frac{d\epsilon}{2\pi}\,&[2\pi i N(0) f(\epsilon+\omega-\mu_1)\Theta(D-|\epsilon+\omega|)(-i\pi)N(0)\Theta(D-|\epsilon|)\\ &+i\pi N(0)\Theta(D-|\epsilon+\omega|)2\pi i N(0) f(\epsilon-\mu_2)\Theta(D-|\epsilon|)]\\ &= -\pi N(0)^2 \int d\epsilon\,[f(\epsilon+\omega-\mu_1)-f(\omega-\mu_2)]\,.\end{aligned}$$

And finally,

$$\begin{aligned}&\mathrm{Re}\left(X_2^1\right)^a(\omega) = -\pi N(0)^2 \int d\epsilon\,[f(\epsilon+\omega-\mu_1)-f(\omega-\mu_2)]\\ &= -\pi N(0)^2 \int d\epsilon\,[f(\epsilon+\omega-\mu_1)\,(1-f(\omega-\mu_2)) - f(\omega-\mu_2)\,(1-f(\omega+\epsilon-\mu_1))]\\ &= \frac{1}{2}\left(X_2^1\right)^<(\omega) - \frac{1}{2}\left(X_2^1\right)^>(\omega),\end{aligned}$$

the relation Eq. (B.8) is proved. Since we only include Re[X] this expression is exact. Actually we would not have needed any assumption for this prove, but now we already have the required equations for later use.

B.2.2 Broadening of the Spin Susceptibility

The Bose function $n_B(x) = 1/(\mathrm{e}^{\beta x}-1)$ is singular at $x=0$, but the product $x n_B(x)$ is finite and in the limit of $x/T \ll 1$ it can be approximated by

$$x n_B(x) = \begin{cases} 0 & \text{if } x > 2T \\ T - \frac{1}{2}x & \text{if } |x| < 2T \\ |x| & \text{if } x < -2T \end{cases}.$$

Using this expression for $x n_B(x)$ we find for small temperatures

$$\begin{aligned}\int_{-\Lambda}^{\Lambda} dx \frac{1}{\pi}\frac{\Gamma}{x^2+\Gamma^2}(a-x)n_B(a-x) = &\int_{a-2T}^{a+2T} dx \frac{1}{\pi}\frac{\Gamma}{x^2+\Gamma^2}\frac{1}{2}\,(x-a+2T)\\ &+\int_{a+2T}^{\Lambda} dx \frac{1}{\pi}\frac{\Gamma}{x^2+\Gamma^2}(x-a).\end{aligned}$$

This can be integrated and provides

$$\begin{aligned}= \frac{1}{2}a\Bigg\{&\left(1-\frac{2T}{a}\right)\frac{1}{\pi}\arctan\left(\frac{a-2T}{\Gamma}\right) + \left(1+\frac{2T}{a}\right)\frac{1}{\pi}\arctan\left(\frac{a+2T}{\Gamma}\right)\\ &-\frac{\Gamma}{a}\frac{1}{2\pi}\ln\left((a-2T)^2+\Gamma^2\right) - \frac{\Gamma}{a}\frac{1}{2\pi}\ln\left((a+2T)^2+\Gamma^2\right)\\ &-\frac{2}{\pi}\arctan\left(\frac{\Lambda}{\Gamma}\right) + \frac{2\Gamma}{a}\frac{1}{2\pi}\ln\left(\Lambda^2+\Gamma^2\right)\Bigg\}.\end{aligned}$$

For a finite Γ this result diverges for $\Lambda \to \infty$. The spectral function falls off too slowly such that the linear part of $xn_B(x)$ gives an increasingly important contribution at $x \to \infty$.

In all physical quantities like in the current in Eq. (4.9), a difference of two contributions enters, e.g. $(X_2^1)^>(\omega) - (X_2^1)^<(\omega)$. Thus the divergent part of the integral cancels out and the problem of the divergence is solved.

Finally we can write in short notation

$$\int_{-\Lambda}^{\Lambda} dx \frac{1}{\pi} \frac{\Gamma}{x^2+\Gamma^2}(a-x)n_B(a-x) = an_B^\Gamma(a)$$

which is of course only valid if there is a difference of two of those terms. The broadened Bose distribution $n_B^\Gamma(a)$ is defined analogous to $n_B(x) = \frac{1}{2}(\coth(\beta x/2) - 1)$,

$$\begin{aligned} n_B^\Gamma(a) &= \frac{1}{2}\left(\tilde{c}(a) - 1\right), \\ \tilde{c}(a) &= \frac{1}{\pi}\left(\arctan\left(\frac{a+2T}{\Gamma}\right) + \arctan\left(\frac{a-2T}{\Gamma}\right)\right) \\ &\quad + \frac{2T}{a}\frac{1}{\pi}\left(\arctan\left(\frac{a+2T}{\Gamma}\right) - \arctan\left(\frac{a-2T}{\Gamma}\right)\right) \\ &\quad - \frac{\Gamma}{2a}\frac{1}{\pi}\left(\ln\left[(a+2T)^2+\Gamma^2\right] + \ln\left[(a-2T)^2+\Gamma^2\right]\right), \end{aligned}$$

which corresponds to the expansion of $\coth(a/2T)$ for $\Gamma \to 0$ and simplifies to

$$\tilde{c}(a) = \frac{2}{\pi}\arctan\left(\frac{a}{\Gamma}\right) - \frac{2}{\pi}\frac{\Gamma}{a}\ln\left[\sqrt{a^2+\Gamma^2}\right]$$

in the case of zero temperature $T = 0$.

B.2.3 Broadening of the Fermi Function

Now we study how the Fermi function changes if it is convoluted with a spectral function including a finite broadening, e.g. in the calculation of the T-matrix. Using $2f(\omega) - 1 = -\tanh(\omega/2T)$ at low temperatures

$$\begin{aligned} &-\int d\epsilon \frac{1}{\pi}\frac{\Gamma}{\epsilon^2+\Gamma^2}\tanh[(\omega+\epsilon-\mu_m)/2T] \\ &= \int_{-D}^{-2T-\omega+\mu_m} d\epsilon \frac{1}{\pi}\frac{\Gamma}{\epsilon^2+\Gamma^2} - \int_{-2T-\omega+\mu_m}^{2T-\omega+\mu_m} d\epsilon \frac{1}{\pi}\frac{\Gamma}{\epsilon^2+\Gamma^2}\frac{\omega+\epsilon-\mu_m}{2T} - \int_{2T-\omega+\mu_m}^{D} d\epsilon \frac{1}{\pi}\frac{\Gamma}{\epsilon^2+\Gamma^2}. \end{aligned}$$

We assume that the temperature is negligible small and therefore the central integration vanishes. Thus we find

$$\approx \frac{1}{\pi}\arctan\left(\frac{-2T-\omega+\mu_m}{\Gamma}\right) + \frac{1}{\pi}\arctan\left(\frac{2T-\omega+\mu_m}{\Gamma}\right) \approx -\frac{2}{\pi}\arctan\left(\frac{\omega-\mu_m}{\Gamma}\right).$$

Thus instead of a $(-\tanh)$ with the width of the temperature T we have a broader function of $(-\arctan)$ and we define a broadened Fermi-function with the broadening Γ

$$f_\Gamma(\omega) = \frac{1}{2}\left(1 - \frac{2}{\pi}\arctan\left(\frac{\omega}{\Gamma}\right)\right)$$
$$\Rightarrow -\frac{2}{\pi}\arctan\left(\frac{\omega}{\Gamma}\right) = 2f_\Gamma(\omega) - 1$$

B.3 Occupation Numbers without Off-Diagonal Contributions

Assuming that the spectral function can be approximated as a δ-function the calculation of the self energy from Eq. (3.29) is simple and we find

$$\begin{aligned}
\Sigma^<_{ss}(\omega_s) =& \frac{i}{16}\left(n_{t_0}Y^<_{L+R}(\omega_s-\omega_{t_0}) + n_{t_+}Y^<_{L+R}(\omega_s-\omega_{t_+}) + n_{t_-}Y^<_{L+R}(\omega_s-\omega_{t_-})\right),\\
\Sigma^<_{t_0t_0}(\omega_{t_0}) =& \frac{i}{16}\left(n_{s}Y^<_{L+R}(\omega_{t_0}-\omega_s) + n_{t_+}Y^<_{L+R}(\omega_{t_0}-\omega_{t_+}) + n_{t_-}Y^<_{L+R}(\omega_{t_0}-\omega_{t_-})\right),\\
\Sigma^<_{t_\pm t_\pm}(\omega_{t_\pm}) =& \frac{i}{16}\left(n_{s}Y^<_{L+R}(\omega_{t_\pm}-\omega_s) + n_{t_0}Y^<_{L+R}(\omega_{t_\pm}-\omega_{t_0}) + n_{t_\pm}Y^<_{L+R}(\omega_{t_\pm}-\omega_{t_\pm})\right),
\end{aligned}$$

where $Y^<_{L+R}(\omega) = Y^<_L(\omega) + Y^<_R(\omega)$.

In the quantum Boltzmann equation we also need Γ, which we calculate like explained in Eq. (3.30).

$$\begin{aligned}
-i\Gamma_{ss}(\omega_s) =& -\frac{1}{16}\left(Y^<_{L+R}(\omega_{t_0}-\omega_s) + Y^<_{L+R}(\omega_{t_+}-\omega_s) + Y^<_{L+R}(\omega_{t_-}-\omega_s)\right),\\
-i\Gamma_{t_0t_0}(\omega_{t_0}) =& -\frac{1}{16}\left(Y^<_{L+R}(\omega_{s}-\omega_{t_0}) + Y^<_{L+R}(\omega_{t_+}-\omega_{t_0}) + Y^<_{L+R}(\omega_{t_-}-\omega_{t_0})\right),\\
-i\Gamma_{t_\pm t_\pm}(\omega_{t_\pm}) =& -\frac{1}{16}\left(Y^<_{L+R}(\omega_{s}-\omega_{t_\pm}) + Y^<_{L+R}(\omega_{t_0}-\omega_{t_\pm}) + Y^<_{L+R}(\omega_{t_\pm}-\omega_{t_\pm})\right).
\end{aligned}$$

The prefactor is the same for $\Sigma^<$ and Γ so we will neglect it in the further calculation since it cancels out in the quantum Boltzmann equation.

Using $\omega_s = -\frac{3}{4}K$, $\omega_{t_0} = \frac{1}{4}K$, $\omega_{t_+} = \frac{1}{4}K - B$ and $\omega_{t_-} = \frac{1}{4}K + B$ we have to solve the following equations

$$\begin{aligned}
&\left(Y^<_{L+R}(K) + Y^<_{L+R}(K-B) + Y^<_{L+R}(K+B)\right)n_s\\
&\quad = n_{t_0}Y^<_{L+R}(-K) + n_{t_+}Y^<_{L+R}(-K+B) + n_{t_-}Y^<_{L+R}(-K-B),\\
&\left(Y^<_{L+R}(-K) + Y^<_{L+R}(-B) + Y^<_{L+R}(B)\right)n_{t_0}\\
&\quad = n_{s}Y^<_{L+R}(K) + n_{t_+}Y^<_{L+R}(B) + n_{t_-}Y^<_{L+R}(-B),\\
&\left(Y^<_{L+R}(-K\pm B) + Y^<_{L+R}(\pm B)\right)n_{t_\pm}\\
&\quad = n_{s}Y^<_{L+R}(K\mp B) + n_{t_0}Y^<_{L+R}(\mp B).
\end{aligned}$$

The set of equations is underdetermined. To find a non-zero solution the information of the pseudo particle constraint,

$$n_s + n_{t_0} + n_{t_+} + n_{t_-} = 1,$$

is important.

The solution is of the following structure

$$n_\gamma = \frac{N_\gamma}{N_s + N_{t_0} + N_{t_+} + N_{t_-}},$$

where

$$\begin{aligned}\Gamma_{t_0} &= Y^<_{L+R}(-K) + Y^<_{L+R}(B) + Y^<_{L+R}(-B),\\ \Gamma_{t_\pm} &= Y^<_{L+R}(-K \pm B) + Y^<_{L+R}(\pm B),\end{aligned}$$

and

$$\begin{aligned}N_s =&\Gamma_{t_0}\Gamma_{t_+}\Gamma_{t_-} - \Gamma_{t_-}Y^<_{L+R}(B)Y^<_{L+R}(-B) - \Gamma_{t_+}Y^<_{L+R}(B)Y^<_{L+R}(-B),\\ N_{t_0} =&\Gamma_{t_-}\Gamma_{t_+}Y^<_{L+R}(K) + \Gamma_{t_+}Y^<_{L+R}(-B)Y^<_{L+R}(B+K) + \Gamma_{t_-}Y^<_{L+R}(B)Y^<_{L+R}(-B+K),\\ N_{t_\pm} =&\Gamma_{t_\mp}\Gamma_{t_0}Y^<_{L+R}(\mp B+K) + \Gamma_{t_\mp}Y^<_{L+R}(\mp B)Y^<_{L+R}(K)\\ &+ Y^<_{L+R}(\mp B)Y^<_{L+R}(\mp B)Y^<_{L+R}(B+K) - Y_{L+R}(\mp B)Y_{L+R}(\pm B)Y^<_{L+R}(\mp B+K).\end{aligned}$$

Please note that N_{t_+} is the same as N_{t_-} just with the sign of B exchanged.

The solution of these equations is discussed in section 4.1.

B.4 Add-Ons to the Calculation of the Current

In this section we prove the relation in Eq. (4.5), $X^r_{\mathrm{DQD}}(\omega) = -\frac{1}{2}X^<_{\mathrm{DQD}}(\omega) + \frac{1}{2}X^>_{\mathrm{DQD}}(\omega)$. From Langreth rules we can show, neglecting all prefactors,

$$\begin{aligned}X^>_{\mathrm{DQD}}(\omega) &\propto \int \frac{d\epsilon}{2\pi}\mathrm{Tr}\left[G^<(\epsilon)T^iG^>(\epsilon+\omega)T^j\right]\\ X^<_{\mathrm{DQD}}(\omega) &\propto \int \frac{d\epsilon}{2\pi}\mathrm{Tr}\left[G^>(\epsilon)T^iG^<(\epsilon+\omega)T^j\right]\\ X^r_{\mathrm{DQD}}(\omega) &\propto \int \frac{d\epsilon}{2\pi}\mathrm{Tr}\left[G^a(\epsilon)T^iG^<(\epsilon+\omega)T^j\right] + \mathrm{Tr}\left[G^<(\epsilon)T^iG^r(\epsilon+\omega)T^j\right]\end{aligned}$$

Always fulfilled is the relation $G^> - G^< = G^r - G^a$. The unknown greater Green's function can consequently be written by $G^> = G^< + G^r - G^a$. The lesser Green's function is proportional to the occupation number and scales with $e^{-\beta\lambda}$ from the constraint on the quasi-particles. A term like $G^<T^iG^<T^j$ is consequently of the order of $e^{-2\beta\lambda}$ and will be projected out by the Abrikosov pseudo particle projection. We already neglect this term now and use in this context $G^> \approx G^r - G^a$.

From the upper expression one can also immediately see the relation

$$X^<_{\mathrm{DQD}}(\omega) = X^>_{\mathrm{DQD}}(-\omega).$$

Next we neglect the real part of the retarded and advanced Green's function. To calculate the current in Eq. (4.4) we need the real part of the correlation function $D^>_{12}$. Thus we also only need the real part of X^r_{DQD}. Now we assume, that the lesser Green's function for the quantum dot system is only imaginary. This is an approximation since we have realized before, that the off-diagonal parts can have real parts as well. Diagonal

parts are purely imaginary and to study the influence of off-diagonal terms on those we use throughout the whole thesis the approximation that all lesser Green's functions are imaginary. With this assumption we only need to take the imaginary part of the retarded $G^r \approx \frac{1}{2}(G^r - G^a)$ and advanced Green's function $G^a \approx -\frac{1}{2}(G^r - G^a)$ to take into account in the calculation of X^r_{DQD}.

$$\begin{aligned} X^r_{\mathrm{DQD}}(\omega) \approx \int \frac{d\epsilon}{2\pi} \Bigg(& -\frac{1}{2}\mathrm{Tr}\left[\left(G^r(\epsilon) - G^a(\epsilon)\right) T^i G^<(\epsilon+\omega) T^j\right] \\ & + \frac{1}{2}\mathrm{Tr}\left[G^<(\epsilon) T^i \left(G^r(\epsilon+\omega) - G^a(\epsilon+\omega)\right) T^j\right] \Bigg) \\ = & -\frac{1}{2} X^<_{\mathrm{DQD}}(\omega) + \frac{1}{2} X^>_{\mathrm{DQD}}(\omega) \end{aligned}$$

Therefore the relation (4.5) holds within the usual assumptions.

B.4.1 Can the Double Quantum Dot System Act as a Switch?

In order to check if the system can work as a switch we have to find a parameter regime where

$$I_L = I_R \quad \text{while} \quad V_L \neq V_R.$$

Thus in the case that there is left-right symmetry we can not distinguish which voltage is applied on which quantum dot if we tune both to the same current.

With the assumption of left-right symmetry we find $g_L = g_R$, where

$$\begin{aligned} g_{11} = g_{22} = g_{12} = g_{21} \equiv g_L, \\ g_{33} = g_{44} = g_{34} = g_{43} \equiv g_R. \end{aligned}$$

The current on the left or right side ($\alpha = L, R$) is defined by

$$I_\alpha = \frac{1}{8}(2\pi)^2 \frac{e}{h} g_\alpha^2 \left[3eV_\alpha + 3p(V_L, V_R) F_3(K, V_\alpha)\right].$$

Thus we have to check if $I_L - I_R = 0$ has a non-trivial solution for V_L and V_R. Assuming left-right symmetry the equation,

$$[V_L + p(V_L, V_R) F_3(K, V_L)] - [V_R + p(V_L, V_R) F_3(K, V_R)] = 0,$$

is to be tested.

The function $F_3(x, V_\alpha)$ describes the step in the differential conductance,

$$F_3(x, V_\alpha) = \frac{1}{2}(x - eV_\alpha) \coth\left[\frac{1}{2}\beta(x - eV_\alpha)\right] - \frac{1}{2}(x + eV_\alpha) \coth\left[\frac{1}{2}\beta(x + eV_\alpha)\right].$$

For temperature $T \to 0$ or $\beta \to \infty$ it can be approximated by

$$F_3(K, V_\alpha) = \begin{cases} -eV_\alpha & \text{for} \quad eV_\alpha < K \\ -K & \text{for} \quad eV_\alpha > K \end{cases}.$$

The polarization p is defined as $p = n_s - n_t$. It is assumed for the following that the spin-spin interaction $K > 0$ is antiferromagnetic. Thus the polarization is nearly 1 (thermodynamic value, exactly 1 for $T \to 0$) in the equilibrium case $eV_L, eV_R < K$ and less than 1 in the case of excited triplet states

$$p \begin{cases} = 1 \text{ for } & eV_L, eV_R < K \\ < 1 & \text{otherwise} \end{cases}.$$

Consequently three different voltage regime have to be distinguished: $eV_L, eV_R < K$, $eV_L < K < eV_R$ and symmetric, and $K < eV_L, eV_R$

First Voltage Regime $eV_L, eV_R < K$

In this case the current is zero,

$$I_L = I_R = 0,$$

and this condition is valid for all V_L, V_R as long as they do not exceed the threshold. This trivial case is not interesting.

Second Voltage Regime $eV_L < K < eV_R$

In this case there is a finite current flowing on the right side and due to the transconductance effect (excited triplet states) also a current on the left side,

$$\begin{aligned} I_L - I_R = [eV_L - p(V_L, V_R)eV_L] - [eV_R - p(V_L, V_R)K] = 0, \\ eV_R = (1-p)eV_L + pK < (1-p)K + pK = K. \end{aligned}$$

Thus the condition for equal current leads to $eV_R < K$. This is in disagreement with the assumption $eV_R < K$. In this regime there is no possibility to have equal current for different voltages.

Third Voltage Regime $K < eV_L, eV_R$

Now both voltages are above the threshold and the condition changes to

$$I_L - I_R = [eV_L - p(V_L, V_R)K] - [eV_R - p(V_L, V_R)K] = eV_L - eV_R \equiv 0.$$

There is only identical current $I_L = I_R$ for equal voltages $eV_L = eV_R$.

Consequently we can state that with this double quantum dot setup in a 4-terminal geometry we cannot build a switch.

B.5 Derivation of the Shot Noise

The lowest order expectation value of the current $\langle I_L(0)\rangle_0$ is zero. On the contrary the product of two current operators in the definition of the noise is finite

$$\begin{aligned} S_L(\tau, \tau') = \left(i\frac{e}{\hbar}\right)^2 \langle T_c \Big(J_{12}\vec{S}_L(\tau)\vec{s}_{12}(\tau) - J_{21}\vec{S}_L(\tau)\vec{s}_{21}(\tau) \Big) \\ \Big(J_{12}\vec{S}_L(\tau')\vec{s}_{12}(\tau') - J_{21}\vec{S}_L(\tau')\vec{s}_{21}(\tau') \Big) \rangle. \end{aligned}$$

This expression is straightforwardly written by

$$S_L(\tau,\tau') = \left(2\pi\frac{e}{h}\right)^2 \langle T_c \vec{S}_L^i(\tau)\vec{S}_L^j(\tau')\rangle \\ \left[J_{12}^i J_{21}^j \langle T_c \vec{s}_{12}^{\,i}(\tau)\vec{s}_{21}^{\,j}(\tau')\rangle + J_{21}^i J_{12}^j \langle T_c \vec{s}_{21}^{\,i}(\tau)\vec{s}_{12}^{\,j}(\tau')\rangle\right].$$

The conduction electron part has already been calculated several times and gives

$$\langle T_c \vec{s}_{12}^{\,i}(\tau)\vec{s}_{21}^{\,j}(\tau')\rangle = -\frac{1}{4}\tau^i_{\sigma'\sigma}\tau^j_{\sigma\sigma'}\frac{1}{(-i)^2}G_{2k\sigma}(\tau,\tau')G_{1k'\sigma'}(\tau',\tau) = -\frac{1}{4}\tau^i_{\sigma'\sigma}\tau^j_{\sigma\sigma'}X_1^2(\tau,\tau'),$$
$$\langle T_c \vec{s}_{21}^{\,i}(\tau)\vec{s}_{12}^{\,j}(\tau')\rangle = -\frac{1}{4}\tau^i_{s's}\tau^j_{ss'}\frac{1}{(-i)^2}G_{1\kappa's}(\tau,\tau')G_{2\kappa s'}(\tau',\tau) = -\frac{1}{4}\tau^i_{\sigma'\sigma}\tau^j_{\sigma\sigma'}X_2^1(\tau,\tau').$$

Since the spin index is negligible in the conduction electron leads, the two expressions are the same besides an exchange from lead index $1 \leftrightarrow 2$, which provides the correct symmetry. This leads to the expression of the noise

$$S_L(\tau,\tau') = \frac{1}{4}\left(2\pi\frac{e}{h}\right)^2 \tau^i_{\sigma'\sigma}\tau^j_{\sigma\sigma'}\langle T_c \vec{S}_L^i(\tau)\vec{S}_L^j(\tau')\rangle \\ \left[J_{12}^i J_{21}^j G_{2k\sigma}(\tau,\tau')G_{1k'\sigma'}(\tau',\tau) + J_{21}^i J_{12}^j G_{1k'\sigma'}(\tau,\tau')G_{2k\sigma}(\tau',\tau)\right].$$

Now we study the contribution from the singlet-triplet states in

$$\langle T_c \vec{S}_L^i(\tau)\vec{S}_L^j(\tau')\rangle = \frac{1}{4}\vec{T}^i_{\gamma'\gamma}\vec{T}^j_{g'g}\langle T_c f^\dagger_{\gamma'}(\tau) f_\gamma(\tau) f^\dagger_{g'}(\tau') f_g(\tau)\rangle \\ = \frac{1}{4}\frac{1}{(-i)^2}\vec{T}^i_{\gamma'\gamma}G_{\gamma g'}(\tau,\tau')\vec{T}^j_{g'g}G_{g\gamma'}(\tau',\tau).$$

The most general expression we can thus write down for the noise is

$$S_L(\tau,\tau') = -\frac{1}{16}\left(2\pi\frac{e}{h}\right)^2 \tau^i_{\sigma'\sigma}\tau^j_{\sigma\sigma'}\vec{T}^i_{\gamma'\gamma}G_{\gamma g'}(\tau,\tau')\vec{T}^j_{g'g}G_{g\gamma'}(\tau',\tau) \\ \left[J_{12}^i J_{21}^j G_{2k\sigma}(\tau,\tau')G_{1k'\sigma'}(\tau',\tau) + J_{21}^i J_{12}^j G_{1k'\sigma'}(\tau,\tau')G_{2k\sigma}(\tau',\tau)\right], \quad \text{(B.11)}$$

which could be used for generalizing this physical quantity to a calculation within the framework of perturbative RG.

Now we concentrate on the result in second order perturbation theory. Therefore we continue with the simpler expression

$$S_L(\tau,\tau') = \frac{1}{8}\left(2\pi\frac{e}{h}\right)^2 J_{12}J_{21}X_{\mathrm{DQD}}(\tau,\tau')\left[X_1^2(\tau,\tau') + X_2^1(\tau,\tau')\right],$$

where

$$X_{\mathrm{DQD}}(\tau,\tau') = \vec{T}_{\gamma'\gamma}G_{\gamma g'}(\tau,\tau')\vec{T}_{g'g}G_{g\gamma'}(\tau',\tau).$$

With the use of $X_n^m(\tau,\tau') = X_m^n(\tau',\tau)$ we can determine the greater component of the noise

$$S_L^>(t,t') = \frac{1}{8}\left(2\pi\frac{e}{h}\right)^2 J_{12}J_{21}X^>_{\mathrm{DQD}}(t,t')\left[\left(X_2^1\right)^<(t',t) + \left(X_1^2\right)^<(t',t)\right]$$
$$\Rightarrow \quad S_L^>(\omega) = \frac{1}{8}\left(2\pi\frac{e}{h}\right)^2 J_{12}J_{21}\int\frac{d\epsilon}{2\pi}X^>_{\mathrm{DQD}}(\epsilon)\left[\left(X_2^1\right)^<(\epsilon-\omega) + \left(X_1^2\right)^<(\epsilon-\omega)\right]$$

With $(X_n^m)^< (\epsilon-\omega) = -2\pi N(0) n_B(\epsilon-\omega+\mu_m-\mu_n)(\epsilon-\omega+\mu_m-\mu_n)$ we only need to find the expression for $X^<_{\rm DQD}$. For the following we assume that $\Sigma_{st_0}=0$ such that we do not have to take into account off-diagonal contributions. This is true in almost any case of finite spin-spin interaction K if the magnetic field $B=0$, the coupling to the left and the right is identical $g_L=g_R$ or the spin-spin interaction K is much larger than the broadening Γ. Then the pseudo particle Green's functions are diagonal and we get

$$\begin{aligned} X^>_{\rm DQD}(t,t') &= \vec{T}_{\gamma'\gamma} G^>_\gamma(t,t') \vec{T}_{\gamma\gamma'} G^<_{\gamma'}(t',t), \\ \Rightarrow \qquad X^>_{\rm DQD}(\epsilon) &= \int \frac{d\omega_\gamma}{2\pi} \vec{T}_{\gamma'\gamma} G^>_\gamma(\omega_\gamma) \vec{T}_{\gamma\gamma'} G^<_{\gamma'}(\omega_\gamma-\epsilon). \end{aligned}$$

Furthermore we use the quasi-particle ansatz for the pseudo particle Green's functions and find

$$X^>_{\rm DQD}(\epsilon) = \vec{T}_{\gamma\gamma'} n_{\gamma'} \vec{T}_{\gamma'\gamma} 2\pi\delta(\epsilon_\gamma - E/\hbar - \epsilon_{\gamma'}),$$

and

$$S^>_L(\omega) = \frac{1}{8}\left(2\pi\frac{e}{h}\right)^2 J_{12}J_{21} \vec{T}^j_{\gamma\gamma'} n_{\gamma'} \vec{T}^i_{\gamma'\gamma} \left[\left(X_2^1\right)^< (\epsilon_\gamma - \epsilon_{\gamma'} - \omega) + \left(X_1^2\right)^< (\epsilon_\gamma - \epsilon_{\gamma'} - \omega) \right].$$

After evaluating the summation over the pseudo particle indices we find

$$\begin{aligned} S^>_L(\omega) = \frac{2\pi}{8}\left(2\pi\frac{e}{h}\right)^2 g_{12}g_{21} \big[& n_s \left(\mathcal{F}_2(K-B-\omega) + \mathcal{F}_2(K+B-\omega) + \mathcal{F}_2(K-\omega)\right) \\ & + n_{t_+} \left(\mathcal{F}_2(-K+B-\omega) + \mathcal{F}_2(B-\omega) + \mathcal{F}_2(-\omega)\right) \\ & + n_{t_0} \left(\mathcal{F}_2(-K-\omega) + \mathcal{F}_2(B-\omega) + \mathcal{F}_2(-B-\omega)\right) \\ & + n_{t_-} \left(\mathcal{F}_2(-K-B-\omega) + \mathcal{F}_2(-B-\omega) + \mathcal{F}_2(-\omega)\right) \big], \end{aligned} \tag{B.12}$$

where

$$\mathcal{F}_2(x) = n_B(x+eV_L)(x+eV_L) + n_B(x-eV_L)(x-eV_L).$$

The function $\mathcal{F}_2(x)$ is symmetric in the voltage,

$$\mathcal{F}_2(x) = \frac{1}{2}(x+eV_L)\coth\left(\frac{1}{2}\beta(x+eV_L)\right) + \frac{1}{2}(x-eV_L)\coth\left(\frac{1}{2}\beta(x-eV_L)\right) - x,$$

and for $V_L=0$ it gives a finite value of $2xn_B(x)$. This temperature dependent value is related to the thermal noise.

Please note, that in the result of $S^<_L(\omega)$ the variable ω has the unit of an energy and is not a frequency. The frequency dependent shot noise as defined in Eq. (4.24) has to be divided by $\hbar$. The prefactor of the noise is

$$\frac{2\pi}{8}\frac{e^2}{\hbar^2} g_{12}g_{21} \cdot 1/\hbar = \frac{(2\pi)^2}{8}\frac{e^2}{h} g_{12}g_{21},$$

which is proportional to the prefactor of the current times the electric charge e.

Additionally we have to calculate

$$S_L^<(t,t') = \frac{1}{8}\left(2\pi\frac{e}{h}\right)^2 J_{12}J_{21}X^<_{\mathrm{DQD}}(t,t')\left[\left(X_2^1\right)^<(t,t') + \left(X_1^2\right)^<(t,t')\right],$$

and

$$X^<_{\mathrm{DQD}}(t,t') = \vec{T}_{\gamma'\gamma}G^<_\gamma(t,t')\vec{T}_{\gamma\gamma'}G^>_{\gamma'}(t',t),$$
$$X^<_{\mathrm{DQD}}(\epsilon) = \int\frac{d\omega_\gamma}{2\pi}\vec{T}_{\gamma'\gamma}G^>_\gamma(\omega_\gamma)\vec{T}_{\gamma\gamma'}G^<_{\gamma'}(\omega_\gamma-\epsilon) = \vec{T}_{\gamma'\gamma}n_\gamma\vec{T}_{\gamma\gamma'}2\pi\delta(\epsilon+\epsilon_{\gamma'}-\epsilon_\gamma).$$

This is similar to the result for $X^>_{\mathrm{DQD}}$ only with the index $\gamma \leftrightarrow \gamma'$ exchanged and a different sign of ω. Thus we find,

$$S_L^<(\omega) = \frac{1}{8}\left(2\pi\frac{e}{h}\right)^2 J_{12}J_{21}\vec{T}^j_{\gamma\gamma'}n_{\gamma'}\vec{T}^i_{\gamma'\gamma}\left[\left(X_2^1\right)^<(\omega+\epsilon_\gamma-\epsilon_{\gamma'}) + \left(X_1^2\right)^<(\omega+\epsilon_\gamma-\epsilon_{\gamma'})\right].$$

For $\omega = 0$ the noise is due to $\langle I_L(t)I_L(t')\rangle + \langle I_L(t')I_L(t)\rangle = S_L^>(t,t') + S_L^<(t,t')$ given by Eq. (B.12) multiplied by a factor of 2.

B.5.1 Further Preliminary Results

As can be seen from Fig. 4.19(a) the noise shows a similar behavior to the current in section 4.2. The Fano factor in the inset of Fig. B.1 shows the typical thermal divergence $\coth(\beta V)$ at small voltages. The noise is most often Poissonian, but close to the transitions between two pseudo particle states we observe a super-poissonian value. In analogy to Ref. [62, 63] we interpret this result as the existence of two states with finite life time. For example if the singlet state is occupied the current is 0 and if the triplet t_+ is occupied the current is finite. The measured current jumps between these two states with a time indirect proportional to the life time of the states. At low frequencies $\omega \to 0$ this enhances the noise power.

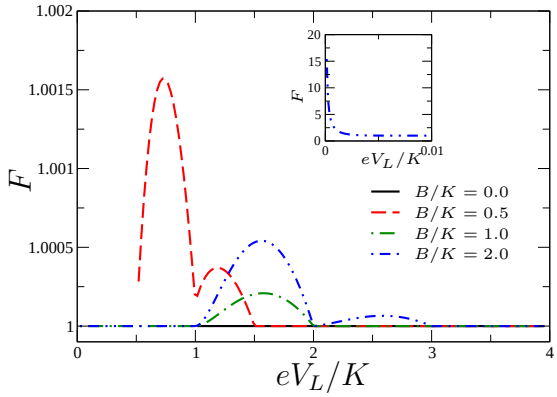

Figure B.1: Fano factor F vs. eV_L/K for finite values of the magnetic field $B/K = 0.0, 0.5, 1.0, 2.0$ at low temperature $T/K = 0.001$, $V_R = 0$ and $g_L = g_R = 0.1$. Inset: The thermal noise is visible only at values of $eV_L \ll k_BT$.

The result in Fig. B.1 is preliminary and the origin of the super-possonian values has to be studied in more detail. Further insight into the physical behavior of the system can be found maybe in the frequency dependent noise $S(\omega)$.

B.6 Derivation of the Current Cross-Correlation

B.6.1 Double Quantum Dot Contribution

For the perturbation H_{int} we introduce the notation

$$\begin{aligned} H_{\text{int}} &= J_{mn}\vec{S}_\alpha(\tau)\vec{s}_{mn}(\tau) \\ &= \frac{1}{4}J_{mn}\vec{T}^{\alpha}_{\gamma'\gamma}\vec{\tau}_{\sigma'\sigma}{}^{a} f^\dagger_{\gamma'}(\tau)^b f_\gamma(\tau)^c c^\dagger_{mk'\sigma'}(\tau)^d c_{nk\sigma}(\tau) \end{aligned} \tag{B.13}$$

where the summation goes over momentum k', k, spin σ', σ, pseudo particle index $\gamma', \gamma \in \{s, t_+, t_0, t_-\}$ and lead indices m, n. a, b, c, d are Keldysh indices and in the time domain we can use the fact, that the interaction can take place only either on the upper contour $a = b = c = d = 1$ or on the lower contour $a = b = c = d = 2$ where an interaction on the inverse time axis leads to an additional minus sign ($\Lambda^{cd}_{ab} = \delta_{ab}\delta_{cd}\tau^3_{ac}$).

The conduction electrons of the left and the right leads are decoupled, thus the only mediation of a current cross-correlation can originate from the spin-spin interaction K of the left with the right impurity spin. Therefore we calculate

$$\langle T_c \vec{S}^i_L(\tau)\vec{S}^{i_1}_L(\tau_1)\vec{S}^{j_2}_R(\tau_2)\vec{S}^j_R(\tau')\rangle$$

in the singlet-triplet representation

$$\begin{aligned} &= \left(\frac{1}{2}\right)^4 \left(\vec{T}^i_L\right)_{\gamma'\gamma}\left(\vec{T}^{i_1}_L\right)_{\gamma'_1\gamma_1}\left(\vec{T}^{j_2}_R\right)_{\gamma'_2\gamma_2}\left(\vec{T}^j_R\right)_{g'g} \\ &\quad \langle T_c{}^a f^\dagger_{\gamma'}(\tau)\,{}^b f_\gamma(\tau)\,{}^{a_1} f^\dagger_{\gamma'_1}(\tau_1)\,{}^{b_1} f_{\gamma_1}(\tau_1)\,{}^{a_2} f^\dagger_{\gamma'_2}(\tau_2)\,{}^{b_2} f_{\gamma_2}(\tau_2)\,{}^{a'} f^\dagger_{g'}(\tau')\,{}^{b'} f_g(\tau')\rangle \end{aligned}$$

where we can use Wicks theorem.

B.6.2 "Vertex" Contributions

The first contribution of the "vertex" type is found for example

$$\begin{aligned} &\frac{1}{16}\left(\vec{T}^i_L\right)_{\gamma'\gamma}\left(\vec{T}^{i_1}_L\right)_{\gamma'_1\gamma_1}\left(\vec{T}^{j_2}_R\right)_{\gamma'_2\gamma_2}\left(\vec{T}^j_R\right)_{g'g} \\ &\langle T_c{}^{b_2} f_{\gamma_2}(\tau_2)\,{}^a f^\dagger_{\gamma'}(\tau)\rangle\ \langle T_c{}^{b'} f_g(\tau')\,{}^{a_1} f^\dagger_{\gamma'_1}(\tau_1)\rangle\ \langle T_c{}^{b_1} f_{\gamma_1}(\tau_1)\,{}^{a_2} f^\dagger_{\gamma'_2}(\tau_2)\rangle\ \langle T_c{}^b f_\gamma(\tau)\,{}^{a'} f^\dagger_{g'}(\tau')\rangle \\ =&\frac{1}{16}\left(\vec{T}^i_L\right)_{\gamma'\gamma} G^{ba'}_\gamma(\tau,\tau')\left(\vec{T}^j_R\right)_{\gamma g} G^{b'a_1}_g(\tau',\tau_1)\left(\vec{T}^{i_1}_L\right)_{g\gamma_1} G^{b_1a_2}_{\gamma_1}(\tau_1,\tau_2)\left(\vec{T}^{j_2}_R\right)_{\gamma_1\gamma'} G^{b_2a}_{\gamma'}(\tau_2,\tau) \end{aligned}$$

neglecting a factor of $-(2\pi e/h)^2\chi_L(\tau,\tau_1)\chi_R(\tau',\tau_2)$.

As discussed in the main text this contribution is denoted "vertex" contribution, since it is similar to a vertex as illustrated in Fig. 4.21(a), see also discussion in section 4.6.2.

We introduce $d(\tau,\tau')$ as the correlation function without the prefactor

$$\mathcal{D}(\tau,\tau') = -\left(2\pi\frac{e}{h}\right)^2 d(\tau,\tau').$$

Before we do the spin index summation, we focus on the Keldysh contour integration.

We are interested in the lesser correlation function

$$\mathcal{D}^{<}(t,t') = \mathcal{D}^{12}(t,t')$$

which implies that $\tau \to t$ is on the upper (= 1) and $\tau' \to t'$ is on the lower contour (= 2). The two contour times τ_1 and τ_2 can be either on the upper or on the lower contour and we have to take into account the four different possibilities. Thereby we have to take into account that we gain an minus sign if one vertex is on the lower contour (= 2).

Since it is easier to calculate with retarded and advanced Green's functions than with time-ordered and anti-time-ordered we use the following relations

$$G^{11}(t,t') = G^{r}(t,t') + G^{<}(t,t') \tag{B.14}$$
$$G^{22}(t,t') = G^{<}(t,t') - G^{a}(t,t') \tag{B.15}$$

Furthermore it is used that the system of contour-ordered Green's functions is over-determined and thus the greater Green's function $G^{>}$,

$$G^{21}(t,t') = G^{>}(t,t') = G^{<}(t,t') + G^{r}(t,t') - G^{a}(t,t'), \tag{B.16}$$

can be expressed in terms of the lesser Green's function $G^{<}$.

Please note, that the constraint allows only for one lesser Green's function in the whole expression. A product of two lesser Green's functions is immediately proportional to $e^{-2\beta\lambda}$ and is projected out in the calculation of a physical observable.

For the first vertex term $d_{v1}(\tau,\tau')$ the analytical continuation is shown in detail, but the derivation is shortened in the procedure afterwards. We have to sum over the Keldysh indices in the expression

$$d_{v1}(\tau,\tau') \propto G_{\gamma}^{12}(\tau,\tau') G_{g}^{2a_1}(\tau',\tau_1) G_{\gamma_1}^{b_1 a_2}(\tau_1,\tau_2) G_{\gamma'}^{b_2 1}(\tau_2,\tau) \chi_{L}^{1c_1}(\tau,\tau_1) \chi_{R}^{2c_2}(\tau',\tau_2)$$

and receive four terms already taking into account an additional minus sign if the interaction takes place on the lower contour.

$$\begin{aligned}
d_{v1}^{12}(t,t') \propto & G_{\gamma}^{12}(t,t') G_{g}^{21}(t',t_1) G_{\gamma_1}^{11}(t_1,t_2) G_{\gamma'}^{11}(t_2,t) \chi_{L}^{11}(t,t_1) \chi_{R}^{21}(t',t_2) \\
& - G_{\gamma}^{12}(t,t') G_{g}^{21}(t',t_1) G_{\gamma_1}^{12}(t_1,t_2) G_{\gamma'}^{21}(t_2,t) \chi_{L}^{11}(t,t_1) \chi_{R}^{22}(t',t_2) \\
& - G_{\gamma}^{12}(t,t') G_{g}^{22}(t',t_1) G_{\gamma_1}^{21}(t_1,t_2) G_{\gamma'}^{11}(t_2,t) \chi_{L}^{12}(t,t_1) \chi_{R}^{21}(t',t_2) \\
& + G_{\gamma}^{12}(t,t') G_{g}^{22}(t',t_1) G_{\gamma_1}^{22}(t_1,t_2) G_{\gamma'}^{21}(t_2,t) \chi_{L}^{12}(t,t_1) \chi_{R}^{22}(t',t_2).
\end{aligned}$$

Inserting the relations for the Green's functions we find,

$$\begin{aligned}
d_{v1}^{12}(t,t') \propto & G_{\gamma}^{<}(t,t') \left(G_{g}^{<}(t',t_1) + G_{g}^{r}(t',t_1) - G_{g}^{a}(t',t_1) \right) \left(G_{\gamma_1}^{<}(t_1,t_2) + G_{\gamma_1}^{r}(t_1,t_2) \right) \\
& \left(G_{\gamma'}^{<}(t_2,t) + G_{\gamma'}^{r}(t_2,t) \right) \chi_{L}^{11}(t,t_1) \chi_{R}^{>}(t',t_2) \\
& - G_{\gamma}^{<}(t,t') \left(G_{g}^{<}(t',t_1) + G_{g}^{r}(t',t_1) - G_{g}^{a}(t',t_1) \right) G_{\gamma_1}^{<}(t_1,t_2) \\
& \left(G_{\gamma'}^{<}(t_2,t) + G_{\gamma'}^{r}(t_2,t) - G_{\gamma'}^{a}(t_2,t) \right) \chi_{L}^{11}(t,t_1) \chi_{R}^{22}(t',t_2) \\
& - G_{\gamma}^{<}(t,t') \left(G_{g}^{<}(t',t_1) - G_{g}^{a}(t',t_1) \right) \left(G_{\gamma_1}^{<}(t_1,t_2) + G_{\gamma_1}^{r}(t_1,t_2) - G_{\gamma_1}^{a}(t_1,t_2) \right) \\
& \left(G_{\gamma'}^{<}(t_2,t) + G_{\gamma'}^{r}(t_2,t) \right) \chi_{L}^{<}(t,t_1) \chi_{R}^{>}(t',t_2) \\
& + G_{\gamma}^{<}(t,t') \left(G_{g}^{<}(t',t_1) - G_{g}^{a}(t',t_1) \right) \left(G_{\gamma_1}^{<}(t_1,t_2) - G_{\gamma_1}^{a}(t_1,t_2) \right) \\
& \left(G_{\gamma'}^{<}(t_2,t) + G_{\gamma'}^{r}(t_2,t) - G_{\gamma'}^{a}(t_2,t) \right) \chi_{L}^{<}(t,t_1) \chi_{R}^{22}(t',t_2)
\end{aligned}$$

Already projecting out non-physical components with more than one occupation number, this expression simplifies to

$$\begin{aligned} d_{v1}^{<}(t,t') \approx & \frac{1}{16}\left(\vec{T}_L^{i}\right)_{\gamma'\gamma}\left(\vec{T}_R^{j}\right)_{\gamma g}\left(\vec{T}_L^{i_1}\right)_{g\gamma_1}\left(\vec{T}_R^{j_2}\right)_{\gamma_1\gamma'}\int dt_1\int dt_2 \\ & \left\{G_\gamma^{<}(t,t')\left(G_g^r(t',t_1)-G_g^a(t',t_1)\right)G_{\gamma_1}^r(t_1,t_2)G_{\gamma'}^r(t_2,t)\chi_L^{11}(t,t_1)\chi_R^{>}(t',t_2)\right. \\ & + G_\gamma^{<}(t,t')G_g^a(t',t_1)\left(G_{\gamma_1}^r(t_1,t_2)-G_{\gamma_1}^a(t_1,t_2)\right)G_{\gamma'}^r(t_2,t)\chi_L^{<}(t,t_1)\chi_R^{>}(t',t_2) \\ & \left.+ G_\gamma^{<}(t,t')G_g^a(t',t_1)G_{\gamma_1}^a(t_1,t_2)\left(G_{\gamma'}^r(t_2,t)-G_{\gamma'}^a(t_2,t)\right)\chi_L^{<}(t,t_1)\chi_R^{22}(t',t_2)\right\} \end{aligned}$$

All Green's function are only dependent on the difference of the two times (time inversion symmetry). It appears to be easier to calculate with the Green's functions in Fourier space thus in a next step the expression for d_{v1} is Fourier transformed,

$$\begin{aligned} & \int dt_1\int dt_2\int d(t-t')\mathrm{e}^{i\omega(t-t')}\int\frac{d\omega_L}{2\pi}\mathrm{e}^{-i\omega_L(t-t_1)}\int\frac{d\omega_R}{2\pi}\mathrm{e}^{-i\omega_R(t'-t_2)} \\ & \int\frac{d\omega_\gamma}{2\pi}\mathrm{e}^{-i\omega_\gamma(t-t')}\int\frac{d\omega_g}{2\pi}\mathrm{e}^{-i\omega_g(t'-t_1)}\int\frac{d\omega_{\gamma_1}}{2\pi}\mathrm{e}^{-i\omega_{\gamma_1}(t_1-t_2)}\int\frac{d\omega_{\gamma'}}{2\pi}\mathrm{e}^{-i\omega_{\gamma'}(t_2-t)} \\ & G_\gamma(\omega_\gamma)G_g(\omega_g)G_{\gamma_1}(\omega_{\gamma_1})G_{\gamma'}(\omega_{\gamma'})\chi_L(\omega_L)\chi_R(\omega_R) \\ = & \int\frac{d\omega_\gamma}{2\pi}\int\frac{d\omega_g}{2\pi}\int\frac{d\omega_{\gamma_1}}{2\pi}\int\frac{d\omega_{\gamma'}}{2\pi}\,2\pi\delta\left(\omega-\omega_\gamma+\omega_g-\omega_{\gamma_1}+\omega_{\gamma'}\right) \\ & G_\gamma(\omega_\gamma)G_g(\omega_g)G_{\gamma_1}(\omega_{\gamma_1})G_{\gamma'}(\omega_{\gamma'})\chi_L(\omega_{\gamma_1}-\omega_g)\chi_R(\omega_{\gamma'}-\omega_{\gamma_1}) \end{aligned}$$

Please note that the ω_γ's is are only placeholders and not the eigenenergy of the state γ. The eigenenergy are in the following denoted by ϵ_γ. The contribution of the first "vertex" contribution can now be determined by the following integral,

$$\begin{aligned} d_{v1}^{<}(\omega) = & \frac{1}{16}\left(\vec{T}_L^{i}\right)_{\gamma'\gamma}\left(\vec{T}_R^{j}\right)_{\gamma g}\left(\vec{T}_L^{i_1}\right)_{g\gamma_1}\left(\vec{T}_R^{j_2}\right)_{\gamma_1\gamma'} \\ & \int\frac{d\omega_\gamma}{2\pi}\int\frac{d\omega_g}{2\pi}\int\frac{d\omega_{\gamma_1}}{2\pi}\int\frac{d\omega_{\gamma'}}{2\pi}\,2\pi\delta\left(\omega-\omega_\gamma+\omega_g-\omega_{\gamma_1}+\omega_{\gamma'}\right) \\ & \left\{G_\gamma^{<}(\omega_\gamma)\left(G_g^r(\omega_g)-G_g^a(\omega_g)\right)G_{\gamma_1}^r(\omega_{\gamma_1})G_{\gamma'}^r(\omega_{\gamma'})\chi_L^{11}(\omega_{\gamma_1}-\omega_g)\chi_R^{>}(\omega_{\gamma'}-\omega_{\gamma_1})\right. \\ & + G_\gamma^{<}(\omega_\gamma)G_g^a(\omega_g)\left(G_{\gamma_1}^r(\omega_{\gamma_1})-G_{\gamma_1}^a(\omega_{\gamma_1})\right)G_{\gamma'}^r(\omega_{\gamma'})\chi_L^{<}(\omega_{\gamma_1}-\omega_g)\chi_R^{>}(\omega_{\gamma'}-\omega_{\gamma_1}) \\ & \left.+ G_\gamma^{<}(\omega_\gamma)G_g^a(\omega_g)G_{\gamma_1}^a(\omega_{\gamma_1})\left(G_{\gamma'}^r(\omega_{\gamma'})-G_{\gamma'}^a(\omega_{\gamma'})\right)\chi_L^{<}(\omega_{\gamma_1}-\omega_g)\chi_R^{22}(\omega_{\gamma'}-\omega_{\gamma_1})\right\}. \end{aligned}$$

If we assume that the pseudo particle Green's functions are only the non-interacting one's, then we can simplify the expression significantly by using $G_\gamma^{<}(\omega) = -in_\gamma^\lambda A_\gamma(\omega)$ and $G_\gamma^r(\omega) - G_\gamma^a(\omega) = -iA_\gamma(\omega)$, where $A_\gamma(\omega) = 2\pi\delta(\omega-\epsilon_\gamma)$. After some simplifications we are left with only one frequency integration,

$$\begin{aligned} d_{v1}^{<}(\omega) = & \frac{1}{16}\left(\vec{T}_L^{i}\right)_{\gamma'\gamma}n_\gamma\left(\vec{T}_R^{j}\right)_{\gamma g}\left(\vec{T}_L^{i_1}\right)_{g\gamma_1}\left(\vec{T}_R^{j_2}\right)_{\gamma_1\gamma'} \\ & \int\frac{d\tilde{\omega}}{2\pi}\left\{G_{\gamma_1}^r(\tilde{\omega}+[\omega-\epsilon_\gamma+\epsilon_g])G_{\gamma'}^r(\tilde{\omega})\chi_L^{11}(\tilde{\omega}-\epsilon_\gamma+\omega)\chi_R^{>}(-\omega+\epsilon_\gamma-\epsilon_g)\right. \\ & \quad + G_g^a(-\tilde{\omega}+[-\omega+\epsilon_\gamma+\epsilon_{\gamma_1}])G_{\gamma'}^r(\tilde{\omega})\chi_L^{<}(\tilde{\omega}-\epsilon_\gamma+\omega)\chi_R^{>}(\tilde{\omega}-\epsilon_{\gamma_1}) \\ & \quad \left.+ G_g^a(\tilde{\omega})G_{\gamma_1}^a(\tilde{\omega}+[\omega-\epsilon_\gamma+\epsilon_{\gamma'}])\chi_L^{<}(\omega-\epsilon_\gamma+\epsilon_{\gamma'})\chi_R^{22}(-\tilde{\omega}+\epsilon_\gamma-\omega)\right\}. \end{aligned}$$

Please note that every of the three terms has the residuum from the retarded or advanced Green's function on the same half plane. Consequently this contribution is negligible.

The second contribution of this type d_{v2} is the time-reversed version of the previous contribution d_{v1}, i. e.

$$=\frac{1}{16}G^{b'a}_{\gamma'}(\tau',\tau)\left(\vec{T}^{i}_{L}\right)_{\gamma'\gamma}G^{ba_2}_{\gamma}(\tau,\tau_2)\left(\vec{T}^{j_2}_{R}\right)_{\gamma\gamma_2}G^{b_2a_1}_{\gamma_2}(\tau_2,\tau_1)\left(\vec{T}^{i_1}_{L}\right)_{\gamma_2 g'}G^{b_1a'}_{g'}(\tau_1,\tau')\left(\vec{T}^{j}_{R}\right)_{g'\gamma'}.$$

Following the same steps than in the calculation of d_{v1} we find that only three terms contribute,

$$\begin{aligned}d^{<}_{v2}(t,t') =&\frac{1}{16}\left(\vec{T}^{i}_{L}\right)_{\gamma'\gamma}\left(\vec{T}^{j_2}_{R}\right)_{\gamma\gamma_2}\left(\vec{T}^{i_1}_{L}\right)_{\gamma_2 g'}\left(\vec{T}^{j}_{R}\right)_{g'\gamma'}\int dt_1\int dt_2\\ &\left\{\left(G^{r}_{\gamma'}(t',t)-G^{a}_{\gamma'}(t',t)\right)G^{r}_{\gamma}(t,t_2)G^{r}_{\gamma_2}(t_2,t_1)G^{<}_{g'}(t_1,t')\chi^{11}_{L}(t,t_1)\chi^{>}_{R}(t',t_2)\right.\\ &+\left(G^{r}_{\gamma'}(t',t)-G^{a}_{\gamma'}(t',t)\right)G^{r}_{\gamma}(t,t_2)G^{<}_{\gamma_2}(t_2,t_1)G^{a}_{g'}(t_1,t')\chi^{<}_{L}(t,t_1)\chi^{>}_{R}(t',t_2)\\ &\left.+\left(G^{r}_{\gamma'}(t',t)-G^{a}_{\gamma'}(t',t)\right)G^{<}_{\gamma}(t,t_2)G^{a}_{\gamma_2}(t_2,t_1)G^{a}_{g'}(t_1,t')\chi^{<}_{L}(t,t_1)\chi^{22}_{R}(t',t_2)\right\}.\end{aligned}$$

Analogous to the other calculation we prefer to calculate in Fourier space, thus we have to Fouriertransform the expression from the time domain,

$$\begin{aligned}=&\int\frac{d\omega_{\gamma'}}{2\pi}\int\frac{d\omega_{\gamma}}{2\pi}\int\frac{d\omega_{\gamma_2}}{2\pi}\int\frac{d\omega_{g'}}{2\pi}\,2\pi\delta\left(\omega-\omega_{\gamma}+\omega_{\gamma'}-\omega_{g'}+\omega_{\gamma_2}\right)\\ &G_{\gamma'}(\omega_{\gamma'})G_{\gamma}(\omega_{\gamma})G_{\gamma_2}(\omega_{\gamma_2})G_{g'}(\omega_{g'})\chi_{L}(\omega_{g'}-\omega_{\gamma_2})\chi_{R}(\omega_{\gamma_2}-\omega_{\gamma}).\end{aligned}$$

By using the zeroth order expression for the lesser Green's functions and the spectral function we yield

$$\begin{aligned}d^{<}_{v2}(t,t') =&\frac{1}{16}\left(\vec{T}^{i}_{L}\right)_{\gamma'\gamma}\left(\vec{T}^{j_2}_{R}\right)_{\gamma\gamma_2}\left(\vec{T}^{i_1}_{L}\right)_{\gamma_2 g'}\left(\vec{T}^{j}_{R}\right)_{g'\gamma'}\\ &\int\frac{d\tilde{\omega}}{2\pi}\left\{G^{r}_{\gamma}(\tilde{\omega}+[\omega+\epsilon_{\gamma'}-\epsilon_{g'}])G^{r}_{\gamma_2}(\tilde{w})n_{g'}\chi^{11}_{L}(\epsilon_{g'}-\tilde{\omega})\chi^{>}_{R}(-\omega+\epsilon_{g'}-\epsilon_{\gamma'})\right.\\ &+G^{r}_{\gamma}(-\tilde{\omega}+[\omega+\epsilon_{\gamma'}+\epsilon_{\gamma_2}])n_{\gamma_2}G^{a}_{g'}(\tilde{\omega})\chi^{<}_{L}(\tilde{\omega}-\epsilon_{\gamma_2})\chi^{>}_{R}(\tilde{\omega}-\omega-\epsilon_{\gamma'})\\ &\left.+n_{\gamma}G^{a}_{\gamma_2}(\tilde{\omega})G^{a}_{g'}(\tilde{\omega}+[\omega-\epsilon_{\gamma}+\epsilon_{\gamma'}])\chi^{<}_{L}(\omega-\epsilon_{\gamma}+\epsilon_{\gamma'})\chi^{22}_{R}(\tilde{\omega}-\epsilon_{\gamma})\right\}.\end{aligned}$$

Again all residues are on the same half plane and the contribution of this integral is negligible. For more discussion of these results we refer the reader to section 4.6.

B.6.3 "Self Energy" Contributions

The four contributions which we collect under the name "self energy" contributions are again split into two groups. We recognize that every contributions shows a combination of $\chi_\alpha(\tau,\tau_i)G(\tau,\tau_i)$. Thus we define the "self energy" like structure $\mathcal{S}$, as discussed in detail in section 4.6.3,

$$\left(\mathcal{S}_L\right)_{\gamma'\gamma_1}(\tau,\tau_1)=\frac{1}{4}\left(\vec{T}^{i}_{L}\right)_{\gamma'\gamma}G_{\gamma}(\tau,\tau_1)\left(\vec{T}^{i_1}_{L}\right)_{\gamma\gamma_1}\chi_{L}(\tau,\tau_1),\tag{B.17}$$

$$\left(\mathcal{S}_R\right)_{g'\gamma_2}(\tau',\tau_2)=\frac{1}{4}\left(\vec{T}^{j}_{R}\right)_{g'g}G_{g}(\tau',\tau_2)\left(\vec{T}^{j_2}_{R}\right)_{g\gamma_2}\chi_{R}(\tau',\tau_2).\tag{B.18}$$

Please note that due to the asymmetry of the bubble Eqs. (4.32) and (4.33), for example

$$\frac{1}{4}\left(\vec{T}_L^{i_1}\right)_{\gamma_1'\gamma'} G_{\gamma'}(\tau_1,\tau)\left(\vec{T}_L^{i}\right)_{\gamma'\gamma} \chi_L(\tau,\tau_1) = -\left(\mathcal{S}_L\right)_{\gamma_1'\gamma}(\tau_1,\tau),$$

the inverse time argument picks up a minus sign.

As every function in Keldysh space the function $\mathcal{S}$ fulfills for example $\mathcal{S}^{>} - \mathcal{S}^{<} = \mathcal{S}^{r} - \mathcal{S}^{a}$. It is also important to notice, that

$$\mathcal{S}^{<}(t_i,t_j) = \frac{1}{4}\vec{T}\,\mathcal{G}^{<}(t_i,t_j)\,\vec{T}\,\chi^{<}(t_i,t_j)$$

is proportional to the lesser Green's function and therefore proportional to $e^{-\beta\lambda}$ from the pseudo particle constraint.

We can now write the four different "self energy" contributions as

$$\begin{aligned}
d_{s1}(\tau,\tau') &= \int_C d\tau_1 \int_C d\tau_2\; \mathcal{S}_L(\tau,\tau_1)\mathcal{G}(\tau_1,\tau_2)\left[-\mathcal{S}_R(\tau_2,\tau')\right]\mathcal{G}(\tau',\tau),\\
d_{s2}(\tau,\tau') &= \int_C d\tau_1 \int_C d\tau_2\; \left[-\mathcal{S}_L(\tau_1,\tau)\right]\mathcal{G}(\tau,\tau')\mathcal{S}_R(\tau',\tau_2)\mathcal{G}(\tau_2,\tau_1),\\
d_{s3}(\tau,\tau') &= \int_C d\tau_1 \int_C d\tau_2\; \mathcal{S}_L(\tau,\tau_1)\mathcal{G}(\tau_1,\tau')\mathcal{S}_R(\tau',\tau_2)\mathcal{G}(\tau_2,\tau),\\
d_{s4}(\tau,\tau') &= \int_C d\tau_1 \int_C d\tau_2\; \left[-\mathcal{S}_L(\tau_1,\tau)\right]\mathcal{G}(\tau,\tau_2)\left[-\mathcal{S}_R(\tau_2,\tau')\right]\mathcal{G}(\tau',\tau_1),
\end{aligned}$$

where we implicitly assume a matrix product over all Keldysh indices and the trace over all singlet-triplet states.

First we evaluate the matrix product in the time domain Keldysh representation where we assume as in the section before, that τ is on the upper contour (= 1)and τ' is on the lower (= 2). Additionally we only write down the terms which are not projected out by the constraint in the end. To limit the amount of written formula we also do the Fourier

transformation in the same step. Thus we find

$$
\begin{aligned}
d_{s1}^{<}(\omega) = -\int \frac{d\tilde{\omega}}{2\pi} \big\{ & \mathcal{S}_L^{11}(\tilde{\omega})\mathcal{G}^{11}(\tilde{\omega})\mathcal{S}_R^{12}(\tilde{\omega})\mathcal{G}^{21}(\tilde{\omega}-\omega) \\
& -\mathcal{S}_L^{11}(\tilde{\omega})\mathcal{G}^{12}(\tilde{\omega})\mathcal{S}_R^{22}(\tilde{\omega})\mathcal{G}^{21}(\tilde{\omega}-\omega) \\
& +\mathcal{S}_L^{12}(\tilde{\omega})\mathcal{G}^{22}(\tilde{\omega})\mathcal{S}_R^{22}(\tilde{\omega})\mathcal{G}^{21}(\tilde{\omega}-\omega)\big\}\,, \\
d_{s2}^{<}(\omega) = -\int \frac{d\tilde{\omega}}{2\pi} \big\{ & \mathcal{S}_L^{11}(\tilde{\omega})\mathcal{G}^{12}(\tilde{\omega}+\omega)\mathcal{S}_R^{21}(\tilde{\omega})\mathcal{G}^{11}(\tilde{\omega}) \\
& -\mathcal{S}_L^{11}(\tilde{\omega})\mathcal{G}^{12}(\tilde{\omega}+\omega)\mathcal{S}_R^{22}(\tilde{\omega})\mathcal{G}^{21}(\tilde{\omega}) \\
& +\mathcal{S}_L^{21}(\tilde{\omega})\mathcal{G}^{12}(\tilde{\omega}+\omega)\mathcal{S}_R^{22}(\tilde{\omega})\mathcal{G}^{22}(\tilde{\omega})\big\}\,, \\
d_{s3}^{<}(\omega) = \int \frac{d\tilde{\omega}}{2\pi} \big\{ & \mathcal{S}_L^{11}(\tilde{\omega}+\omega)\mathcal{G}^{12}(\tilde{\omega}+\omega)\mathcal{S}_R^{21}(\tilde{\omega})\mathcal{G}^{11}(\tilde{\omega}) \\
& -\mathcal{S}_L^{11}(\tilde{\omega}+\omega)\mathcal{G}^{12}(\tilde{\omega}+\omega)\mathcal{S}_R^{22}(\tilde{\omega})\mathcal{G}^{21}(\tilde{\omega}) \\
& -\mathcal{S}_L^{12}(\tilde{\omega}+\omega)\mathcal{G}^{22}(\tilde{\omega}+\omega)\mathcal{S}_R^{21}(\tilde{\omega})\mathcal{G}^{11}(\tilde{\omega}) \\
& +\mathcal{S}_L^{12}(\tilde{\omega}+\omega)\mathcal{G}^{22}(\tilde{\omega}+\omega)\mathcal{S}_R^{22}(\tilde{\omega})\mathcal{G}^{21}(\tilde{\omega})\big\}\,, \\
d_{s4}^{<}(\omega) = \int \frac{d\tilde{\omega}}{2\pi} \big\{ & \mathcal{S}_L^{11}(\tilde{\omega})\mathcal{G}^{11}(\tilde{\omega}+\omega)\mathcal{S}_R^{12}(\tilde{\omega}+\omega)\mathcal{G}^{21}(\tilde{\omega}) \\
& -\mathcal{S}_L^{11}(\tilde{\omega})\mathcal{G}^{12}(\tilde{\omega}+\omega)\mathcal{S}_R^{22}(\tilde{\omega}+\omega)\mathcal{G}^{21}(\tilde{\omega}) \\
& -\mathcal{S}_L^{21}(\tilde{\omega})\mathcal{G}^{11}(\tilde{\omega}+\omega)\mathcal{S}_R^{12}(\tilde{\omega}+\omega)\mathcal{G}^{22}(\tilde{\omega}) \\
& +\mathcal{S}_L^{21}(\tilde{\omega})\mathcal{G}^{12}(\tilde{\omega}+\omega)\mathcal{S}_R^{22}(\tilde{\omega}+\omega)\mathcal{G}^{22}(\tilde{\omega})\big\}\,.
\end{aligned}
$$

The result of $\langle I_L I_R \rangle$ is the sum of all. Now we sort the result to get an impression of the different kind of contributions. Further discussion of these expressions and preliminary results are given in section 4.6.

C Degenerate Perturbation Theory

The singlet-triplet representation of a double quantum dot setup is not able to describe the physical behavior of the system for a very small exchange interaction K. In this chapter we try to provide a calculational tool how to circumvent this problem.

C.1 Retarded Green's function

As has already been discussed in the main text the off-diagonal self energy elements can play a major role in the physics of a double quantum dot system if the singlet-triplet energy gap K is small. In this section we therefore propose a scheme in which the off-diagonal elements can be included. The eigenstates of the retarded Green's function in section C.1.2 and of the advanced Green's function are calculated in section C.1.4. We show some examples and discuss the regimes where the proposed rotation becomes important and then continue with the importance of off-diagonal elements on the lesser Green's function $\mathcal{G}^<$ in section C.2.

C.1.1 Special Case: Spin-Spin Interaction $K = 0$

First we concentrate on the special case that $K = 0$. The singlet s and the triplet state t_0 are in this case degenerate. The ambiguity between the singlet-triplet and product state representation was already discussed in section 2.1. The unperturbed retarded Green's functions are in consequence identical,

$$G^{(0),r}_{ss}(\omega) = G^{(0),r}_{t_0t_0}(\omega) = \frac{1}{\omega + i\delta},$$

since $\omega_s = -3/4K = 0$ and $\omega_{t_0} = 1/4K = 0$. This degeneracy has also an effect if K is small but not zero, as discussed in section C.1.2. Here we discuss the special case for $K = 0$ since we can show for this special case some analytical insight into the importance of the off-diagonal components.

From the equations for the self energy in section 3.3.2 we find, that for $K = 0$ and $G^r_{ss} = G^r_{t_0t_0}$ consequently $\Sigma^r_{ss} = \Sigma^r_{t_0t_0}$ and $\Sigma^r_{st_0} = \Sigma^r_{t_0s}$ at least in lowest order. This is also true in higher order due to an iterative argument and we can therefore state that $G^r_{st_0} = G^r_{t_0s}$.

The expression for the determinant det, Eq. (3.33), can in this case be simplified to

$$\begin{aligned}\det &= \left(\omega - \omega_{t_0} - \Sigma^r_{t_0t_0}\right)\left(\omega - \omega_s - \Sigma^r_{ss}\right) - \Sigma^r_{st_0}\Sigma^r_{t_0s} \\ &= \left(\omega - \Sigma^r_{ss}\right)^2 - \left(\Sigma^r_{st_0}\right)^2 = \left(\omega - \Sigma^r_{ss} - \Sigma^r_{st_0}\right)\left(\omega - \Sigma^r_{ss} + \Sigma^r_{st_0}\right).\end{aligned}$$

The retarded Green's function $G^r_{ss}(\omega)$ for the singlet state is consequently for $K = 0$ given by

$$\begin{aligned} G^r_{ss}(\omega) &= \frac{\left(\omega - \omega_{t_0} - \Sigma^r_{t_0 t_0}\right)}{\det} = \frac{\left(\omega - \Sigma^r_{ss}\right)}{\left(\omega - \Sigma^r_{ss} - \Sigma^r_{st_0}\right)\left(\omega - \Sigma^r_{ss} + \Sigma^r_{st_0}\right)} \\ &= \frac{1}{2}\frac{2\left(\omega - \Sigma^r_{ss}\right) - \Sigma^r_{st_0} + \Sigma^r_{st_0}}{\left(\omega - \Sigma^r_{ss} - \Sigma^r_{st_0}\right)\left(\omega - \Sigma^r_{ss} + \Sigma^r_{st_0}\right)} \\ &= \frac{1}{2}\left(\frac{1}{\omega - \left(\Sigma^r_{ss} - \Sigma^r_{st_0}\right)} + \frac{1}{\omega - \left(\Sigma^r_{ss} + \Sigma^r_{st_0}\right)}\right). \end{aligned} \tag{C.1}$$

In the same manner the off-diagonal $G^r_{st_0}(\omega)$ is given by

$$\begin{aligned} G^r_{st_0}(\omega) &= \frac{\Sigma^r_{st_0}}{\det} = \frac{\Sigma^r_{st_0}}{\left(\omega - \Sigma^r_{ss} - \Sigma^r_{st_0}\right)\left(\omega - \Sigma^r_{ss} + \Sigma^r_{st_0}\right)} \\ &= \frac{1}{2}\frac{\left(\omega - \Sigma^r_{ss}\right) - \left(\omega + \Sigma^r_{ss}\right) + 2\Sigma^r_{st_0}}{\left(\omega - \Sigma^r_{ss} - \Sigma^r_{st_0}\right)\left(\omega - \Sigma^r_{ss} + \Sigma^r_{st_0}\right)} \\ &= \frac{1}{2}\left(\frac{1}{\omega - \left(\Sigma^r_{ss} + \Sigma^r_{st_0}\right)} - \frac{1}{\omega - \left(\Sigma^r_{ss} - \Sigma^r_{st_0}\right)}\right). \end{aligned} \tag{C.2}$$

In the case of zero exchange interaction $K = 0$ the singlet Green's function is the sum of two Lorentzians with two different broadenings $(\Gamma_{ss}(0) + \Gamma_{st_0}(0))/2$ and $(\Gamma^r_{ss}(0) - \Gamma^r_{st_0}(0))/2$ at the resonance, $\epsilon_0 = 0$.

At the same time there exists an off-diagonal Green's function G_{st_0}, Eq. (C.2), which is in contrast given by the difference of the two Lorentzians. The real part of the retarded self energy can become important, see for example Ref. [53]. Thus it has to be included as will be done in a numerical routine.

The result of the two retarded Green's functions in Eqs. (C.1) and (C.2) can be interpreted such that each Lorentzian represents a state. These two states can have different life times corresponding to the different broadenings. The singlet is the symmetric and the off-diagonal is the antisymmetric combination of these two states.

In order to discuss the shape of the two Lorentzians we have to find out which system parameters determine the broadening,

$$\begin{aligned} \Gamma_{ss}(\omega = 0) &= \int \frac{d\epsilon}{2\pi}\left(A_{ss}(\epsilon) + A_{t_- t_-}(\epsilon) + A_{t_+ t_+}(\epsilon)\right)\left(Y^<_L(\epsilon) + Y^<_R(\epsilon)\right), \\ \Gamma_{st_0}(\omega = 0) &= \int \frac{d\epsilon}{2\pi}\left(A_{t_- t_-}(\epsilon) - A_{t_+ t_+}(\epsilon)\right)\left(Y^<_L(\epsilon) - Y^<_R(\epsilon)\right). \end{aligned}$$

If we assume in a first approximation, that the spectral functions are δ function at the resonances $\omega_s = 0$, $\omega_{t_+} = -B$ and $\omega_{t_-} = B$. Thus we find,

$$\begin{aligned} \Gamma_{ss}(0) + \Gamma_{st_0}(0) &= \left(Y^<_L(0) + Y^<_R(0)\right) + 2Y^<_L(B) + 2Y^<_R(-B), \\ \Gamma_{ss}(0) - \Gamma_{st_0}(0) &= \left(Y^<_L(0) + Y^<_R(0)\right) + 2Y^<_L(-B) + 2Y^<_R(B). \end{aligned}$$

Assuming $V_L = V_R = 0$ we find

$$\begin{aligned} \Gamma_{ss}(0) + \Gamma_{st_0}(0) &\propto 2g^2_{\text{all}}T + 4\ 4g^2_L B n_B(B) + 4\ 4g^2_R(-B) n_B(-B), \\ \Gamma_{ss}(0) - \Gamma_{st_0}(0) &\propto 2g^2_{\text{all}}T + 4\ 4g^2_L(-B) n_B(-B) + 4\ 4g^2_R B n_B(B). \end{aligned}$$

If the magnetic field B is larger than the temperature T then the dominant contribution comes from $n_B(-B) \approx -1$,

$$\Gamma_{ss}(0) + \Gamma_{st_0}(0) \propto 4\, 4 g_R^2\, B,$$
$$\Gamma_{ss}(0) - \Gamma_{st_0}(0) \propto 4\, 4 g_L^2\, B.$$

The level width is directly proportional to the magnetic field B and a combination of the Kondo couplings of the left or the right side. If $g_L^2 = g_R^2$ then both broadenings are identical and the off-diagonal vanishes as already discussed in section 3.3.3.

Thus the two Lorentzians can be interpreted as two particles, one connected to the left leads and one to the right leads. This supports the interpretation that the product states of the left spin and right spin is the basis which describes the physics at $K = 0$. The problems in the singlet-triplet representation appears if the life time of the particle coupled to the left leads is different than the life time of a particle to the right leads. Note that this is not an effect of finite voltage, by contrast, it is observed that Γ_{st_0} does not depend on the voltage if $V \gg B$, since the difference between two triplet states enters the expression.

As we have seen before, $G^r_{st_0}$ vanishes if the magnetic field $B = 0$. The width of the Green's function G^r_{ss} is in this case determined by the temperature T.

We have demonstrated in this section that the off-diagonal components are of the same order as the diagonals and therefore important to include into the calculation for small K. How to include them into the calculation is suggested in the next section.

For the following we concentrate on the s-t_0 subspace. In principle the rotation is dependent on the frequency ω. Until we introduce the frequency dependence again, it is assumed that there is an arbitrary but fixed ω which is not written explicitly.

C.1.2 Diagonalization of the Retarded Green's Function $\mathcal{G}^r$

The general solution of the retarded Green's function was shown in Eq. (3.32) on page 48. In principle this is already the solution and we could just continue with the calculation including the off-diagonals. The simple idea we want to put forward here is a rotation of the basis states that make the retarded Green's function diagonal. Therefore we first determine the eigenvalues of the retarded Green's function matrix $\mathcal{G}^r$, i.e. determine the eigenstates of the double quantum dot with the leads. In a finite magnetic field the triplet is non-degenerate and cotunneling will mix the triplet-component $|t_0\rangle$ with the singlet $|s\rangle$. This leads to renormalized spin-excitations at energies $\omega_{1,2}$, corresponding to poles of the retarded Green's functions.

Eigenvalues

The retarded Green's function in the s-t_0 subspace is known to fulfill,

$$\mathcal{G}^r(\omega) = \frac{1}{\det} \begin{pmatrix} T_0 & \Sigma^r_{st_0} \\ \Sigma^r_{t_0 s} & S \end{pmatrix},$$

where

$$S = \omega - \tilde{\omega}_s, \qquad \tilde{\omega}_s = \omega_s + \Sigma^r_{ss}, \qquad \omega_s = -\frac{3}{4}K, \tag{C.3}$$

$$T_0 = \omega - \tilde{\omega}_{t_0}, \qquad \tilde{\omega}_{t_0} = \omega_{t_0} + \Sigma^r_{t_0 t_0}, \qquad \omega_{t_0} = \frac{1}{4}K. \tag{C.4}$$

Thus the determinant det, Eq. (3.33), can be rewritten by

$$\begin{aligned} \det &= \left(\omega - \omega_{t_0} - \Sigma^r_{t_0 t_0}\right)\left(\omega - \omega_s - \Sigma^r_{ss}\right) - \Sigma^r_{st_0}\Sigma^r_{t_0 s} && \text{(C.5)} \\ &= T_0\, S - \Sigma^r_{st_0}\Sigma^r_{t_0 s} = \left(\omega - \omega_1\right)\left(\omega - \omega_2\right), && \text{(C.6)} \end{aligned}$$

where

$$\omega_{1,2} = \frac{1}{2}\left(\tilde{\omega}_{t_0} + \tilde{\omega}_s\right) \mp \frac{1}{2}\sqrt{\left(\tilde{\omega}_{t_0} - \tilde{\omega}_s\right)^2 + 4\Sigma^r_{st_0}\Sigma^r_{t_0 s}}. \tag{C.7}$$

Please note

$$\begin{aligned} \omega_1 + \omega_2 &= \tilde{\omega}_s + \tilde{\omega}_{t_0}, \\ \omega_1 - \omega_2 &= \sqrt{\left(\tilde{\omega}_{t_0} - \tilde{\omega}_s\right)^2 + 4\Sigma^r_{st_0}\Sigma^r_{t_0 s}}. \end{aligned}$$

The eigenvalues of $\mathcal{G}^r$ are two different retarded Green's functions $G^r_{1/2}$

$$\begin{aligned} \det \cdot\, G^r_{1/2} &= \frac{1}{2}\left(S + T_0\right) \mp \frac{1}{2}\sqrt{(S - T_0)^2 + 4\Sigma^r_{st_0}\Sigma^r_{t_0 s}} && \text{(C.8)} \\ &= \omega - \frac{1}{2}\left(\tilde{\omega}_{t_0} + \tilde{\omega}_s\right) \mp \frac{1}{2}\sqrt{\left(\tilde{\omega}_{t_0} - \tilde{\omega}_s\right)^2 + 4\Sigma_{st_0}\Sigma_{t_0 s}} && \text{(C.9)} \end{aligned}$$

Therefore these two eigenvalues correspond to

$$G^r_1 = \frac{\omega - \omega_2}{\det} = \frac{1}{\omega - \omega_1}, \tag{C.10}$$

$$G^r_2 = \frac{\omega - \omega_1}{\det} = \frac{1}{\omega - \omega_2}. \tag{C.11}$$

The eigenvalues of the retarded Green's functions are thus two retarded functions with the resonances at $\mathrm{Re}[\omega_1]$ and $\mathrm{Re}[\omega_2]$ and the broadening $\mathrm{Im}[\omega_1]$ and $\mathrm{Im}[\omega_2]$ respectively,

$$G^r_D(\omega) = \begin{pmatrix} \frac{1}{\omega - \mathrm{Re}[\omega_1(\omega)] - i\mathrm{Im}[\omega_1(\omega)]} & 0 \\ 0 & \frac{1}{\omega - \mathrm{Re}[\omega_2(\omega)] - i\mathrm{Im}[\omega_2(\omega)]} \end{pmatrix}.$$

Both have a finite broadening which can be different as discussed in the special case of $K = 0$ see section C.1.1. Now the eigenvectors regarding to the two eigenvalues are calculated and the basis states that diagonalize the system for different parameter regimes are discussed.

Eigenvectors

In section B.1 we found that $\left[G^r_{st_0}\right]^\dagger = G^a_{t_0 s} = \left[G^r_{t_0 s}\right]^*$. Thus the retarded matrix Green's function is a symmetric $\mathcal{G}^r = [\mathcal{G}^r]^T$, but not hermitian matrix. Therefore the eigenvalues do not have to be real and we have to take care that the eigenvectors from the left and from the right can be different.

The right eigenvectors for $\mathcal{G}^r \vec{r}_{1,2} = G^r_{1,2}\vec{r}_{1,2}$ have to fulfill

$$\begin{aligned}\left(T_0 - \det \cdot G^r_{1,2}\right) x'_{1,2} + \Sigma^r_{st_0}\, y'_{1,2} = 0,\\ \Sigma^r_{t_0 s}\, x'_{1,2} + \left(S - \det \cdot G^r_{1,2}\right) y'_{1,2} = 0.\end{aligned}$$

The eigenvectors are chosen such that in the symmetric case where $\Sigma^r_{st_0} = 0$ they correspond to the vectors in the unrotated basis $\vec{r}_1 = (1,0)^T$ and $\vec{r}_2 = (0,1)^T$,

$$x'_1 = S - \det \cdot G^r_1, \qquad y'_1 = -\Sigma^r_{t_0 s}, \tag{C.12}$$

and

$$x'_2 = \Sigma^r_{st_0}, \qquad y'_2 = -T_0 + \det \cdot G^r_2. \tag{C.13}$$

These definitions imply,

$$\begin{aligned} x'_1 = y'_2 &= \frac{1}{2}\left(\tilde{\omega}_{t_0} - \tilde{\omega}_s\right) + \frac{1}{2}\sqrt{\left(\tilde{\omega}_{t_0} - \tilde{\omega}_s\right)^2 + 4\Sigma^r_{st_0}\Sigma^r_{t_0 s}}, \\ &= \frac{1}{2}\left(S - T_0\right) + \frac{1}{2}\sqrt{\left(S - T_0\right)^2 + 4\Sigma^r_{st_0}\Sigma^r_{t_0 s}}. \end{aligned} \tag{C.14}$$

The left eigenvectors $\underline{l}_i\, \mathcal{G}^r = \lambda_{1,2}\, \underline{l}_{1,2}$ have to fulfill a similar equation,

$$\begin{aligned}\left(T_0 - \det \cdot G^r_{1,2}\right) x'_{1,2} + \Sigma^r_{t_0 s}\, y'_{1,2} = 0,\\ \Sigma^r_{st_0}\, x'_{1,2} + \left(S - \det \cdot G^r_{1,2}\right) y'_{1,2} = 0.\end{aligned}$$

We find the left eigenvectors to be closely related to the eigenvectors from the right

$$\begin{aligned}\underline{l}_1 &= \left(x'_1, -\Sigma^r_{st_0}\right)\\ \underline{l}_2 &= \left(\Sigma^r_{t_0 s}, x'_1\right)\end{aligned}$$

The left and the right eigenvectors are orthogonal and therefore span a vector space denoted as the 1-2 eigenspace or product state basis,

$$\begin{aligned}\underline{l}_1\, \vec{r}_1 &= \left(x'_1, -\Sigma^r_{st_0}\right)\begin{pmatrix} x'_1 \\ -\Sigma^r_{t_0 s}\end{pmatrix} = (x'_1)^2 + \Sigma^r_{st_0}\Sigma^r_{t_0 s} = \mathcal{N}^2,\\ \underline{l}_1\, \vec{r}_2 &= \left(x'_1, -\Sigma^r_{st_0}\right)\begin{pmatrix} \Sigma^r_{st_0} \\ x'_1\end{pmatrix} = x'_1\Sigma^r_{st_0} - \Sigma^r_{st_0}x'_1 = 0.\end{aligned}$$

In order to have an orthonormal basis, we have to normalize all eigenvectors by the normalization constant $\mathcal{N}$ which is defined as [1]

$$\mathcal{N} = \sqrt{(x'_1)^2 + \Sigma^r_{st_0}\Sigma^r_{t_0 s}}. \tag{C.15}$$

[1] The square root of the complex number $\mathcal{N}^2$ is assumed to be taken on the first "Riemann sheet", i.e. the square root is chosen with a positive sign.

We define new normalized coordinates

$$x_1 = x_1'/\mathcal{N}, \tag{C.16}$$
$$x_2^2 = \Sigma^r_{st_0}\Sigma^r_{t_0 s}/\mathcal{N}^2, \tag{C.17}$$

which obey $x_1^2 + x_2^2 = 1$.

Transformation of Retarded Green's Function

The transformation matrix U which transforms the symmetric matrix $\mathcal{G}^r$ into a diagonal matrix G^r_D,

$$G^r_D = \begin{pmatrix} G^r_1 & 0 \\ 0 & G^r_2 \end{pmatrix},$$

is defined by the orthonormal eigenvectors. The rotation is defined by,

$$G^r_D = U^{-1}\mathcal{G}^r U, \tag{C.18}$$
$$\mathcal{G}^r = U G^r_D U^{-1}, \tag{C.19}$$

where

$$U_{\text{left}} = U = \begin{pmatrix} x_1 & \Sigma^r_{st_0}/\mathcal{N} \\ -\Sigma^r_{t_0 s}/\mathcal{N} & x_1 \end{pmatrix}, \tag{C.20}$$
$$U_{\text{right}} = U^{-1} = \begin{pmatrix} x_1 & -\Sigma^r_{st_0}/\mathcal{N} \\ \Sigma^r_{t_0 s}/\mathcal{N} & x_1 \end{pmatrix}. \tag{C.21}$$

For a proof that this rotation provides the correct result, see section C.1.3. U_{left} is created by the two left eigenvectors and U_{right} from the two right eigenvectors. As can be seen from the two equations Eq. (C.20) and (C.21) the two matrices are just the inverse of each other.

For later use it should be remarked here that

$$(G^r_D)^{-1} = \left(U^{-1}\mathcal{G}^r U\right)^{-1} = U^{-1}\left(\mathcal{G}^r\right)^{-1} U.$$

Within the framework of this rotation we can now express the diagonal and off-diagonal retarded Green's functions by the two orthogonal retarded Green's functions G^r_1 and G^r_2. The equivalence is given by

$$\begin{aligned} G^r_{ss} &= x_1^2\, G^r_1 + x_2^2\, G^r_2, \\ G^r_{st_0} &= x_1 \Sigma^r_{st_0}/\mathcal{N}\ \left(G^r_2 - G^r_1\right), \\ G^r_{t_0 s} &= x_1 \Sigma^r_{t_0 s}/\mathcal{N}\ \left(G^r_2 - G^r_1\right), \\ G^r_{t_0 t_0} &= x_2^2\, G^r_1 + x_1^2\, G^r_2. \end{aligned}$$

For example for $\Sigma^r_{st_0} = \Sigma^r_{t_0 s} = 0$ using the definitions of x_1 (Eq. (C.16)) and $\mathcal{N}$ (Eq. (C.15)) we find,

$$G^r_{ss} = G^r_1, \qquad G^r_{st_0} = G^r_{t_0 s} = 0, \qquad G^r_{t_0 t_0} = G^r_2.$$

The eigenvalues $\omega_{1/2} = \frac{1}{2}(\tilde{\omega}_{t_0} - \tilde{\omega}_s) \mp |\tilde{\omega}_{t_0} - \tilde{\omega}_s|$ are given for the upper branch of the square root by $\omega_1 = \tilde{\omega}_s$ and $\omega_2 = \tilde{\omega}_{t_0}$ in this special case. It is also obvious from the eigenvectors $\vec{r}_1 = (1,0)^T$ and $\vec{r}_2 = (0,1)^T$ that the eigenstates thus correspond to the singlet and triplet states.

In the case of zero interaction $K = 0$ the singlet s and triplet t_0 are identical and consequently also $S = T_0$. Additionally it can be assumed that the off-diagonal terms fulfills $\Sigma^r_{st_0} = \Sigma^r_{t_0 s}$ from an iterative argument. The parameters of the transformation are consequently given by $x'_1 = \Sigma^r_{st_0}$, $\mathcal{N} = 2\Sigma^r_{st_0}$ and thus $x_1 = 1/\sqrt{2}$, $x_2^2 = 1/2$. For zero spin-spin interaction we find

$$G^r_{ss} = G^r_{t_0 t_0} = \frac{1}{2}\left(G^r_1 + G^r_2\right),$$
$$G^r_{st_0} = G^r_{t_0 s} = \frac{1}{2}\left(G^r_2 - G^r_1\right).$$

This result is similar to the expression found in section C.1.1. The eigenvectors in the case of $K = 0$ are

$$\vec{r}_1 = \frac{1}{\sqrt{2}}\begin{pmatrix}1\\-1\end{pmatrix} \equiv \frac{1}{\sqrt{2}}\left(|s\rangle - |t_0\rangle\right),$$
$$\vec{r}_2 = \frac{1}{\sqrt{2}}\begin{pmatrix}1\\1\end{pmatrix} \equiv \frac{1}{\sqrt{2}}\left(|s\rangle + |t_0\rangle\right).$$

The state $\vec{r}_2$ corresponds to $|\downarrow\rangle_L|\uparrow\rangle_R$ and $\vec{r}_2$ corresponds to $-|\uparrow\rangle_L|\downarrow\rangle_R$, from the definition of the singlet and triplet states in section 2.1. Thus in the case of $K = 0$ the eigenstates of the retarded Green's function are the states of the product basis.

C.1.3 Proof of the Rotation

We want to prove that the statement

$$\begin{pmatrix} G^r_1 & 0 \\ 0 & G^r_2 \end{pmatrix} = \frac{1}{\mathcal{N}^2}\begin{pmatrix} x'_1 & -\Sigma^r_{st_0} \\ \Sigma^r_{t_0 s} & x'_1 \end{pmatrix}\begin{pmatrix} G^r_{ss} & G^r_{st_0} \\ G^r_{t_0 s} & G^r_{t_0 t_0} \end{pmatrix}\begin{pmatrix} x'_1 & \Sigma^r_{st_0} \\ -\Sigma^r_{t_0 s} & x'_1 \end{pmatrix}$$

is correct. Therefore we check the equivalence of the component $(1,1)$ on the left and right side of the expression

$$\begin{aligned}
& G^r_1 \cdot \mathcal{N}^2 = (x'_1)^2 G^r_{ss} - x'_1\Sigma^r_{t_0 s}G^r_{st_0} - x'_1\Sigma^r_{st_0}G^r_{t_0 s} + \Sigma^r_{st_0}\Sigma^r_{t_0 s}G^r_{t_0 t_0} \\
\Leftrightarrow\ & (G^r_1 \cdot \det)\cdot\mathcal{N}^2 = (x'_1)^2 T_0 - 2x'_1\Sigma^r_{st_0}\Sigma^r_{t_0 s} + \Sigma^r_{st_0}\Sigma^r_{t_0 s}S \\
\Leftrightarrow\ & (S - x'_1)\left[(x'_1)^2 + \Sigma^r_{st_0}\Sigma^r_{t_0 s}\right] = (x'_1)^2 T_0 - 2x'_1\Sigma^r_{st_0}\Sigma^r_{t_0 s} + \Sigma^r_{st_0}\Sigma^r_{t_0 s}S \\
\Leftrightarrow\ & 0 = (x'_1)^2\left[T_0 - S + x'_1\right] + \Sigma^r_{st_0}\Sigma^r_{t_0 s}\left[-2x'_1 + S - S + x'_1\right] \\
\Leftrightarrow\ & 0 = \left[\frac{1}{2}(S - T_0) + \frac{1}{2}\sqrt{\cdots}\right]\left[\frac{1}{2}(T_0 - S) + \frac{1}{2}\sqrt{\cdots}\right] - \Sigma^r_{st_0}\Sigma^r_{t_0 s} \\
\Leftrightarrow\ & 0 = -\frac{1}{4}(S - T_0)^2 + \frac{1}{4}(S - T_0)^2 + \frac{1}{4}4\Sigma^r_{st_0}\Sigma^r_{t_0 s} - \Sigma^r_{st_0}\Sigma^r_{t_0 s}.
\end{aligned}$$

Thus we demonstrated that the statement is true. The transformation produces the diagonal retarded Green's function G^r_1 in the component $(1,1)$.

Additionally we have to show, that the off-diagonal components are zero. For example the entry $(2,1)$ in the matrix gives

$$\begin{aligned}
0 &= (x_1'\Sigma^r_{t_0s}G^r_{ss} - \Sigma^2_{t_0s}G^r_{st_0} + (x_1')^2 G^r_{t_0s} - x_1'\Sigma^r_{t_0s}G_{t_0t_0})/\mathcal{N}^2 \\
\Leftrightarrow 0 &= x_1'(T_0 - S) - \Sigma^r_{st_0}\Sigma^r_{t_0s} + (x_1')^2 \\
\Leftrightarrow 0 &= x_1'(T_0 - S + x_1') - \Sigma^r_{st_0}\Sigma^r_{t_0s} \\
\Leftrightarrow 0 &= \left[\frac{1}{2}(S - T_0) + \frac{1}{2}\sqrt{\dots}\right]\left[\frac{1}{2}(T_0 - S) + \frac{1}{2}\sqrt{\dots}\right] - \Sigma^r_{st_0}\Sigma^r_{t_0s}.
\end{aligned}$$

We reduced the relation to an expression of which we already know that it gives zero.

The other two components $(1,2)$ and $(2,2)$ work out analogously. This proves that we found the right transformation.

C.1.4 Diagonalization of Advanced Green's Function $\mathcal{G}^a$

The advanced Green's function is rotated similarly to the retarded Green's function, but since the Dyson equation $G^a = G^a_0 + G^a_0\Sigma^a G^a$ now includes only the advanced self energy we have to replace every retarded by an advanced in the previous calculation. Then we find new eigenresonances,

$$\omega^a_{1,2} = \frac{1}{2}\left(\omega_{t_0} + \Sigma^a_{t_0t_0} + \omega_s + \Sigma^a_{ss}\right) \mp \frac{1}{2}\sqrt{\left(\omega_{t_0} + \Sigma^a_{t_0t_0} - \omega_s - \Sigma^a_{ss}\right)^2 + 4\Sigma^a_{st_0}\Sigma^a_{t_0s}},$$

and consequently have to change the definition by

$$\begin{aligned}
(x^a_1)' &= \frac{1}{2}\left(\omega_{t_0} + \Sigma^a_{t_0t_0} - \omega_s - \Sigma^a_{ss}\right) + \frac{1}{2}\sqrt{\left(\omega_{t_0} + \Sigma^a_{t_0t_0} - \omega_s - \Sigma^a_{ss}\right)^2 + 4\Sigma^a_{st_0}\Sigma^a_{t_0s}}, \\
\mathcal{N}^a &= \sqrt{[(x^a_1)']^2 + \Sigma^a_{st_0}\Sigma^a_{t_0s}}, \\
x^a_1 &= (x^a_1)'/\mathcal{N}^a.
\end{aligned}$$

Thus the rotation is given by

$$G^a_D = (U^a)^{-1}\mathcal{G}^a U^a, \tag{C.22}$$

$$\mathcal{G}^a = U^a G^a_D (U^a)^{-1}, \tag{C.23}$$

where

$$U^a = \begin{pmatrix} x^a_1 & \Sigma^a_{st_0}/\mathcal{N} \\ -\Sigma^a_{t_0s}/\mathcal{N} & x^a_1 \end{pmatrix}, \tag{C.24}$$

$$(U^a)^{-1} = \begin{pmatrix} x^a_1 & -\Sigma^a_{st_0}/\mathcal{N} \\ \Sigma^a_{t_0s}/\mathcal{N} & x^a_1 \end{pmatrix}.$$

If the real part of the self energy is neglected, then we find using $\mathrm{Im}\Sigma^a = -i(\mathrm{Im}\Sigma^r)^*$ that $U^a = U^*$. This will be used in the numerical routine later on.

C.2 Lesser Green's Function or the Quantum Boltzmann Equation

C.2.1 Special case for Zero Exchange Interaction $K = 0$

In the special case of $K = 0$ we know, that $A_{ss} = A_{t_0t_0}$ and consequently $G^<_{ss} = G^<_{t_0t_0}$ since $\Sigma^<_{ss} = \Sigma^<_{t_0t_0}$ and $\Gamma_{ss} = \Gamma_{t_0t_0}$. Additionally we find $G^<_{st_0} = G^<_{t_0s}$ also from iterative arguments.

Due to the degeneracy at the special point $K = 0$ we only have to solve two independent equations,

$$\begin{aligned}&\left[(G^r)^{-1}_{ss} - (G^a)^{-1}_{ss}\right] G^<_{ss} + \left[(G^r)^{-1}_{st_0} - (G^a)^{-1}_{st_0}\right] G^<_{st_0}\\ =&\Sigma^<_{ss}\left[G^a_{ss} - G^r_{ss}\right] + \Sigma^<_{st_0}\left[G^a_{st_0} - G^r_{st_0}\right]\end{aligned}$$

and

$$\begin{aligned}&\left[(G^r)^{-1}_{ss} - (G^a)^{-1}_{ss}\right] G^<_{st_0} + \left[(G^r)^{-1}_{st_0} - (G^a)^{-1}_{st_0}\right] G^<_{ss}\\ =&\Sigma^<_{ss}\left[G^a_{st_0} - G^r_{st_0}\right] + \Sigma^<_{st_0}\left[G^a_{ss} - G^r_{ss}\right].\end{aligned}$$

Now we assume $G^r - G^a = -iA$ and $(G^r)^{-1} - (G^a)^{-1} = -2i\Gamma$ and find

$$2\Gamma_{ss}G^<_{ss} + 2\Gamma_{st_0}G^<_{st_0} = 2\Sigma^<_{ss}A_{ss} + 2\Sigma^<_{st_0}A_{st_0}, \tag{C.25}$$

$$2\Gamma_{ss}G^<_{st_0} + 2\Gamma_{st_0}G^<_{ss} = 2\Sigma^<_{ss}A_{st_0} + 2\Sigma^<_{st_0}A_{ss}. \tag{C.26}$$

In a previous calculation in section C.1.1 we already used the linear combinations for the retarded Green's functions

$$A_{ss} = \frac{1}{2}(A_+ + A_-) \qquad A_{st_0} = \frac{1}{2}(A_+ - A_-)$$

or

$$A_+ = A_{ss} + A_{st_0} \qquad A_- = A_{ss} - A_{st_0} \tag{C.27}$$

Now we define similarly for the lesser Green's functions

$$G^<_+ = G^<_{ss} + G^<_{st_0} \qquad G^<_- = G^<_{ss} - G^<_{st_0}$$

or

$$G^<_{ss} = \frac{1}{2}\left(G^<_+ + G^<_-\right) \qquad G^<_{st_0} = \frac{1}{2}\left(G^<_+ - G^<_-\right) \tag{C.28}$$

If we take the sum and the difference of Eqs. (C.25) and (C.26), we find

$$\begin{aligned}2\left(\Gamma_{ss} + \Gamma_{st_0}\right)\left(G^<_{ss} + G^<_{st_0}\right) &= 2\left(\Sigma^<_{ss} + \Sigma^<_{st_0}\right)\left(A_{ss} + A_{st_0}\right),\\ 2\left(\Gamma_{ss} - \Gamma_{st_0}\right)\left(G^<_{ss} - G^<_{st_0}\right) &= 2\left(\Sigma^<_{ss} - \Sigma^<_{st_0}\right)\left(A_{ss} - A_{st_0}\right).\end{aligned}$$

Using the definitions from Eq. (C.27) and Eq. (C.28), we receive a set of diagonal equations,

$$\begin{aligned}(\Gamma_{ss} + \Gamma_{st_0})\, G_+^< &= \left(\Sigma_{ss}^< + \Sigma_{st_0}^<\right) A_+, \\ (\Gamma_{ss} - \Gamma_{st_0})\, G_-^< &= \left(\Sigma_{ss}^< - \Sigma_{st_0}^<\right) A_-.\end{aligned}$$

With the second order self energies from Eqs. (3.14) to (3.19) we receive the following set of equations,

$$\begin{aligned}&\int \frac{d\epsilon}{2\pi} \big[2A_{t_-}(\epsilon) Y_L^<(\epsilon-\omega) + 2A_{t_+}(\epsilon) Y_R^<(\epsilon-\omega) \\ &\qquad + A_+(\epsilon)\left(Y_L^< + Y_R^<\right)(\epsilon-\omega)\big]\, n_+(\omega) A_+(\omega) \\ =&\int \frac{d\epsilon}{2\pi} \big[2n_{t_-}(\epsilon) A_{t_-}(\epsilon) Y_L^<(\omega-\epsilon) + 2n_{t_+}(\epsilon) A_{t_+}(\epsilon) Y_R^<(\omega-\epsilon) \\ &\qquad + n_+(\epsilon) A_+(\epsilon)\left(Y_L^< + Y_R^<\right)(\omega-\epsilon)\big]\, A_+(\omega), \qquad \text{(C.29)} \\ &\int \frac{d\epsilon}{2\pi} \big[2A_{t_-}(\epsilon) Y_R^<(\epsilon-\omega) + 2A_{t_+}(\epsilon) Y_L^<(\epsilon-\omega) \\ &\qquad + A_-(\epsilon)\left(Y_L^< + Y_R^<\right)(\epsilon-\omega)\big]\, n_-(\omega) A_-(\omega) \\ =&\int \frac{d\epsilon}{2\pi} \big[2n_{t_-}(\epsilon) A_{t_-}(\epsilon) Y_R^<(\omega-\epsilon) + 2n_{t_+}(\epsilon) A_{t_+}(\epsilon) Y_L^<(\omega-\epsilon) \\ &\qquad + n_-(\epsilon) A_-(\epsilon)\left(Y_L^< + Y_R^<\right)(\omega-\epsilon)\big]\, A_-(\omega), \qquad \text{(C.30)}\end{aligned}$$

$$\begin{aligned}&\int \frac{d\epsilon}{2\pi} \big[2A_+(\epsilon) Y_R^<(\epsilon-\omega) + 2A_-(\epsilon) Y_L^<(\epsilon-\omega) \\ &\qquad + A_{t_+}(\epsilon)\left(Y_L^< + Y_R^<\right)(\epsilon-\omega)\big]\, n_{t_+}(\omega) A_{t_+}(\omega) \\ =&\int \frac{d\epsilon}{2\pi} \big[2n_+(\epsilon) A_+(\epsilon) Y_R^<(\omega-\epsilon) + 2n_-(\epsilon) A_-(\epsilon) Y_L^<(\omega-\epsilon) \\ &\qquad + n_{t_+}(\epsilon) A_{t_+}(\epsilon)\left(Y_L^< + Y_R^<\right)(\omega-\epsilon)\big]\, A_{t_+}(\omega), \qquad \text{(C.31)} \\ &\int \frac{d\epsilon}{2\pi} \big[2A_+(\epsilon) Y_L^<(\epsilon-\omega) + 2A_-(\epsilon) Y_R^<(\epsilon-\omega) \\ &\qquad + A_{t_-}(\epsilon)\left(Y_L^< + Y_R^<\right)(\epsilon-\omega)\big]\, n_{t_-}(\omega) A_{t_-}(\omega) \\ =&\int \frac{d\epsilon}{2\pi} \big[2n_+(\epsilon) A_+(\epsilon) Y_L^<(\omega-\epsilon) + 2n_-(\epsilon) A_-(\epsilon) Y_R^<(\omega-\epsilon) \\ &\qquad + n_{t_-}(\epsilon) A_{t_-}(\epsilon)\left(Y_L^< + Y_R^<\right)(\omega-\epsilon)\big]\, A_{t_-}(\omega). \qquad \text{(C.32)}\end{aligned}$$

This is only valid in the case of $K = 0$. Please note, that one can immediately see from this set of equations that for $Y_L^< = Y_R^<$ the distribution functions n_+ and n_- fulfill the same equations.

This representation is diagonal in the spectral functions $A_+, A_-, A_{t_+}, A_{t_-}$. Thus we can cancel $A_i(\omega)$ on each side of each equation and still the equation is valid for every frequency ω.

For the constraint we use $G_{ss}^< + G_{t_0t_0}^< = 2\,\frac{1}{2}\left(G_+^< + G_-^<\right)$

$$\int \frac{d\epsilon}{2\pi} \left[n_+(\epsilon) A_+(\epsilon) + n_-(\epsilon) A_-(\epsilon) + n_{t_-}(\epsilon) A_{t_-}(\epsilon) + n_{t_+}(\epsilon) A_{t_+}(\epsilon)\right] = 1 \qquad \text{(C.33)}$$

We assume $G_i^<(\omega) = -in_i(\omega_i)A_i(\omega)$. The distribution functions are assumed to be frequency independent and the equations are considered at $\omega = \omega_i$. We introduce for the coefficients two different expressions for the two different convolutions

$$a_i^\alpha(\omega) = \int \frac{d\epsilon}{2\pi} A_i(\epsilon) Y_\alpha^<(\omega - \epsilon), \tag{C.34}$$

$$b_i^\alpha(\omega) = \int \frac{d\epsilon}{2\pi} A_i(\epsilon) Y_\alpha^<(\epsilon - \omega). \tag{C.35}$$

and can then rewrite the set of equations Eqs. (C.29), (C.30), (C.31), and (C.32) by

$$\left(b_{t_-}^L(-\omega_+) + b_{t_+}^R(-\omega_+)\right) n_+ = a_{t_-}^L(\omega_+) n_{t_-} + a_{t_+}^R(\omega_+) n_{t_+}, \tag{C.36}$$

$$\left(b_{t_-}^R(-\omega_-) + b_{t_+}^L(-\omega_-)\right) n_- = a_{t_-}^R(\omega_-) n_{t_-} + a_{t_+}^L(\omega_-) n_{t_+}, \tag{C.37}$$

$$\left(b_{+}^R(-\omega_{t_+}) + b_{-}^L(-\omega_{t_+})\right) n_{t_+} = a_{+}^R(\omega_{t_+}) n_+ + a_{-}^L(\omega_{t_+}) n_-, \tag{C.38}$$

$$\left(b_{+}^L(-\omega_{t_-}) + b_{-}^R(-\omega_{t_-})\right) n_{t_-} = a_{+}^L(\omega_{t_-}) n_+ + a_{-}^R(\omega_{t_-}) n_-, \tag{C.39}$$

and the constraint

$$n_+ + n_- + n_{t_+} + n_{t_-} = 1. \tag{C.40}$$

If the magnetic field B is large, the width of the spectral function of t_+ and t_- is not important and we can approximate it by a δ-function at the corresponding resonance. In A_+ and A_- the width is important. Nevertheless we can neglect the width of A_+ and A_- in a_i^α and b_i^α, because the width is much smaller than the energy scale on which Y_α changes.

$$a_i^\alpha(\omega) \approx Y_\alpha^<(\omega - \omega_i),$$
$$b_i^\alpha(\omega) \approx Y_\alpha^<(\omega_i - \omega).$$

Since the exchange interaction is zero, $K = 0$, the resonances are given by $\omega_+ = 0$, $\omega_- = 0$, $\omega_{t_+} = -B$ and $\omega_{t_-} = B$. The set of equations (C.36), (C.37), (C.38) and (C.39) now becomes

$$\left(Y_L^<(B) + Y_R^<(-B)\right) n_+ = Y_L^<(-B) n_{t_-} + Y_R^<(B) n_{t_+}, \tag{C.41}$$

$$\left(Y_L^<(-B) + Y_R^<(B)\right) n_- = Y_R^<(-B) n_{t_-} + Y_L^<(B) n_{t_+}, \tag{C.42}$$

$$\left(Y_L^<(B) + Y_R^<(B)\right) n_{t_+} = Y_R^<(-B) n_+ + Y_L^<(-B) n_-, \tag{C.43}$$

$$\left(Y_L^<(-B) + Y_R^<(-B)\right) n_{t_-} = Y_L^<(B) n_+ + Y_R^<(B) n_-. \tag{C.44}$$

Please note, that the sum of Eq. (C.41) and Eq. (C.42) is equal to the sum of of Eq. (C.43) and Eq. (C.44). The system of equations is underdetermined. We need the additional information of the constraint Eq. (C.40) to find solutions for the distribution functions.

The solutions are

$$n_+ = \frac{Y_L(-B)Y_R(B)}{\left(Y_L(-B) + Y_L(B)\right)\left(Y_R(-B) + Y_R(B)\right)}, \tag{C.45}$$

$$n_- = \frac{Y_L(B)Y_R(-B)}{\left(Y_L(-B) + Y_L(B)\right)\left(Y_R(-B) + Y_R(B)\right)}, \tag{C.46}$$

$$n_{t_-} = \frac{Y_L(B)Y_R(B)}{\left(Y_L(-B) + Y_L(B)\right)\left(Y_R(-B) + Y_R(B)\right)}, \tag{C.47}$$

$$n_{t_+} = \frac{Y_L(-B)Y_R(-B)}{\left(Y_L(-B) + Y_L(B)\right)\left(Y_R(-B) + Y_R(B)\right)}. \tag{C.48}$$

One can immediately see that the solution is in principle the occupation of product states, for example the expression

$$n_+ = \frac{Y_L(-B)}{(Y_L(-B)+Y_L(B))} \cdot \frac{Y_R(B)}{(Y_R(-B)+Y_R(B))}$$

represents the state $|1\rangle = |\uparrow\rangle_L|\downarrow\rangle_R$ and the occupation is just the product of the known distribution for spin $\uparrow$ left and spin $\downarrow$ right.

For example the magnetization of the whole spin system is

$$\begin{aligned} M_{\text{tot}} &= 2\langle \vec{S}_L^z + \vec{S}_R^z \rangle = 2\langle t_+ t_+ - t_- t_- \rangle \\ &= 2\frac{Y_L(-B)Y_R(-B) - Y_L(B)Y_R(B)}{(Y_L(-B)+Y_L(B))\,(Y_R(-B)+Y_R(B))} \end{aligned}$$

The total magnetization depends on both the left and the right side.

Now we calculate the magnetization only of one quantum dot, which is most reasonable since for $K = 0$ both spins are not coupled. The z component of the left impurity spin is defined by (see Eq. (2.4) in section 2.1 on page 11)

$$\vec{S}_L^z = \frac{1}{2}\left(s^\dagger t_0 + t_0^\dagger s + t_+^\dagger t_+ - t_-^\dagger t_-\right).$$

If we neglect the st_0 contributions, then M_L would be exactly the same as $M_{\text{tot}}/2$ and consequently dependent on the properties of the right dot. It is important that for small or zero K interaction the off-diagonal contributions have to be taken into account. Thus we find in this chapter that $\langle s^\dagger t_0 + t_0^\dagger s\rangle$ is finite and gives,

$$\begin{aligned} \langle s^\dagger t_0 + t_0^\dagger s\rangle = \langle \vec{S}_L - \vec{S}_R\rangle &= 2\int d\omega \frac{1}{2}\left(G_+^< - G_-^<\right) = n_+ - n_- \\ &= \frac{Y_L(-B)Y_R(B) - Y_L(B)Y_R(-B)}{(Y_L(-B)+Y_L(B))\,(Y_R(-B)+Y_R(B))}. \end{aligned}$$

Please note that this average, which is proportional to $n_+ - n_-$ is of the same order of magnitude as $n_{t_+} - n_{t_-}$.

Finally taking into account this additional contribution, we get for the magnetization of the left and the right impurity

$$\begin{aligned} M_L = 2\langle S_L^z\rangle &= n_+ - n_- + n_{t_+} - n_{t_-} = \frac{Y_L(-B) - Y_L(B)}{Y_L(-B) + Y_L(B)} \\ M_R = 2\langle S_R^z\rangle &= -n_+ + n_- + n_{t_+} - n_{t_-} = \frac{Y_R(-B) - Y_R(B)}{Y_R(-B) + Y_R(B)} \end{aligned}$$

This is exactly the result we would expect for uncoupled quantum dots. The magnetization on the left and right impurity are decoupled from each other. By using the new basis states + and − and taking into account all off-diagonal terms we could show, that the basis of singlet-triplet does not give wrong results even for $K = 0$ although a level system with singlet and triplets by itself does no longer exist.

C.2.2 General Case for Finite K

So far the Dyson equation was solved for the retarded and advanced Green's functions. In order to find a solution for the lesser Green's function we have to solve the following matrix equation, Eq. (3.36),

$$\Sigma^{<}\mathcal{G}^{a} - \mathcal{G}^{r}\Sigma^{<} = (\mathcal{G}^{r})^{-1}\,\mathcal{G}^{<} - \mathcal{G}^{<}\,(\mathcal{G}^{a})^{-1}\,.$$

To make use of the diagonalized functions introduced above, we multiply this expression by U^r from the left and $(U^a)^{-1}$ from the right. Thus we find

$$\tilde{\Sigma}^{<}G_D^a - G_D^r\tilde{\Sigma}^{<} = (G_D^r)^{-1}\,\tilde{G}^{<} - \tilde{G}^{<}\,(G_D^a)^{-1}\,, \tag{C.49}$$

where

$$\tilde{\Sigma}^{<} = U^r\Sigma^{<}(U^a)^{-1}, \tag{C.50}$$
$$\tilde{G}^{<} = U^r\mathcal{G}^{<}(U^a)^{-1}, \tag{C.51}$$

and vice versa

$$\Sigma^{<} = (U^r)^{-1}\tilde{\Sigma}^{<}U^a,$$
$$\mathcal{G}^{<} = (U^r)^{-1}\tilde{G}^{<}U^a.$$

This implies for the lesser Green's functions in s-t_0 space,

$$\begin{aligned}
G^{<}_{ss} &= \left(x_1^r x_1^a G^{<}_{(1,1)} - x_1^r\Sigma^{a'}_{t_0 s}G^{<}_{(1,2)} - \Sigma^{r'}_{t_0 s}x_1^a G^{<}_{(2,1)} + \Sigma^{r'}_{st_0}\Sigma^{a'}_{t_0 s}G^{<}_{(2,2)}\right),\\
G^{<}_{st_0} &= \left(x_1^r\Sigma^{a'}_{st_0}G^{<}_{(1,1)} + x_1^r x_1^a G^{<}_{(1,2)} - \Sigma^{r'}_{st_0}\Sigma^{a'}_{t_0 s}G^{<}_{(2,1)} - \Sigma^{r'}_{st_0}x_1^a G^{<}_{(2,2)}\right),\\
G^{<}_{t_0 s} &= \left(\Sigma^{r'}_{t_0 s}x_1^a G^{<}_{(1,1)} - \Sigma^{r'}_{t_0 s}\Sigma^{a'}_{st_0}G^{<}_{(1,2)} + x_1^r x_1^a G^{<}_{(2,1)} - x_1^r\Sigma^{a'}_{t_0 s}G^{<}_{(2,2)}\right),\\
G^{<}_{t_0 t_0} &= \left(\Sigma^{r'}_{t_0 s}\Sigma^{a'}_{st_0}G^{<}_{(1,1)} + \Sigma^{r'}_{t_0 s}x_1^a G^{<}_{(1,2)} + x_1^r\Sigma^{a'}_{st_0}G^{<}_{(2,1)} + x_1^r x_1^a G^{<}_{(2,2)}\right),
\end{aligned}$$

where $\Sigma^{r'} = \Sigma^r/\mathcal{N}^r$ and $\Sigma^{a'} = \Sigma^a/\mathcal{N}^a$.

Expression for $\tilde{\Sigma}$

Next step would be to calculate the new self energy matrix $\tilde{\Sigma}$ by doing the rotation $U^r\Sigma(U^a)^{-1}$ and then inserting the expression for the Green's function G_{ss} etc.

Alternatively, the self energy can be calculated from a matrix product as defined in Eq. (3.13) on page 44,

$$\Sigma(\tau_1,\tau_2) = -\frac{1}{16}\sum_\alpha Y_\alpha(\tau_1,\tau_2)\vec{\mathbf{T}}_\alpha\mathcal{G}(\tau_1,\tau_2)\vec{\mathbf{T}}_\alpha,$$

in the general matrix representation.

Thus the self energy matrix which has to be transformed by $U^r\Sigma^{<}(U^a)^{-1}$ becomes under inserting $\mathcal{G} = (U^r)^{-1}\tilde{G}U^a$

$$\begin{aligned}
&\mathbf{U}^r\boldsymbol{\Sigma}(\omega)(\mathbf{U}^a)^{-1}\\
&= -\frac{1}{16}\sum_\alpha\int\frac{d\epsilon}{2\pi}Y^{<}_\alpha(\omega-\epsilon)\mathbf{U}^r(\omega)\vec{\mathbf{T}}^i_\alpha(\mathbf{U}^r)^{-1}(\epsilon)\tilde{G}^{<}(\epsilon)\mathbf{U}^a(\epsilon)\vec{\mathbf{T}}^j_\alpha(\mathbf{U}^a)^{-1}(\omega)
\end{aligned}$$

Consequently the self energy can be written in a new form, where only the pseudo Pauli matrices are changed,

$$\begin{aligned}\tilde{\mathbf{\Sigma}}^{<}(\omega) =& \mathbf{U}^r(\omega)\Sigma^{<}(\omega)(\mathbf{U}^a)^{-1}(\omega) \\ =& -\frac{1}{16}\int\frac{d\epsilon}{2\pi}\left(\tilde{\mathbf{T}}^i_L(\omega,\epsilon)\right)^r\tilde{\mathbf{G}}(\epsilon)\left(\tilde{\mathbf{T}}^j_L(\epsilon,\omega)\right)^a\tau^i_{\sigma\sigma'}\tau^j_{\sigma'\sigma}Y_L(\omega-\epsilon) \\ & -\frac{1}{16}\int\frac{d\epsilon}{2\pi}\left(\tilde{\mathbf{T}}^i_R(\omega,\epsilon)\right)^r\tilde{\mathbf{G}}(\epsilon)\left(\tilde{\mathbf{T}}^j_R(\epsilon,\omega)\right)^a\tau^i_{\sigma\sigma'}\tau^j_{\sigma'\sigma}Y_R(\omega-\epsilon),\end{aligned}$$

where

$$\begin{aligned}\left(\tilde{\mathbf{T}}_\alpha(\omega,\epsilon)\right)^r &= \mathbf{U}^r(\omega)\,\mathbf{T}^i_\alpha\,(\mathbf{U}^r)^{-1}(\epsilon), \\ \left(\tilde{\mathbf{T}}_\alpha(\omega,\epsilon)\right)^a &= \mathbf{U}^a(\omega)\,\mathbf{T}^i_\alpha\,(\mathbf{U}^a)^{-1}(\epsilon).\end{aligned}$$

To simplify the expression it is assumed in the following that the real part of the retarded and advanced self energy is negligible. Thus $i\mathrm{Im}\Sigma^r_{st_0} = -i\mathrm{Im}\Sigma^a_{st_0}$ and the two rotations U^r and U^a are related to each other by the complex conjugate. It is also assumed that $\Gamma_{st_0} = \Gamma_{t_0 s}$. Using these assumptions we find

$$\tilde{\mathbf{T}}^z_L(\omega,\epsilon) = \begin{pmatrix} A(\omega,\epsilon) & 0 & B(\omega,\epsilon) & 0 \\ 0 & 1 & 0 & 0 \\ B(\omega,\epsilon) & 0 & -A(\omega,\epsilon) & 0 \\ 0 & 0 & 0 & -1 \end{pmatrix} \qquad \tilde{\mathbf{T}}^z_R(\omega,\epsilon) = \begin{pmatrix} -A(\omega,\epsilon) & 0 & -B(\omega,\epsilon) & 0 \\ 0 & 1 & 0 & 0 \\ -B(\omega,\epsilon) & 0 & A(\omega,\epsilon) & 0 \\ 0 & 0 & 0 & -1 \end{pmatrix}$$

$$\tilde{\mathbf{T}}^+_L(\omega,\epsilon) = \begin{pmatrix} 0 & 0 & 0 & a(\omega) \\ -b(\epsilon) & 0 & a(\epsilon) & 0 \\ 0 & 0 & 0 & b(\omega) \\ 0 & 0 & 0 & 0 \end{pmatrix} \qquad \tilde{\mathbf{T}}^+_R(\omega,\epsilon) = \begin{pmatrix} 0 & 0 & 0 & -b(\omega) \\ a(\epsilon) & 0 & b(\epsilon) & 0 \\ 0 & 0 & 0 & a(\omega) \\ 0 & 0 & 0 & 0 \end{pmatrix}$$

$$\tilde{\mathbf{T}}^-_L(\omega,\epsilon) = \begin{pmatrix} 0 & -b(\omega) & 0 & 0 \\ 0 & 0 & 0 & 0 \\ 0 & a(\omega) & 0 & 0 \\ a(\epsilon) & 0 & b(\epsilon) & 0 \end{pmatrix} \qquad \tilde{\mathbf{T}}^-_R(\omega,\epsilon) = \begin{pmatrix} 0 & a(\omega) & 0 & 0 \\ 0 & 0 & 0 & 0 \\ 0 & b(\omega) & 0 & 0 \\ -b(\epsilon) & 0 & a(\epsilon) & 0 \end{pmatrix}$$

After the transformation the difference between left and right pseudo Pauli matrix is even more significant, which is consistent with the observation that the product states become most important if there is a left-right asymmetry.

In the definition of $\tilde{T}_\alpha$ the following notations were used

$$\begin{aligned}a(\omega) &= \left(x_2(\omega) + x_1(\omega)\right), \\ b(\omega) &= \left(x_1(\omega) - x_2(\omega)\right),\end{aligned}$$

and

$$\begin{aligned}A(\omega,\epsilon) &= \frac{1}{2}\left(a(\omega)a(\epsilon) - b(\omega)b(\epsilon)\right), \\ B(\omega,\epsilon) &= \frac{1}{2}\left(a(\omega)b(\epsilon) + b(\omega)a(\epsilon)\right).\end{aligned}$$

Furthermore

$$x_1'(\omega) = \frac{1}{2}(S(\omega) - T_0(\omega)) + \frac{1}{2}\sqrt{(S(\omega) - T_0(\omega))^2 - \Gamma_{st_0}^2(\omega)}$$
$$x_2'(\omega) = -i\Gamma_{st_0}(\omega)/2$$

where $S(\omega) = \omega - \omega_s + i\Gamma_{ss}(\omega)/2$ and $T_0(\omega) = \omega - \omega_{t_0} + i\Gamma_{t_0t_0}(\omega)/2$. Analogous to previous calculations we define the normalized values,

$$x_1 = \frac{x_1'}{(x_1')^2 + (x_2')^2}, \qquad x_2 = \frac{x_2'}{(x_1')^2 + (x_2')^2}.$$

Please note, that a, b, A and B are in general complex functions of the frequency arguments. The following symmetry relations hold

$$A(\omega, \epsilon) = A(\epsilon, \omega),$$
$$B(\omega, \epsilon) = B(\epsilon, \omega).$$

Due to the normalization $x_1^2 + x_2^2 = 1$ we find

$$a^2(\omega) + b^2(\omega) = 2.$$

In the two limiting cases these complex functions simplify to numbers. For example in the case of the off-diagonal $\Gamma_{st_0} = 0$ and therefore $x_2 = 0$, the rotation is just the unity operation,

$$a(\omega) = 1, \qquad b(\omega) = 1, \qquad A(\omega, \epsilon) = 0, \qquad B(\omega, \epsilon) = 1.$$

Thus $\tilde{T}$ is identical to the initial T. In this case the singlet-triplet states are the right basis choice and we find the result for the occupation numbers like states in section 4.1.

And if the exchange interaction $K = 0$ is zero than $x_1 = -x_2$ and we find

$$a(\omega) = 0, \qquad b(\omega) = \sqrt{2}, \qquad A(\omega, \epsilon) = -1, \qquad B(\omega, \epsilon) = 0.$$

Now left and right quantum dot spin couple to completely different states already observed in section C.2.1.

C.2.3 Explicit Expressions of Self Energies

The diagonal parts of the transformed self energy are given by

$$\begin{aligned}\tilde{\Sigma}_{(1,1)}^{<}(\omega) = \int d\epsilon \Big[& A(\omega,\epsilon)A^*(\epsilon,\omega)\left(Y_L^<(\omega-\epsilon) + Y_R^<(\omega-\epsilon)\right) G_{(1,1)}^<(\epsilon) \\ & + A(\omega,\epsilon)B^*(\epsilon,\omega)\left(Y_L^<(\omega-\epsilon) + Y_R^<(\omega-\epsilon)\right) G_{(1,2)}^<(\epsilon) \\ & + B(\omega,\epsilon)A^*(\epsilon,\omega)\left(Y_L^<(\omega-\epsilon) + Y_R^<(\omega-\epsilon)\right) G_{(2,1)}^<(\epsilon) \\ & + B(\omega,\epsilon)B^*(\epsilon,\omega)\left(Y_L^<(\omega-\epsilon) + Y_R^<(\omega-\epsilon)\right) G_{(2,2)}^<(\epsilon) \\ & + \left(a(\omega)a^*(\omega)Y_L^<(\omega-\epsilon) + b(\omega)b^*(\omega)Y_R^<(\omega-\epsilon)\right) G_{t_-}^<(\epsilon) \\ & + \left(b(\omega)b^*(\omega)Y_L^<(\omega-\epsilon) + a(\omega)a^*(\omega)Y_R^<(\omega-\epsilon)\right) G_{t_+}^<(\epsilon)\Big], \end{aligned} \tag{C.52}$$

$$\begin{aligned}\tilde{\Sigma}^<_{(2,2)}(\omega) = \int d\epsilon \Big[& B(\omega,\epsilon)B^*(\epsilon,\omega)\left(Y_L^<(\omega-\epsilon)+Y_R^<(\omega-\epsilon)\right)G^<_{(1,1)}(\epsilon) \\ & -B(\omega,\epsilon)A^*(\epsilon,\omega)\left(Y_L^<(\omega-\epsilon)+Y_R^<(\omega-\epsilon)\right)G^<_{(1,2)}(\epsilon) \\ & -A(\omega,\epsilon)B^*(\epsilon,\omega)\left(Y_L^<(\omega-\epsilon)+Y_R^<(\omega-\epsilon)\right)G^<_{(2,1)}(\epsilon) \\ & +A(\omega,\epsilon)A^*(\epsilon,\omega)\left(Y_L^<(\omega-\epsilon)+Y_R^<(\omega-\epsilon)\right)G^<_{(2,2)}(\epsilon) \\ & +\left(b(\omega)b^*(\omega)Y_L^<(\omega-\epsilon)+a(\omega)a^*(\omega)Y_R^<(\omega-\epsilon)\right)G^<_{t_-}(\epsilon) \\ & +\left(a(\omega)a^*(\omega)Y_L^<(\omega-\epsilon)+b(\omega)b^*(\omega)Y_R^<(\omega-\epsilon)\right)G^<_{t_+}(\epsilon)\Big], \end{aligned} \tag{C.53}$$

and the off-diagonal parts are found

$$\begin{aligned}\tilde{\Sigma}^<_{(1,2)}(\omega) = \int d\epsilon \Big[& A(\omega,\epsilon)B^*(\epsilon,\omega)\left(Y_L^<(\omega-\epsilon)+Y_R^<(\omega-\epsilon)\right)G^<_{(1,1)}(\epsilon) \\ & -A(\omega,\epsilon)A^*(\epsilon,\omega)\left(Y_L^<(\omega-\epsilon)+Y_R^<(\omega-\epsilon)\right)G^<_{(1,2)}(\epsilon) \\ & +B(\omega,\epsilon)B^*(\epsilon,\omega)\left(Y_L^<(\omega-\epsilon)+Y_R^<(\omega-\epsilon)\right)G^<_{(2,1)}(\epsilon) \\ & +B(\omega,\epsilon)A^*(\epsilon,\omega)\left(Y_L^<(\omega-\epsilon)+Y_R^<(\omega-\epsilon)\right)G^<_{(2,2)}(\epsilon) \\ & +\left(a(\omega)b^*(\omega)Y_L^<(\omega-\epsilon)-b(\omega)a^*(\omega)Y_R^<(\omega-\epsilon)\right)G^<_{t_-}(\epsilon) \\ & +\left(-b(\omega)a^*(\omega)Y_L^<(\omega-\epsilon)+a(\omega)b^*(\omega)Y_R^<(\omega-\epsilon)\right)G^<_{t_+}(\epsilon)\Big], \end{aligned} \tag{C.54}$$

$$\begin{aligned}\tilde{\Sigma}^<_{(2,1)}(\omega) = \int d\epsilon \Big[& B(\omega,\epsilon)A^*(\epsilon,\omega)\left(Y_L^<(\omega-\epsilon)+Y_R^<(\omega-\epsilon)\right)G^<_{(1,1)}(\epsilon) \\ & +B(\omega,\epsilon)B^*(\epsilon,\omega)\left(Y_L^<(\omega-\epsilon)+Y_R^<(\omega-\epsilon)\right)G^<_{(1,2)}(\epsilon) \\ & -A(\omega,\epsilon)A^*(\epsilon,\omega)\left(Y_L^<(\omega-\epsilon)+Y_R^<(\omega-\epsilon)\right)G^<_{(2,1)}(\epsilon) \\ & -A(\omega,\epsilon)B^*(\epsilon,\omega)\left(Y_L^<(\omega-\epsilon)+Y_R^<(\omega-\epsilon)\right)G^<_{(2,2)}(\epsilon) \\ & +\left(b(\omega)a^*(\omega)Y_L^<(\omega-\epsilon)-a(\omega)b^*(\omega)Y_R^<(\omega-\epsilon)\right)G^<_{t_-}(\epsilon) \\ & +\left(-a(\omega)b^*(\omega)Y_L^<(\omega-\epsilon)+b(\omega)a^*(\omega)Y_R^<(\omega-\epsilon)\right)G^<_{t_+}(\epsilon)\Big]. \end{aligned} \tag{C.55}$$

The non-degenerate triplets t_+ and t_- also change

$$\begin{aligned}\tilde{\Sigma}^<_{t_+t_+}(\omega) = \int d\epsilon \Big[& \left(b(\epsilon)b^*(\epsilon)Y_L^<(\omega-\epsilon)+a(\epsilon)a^*(\epsilon)Y_R^<(\omega-\epsilon)\right)G^<_{(1,1)}(\epsilon) \\ & +\left(-b(\epsilon)a^*(\epsilon)Y_L^<(\omega-\epsilon)+a(\epsilon)b^*(\epsilon)Y_R^<(\omega-\epsilon)\right)G^<_{(1,2)}(\epsilon) \\ & +\left(-a(\epsilon)b^*(\epsilon)Y_L^<(\omega-\epsilon)+b(\epsilon)a^*(\epsilon)Y_R^<(\omega-\epsilon)\right)G^<_{(2,1)}(\epsilon) \\ & +\left(a(\epsilon)a^*(\epsilon)Y_L^<(\omega-\epsilon)+b(\epsilon)b^*(\epsilon)Y_R^<(\omega-\epsilon)\right)G^<_{(2,2)}(\epsilon) \\ & +\left(Y_L^<(\omega-\epsilon)+Y_R^<(\omega-\epsilon)\right)G^<_{t_+}(\epsilon)\Big], \end{aligned} \tag{C.56}$$

$$\begin{aligned}\tilde{\Sigma}^<_{t_-t_-}(\omega) = \int d\epsilon \Big[& \left(a(\epsilon)a^*(\epsilon)Y_L^<(\omega-\epsilon)+b(\epsilon)b^*(\epsilon)Y_R^<(\omega-\epsilon)\right)G^<_{(1,1)}(\epsilon) \\ & +\left(a(\epsilon)b^*(\epsilon)Y_L^<(\omega-\epsilon)-b(\epsilon)a^*(\epsilon)Y_R^<(\omega-\epsilon)\right)G^<_{(1,2)}(\epsilon) \\ & +\left(b(\epsilon)a^*(\epsilon)Y_L^<(\omega-\epsilon)-a(\epsilon)b^*(\epsilon)Y_R^<(\omega-\epsilon)\right)G^<_{(2,1)}(\epsilon) \\ & +\left(b(\epsilon)b^*(\epsilon)Y_L^<(\omega-\epsilon)+a(\epsilon)a^*(\epsilon)Y_R^<(\omega-\epsilon)\right)G^<_{(2,2)}(\epsilon) \\ & +\left(Y_L^<(\omega-\epsilon)+Y_R^<(\omega-\epsilon)\right)G^<_{t_-}(\epsilon)\Big]. \end{aligned} \tag{C.57}$$

In the sum of $\Sigma^<_{(1,1)}$ (C.52) and $\Sigma^<_{(2,2)}$ (C.53) all the contributions from the off-diagonals vanish. Same happens if one adds $\Sigma^<_{t_+t_+}$ (C.56) to $\Sigma^<_{t_-t_-}$ (C.57). Looking into the quantum Boltzmann equation for the diagonal function one can observe, that this leads in direct consequence to the fact, that the system of equations is underdetermined and the constraint is important to get a non-trivial result.

Additionally to the quantum Boltzmann equation the constraint applies,

$$\int \frac{d\epsilon}{2\pi} \mathrm{Tr}\left[G^<(\epsilon)\right] = 1.$$

Performing the transformation and evaluating only the trace we find

$$\begin{aligned} 1 = \int \frac{d\epsilon}{2\pi} \Bigg[& \frac{1}{2}\left(a(\epsilon)a^*(\epsilon) + b(\epsilon)b^*(\epsilon)\right)\left(G^<_{(1,1)}(\epsilon) + G^<_{(2,2)}(\epsilon)\right) + G^<_{t_+}(\epsilon) + G^<_{t_-}(\epsilon) \\ & + \frac{1}{2}\left(a(\epsilon)b^*(\epsilon) - b(\epsilon)a^*(\epsilon)\right)\left(G^<_{(1,2)}(\epsilon) - G^<_{(2,1)}(\epsilon)\right)\Bigg] \end{aligned} \tag{C.58}$$

We introduce

$$d(\epsilon) = \frac{1}{2}\left(a(\epsilon)a^*(\epsilon) + b(\epsilon)b^*(\epsilon)\right) \tag{C.59}$$

for later use.

C.2.4 Ansatz for Lesser Green's Functions

In the 1-2 subspace we get four equations from the rotated quantum Boltzmann equation, two for the diagonal Green's functions and still two off-diagonal. The off-diagonals $G^<_{(1,2)}$ and $G^<_{(2,1)}$ describe different physics compared to $G^<_{st_0}$ and $G^<_{t_0s}$ as is discussed later. For example the equation (C.49) for $(1,1)$ yields

$$\begin{aligned} \tilde{\Sigma}^<_{(1,1)}\left(G^a_1 - G^r_1\right) &= \left((G^r_1)^{-1} - (G^a_1)^{-1}\right)\tilde{G}^<_{(1,1)}, \\ \tilde{\Sigma}^<_{(1,1)} \frac{-2i\mathrm{Im}[\omega_1]}{\left(\omega - \mathrm{Re}[\omega_1]\right)^2 + \left(\mathrm{Im}[\omega_1]\right)^2} &= \tilde{G}^<_{(1,1)}\left(-2i\mathrm{Im}[\omega_1]\right), \\ -i\tilde{\Sigma}^<_{(1,1)}A_1(\omega) &= \tilde{G}^<_{(1,1)}\left(\omega^a_1 - \omega^r_1\right). \end{aligned} \tag{C.60}$$

The equation for $(2,2)$ works analogous.

In equilibrium we now, that the lesser Green's function takes the form

$$G^<(\omega) = -in(\omega)A(\omega),$$

where $A(\omega)$ is the spectral weight, $A(\omega) = i(G^r(\omega) - G^a(\omega))$, and $n(\omega)$ is in general a frequency dependent distribution function. If $A(\omega)$ is a delta function, $n(\omega)$ can be assumed to be a frequency independent number n. Even if $A(\omega)$ has a finite width, then it can be assumed that $n(\omega)$ is a frequency independent occupation number if it varies on a larger energy scale than the broadening. In the case here the spectral function $A_{(1,1)}$ is a Lorentzian with the resonance position at $\mathrm{Re}[\omega_1]$ and the width $\mathrm{Im}[\omega_1]$. As discussed before $A_{(1,1)}$ can be approximated by a δ-function in an integration with another function that varies on a larger energy scale than Γ.

Thus we make the ansatz for all diagonal lesser Green's functions,

$$\begin{aligned} G^<_{(1,1)}(\omega) &= -in_1 A_1(\omega), \\ G^<_{(2,2)}(\omega) &= -in_2 A_2(\omega), \\ G^<_{t_+t_+}(\omega) &= -in_{t_+} A_{t_+}(\omega), \\ G^<_{t_-t_-}(\omega) &= -in_{t_-} A_{t_-}(\omega). \end{aligned}$$

Please note, that all these lesser functions are from sum rule considerations only imaginary see section B.1.

It is known from Eq. (B.4) on page 177 that $G^<_{ss} = -[G^<_{ss}]^\dagger$ and $G^<_{st_0}(\omega) = -\left[G^<_{t_0 s}(\omega)\right]^\dagger$. Thus we find accordingly for the off-diagonal Green's function in the rotated subspace,

$$\tilde{G}^<_{(1,2)}(\omega) = -\left[\tilde{G}^<_{(2,1)}(\omega)\right]^\dagger. \tag{C.61}$$

The equation of motion for $G^<_{(2,1)}(\omega)$ is only the complex conjugate of the equation for $G^<_{(1,2)}(\omega)$ since also

$$\tilde{\Sigma}^<_{(1,2)} = -\left[\tilde{\Sigma}^<_{(2,1)}\right]^\dagger.$$

In contrast to the diagonal Green's functions $\tilde{G}^<_{(1,1)} = -\left[\tilde{G}^<_{(1,1)}\right]^\dagger$ which are purely imaginary, the off-diagonal Green's function $\tilde{G}^<_{(1,2)}$ can also have a real part.

Please note, that $G^<_{(1,2)}$ does not have a spectral weight since $A_{(1,2)} = 0$. It is important not to mistake $A_{(1,2)}$ for A_{st_0}, which as shown in the previous section has a finite spectral weight at the resonances. $G^<_{(1,2)}$ is proportional to a combination of the two spectral function A_1 and A_2. Since the diagonal functions do not have a real part, we will neglect the real part of the off-diagonal functions since we are most interested in the change of the diagonal functions if we take into account the off-diagonal contributions. Consequently the Green's function in the transformed space is diagonal and $G^<_{(1,2)} = G^<_{(2,1)}$. Using the approximation that $\tilde{G}^<_{(1,2)}$ is only imaginary, we thus neglect all real components of $\tilde{G}^<_{(1,2)}$.

In the special case of $K = 0$ we found that $G^<_{(1,2)} = 0$ and also in the case of $\Sigma_{st_0} = 0$ the off-diagonal component does not contribute. Thus it seems that it is only important in the intermediate regime.

The off-diagonal components $G^<_{(1,2)}$ and $G^<_{(2,1)}$ obey a different quantum Boltzmann equation than the diagonal components. We find

$$\begin{aligned} \tilde{\Sigma}^<_{(1,2)}\left(G^a_2 - G^r_1\right) &= \left((G^r_1)^{-1} - (G^a_2)^{-1}\right)\tilde{G}^<_{(1,2)}, \\ \tilde{\Sigma}^<_{(1,2)}\left(\mathrm{Re}[G_2] - \mathrm{Re}[G_1]\right) + i\tilde{\Sigma}^<_{(1,2)}\left(A_2 + A_1\right) &= \left(\omega^a_2 - \omega^r_1\right)\tilde{G}^<_{(1,2)}. \end{aligned} \tag{C.62}$$

where

$$\begin{aligned} \omega^a_2 - \omega^r_1 &= \frac{1}{2}\left(\omega^a_2 - \omega^a_1 + \omega^r_2 - \omega^r_1\right) + \frac{1}{2}\left(\omega^a_2 + \omega^a_1 - \omega^r_2 - \omega^r_1\right) \\ &= \frac{1}{2}\left(\sqrt{\ldots}^a + \sqrt{\ldots}^r\right) + i\left(\Gamma_{t_0 t_0} - \Gamma_{ss}\right). \end{aligned}$$

The approximation is used that $\tilde{G}^<_{(1,2)}$ is only imaginary. Therefore we neglect the real part of G^r_1 and G^r_2 with the physical argument, that the diagonal Green's functions have their importance only on the imaginary axis and if the off-diagonal can have an influence on them, then it is sufficient to look into the imaginary part and neglect the real contributions. The ansatz which we use for $G^<_{(1,2)}$ can be straightforwardly seen from the Quantum Boltzmann equation Eq. (C.62)

$$\begin{aligned}\tilde{\Sigma}^<_{(1,2)}\left(iA_2 + iA_1\right) &= 2i\mathrm{Im}\left[\omega_2^a - \omega_1^r\right]\tilde{G}^<_{(1,2)},\\ \Rightarrow i\tilde{G}^<_{(1,2)} = n_3A_1 + n_4A_2 &= \frac{i\tilde{\Sigma}^<_{(1,2)}}{2\mathrm{Im}\left[\omega_2^a - \omega_1^r\right]}\left(A_2 + A_1\right).\end{aligned}$$

C.2.5 Remark on the Numerical Calculation

In the following it is assumed, that the spectral weight is stronger peaked than any other physical quantity. In order to calculate the self energy we need to derive the convolution of $A(\epsilon)$ with e.g. $Y^<_L(\omega-\epsilon)$. Thus the broadening of A is negligible compared to the scale on which $Y^<_L$ changes in the integral

$$\int d\epsilon\, Y^<_L(\omega-\epsilon)A_i(\epsilon) \approx Y^<_L(\omega-\omega_i).$$

We now write down the diagonal lesser self energies $\Sigma^<_{(i,i)}$ only at the frequency ω_i where the corresponding spectral function is peaked. From Eq. (C.52) we derive

$$\begin{aligned}i\tilde{\Sigma}^<_{(1,1)}(\omega_1) =& A(\omega_1,w_1)A^*(\omega_1,\omega_1)\left(Y^<_L(\omega_1-\omega_1)+Y^<_R(\omega_1-\omega_1)\right)n_1\\ &+\left(A(\omega_1,\omega_1)B^*(\omega_1,\omega_1)+B(\omega_1,\omega_1)A^*(\omega_1,\omega_1)\right)\\ &\quad\left(Y^<_L(\omega_1-\omega_1)+Y^<_R(\omega_1-\omega_1)\right)n_3\\ &+\left(A(\omega_1,\omega_2)B^*(\omega_2,\omega_1)+B(\omega_1,\omega_2)A^*(\omega_2,\omega_1)\right)\\ &\quad\left(Y^<_L(\omega_1-\omega_2)+Y^<_R(\omega_1-\omega_2)\right)n_4\\ &+B(\omega_1,\omega_2)B^*(\omega_2,\omega_1)\left(Y^<_L(\omega_1-\omega_2)+Y^<_R(\omega_1-\omega_2)\right)n_2\\ &+\left(a(\omega_1)a^*(\omega_1)Y^<_L(\omega_1-\omega_{t_-})+b(\omega_1)b^*(\omega_1)Y^<_R(\omega_1-\omega_{t_-})\right)n_{t_-}\\ &+\left(b(\omega_1)b^*(\omega_1)Y^<_L(\omega_1-\omega_{t_+})+a(\omega_1)a^*(\omega_1)Y^<_R(\omega_1-\omega_{t_+})\right)n_{t_+}.\end{aligned}$$

Please note that in this example all prefactors are real numbers. We do not write down the other expression but assume that the reader can produce the simplified version of Eq. (C.53), (C.54), (C.55), (C.56) and (C.57).

With this ansatz the Quantum Boltzmann equations for the diagonal contributions result in

$$\begin{aligned}i\tilde{\Sigma}^<_{(1,1)}(\omega_1) &= \mathrm{Im}[\omega_1(\omega_1)]n_1,\\ i\tilde{\Sigma}^<_{(2,2)}(\omega_1) &= \mathrm{Im}[\omega_2(\omega_2)]n_2,\\ i\tilde{\Sigma}^<_{t_+t_+}(\omega_1) &= \Gamma_{t_+t_+}n_{t_+},\\ i\tilde{\Sigma}^<_{t_-t_-}(\omega_1) &= \Gamma_{t_-t_-}n_{t_-}.\end{aligned}$$

From the quantum Boltzmann equation of $G_{(1,2)}$ Eq. (C.62) and the discussion in the previous section, we use the ansatz,

$$\begin{aligned} G^{<}_{(1,2)} &= -in_3 A_1(\omega) - in_4 A_2(\omega), \\ G^{<}_{(2,1)} &= -in_3 A_1(\omega) - in_4 A_2(\omega). \end{aligned} \tag{C.63}$$

With this ansatz the constraint Eq. (C.58) is no longer an integral equation,

$$1 = d(\omega_1)\, n_1 + d(\omega_2)\, n_2 + n_{t_+} + n_{t_-}, \tag{C.64}$$

and is not dependent on any off-diagonals. A real part of $G_{(1,2)}$ or an imaginary part of n_3 or n_4 would contribute to the constraint but as we discussed above, this is not of physical interest.

As obvious from the discussion this chapter is on-going work. A manuscript is in preparation and at the moment we test the different approximations. Therefore no preliminary results are shown.

C.3 Calculation of the Non-Equilibrium Current

In the general case of finite B and finite K we have to implement the transformation into the equation for the current. This means that we have to calculate $X^{>}_{\mathrm{DQD}}$ and $X^{<}_{\mathrm{DQD}}$ within the new basis instead of the singlet-triplet states, as discussed in section C.1.

C.3.1 Calculation of the Current for General Case

We know that the current is given by

$$I = \frac{e}{h} \int d\omega \frac{1}{4} J_{12} \frac{1}{4} J_{21} \left(X^{>}_{\mathrm{DQD}}(\omega) \left(X^1_2\right)^{<}(\omega) - X^{<}_{\mathrm{DQD}}(\omega) \left(X^1_2\right)^{>}(\omega) \right).$$

Using $X^{<}_{\mathrm{DQD}}(-\omega) = X^{>}_{\mathrm{DQD}}(\omega)$, we can write

$$I = -2\pi \frac{e}{h} \int d\omega \int d\epsilon \frac{1}{4} g_{12} \frac{1}{4} g_{21} X^{>}_{\mathrm{DQD}}(\omega) \left(f(\epsilon + \omega - \mu_1) \left(1 - f(\epsilon - \mu_2)\right) - \{1 \leftrightarrow 2\} \right). \tag{C.65}$$

Using the function $F_3(\omega, V)$ from Eq. (4.11) we result in the simple expression

$$I = -2\pi \frac{e}{h} \int d\omega \frac{1}{4} g_{12} \frac{1}{4} g_{21} \left(V + F_3(\omega, V)\right) X^{>}_{\mathrm{DQD}}(\omega).$$

Finally, we solely have to calculate $X^{>}_{\mathrm{DQD}}$. This calculation is not shown here. We only state the result in the next section.

Explicit Expression

The expression for X_{DQD} is lengthy and is thus omitted.

The result can be written in a similar fashion to the result we already know from the unrotated system and we find

$$\begin{aligned} I = (2\pi)^2 \frac{e}{h} \frac{1}{8} g_{12}^2 \, [3V + \mathcal{C}_V V + \mathcal{C}_{3,4} + \mathcal{C}_f \\ + \mathrm{Re}[a^2(\epsilon_1)] \left(d(\epsilon_1) n_1 - n_{t_-} \right) F_3(\epsilon_{t_-} - \epsilon_1, V_L) \\ + \mathrm{Re}[b^2(\epsilon_2)] \left(d(\epsilon_2) n_2 - n_{t_-} \right) F_3(\epsilon_{t_-} - \epsilon_2, V_L) \\ + \mathrm{Re}[b^2(\epsilon_1)] \left(d(\epsilon_1) n_1 - n_{t_+} \right) F_3(\epsilon_{t_+} - \epsilon_1, V_L) \\ + \mathrm{Re}[a^2(\epsilon_2)] \left(d(\epsilon_2) n_2 - n_{t_+} \right) F_3(\epsilon_{t_+} - \epsilon_2, V_L) \\ + \mathrm{Re}[B^2(\epsilon_1, \epsilon_2)] \left(d(\epsilon_1) n_1 - d(\epsilon_2) n_2 \right) F_3(\epsilon_2 - \epsilon_1, V_L) \big] \,, \end{aligned} \tag{C.66}$$

where the additional terms $\mathcal{C}$ are correction terms, which we assume to be small. They are explicitly stated at the end of this section.

The quantity $d(\omega)$ was already defined (Eq. (C.59)) in context with the constraint in the degenerate perturbation theory and f is given by

$$\begin{aligned} d(\omega) &= \frac{1}{2} \left(a^*(\omega) a(\omega) + b^*(\omega) b(\omega) \right), \\ f(\omega) &= \frac{1}{2} \left(b^*(\omega) a(\omega) - a^*(\omega) b(\omega) \right). \end{aligned}$$

Please note that

$$\begin{aligned} d(\omega)^\dagger &= d(\omega), \\ f(\omega)^\dagger &= -f(\omega), \end{aligned}$$

where $d(\omega)$ is a real and $f(\omega)$ an imaginary number.

There is a contribution to the linear term in the voltage from

$$\begin{aligned} \mathcal{C}_V = {} & d(\epsilon_1) n_1 \mathrm{Re}[A^2(\epsilon_1, \epsilon_1) + B^2(\epsilon_1, \epsilon_2) - 1] + d(\epsilon_2) n_2 \mathrm{Re}[A^2(\epsilon_2, \epsilon_2) + B^2(\epsilon_1, \epsilon_2) - 1] \\ & + n_{t_+} \mathrm{Re}[a^2(\epsilon_2) + b^2(\epsilon_1) - 2] + n_{t_-} \mathrm{Re}[a^2(\epsilon_1) + b^2(\epsilon_2) - 2] \\ & + 2 d(\epsilon_1) n_3 \mathrm{Re}[A(\epsilon_1, \epsilon_1) B(\epsilon_1, \epsilon_1) - A(\epsilon_1, \epsilon_2) B(\epsilon_2, \epsilon_1)] \\ & - 2 d(\epsilon_2) n_4 \mathrm{Re}[A(\epsilon_2, \epsilon_2) B(\epsilon_2, \epsilon_2) - A(\epsilon_2, \epsilon_1) B(\epsilon_1, \epsilon_2)] \\ & - \mathrm{Im}[f(\epsilon_1)] n_1 \mathrm{Im}[B(\epsilon_1, \epsilon_2) A(\epsilon_2, \epsilon_1) - B(\epsilon_1, \epsilon_1) A(\epsilon_1, \epsilon_1)] \\ & - \mathrm{Im}[f(\epsilon_2)] n_2 \mathrm{Im}[B(\epsilon_2, \epsilon_1) A(\epsilon_1, \epsilon_2) - B(\epsilon_2, \epsilon_2) A(\epsilon_2, \epsilon_2)] \\ & - \mathrm{Im}[f(\epsilon_1)] n_3 \mathrm{Im}[A^2(\epsilon_1, \epsilon_1) - A^2(\epsilon_1, \epsilon_2) - B^2(\epsilon_1, \epsilon_1) + B^2(\epsilon_1, \epsilon_2)] \\ & - \mathrm{Im}[f(\epsilon_2)] n_4 \mathrm{Im}[A^2(\epsilon_1, \epsilon_2) - A^2(\epsilon_2, \epsilon_2) + B^2(\epsilon_2, \epsilon_2) - B^2(\epsilon_1, \epsilon_2)], \end{aligned}$$

and a contribution from the off-diagonal occupation numbers

$$\begin{aligned} \mathcal{C}_{3,4} = {} & - \mathrm{Re}[A(\epsilon_1, \epsilon_2) B(\epsilon_2, \epsilon_1)] \left(d(\epsilon_1) n_3 + d(\epsilon_2) n_4 \right) F_3(\epsilon_2 - \epsilon_1, V) \\ & + \mathrm{Re}[a(\epsilon_1) b(\epsilon_1)] 2 d(\epsilon_1) n_3 \left(F_3(\epsilon_{t_-} - \epsilon_1, V) - F_3(\epsilon_{t_+} - \epsilon_1, V) \right) \\ & + \mathrm{Re}[a(\epsilon_2) b(\epsilon_2)] 2 d(\epsilon_2) n_4 \left(F_3(\epsilon_{t_-} - \epsilon_2, V) - F_3(\epsilon_{t_+} - \epsilon_2, V) \right), \end{aligned}$$

and finally from the f contribution

$$\begin{aligned}
\mathcal{C}_f = &- \mathrm{Im}[A(\epsilon_1,\epsilon_2)B(\epsilon_2,\epsilon_1)]\,(\mathrm{Im}[f(\epsilon_1)]n_1 - \mathrm{Im}[f(\epsilon_2)]n_2)\,F_3(\epsilon_2-\epsilon_1,V)\\
&- \mathrm{Im}[B^2(\epsilon_1,\epsilon_2) - A^2(\epsilon_2,\epsilon_1)]\,(\mathrm{Im}[f(\epsilon_1)]n_3 + \mathrm{Im}[f(\epsilon_2)]n_4)\,F_3(\epsilon_2-\epsilon_1,V)\\
&- \mathrm{Im}[a(\epsilon_1)b(\epsilon_1)]\mathrm{Im}[f(\epsilon_1)]n_1\left(-F_3(\epsilon_{t_-}-\epsilon_1,V) + F_3(\epsilon_{t_+}-\epsilon_1,V)\right)\\
&- \mathrm{Im}[a(\epsilon_2)b(\epsilon_2)]\mathrm{Im}[f(\epsilon_2)]n_2\left(F_3(\epsilon_{t_-}-\epsilon_2,V) - F_3(\epsilon_{t_+}-\epsilon_2,V)\right)\\
&- \mathrm{Im}[a^2(\epsilon_1) - b^2(\epsilon_1)]\mathrm{Im}[f(\epsilon_1)]n_3\left(F_3(\epsilon_{t_-}-\epsilon_1,V) - F_3(\epsilon_{t_+}-\epsilon_1,V)\right)\\
&- \mathrm{Im}[a^2(\epsilon_2) - b^2(\epsilon_2)]\mathrm{Im}[f(\epsilon_2)]n_4\left(F_3(\epsilon_{t_-}-\epsilon_2,V) - F_3(\epsilon_{t_+}-\epsilon_2,V)\right).
\end{aligned}$$

An analysis of the expression (C.66) is work in progress. As already mentioned we are working on a manuscript on the subject of "Non-equilibrium perturbation theory with almost degenerate levels".

D Additional Calculations to Chapter 5

D.1 Derivation of an RG Equations as an Example

D.1.1 Spin Structure of the Conduction Electrons

Spin Structure of Cooper Contribution

For evaluating the spin product $\tau^i_{\sigma' s}\tau^j_{s\sigma}$ the following relations are useful,

$$\begin{aligned}
&\tau^z_{\sigma' s}\tau^z_{s\sigma} = \delta_{\sigma',\sigma}, && \\
&\tau^+_{\sigma' s}\tau^-_{s\sigma} = \delta_{\sigma',\sigma} + \tau^z_{\sigma'\sigma}, && \tau^-_{\sigma' s}\tau^+_{s\sigma} = \delta_{\sigma',\sigma} - \tau^z_{\sigma'\sigma}, \\
&\tau^+_{\sigma' s}\tau^z_{s\sigma} = -\tau^+_{\sigma',\sigma}, && \tau^z_{\sigma' s}\tau^+_{s\sigma} = \tau^+_{\sigma',\sigma}, \\
&\tau^-_{\sigma' s}\tau^z_{s\sigma} = \tau^-_{\sigma',\sigma}, && \tau^z_{\sigma' s}\tau^-_{s\sigma} = -\tau^-_{\sigma',\sigma}.
\end{aligned}$$

Here one can already see the spin "dynamics" of the Kondo physics. Two spin-flip processes lead to a non spin-flip process and a spin-flip process is generated out of one with and one without spin-flip.

In order to not get lost with all the indices, we will leave out for the following the momentum indices k, k'. To calculate the Cooper contribution we perform the summation over the conduction electron spin and find

$$\begin{aligned}
&\tau^i_{\sigma' s}\tau^j_{s\sigma} J^{\nu s;m\sigma'}_{\eta;\gamma'} \mathbf{C}^{\nu s}_{\eta} J^{n\sigma;\nu s}_{\gamma;\eta} \left(\vec{T}_\alpha\right)^i_{\gamma'\eta} \left(\vec{T}_\alpha\right)^j_{\eta\gamma} \\
= \;& \tau^z_{\uparrow\uparrow} J^{\nu\downarrow;m\uparrow}_{\eta;\gamma'} \mathbf{C}^{\downarrow}_{\eta} J^{n\uparrow;\nu\downarrow}_{\gamma;\eta} \left(\vec{T}_\alpha\right)^-_{\gamma'\eta} \left(\vec{T}_\alpha\right)^+_{\eta\gamma} - \tau^z_{\downarrow\downarrow} J^{\nu\uparrow;m\downarrow}_{\eta;\gamma'} \mathbf{C}^{\uparrow}_{\eta} J^{n\downarrow;\nu\uparrow}_{\gamma;\eta} \left(\vec{T}_\alpha\right)^+_{\gamma'\eta} \left(\vec{T}_\alpha\right)^-_{\eta\gamma} \\
&- \tau^+_{\uparrow\downarrow} J^{\nu\downarrow;m\uparrow}_{\eta;\gamma'} \mathbf{C}^{\downarrow}_{\eta} J^{n\downarrow;\nu\downarrow}_{\gamma;\eta} \left(\vec{T}_\alpha\right)^-_{\gamma'\eta} \left(\vec{T}_\alpha\right)^z_{\eta\gamma} + \tau^+_{\uparrow\downarrow} J^{\nu\uparrow;m\uparrow}_{\eta;\gamma'} \mathbf{C}^{\uparrow}_{\eta} J^{n\downarrow;\nu\uparrow}_{\gamma;\eta} \left(\vec{T}_\alpha\right)^z_{\gamma'\eta} \left(\vec{T}_\alpha\right)^-_{\eta\gamma} \\
&+ \tau^-_{\downarrow\uparrow} J^{\nu\uparrow;m\downarrow}_{\eta;\gamma'} \mathbf{C}^{\uparrow}_{\eta} J^{n\uparrow;\nu\uparrow}_{\gamma;\eta} \left(\vec{T}_\alpha\right)^+_{\gamma'\eta} \left(\vec{T}_\alpha\right)^z_{\eta\gamma} - \tau^-_{\downarrow\uparrow} J^{\nu\downarrow;m\downarrow}_{\eta;\gamma'} \mathbf{C}^{\downarrow}_{\eta} J^{n\uparrow;\nu\downarrow}_{\gamma;\eta} \left(\vec{T}_\alpha\right)^z_{\gamma'\eta} \left(\vec{T}_\alpha\right)^+_{\eta\gamma}.
\end{aligned}$$

Additionally there are potential scattering terms,

$$\begin{aligned}
&\delta_{\uparrow\uparrow} J^{\nu\downarrow;m\uparrow}_{\eta;\gamma'} \mathbf{C}^{\downarrow}_{\eta} J^{n\uparrow;\nu\downarrow}_{\gamma;\eta} \left(\vec{T}_\alpha\right)^-_{\gamma'\eta} \left(\vec{T}_\alpha\right)^+_{\eta\gamma} + \delta_{\downarrow\downarrow} J^{\nu\uparrow;m\downarrow}_{\eta;\gamma'} \mathbf{C}^{\uparrow}_{\eta} J^{n\downarrow;\nu\uparrow}_{\gamma;\eta} \left(\vec{T}_\alpha\right)^+_{\gamma'\eta} \left(\vec{T}_\alpha\right)^-_{\eta\gamma} \\
&+ \delta_{\sigma\sigma} J^{\nu\sigma;m\sigma}_{\eta;\gamma'} \mathbf{C}^{\sigma}_{\eta} J^{n\sigma;\nu\sigma}_{\gamma;\eta} \left(\vec{T}_\alpha\right)^z_{\gamma'\eta} \left(\vec{T}_\alpha\right)^z_{\eta\gamma}.
\end{aligned}$$

It can be shown analytically and numerically, although not illustrated explicitly here, that the potential scattering terms do not contribute to leading logarithmic order. Thus they are neglected.

Spin Structure of Peierls Contribution

Not the same, but similar is the spin combination for the Peierls contribution. Thus we find,

$$\begin{aligned}
&\tau^j_{\sigma' s}\tau^i_{s\sigma}J^{n\sigma;\nu s}_{\eta;\gamma'}\mathbf{P}^{\nu s}_{\eta}J^{\nu s;m\sigma'}_{\gamma;\eta}\left(\vec{T}_\alpha\right)^i_{\gamma'\eta}\left(\vec{T}_\alpha\right)^j_{\eta\gamma}\\
=\;&\tau^z_{\uparrow\uparrow}J^{n\uparrow;\nu\downarrow}_{\eta;\gamma'}\mathbf{P}^{\downarrow}_{\eta}J^{\nu\downarrow;m\uparrow}_{\gamma;\eta}\left(\vec{T}_\alpha\right)^+_{\gamma'\eta}\left(\vec{T}_\alpha\right)^-_{\eta\gamma}-\tau^z_{\downarrow\downarrow}J^{n\downarrow;\nu\uparrow}_{\eta;\gamma'}\mathbf{P}^{\uparrow}_{\eta}J^{\nu\uparrow;m\downarrow}_{\gamma;\eta}\left(\vec{T}_\alpha\right)^-_{\gamma'\eta}\left(\vec{T}_\alpha\right)^+_{\eta\gamma}\\
&-\tau^+_{\uparrow\downarrow}J^{n\downarrow;\nu\downarrow}_{\eta;\gamma'}\mathbf{P}^{\downarrow}_{\eta}J^{\nu\downarrow;m\uparrow}_{\gamma;\eta}\left(\vec{T}_\alpha\right)^z_{\gamma'\eta}\left(\vec{T}_\alpha\right)^-_{\eta\gamma}+\tau^+_{\uparrow\downarrow}J^{n\downarrow;\nu\uparrow}_{\eta;\gamma'}\mathbf{P}^{\uparrow}_{\eta}J^{\nu\uparrow;m\uparrow}_{\gamma;\eta}\left(\vec{T}_\alpha\right)^-_{\gamma'\eta}\left(\vec{T}_\alpha\right)^z_{\eta\gamma}\\
&+\tau^-_{\downarrow\uparrow}J^{n\uparrow;\nu\uparrow}_{\eta;\gamma'}\mathbf{P}^{\uparrow}_{\eta}J^{\nu\uparrow;m\downarrow}_{\gamma;\eta}\left(\vec{T}_\alpha\right)^z_{\gamma'\eta}\left(\vec{T}_\alpha\right)^+_{\eta\gamma}-\tau^-_{\downarrow\uparrow}J^{n\uparrow;\nu\downarrow}_{\eta;\gamma'}\mathbf{P}^{\downarrow}_{\eta}J^{\nu\downarrow;m\downarrow}_{\gamma;\eta}\left(\vec{T}_\alpha\right)^+_{\gamma'\eta}\left(\vec{T}_\alpha\right)^z_{\eta\gamma}.
\end{aligned}$$

D.1.2 Calculation of the RG Equations for the Double Quantum Dot System

The only thing that is left to do is calculate the matrix product $\left(\vec{T}_\alpha\right)^i_{\gamma'\eta}\mathbf{C}_\eta\left(\vec{T}_\alpha\right)^j_{\eta,\gamma}$ and $\left(\vec{T}_\alpha\right)^j_{\gamma'\eta}\mathbf{P}_\eta\left(\vec{T}_\alpha\right)^i_{\eta,\gamma}$. This is a straightforward exercise. We find for example for the spin-flip terms

$$\begin{aligned}
T^-_{\gamma'\eta}T^z_{\eta\gamma}&=\begin{pmatrix}0&-\delta_{\gamma',s}\delta_{\eta,t_+}\delta_{\gamma,t_+}&0&0\\0&0&0&0\\0&\delta_{\gamma',t_0}\delta_{\eta,t_+}\delta_{\gamma,t_+}&0&0\\\delta_{\gamma',t_-}\delta_{\eta,t_0}\delta_{\gamma,s}&0&\delta_{\gamma',t_-}\delta_{\eta,s}\delta_{\gamma,t_0}&0\end{pmatrix}\\
-T^z_{\gamma'\eta}T^-_{\eta\gamma}&=\begin{pmatrix}0&-\delta_{\gamma',s}\delta_{\eta,t_0}\delta_{\gamma,t_+}&0&0\\0&0&0&0\\0&\delta_{\gamma',t_0}\delta_{\eta,s}\delta_{\gamma,t_+}&0&0\\\delta_{\gamma',t_-}\delta_{\eta,t_-}\delta_{\gamma,s}&0&\delta_{\gamma',t_-}\delta_{\eta,t_-}\delta_{\gamma,t_0}&0\end{pmatrix}
\end{aligned}$$

Thus we get for example for the $\gamma'=s$ and $\gamma=t_+$ coupling

$$-J^{\nu\downarrow;m\uparrow}_{t_+;s}\mathbf{C}^{\nu\downarrow}_{t_+}J^{n\downarrow;\nu\downarrow}_{t_+;t_+}+J^{n\downarrow;\nu\uparrow}_{t_+;s}\mathbf{P}^{\nu\uparrow}_{t_+}J^{\nu\uparrow;m\uparrow}_{t_+;t_+}-J^{\nu\uparrow;m\uparrow}_{t_0;s}\mathbf{C}^{\nu\uparrow}_{t_0}J^{n\downarrow;\nu\uparrow}_{t_+;t_0}+J^{n\downarrow;\nu\downarrow}_{t_0;s}\mathbf{P}^{\nu\downarrow}_{t_0}J^{\nu\downarrow;m\uparrow}_{t_+;t_0}$$

Please note, that $T_{st_+}=-1$ and thus we get an additional minus sign. Using the calculated expressions for the Cooper and Peierls contribution we finally find,

$$\begin{aligned}
\frac{\partial g^{n\downarrow;m\uparrow}_{s;t_+}}{\partial\ln D}=-\frac{1}{2}\Big(&g^{\nu\downarrow;m\uparrow}_{t_+;s}g^{n\downarrow;\nu\downarrow}_{t_+;t_+}\Theta_{\omega_c+\omega_{t_+}-\mu_\nu-\omega_{t_+}}+g^{n\downarrow;\nu\uparrow}_{t_+;s}g^{\nu\uparrow;m\uparrow}_{t_+;t_+}\Theta_{\omega_s-\omega_c+\mu_\nu-\omega_{t_+}}\\
&+g^{\nu\uparrow;m\uparrow}_{t_0;s}g^{n\downarrow;\nu\uparrow}_{t_+;t_0}\Theta_{\omega_c+\omega_{t_+}-\mu_\nu-\omega_{t_0}}+g^{n\downarrow;\nu\downarrow}_{t_0;s}g^{\nu\downarrow;m\uparrow}_{t_+;t_0}\Theta_{\omega_s-\omega_c+\mu_\nu-\omega_{t_0}}\Big).
\end{aligned}$$

This expression is discussed further in section 5.2.3.

D.2 Flow of the Couplings

The RG equations are

$$\begin{aligned}\frac{\partial g_{ts}^{nm}(\omega)}{\partial \ln D} = -\frac{1}{2}\,&(2g_{ts}^{\nu m}(\mu_\nu)g_{tt}^{n\nu}(\mu_\nu)\Theta_{\omega-\mu_\nu} \\ &+2g_{ts}^{n\nu}(\mu_\nu - K)g_{tt}^{\nu m}(\mu_\nu)\Theta_{\omega-\mu_\nu+K})\,,\end{aligned}$$

$$\begin{aligned}\frac{\partial g_{tt}^{nm}(\omega)}{\partial \ln D} = -\frac{1}{2}\,&(g_{st}^{\nu m}(\mu_\nu)g_{ts}^{n\nu}(\mu_\nu - K)\Theta_{\omega-\mu_\nu+K} \\ &+g_{st}^{n\nu}(\mu_\nu + K)g_{ts}^{\nu m}(\mu_\nu)\Theta_{\omega-\mu_\nu-K} \\ &+2g_{tt}^{\nu m}(\mu_\nu)g_{tt}^{n\nu}(\mu_\nu)\Theta_{\omega-\mu_\nu})\,.\end{aligned}$$

For the following it is assumed that $V_L = 0$. The coupling from lead 1 and 2 are thus in equilibrium. It turns out that only the three couplings $g_{ts}^{nm}(0), g_{ts}^{nm}(-K)$ and $g_{tt}^{nm}(0)$ are of interest.

D.2.1 Flow in the Energy Regime $D_0 > D > K$

The cutoff D_0 is the largest energy scale of the system. In the RG equations two different cut-off regimes, Θ_K and Θ_Γ, appear since the broadening cuts off the flow when there is no other energy scale left. The initial couplings are frequency independent and until the scale $D^* = K$ no frequency dependence shows up. Therefore we can neglect the frequency argument in the RG flow. All Θ functions are 1 in the regime $D_0 > D > K$,

$$\frac{\partial g_{ts}^{nm}}{\partial \ln D} = -\frac{1}{2}\,(2g_{ts}^{\nu m}g_{tt}^{n\nu} + 2g_{ts}^{n\nu}g_{tt}^{\nu m})\,,$$

$$\frac{\partial g_{tt}^{nm}}{\partial \ln D} = -\frac{1}{2}\,(g_{st}^{\nu m}g_{ts}^{n\nu} + g_{st}^{n\nu}g_{ts}^{\nu m} + 2g_{tt}^{\nu m}g_{tt}^{n\nu})\,.$$

We have on the one hand side the indices tt, st and ts and also the lead indices from the conduction electrons 11, 12, 21 and 22.

Since $g_{st}^{mn}(\omega) = g_{ts}^{nm}(\omega - K)$ and the energy argument is negligible in the chosen regime, we find

$$\begin{aligned}g_{st}^{nn} &= g_{ts}^{nn}\,,\\ g_{st}^{12} &= g_{ts}^{21}.\end{aligned}$$

Same argument for g_{tt} leads to

$$g_{tt}^{12} = g_{tt}^{21}.$$

Thus we receive the following RG equations,

$$\begin{aligned}\frac{\partial g_{ts}^{11}}{\partial \ln D} &= -\left(g_{ts}^{11}g_{tt}^{11} + g_{ts}^{11}g_{tt}^{11} + g_{ts}^{21}g_{tt}^{12} + g_{ts}^{12}g_{tt}^{21}\right),\\ \frac{\partial g_{ts}^{12}}{\partial \ln D} &= -\left(g_{ts}^{12}g_{tt}^{11} + g_{ts}^{11}g_{tt}^{12} + g_{ts}^{22}g_{tt}^{12} + g_{ts}^{12}g_{tt}^{22}\right),\\ \frac{\partial g_{ts}^{21}}{\partial \ln D} &= -\left(g_{ts}^{11}g_{tt}^{21} + g_{ts}^{21}g_{tt}^{11} + g_{ts}^{21}g_{tt}^{22} + g_{ts}^{22}g_{tt}^{21}\right),\\ \frac{\partial g_{ts}^{22}}{\partial \ln D} &= -\left(g_{ts}^{12}g_{tt}^{21} + g_{ts}^{21}g_{tt}^{12} + g_{ts}^{22}g_{tt}^{22} + g_{ts}^{22}g_{tt}^{22}\right).\end{aligned}$$

We observe that g^{22}_{ts} and g^{11}_{ts} fulfill the same equations. If they start with the same initial value, they will be the same during the flow and we define a diagonal coupling,

$$g^d_{ts} \equiv g^{11}_{ts} = g^{22}_{ts}.$$

Thus we can rewrite

$$\begin{aligned}\frac{\partial g^{12}_{ts}}{\partial \ln D} &= -\left(g^{12}_{ts}(g^{11}_{tt} + g^{22}_{tt}) + 2g^d_{ts}g^{12}_{tt}\right), \\ \frac{\partial g^{21}_{ts}}{\partial \ln D} &= -\left(2g^d_{ts}g^{21}_{tt} + g^{21}_{ts}(g^{11}_{tt} + g^{22}_{tt})\right).\end{aligned}$$

Due to the same arguments we define a transport coupling

$$g^t_{ts} \equiv g^{12}_{ts} = g^{21}_{ts}.$$

Since $g^{12}_{st} = g^{21}_{ts} = g^{12}_{ts}$ we do not have to distinguish between st and ts. This is completely reasonable since we do not have frequency arguments in the regime of $D_0 > D > K$.

All the above considerations hold for g_{tt} as well and we define correspondingly

$$\begin{aligned}g^t_{tt} &\equiv g^{12}_{tt} = g^{21}_{tt}, \\ g^d_{tt} &\equiv g^{11}_{tt} = g^{22}_{tt}.\end{aligned}$$

The equations for $g^d_{\gamma\gamma'}$ and $g^t_{\gamma\gamma'}$ are still coupled.

$$\begin{aligned}\frac{\partial g^d_{ts}}{\partial \ln D} &= -\left(2g^t_{ts}g^t_{tt} + 2g^d_{ts}g^d_{tt}\right), \\ \frac{\partial g^t_{ts}}{\partial \ln D} &= -\left(2g^t_{ts}g^d_{tt} + 2g^d_{ts}g^t_{tt}\right).\end{aligned}$$

We can decouple them by introducing

$$\begin{aligned}g^+_{ts} &= g^d_{ts} + g^t_{ts}, \\ g^-_{ts} &= g^d_{ts} - g^t_{ts},\end{aligned}$$

which fulfill the equations

$$\begin{aligned}\frac{\partial g^+_{ts}}{\partial \ln D} &= -2g^+_{ts}g^+_{tt}, \\ \frac{\partial g^-_{ts}}{\partial \ln D} &= -2g^-_{ts}g^-_{tt}.\end{aligned}$$

Thus the conduction electron leads are decoupled, but we still have a coupled equation for the singlet-triplet pseudo particle index. Therefore we have to derive the RG equations for g^+_{tt} and g^-_{tt} in the same manner. We shorten the derivation and just write down

$$\begin{aligned}\frac{\partial g^+_{tt}}{\partial \ln D} &= -\left(g^+_{ts}\right)^2 - \left(g^+_{tt}\right)^2 \\ \frac{\partial g^-_{tt}}{\partial \ln D} &= -\left(g^-_{ts}\right)^2 - \left(g^-_{tt}\right)^2\end{aligned}$$

Now we can define further symmetric combinations of the coupling,

$$\begin{aligned}
g_+^+ &= g_{tt}^+ + g_{ts}^+ = g_{tt}^d + g_{tt}^t + g_{st}^d + g_{st}^t, \\
g_-^+ &= g_{tt}^+ - g_{ts}^+ = g_{tt}^d + g_{tt}^t - g_{st}^d - g_{st}^t, \\
g_+^- &= g_{tt}^- + g_{ts}^- = g_{tt}^d - g_{tt}^t + g_{st}^d - g_{st}^t, \\
g_-^- &= g_{tt}^- - g_{ts}^- = g_{tt}^d - g_{tt}^t - g_{st}^d + g_{st}^t.
\end{aligned}$$

Then all equation have the same form

$$\begin{aligned}
\frac{\partial g_+^+}{\partial \ln D} &= -\left(g_+^+\right)^2, \\
\frac{\partial g_-^+}{\partial \ln D} &= -\left(g_-^+\right)^2, \\
\frac{\partial g_+^-}{\partial \ln D} &= -\left(g_+^-\right)^2, \\
\frac{\partial g_-^-}{\partial \ln D} &= -\left(g_-^-\right)^2.
\end{aligned}$$

For example the solution for the differential equation g_+^+ is

$$g_+^+(D) = \frac{1}{\frac{1}{g_+^+(D_0)} + \ln\left(D/D_0\right)}.$$

This coupling is divergent on the energy scale T_K,

$$\begin{aligned}
\ln\left(T_K/D_0\right) &= -\frac{1}{g_+^+(D_0)}, \\
T_K &= D_0\, \mathrm{e}^{-1/g_+^+(D_0)}.
\end{aligned}$$

Altogether we have four different energy scales on which the four different coupling diverge. Of importance is only the largest energy scale, which originates from the largest coupling. From the definitions we can see, that this is g_+^+ since it is the sum of four couplings. All other couplings contain a difference of couplings. Finally we find for $D_0 > D > K$,

$$\begin{aligned}
g_+^+(D) &= \frac{1}{\ln\left(\frac{D}{T_K}\right)}, \\
g_-^+(D) &= \frac{1}{\frac{1}{g_+^{eff}} + \ln\left(\frac{D}{T_K}\right)}, \qquad \text{where} \qquad \frac{1}{g_+^{eff}} = \frac{1}{g_-^+(D_0)} - \frac{1}{g_+^+(D_0)}, \\
g_+^-(D) &= \frac{1}{\frac{1}{g_{eff}^+} + \ln\left(\frac{D}{T_K}\right)}, \qquad \text{where} \qquad \frac{1}{g_{eff}^+} = \frac{1}{g_+^-(D_0)} - \frac{1}{g_+^+(D_0)}, \\
g_-^-(D) &= \frac{1}{\frac{1}{g_{eff}^{eff}} + \ln\left(\frac{D}{T_K}\right)}, \qquad \text{where} \qquad \frac{1}{g_{eff}^{eff}} = \frac{1}{g_-^-(D_0)} - \frac{1}{g_+^+(D_0)}.
\end{aligned}$$

By taking sum and difference of these four couplings we get explicit expressions for g^d_{tt}, g^t_{tt}, g^d_{ts} and g^t_{ts},

$$\begin{aligned} g^d_{tt} &= \frac{1}{4}\left(g^+_+ + g^+_- + g^-_+ + g^-_-\right), \\ g^t_{tt} &= \frac{1}{4}\left(g^+_+ + g^+_- - g^-_+ - g^-_-\right), \\ g^d_{st} &= \frac{1}{4}\left(g^+_+ - g^+_- + g^-_+ - g^-_-\right), \\ g^t_{tt} &= \frac{1}{4}\left(g^+_+ - g^+_- - g^-_+ + g^-_-\right). \end{aligned}$$

This will become arbitrarily difficult and we focus from now on a simplified case. It is assumed that all couplings are the same in the beginning of the flow,

$$g^{mn}_{tt}(D_0) = g^{mn}_{st}(D_0) = g^{mn}_{ts}(D_0) = g.$$

This leads to quite a severe simplification of the equations,

$$\begin{aligned} & g^+_+(D_0) = 4g, \\ & g^+_-(D_0) = g^-_+(D_0) = g^-_-(D_0) = 0, \\ \Rightarrow \quad & g^+_+(D) = \frac{1}{\ln(D/T_K)}, \\ & g^+_-(D) = g^-_+(D) = g^-_-(D) = 0, \end{aligned}$$

and a Kondo temperature of

$$T_K = D_0\, \mathrm{e}^{-1/4g}.$$

And since all couplings are the same in the beginning of the flow, they are also the same at D,

$$g^d_{tt} = g^t_{tt} = g^d_{st} = g^t_{tt} = \frac{1}{4\ln\left(D/T_K\right)}.$$

D.2.2 Flow in the Energy Regime $K > D > \Gamma$

After we reduced the cutoff to the scale of K, some of the Θ functions are 0. Now we have to take care about frequency arguments. The RG equations are for $V_L = 0$,

$$\begin{aligned} \frac{\partial g^{nm}_{ts}(\omega)}{\partial \ln D} = -\frac{1}{2}\,&(2g^{\nu m}_{ts}(0)g^{n\nu}_{tt}(0)\Theta_\omega \\ &+2g^{n\nu}_{ts}(-K)g^{\nu m}_{tt}(0)\Theta_{\omega+K}), \end{aligned}$$

$$\begin{aligned} \frac{\partial g^{nm}_{tt}(\omega)}{\partial \ln D} = -\frac{1}{2}\,&(g^{\nu m}_{st}(0)g^{n\nu}_{ts}(-K)\Theta_{\omega+K} \\ &+g^{n\nu}_{st}(K)g^{\nu m}_{ts}(0)\Theta_{\omega-K} \\ &+2g^{\nu m}_{tt}(0)g^{n\nu}_{tt}(0)\Theta_\omega). \end{aligned}$$

The triplet-triplet coupling appears only with the frequency 0. It has to obey the equation

$$\frac{\partial g_{tt}^{11}(0)}{\partial \ln D} = -g_{tt}^{11}(0)g_{tt}^{11}(0) - g_{tt}^{21}(0)g_{tt}^{12}(0),$$
$$\frac{\partial g_{tt}^{12}(0)}{\partial \ln D} = -g_{tt}^{12}(0)g_{tt}^{11}(0) - g_{tt}^{22}(0)g_{tt}^{12}(0).$$

Without showing it, we use again $g_{tt}^{t} = g_{tt}^{12} = g_{tt}^{21}$ and $g_{tt}^{d} = g_{tt}^{11} = g_{tt}^{22}$. The two functions are coupled, but the sum $g_{tt}^{+} = g_{tt}^{d} + g_{tt}^{t}$ and difference $g_{tt}^{-} = g_{tt}^{d} - g_{tt}^{t}$ are not,

$$\frac{\partial g_{tt}^{+}(0)}{\partial \ln D} = -\left(g_{tt}^{+}(0)\right)^2,$$
$$\frac{\partial g_{tt}^{-}(0)}{\partial \ln D} = -\left(g_{tt}^{-}(0)\right)^2.$$

We can solve this differential equation and get

$$g_{tt}^{+}(0,D) = \frac{1}{\ln\left(\frac{D}{T^*}\right)},$$
$$g_{tt}^{-}(0,D) = \frac{g_{tt}^{-}(0,D^*)}{1+g_{tt}^{-}(0,D^*)} = \frac{1}{\frac{1}{g_{tt}^{-}(0,D^*)} - \frac{1}{g_{tt}^{+}(0,D^*)} + \ln\left(\frac{D}{T^*}\right)}.$$

The upper energy scale where the flow starts is $D^* = K$, and thus

$$g_{tt}^{+}(0,D^*) = g_{tt}^{d}(0,K) + g_{tt}^{t}(0,K) = \frac{1}{2\ln\left(\frac{K}{T_K}\right)},$$
$$T^* = D^* \mathrm{e}^{-1/g_{tt}^{+}(0,D^*)} = K\mathrm{e}^{-2\ln\left(\frac{K}{T_K}\right)} = K\left(\frac{1}{K/T_K}\right)^2 = T_K\,\frac{T_K}{K}.$$

The coupling g_{tt}^{-} does not flow since $g_{tt}^{-}(0,D^*) = 0$. Thus we find a solution for the triplet couplings for $K > D > \Gamma$,

$$g_{tt}^{d}(0,D) = g_{tt}^{t}(0,D) = \frac{1}{2\ln\left(\frac{D}{T^*}\right)}.$$

The equations for g_{ts} include g_{tt}, but now we can put in the solution of g_{tt} and find

$$\frac{\partial g_{ts}^{12}(0)}{\partial \ln D} = -g_{ts}^{12}(0)g_{tt}^{d}(0) - g_{ts}^{22}(0)g_{tt}^{t}(0) = -\left(g_{ts}^{12}(0) + g_{ts}^{22}(0)\right)\frac{1}{2\ln(D/T^*)},$$
$$\frac{\partial g_{ts}^{21}(-K)}{\partial \ln D} = -g_{ts}^{21}(-K)g_{tt}^{d}(0) - g_{ts}^{d}(-K)g_{tt}^{21}(0)$$
$$= -\left(g_{ts}^{21}(-K) + g_{ts}^{22}(-K)\right)\frac{1}{2\ln(D/T^*)}.$$

Unfortunately again we have to also calculate the $d = 11 = 22$ component,

$$\frac{\partial g_{ts}^{22}(0)}{\partial \ln D} = -g_{ts}^{12}(0)g_{tt}^{t}(0) - g_{ts}^{22}(0)g_{tt}^{d}(0) = -\left(g_{ts}^{12}(0) + g_{ts}^{22}(0)\right)\frac{1}{2\ln(D/T^*)},$$
$$\frac{\partial g_{ts}^{22}(-K)}{\partial \ln D} = -g_{ts}^{21}(-K)g_{tt}^{t}(0) - g_{ts}^{22}(-K)g_{tt}^{d}(0)$$
$$= -\left(g_{ts}^{21}(-K) + g_{ts}^{22}(-K)\right)\frac{1}{2\ln(D/T^*)}.$$

With the same initial conditions the difference $g_{ts}^{-}(0)$ and $g_{ts}^{-}(-K)$ do not flow. The flowing couplings are $g_{ts}^{+}(0) = g_{ts}^{d}(0) + g_{st}^{t}(0)$ and $g_{ts}^{+}(-K) = g_{ts}^{d}(-K) + g_{ts}^{t}(-K)$,

$$\frac{\partial g_{ts}^{+}(0)}{\partial \ln D} = -g_{ts}^{+}(0)\frac{1}{\ln(D/T^*)},$$
$$\frac{\partial g_{ts}^{+}(-K)}{\partial \ln D} = -g_{ts}^{+}(-K)\frac{1}{\ln(D/T^*)}.$$

These differential equations can be solved again

$$\frac{\partial g_{ts}^{+}(0,D)}{g_{ts}^{+}(0,D)} = -\frac{\partial \ln D}{\ln D - \ln T^*} \qquad |\cdot \int_{D^*}^{D}$$
$$\Rightarrow \quad \ln \frac{g_{ts}^{+}(0,D)}{g_{ts}^{+}(0,D^*)} = -\ln\left(\frac{\ln D/T^*}{\ln D^*/T^*}\right)$$
$$\Leftrightarrow \quad g_{ts}^{+}(0,D) = g_{ts}^{+}(0,D^*)\frac{\ln D^*/T^*}{\ln D/T^*}.$$

With $g_{ts}^{+}(0,D^*) = 1/\ln(D^*/T^*)$[1], $g_{ts}^{t}(0) = \frac{1}{2}g_{ts}^{+}(0,D)$ and an analogous calculation for $g_{ts}^{t}(-K)$ we find

$$g_{ts}^{t}(0,D) = \frac{1}{2\ \ln D/T^*},$$
$$g_{ts}^{t}(-K,D) = \frac{1}{2\ \ln D/T^*}.$$

With the assumption that all coupling start with the same value, also in the regime of $K > D > \Gamma$ all couplings flow the same

$$g_{ts}^{d/t}(0,D) = g_{ts}^{d/t}(-K,D) = g_{tt}^{d/t}(0,D) = \frac{1}{2\ \ln D/T^*}$$
$$= \frac{1}{2\ \ln D/T_K + 2\ \ln K/T_K}.$$

D.2.3 Flow in the Energy Regime $D < \Gamma$

If the band width is reduced below the lowest energy scale, none of the couplings flows any more. They take the value

$$g_{ts}^{d/t}(0,D=0) = g_{ts}^{d/t}(-K,D=0) = g_{tt}^{d/t}(0,D=0) = \frac{1}{2\ \ln \Gamma/T_K + 2\ \ln K/T_K}.$$

For a discussion and illustration of this frequency-dependent flow of the couplings please see section 5.3.

[1] actually we only know that $g_{tt} = 1/\ln$ but since all couplings are the same until the flow to D^* we can use the latter assumption.

E Additional Calculations to Chapter 6

E.1 Useful Commutators

E.1.1 Useful Commutators for the Lead Operators

For fermions in normal ordering the following commutator applies,

$$\left[: c_{1'}^\dagger c_1 :, : c_{2'}^\dagger c_2 :\right] = \delta_{1,2'} : c_{1'}^\dagger c_2 : - \delta_{1',2} : c_{2'}^\dagger c_1 : + \delta_{1',2}\delta_{1,2'} \left(n(1') - n(1)\right).$$

Lowest Order

The following case is found often,

$$\begin{aligned}\left[: \vec{s}_{(k'i)(ki)} :, H_{\text{kin}}\right] &= \sum_{\kappa,j,\alpha} \epsilon_{\kappa,j} \left[: \vec{s}_{(k'i)(ki)} :, : c_{\kappa,j,\alpha}^\dagger c_{\kappa,j,\alpha} :\right] \\ &= -\left(\epsilon_{k',i} - \epsilon_{k,i}\right) : \vec{s}_{(k'i)(ki)} : .\end{aligned}$$

Higher Orders

In higher orders the commutator between two conduction electrons appears,

$$\begin{aligned}\left[: \vec{s}^{\alpha}_{(k'j)(kj)} :, : \vec{s}^{\alpha}_{(p'n)(pn)} :\right]_- = &\sum_s \frac{1}{4}\delta_{a,\alpha}\delta_{j,n} \left(\delta_{k,p'} : c_{k'js}^\dagger c_{pjs} : - \delta_{k'p} : c_{p'js}^\dagger c_{kjs} :\right) \\ &+ \frac{1}{2}\delta_{a,\alpha}\delta_{j,n}\delta_{k,p'}\delta_{k'p} \left(n(k'j) - n(kj)\right) \\ &+ \frac{1}{2} i \delta_{j,n}\delta_{k,p'}\epsilon_{a\alpha b} : s^b_{(k'j)(pj)} : \\ &+ \frac{1}{2} i \delta_{j,n}\delta_{k',p}\epsilon_{a\alpha b} : s^b_{(p'j)(kj)} : .\end{aligned}$$

Apart from the commutator also the following property is used,

$$\begin{aligned}: c_{1'}^\dagger c_1 :: c_{2'}^\dagger c_2 : = &: c_{1'}^\dagger c_1 c_{2'}^\dagger c_2 : + \delta_{1,2'} : c_{1'}^\dagger c_2 : \left(1 - n(1)\right) \\ &- \delta_{1',2} : c_{2'}^\dagger c_1 : n(1') + \delta_{1',2}\delta_{1,2'} n(1') \left(1 - n(1)\right).\end{aligned}$$

Thus we find for the anticommutator,

$$\begin{aligned}
&\left\{ :\vec{s}^{\,a}_{(k'j)(kj)}:, :\vec{s}^{\,\alpha}_{(p'n)(pn)}: \right\}_+ \\
=&2 : \vec{s}^{\,a}_{(k'j)(kj)} \vec{s}^{\,\alpha}_{(p'n)(pn)} : \\
&+ \sum_s \frac{1}{4}\delta_{a,\alpha}\delta_{j,n}\left(\delta_{k,p'} : c^\dagger_{k'js}c_{pjs} : (1-2n(kj)) - \delta_{k'p} : c^\dagger_{p'js}c_{kjs} : (1-2n(k'j))\right) \\
&+ i\frac{1}{2}\delta_{j,n}\delta_{k,p'}\epsilon_{a\alpha b} : \vec{s}^{\,b}_{(k'j)(pj)} : (1-2n(kj)) \\
&- i\frac{1}{2}\delta_{j,n}\delta_{k',p}\epsilon_{a\alpha b} : \vec{s}^{\,b}_{(p'j)(kj)} : (1-2n(k'j)) \\
&+ \frac{1}{2}\delta_{a,\alpha}\delta_{j,n}\delta_{k,p'}\delta_{k'p}\left(n(k'j)(1-n(kj)) + n(kj)(1-n(k'j))\right).
\end{aligned}$$

E.1.2 Useful Commutators for the Spin Operators

Lowest Order

In lowest order there are contributions from

$$[\vec{S}_L\vec{S}_R, \vec{S}^\alpha_L] = [\vec{S}^a_L\vec{S}^a_R, \vec{S}^\alpha_L] = i\epsilon_{a\alpha b}\vec{S}^b_L\vec{S}^a_R = i\epsilon_{\alpha ba}\vec{S}^b_L\vec{S}^a_R = i\left(\vec{S}_L\times\vec{S}_R\right)^\alpha$$

and

$$[\vec{S}_L\vec{S}_R, \vec{S}^\alpha_R] = -i\left(\vec{S}_L\times\vec{S}_R\right)^\alpha.$$

Further the relation applies,

$$\begin{aligned}
&[\left(\vec{S}_L\times\vec{S}_R\right)^a, \vec{S}_L\vec{S}_R] = \epsilon_{abc}[\vec{S}^b_L\vec{S}^c_R, \vec{S}^\alpha_L\vec{S}^\alpha_R] \\
&= \epsilon_{abc}\left(\vec{S}^b_L[\vec{S}^c_R, \vec{S}^\alpha_L\vec{S}^\alpha_R] + [\vec{S}^b_L, \vec{S}^\alpha_L\vec{S}^\alpha_R]\vec{S}^c_R\right) \\
&= \epsilon_{abc}\left(\vec{S}^b_L\vec{S}^\alpha_L[\vec{S}^c_R, \vec{S}^\alpha_R] + [\vec{S}^b_L, \vec{S}^\alpha_L]\vec{S}^\alpha_R\vec{S}^c_R\right) \\
&= \epsilon_{abc}\left[\left(\frac{1}{4}\delta_{b,\alpha} + \frac{1}{2}i\epsilon_{b\alpha\beta}\vec{S}^\beta_L\right)i\epsilon_{c\alpha\gamma}\vec{S}^\gamma_R + i\epsilon_{b\alpha\beta}\vec{S}^\beta_L\left(\frac{1}{4}\delta_{\alpha,c} + \frac{1}{2}i\epsilon_{\alpha c\gamma}\vec{S}^\gamma_R\right)\right] \\
&= \frac{1}{4}i\epsilon_{abc}\epsilon_{bc\beta}\left(-\vec{S}^\beta_R + \vec{S}^\beta_L\right) = \frac{1}{2}i\left(-\vec{S}^a_R + \vec{S}^a_L\right),
\end{aligned}$$

where

$$\sum_{b,c}\epsilon_{abc}\epsilon_{bc\beta} = \sum_{b,c}\epsilon_{abc}\epsilon_{\beta bc} = \sum_b \delta_{a,\beta}\delta_{b,b} - \delta_{a,b}\delta_{\beta,b} = 3\delta_{a,\beta} - \delta_{a,\beta} = 2\delta_{a,\beta}.$$

Higher Orders

It is used that

$$\left(\vec{S}_L\times\vec{S}_R\right)^a\left(\vec{S}_L\times\vec{S}_R\right)^\alpha = \frac{1}{8}\delta_{a,\alpha} - \frac{1}{4}\left(S^a_LS^\alpha_R + S^\alpha_LS^a_R\right) + \frac{1}{8}i\epsilon_{a\alpha d}\left(S^d_R + S^d_L\right),$$

and

$$\left(\vec{S}_L \times \vec{S}_R\right)^\alpha \left(\vec{S}_L \times \vec{S}_R\right)^a = \frac{1}{8}\delta_{a,\alpha} - \frac{1}{4}\left(S_L^a S_R^\alpha + S_L^\alpha S_R^a\right) - \frac{1}{8} i\epsilon_{a\alpha d}\left(S_R^d + S_L^d\right).$$

Additionally we find

$$\left(\vec{S}_L \times \vec{S}_R\right)^a \vec{S}_L^\alpha = \frac{1}{4}\epsilon_{a\alpha c} S_R^c + \frac{1}{2} i S_L^a S_R^\alpha - \frac{1}{2} i\delta_{a,\alpha}\vec{S}_L\vec{S}_R,$$

and

$$\vec{S}_L^\alpha \left(\vec{S}_L \times \vec{S}_R\right)^a = \frac{1}{4}\epsilon_{a\alpha c} S_R^c - \frac{1}{2} i S_L^a S_R^\alpha + \frac{1}{2} i\delta_{a,\alpha}\vec{S}_L\vec{S}_R.$$

E.2 Add-Ons to the One-Loop Order Calculation

E.2.1 Explicit Expression for $J^{\mathrm{sum},j}_{k'k}$

Inserting the canonical generator, Eq. (6.10), in the scaling equation for $J^{\mathrm{sum},j}_{k'k}$, we find

$$\begin{aligned}
\frac{dJ^{\mathrm{sum},j}_{k'k}(B)}{dB} =& -\left(\epsilon_{k'} - \epsilon_k\right)^2 J^{\mathrm{sum},j}_{k'k}(B) \\
&- \frac{1}{2}\sum_v \left(1 - 2n(vj)\right)\left(\left(\epsilon_{k'} - \epsilon_v\right) - \left(\epsilon_v - \epsilon_k\right)\right) J^{\mathrm{sum},j}_{k'v}(B) J^{\mathrm{sum},j}_{vk}(B) \\
&- \frac{1}{2}\sum_v \left(1 - 2n(vj)\right)\left(\left(\epsilon_{k'} - \epsilon_v + K\right) - \left(\epsilon_v - \epsilon_k + K\right)\right) P^j_{k'v}(B) P^j_{vk}(B) \\
&- \frac{1}{2}\sum_v \left(1 - 2n(vj)\right)\left(\left(\epsilon_{k'} - \epsilon_v + K\right) - \left(\epsilon_v - \epsilon_k - K\right)\right) P^j_{k'v}(B) M^j_{vk}(B) \\
&- \frac{1}{2}\sum_v \left(1 - 2n(vj)\right)\left(\left(\epsilon_{k'} - \epsilon_v - K\right) - \left(\epsilon_v - \epsilon_k + K\right)\right) M^j_{k'v}(B) P^j_{vk}(B) \\
&- \frac{1}{2}\sum_v \left(1 - 2n(vj)\right)\left(\left(\epsilon_{k'} - \epsilon_v - K\right) - \left(\epsilon_v - \epsilon_k - K\right)\right) M^j_{k'v}(B) M^j_{vk}(B)
\end{aligned} \tag{E.1}$$

$$
\begin{aligned}
&+\frac{1}{2}\sum_v \left((\epsilon_{k'}-\epsilon_v+K)-(\epsilon_v-\epsilon_k+K)\right) P^j_{k'v}(B)P^j_{vk}(B)\\
&-\frac{1}{2}\sum_v \left((\epsilon_{k'}-\epsilon_v+K)-(\epsilon_v-\epsilon_k-K)\right) P^j_{k'v}(B)M^j_{vk}(B)\\
&-\frac{1}{2}\sum_v \left((\epsilon_{k'}-\epsilon_v-K)-(\epsilon_v-\epsilon_k+K)\right) M^j_{k'v}(B)P^j_{vk}(B)\\
&+\frac{1}{2}\sum_v \left((\epsilon_{k'}-\epsilon_v-K)-(\epsilon_v-\epsilon_k-K)\right) M^j_{k'v}(B)M^j_{vk}(B)\\
&+\frac{1}{2}\sum_v \left((\epsilon_{k'}-\epsilon_v)-(\epsilon_v-\epsilon_k+K)\right) J^{\mathrm{sum},j}_{k'v}(B)P^j_{vk}(B)\\
&-\frac{1}{2}\sum_v \left((\epsilon_{k'}-\epsilon_v)-(\epsilon_v-\epsilon_k-K)\right) J^{\mathrm{sum},j}_{k'v}(B)M^j_{vk}(B)\\
&-\frac{1}{2}\sum_v \left((\epsilon_{k'}-\epsilon_v+K)-(\epsilon_v-\epsilon_k)\right) P^j_{k'v}(B)J^{\mathrm{sum},j}_{vk}(B)\\
&+\frac{1}{2}\sum_v \left((\epsilon_{k'}-\epsilon_v-K)-(\epsilon_v-\epsilon_k)\right) M^j_{k'v}(B)J^{\mathrm{sum},j}_{vk}(B)
\end{aligned}
$$

If we insert the diagonal parametrization, Eqs. (6.24) and (6.25), into the flow equation of the coupling $J^{\mathrm{sum},j}_{k'k}$ each term is similar to

$$
\begin{aligned}
&\left((\epsilon_{k'}-\epsilon_v+\alpha K)-(\epsilon_v-\epsilon_k+\beta K)\right)\mathrm{e}^{-B(\epsilon_{k'}-\epsilon_v+\alpha K)^2}\mathrm{e}^{-B(\epsilon_v-\epsilon_k+\beta K)^2}\\
=&\frac{1}{2B}\frac{d}{d\,\epsilon_v}\mathrm{e}^{-B(\epsilon_{k'}-\epsilon_v+\alpha K)^2}\mathrm{e}^{-B(\epsilon_v-\epsilon_k+\beta K)^2},
\end{aligned}
$$

where $\alpha,\beta=0,\pm1$.

The two different types of integrations thus give

$$
\sum_v \frac{d}{d\,\epsilon_v}f(\epsilon_v)=\int_{-D}^{D} d\epsilon\rho\frac{d}{d\,\epsilon}f(\epsilon)=\rho f(\epsilon_v=D)-\rho f(\epsilon_v=-D)
$$

and

$$
\begin{aligned}
\sum_v \left(1-2\,n(vj)\right)\frac{d}{d\,\epsilon_v}f(\epsilon_v)&=\int_{-D}^{0} d\epsilon_v\rho\left(1-2\cdot1\right)\frac{d}{d\,\epsilon_v}f(\epsilon_v)+\int_{0}^{D} d\epsilon_v\rho\left(1-2\cdot0\right)\frac{d}{d\,\epsilon_v}f(\epsilon_v)\\
&=-2\rho\,f(\epsilon_v=0)+\rho\,f(\epsilon_v=-D)+\rho\,f(\epsilon_v=D),
\end{aligned}
$$

where ρ is the density of states which is assumed to be constant. The second integration is characteristic for a Kondo spin interaction. Due to the spin algebra and the discontinuity at the Fermi surface the function $f(\epsilon_v=0)$ is not cancelled like in the first integration.

The following scaling equation is obtained,

$$\begin{aligned}\mathrm{e}^{-B(\epsilon_{k'}-\epsilon_k)^2}\ \frac{d\overline{J^{\mathrm{sum},j}_{k'k}}(B)}{dB} &= \frac{1}{2B}\,\mathrm{e}^{-B(\epsilon_{k'})^2}\mathrm{e}^{-B(-\epsilon_k)^2}\overline{J^{\mathrm{sum},j}_{k'0}}(B)\ \overline{J^{\mathrm{sum},j}_{0k}}(B)\\ &+\frac{1}{2B}\left(\mathrm{e}^{-B(\epsilon_{k'}+K)^2}\overline{P^j_{k'0}}(B)+\mathrm{e}^{-B(\epsilon_{k'}-K)^2}\overline{M^j_{k'0}}(B)\right)\\ &\quad\left(\mathrm{e}^{-B(-\epsilon_k+K)^2}\overline{P^j_{0k}}(B)+\mathrm{e}^{-B(-\epsilon_k-K)^2}\overline{M^j_{0k}}(B)\right),\end{aligned}$$

with some additional terms to mention just a few,

$$\begin{aligned}\mathrm{e}^{-B(\epsilon_{k'}-\epsilon_k)^2}\ \frac{d\overline{J^{\mathrm{sum}}_{k'k}}(B)}{dB} &= -\frac{1}{2}\mathrm{e}^{-B(\epsilon_{k'}-D)^2}\mathrm{e}^{-B(D-\epsilon_k)^2}J^{\mathrm{sum},j}_{k',D}J^{\mathrm{sum},j}_{D,k}\\ &\quad-\frac{1}{2}\mathrm{e}^{-B(\epsilon_{k'}-(-D))^2}\mathrm{e}^{-B((-D)-\epsilon_k)^2}J^{\mathrm{sum},j}_{k',-D}J^{\mathrm{sum},j}_{-D,k}\\ &\quad-\ldots.\end{aligned}$$

Since $\epsilon_k, \epsilon_{k'} \ll D$ these additional terms scale like e^{-2BD^2}. Please see section 6.4 in the main text for a discussion why the contributions proportional to e^{-BD^2} can be neglected.

E.3 Add-Ons to the Two-Loop Order Calculation

E.3.1 Neglected Higher Order Terms

To first-loop order also new interaction terms are created. To second order in the coupling J the potential scattering is found,

$$\sum\sum_s V^j_{k'k} : c^\dagger_{k'js}c_{kjs} : + \sum\left(\vec{S}_L\vec{S}_R\right)\sum_s W^j_{k'k} : c^\dagger_{k'js}c_{kjs} :,$$

and the flow of $V^j_{k'k}(B)$ and $W^j_{k'k}(B)$ is given by

$$\begin{aligned}\frac{dV^j_{k'k}}{dB} &= \frac{1}{4}\frac{3}{4}\sum_v\left[\left(\eta^{Lj}_{k'v}J^{Lj}_{vk}-J^{Lj}_{k'v}\eta^{Lj}_{vk}+\eta^{Rj}_{k'v}J^{Rj}_{vk}-J^{Rj}_{k'v}\eta^{Rj}_{vk}\right)-2\left(\gamma^j_{k'v}Q^j_{vk}-Q^j_{k'v}\gamma^j_{vk}\right)\right],\\ \frac{dW^j_{k'k}}{dB} &= \frac{1}{4}\sum_v\left[\left(\eta^{Lj}_{k'v}J^{Rj}_{vk}-J^{Rj}_{k'v}\eta^{Lj}_{vk}+\eta^{Rj}_{k'v}J^{Lj}_{vk}-J^{Lj}_{k'v}\eta^{Rj}_{vk}\right)+2\left(\gamma^j_{k'v}Q^j_{vk}-Q^j_{k'v}\gamma^j_{vk}\right)\right]\\ &\quad-\frac{1}{2}\sum_v(1-2n(vj))\left[\gamma^j_{k'v}(J^{Lj}_{vk}-J^{Rj}_{vk})-(J^{Lj}_{k'v}-J^{Rj}_{k'v})\gamma^j_{vk}\right.\\ &\qquad\left.-(\eta^{Lj}_{k'v}-\eta^{Rj}_{k'v})Q^j_{vk}+Q^j_{k'v}(\eta^{Lj}_{vk}-\eta^{Rj}_{vk})\right].\end{aligned}$$

Additionally the singlet-triplet gap K is renormalized and a constant energy term arises,

$$
\begin{aligned}
&- \sum \gamma^j_{k'k} Q^j_{kk'} \left(n(k'j) - n(kj)\right) \left(\frac{3}{4} - \vec{S}_L \vec{S}_R\right) \\
&+ \sum \left(\gamma^j_{k'k} (J^{Lj}_{kk'} - J^{Rj}_{kk'}) - (\eta^{Lj}_{k'k} - \eta^{Rj}_{k'k}) Q^j_{kk'}\right) \\
&\qquad \left(n(k'j)(1-n(kj)) + n(kj)(1-n(k'j))\right) \left(\vec{S}_L \vec{S}_R\right) \\
&+ \frac{1}{2} \sum \left(\eta^{Lj}_{k'k} J^{Rj}_{kk'} + \eta^{Rj}_{k'k} J^{Lj}_{kk'}\right) \left(n(k'j) - n(kj)\right) \left(\vec{S}_L \vec{S}_R\right) \\
&+ \frac{1}{2}\frac{3}{4} \sum \left(\eta^{Lj}_{k'k} J^{Lj}_{kk'} + \eta^{Rj}_{k'k} J^{Rj}_{kk'}\right) \left(n(k'j) - n(kj)\right).
\end{aligned}
$$

Thus the coupling $\mathcal{K} \vec{S}_L \vec{S}_R$ flows like

$$
\begin{aligned}
\frac{d\mathcal{K}(B)}{dB} = &+ \frac{1}{2} \sum_{k'k} \left(\eta^{Lj}_{k'k} J^{Rj}_{kk'} + \eta^{Rj}_{k'k} J^{Lj}_{kk'} + 2\gamma^j_{k'k} Q^j_{kk'}\right) \left(n(k'j) - n(kj)\right) \\
&+ \sum_{k'k} \left(\gamma^j_{k'k} (J^{Lj}_{kk'} - J^{Rj}_{kk'}) - (\eta^{Lj}_{k'k} - \eta^{Rj}_{k'k}) Q^j_{kk'}\right) \\
&\qquad \left(n(k'j)(1-n(kj)) + n(kj)(1-n(k'j))\right).
\end{aligned}
$$

To study these couplings in more detail will be the task of future investigations. For the rest of this thesis they are neglected since the flow of the potential scattering or the coupling K is not to leading logarithmic order.

E.3.2 Higher Order Contributions from 2nd Order

Some two-particle interactions are created to 2nd order in the coupling to the leads. To calculate the 3rd order contributions to the flow equations the following terms are included,

$$
\begin{aligned}
&\sum \left(\eta^{Lj}_{k'k} g^{Ln}_{p'p} - \gamma^j_{k'k} Q^n_{p'p}\right) : i\vec{S}_L \left(\vec{s}_{(k'j)(kj)} \times \vec{s}_{(p'n)(pn)}\right) : \\
&+ \sum \left(\eta^{Rj}_{k'k} g^{Rn}_{p'p} - \gamma^j_{k'k} Q^n_{p'p}\right) : i\vec{S}_R \left(\vec{s}_{(k'j)(kj)} \times \vec{s}_{(p'n)(pn)}\right) : \\
&+ \sum \left(\gamma^j_{k'k} g^{Ln}_{p'p} - \gamma^j_{k'k} g^{Rn}_{p'p} - \eta^{Lj}_{k'k} Q^n_{p'p} + \eta^{Rj}_{k'k} Q^n_{p'p}\right) : 2 \left(\vec{S}_L \vec{S}_R\right) \left(\vec{s}_{(k'j)(kj)} \vec{s}_{(p'n)(pn)}\right) : \\
&+ \sum \left(-\gamma^j_{k'k} g^{Ln}_{p'p} - \eta^{Rj}_{k'k} Q^n_{p'p}\right) : 2 \left(\vec{S}_L \vec{s}_{(k'j)(kj)}\right) \left(\vec{S}_R \vec{s}_{(p'n)(pn)}\right) : \\
&+ \sum \left(\gamma^j_{k'k} g^{Rn}_{p'p} + \eta^{Lj}_{k'k} Q^n_{p'p}\right) : 2 \left(\vec{S}_R \vec{s}_{(k'j)(kj)}\right) \left(\vec{S}_L \vec{s}_{(p'n)(pn)}\right) : .
\end{aligned}
$$

The Hamiltonian $H^{(2)}_{\text{int}}$ is given by

$$
\begin{aligned}
H^{(2)}_{\text{int}} = &\sum_{i,j,n=L,R} \sum_{k'k} \sum_{p'p} K^i_{(k'j)(kj);(p'n)(pn)} : i\vec{S}_i \left(\vec{s}_{(k'j)(kj)} \times \vec{s}_{(p'n)(pn)}\right) : \\
&+ \sum_{i,j,n=L,R} \sum_{k'k} \sum_{p'p} {}^{(2)}K^i_{(k'j)(kj);(p'n)(pn)} : 2 \left(\vec{S}_{!i} \vec{s}_{(k'j)(kj)}\right) \left(\vec{S}_i \vec{s}_{(p'n)(pn)}\right) : \\
&+ \sum_{j,n=L,R} \sum_{k'k} \sum_{p'p} {}^{(3)}K_{(k'j)(kj);(p'n)(pn)} : 2 \left(\vec{S}_L \vec{S}_R\right) \left(\vec{s}_{(k'j)(kj)} \vec{s}_{(p'n)(pn)}\right) : .
\end{aligned} \tag{E.2}
$$

We should take into account the symmetry relations,

$$K^i_{(k'j)(kj);(p'n)(pn)} = -K^i_{(kj)(k'j);(pn)(p'n)}, \tag{E.3a}$$
$${}^{(2)}K^i_{(k'j)(kj);(p'n)(pn)} =^{(2)} K^i_{(kj)(k'j);(pn)(p'n)}, \tag{E.3b}$$
$${}^{(3)}K_{(k'j)(kj);(p'n)(pn)} =^{(3)} K_{(kj)(k'j);(pn)(p'n)}, \tag{E.3c}$$

due to the hermiticity of the Hamiltonian.

Since the summation is over both $k'k$ and $p'p$ we find some additional symmetry relations from exchanging the indices

$$K^i_{(k'j)(kj);(p'n)(pn)} = -K^i_{(p'n)(pn);(k'j)(kj)}, \tag{E.4a}$$
$${}^{(2)}K^i_{(k'j)(kj);(p'n)(pn)} =^{(2)} K^{!i}_{(p'n)(pn);(k'j)(kj)}, \tag{E.4b}$$
$${}^{(3)}K_{(k'j)(kj);(p'n)(pn)} =^{(3)} K_{(p'n)(pn);(k'j)(kj)}. \tag{E.4c}$$

The couplings K are created to second order in g^2. The initial value is 0.

E.3.3 Canonical Generator to 3rd Order

Since the interaction Hamiltonian has been changed by adding higher-order terms, $H^{(2)}_{\rm int}$, the canonical generator $\eta = [H_0, H_{\rm int}]$ has to be calculated correspondingly. The contribution $\eta^{(2)}$ is found,

$$\begin{aligned}\eta^{(2)} = &\sum_{i,j,n=L,R}\sum_{k'k}\sum_{p'p} {}^{(1)}\zeta^i_{(k'j)(kj);(p'n)(pn)} : i\vec{S}_i \left(\vec{s}_{(k'j)(kj)} \times \vec{s}_{(p'n)(pn)}\right) : \\ &+ \sum_{i,j,n=L,R}\sum_{k'k}\sum_{p'p} {}^{(2)}\zeta^i_{(k'j)(kj);(p'n)(pn)} : 2\left(\vec{S}_{!i}\vec{s}_{(k'j)(kj)}\right)\left(\vec{S}_i\vec{s}_{(p'n)(pn)}\right) : \\ &+ \sum_{j,n=L,R}\sum_{k'k}\sum_{p'p} {}^{(3)}\zeta_{(k'j)(kj);(p'n)(pn)} : 2\left(\vec{S}_L\vec{S}_R\right)\left(\vec{s}_{(k'j)(kj)}\vec{s}_{(p'n)(pn)}\right) :,\end{aligned} \tag{E.5}$$

where

$$\begin{aligned}{}^{(1)}\zeta^{L/R}_{(k'j)(kj);(p'n)(pn)} &= \left(\epsilon_{k'j} - \epsilon_{kj} + \epsilon_{p'n} - \epsilon_{pn}\right) K^{L/R}_{(k'j)(kj);(p'n)(pn)} \\ &\quad \pm \frac{1}{2}K\left({}^{(2)}K^L_{(k'j)(kj);(p'n)(pn)} - {}^{(2)}K^R_{(k'j)(kj);(p'n)(pn)}\right), \\ {}^{(2)}\zeta^{L/R}_{(k'j)(kj);(p'n)(pn)} &= \left(\epsilon_{k'j} - \epsilon_{kj} + \epsilon_{p'n} - \epsilon_{pn}\right)^{(2)} K^{L/R}_{(k'j)(kj);(p'n)(pn)} \\ &\quad \pm \frac{1}{2}K\left(K^L_{(k'j)(kj);(p'n)(pn)} - K^R_{(k'j)(kj);(p'n)(pn)}\right), \\ {}^{(3)}\zeta_{(k'j)(kj);(p'n)(pn)} &= \left(\epsilon_{k'j} - \epsilon_{kj} + \epsilon_{p'n} - \epsilon_{pn}\right)^{(3)} K_{(k'j)(kj);(p'n)(pn)}.\end{aligned}$$

The generator is antihermitian, which leads to similar symmetry relations for $\zeta^i_{(k'j)(kj);(q'v)(qv)}$ than for $K^i_{(k'j)(kj);(q'v)(qv)}$ but with opposite sign than in Eq. (E.3).

E.3.4 Flow of the Coupling to 3rd Order

We redefine the couplings to take respect to their symmetry and the way they are found in the flow equations. We use the notation $K^{L\pm R} = K^L \pm K^R$ and find

$$\begin{aligned}
(k_1^a)_{(k'j)(kj);(q'\nu)(q\nu)} &= K^{L+R}_{(k'j)(kj);(q'\nu)(q\nu)} - K^{L+R}_{(q'\nu)(q\nu);(k'j)(kj)},\\
(k_2^a)_{(k'j)(kj);(q'\nu)(q\nu)} &= K^{L-R}_{(k'j)(kj);(q'\nu)(q\nu)} - K^{L-R}_{(q'\nu)(q\nu);(k'j)(kj)},\\
(k_3^s)_{(k'j)(kj);(q'\nu)(q\nu)} &=^{(2)} K^{L+R}_{(k'j)(kj);(q'\nu)(q\nu)} +^{(2)} K^{L+R}_{(q'\nu)(q\nu);(k'j)(kj)},\\
(k_4^a)_{(k'j)(kj);(q'\nu)(q\nu)} &=^{(2)} K^{L-R}_{(k'j)(kj);(q'\nu)(q\nu)} -^{(2)} K^{L-R}_{(q'\nu)(q\nu);(k'j)(kj)},\\
(k_5^s)_{(k'j)(kj);(q'\nu)(q\nu)} &=^{(3)} K_{(k'j)(kj);(q'\nu)(q\nu)} +^{(3)} K_{(q'\nu)(q\nu);(k'j)(kj)},
\end{aligned}$$

where s is the symmetric and a the antisymmetric version with respect to interchanging the index q with k.

From the symmetry relations in Eq. (E.3) and (E.4), the following combinations are zero,

$$k_1^s = k_2^s = k_3^a = k_4^s = k_5^a = 0.$$

So far all couplings are denoted by the energy $(k'j)(kj);(q'\nu)(q\nu)$. In the flow equations we also find contributions from the combination $(k'j)(qj);(q'j)(kj)$ and define

$$\begin{aligned}
k_6 &=^{(3)} K_{(k'j)(qj);(q'j)(kj)} +^{(3)} K_{(q'j)(kj);(k'j)(qj)},\\
k_6' &=^{(2)} K^{L+R}_{(k'j)(qj);(q'j)(kj)} +^{(2)} K^{L+R}_{(q'j)(kj);(k'j)(qj)}.
\end{aligned}$$

The flow equations for k_1, k_3 and k_5 are given by

$$\begin{aligned}
\frac{d(k_1^a)_{(k'j)(kj);(q'v)(qv)}}{dB} &= -(\epsilon_{k'} - \epsilon_k + \epsilon_{q'} - \epsilon_q)^2 k_1^a\\
&\quad + 2\left[(\epsilon_{k'} - \epsilon_k) - (\epsilon_{q'} - \epsilon_q)\right] g^{\mathrm{sum},j}_{k'k} g^{\mathrm{sum},v}_{q'q}\\
&\quad + 4\left[(\epsilon_{k'} - \epsilon_k + K) - (\epsilon_{q'} - \epsilon_q - K)\right] p^j_{k'k} m^v_{q'q}\\
&\quad + 4\left[(\epsilon_{k'} - \epsilon_k - K) - (\epsilon_{q'} - \epsilon_q + K)\right] m^j_{k'k} p^v_{q'q},
\end{aligned}$$

$$\begin{aligned}
\frac{d(k_3^s)_{(k'j)(kj);(q'v)(qv)}}{dB} &= -(\epsilon_{k'} - \epsilon_k + \epsilon_{q'} - \epsilon_q)^2 k_3^s\\
&\quad - 4\left[(\epsilon_{k'} - \epsilon_k + K) - (\epsilon_{q'} - \epsilon_q - K)\right] p^j_{k'k} m^v_{q'q}\\
&\quad + 4\left[(\epsilon_{k'} - \epsilon_k - K) - (\epsilon_{q'} - \epsilon_q + K)\right] m^j_{k'k} p^v_{q'q},
\end{aligned}$$

where the equation for k_5 gives $k_5^s = -k_3^s$. Furthermore $k_2 \pm k_4$ flow like

$$\begin{aligned}
\frac{d(k_2^a + k_4^a)_{(k'j)(kj);(q'v)(qv)}}{dB} &= -(\epsilon_{k'} - \epsilon_k + \epsilon_{q'} - \epsilon_q + K)^2 (k_2^a + k_4^a)\\
&\quad + 4\left[(\epsilon_{k'} - \epsilon_k) - (\epsilon_{q'} - \epsilon_q + K)\right] g^{\mathrm{sum},j}_{k'k} p^v_{q'q}\\
&\quad + 4\left[(\epsilon_{k'} - \epsilon_k + K) - (\epsilon_{q'} - \epsilon_q)\right] p^j_{k'k} g^{\mathrm{sum},v}_{q'q}
\end{aligned}$$

and

$$\begin{aligned}\frac{d(k_2^a - k_4^a)_{(k'j)(kj);(q'v)(qv)}}{dB} &= -(\epsilon_{k'} - \epsilon_k + \epsilon_{q'} - \epsilon_q - K)^2 (k_2^a - k_4^a) \\ &+ 4\left[(\epsilon_{k'} - \epsilon_k) - (\epsilon_{q'} - \epsilon_q - K)\right] g^{\mathrm{sum},j}_{k'k} m^v_{q'q} \\ &+ 4\left[(\epsilon_{k'} - \epsilon_k - K) - (\epsilon_{q'} - \epsilon_q)\right] m^j_{k'k} g^{\mathrm{sum},v}_{q'q}.\end{aligned}$$

Finally,

$$\begin{aligned}\frac{d(k_6)_{(k'j)(qj);(q'j)(kj)}}{dB} &= -(\epsilon_{k'} - \epsilon_k + \epsilon_{q'} - \epsilon_q - K)^2 k_6 \\ &+ 4\left[(\epsilon_{k'} - \epsilon_q + K) - (\epsilon_{q'} - \epsilon_k - K)\right] p^j_{k'k} m^v_{q'q} \\ &- 4\left[(\epsilon_{k'} - \epsilon_q - K) - (\epsilon_{q'} - \epsilon_k + K)\right] m^j_{k'k} p^v_{q'q},\end{aligned}$$

and $k_6' = -k_6$.

The coupling to the total spin flows like

$$\begin{aligned}\frac{dg^{\mathrm{sum},j}_{k'k}}{dB} &= \ldots + \\ &[n(q'v)(1-n(qv)) + n(qv)(1-n(q'v))] \\ &\left\{\frac{1}{4}\left(\epsilon_{k'} - \epsilon_k + \epsilon_{q'} - \epsilon_q - (\epsilon_q - \epsilon_{q'})\right) k_1^a g^{\mathrm{sum},v}_{qq'}\right. \\ &+ \frac{1}{4}\left(\epsilon_{k'} - \epsilon_k + \epsilon_{q'} - \epsilon_q - K - (\epsilon_q - \epsilon_{q'} + K)\right)(k_2^a - k_4^a)\, p^v_{qq'} \\ &\left.+\frac{1}{4}\left(\epsilon_{k'} - \epsilon_k + \epsilon_{q'} - \epsilon_q + K - (\epsilon_q - \epsilon_{q'} - K)\right)(k_2^a + k_4^a)\, m^v_{qq'}\right\}\end{aligned}$$

and

$$\begin{aligned}\frac{dp^j_{k'k}}{dB} &= \ldots + \\ &[n(q'v)(1-n(qv)) + n(qv)(1-n(q'v))] \\ &\left\{\frac{1}{8}\left(\epsilon_{q'} - \epsilon_q + \epsilon_{k'} - \epsilon_k + K - (\epsilon_q - \epsilon_{q'})\right)(k_2^a + k_4^a)\, g^{\mathrm{sum},v}_{qq'}\right. \\ &+ \frac{1}{4}\left(\epsilon_{q'} - \epsilon_q + \epsilon_{k'} - \epsilon_k - (\epsilon_q - \epsilon_{q'} + K)\right)(k_1^a - 3k_3^s)\, p^v_{qq'} \\ &\left.+\frac{1}{4}\delta_{v,j}\left(\epsilon_{q'} - \epsilon_q + \epsilon_{k'} - \epsilon_k - (\epsilon_q - \epsilon_{q'} + K)\right)(2k_6' + k_6)\, p^i_{qq'}\right\},\end{aligned}$$

where $k_5^s = -k_3^s$ is used. The hermiticity is fulfilled, which provides a check on the calculations.

There is also a contribution from $(n(q') - n(q))$ to the flow of $g^{\mathrm{sum}}_{k'k}$. Since terms including $(n(q') - n(q))$ are only proportional to the phase space between q' and q, these terms will be neglected.

In general one has to solve the set of differential equations for $g^{\mathrm{sum},j}_{k'k}$, p^j, $k_1 ... k_5$. For an analytical result we perform the calculation in two steps. First the flow equations for the couplings $k_1 - k_6$ are integrated over B and the result is inserted into the differential equation for $g^{\mathrm{sum},j}_{k'k}$.

With the same assumption for k_1^a as for the diagonal parametrization

$$k_1^a(B) = e^{-B(\epsilon_{k'}-\epsilon_k+\epsilon_{q'}-\epsilon_q)^2}\ \overline{k_1^a}(B)$$

we find that $\overline{k_1^a}$ is given by inserting the diagonal representation of $g_{k'k}^{\mathrm{sum},j}$ and $p_{k'k}^j$

$$\begin{aligned}\overline{k_1^a}(B) = \int_{B_0}^{B} d\tilde{B} \Big\{ & 2\left[(\epsilon_{k'}-\epsilon_k)-(\epsilon_{q'}-\epsilon_q)\right] e^{2\tilde{B}(\epsilon_{k'}-\epsilon_k)(\epsilon_{q'}-\epsilon_q)} \overline{g_{k'k}^{\mathrm{sum},j}}\ \overline{g_{q'q}^{\mathrm{sum},v}} \\ & + 4\left[(\epsilon_{k'}-\epsilon_k+K)-(\epsilon_{q'}-\epsilon_q-K)\right] e^{2\tilde{B}(\epsilon_{k'}-\epsilon_k+K)(\epsilon_{q'}-\epsilon_q-K)} \overline{p_{k'k}^j}\ \overline{m_{q'q}^v} \\ & +4\left[(\epsilon_{k'}-\epsilon_k-K)-(\epsilon_{q'}-\epsilon_q+K)\right] e^{2\tilde{B}(\epsilon_{k'}-\epsilon_k-K)(\epsilon_{q'}-\epsilon_q+K)} \overline{m_{k'k}^j}\ \overline{p_{q'q}^v} \Big\}\end{aligned}$$

Each of the three terms is of the form of

$$e^{-B\left(\epsilon_{k'}-\epsilon_k+a+\epsilon_{q'}-\epsilon_q+b\right)^2} \int_{B_0}^{B} d\tilde{B}\left[(\epsilon_{k'}-\epsilon_k+a)-(\epsilon_{q'}-\epsilon_q+b)\right] e^{2\tilde{B}(\epsilon_{k'}-\epsilon_k+a)(\epsilon_{q'}-\epsilon_q+b)}$$

where $a/b = 0, \pm K$. If $\epsilon_{k'}-\epsilon_k+a=0$ the e-function vanishes and the integration is trivial. We find

$$-\left(\epsilon_{q'}-\epsilon_q+b\right) e^{-B\left(\epsilon_{q'}-\epsilon_q+b\right)^2} * (B-B_0)$$

The assumption that $\epsilon_{k'}-\epsilon_k+a=0$ is always valid if we use the diagonal representation.

However, for this integration it is assumed that the B-dependence of the couplings can be neglected in the integration, since it flows slowly, i.e. proportional to $g(B) \propto 1/\ln$. Thus the result is valid only to leading log order.

E.3.5 Explicit Expression for $g^{\mathrm{sum},j}$ in 3rd Order

In the same way as shown for k_1 the other higher order couplings $k_2 - k_6$ can be derived. If we insert them into the scaling equation for $g^{\mathrm{sum},j}_{k'k}$ we find

$$
\begin{aligned}
\frac{dg^{\mathrm{sum},j}_{k'k}}{dB} = \ldots + \\
&[n(q'v)(1-n(qv)) + n(qv)(1-n(q'v))] \\
&\Big\{ \frac{1}{2} \left[(\epsilon_{k'} - \epsilon_k) - (\epsilon_{q'} - \epsilon_q) \right] \left[(\epsilon_{k'} - \epsilon_k) + (\epsilon_{q'} - \epsilon_q) - (\epsilon_q - \epsilon_{q'}) \right] \\
&\quad e^{-B\left((\epsilon_{k'}-\epsilon_k)+(\epsilon_{q'}-\epsilon_q)\right)^2} e^{-B\left(\epsilon_q-\epsilon_{q'}\right)^2} \\
&\quad \overline{g^{\mathrm{sum},j}_{k'k}}\ \overline{g^{\mathrm{sum},v}_{q'q}}\ \overline{g^{\mathrm{sum},v}_{qq'}} \int_{B_0}^{B} d\tilde{B}\ e^{2\tilde{B}(\epsilon_{k'}-\epsilon_k)\left(\epsilon_{q'}-\epsilon_q\right)} \\
&+ \left[(\epsilon_{k'} - \epsilon_k + K) - (\epsilon_{q'} - \epsilon_q - K) \right] \\
&\quad \left[(\epsilon_{k'} - \epsilon_k + K) + (\epsilon_{q'} - \epsilon_q - K) - (\epsilon_q - \epsilon_{q'}) \right] \\
&\quad e^{-B\left((\epsilon_{k'}-\epsilon_k+K)+(\epsilon_{q'}-\epsilon_q-K)\right)^2} e^{-B\left(\epsilon_q-\epsilon_{q'}\right)^2} \\
&\quad \overline{p^{j}_{k'k}}\ \overline{m^{v}_{q'q}}\ \overline{g^{\mathrm{sum},v}_{qq'}} \int_{B_0}^{B} d\tilde{B}\ e^{2\tilde{B}(\epsilon_{k'}-\epsilon_k+K)\left(\epsilon_{q'}-\epsilon_q-K\right)} \\
&+ \left[(\epsilon_{k'} - \epsilon_k - K) - (\epsilon_{q'} - \epsilon_q + K) \right] \\
&\quad \left[(\epsilon_{k'} - \epsilon_k - K) + (\epsilon_{q'} - \epsilon_q + K) - (\epsilon_q - \epsilon_{q'}) \right] \\
&\quad e^{-B\left((\epsilon_{k'}-\epsilon_k-K)+(\epsilon_{q'}-\epsilon_q+K)\right)^2} e^{-B\left(\epsilon_q-\epsilon_{q'}\right)^2} \\
&\quad \overline{m^{j}_{k'k}}\ \overline{p^{v}_{q'q}}\ \overline{g^{\mathrm{sum},v}_{qq'}} \int_{B_0}^{B} d\tilde{B}\ e^{2\tilde{B}(\epsilon_{k'}-\epsilon_k-K)\left(\epsilon_{q'}-\epsilon_q+K\right)} \\
&+ \left[(\epsilon_{k'} - \epsilon_k) - (\epsilon_{q'} - \epsilon_q - K) \right] \\
&\quad \left[(\epsilon_{k'} - \epsilon_k) + (\epsilon_{q'} - \epsilon_q - K) - (\epsilon_q - \epsilon_{q'} + K) \right] \\
&\quad e^{-B\left((\epsilon_{k'}-\epsilon_k)+(\epsilon_{q'}-\epsilon_q-K)\right)^2} e^{-B\left(\epsilon_q-\epsilon_{q'}+K\right)^2} \\
&\quad \overline{g^{\mathrm{sum},j}_{k'k}}\ \overline{m^{v}_{q'q}}\ \overline{p^{v}_{qq'}} \int_{B_0}^{B} d\tilde{B}\ e^{2\tilde{B}(\epsilon_{k'}-\epsilon_k)\left(\epsilon_{q'}-\epsilon_q-K\right)} \\
&+ \left[(\epsilon_{k'} - \epsilon_k) - (\epsilon_{q'} - \epsilon_q + K) \right] \\
&\quad \left[(\epsilon_{k'} - \epsilon_k) + (\epsilon_{q'} - \epsilon_q + K) - (\epsilon_q - \epsilon_{q'} - K) \right] \\
&\quad e^{-B\left((\epsilon_{k'}-\epsilon_k)+(\epsilon_{q'}-\epsilon_q+K)\right)^2} e^{-B\left(\epsilon_q-\epsilon_{q'}-K\right)^2} \\
&\quad \overline{g^{\mathrm{sum},j}_{k'k}}\ \overline{p^{v}_{q'q}}\ \overline{m^{v}_{qq'}} \int_{B_0}^{B} d\tilde{B}\ e^{2\tilde{B}(\epsilon_{k'}-\epsilon_k)\left(\epsilon_{q'}-\epsilon_q+K\right)}
\end{aligned}
$$

$$
\begin{aligned}
&+ [(\epsilon_{k'} - \epsilon_k - K) - (\epsilon_{q'} - \epsilon_q)] \\
&\quad [(\epsilon_{k'} - \epsilon_k - K) + (\epsilon_{q'} - \epsilon_q) - (\epsilon_q - \epsilon_{q'} + K)] \\
&\quad e^{-B\left((\epsilon_{k'} - \epsilon_k - K) + (\epsilon_{q'} - \epsilon_q)\right)^2} e^{-B\left(\epsilon_q - \epsilon_{q'} + K\right)^2} \\
&\quad \overline{m^j_{k'k}}\ \overline{g^{\mathrm{sum},v}_{q'q}}\ \overline{p^v_{qq'}} \int_{B_0}^{B} d\tilde{B}\ e^{2\tilde{B}(\epsilon_{k'} - \epsilon_k - K)\left(\epsilon_{q'} - \epsilon_q\right)} \\
&+ [(\epsilon_{k'} - \epsilon_k + K) - (\epsilon_{q'} - \epsilon_q)] \\
&\quad [(\epsilon_{k'} - \epsilon_k + K) + (\epsilon_{q'} - \epsilon_q) - (\epsilon_q - \epsilon_{q'} - K)] \\
&\quad e^{-B\left((\epsilon_{k'} - \epsilon_k + K) + (\epsilon_{q'} - \epsilon_q)\right)^2} e^{-B\left(\epsilon_q - \epsilon_{q'} - K\right)^2} \\
&\quad \overline{p^j_{k'k}}\ \overline{g^{\mathrm{sum},v}_{q'q}}\ \overline{m^v_{qq'}} \int_{B_0}^{B} d\tilde{B}\ e^{2\tilde{B}(\epsilon_{k'} - \epsilon_k + K)\left(\epsilon_{q'} - \epsilon_q\right)} \Big\}
\end{aligned}
\tag{E.6}
$$

E.3.6 Discussion of the Flow to 3rd Order

The elastic coupling is calculated in the diagonal parametrization. In the following we are thus only interested in contributions from $\epsilon_{k'} = \epsilon_k$. Inserting $k' = k$ in the Eq. (E.6) we find,

$$
\begin{aligned}
\frac{dg^{\mathrm{sum},j}_{kk}}{dB} = \ldots + \\
&[n(q'v)(1 - n(qv)) + n(qv)(1 - n(q'v))] \\
&\Big\{ - (\epsilon_{q'} - \epsilon_q)^2 e^{-2B\left(\epsilon_{q'} - \epsilon_q\right)^2} \overline{g^{\mathrm{sum},j}_{kk}}\ \overline{g^{\mathrm{sum},v}_{q'q}}\ \overline{g^{\mathrm{sum},v}_{qq'}}\ (B - B_0) \\
&- 2(\epsilon_{q'} - \epsilon_q - K)^2 e^{-2B\left(\epsilon_{q'} - \epsilon_q - K\right)^2} \overline{g^{\mathrm{sum},j}_{kk}}\ \overline{m^v_{q'q}}\ \overline{p^v_{qq'}}\ (B - B_0) \\
&- 2(\epsilon_{q'} - \epsilon_q + K)^2 e^{-2B\left(\epsilon_{q'} - \epsilon_q + K\right)^2} \overline{g^{\mathrm{sum},j}_{kk}}\ \overline{p^v_{q'q}}\ \overline{m^v_{qq'}}\ (B - B_0) \\
&+ \mathcal{O}\left(\mathrm{e}^{-BK^2}\right) \Big\}.
\end{aligned}
$$

The other terms are proportional to e^{-BK^2} and can be neglected if the flow is only studied for $B \gg 1/K^2$, see also discussion in main text.

Please note that with the definition of a function

$$
F(y) = \frac{y}{8B} \frac{\sqrt{\pi}}{\sqrt{2B}} \operatorname{erf}\left(\sqrt{2B}\, y\right) + \frac{1}{2(2B)^2}\, \mathrm{e}^{-2By^2}
$$

the scaling equation can be written in equilibrium ($T = 0$, $V = 0$) by

$$
\begin{aligned}
\frac{dg^{\mathrm{sum},j}_{k'k}}{dB} = \ldots &- 2BF(0) \overline{g^{\mathrm{sum},j}_{k'k}}\ \overline{g^{\mathrm{sum},v}_{q'q}}\ \overline{g^{\mathrm{sum},v}_{qq'}} \\
&- 4BF(-K) \overline{g^{\mathrm{sum},j}_{k'k}}\ \overline{m^v_{q'q}}\ \overline{p^v_{qq'}}\ - 4BF(K) \overline{g^{\mathrm{sum},j}_{k'k}}\ \overline{p^v_{q'q}}\ \overline{m^v_{qq'}}
\end{aligned}
$$

We find that all contributions of the band cutoff vanish for $B \gg 1/D^2$. Thus it is assumed that flow starts at $B_0 = 1/D^2$ with some initial value of the coupling. The two terms $F(K) = F(-K)$ are both proportional to e^{-BK^2} and will thus not be discussed in the regime of $B \gg 1/K^2$. Please see main text for further discussions of the flow equations and numerical results.

Acknowledgment

This work would have not been possible without a lot of support from other people and I apologize that it is not possible to mention you all.

I would like to thank Prof. P. Wölfle and Prof. A. Mirlin for refereeing this thesis.

I would like to thank Prof. P. Wölfle for his support, scientifically and financially, and for introducing me to this interesting topic. Thanks for many enlightening discussions, inspiring ideas, and for teaching me the scientific way of working.

A special thanks goes to Assoc. Prof. J. Paaske. Thanks for your support and for providing many insights into the world of non-equilibrium theory. Thanks for the numerous phone calls, emails, and discussions on every possible occasion, your neverending interest in my calculations, and for keeping up the good spirit even to fourth order.

I would also like to thank Prof. S. Kehrein and his group, in particular Peter Fritsch, for introducing me to the flow equation method. Thanks for many useful discussions, support and help, and providing inside information on both non-equilibrium scaling methods.

I would like to thank the people at the "Institut für Theorie der Kondensierten Materie" for a nice daily atmosphere, especially Rose Schrempp for all her support. Thanks to all my colleagues for useful discussions, providing physical insights, explanations and calculational tricks, help and technical support, and nice coffee breaks.

While writing this thesis I was lucky to be supported by Dan Bohr, Jan Brinckman, Peter Fritsch, Christine Köhler, Jens Paaske, Stefan Schmaus, Holger Schmidt, and Benjamin Schmidt.

I would also like to thank Dan Bohr for making this thesis possible at all. Thanks for standing by my side and for providing the right support at the right time.

Finally thanks goes to my family for your backup and encouragement in good times and bad times. It is hard to express my gratitude, but I hope you can be as proud of me as I am of you.

Bibliography

[1] J. Kondo, "Resistance minimum in dilute magnetic alloys," *Prog. Theor. Phys.*, vol. 32, no. 1, pp. 37–49, 1964.

[2] A. C. Hewson, *The Kondo Problem to Heavy Fermions*. Cambridge University Press, 1993.

[3] L. Kouwenhoven and L. Glazman, "Revival of the kondo effect," *Physics World*, p. 33, January 2001.

[4] P. Coleman, "Local moment physics in heavy electron systems." cond-mat/0206003v3, June 2002.

[5] L. I. Glazman and M. Pustilnik, "Low-temperature transport through a quantum dot." cond-mat/0501007v2, January 2005.

[6] M. Grobis, I. G. Rau, R. M. Potok, and D. Goldhaber-Gordon, "Kondo effect in mesoscopic quantum dots." cond-mat/0611480v1, November 2006.

[7] P. W. Anderson, "Localized magnetic states in metals," *Phys. Rev.*, vol. 124, pp. 41–53, October 1961.

[8] J. R. Schrieffer and P. A. Wolff, "Relation between the anderson and kondo hamiltonians," *Phys. Rev.*, vol. 149, pp. 491–492, September 1966.

[9] P. Nozières, "A "fermi-liquid" description of the kondo problem at low temperatures," *Journal of Low Temperature Physics*, vol. 17, pp. 31–42, October 1974.

[10] P. W. Anderson, "Poor man's scaling," *J. Phys. C*, vol. 3, p. 2436, 1966.

[11] K. G. Wilson, "The renormalization group: Critical phenomena and the kondo problem," *Rev. Mod. Phys.*, vol. 47, p. 773, October 1975.

[12] C. Jayaprakash, H. R. Krishnamurthy, and J. W. Wilkins, "Two-impurity kondo problem," *Phys. Rev. Lett.*, vol. 47, p. 737, September 1981.

[13] B. A. Jones and C. M. Varma, "Study of two magnetic impurities in a fermi gas," *Phys. Rev. Lett.*, vol. 58, p. 843, March 1987.

[14] B. A. Jones, C. M. Varma, and J. W. Wilkins, "Low-temperature properties of the two-impurity kondo hamiltonian," *Phys. Rev. Lett.*, vol. 61, p. 2819, December 1988.

[15] R. M. Fye and J. E. Hirsch, "Quantum monte carlo study of the two-impurity kondo hamiltonian," *Phys. Rev. B*, vol. 40, p. 4780, September 1989.

[16] I. Affleck, A. W. W. Ludwig, and B. A. Jones, "Conformal-field-theory approach to the two-impurity kondo problem: Comparison with numerical renormalization-group results," *Phys. Rev. B*, vol. 52, p. 9528, October 1995.

[17] L. Zhu and C. M. Varma, "Coherence in the two impurity kondo problem." cond-mat/0607426v2, January 2007.

[18] C. Kittel, *Quantum Theory of Solids*. John Wiley & Sons. Inc., 1967.

[19] D. Goldhaber-Gordon, H. Shtrikman, D. Mahalu, D. Abusch-Magder, U. Meirav, and M. A. Kastner, "Kondo effect in a single-electron transistor," *Nature*, vol. 391, p. 156, January 1998.

[20] S. M. Cronenwatt, T. H. Oosterkamp, and L. P. Kouwenhoven, "A tunable kondo effect in quantum dots," *Science*, vol. 281, p. 540, 1998.

[21] W. G. van der Wiel, S. Franceschi, T. Fujisawa, J. M. Elzerman, S. Tarucha, and L. P. Kouwenhoven, "The kondo effect in the unitary limit," *Science*, vol. 289, p. 210, September 2000.

[22] H. Bruus and K. Flensberg, *Many-Body Quantum Theory in Condensed Matter Physics*. Oxford University Press, 2004.

[23] L. I. Glazman and M. E. Raikh, "Resonant kondo transparency of a barrier with quasilocal impurity states," *JETP Letters*, vol. 47, p. 452, 1988.

[24] T. K. Ng and P. A. Lee, "On-site coulomb repulsion and resonant tunneling," *Phys. Rev. Lett.*, vol. 61, p. 1768, October 1988.

[25] D. C. Ralph and R. A. Buhrmann, "Kondo-assisted and resonant tunneling via a single charge trap: A realization of the anderson model out of equilibrium," *Phys. Rev. Lett.*, vol. 72, no. 21, p. 3401, 1994.

[26] W. G. van der Wiel, S. De Franceschi, J. M. Elzerman, T. Fujisawa, S. Tarucha, and L. P. Kouwenhoven, "Electron transport through double quantum dots," *Rev. Mod. Phys.*, vol. 75, pp. 1–22, December 2002.

[27] N. J. Craig, J. M. Taylor, E. A. Lester, C. M. Marcus, M. P. Hanson, and A. C. Gossard, "Tunable nonlocal spin control in a coupled-quantum dot system," *Science*, vol. 304, p. 565, 2004.

[28] H. B. Heersche, Z. de Groot, J. A. Folk, L. P. Kouwenhoven, H. S. J. van der Zant, A. A. Houck, J. Labaziewski, and I. L. Chuang, "The kondo effect in the presence of magnetic impurities." cond-mat/0508395v1, August 2005.

[29] S. Sasaki, S. Kang, K. Kitagawa, M. Yamaguchi, S. Miyashita, T. Maruyama, H. Tamura, T. Akazaki, Y. Hirayama, and H. Takayanagi, "Nonlocal control of the kondo effect in a double quantum dot-wire coupled system," *Phys. Rev. B*, vol. 73, p. 161303(R), 2006.

[30] M. G. Vavilov and L. I. Glazman, "Transport spectroscopy of kondo quantum dots coupled by rkky interaction," *Phys. Rev. Lett.*, vol. 94, p. 086805, March 2005.

[31] P. Simon, R. López, and Y. Oreg, "Rudermann-kittel-kasuya-yoshida and magnetic-field interactions in coupled kondo quantum dots," *Phys. Rev. Lett.*, vol. 94, p. 086602, March 2005.

[32] J. Rammer and H. Smith, "Quantum field-theoretical methods in transport theory of metals," *Rev. Mod. Phys.*, vol. 58, p. 323, April 1986.

[33] G. D. Mahan, *Many-Particle Physics*. Plenum Press, second edition ed., 1990.

[34] H. Haug and A.-P. Jauho, *Quantum Kinetics in Transport and Optics of Semiconductors*. Springer Series in Solid-State Sciences, Springer-Verlag, 1996.

[35] A. Rosch, J. Paaske, J. Kroha, and P. Wölfle, "Nonequilibrium transport through a kondo dot in a magnetic field: Perturbation theory and poor man's scaling," *Phys. Rev. Lett.*, vol. 90, no. 7, p. 076804, 2003.

[36] A. Rosch, J. Paaske, J. Kroha, and P. Wölfle, "The kondo effect in non-equilibrium quantum dots: Perturbative renormalization group," *Journal of the Phys. Society of Japan*, vol. 74, no. 1, p. 118, 2005.

[37] S. Kehrein, "Scaling and decoherence in the nonequilibrium kondo model," *Phys. Rev. Lett.*, vol. 95, no. 5, p. 056602, 2005.

[38] S. Kehrein, *The Flow Equation Approach to Many-Particle Systems*. Springer Tracts in Modern Physics, Springer-Verlag, 2006.

[39] T. Korb, F. Reininghaus, H. Schoeller, and J. König, "Real-time renormalization group and cutoff scales in nonequilibrium applied to an arbitrary quantum dot in the coulomb blockade regime," *Phys. Rev. B*, vol. 76, no. 16, p. 165316, 2007.

[40] S. G. Jakobs, V. Meden, and H. Schoeller, "Nonequilibrium functional renormalization group for interacting quantum systems," *Phys. Rev. Lett.*, vol. 99, no. 15, p. 150603, 2007.

[41] J. Paaske, A. Rosch, J. Kroha, and P. Wölfle, "Nonequilibrium transport through a kondo dot: Decoherence effects," *Phys. Rev. B*, vol. 70, p. 155301, 2004.

[42] A. A. Abrikosov, "Electron scattering on magnetic impurities in metals and anomalous resistivity effects," *Physics (N.Y.)*, vol. 2, no. 1, p. 5, 1965.

[43] P. Coleman, "New approach to the mixed-valence problem," *Phys. Rev. B*, vol. 29, p. 3035, March 1984.

[44] S. Sachdev and R. N. Bhatt, "Bond-operator representation of quantum spins: Mean-field theory of frustrated quantum heisenberg antiferromagnets," *Phys. Rev. B*, vol. 41, p. 9323, May 1990.

[45] M. Pustilnik and L. I. Glazman, "Kondo effect induced by a magnetic field," *Phys. Rev. B*, vol. 64, p. 045328, 2001.

[46] V. N. Golovach and D. Loss, "Kondo effect and singlet-triplet splitting in coupled quantum dots in a magnetic field," *Europhy. Lett.*, vol. 62, no. 1, pp. 83–89, 2003.

[47] V. N. Golovach and D. Loss, "Transport through a double quantum dot in the sequential tunneling and cotunneling regimes," *Phys. Rev. B*, vol. 69, p. 245327, 2004.

[48] J. Paaske, A. Rosch, P. Wölfle, N. Mason, C. M. Marcus, and J. Nygård, "Non-equilibrium singlet-triplet kondo effect in carbon nanotubes," *Nature Physics*, vol. 2, p. 460, 2006.

[49] S. Schmaus, "Elektronentransport durch halbleiternanodrähte im kondo regime," Master's thesis, Universität Karlsruhe, August 2007.

[50] L. P. Keldysh, "Diagram technique for nonequilibriun processes," *Sov. Phys. JETP*, vol. 20, p. 1018, 1965.

[51] L. P. Kadanoff and G. Baym, *Quantum Statistical Mechanics*. Benjamin, New York, 1962.

[52] J. Paaske, A. Rosch, and P. Wölfle, "Nonequilibrium transport through a kondo dot in a magnetic field: Perturbation theory," *Phys. Rev. B*, vol. 69, p. 155330, 2004.

[53] T. Langenbruch, "Two-channel kondo nonequilibrium signatures of multiorbital impurities," Master's thesis, University Bonn, March 2006.

[54] O. Parcollet and C. Hooley, "Perturbative expansion of the magnetization in the out-of-equilibrium kondo model," *Phys. Rev. B*, vol. 66, p. 085315, 2002.

[55] Y. Meir and N. S. Wingreen, "Landauer formula for the current through an interacting electron region," *Phys. Rev. Lett.*, vol. 68, p. 2512, April 1992.

[56] Y. Meir, N. S. Wingreen, and P. A. Lee, "Low-temperature transport through a quantum dot: The anderson model out of equilibrium," *Phys. Rev. Lett.*, vol. 70, p. 2601, April 1993.

[57] N. S. Wingreen and Y. Meir, "Anderson model out of equilibrium: Noncrossing-approximation approach to transport through a quantum dot," *Phys. Rev. B*, vol. 49, p. 11040, April 1994.

[58] T. A. Costi, "Kondo effect in a magnetic field and the magnetoresistivity of kondo alloys," *Phys. Rev. Lett.*, vol. 85, p. 1504, August 2000.

[59] A. Rosch, T. A. Costi, J. Paaske, and P. Wölfle, "Spectral function of the kondo model in high magnetic fields," *Phys. Rev. B*, vol. 68, p. 014430, 2003.

[60] Y. M. Blanter and M. Büttiker, "Shot noise in mesoscopic conductors," *Physics Reports*, vol. 336, pp. 1–166, 2000.

[61] M. J. M. D. Jong and C. W. J. Beenakker, *Shot noise in mesoscopic systems*, pp. 225–258. Kluwer Academic Press, 1997.

[62] W. Belzig, "Full counting statistics of super-poissonian shot noise in multilevel quantum dots," *Phys. Rev. B*, vol. 71, no. 16, p. 161301, 2005.

[63] S. S. Safonov, A. K. Savchenko, D. A. Bagrets, O. N. Jouravlev, Y. V. Nazarov, E. H. Linfield, and D. A. Ritchie, "Enhanced shot noise in resonant tunneling via interacting localized states," *Phys. Rev. Lett.*, vol. 91, p. 136801, September 2003.

[64] A. Cottet, W. Belzig, and C. Bruder, "Positive cross-correlations due to dynamical channel blockade in a three-terminal quantum dot," *Phys. Rev. B*, vol. 70, no. 11, p. 115315, 2004.

[65] V. Koerting, P. Wölfle, and J. Paaske, "Transconductance of a double quantum dot system in the kondo regime," *Phys. Rev. Lett.*, vol. 99, no. 3, p. 036807, 2007.

[66] D. T. McClure, L. DiCarlo, Y. Zhang, H.-A. Engel, C. M. Marcus, M. P. Hanson, and A. C. Gossard, "Tunable noise cross correlations in a double quantum dot," *Phys. Rev. Lett.*, vol. 98, p. 056801, 2007.

[67] Y. Zhang, L. DiCarlo, D. T. McClure, M. Yamamoto, S. Tarucha, C. M. Marcus, M. P. Hanson, and A. C. Gossard, "Noise correlations in a coulomb-blockaded quantum dot," *Phys. Rev. Lett.*, vol. 99, p. 036603, 2007.

[68] P. W. Anderson, *Basic Notations of Condensed Matter Physcis*. Westview Press, 1997.

[69] M. N. Kiselev, K. Kikoin, and L. W. Molenkamp, "Resonance tunneling through a double quantum dot at finite bias," *Phys. Rev. B*, vol. 68, p. 155323, 2003.

[70] Y.-F. Yang and K. Held, "Nonequilibrium transport through parallel double quantum dots in the kondo regime," *Phys. Rev. B*, vol. 72, p. 235308, 2005.

[71] C.-H. Chung and W. Hofstetter, "Kondo effect in coupled quantum dots with rkky interaction: Finite temperature and magnetic field effects." cond-mat/0607772, July 2006.